PhD thesis

Relaxation in Supercooled Liquids

Linear and Nonlinear, Mechanical and Dielectric Studies of Molecular Liquids

Author:
Tina Hecksher

Supervisor:
Jeppe Dyre

Danish National Research Foundation Centre "Glass and Time",
IMFUFA, Department of Science, Systems, and Models
Roskilde University, Denmark

Abstract in English

In the present PhD thesis dissertation three themes of viscous liquids dynamics are treated: (1) the visco-elastic properties studied via mechanical measurements, (2) the temperature dependence of the (dielectric) relaxation time, and (3) non-linear relaxation. The first part is based on own measurements of molecular liquids, in particular 5-phenyl-4-ether (PPE) and tetramethyl-tetraphenyl-trisiloxane (DC704), while part 2 and 3 are based on analyses of measurements by others.

The mechanical measurements in the first part consist of bulk and shear modulus measurements with unique methods developed in the Glass & Time group at Roskilde University. The measurements were carried out under identical experimental conditions in the same cryostat thus eliminating most uncertainties associated with comparing different measured properties of viscous liquids, the temperature calibration being the most problematic. We found that the spectral shape of the bulk and shear modulus relaxation is identical within experimental uncertainty for PPE and DC704, respectively, while the bulk modulus relaxes slower than the shear modulus. Bulk and shear modulus relaxation times, as well as relaxation times of three other response functions, are however proportional in the entire temperature interval studied.
Measurements on DC704 were combined with mechanical measurements at higher frequencies carried out by our collaborators from Massachusetts Institute of Technology in the USA to compile "the widest mechanical spectrum in the world". A total of six different techniques covers 14 orders of magnitude in frequency and 250 Kelvin in temperature. The good agreement between the results from all these methods can be seen as a mutual confirmation of the absolute values measured by the individual methods.

In the second part Adam-Gibbs entropy model is challenged. The model predicts a phase transition to an "ideal glassy state" with infinite relaxation time. An analysis of the temperature dependence of the dielectric relaxation time for 42 liquids show that data do not favor this picture.

In the third part, a series of non-linear relaxation measurements on five different molecular liquids. It is shown that the non-linear relaxation can be linearized via the Tool-Narayanaswamy formalism. The high resolution of the measurements indicates that the linearized relaxation at long times follow a simple exponential, while the relaxation at short times is "stretched". This discovery lead to a new single-parameter fitting function for the relaxation of viscous liquids. The function was fitted to the (linear) dielectric relaxation spectra for 53 liquids and it was found to fit as well as the "standard" fitting function, the stretched exponential.

Abstract in Danish

Denne Ph.D. afhandling behandler tre temaer inden for seje væskers dynamik: (1) visko-elastiske egenskaber studeret via mekaniske målinger, (2) temperaturafhængigheden af (den dielektriske) relaxations tid og (3) ikke-lineær relaxation. Første del er baseret på egne målinger af især to organiske væsker: PPE (5-phenyl-4-ether) og DC704 (tetramethyl tetraphenyl trisiloxane), mens anden og tredje del er analyser af andres målinger.

De mekaniske målinger i første del består af shear- og bulkmodul målinger udført med unikke metoder udviklet i Glas & Tid gruppen på Roskilde Universitet. Målingerne er udført under samme eksperimentelle forhold i den samme cryostat, hvilket eliminerer de fleste usikkerheder der ellers er forbundet med sammenligning af forskellige målte størrelser, hvoraf den mest problematiske er den absolutte temperaturkalibrering. Overordnet set kan det konkluderes, at den spektrale form af bulk- og shearmodulets relaxation er identisk inden for måleusikkerheden i de to undersøgte stoffer henholdsvis, mens bulk modulet relaxerer langsommere end shear modulet. Relaxationstiderne for bulk og shear modulet, samt 3 andre responsfunktioner følges ad i hele det undersøgte temperaturområde.
Målinger på DC704 blev forbundet med mekaniske målinger ved højere frekvenser udført af vores samarbejdspartnere fra Massachusetts Institute of Technology i USA, for at samle "verden længste mekaniske spektrum". I alt seks forskellige måleteknikker spænder over 14 størrelsesordener i frekvens og 250 Kelvin i temperatur. Den fine overensstemmelse mellem disse målinger kan ses som en gensidig bekræftelse af de enkelte metoders absolutte niveauer.

I del 2 udfordres den populære entropi model for temperaturafhængigheden af viskositeten i seje væsker. Modellen forudsiger en faseovergang til en "ideel glastilstand" med uendelig relaxationstid. En analyse af temperaturafhængigheden af den dielektriske relaxationstid for 42 væsker viser imidlertid, at data ikke specifikt understøtter denne model.

Endelig analyseres i tredje del en række meget præcise dielektriske målinger af relaxationen i 5 væsker efter ikke-lineære temperaturstep. Det vises, at den ikke-lineære relaxation kan lineariseres ved Tool-Narayanaswamy-formalismen. Den høje opløsning af de eksperimentelle data indikerer, at den linariserede relaxationskurve afsluttes exponentielt, mens relaxationen til korte tider er "stretched". Dette førte til fødslen af en ny én-parameter relaxationsfunktion. Denne funktion blev efterfølgende testet på dielektriske relaxationsspektre for 53 væsker ligesom 3 øvrige én-parameter fittefunktioner for ikke-exponentielt henfald. Funktionen viser sig at fitte data lige så godt som standard fittefuntionen, "stretched exponential".

Acknowledgements

This dissertation represents the work accumulated since I started as a PhD student in the Danish National Research Foundation Centre 'Glass & Time' at Roskilde University. During my time as PhD student in the Glass & Time group, I have been surrounded by many skilled and – equally important – nice colleagues, both within the group and in the department (IMFUFA) in general. I have always felt that all doors were open and people were always willing to help or discuss. This goes for other PhD student as well as for postdocs and professors. I thank you all jointly for creating such a both welcoming and intellectually stimulating atmosphere. Naturally there is a list of people who I feel have had a particularly great impact on the course of my PhD.

First of all I would like to thank my supervisor Jeppe Dyre for his whole-hearted support and mentoring – not just during my PhD studies, but also years before. I especially appreciate the freedom I have enjoyed under his supervision that has allowed me to pursue the topics that I felt was the most interesting or important. This, I believe, is a manifestation of the confidence and faith he has in his students.

I would also like to thank Tage Christensen for his willingness to share his idea, knowledge, and experience in general and about the experimental techniques in particular. And Niels Boye Olsen whose intuition and experience from a lifetime in the lab has been a great inspiration.

I owe a special thank you to Albena Nielsen, a former PhD student in our group, who on many occasions has nursed my measurements and refilled nitrogen in my cryostat and to Claudio Maggi, my former office mate, now a full-fledged doctor somewhere in Italy, for good company. I have also worked closely together with Albena on several projects and it has always been a pleasure.

Our collaborators at Massachusetts Institute of Technology, Christoph Klieber, Darius Tochinsky, Jeremy Johnson, and Kara Manke in the group of Keith Nelson, and Maria Cutroni and Andrea Mandanici from University of Messina are all acknowledged for the their hard work and enthusiasm for our collaborative project.

The technical staff at IMFUFA, Torben Rasmussen, Ebbe H. Larsen, Preben Olsen, Ib Høst, and Heine Larsen, have all contributed in some way to my project (and otherwise: thank you for fixing my sons push chair and various toys of his!).

It is a rare luxury to work so closely together with the workshop, not only in the day-to-day experimental issues (where I personally have benefitted greatly from Torben and Ib's combined effort to help me find the source of several never-seen-before errors), but also in the developing and designing phases of planning new experiments.

Heine has been indispensable in the final stages of the thesis writing, fixing all possible – and impossible – kinds problems with LaTex, Linux, SVN, scanning, etc. etc. – and

doing it with a smile.

I am most grateful that Sif Skjoldager and, especially, Thomas Hecksher, took the time for reading and commenting parts of my thesis (in Thomas' case *all* of the thesis). I am sure, this has greatly improved the quality!

Finally, I am deeply indebted to my family for moral support over the years, especially, from the two most important people in my life: my husband Henrik, and my son, Ro. Henrik has always been there whenever things are falling apart (which they do frequently...) and has shown an immense amount of patience, understanding, and flexibility during the my thesis writing, while struggling with his own PhD thesis. Ro robbed much of my night's sleep in the first years of my PhD study, but in the end I feel that he has taught me more about the value of time, than many years in school.

Tina Hecksher

November, 2010

List of commonly used notation

$\mathbf{u}$	displacement vector
δ_{ij}	Kronecker delta
ϵ_{ij}	strain tensor
σ_{ij}	stress tensor
c_{ijkl}	elasticity tensor
K, $K(\omega)$	(complex) bulk modulus
G, $G(\omega)$	(complex) shear modulus
M, $M(\omega)$	(complex) longitudinal modulus
E, $E(\omega)$	(complex) Young's modulus
ν, $\nu(\omega)$	(complex) Poisson's ratio
c_l	longitudinal sound velocity
c_t	transverse sound velocity
K_∞, G_∞, c_∞	instantaneous (high frequency) moduli/sound velocities
K_0, G_0, c_0	DC (low frequency) moduli/sound velocities
$\tilde{Z}$,$\tilde{Y}$	(generalized) impedence/admittance
q (q_h, q_c)	heating/cooling rates, $\frac{\partial T}{\partial t}$
T	temperature
T_g	glass transition temperature
k_B	Boltzmann's constant
ΔE	(free) energy of activation
τ	relaxation time
η	viscosity
k	wave vector
ω	angular frequency (s^{-1})
f	frequency (Hz)
$f_{\max}$ ($\omega_{\max}$)	loss peak (angular) frequency
$(-)'$	real part of $(-)$
$(-)''$	imaginary part of $(-)$
$\dot{(-)}$	time derivative of $(-)$

Contents

1 Introduction to the thesis

The topic in this thesis is the dynamics of viscous liquids and glasses. This research field is very broad and interdisciplinary; it is just as likely to find a physicist as a chemist, an engineer, or a materials scientist, and even biologists and food scientists are frequently encountered. This is because the field of viscous liquids and glasses does not only present significant fundamental challenges, it is also of great importance in many practical applications. The optical and physical properties of glass make it suitable for many engineering applications such as window glass, container glass, laboratory equipment, fibers and optics. In addition to these familiar glass applications, most plastic materials in our everyday lives are glassy polymers. The glassy state has also proven to be important in more surprising areas [1] such as pharmaceuticals [2] and storage and preservation of food [3]. The properties of metallic glasses make them superior to classic metals materials especially for micro engineering purposes.

In this thesis the focus is on the fundamental aspects of the dynamics of viscous liquids and glasses.

1.1 Reading guide and composition

The thesis consists of three parts with separate titles: Part I "Mechanical relaxation spectra of viscous liquids", Part II "Temperature dependence of the dielectric relaxation time", and Part III "Linear and non-linear relaxation" with separate reference lists. The first and the last part include several chapters. I chose to do so, because there is very little overlap between the three parts and there was no obvious link between the three although of course they fall in the area the viscous liquid dynamics.

Before the three parts of the thesis there is a short general introduction to the field, explaining what a glass is, the phenomenology of the viscous liquids and glasses, and stating the "big questions" of the field, that ultimately we aim to answer. Then each part of the thesis will have its own introduction to the specific subtopic that it is concerned with. In the end I will give a summary and outlook, including an overview of what I believe to be the most important outcome of my work.

Part I consists of a total of seven chapters. First an introductory chapter about mechanical measurements in general and an overview of the methods used and the liquids studied. The following three chapters (chapter 4, 5, and 6) are devoted to presenting the experimental techniques and the data. The first of the three concerns the bulks modulus measurement and is by far the most extensive, reflecting that it is a relatively unexplored technique – despite the fact that it was developed more than 15 years ago – and only a short description exists. The chapter on the shear modulus measurement is brief where the main new contribution to the discussion of the technique is thor-

ough investigation of the reproducibility of the measurement, and the third chapter on the new measurement is merely a proof of concept. Then three chapters follows that will utilize these data in different ways. In chapter 7 various characteristic properties are derived from the different measurements and compared. Chapter 8 connects the measurements on DC704 with high-frequency mechanical measurements to compile a broadband mechanical spectrum, and in chapter 9 the so-called Cauchy relation is examined.

Part II is just one chapter, which in essence presents the content of Paper I (enclosed on page 259). Paper I presented a systematic investigation of the temperature dependence of the (dielectric) relaxation time arguing against the existence of a dynamic divergence at a finite temperature. The chapter features many details not included in the paper, in particular an analysis of the stability of the fitting routines that the analysis is based on, as well as new observations.

Part III consists of three chapters. The first chapter (chapter 11) is an introduction to relaxation in the glass, i.e. when the liquid is quenched out of equilibrium. This chapter also introduces the traditional formulation of Tool-Narayanaswamy model for non-linear relaxation. Second chapter (chapter 12) is an analysis of a series of non-linear temperature step experiments, formulating a test of the inner clock hypothesis. Chapter 13 concludes – much in the spirit of part II – this part by comparison various single parameter functions for non-exponential relaxation.

Five papers are enclosed in chronological order. Some parts of the thesis are based heavily on Paper I (p. 259) and Paper III (p. 269), while Paper II (p. 265), IV (p. 283), and V (p. 289) are only peripherally covered.

Throughout the thesis writing process it was my intension that the written output should be a useful tool for the next PhD student. Consequently, the thesis ended up being quite detailed (and long!). On the other hand, I have split each part into relatively self-contained chapters to ease the reading. And I have not been shy about using illustrations; whenever I felt a point would benefit from some kind of illustration it was included. So the thesis may almost be read as a cartoon.

1.1.1 Prerequisites and notation

In several of the chapters a familiarity with the theory of elasticity is required. Landau & Lifshitz [4] is a standard reference and can be recommended. Notation used here (adopted from Landau & Lifshitz [4]) is the Einstein notation, i.e. summation over repeated indices (unless otherwise explicitly stated). For instance σ_{ii} should be read as sum of the diagonal elements.

Knowledge of linear response theory in the time and frequency domain and equivalent diagrams as a modelling tool is also assumed. In appendix A a short summary of this can be found.

I have aimed at being consistent in the use of symbols. The list of symbols included on page vi should be valid unless something else is explicitly stated. Symbols will be explained (at least) the first time they are used.

1.2 General reflections on the thesis

While there is little overlap between the different parts of the thesis in phenomenology, I think that they do have a macroscopic and phenomenological approach in common. Probably, this approach is natural for an experimentalist, because what we measure are typically macroscopic quantities. Thus much of the work in the present thesis consists of relating and comparing measurable macroscopic quantities to each other.

The methods in this thesis change between the in-depth investigation of few (representative) examples and the very broad study of many data sets. Both approaches are useful and necessary.

A underlying point in the thesis is that careful and precise measurements are a necessity for testing existing models, but also for generating new ideas or for new discoveries. Measurements with much scatter are not well-suited to distinguish between models. And if we are not careful with experiments, spurious effects may be misinterpreted as physical features.

The broad studies of many data sets can be used to test models and new ideas generated from the more focussed studies, to see how general some observation is or how well a model in general describes data.

2 Phenomenology of Glasses and Glass-Forming Liquids

What is a glass? In the everyday understanding, glass is the material that for instance windows or bottles are made of. As a scientific research topic, glass has a much broader meaning: glass is state of matter (almost) on par with gaseous, liquid, and crystalline phases of matter [1], in the sense that apparently all liquids can form glasses [1, 5–7]. Some liquids (like glycerol or silica) are actually difficult to crystallize, while others are very difficult to vitrify (like water or metals).

A glass macroscopically behaves like a crystalline solid, but microscopically lacks the order of the crystal – the structure of a glass is disordered like the (super-cooled) liquid. *Glass* or *glassy* usually refers to structural disorder, but sometimes also other kinds of disorder, for instance models with spatial order but energetic disorder (lattice-gas models) or spin disorder (spin-glass models) or plastic crystals (with disordered dipoles). We will only use the term in the first sense.

2.1 Producing a glass

The most common way to produce a glass is by cooling. Figure 2.1 is a schematic illustration of some thermodynamic property (for instance volume or enthalpy) of the liquid of the liquid as a function of temperature when cooled at some constant cooling rate $q := \frac{dT}{dt}$. Starting above the melting point the liquid contracts and volume decreases when the temperature is lowered. At the melting temperature T_M the liquid can crystallize in which case this property will undergo a discontinuous change and then – upon further cooling – contract at slightly slower rate, reflecting the fact the expansion coefficient of a crystal normally is lower than that of the liquid. This is illustrated with the blue curve.

If instead the liquid is cooled fast enough to prevent crystallization, it continues to contract at the same rate as the liquid. The liquid is now *super-cooled* and the state is a *meta-stable* equilibrium state – the crystal of course being the true equilibrium state. The viscosity η and relaxation time τ now increases dramatically, and eventually the liquid will not have time to relax fully to equilibrium and it forms a glass. In the (T, V)-plot this will show up as a gradual deviation from the equilibrium liquid line eventually settling to a line roughly parallel to the crystal line.

The glass-transition temperature T_g is defined as the temperature where the glass and liquid line intersect. This temperature is however not a material constant like the melting temperature, but a "dynamic" temperature that will depend on the cooling rate: a fast cooling rate will give a high T_g and a slow cooling rate will result in a lower

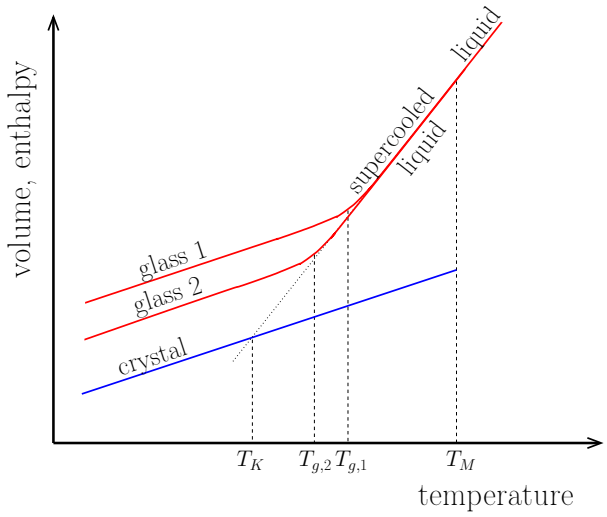

Figure 2.1 The canonical schematic illustration of some measured property of liquid, for instance volume or enthalpy, as a function of temperature when cooled at some constant cooling rate q.

T_g. The cooling rate is defined by $q = dT/dt$. If the cooling process is viewed as a series of temperature steps, then the cooling rate expresses how much time is spent at each new temperature $\Delta t = \Delta T/q$. Thus the liquid falls out of equilibrium when Δt is smaller than the relaxation time τ

$$\begin{aligned} \Delta t \gg \tau &\rightarrow \text{ (supercooled) liquid} \\ \Delta t \approx \tau &\rightarrow \text{ glasstransition} \\ \Delta t \ll \tau &\rightarrow \text{ glass} \end{aligned}$$

Evidently, the glass is not a unique state but a state that depends on the temperature (and also pressure) history.

That the glass transition is a dynamic temperature that depends on the cooling rate has been showed clearly by experiments (e.g. by Kovacs [8] and Moynihan *et al* [9]), however if the cooling rates are not varied wildly the different T_g's will fall within a narrow range of temperatures. So, as long as the cooling rate is in the range 0.1-100K/min it is thus still meaningful and relatively well-defined to talk about the glass transition temperature. Since the viscosity of the liquid is roughly 10^{12} when falling out of equilibrium at these moderate cooling rates, T_g is sometimes pragmatically defined through the viscosity

$$\eta(T_g) = 10^{12}\text{Pas}. \tag{2.1}$$

If we were very patient and cooled the liquid at an increasingly slower rate we could in principle stay on the equilibrium liquid line. At some finite temperature (called the *Kauzmann temperature* T_K) this line – since it is steeper – will cross the crystal line, see Fig. 2.1. This is the *Kauzmann paradox*: the volume (and also entropy) of the liquid will be lower than that of the crystal which is the true thermodynamic

equilibrium state. In practice this point has never been reached and is always avoided by the kinetic glass transition. Still, a lot of theoretical work in this field has been dedicated to solving this paradox [10–12].

2.1.1 Not really liquid – not really solid

The properties of a viscous liquid are *visco-elastic*, i.e. they are time or frequency dependent. If the liquid is perturbed, the short time or high frequency response will be *elastic* (solid-like), while the long time or low frequency response will be *viscous* (liquid-like). The viscosity of a Newtonian liquid is defined by $\sigma = \eta\dot{\epsilon}_N$, while Hooke's law for an elastic solid states $\sigma = G_\infty \epsilon_H$

The Maxwell model [13, 14] extrapolates between the liquid and solid behavior by assuming

$$\dot{\epsilon} = \dot{\epsilon}_N + \dot{\epsilon}_H = \frac{\sigma}{\eta} + \frac{\dot{\sigma}}{G_\infty} \tag{2.2}$$

The constitutive equation of the Maxwell model can thus be written $\eta\dot{\epsilon} = \sigma + \eta/G_\infty\dot{\sigma}$, where the ratio η/G_∞ has the dimensions of time and is called the Maxwell relaxation time

$$\tau_M = \frac{\eta}{G_\infty}\,. \tag{2.3}$$

This relation that tells us that the relaxation time of the liquid is roughly proportional to the viscosity, since the temperature dependence of G_∞ is much less dramatic than that of the viscosity. Visco-elastic effects can in principle be observed in a liquid at any temperature, but at high temperatures this is an experimentally quite challenging task that requires an extremely good time resolution. At lower temperatures the relaxation takes place over minutes or hours.

The Maxwell model can be illustrated by a electrical circuit with a resistor and a capacitance in parallel, see Fig. 2.2. The resistor models the dissipative property of

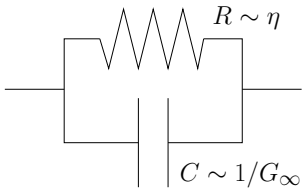

Figure 2.2 Maxwell model of visco-elastic behavior in terms of an electrical network.

the liquid and the capacitor the elastic (energy storing) property. This model has the correct limiting behavior: at high frequencies only the capacitor is seen while at low frequencies the capacitor blocks the current and only the resistor is seen. The mechanical equivalent of voltage and current are the (shear) stress and the (shear) strain rate. The impedance of the network is given by

$$\tilde{Z}_M = \frac{1}{\tilde{Y}_M} = \frac{1}{\tilde{Y}_R + \tilde{Y}_C} = \frac{1}{\frac{1}{R} + i\omega C} = \frac{R}{1 + i\omega RC} \tag{2.4}$$

and we recover the Maxwell relaxation time as the time constant of electrical circuit $\tau_M = RC = \frac{\eta}{G_\infty}$.

A more detailed and technical introduction to visco-elasticity is given in chapter 3 as an introduction to the mechanical measurements presented subsequently.

2.2 Universal properties of viscous liquids

The ultra-viscous liquid phase preceding glass formation has universal physical properties, independent of the nature of the chemical bonds involved. These universal features [1, 15–19] may be summarized into three non's: Non-Arrhenius temperature dependence of the average relaxation time, non-exponential relaxations, and non-linearity of relaxations upon even small temperature jumps (e.g., 1 %).

2.2.1 Non-Arrhenius

One of the hallmark features of the supercooled liquid is the dramatic increase in relaxation time and viscosity. In Fig. 2.3 the dielectric relaxation time data for some liquids is plotted as a function of temperature. As the temperature is lowered the relaxation times increase rapidly. Even when plotted on a logarithmic scale, the increase in relaxation time is dramatic increasing many orders of magnitude with a 10% change in temperature that is shown here.

The Arrhenius equation gives the temperature dependence of activated processes such as instance chemical reaction rates, and gives rise to similar dramatic temperature dependences.

Already in the 1930's Eyring [20] showed that many physical processes in condensed phases involve passages over free energy barriers. Among these processes are plastic flow, molecular diffusion, and dielectric relaxation. Kauzmann [21] therefore argued, that we must expect metastable states to occur supported by the free energy barriers involved in these processes [21].

If we adopt the view that the viscous flow in a supercooled liquid is an activated process, then the increase in viscosity should be described by the Arrhenius equation

$$\eta = \eta_0 \exp\left\{\frac{\Delta E}{k_B T}\right\} \tag{2.5}$$

where ΔE is the free energy of activation, the prefactor η_0 is the high temperature limit of the viscosity (usually taken to be $\sim 10^{-4}$Pas), k_B is Boltzmanns constant, and T is temperature. Usually, what is observed is that the free energy of activation is an increasing function of temperature $\Delta E = \Delta E(T)$. This is illustrated in Fig. 2.4, where log viscosity of several glass-forming liquids is plotted against the inverse temperature scaled with T_g. In this plot all curves have two common points: the glass transition ($\eta = 10^{12}$Pas) and the high temperature limit ($\eta_0 = 10^{-4}$Pas). In between there are a variety of different behaviors from nearly Arrhenius (i.e. a straight line in this plot) to extremely non-Arrhenius.

Based on this representation, Angell [22] suggested a classification of the liquids based on the steepness of their curve at T_g in the Arrhenius plot. Near Arrhenius liquids are

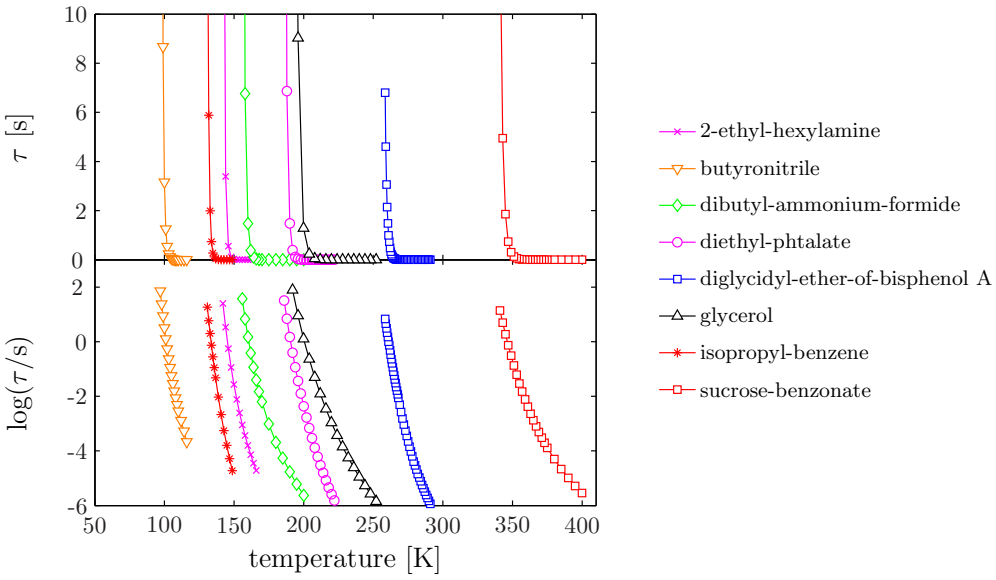

Figure 2.3 Dielectric relaxation times of eight liquids plotted as a function of temperature. Top panel shows simply the relaxation time versus temperature, while bottom panel show the logarithmic relaxation time versus temperature. Obviously, the relaxation time is extremely sensitive to temperature in these supercooled liquids – even plotted on a logarithmic scale the increase upon cooling appears quite dramatic increasing 6-8 orders of magnitude in a relatively small temperature interval. (See table 10.1, p. 157, for further informations on the liquids.)

termed *strong* liquids and super-Arrhenius liquids *fragile*. The *fragility index* is defined by

$$m_A = \left.\frac{d\log\eta}{d(T_g/T)}\right|_{T=T_g} . \tag{2.6}$$

If $\log\eta_0 = -4$ and $\log\eta(T_g) = 12$, Arrhenius behavior corresponds to $m_A = 16$. The prototypical glassformer glycerol has a fragility index of ~ 50. The highest measured fragility is of decahydro isoquinoline [23], which has a fragility index of 158 [24].

The Arrhenius model has more or less become the standard model and quest of explaining the dramatic increase in relaxation time and viscosity has to a high degree become a search of what controls the temperature dependence of the activations energy (at least in the more phenomenological models). There are a number of different models and purely empirical functions for the non-Arrhenius temperature dependence of the viscosity, some of which we introduce in part II (chapter 10).

2.2.2 Non-exponential

In a viscous liquid the relaxation towards equilibrium following a step-like perturbation is almost always non-exponential [25–27]. Theoretically it is not well-understood why this is. There are two possible scenarios to explain: either the relaxation is in-

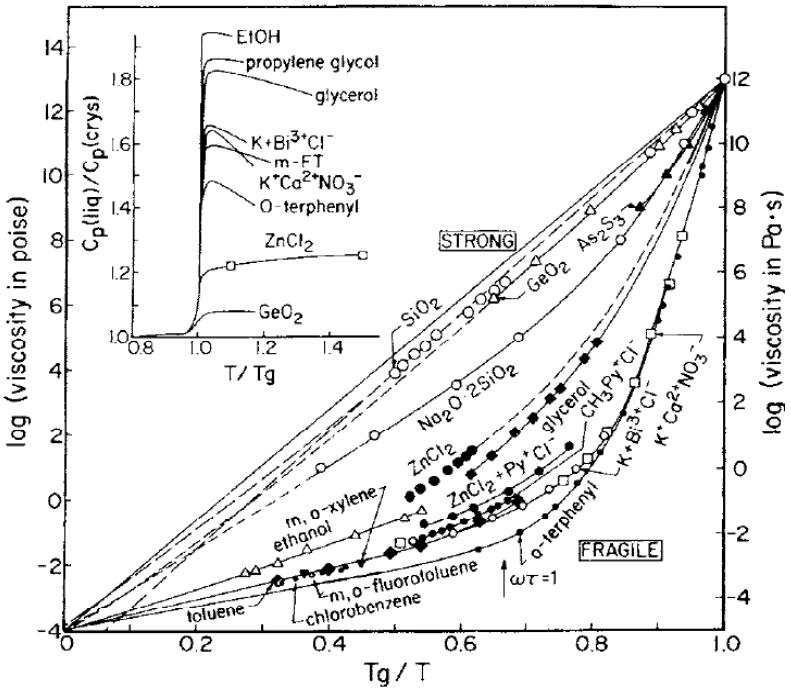

Figure 2.4 Arrhenius plot of the viscosity of various glass forming liquids with the temperature axis scaled with T_g. Liquids range from a near Arrhenius behavior represented by a straight line in this plot (termed "strong" liquids) to an extremely non-Arrhenius behavior giving a high curvature traces between the two fixed points (termed "fragile" liquids). The inset show the specific heat jumps at the glass transition. From [22]

herently non-exponential (the "homogeneous" picture) or the macroscopically observed non-exponentiality is a superposition of microscopic domains with exponential relaxation of different relaxation times (the "heterogeneous" picture). These scenarios were illustrated by Richert [28], which we show in Fig. 2.5. Experiments primarily provide support for the heterogeneous picture [29].

The standard fitting functions in the time domain is the stretched exponential [30, 31]

$$r(t) = \exp\left(-\left(t/\tau\right)^{\beta_{SE}}\right) \tag{2.7}$$

where the stretching parameter, β_{SE} varies between 0 and 1. For $\beta_{SE} = 1$ this gives a simple exponential relaxation. $r(t)$ represents a response in time after a step input.

Many linear experiments are conducted in the frequency domain, where the perturbation is periodic. In the frequency domain the "stretching" of the relaxation shows up as a characteristic asymmetric loss peak, where the low frequency side of the alpha relaxation peak is Debye like with $\varepsilon'' \propto \omega^1$, while on the high frequency side we typically have $\varepsilon'' \propto \omega^{-n}$ where $0 < n < 1$. A popular fitting function in the frequency domain

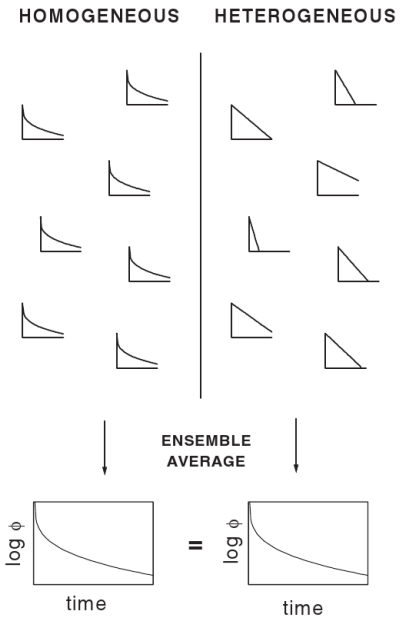

(a) From [28]

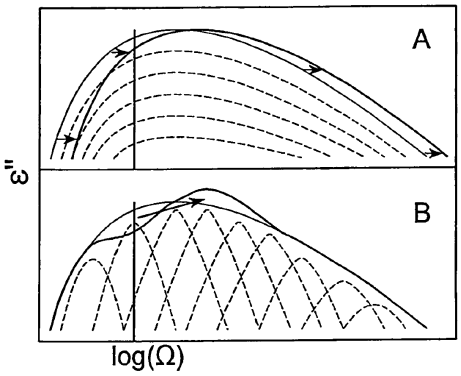

(b) From [27]

Figure 2.5 An illustration of the difference between the "homogeneous" and the "heterogeneous" explanation for the non-exponential relaxation observed in most viscous liquids. In the heterogeneous picture the source of non-exponentiality is a superposition (ensemble average) of individual Debye processes with different relaxation times. (a) Illustration by Richert [28] in the time domain. Φ represents a the measured time domain response function. (b) Illustration by Chamberlin [27] in the frequency domain. This illustration also suggests the outcome of an 'hole-burning' experiment in the two cases: If a pump field is applied at selected frequency (here Ω), then in (A) energy is absorbed homogeneously yielding a uniform shift in the spectrum of response. In (B) domains with significant absorption at R are selectively modified, and a spectral hole develops

is the Cole-Davidson fitting function [32, 33]

$$\chi(\omega) = \frac{1}{(1 + i\omega\tau)^{\beta_{CD}}} \tag{2.8}$$

where χ denotes any normalized response function in the frequency domain. This function has the required behavior for $0 < \beta_{CD} < 1$.

In Fig. 2.6 the exponential and stretched exponential relaxation functions is schematically depicted in the time domain and in the frequency domain the Cole-Davidson fitting function is shown in addition to the (Laplace transform of the) two first.

Often, it is observed that the stretching increases with decreasing temperature, from a Debye like relaxation at high temperatures to a broader relaxation shape at low temperatures [18]. Close to the glass transition however, many liquids obey the time-temperature-superposition principle (TTS), i.e. the relaxation shape is temperature independent in some temperature interval. It was suggested by Olsen *et al* [35] that a high-frequency $\omega^{-1/2}$ dielectric loss spectrum is valid whenever TTS is obeyed. This

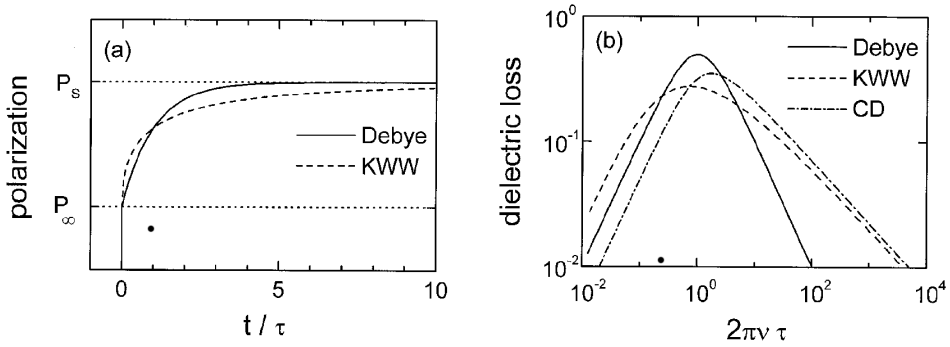

Figure 2.6 Stretched relaxation in the time and frequency domain. In the time domain the relaxation stretched compared to a simple exponential. In the frequency domain the "stretching" shows up as an asymmetric shape of the imaginary part of the dielectric constant. The imaginary part of a Debye (exponential) relaxation, a stretched exponential (KWW) and a Cole-Davidson function (CD) with the same relaxation time τ is shown. From [34]

was further supported by Nielsen *et al* [36], who for a large number of liquids showed that a slope of $-1/2$ may be generic.

If (and in that case how) the non-Arrhenius temperature dependence of the relaxation time and the non-exponential relaxation is connected is not known, although a strong correlation between the fragility index m_A and the stretching parameter β_{SE} of the stretched exponential has been reported [26, 27].

The topic of non-exponential relaxation enters in several parts of the thesis. In part III (chapter 13) Eq. (2.7) and (2.8) and other single-parameter relaxation functions are compared for a large set of dielectric data (collected by Albena Nielsen). And indirectly in the characterization of the mechanical relaxation spectra in part I.

2.2.3 Non-linearity

Non-linearity refers to the fact the relaxation in the liquid near (and below) T_g following even quite small temperature jumps is highly non-linear in the sense that the response to a step in temperature depends both on the sign and the magnitude of the jump.

In Fig. 2.7(a) a schematic representation of a typical protocol for a nonlinear relaxation measurement is illustrated by a temperature up-jump and a temperature down-jump to the same temperature. In both up- and down-jumps the liquids responds by an instantaneous (solid) change – as in the Maxwell model – followed by a slow relaxation toward the (metastable) equilibrium line. Fig. 2.7(b) shows Kovacs data on glucose [37] following such a protocol. The up and down jump are clearly not symmetric in their approach to equilibrium.

This topic is explored in part III, where chapter 11 gives a much more detailed introduction to the out-of-equilibrium dynamics. In chapter 12 is testing a standard formalism for addressing non-linear relaxation (the Tool-Narayanaswamy formalism).

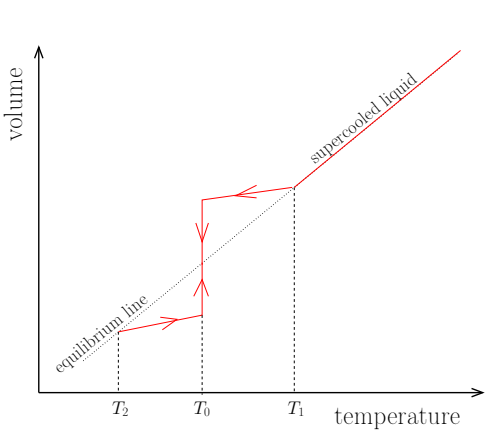

(a) Schematic representation of a temperature jump experiment

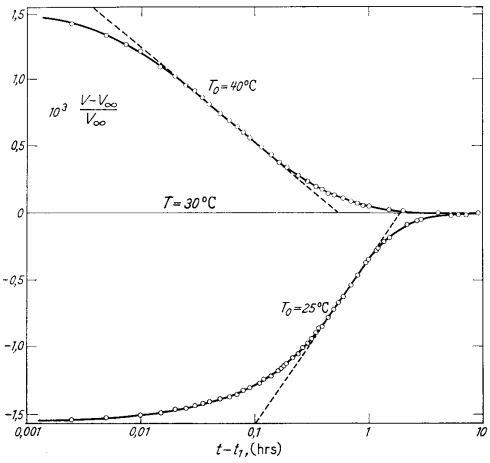

(b) Data obtained by following such protocol

Figure 2.7 A temperature jump experiment. (a) A schematic representation of two temperature jumps to a target temperature (T_0) from initial temperatures above (T_1) and below (T_2). (b) The data of Kovacs [37] on glucose following such a protocol. The volume change in the system is measured after a 5K up-jump (corresponding to $\sim 1.6\%$) and a 10K down-jump (corresponding to $\sim 3.3\%$) to 30°C. Obviously, the temperature down-jump reaches equilibrium faster and is much flatter (or stretched) than the temperature up-jump. From [37]

2.3 Concluding remarks

The ability to form a glass is universal and the properties of the viscous phase preceding the glass formation are universal and non-trivial. The universality and the general lack of basic understanding continue to make this research field attractive to physicists. The hope is of course that behind this universality, a theory exists for viscous liquid that explains these main questions, here posed in form of the three non's.

Several phenomenological models and more fundamental theories have been proposed that allegedly solves the problem of non-Arrhenius behavior of the relaxation time, as well as some first principles approaches. But no consensus has been reached so far.

The lack of order in some respects make things simpler. The lack of crystalline order for instance has the consequence that viscous liquids and glasses are isotropic, which for instance simplifies their mechanical properties compared to crystalline solids. And since the glass transition phenomena are universal, i.e. insensitive to the microscopic details of the molecules and the chemical bonds involved, it has been proposed that cause of the universality is the lack of long-range order [38].

Bibliography

[1] J. C. Dyre. The glass transition and elastic models of glass-forming liquids. *Reviews of Modern Physics*, 78(3):953–972, 2006.

[2] G. P. Johari and D. Pyke. On the glassy and supercooled liquid states of a common medicament: Aspirin. *Physical Chemistry Chemical Physics*, 2:5479–5484, 2000.

[3] M. Le Meste, D. Champion, G. Roudaut, G. Blond, and D. Simatos. Glass transition and food technology: A critical appraisal. *Journal of Food Science*, 67:2444–2458, 2002.

[4] L. D. Landau and E. M. Lifshitz. *Theory of Elasticity.* Elsevier, 1986.

[5] M. Goldstein. Viscous liquids and the glass transition: A potential energy barrier picture. *Journal of Chemical Physics*, 51:3728–3739, 1969.

[6] J. Jäckle. Models of the glass transition. *Reports on Progess in Physics*, 49:171–231, 1986.

[7] J. C. Dyre. Source of the non-Arrhenius average relaxation time in glass-forming liquids. *Journal of Non-Crystalline Solids*, 235-237:142–149, 1998.

[8] A. J. Kovacs. La contraction isotherme du volume des polymères amorphes. *Journal of Polymer Science*, 30:131–147, 1958.

[9] C. T. Moynihan, A. J. Easteal, M.a. DeBolt, and J. Tucker. Dependence of the fictive temperature of glass on cooling rate. *American Ceramic Society*, 59:12–16, 1976.

[10] G. Adams and J. H. Gibbs. On the temperature dependence of cooperative relaxation properties in glass-forming liquids. *Journal of Chemical Physics*, 43(1):139–146, 1965.

[11] F. H. Stillinger and P. G. Debenedetti. The Kauzmann paradox revisited. *Journal of Physical Chemistry B*, 105:11809–11816, 2001.

[12] R. J. Speedy. Kauzmann's paradox and the glass transition. *Biophysical Chemistry*, 105:411–420, 2003.

[13] J. C. Maxwell. On the dynamical theory of gases. *Philosophical Transactions of the Royal Society of London*, 157:49–88, 1867.

[14] G. Harrison. *The Dynamic Properties of Supercooled Liquids.* Academic Press, 1976.

[15] S. Brawer. *Relaxation in Viscous Liquids and Glasses.* Columbus OH: American Ceramic Society, 1985.

[16] P. G. Debenedetti. *Metastable liquids : concepts and principles.* Princeton, N.J. : Princeton University Press, 1996.

[17] M. D. Ediger, C. A. Angell, and S. R. Nagel. Supercooled liquids and glasses. *Journal of Chemical Physics*, 100:13200–13212, 1996.

[18] C. A. Angell, K. L. Ngai, G. B. McKenna, P. F. McMillan, and S. W. Martin. Relaxation in glassforming liquids and amorphous solids. *Journal of Applied Physics*, 88:3113–3157, 2000.

[19] P. G. Debenedetti and F. H. Stillinger. Supercooled liquids and the glass transition. *Nature*, 410:259–267, 2001.

[20] H. Eyring. Viscosity, plasticity, and diffusion as examples of absolute reaction rates. *Journal of Chemical Physics*, 4:283–291, 1936.

[21] Walter Kauzmann. The nature of the glassy state and the behavior of liquids at low temperatures. *Chemical Review*, 43:219–256, 1948.

[22] C. A. Angell. Perspective on the glass transition. *Journal of Physics and Chemistry of Solids*, 49(8):863–871, 1988.

[23] R. Casalini, M. J. McGrath, and C. M. Roland. Isobaric and isochoric properties of decahydroisoquinoline, an extremely fragile glass-former. *Journal of Non-Crystalline Solids*, 352:4905–4909, 2006.

[24] R. Richert, K. Duvvuri, and L.-T. Duong. Dynamics of glass-forming liquids. VII. Dielectric relaxation of supercooled tris-naphthylbenzene, squalane and decahydroisoquinoline. *Journal of Chemical Physics*, 118(4):1828–1836, 2003.

[25] O. V. Mazurin. Relaxation phenomena in glass. *Journal of Non-Crystalline Solids*, 25:129–169, 1977.

[26] R. Böhmer, K. L. Ngai, C. A. Angell, and D. J. Plazek. Nonexponential relaxation in strong and fragile glass-formers. *Journal of Chemical Physics*, 99:4201, 1993.

[27] R. V. Chamberlin. Experiments and theory of the nonexponential relaxation in liquids, glasses, polymers and crystals. *Phase Transitions*, 65:169–209, 1998.

[28] R. Richert. Heterogeneous dynamics in liquids: fluctuations in space and time. *Journal of Physics: Condensed Matter*, 14:R703–R738, 2002.

[29] R. Böhmer, R. V. Chamberlin, G. Diezemann, B. Geil, A. Heuer, G. Hinze, S. C. Kuebler, R. Richert, B. Schiener, H. Sillescu, H. W. Spiess, U. Tracht, and M. Wilhelm. Nature of the non-exponential primary relaxation in structural glass-formers probed by dynamically selective experiments. *Journal of Non-Crystalline Solids*, 235-237:1–9, 1998.

[30] R. Kohlrausch. Theorie des elektrischen Rückstandes in der Leidner Flasche. *Annalen der Physik und Chemie (Poggendorff)*, 91:179–213, 1854.

[31] G. Williams and D. C. Watts. Non-symmetrical dielectric relaxation behavior arising from a simple empirical decay function. *Transaction of the Faraday Society*, 66:80, 1970.

[32] D. W. Davidson and R. H. Cole. Dielectric relaxation in glycerine. *Journal of Chemical Physics*, 18:1417–1417, 1950.

[33] D. W. Davidson and R. H. Cole. Dielectric relaxation in glycerol, propylene glycol and *n*-propanol. *Journal of Chemical Physics*, 19:1484–1490, 1951.

[34] P. Lunkenheimer, U. Schneider, R. Brand, and A. Loidl. Glassy dynamics. *Contemporary Physics*, 41:15–36, 2000.

[35] N. B. Olsen, T. Christensen, and J. C. Dyre. Time-temperature superposition in viscous liquids. *Physical Review Letters*, 86(7):1271–1274, 2001.

[36] A. I. Nielsen, T. Christensen, B. Jakobsen, K. Niss, N. B. Olsen, R. Richert, and J. C. Dyre. Prevalence of approximate $\sqrt{t}$ relaxation for the dielectric alpha process in viscous organic liquids. *Journal of Chemical Physics*, 130:154508, 2009.

[37] A. J. Kovacs. Transition vitreuse dans les polymeres amorphes. Etude phenomenologique. *Fortschritte der Hochpolymeren-Forschung*, 3(3):394–507, 1963.

[38] J. C. Dyre. Solidity of viscous liquids. IV.density fluctuations. *Physical Review E*, 74:021502, 2006.

Part I

Mechanical relaxation spectra of viscous liquids

3 Introduction

This part of the thesis has roots back in my master thesis work, which was carried out in the Nelson group at the Department of Chemistry at Massachusetts Institute of Technology (MIT). In this group several techniques for measuring the ultra-fast properties of (disordered) matter through the interaction with laser light. A subset of the techniques are focussed on measuring the mechanical properties of especially (but not restricted to) glass-forming liquids.

The idea in my master thesis was to combine these high frequency techniques with the techniques developed here at Roskilde University to compile a mechanical counterpart of the broadband spectra that is accessible with dielectric spectroscopy. That turned out to be a too ambitious goal for the time-frame of a master thesis work and it seemed obvious to finish this project as a part of my PHD work. Among the challenges for this has been to get reproducible results and estimate the error on the absolute values of the measured mechanical moduli in order to be able to compare with results from other labs and different techniques – a discipline that has not been explored too much in the literature.

This initial idea has given rise to a number of other activities. In particular, one spin-off from this was the development of a new mechanical spectroscopy technique. This new technique is really rather a modification of one the existing techniques, which was an old idea of Tage Christensen and Niels Boye Olsen. A set of high quality data can also be used in other contexts than what they were originally intended for. As a result this part of the thesis kept growing in size to the point where it actually became the main part of the thesis.

In the present chapter we give a short introduction to mechanical spectroscopy in general and a brief review of existing techniques. Then an overview of the experimental work done in connection with this thesis follows including a presentation of the liquids studied.

3.1 Mechanical spectroscopy in general

If we want to observe the visco-elastic effects (mechanical relaxation) in a liquid, the frequency or time window of the technique needs to be carefully matched with the relaxation time of the liquid. The relaxation time of the liquid is strongly temperature dependent and since viscosity is roughly proportional to the relaxation time, a specific technique will typically select out a certain interval of viscosities and should be sensitive to these viscosities. Low frequencies correspond to long relaxation times and high viscosities, and high frequencies to short relaxation times and low viscosities.

The frequency or time window in combination with the temperature at which the technique can be operated limits the liquids that can be studied by a specific technique.

Mechanical measurements on viscous liquids are not easy, because – if kept above the glass transition temperature – they eventually flow. Thus they must contained and are not easily "pulled", "bent", or "squeezed".

We restrict our review of the existing techniques for measuring the shear and bulk mechanical properties of viscous liquids to the methods that operate roughly in the frequency range of our own methods, the Piezo-electric Shear Gauge (PSG) [1] and the Piezo-electric Bulk Gauge (PBG) [2] developed by Niels Boye Olsen and Tage Christensen. For slightly higher frequencies we refer to Harrison [3, Ch. 6] reviewing mechanical spectroscopy techniques at frequencies $>$ 10kHz and in chapter 8 of this thesis a few optical techniques for measuring sound velocity and sound attenuation at high frequencies (10MHz-100GHz) are described.

Ferry [4] and chapter 1 of [5] by Read, Dean & Duncan very thoroughly covers most of the low frequency techniques ($<$ 5kHz). The following is largely based on these references supplemented with some newer developments.

3.1.1 Relaxation, creep, modulus, or compliance?

Mechanical measurements in general relates components of the stress tensor, σ, to components of the strain tensor, ϵ. The experimental geometry determines the relevant components.

The linear stress-strain relation is a generalized Hooke's law

$$\sigma_{ij} = c_{ijkl}\epsilon_{kl} \tag{3.1}$$

where c_{ijkl} and every index i, j, k, l runs through the x, y, z directions. The elasticity tensor c thus contains 81 entries. Through symmetry relations this number is however dramatically decreased and for isotropic solids there are only two independent elastic constants. These can be expressed as a combination of any two moduli (bulk modulus K, Young's modulus E, Poisson's ratio ν, shear modulus G, and longitudinal modulus M), but we like to think of the two fundamental elastic moduli as the bulk K and shear G moduli, which relates the diagonal and deviatoric parts of the stress and strain tensors respectively [6]

$$\sigma_{ii} = 3K\epsilon_{ii}, \quad \sigma_{ij} = 2G(\epsilon_{ij} - \frac{1}{3}\delta_{ij}\epsilon_{ll}) \tag{3.2}$$

where δ_{ij} is the Kronecker delta. This means that the bulk modulus K is the response to a shape preserving volume deformation (homogeneous compression), while the shear modulus is the response to a volume preserving deformation. Since the hydrostatic pressure is given by $\delta p = {}^1\!/_3\sigma_{ii}$ and for small displacements the trace of the strain tensor gives the relative volume change $\delta V/V = \epsilon_{ii}$, we have

$$K = V\frac{\delta p}{\delta V}\,. \tag{3.3}$$

There are two different boundary conditions under which the bulk modulus may be measured, namely isothermal and adiabatic. Whether K_T or K_S is measured depends

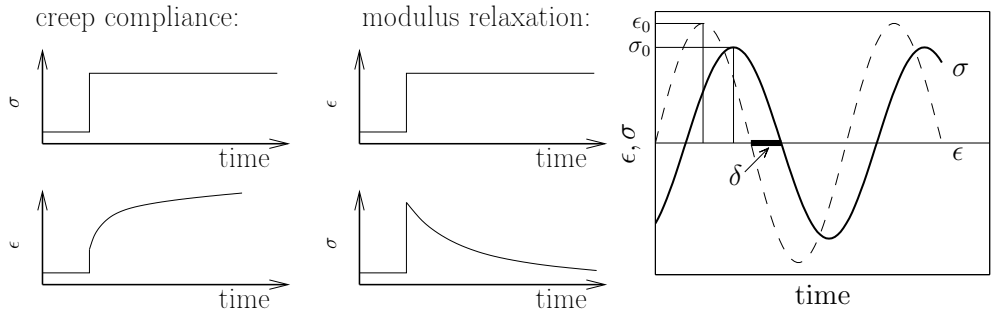

Figure 3.1 Schematic representation of the different input/output relations of mechanical measurements of visco-elastic materials. Left: applying a step in stress and measuring the time dependence of the strain (creep compliance). Middle: applying a step in strain and measuring the stress relaxation (modulus relaxation). Right: applying a harmonic stress/strain input and measuring the phase δ and amplitude of the strain/stress giving the complex compliance/modulus. All of these quantities are of course mathematically equivalent and what is measured in an experiment depends on what geometry is convenient.

on experimental details, more specifically on sample dimensions L compared to heat diffusion lengths l_D at the measured frequencies. If $L < l_D$ then the isothermal bulk modulus is measured, and if $L > l_D$ then the adiabatic bulk modulus is measured.

For visco-elastic/relaxing systems the response to some input is time-dependent. The full linear stress response is to an arbitrary deformation for an isotropic material is defined by

$$\sigma_{ij}(t) = \int_{-\infty}^{t} \left(2G(t'-t) \left[\dot{\epsilon}_{ij}(t') - \frac{1}{3}\delta_{ij}\dot{\epsilon}_{ll}(t') \right] + 3K(t'-t)\dot{\epsilon}_{ij}\delta_{ij} \right) dt' \,, \tag{3.4}$$

which in most realized experimental geometries will look much simpler. A similar expression can be written for the stress input.

In Fig. 3.1 we sketch different possibilities of inputs and corresponding responses, when we measure the mechanical properties of visco-elastic materials. For simplicity we have assumed that only component of the stress and strain tensors are involved. The most common modes of operation are step inputs or harmonic inputs. The response to a step input in strain is termed *creep compliance*, the response to a strain step input is called *stress relaxation* or *modulus relaxation*. Response to a harmonic input is called *complex modulus* (if the input is strain) and *complex compliance* (if the input is stress).

For a certain pair of stress and strain components all of these quantities are of course mathematically equivalent. The frequency domain response functions are Fourier transforms of the derivative of the equivalent time domain response functions. In the frequency domain the complex compliance is simply the inverse of the complex modulus

$$\tilde{J} = \frac{1}{\tilde{M}} \tag{3.5}$$

where $\tilde{M}$ here should be interpreted as a generalized complex modulus and $\tilde{J}$ as a generalized complex compliance.

3.1.2 Shearing techniques

Figure 3.2 (from [4]) shows six geometries for probing shear mechanical properties of viscous liquids. The first one (a) is a simple parallel plate (our own in-house developed technique belongs to this category), then there are two torsional geometries (d and e), and three techniques that are based a coaxial cylinder geometry, (b, c, and f).

All of these geometries give equivalent information of the stress-strain relation in the liquid, and all of them can (in principle at least) be operated in a compliance/creep mode (the stress or torque is controlled and displacement or angle relaxation is measured) or a modulus/stress relaxation mode (where the displacement or angle is controlled and the time dependent stress is measured).

Several of these geometries are available as commercial instruments, where probably the two torsional geometries are the most common for measuring on viscous liquids. The vast majority of published shear data, are data on polymeric systems. The frequency span of data on molecular liquids reported in the literature are typically 3-5 decades, for instance $10^{-3} - 10^{1}$Hz measured on a Rheometrics RMS 800 mechanical spectrometer by Deegan *et al* [7] and ARES Rheometric Scientific mechanical spectrometer in the frequency range $10^{-3} - 30$Hz by Mandanici *et al* [8] (both are realization of geometry (e) of Fig. 3.2).

Most of these techniques are limited to frequencies less than $\sim$100-1000Hz due to resonances in the apparatus.

One problem with many of the realizations of these geometries when measuring the mechanical properties of glass forming liquids close to the glass transition, is that the rigidity of the liquid becomes comparable to that of the rheometer, leading to a deformation of the rheometer itself. This can be corrected through proper modelling of the apparatus compliance as shown by McKenna and coworkers [9, 10], but it is a nuisance.

Harrison [3, p. 90] mentions a resonance technique covering the 20-100kHz range. The shear impedance of a liquid can be determined by measuring the loading effect on a transducer immersed in the liquid. The resonant frequency of a cylindrical quartz rod vibrating in torsion is determined first in vacuum and then immersed in the liquid. The changes in resonance frequency and resistance can be converted into components of the shear modulus. This technique however only work for low viscosities (< 20Pas) [3].

3.1.3 Compression techniques

When it comes to the dynamic bulk modulus, bulk compliance, bulk relaxation or bulk creep, the methods and data are very scarce. The bulk modulus has in several cases been determined through a combination of other measured moduli, see for instance Yee and Takemori [11] and references therein. Yee and Takemori [11] themselves developed a method for measuring Young's modulus and Poisson's ratio simultaneously, and used that to calculate the bulk and shear moduli at frequencies $0.01-10$Hz. Most other works combine ultrasonic acoustic measurements of longitudinal and shear sound velocities and sound attenuation to obtain the bulk modulus in the MHz region, see for instance [12–14].

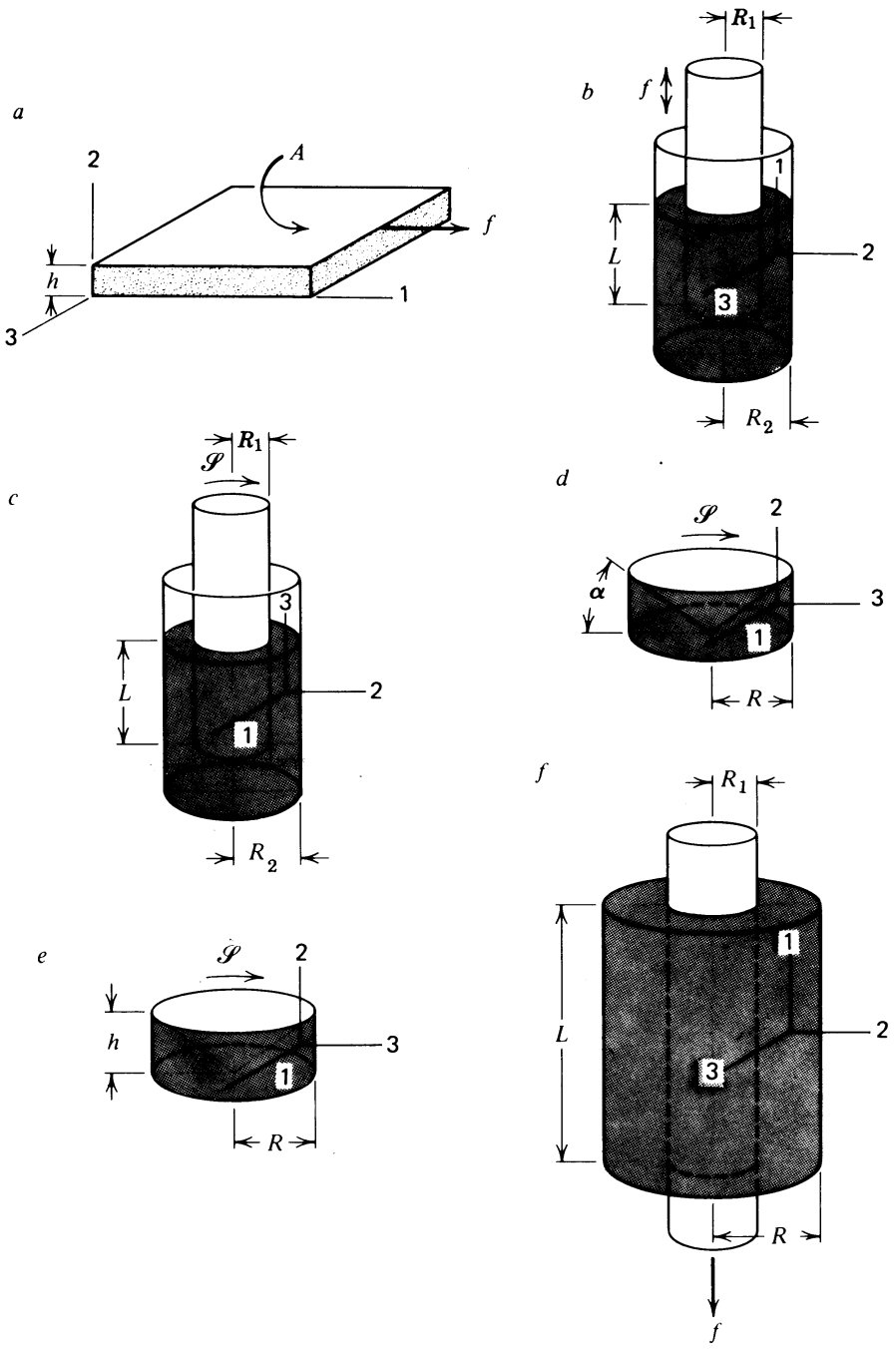

Figure 3.2 Illustration from [4] showing possible experimental geometries for measuring shear properties of viscous liquids. (a) parallel plate simple shear (b) annular pumping (c) rotation between coaxial cylinders (d) torsion between cone and plate (e) torsion between parallel plates (f) axial motion between coaxial cylinders.

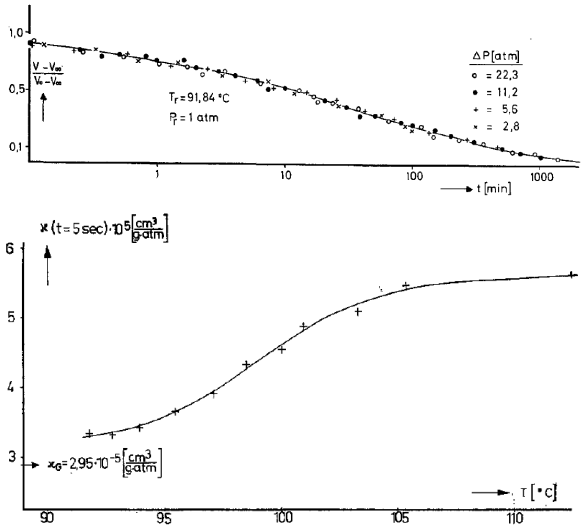

Figure 3.3 Data of Goldbach & Rehage [15] on polystyrol. Top figure show the data collapse of volume relaxation following several pressure jumps of different magnitude, thus confirming that the response is linear. Bottom figure shows the corresponding compressibility (bulk compliance) calculated at different temperatures for $t = 5$s.

Direct measurements of the bulk properties are rare. Experimentally it is a difficult task to create a pure volume deformation and at the same time measure the pressure relaxation or create a pure hydrostatic compression and at the same time measure the volume relaxation.

We have found only two principles of operation for measuring visco-elastic bulk properties (besides our own): one that we will call the dilatometric method [15, 16] and one we will call the acoustic method which was pioneered by McKinney *et al* [17] and later refined by Knauss and coworkers [18, 19].

Dilatometric method

The dilatometric method is a time domain technique. A dilatometer measures volume changes very precisely by the height of a fluid in a capillary that is connected to the sample chamber, analogously to a mercury thermometer. If a sample is placed in contact with (or inside) the liquid, volume changes of the sample can be measured quite accurately. Normally this technique is used for measuring the volume response following a temperature step or simply the volume as a function temperature. But used in conjunction with a pressure generating unit, it can be used to monitor the volume change after a step in pressure.

Goldbach & Rehage [15] published bulk creep results on polystyrene using this method already in 1967. We show some of their results in Fig. 3.3. They demonstrated that their measurement was linear by a perfect superposition of the normalized volume relaxation curves following different pressure jumps (top figure in Fig. 3.3).

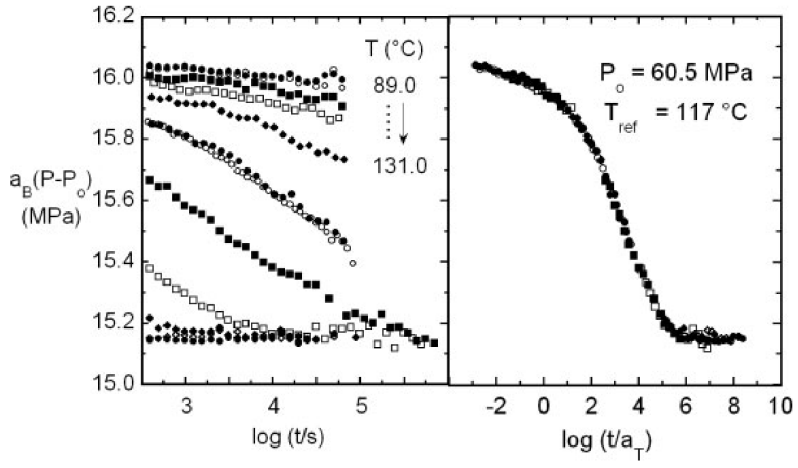

Figure 3.4 Data of Meng & Simon [20]. Left figure shows the time dependent pressure for different temperatures. Right figure show the same data now shifted by some factor a_T with respect to a reference temperature to compile a master curve.

More recently, Meng *et al* [16, 20] published results using a similar technique which is capable of controlling the static pressure up to 250MPa in addition to temperature. They added a pressure gauge with a feedback mechanism to the working principle described above and thus they were able to monitor the pressure relaxation following a volume jump in polystyrene [20], i.e. bulk modulus relaxation instead of bulk creep compliance. We show an example of their data in Fig. 3.4.

These techniques measures isothermal bulk modulus/compliance, because they measure at fairly long times: the time interval reported by Meng & Simon is $\sim 300 - 10^6$s, and slightly shorter for Goldbach & Rehage, $\sim 6 - 10^5$s. Meng & Simon report bulk relaxation in the MPa range.

Acoustic method

Variations in pressure are imposed on a sample contained in a small cavity by a compression wave can be regarded hydrostatic in the cavity if the wavelength of the compression wave is large compared to the size of the cavity (the quasi static limit). Such a pressure wave can be generated by a piezo-electric plate.

Figure 3.5 illustrated the principle of a such an experimental geometry by Sane & Knauss [19]. The sample is suspended in a liquid (an oil) inside a small cavity. Two piezo electric plates on either side of the sample act as transmitter and receiver. An oscillating field is applied to the transmitter creating pressure variations, and the receiver transducer detects the volume variations. The compliance of the suspension liquid and the apparatus is calibrated without sample. The bulk compliance is subsequently determined through the ratio of the complex voltages of the two piezo-electric discs.

Figure 3.6 shows the data of Sane & Knauss [19] on PVAc and PMMA, and we notice

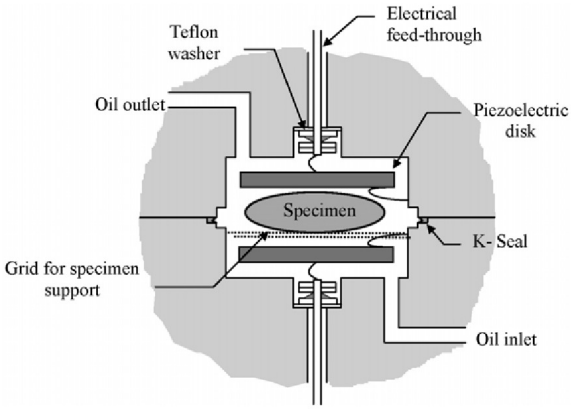

Figure 3.5 Principle of the "acoutic method" for measuring bulk compliance. A sample is suspended in liquid inside a small cavity between two piezo-electric plates. One of the plates acts as a transmitter generating a compression wave when a voltage is applied, and the other as a receiver recording the induced volume variations. From [19].

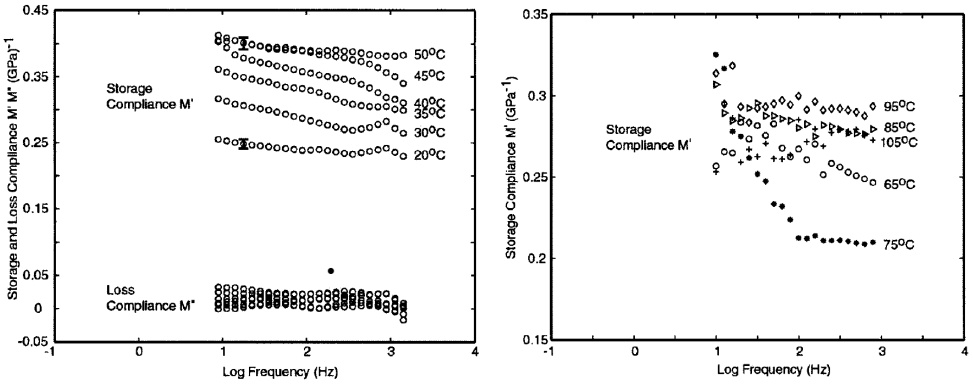

Figure 3.6 Bulk compliance data of PVAc (left) and PMMA (right) obtained with the "acoustic method". From [19].

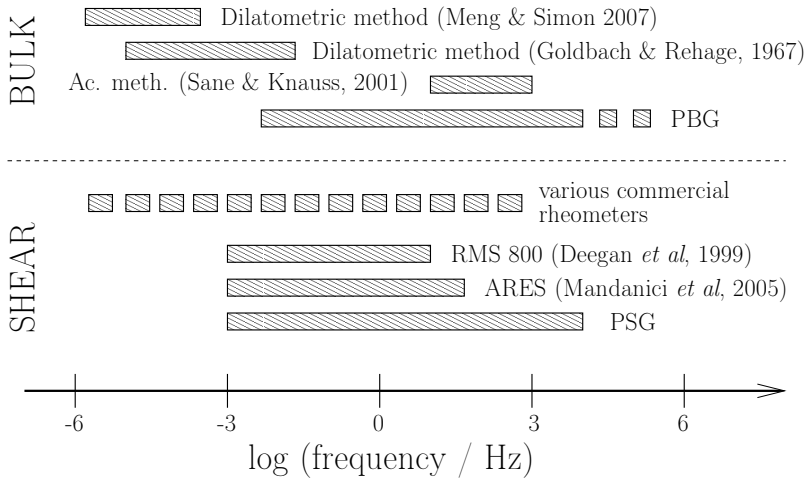

Figure 3.7 Overview of the techniques discussed in the previous subsections. Where the techniques operates in the time domain the time interval have been converted to a frequency interval through the relation $f = \frac{1}{2\pi t}$. We have shown two representative examples of shear measurements on molecular liquids found in the literature, Deegan *et al* [7] who measured on tricresyl phosphate and squalane and Mandanici *et al* [8] who measured on *m*-toluidine. Most shear measurements are carried out on commercial rheometers that typically cover 3-5 decades in frequency below 1kHz. Our own method (PSG) covers 7 decades from 1mHz to 10kHz. There are three different types of bulk measurements with very little overlap in frequency or temperature span. The PBG has a very broad dynamical range extending well into the kHz region for the resonance mode (more details on the technique can be found in chapter 4). The two other techniques are able to go to much higher temperatures than the PBG and they can measure at elevated static pressures.

that the method is sensitive to inverse GPa which means that it is applicable to quite hard materials. This method measures the adiabatic bulk compliance (compressibility).

3.1.4 Summary

Figure 3.7 gives an overview of the techniques for measuring bulk and shear properties of viscous liquids and the range of frequencies that each technique covers. Where the techniques operates in the time domain the time interval have been converted to a frequency interval through the relation $f = \frac{1}{2\pi t}$.

There are several different working principles for measuring shear properties of liquids in the sub kHz region. Not many techniques can measure in the kHz region. Our method (PSG) has a broad dynamical window covering seven decades in frequency from 1mHz to 10kHz, i.e. into the kHz region. This is due to the small size of the device pushing the natural resonance of the device to higher frequencies.

The greatest advantage of the PSG measurements over conventional rheological measurements is that in the PSG the deformation of the measuring gauge is an integrated part of the method. Other advantages include very small strains (approximately 10^{-6}), thus ensuring linearity in the measurements [1].

In contrast to the abundance of shear mechanical methods we found only two different methods of measuring the bulk mechanical properties, working at quite different timescales. All reported data using these methods were on polymers, and it is questionable whether these two methods would be applicable to liquids that are fluid at room temperature, where the loading of the sample is normally carried out.

Our method (the PBG) was developed to measure liquids with low T_g and is not suited for measuring at temperature much above room temperature. Thus there is very little overlap in the working range and applicability range of the existing bulk techniques.

3.2 Experimental overview of the thesis

3.2.1 Techniques and measurements

Low-frequency (i.e. from 1mHz to 10kHz-1MHz) measurements presented in this part are performed at the experimental set-ups at IMFUFA described in detail by Igarashi *et al.* [21, 22]. These set-ups include home-build cryostats with very good temperature control; the temperature is stable within 10mK with a calibration error of $\pm$0.1K in the working range of the cryostat ($\sim$ 95-300K) [21].

Mechanical measurements were performed with the piezo-electric shear gauge (PSG) [1] and the piezo-electric bulk gauge (PBG) [2] developed by Tage Christensen and Niels Boye Olsen in our group as well as a newly developed device which is a modification of the PSG. The transducers were designed for measuring high moduli relaxation in glass-forming liquids near T_g and both rely on the piezo-electric effect, i.e. the conversion of a electric input to a mechanical output (and vice versa).

Dielectric measurements were performed with a multi-layer, gold coated disc capacitor with a capacitance of approximately 20pF (also made in-house), that fits in the same cryostats as the mechanical measuring cells.

In table 3.2 we have listed the measurements that exist on the chosen liquids. In this table an 'X' means that the measurement were performed for this study, 'o' means the measurement has been carried out in another connection, '%' means data for this measurement do not exist, and the superscripts mark in which cryostat(s) the measurement was taken ('c' stands for cryostat and the digit refers to our internal numbering of set-ups). When this is not provided the information is not available.

This last point is important because there are minor differences in the absolute temperature calibration and the data acquisition equipment between the set-ups. This means that a measurement may be completely reproducible in one cryostat, but minor deviations occur when the measurement is moved to a different cryostat. The data produced for this work were obtained in two different cryostats: CRYO 3 which is nitrogen cooled cryostat and CRYO 5 which is a closed cycle pump cryostat. Appendix B for documents the temperature stability of the two set-ups and a discusses of how to compare measurements from the two.

Name	Abbreviation	T_g	m_A
Tetraphenyltetramethyltrisiloxane	DC704	210K	82
5-phenyl-4-ether	PPE	245K	81
Dibuthylphtalate	DBP	177K	68
Pentaphenyltrimethyltrisiloxane	DC705	230K	77
Diethylphtalate	DEP	185K	70
1,2-propanediol	PG	165K	40

Table 3.1 The table shows some relevant information on the liquids used in this study. The glass transition temperatures in this table is determined as the temperature where the dielectric loss peak is at 1mHz (corresponding roughly to the standard definition of T_g through the equation $\tau(T_g) = 100$s). m_A is the fragility index (see Eq. (2.6)). The value reported here is also based on the dielectric loss peak frequencies.

	Bulk	Shear	Longitudinal	Dielectric	Heat-capacity	Expansion
DC704	X^{c5}	X^{c5}	X^{c3}	o^{c5}	o^{c5}	o^{c8}
PPE	X^{c5}	$X^{c3,c5}$	X^{c3}	$X^{c3,c5}$	o^{c5}	%
DEP	%	X^{c5}	X^{c3}	o	%	%
DBP	o	o	X^{c3}	o	%	%
DC705	o	o	X^{c3}	o	%	%
PG	o	o	X^{c5}	o	%	%

Table 3.2 In the table we have listed which measurements were performed on which liquids (more information about the liquids can be found in table 3.1 and Fig. 3.8). X means the measurement was carried out for this thesis, o means that measurements exists (but made by others in the group), and % means that this measurement has not been carried out yet. The superscript indicates which cryostat(s), the measurements were performed: c3 for cryostat 3 (CRYO 3), c5 for cryostat 5 (CRYO 5). Where nothing is indicated the information was lost.

3.2.2 Liquids

All the liquids in this study are organic molecular liquids with relatively low glass transition temperatures. This type of liquid is well-suited for our experimental set-ups. Table 3.1 lists the liquids used in this study, the abbreviations used, and some characteristic quantities. Figure 3.8 gives the molecular structures, chemical formulas and molecular weights.

The choice of liquids is mostly a choice of convenience. For the bulk measurement it is crucial that the liquid never crystallizes during the measurement since a crystallization will destroy the measuring cell. Thus we had to choose some liquids that were extremely good glass-formers. Since I had already started measuring on DC704 during my stay with the Nelson group it was natural to continue with this liquid for the collaborative project of compiling a broadband mechanical spectrum. DEP and PPE were both chosen based on the signal strength of the high frequency (ISS) shear signal, and the rest of the list is chosen based on availability of other in-house measurements (shear and bulk modulus, dielectric, heat-capacity or preferably all).

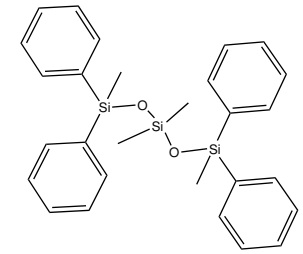

1,3,3,5-tetramethyl-1,1,5,5-tetraphenyltrisiloxane
Chemical Formula: $C_{28}H_{32}O_2Si_3$
Molecular Weight: 484,81

(a) DC704

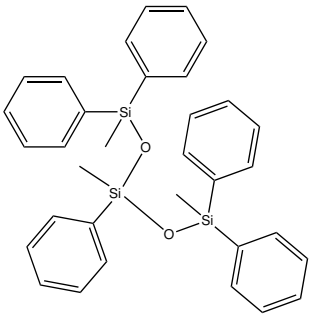

1,3,5-trimethyl-1,1,3,5,5-pentaphenyltrisiloxane
Chemical Formula: $C_{33}H_{34}O_2Si_3$
Molecular Weight: 546,88

(b) DC705

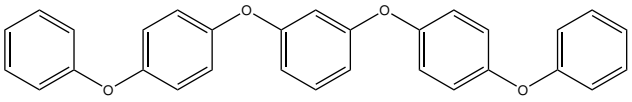

1,3-bis(4-phenoxyphenoxy)benzene
Chemical Formula: $C_{30}H_{22}O_4$
Molecular Weight: 446,49

(c) PPE

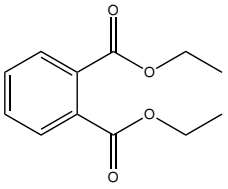

diethyl phthalate
Chemical Formula: $C_{12}H_{14}O_4$
Molecular Weight: 222,24

(d) DEP

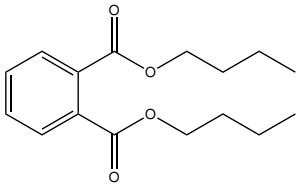

dibutyl phthalate
Chemical Formula: $C_{16}H_{22}O_4$
Molecular Weight: 278,34

(e) DBP

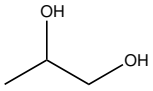

propane-1,2-diol
Chemical Formula: $C_3H_8O_2$
Molecular Weight: 76,09

(f) PG

Figure 3.8 Molecular structures of the liquids used as well as IUPAC names, chemical formulas and molecular weights. In the case of DC704 and DC705 different isoforms of the molecule exists.

Obviously, the chosen liquids do not represent a very broad range of T_g's or fragilities. But this study was not intended to be a broad study of mechanical relaxation behavior of liquids, but an in-depth and thorough investigation of a few liquids, the main focus being primarily on DC704 and PPE due to the collaboration with the Nelson group. We do thus not see this as a problem. For future measurements and investigations, however, a more systematic approach for choosing liquids would probably be desirable.

4 Bulk modulus measurements

The bulk modulus measurement is in some regards the simplest of the three mechanical measurements. The geometry of the measuring cell makes the modeling relatively simple and the results are easy to interpret. At the same time this measurement is extremely cumbersome, lengthy, and sometimes frustrating.

In this chapter we will go over the method in detail from the measurement protocol over the conversion from a measured capacitance to a bulk modulus to results and error estimates. This is mainly because although only little documentation of the method exists. In particular, there no analysis of errors and reproducibilities have been given before.

4.1 The bulk transducer

A schematic drawing of the bulk transducer is shown in Fig. 4.1. It consists of a spherical shell of a piezo electric ceramic material polarized in the radial direction. The shell is covered by an electrode material both on the inside and the outside. Applying an electric field to the capacitor that these electrodes constitute will deform (expand or contract depending on the direction of the field) the ceramic and effectively change the inner volume of the sphere. A liquid inside the shell will oppose this deformation

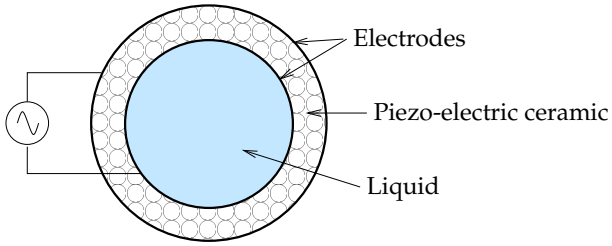

Figure 4.1 Schematic drawing of the bulk transducer. When an electric field is applied the ceramic material between the electrodes contract or expand, which effectively changes the internal volume.

and thus change the measured capacitance. The difference in capacitance between the empty (and freely moving) shell and the partially clamped shell can be related to the bulk modulus of the liquid. The geometry is exactly what makes it a bulk modulus gauge; the deformation is radial and thus a pure volume change with no shearing of the liquid. However, as the analysis of forced vibrations in a visco-elastic sphere below shows, this is only true in the low frequency region of the measurement.

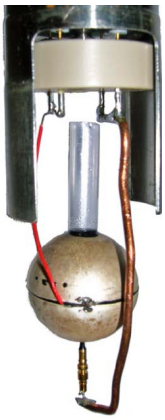

Figure 4.2 A photograph of the bulk-transducer. It is mounted on a special foot and attached to the holder. The holder is 2.5cm in diameter, and the piezo-ceramic shell is 1.9cm in diameter.

In order to be able to fill the PSG with liquid a hole is drilled in the shell. The hole breaks the symmetry and can of course not be too big. A pipe is attached over the hole drilled in the shell. Filling this pipe as well as the shell allows the liquid to "suck" in extra liquid when liquid contracts during cooling. Thus the liquid volume is assumed to be constant in this experiment.

In Fig. 4.2 we show a photo of the bulk-transducer mounted on a foot that fits in the cryostat holder.

4.2 Measurement protocol

The properties of the ceramic that constitute the measuring cells are both temperature dependent and dependent on the thermal history; the ceramic is "aging". It is thus necessary to do all measurements twice: once with liquid in the cell, and once without liquid (the "reference"). This means repeating the entire measurement, i.e. the complete thermal cycle including waiting times for equilibration of the liquid. In addition we found that starting the measurement by heating the cell slightly for ∼10-20 hours to "erase" the memory of the ceramic, increased the reproducibility. In the case of the bulk measurement the initial heat treatment was at 315K, which about the limit of what the cryostat can do.

With the PBG we are also hindered by the flow-time through the drilled hole. This has several implications that we will return to below. For now it suffices to say that it is necessary to make the temperature cycle symmetric (at least up to a certain viscosity), i.e. give the liquid the same time to flow out of the sphere when heating as it spent flowing in during cooling. Otherwise we ultimately risk a cracking of the cell due to rapid (compared to flow-time) thermal expansion of the liquid inside. As a result, bulk modulus measurements are quite lengthy if we want to measure close to the glass transition (which is what we normally want).

It is also important to be careful when choosing which temperatures to measure. We can not go too close to the glass transition, as we risk that cooling too much will cause the liquid to "crack" and destroy the cell in the process. If the sample is not too well known it is recommended to do a heating rate analysis to determine glass transition temperature and also to see how the liquid handles the thermal cycling, if it cracks too easily or crystallizes it should probably not be used in the bulk modulus measurement.

Even extending the waiting times and measuring times may not be a solution, because if we heat the sample too slowly, we risk crystallization of the liquid during the heating.

In table 4.1 we show an example of a measurement cycle for DC704 (the one used for the latest measurement). At all temperatures a logarithmic scan in frequency is performed from between 0.001Hz and 0.1Hz (depending on temperature and thus where the interesting dynamics is taking place) through 1MHz is performed, as well as a scan that is linear in frequency starting at 0.5-1kHz. Column one gives the temperature, column two the waiting time at that temperature, column three states the approximate time the measurement takes, column four gives the number of times the measurement was repeated, and the last column gives the total time spent at each temperature. In the bottom the total time of the entire cycle.

Here we have repeated the measurements at the lowest temperatures to check if the liquid had reached equilibrium. If equilibrium was not established before the first measurement, the repeated measurement will not reproduce the first. In principle this is always a good idea, and should perhaps be included in future protocols for all temperatures.

While this is certainly time consuming in terms of measuring time, it does not require constant monitoring, since the temperature control, the switching between different voltmeters, the saving of data, etc., is completely automated and controlled via MatLab routines.

4.2.1 Filling the cell

The cell was filled via a syringe with a needle long enough to go through the tube and half way down in the cell. The filling has to be done very slowly; how slowly depends on the viscosity of the liquid at ambient temperature.

In practice this was always done in a low-tech automated way: the syringe was fixed in position in the PBG and weights were added on top to force the piston down. This way the filling speed could be controlled by the amount of weight added to the piston.

If the cell is filled too quickly, air bubbles can form inside and sometimes get stuck inside the cell (especially if the liquid is viscous at ambient conditions). These air bubbles will show up in the spectrum as small extra resonances. If a bubble gets stuck inside (this is only revealed through a measurement) it is sometimes necessary to empty the cell and start over, but sometimes it can be "gassed out" by heating the cell over a period of time (usually a couple of days).

Temp (K)	t_{wait} (hrs)	t_{measure} (hrs)	repeat	t_{total} (hrs)
315	10	10.	1x	20.
310	2	0.1	1x	2.1
305	2	0.1	1x	2.1
300	2	0.1	1x	2.1
295	2	0.1	1x	2.1
290	2	0.1	1x	2.1
285	2	0.1	1x	2.1
280	2	0.1	1x	2.1
275	2	0.1	1x	2.1
270	2	0.1	1x	2.1
265	2	0.1	1x	2.1
260	2	0.1	1x	2.1
255	2	0.1	1x	2.1
250	2	0.1	1x	2.1
245	2	0.1	1x	2.1
242	2	0.1	1x	2.1
240	2	0.1	1x	2.1
238	2	1.	1x	3.
236	2	1.	1x	3.
234	2	1.	1x	3.
232	2	1.	1x	3.
230	2	1.	1x	3.
228	2	1.	1x	3.
226	2	1.	1x	3.
224	2	1.	1x	3.
222	2	10.	1x	12.
220	2	10.	1x	12.
218	2	10.	2x	22.
216	2	10.	2x	22.
214	2	10.	2x	22.
216	2	10.	2x	22.
218	2	10.	2x	22.
220	2	10.	1x	12.
222	2	10.	1x	12.
224	2	1.	1x	3.
226	2	1.	1x	3.
228	2	1.	1x	3.
230	2	1.	1x	3.
232	2	1.	1x	3.
240	2	0.1	1x	2.1
295	2	0.1	1x	2.1
Total		.		254.8

Table 4.1 Example of a measurement protocol (for the latest measurement on DC704). In total this protocol takes approximately 255 hours $\simeq$ 10.6 days. This cycle must be performed for the liquid-filled cell as well as the empty cell.

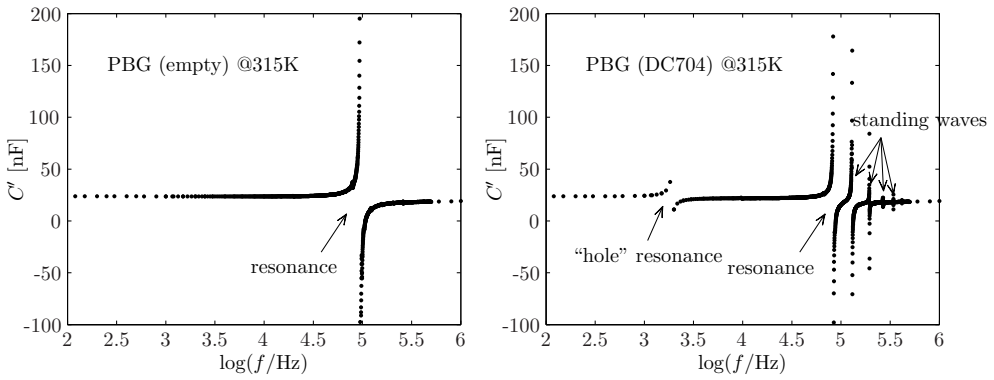

Figure 4.3 Example of (the real part of) raw data of an empty (left) and a liquid filled bulk transducer (right). In the spectrum of the empty transducer we see the first resonance of the shell. The "thickness" resonances are out of the frequency window of this technique. In the liquid-filled spectrum (right) we have a few more features: the first "resonance" is due to liquid flowing though the hole drilled in the shell, second (big) resonance is the first resonance of the combined shell+liquid system, the higher resonances correspond to standing waves in the liquid.

4.3 Raw data

In Fig. 4.3 we show an example of a logarithmic scan of an empty as well as liquid-filled bulk transducer at room temperature.

In the figure we have plotted the real part of the measured capacitance. The spectrum of the empty transducer contains one resonance at (around 100kHz); the overtones are out of the frequency window of this technique. The first resonance in the liquid-filled spectrum (around 5kHz) is due to the liquid flowing in the hole, the second (slightly below 100kHz) is a mixture of the first mechanical resonance of the transducer and the liquid. The additional resonances above this are standing waves in the liquid.

It is these features that we should capture when we model the system.

4.4 Model of the PBG

If the thickness of the ceramic shell is assumed to be vanishing we can model the bulk transducer by an electrical circuit. The model presented here is completely equivalent to the model derived by Christensen and Olsen [2], even though they did not explicitly state the electrical circuit model for the PBG.

Fig. 4.4 shows the electrical circuit equivalent diagram of the piezo ceramic shell that illustrates how we model the bulk transducer. The model has an electrical side (left) that models the electrical input, the capacitor models the electrodes of the shell. On the right side the mechanical properties of the ceramic is modelled and the conversion from electrical to mechanical energy happens through the transducer element. On the mechanical side the capacitor models the elastic properties of the ceramic, the

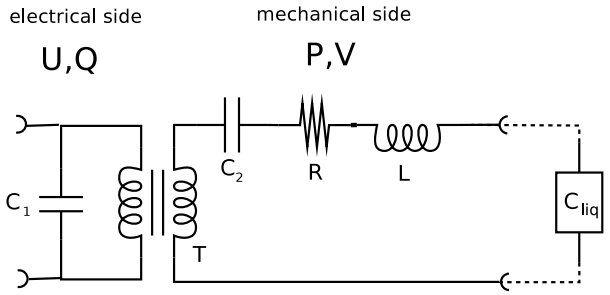

Figure 4.4 Model of the bulktransducer. The electrical part (the capacitor) models the electrodes on the piezo-ceramic shell, the transformer models the conversion from electric displacement (charge) to deformation (volume change) in the ceramic. The RCL series models the mechanical properties of the pz shell itself. For the empty tranducer the mechanical part is short-circuited (i.e. free to move), while a filled transducer will add an extra element (black box) in series with the RCL series.

inductance models the mass (or inertance), and the resistor models the friction (loss due to heating of the ceramic). Seen from the electrical side, the mechanical and electrical side are connected in parallel. This results from a consideration of limits: at high frequencies where the ceramic is mechanically clamped there is still charge on electrodes, thus the electrical capacitor can not be in series with the mechanical side. The mechanical elements are connected in series because they are all subjected to the same volume change (the mechanical equivalent of charge).

With this electrical circuit established it is easy to construct the mathematical expression that gives the measured capacitance (admittance in parallel are added, while impedances in series are added) for the empty transducer

$$C_m^{\mathrm{emp}}(\omega) = C_1 + T^2 \frac{1}{\frac{1}{C_2} + i\omega R - \omega^2 L}. \tag{4.1}$$

In the high frequency limit ($\omega \to \infty$) of this model the resistor and inductor terms will grow effectively blocking the current. This correspond to a mechanical clamping of the ceramic shell and thus we define

$$C_{\mathrm{cl}} = C_1. \tag{4.2}$$

In the low frequency limit ($\omega \to 0$) these two terms vanish. Mechanically this corresponds to the ceramic shell moving freely (without resistance). We define

$$C_{\mathrm{fr}} = C_1 + T^2 C_2. \tag{4.3}$$

We will rewrite this Eq. 4.1 with some more familiar and recognizable quantities,

$$C_m^{\mathrm{emp}}(\omega) = C_{\mathrm{cl}} + \frac{C_{\mathrm{fr}} - C_{\mathrm{cl}}}{1 + i\frac{\omega}{\omega_0}\frac{1}{Q} - \left(\frac{\omega}{\omega_0}\right)^2} \tag{4.4}$$

where $\omega_0 = \sqrt{\frac{1}{LC_2}}$ is the resonance frequency, and $Q = \frac{1}{R}\sqrt{\frac{L}{C_2}}$ is the quality factor.

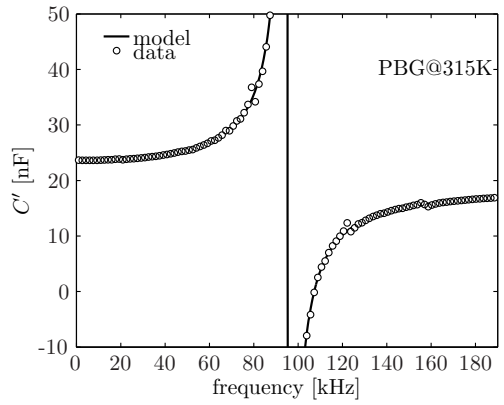

Figure 4.5 Spectrum of the empty transducer at 315K (circles) and the fitted model (full line). The model fits the data well. The "jitter" on the high frequency side of the resonance is probably some extra resonance modes due to a slightly imperfect spherical geometry.

From fitting this expression to the spectrum of the empty capacitor we can determine the 4 quantities: $C_{\rm fr}$, $C_{\rm cl}$, Q, and ω_0. An example of the fit is shown in Fig. 4.5 and the model (full line) fits the data (circles) very well.

According to our model, the measured capacitance for the liquid-filled transducer is

$$C_m^{\rm liq}(\omega) = C_{\rm cl} + \frac{C_{\rm fr} - C_{\rm cl}}{1 + i\frac{\omega}{\omega_0}\frac{1}{Q} - \left(\frac{\omega}{\omega_0}\right)^2 + \frac{C_2}{C_{\rm liq}}} \tag{4.5}$$

i.e. in order to de-convolve the stiffness of the liquid we need to determine C_2. With only four fitted parameters and five in the model we need to determine the fifth by another method. Luckily, the inductance L can be determined by measuring dimension and weight of the transducer. For simplicity we will define the dimensionless measured capacitance

$$F = \frac{C_m^{\rm liq}(\omega) - C_{\rm cl}}{C_{\rm fr} - C_{\rm cl}}\,, \tag{4.6}$$

And finally the stiffness of the liquid (inverse of the capacitance) can be expressed in terms of the four fitted parameters and L

$$S_{\rm liq}(\omega) = \frac{1}{C_{\rm liq}(\omega)} = L\omega_0^2\left\{\frac{1}{F} - 1 - i\frac{\omega}{\omega_0}\frac{1}{Q} + \left(\frac{\omega}{\omega_0}\right)^2\right\}. \tag{4.7}$$

4.4.1 Dispersion in the ceramics

As we can see in the logarithmic scan shown in Fig. 4.6 the measured "free" capacitance is not a constant, it increases with decreasing frequency. This is due to dispersion in the dielectric constant of the ceramics, and for the modelling this represents a problems because we do not know the functional form of the dispersion. This will also influence the "clamped" capacitance. Two assumptions can compensate for that.

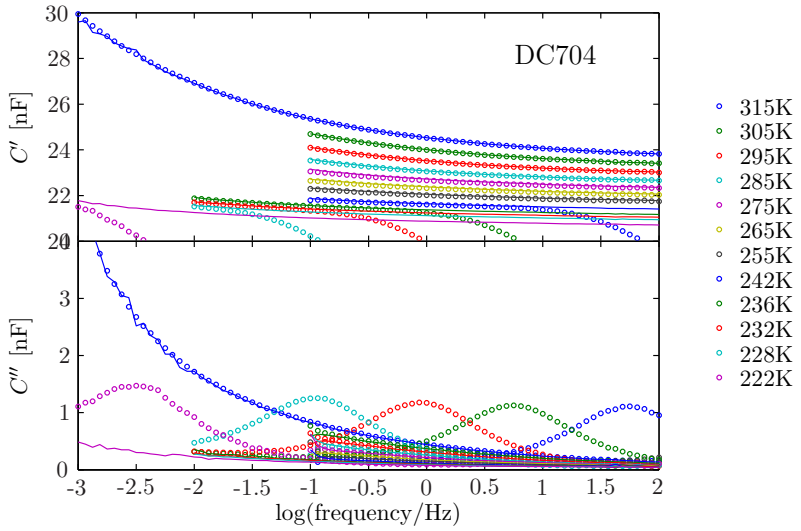

Figure 4.6 Measured capacitance of liquid-filled the bulk transducer (symbols) and the empty reference (lines). Different colors correspond to different temperatures. There is almost perfect overlap at low frequencies of the empty and liquid-filled spectrum, which is one of the central requirements for the method to work.

We have that

$$C_{\rm fr} = C_{\rm fr}(\omega), \;\; C_{\rm cl} = C_{\rm cl}(\omega). \tag{4.8}$$

If we now assume that the frequency-dependence of $C_{\rm fr}$ and $C_{\rm cl}$ is the same, i.e.

$$C_{\rm fr}(\omega) = C^*_{\rm fr} f(\omega), \;\; C_{\rm cl}(\omega) = C^*_{\rm cl} f(\omega) \tag{4.9}$$

then the ratio of the two is constant. This results in the following

$$F(\omega) = \frac{C^{\rm liq}_m(\omega)/C_{\rm fr}(\omega) - C^*_{\rm cl}/C^*_{\rm fr}}{1 - C^*_{\rm cl}/C^*_{\rm fr}} \tag{4.10}$$

This assumption may seem somewhat ad hoc, but will be considered justified if it leads to frequency independent plateau values of the bulk modulus.

But we still do not know what the frequency dependence of $C_{\rm fr}$ is and thus we need the second assumption, namely that the frequency dependence of $C_{\rm fr}$ is the same in the empty $C^{\rm emp}_m$ and the liquid-filled measurement $C^{\rm liq}_m$. In contrast to the first assumption, this assumption is easily justified by inspecting the plots in Fig. 4.6. Indeed the two curves overlap in the low frequency region at all temperatures.

Omitting the $*$-superscripts, we end up with the following expression for the stiffness of the liquid

$$S_{\rm liq}(\omega) = L\omega_0^2 \left\{ \frac{1 - C_{cl}/C_{fr}}{C^{\rm liq}_m(\omega)/C^{\rm emp}_m(\omega) - C_{cl}/C_{fr}} - 1 - i\frac{\omega}{\omega_0}\frac{1}{Q} + \left(\frac{\omega}{\omega_0}\right) \right\} \tag{4.11}$$

4.4.2 Determining inertance L

L is the constant of proportionality between the (generalized) voltage and charge acceleration, which expressed in mechanical variables is pressure difference δp and volume acceleration $\delta\ddot{V}$

$$\delta p = L\delta\ddot{V}\,. \tag{4.12}$$

L is a constant connected to the specific bulk transducer and should be temperature independent. This means we only need to determine this number once for each bulk transducer.

Expressing δp as a force pr. unit area, this force will be given by mass times acceleration, i.e. $\delta p = m\ddot{u_r}/A$. Since the displacement is small we can approximate the change in volume by $\delta V \approx Au_r$. In total we get the following

$$L = \frac{\delta p}{\delta\ddot{V}} \approx \frac{\ddot{u}m/A}{A\ddot{u}} = \frac{m}{A^2}\,. \tag{4.13}$$

An estimate of the mass of the piezo ceramic shell can be found by weighting the bulk transducer and subtracting the mass of the attached pipe. For the surface area we need to be a little more careful: the model of the PBG assumes vanishing thickness of pz shell, but this is of course just an approximation. Thus we should find an "effective" surface area which will be between the outer and inner surface of the shell. Assuming an average of the two will provide us with a good estimate of L.

We can however see from Eq. (4.11) that ultimately the numerical value of this number is quite crucial for the absolute values of the liquid stiffness determined through this model.

Fitting the resonances (see section 4.7.1) at a high temperature (where we can assume the a vanishing shear modulus, $G = 0$) varying L and the bulk modulus, K, we can optimize the estimate of L. Repeating the procedure for different liquids in the same bulk transducer provides us with an estimate of the error on the fitted values. The fitted values of L for the transducers used here can be found in table 4.2.

PBG	P1	P3	14
L $\left[10^3\,\frac{\mathrm{kg}}{\mathrm{m}^4}\right]$	3.8±0.15	3.5±0.1	4.2±+0.1

Table 4.2 Values of L for the bulk transducers used.

4.4.3 Modelling flow through the hole

At high frequencies the hole is essentially closed because the liquid does not have time to flow in and out during one frequency cycle. In that case we can consider the liquid inside a perfect spherical "ball".

At high temperatures (far above T_g) the liquid flowing in the hole is a real resonance, but as the temperature is lowered this resonance gets damped due to the increase in viscosity. When the resonance gets critically damped it will move down in frequency upon further cooling. In Fig. 4.7 this is shown for DC704.

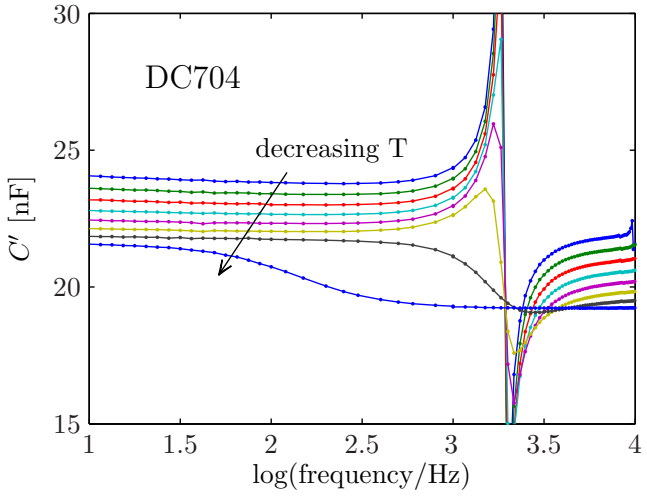

Figure 4.7 The measured capacitance of DC704. At high temperatures the liquid flowing in and out of the drilled hole gives rise to a resonance. When the temperature is lowered this resonance gets damped because the viscosity of the liquid increases.

At low enough frequencies (the definition of low of course depends on the temperature and viscosity of the liquid) the liquid will be able to flow out of the hole drilled in the ceramic shell. This flow can be assumed inertia free since it is extremely slow and can thus be modelled as a Poiseuille flow. A Poiseuille flow describes the laminar flow of fluid in a pipe with radius a and length l ($l > a$) with a no-slip boundary condition at the walls of the pipe.

For a Poiseuille flow the volume flow is given by the following expression (for a derivation see e.g. [23])

$$\dot{V} = \frac{\pi a^4 \delta p}{8\eta l} \tag{4.14}$$

where η the (shear) viscosity, $\dot{V}$ is the volume flow-rate, δp is the pressure difference across the "pipe".

In the framework of the electrical network model this flow can be added as a resistor in parallel with the liquid, since it is subjected to the same pressure difference. (Here we will ignore the mass since the flow is so slow that inertial effects are vanishing). This is illustrated in Fig. 4.8.

From equation (4.14) we obtain an expression for this resistor which is basically the shear viscosity times a geometric factor

$$R_h = \frac{\delta p}{\dot{V}} = \frac{8l}{\pi a^4}\eta_{\text{shear}}. \tag{4.15}$$

which we will use later (in chapter 7).

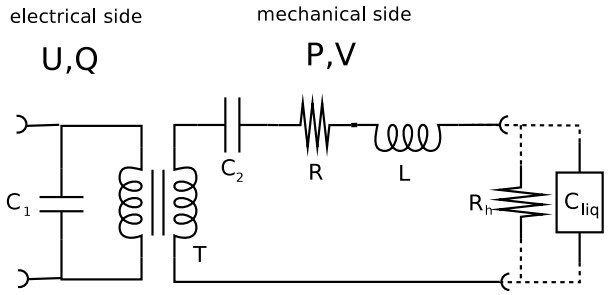

Figure 4.8 The electrical network model of the PBG with an extra element added (compare Fig. 4.4) to model the flow through the hole.

We determine R_h through the mechanical impedance of the measured signal ($\tilde{Z} = 1/i\omega\tilde{J} = 1/i\omega C_m$). The impedance of the signal coming from the liquid is given by

$$\tilde{Z} = \frac{1}{1/R_h + i\omega C_{\text{liq}}} = R_h \frac{1}{1 + i\omega\tau} \tag{4.16}$$

where $\tau = R_h C_{\text{liq}}$. The flow through the hole is thus described by a pure exponential, and plotting the imaginary part versus the real part will describe a semi-circle with R as the high frequency foot point. An example of this is shown in Fig. 4.9, where the red circles are data points and the black dashed line shows the exponential fit. Because the data trace out a semi-circle, R_h can also be found as twice the value of Z' at the top point

$$R_h = 2Z'(\omega_{\max}) \tag{4.17}$$

which is easy to determine.

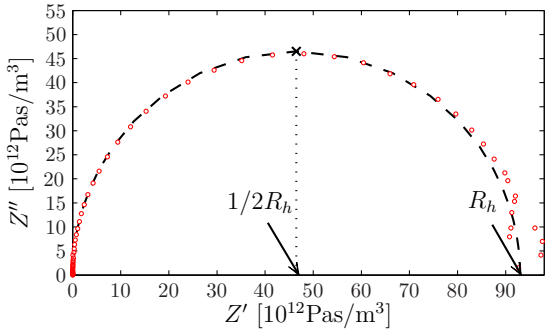

Figure 4.9 Determining the flow resistance (R_h) from the "breathing mode". The mechanical impedance of DC704 at 232K is shown in red symbols, the black dashed line shows a Debye process, and the arrows show how R can be determined.

Now we can subtract this contribution from the signal to extend the frequency range of signal from the liquid. The final expression for the stiffness of the liquid measured

is

$$S_{\text{liq}}(\omega) = \left\{ \left[L\omega_0^2 \left(\frac{1}{F} - 1 - i\frac{\omega}{\omega_0}\frac{1}{Q} + \left(\frac{\omega}{\omega_0}\right)^2 \right) \right]^{-1} - \frac{1}{i\omega R_h} \right\}^{-1} . \tag{4.18}$$

based on the model in Fig. 4.8.

4.5 Stiffness of a visco-elastic sphere

What remains to be determined is an expression for the stiffness of isotropic sphere of liquid that we can insert in the model developed above. The stiffness in the mechanical variables is given by change in pressure divided by the change in volume

$$S = \frac{\delta p}{\delta V} . \tag{4.19}$$

The change in pressure in our case where the displacement is purely radial, is the radial stress at the surface $\sigma_{rr}(r_0)$ and the change in volume for small displacement amplitudes u_0 is simply the surface of the sphere times the displacement

$$\delta V = 4\pi r_0^2 u_0 . \tag{4.20}$$

Thus to determine the stiffness we must solve the equations of motion for the sphere to determine the displacement and the stress. Below we will sketch the crucial steps in this derivation. The reader who is not interested in the details of the derivation may skip this and go directly to the solution (which is also given by Christensen & Olsen in [24]) in Eq. (4.31).

The general equation of motion for an isotropic medium is given by Landau & Lifshitz [6, p. 87]

$$(K + {}^4\!/_3 G)\nabla(\nabla \cdot \mathbf{u}) - G\nabla \times \nabla \times \mathbf{u} = \rho\ddot{\mathbf{u}} \tag{4.21}$$

where $\mathbf{u}$ is the displacement field, ρ is the density, and K and G are the bulk and shear moduli. In our case, the K is the adiabatic K_s as long as the heat diffusion length $l_D \equiv \sqrt{\frac{D}{i\omega}}$ is larger than the sample dimension (i.e. the radius of the sphere). For liquids D is on the order of $10^{-7}\frac{\text{m}^2}{\text{s}}$. The frequency window in the measurement is $10^{-3} - 10^4$Hz which gives $2.8\text{mm} < l_D < 9.0 \cdot 10^{-4}\text{mm}$. The inner radius of the pz shell is 9mm and thus we are in the adiabatic region for all frequencies.

Assuming a harmonically varying input and using the fact that in our case the displacement is purely radial the displacement field can simply be written

$$\mathbf{u} = u_r e^{i\omega t} \tag{4.22}$$

and Eq. (4.21) reduces to

$$\frac{\partial}{\partial r}\left(\frac{1}{r^2}\frac{\partial}{\partial r}\left(r^2 u_r\right) \right) = -\frac{\omega^2\rho}{M_s} u_r , \tag{4.23}$$

where $M_s = K_s + 4/3G$ is the (adiabatic) longitudinal modulus.

The boundary conditions of is zero displacement at the center of the sphere and a fixed amplitude at the surface

$$u_r(0) = 0, \;\; u_r(r_0) = u_0. \tag{4.24}$$

If we define $k^2 = \frac{\omega^2 \rho}{M}$ the general solution to Eq. 4.23 is given by

$$u_r(r) = c_1 \frac{\partial}{\partial r} \frac{e^{ikr}}{r} + c_2 \frac{\partial}{\partial r} \frac{e^{-ikr}}{r} \tag{4.25}$$

where the first boundary condition gives $c_1 = -c_2 =: c$. Thus we can write the solution in the following way

$$\begin{aligned} u_r(r) &= c \frac{\partial}{\partial r} \left(\frac{e^{ikr} - e^{-ikr}}{r} \right) = c \frac{\partial}{\partial r} \left(\frac{2i \sin(kr)}{r} \right) \\ &= 2ick^2 \frac{kr \cos(kr) - \sin(kr)}{(kr)^2} \end{aligned} \tag{4.26}$$

The second boundary condition gives $c = \frac{u_0}{2ik^2} \frac{(kr_0)^2}{2(r_0 \cos(kr_0) - \sin(kr_0))}$.

The stiffness of is given by

$$S = \frac{\delta p_r}{\delta V} = \frac{-\sigma_{rr}(r_0)}{4\pi r_0^2 u_0} \,. \tag{4.27}$$

where σ_{rr} is the radial stress. The radial stress can be expressed in terms of the displacement field through the stress-strain relations for an isotropic medium [6, p. 11]

$$\begin{aligned} &\sigma_{ij} - \frac{1}{3}\sigma_{kk}\delta_{ij} = 2G \left(\epsilon_{ij} - \frac{1}{3}\epsilon_{kk}\delta_{ij} \right) , \\ &\sigma_{ii} = 3K\epsilon_{ii} \end{aligned} \tag{4.28}$$

Since the displacement is purely radial we have the diagonal elements of the strain tensor in spherical coordinates are simple

$$\epsilon_{rr} = \frac{\partial u_r}{\partial r}, \;\; \epsilon_{\theta\theta} = \epsilon_{\phi\phi} = \frac{u_r}{r} \tag{4.29}$$

Combining Eq. (4.28) and (4.29) it can be shown that

$$\sigma_{rr} = -M_s \frac{\partial u_r}{\partial r} - (3K_s - M_s) \frac{u_r}{r} \,. \tag{4.30}$$

Substituting the expression for the radial displacement field (Eq. (4.26)) in Eq. (4.30), then by the definition of stiffness (Eq. (4.27)) we finally arrive at the following expression for the stiffness of an isotropic viscoelastic sphere

$$S_{\text{liq}}(\omega) = \frac{1}{V} \left[K_s - M_s \left(1 + \frac{1}{3} \frac{(kr_0)^2 \sin(kr_0)}{(kr_0)\cos(kr_0) - \sin(kr_0)} \right) \right] \,. \tag{4.31}$$

4.5.1 Quasi-static region

At low frequencies, $\omega \longrightarrow 0$, we obtain by using the l'Hôpital rule (for simplicity we define $x = \sqrt{\rho/M_s}\omega r$ and then $x \to 0$ is equivalent to $\omega \longrightarrow 0$)

$$\begin{aligned} \lim_{x \to 0} \frac{x^2 \sin x}{x \cos x - \sin x} &= \lim_{x \to 0} \frac{2 \sin x + 4x \cos x - x^2 \sin x}{-\sin x - x \cos x} \\ &= \lim_{x \to 0} \frac{6 \cos x + 6x \sin x - x^2 \cos x}{-2 \cos x + x \sin x} \\ &= \frac{6}{-2} = -3 \end{aligned} \tag{4.32}$$

which means that eq. 4.31 reduces to

$$S(\omega) = \frac{1}{V}K \tag{4.33}$$

at sufficiently low frequencies. This we will called the *quasi-static* region. At these frequencies the stiffness element in the model is directly proportional to the bulk modulus.

A correction for moderately high frequencies, i.e. towards the end of the quasi-static region just before the first resonance of the system can be obtained by a Taylor-expansion to the first order of the

$$\frac{x^2 \sin x}{x \cos x - \sin x} \approx \frac{1}{5}x^2 - 3 \tag{4.34}$$

which

$$S_{\text{liq}}(\omega) = \frac{1}{V}\left\{K_s - \frac{1}{15}\rho\omega^2 r_0^2\right\} \tag{4.35}$$

This correction was implemented in the inversion procedure, but it makes very little difference, thus confirming that quasi-static assumption is indeed valid.

4.5.2 Resonance region

At higher frequencies the stiffness becomes a mixture of the bulk modulus and the longitudinal modulus (M_s). Equation (4.31) can be used to determine the mixed modulus at the discrete resonance frequencies.

At high temperatures and low viscosities $G = 0$ and $M_s = M_{s_0} = K_{s_0}$ eq. 4.31 reduces to

$$S(\omega) = -\frac{K_0}{3V}\frac{(kr_0)^2 \sin(kr_0)}{(kr_0)\cos(kr_0) - \sin(kr_0)} \tag{4.36}$$

i.e. there is essentially no loss (imaginary part of the modulus is vanishing).

At lower temperatures these approximations are not valid in general and we have used the full expression from Eq. (4.31) where both K_s and M_s are now complex and frequency dependent.

4.6 Data obtained with the quasi-static method

In Fig. 4.10 we show real and imaginary part of the bulk modulus of DC704 and PPE for a range of temperatures close to T_g determined by the quasi-static method.

It is evident that we encounter noise problems in the low-temperature and low-frequency end of the spectrum; more obvious in the imaginary part because the absolute levels are lower than the real part and worse for PPE than for DC704. We do currently not have a good explanation for this, but it seems to be connected to this particular method and is not seen in other measurements that are performed with the same experimental set-up (except maybe the longitudinal measurement, see chapter 6). We are thus guessing that it may have some mechanical origin that has to do with the particular

shape and size of the PBG. The noise around 50-100Hz is the electrical power network coupling into the electronics.

In general the noise level in this measurement is quite high compared to i.e. dielectric measurements and the shear measurement made in-house, but not compared to other mechanical measurements in the literature. In general the noise level in all our capacitance measurements is roughly the same, but the signal compared to background varies. In chapter 6 (section 6.3) we compare the raw signal (the measured capacitance) in the three mechanical measurements.

In the PPE the K_{s_0} and K_∞ levels are slightly slanted instead of completely flat. This is an artifact of the data treatment and reflects the fact that the liquid measurement and the reference measurement may not have had a perfect low-frequency overlap, i.e. the assumption $C_{\mathrm{fr}}^{\mathrm{liq}}(\omega \to 0) = C_{\mathrm{fr}}^{\mathrm{emp}}(\omega \to 0)$ was not entirely obeyed in this case. But it is very small effect.

The slight up-turn at towards the highest frequencies in the window is also an artifact of the data treatment. The presence of liquid shifts the position of the first mechanical resonance slightly down in frequency and thus $C_{\mathrm{m}}^{\mathrm{liq}}(\omega)$ starts to curve when the resonance frequency is approached while $C_{\mathrm{m}}^{\mathrm{emp}}(\omega)$ is still relatively flat. We should in principle be able to correct for that, which will be part of an ongoing refinement of the data treatment procedure.

4.7 Data obtained with the resonance method

In section 4.5.2 it was sketched how we can determine $M_0 = K_0$ at high temperatures from the resonances using Eq. (4.36). To extend the temperature region of this method some, we can introduce the complex modulus

$$K_s = K' + i\omega\eta^K \tag{4.37}$$

where K and η^K are real constants. η^K is the bulk viscosity (in some texts it is referred to as the volume viscosity e.g. in [3]) and is different from the more familiar shear viscosity. This will then work for temperatures where the imaginary part is non-zero, but η constant, i.e. as long as we are on the low frequency side of the alpha relaxation at the given temperature. We will refer to this as Model 1.

When the temperature is lowered we should in principle use the full expression in Eq. (4.31), since the shear modulus will start to be of significance. The resonance spectrum does however not hold enough information to extract the full frequency dependence of the both bulk and longitudinal moduli. If we still assume to be on the low frequency side of the alpha relaxation, we can write

$$M_s = M' + i\omega\eta^M \tag{4.38}$$

in analogy with Eq. (4.37). If we in addition assume that the relaxation of the shear modulus is faster, i.e. occurs at higher frequencies compared to the bulk modulus at the same temperature (at least for the liquids studied here this is definitely the case which is shown in chapter 7) we have

$$K_s = K_0. \tag{4.39}$$

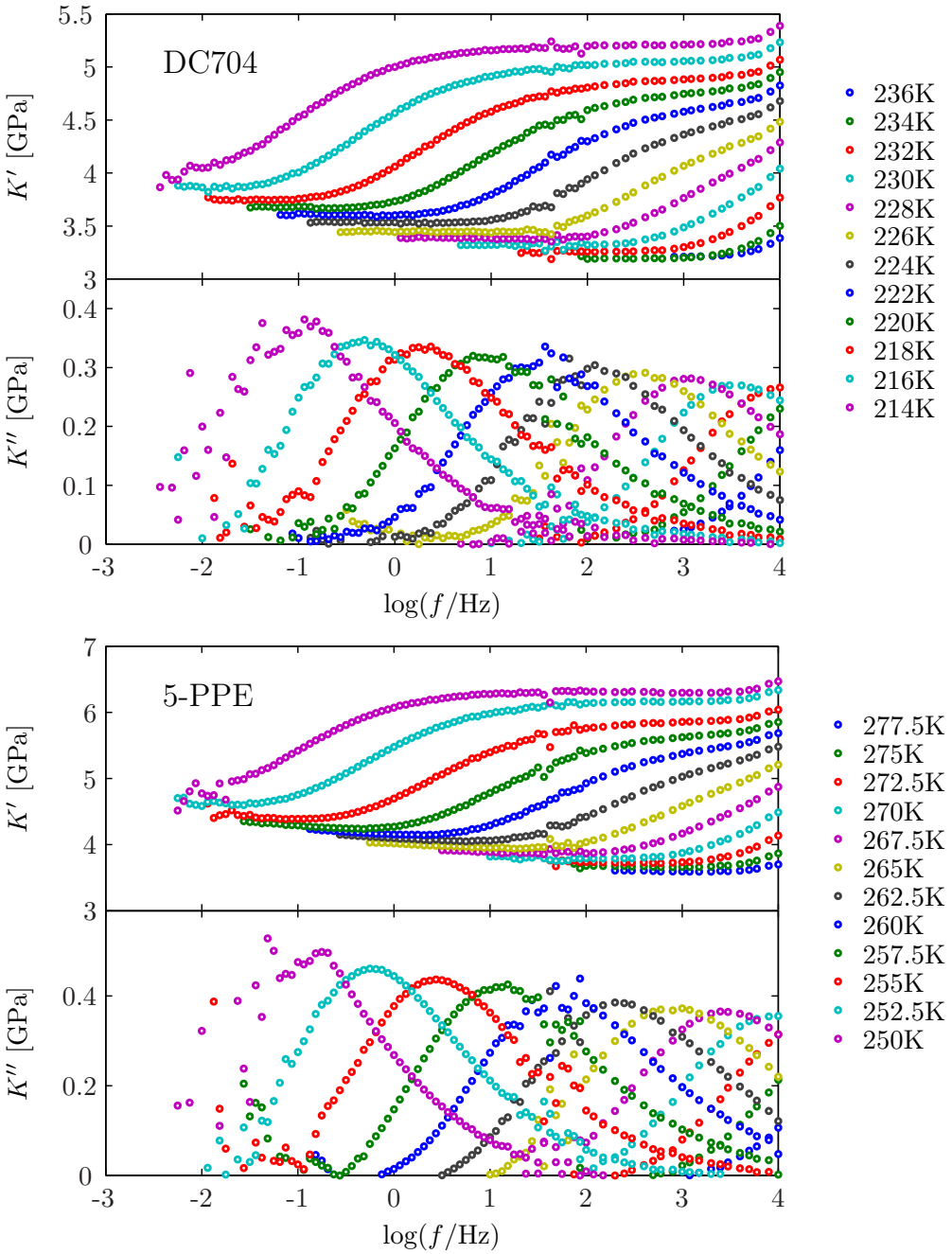

Figure 4.10 Real and imaginary part of the bulk modulus of DC704 and PPE for a range of temperatures close to T_g. It is evident that we encounter noise problems in the low-temperature and low-frequency end of the spectrum (clearly seen in the imaginary part because the absolute levels are lower than the real part), but we do currently not have a good explanation for this. The noise around 50-100Hz is probably the electrical power network coupling into the electronics of the set-up.

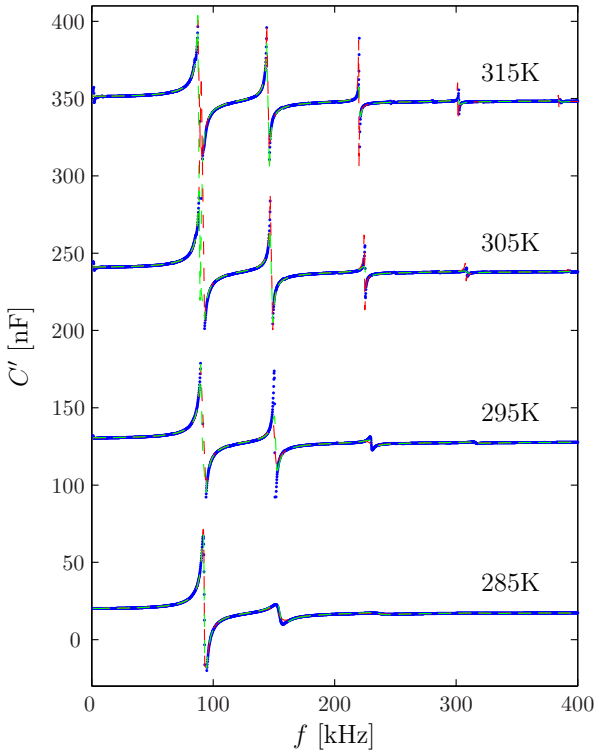

Figure 4.11 Examples of fits to the resonances of PPE with Eq. (4.31) and model assumptions, see section 4.7 for details. The data is shown as blue dots and the model fit in green dashed line (Model 1) and red dashed line (Model 2). Lowest curve is at actual measured values for the capacitance, other curves are shifted for clarity. The models give very good fits to the data, although sometimes overestimating the viscosity.

This gives 3 fitting (real) parameters: K_0, $M'(= K_0 + 4/3G')$ and η^M. We refer to this as Model 2.

It should be noted that the interpretation of the viscosity in Model 1 and 2 is not quite the same. In Model 1 the viscosity must be interpreted as a bulk viscosity, while in Model 2 the longitudinal viscosity, $\eta_M = \eta_K + 4/3\eta_K$, enters.

Figure 4.11 shows examples of fits of data to Model 1 (in green) and Model 2 (in red). We observe that the resonances move a little bit up in frequency as the temperature is lowered and at the same time they get more and more damped. There is near perfect overlap of the model curve and data points, which gives credibility to the assumptions in the model. Fits of data using Model 1 gives nearly identical curves for the temperatures shown here, at lower temperatures the models give visibly different fits.

The low frequency limiting modulus obtained in the quasi-static method can be compared to the values obtained by the resonance method. The two methods are independent ways of determining the temperature dependence of K_0. In figure 4.12 the bulk modulus at fixed frequencies determined through the quasi static method is plotted

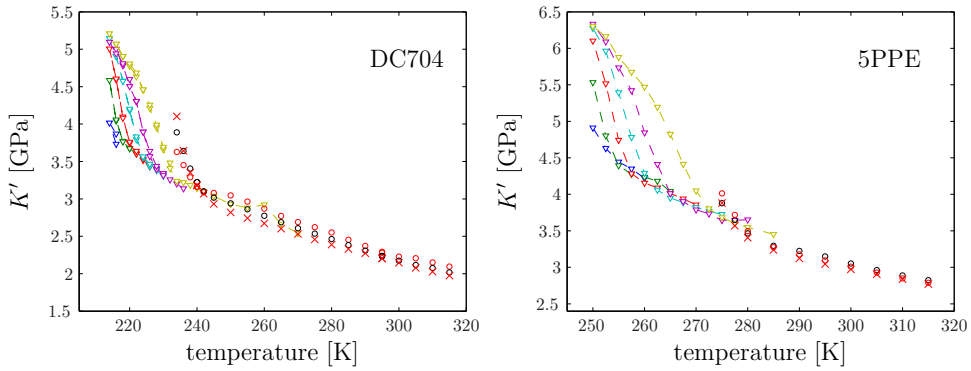

Figure 4.12 Combining results from quasi-static method with result from the resonance method. The bulk modulus data obtained with the quasi static method are plotted as a function of temperature for selected frequencies (colored triangles, each color correspond to a different frequency), the fitted K' of Model 1 (black circles) and the fitted K_0 (red circles) and M' (red crosses) of Model 2. All results agree well for PPE. In DC704 there is excellent agreement between the quasi static results and the fitted results of Model 1, while Model 2 gives a less perfect match.

as a function of temperature (each color correspond to a frequency) as well as K' of Model 1 and M' and K_0 of Model 2. The result from the two methods match up almost perfectly (see however section 4.8 and Fig. 4.14).

4.7.1 Resonance method - the simple way

In [2] a somewhat simpler way of using the resonances to determine M is mentioned. We include this here for comparison.

The resonances of a viscoelastic sphere occurs when the denominator in Eq. 4.31 is zero, i.e. whenever

$$\tan x = x \tag{4.40}$$

where again $x = \sqrt{\rho/M_s}\omega r$.

These resonances are moved due to the mechanical coupling to the PBG but this is only for important for the lowest lying resonances. If Eq. 4.40 is solved graphically we see that for sufficiently high x, the solution is simply where $\cos x = 0$, i.e. for $x = \frac{\pi}{2}, \frac{3\pi}{2}, \frac{5\pi}{2}$ ect. We have

$$\tan x = x \Rightarrow x = \frac{1+2n}{2}\pi, \quad \text{for } n \text{ high} \tag{4.41}$$

where n is an integer. Thus for the resonance frequency ω_n, where $n \geq 3$, the longitudinal modulus is to a good approximation given by

$$M \approx \left(\frac{2}{\pi(2n-1)}\right)^2 \rho\omega_n^2 r^2 = \frac{16}{(2n-1)^2}\rho\nu_n^2 r^2 \tag{4.42}$$

where $\nu_n = 2\pi\omega_n$ is the n^{th} resonance frequency in Hz.

4.8 Reproducibility

The reproducibility of these measurements is a matter of some debate. In the master thesis of Jakobsen & Niss [25] the issue was discussed for the shear modulus measurement, and they concluded that the shapes and peak positions reproduced very well, but their very conservative estimate on the errorbars on the *absolute* numbers based on repeated measurements was as large as ±50%.

4.8.1 Reproducibility of the quasi-static measurement

To arrive at "perfect conditions" for the quasi-static measurement we have repeated the measurement several times, and the results presented in Fig. 4.10 represents the final iteration. Some measurements have been discarded even before the data treatment procedure started, because it was simply impossible to get a liquid and a reference measurement to match.

Figure 4.13 show three different measurement series on each of the liquids. In the case of PPE, two of the measurements were carried out in the same transducer and the same cryostat (black and red curves) while the last measurement (in blue) was taken with a different transducer in a different cryostat. For DC704, the red and black curves are measurements in the same cryostat, but with different transducers, and the blue curves are an old measurement (by Niels Boye Olsen) with a shorter frequency range. In all cases there is reasonable agreement between the different measurements, although the reproduction is not near perfect.

A few comment should be made in this connection:

In the case of PPE, we have measured on two different bottles of the chemical, which actually makes small difference in peak positions and shape of the relaxation. The newest measurement (presented in Fig. 4.10) is the same bottle that was used for measuring heat capacity (see chapter 7). The actual reproducibility for the same bottle of chemical may thus be slightly better than what is inferred from Fig. 4.13(b).

The reproducibility increased enormously with the fabrication of new bulk transducers (by our very competent workshop). The first many tries with measuring bulk modulus on DC704 with old transducers amounted to only one usable match of reference and liquid measurement (the black curves of Fig. 4.13(a)). It is likely that a repeated measurement with one of the new transducers would reproduce better.

4.8.2 Reproducibility of the resonance method

The problems with low frequency dispersion of the ceramics and determination of inertance L have very little influence on the resonance results, which can be inspected in Fig. 4.14. Here we have plotted the fitted values of K', G', and η for several different measurements. The fitted values for K' for both Model 1 and 2 (section 4.7) are very stable – even for measurements that were discarded for the quasi-static method. It shows that the resonance method is less influenced by reproducibility problems.

This is very encouraging, because it means that the resonance results can be used to determine how correct the results from the quasi-static measurement are. The results

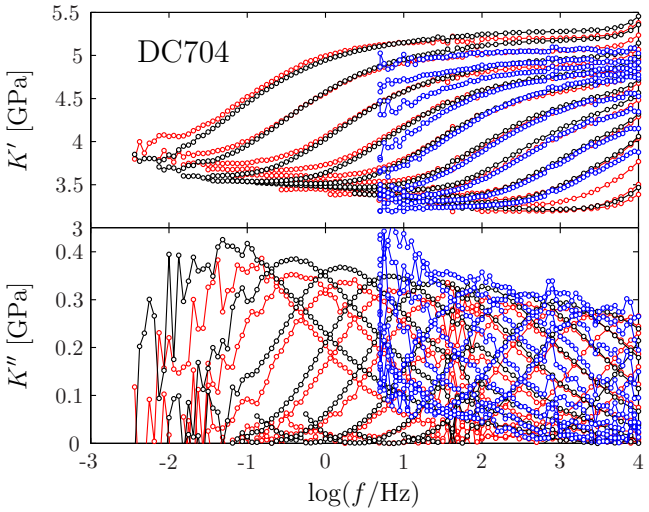

(a) Three different quasi-static bulk modulus measurements on DC704. Red curves are taken with the P3 transducer, the black with an old transducer labeled 14 both in CRYO 5, and the blue curves are from an old measurement (made by N. B. Olsen), transducer and cryostat unknown.

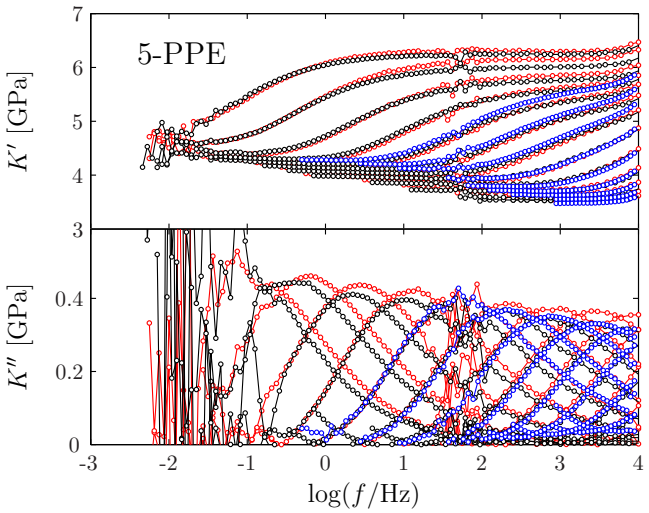

(b) Three different quasi-static bulk modulus measurements on PPE. Black and red curves are taken with the P3 transducer four month apart in CRYO 5, and the blue curves with P1 transducer in CRYO 3.

Figure 4.13 Reproducibility of the bulk modulus measurement. The red curves are the data presented in Fig. 4.10 and represent the final iteration of measurements.

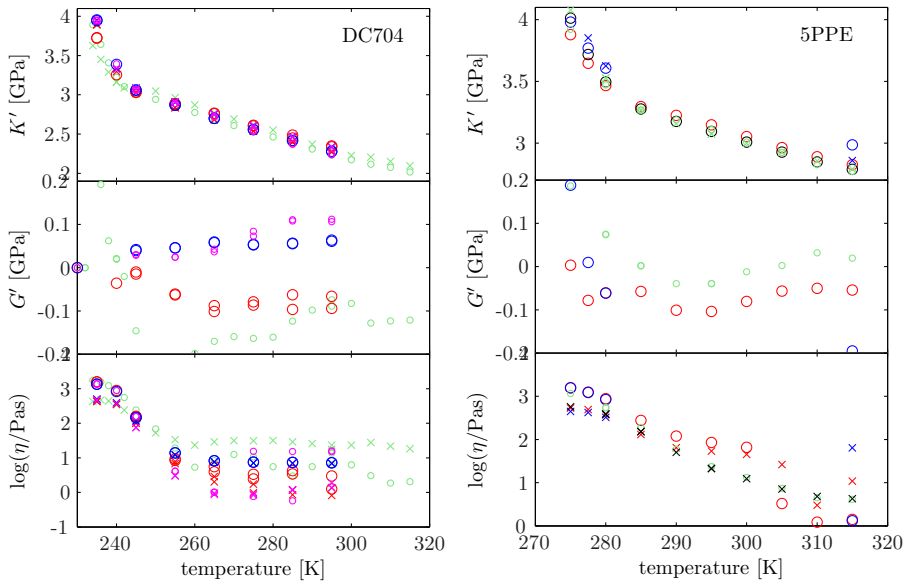

Figure 4.14 Fit parameters of Model 1 and 2 (see section 4.7) fitted to the resonances at high frequencies. Each color represents a different measurement. The fitted values of K' all agree reasonably, while the fitted values of G' (only Model 2) in some cases becomes unphysical (negative). The values of η are not in all cases monotonic which we would expect, but they agree more or less. By inspecting the fits directly it seems that the fitting algorithm tends to overestimate the viscosity. We do not currently have a good explanation for that.

of the resonance method can be used as a guidance for the K_0 level of the quasi static measurement.

The fitted values for G' are in some cases negative, which is of course unphysical. Probably, the K and M parameters (in Model 2) are too correlated to always make a meaningful fit: a low value for M can be balanced in the fit by a correspondingly higher value of K. This notion is further supported by the fact that apparently a negative value of G is preferred at high temperatures.

4.9 Uncertainty of the measurement

One way of examining the sensitivity of the of the determined bulk modulus to the parameters of the model is looking at the logarithmic derivatives of Eq. (4.31). The logarithmic derivative of a function $f(x)$ is given by

$$\frac{d\ln f}{d\ln x} = \frac{df/f}{dx/x} \tag{4.43}$$

and thus it directly tells us what the relative change in f is given a relative change in x.

The bulk modulus in the quasi-static limit is given by Eq. (4.11) combined with Eq.

(4.33). In this function we have 5 variables: L, ω_0, Q, C_{cl}, and C_{fr}. For the quasi static range $\omega \ll \omega_0$ and terms with ω/ω_0 vanish. Consequently, the quasi static measurement is insensitive to the value of Q. For this analysis we will ignore the dispersion. The function we are looking at is thus the following

$$K = V \cdot S = VL\omega_0 \left(\frac{C_{fr} - C_{cl}}{C_m - C_{cl}} - 1 \right), \tag{4.44}$$

where C_m is the measured capacitance of the liquid filled transducer.

The derivatives of Eq. (4.31) is given by

$$\begin{aligned} \frac{\partial K}{\partial C_{cl}} &= VL\omega_0^2 \frac{C_{fr} - C_m}{(C_m - C_{cl})^2}, \quad \frac{\partial K}{\partial L} = V\omega_0^2 \left(\frac{C_{fr} - C_m}{C_m - C_{cl}} - 1 \right) \\ \frac{\partial K}{\partial C_{fr}} &= VL\omega_0^2 \frac{1}{C_m - C_{cl}}, \quad \frac{\partial K}{\partial \omega_0} = 2VL\omega_0 \left(\frac{C_{fr} - C_{cl}}{C_m - C_{cl}} - 1 \right) \end{aligned} \tag{4.45}$$

which gives the following logarithmic derivatives

$$\begin{aligned} \frac{\partial \ln K}{\partial \ln C_{cl}} &= \frac{C_{cl}}{C_{fr} - C_{cl}} \frac{C_{fr} - C_m}{C_m - C_{cl}}, \quad \frac{\partial \ln K}{\partial \ln L} = 1 \\ \frac{\partial \ln K}{\partial \ln C_{fr}} &= \frac{C_{fr}}{C_{fr} - C_{cl}}, \quad \frac{\partial \ln K}{\partial \ln \omega_0} = 2 \end{aligned} \tag{4.46}$$

Thus we can see that if we change L or ω_0 by 1% it will change the resulting bulk modulus by 1%, respectively 2%. The sensitivity to changes in C_{fr} and C_{cl} is more involved and depends both on the actual values of C_{fr} and C_{cl}, as well as their difference and the difference between them and the measured C_m.

The difference between C_{fr} and C_{cl} is determined by the coupling constant of the piezo ceramic material and is temperature dependent since both C_{fr} and C_{cl} are temperature dependent. Both are however decreasing with decreasing temperature so it is reasonable to assume that their difference is roughly temperature independent. Typical values C_{fr} and C_{cl} of $C_{fr} = 22\text{nF}$ and $C_{cl} = 17\text{nF}$. Thus at this temperature a 1% change in C_{fr} leads to a 4.4% change in K.

The difference between C_m and C_{fr} and C_{cl} depends on the stiffness of the sample: a very hard material will lead to $C_m \approx C_{cl}$ while a very soft material will lead to $C_m \approx C_{fr}$. Thus a soft material leads to a small uncertainty in C_{cl} (but then we have little signal) while a hard material will give a large uncertainty in C_{cl}[1]. In our case a typical value of C_m is 19nF. A 1% change in C_{cl} thus leads to a 5.1% change in K.

The result of the quasi-static bulk modulus measurement thus quite sensitive to values of C_{fr} and C_{cl} and their difference (i.e. the properties of the transducer) and how large the bulk modulus of the measured sample is.

The absolute level of the reference measurement is also critical for the outcome of the quasi static measurement. Even a small scaling (in the per mille range) of the reference can shift the results. Preferably, it should not be necessary with any corrections or

1 strictly speaking there is also a frequency dependence of C_m but this will only be of significance if the relaxation strength of the sample is very large

scaling of the reference measurement. So if the conditions are less than perfect it is easy get erroneous results.

No scaling of the reference measurement was used for the data presented in Fig. 4.10.

4.9.1 Estimate of the error based on propagation of uncertainties

The propagation of errors and uncertainties for uncorrelated errors of a function of many variables, $f(x_1, x_2, x_3, ...)$ is given by

$$\Delta f^2 = \left|\frac{\partial f}{\partial x_1}\right|^2 \Delta x_1^2 + \left|\frac{\partial f}{\partial x_2}\right|^2 \Delta x_2^2 + \left|\frac{\partial f}{\partial x_3}\right|^2 \Delta x_3^2 + \dots \tag{4.47}$$

Using the derivatives from Eq. (4.45) we just need to plug in numbers and uncertainties to give an estimate of the error. Strictly speaking many of the quantities depend both in temperature and frequency, but that will be minor corrections.

The resonance frequency is roughly 100kHz, thus $\omega_0 = 2\pi 100\text{s}^{-1}$. The uncertainty on the resonance frequency is very small, since this is a very well defined quantity. f_0 is determined with roughly 1kHz accuracy which gives an error of approximately 1%. The estimated uncertainty of the inertance L was stated in table 4.2. Here we will use the value of the p3 transducer (which was used for the measurements presented in Fig. 4.10), i.e. $\sim$2.8% with $L = 3500$.

Using Fig. 4.7 (lowest curve) we can give some typical values of $C_{fr} = 22\text{nF}$ and $C_m = 19\text{nF}$. The value for $C_{cl} =$ is roughly $C_{cl} = 17\text{nF}$. A conservative estimate on the error of these quantities is between 1 and 2%.

Finally we arrive at an estimate of the bulk modulus

$$0.2\text{GPa} < \Delta K < 0.4\text{GPa}\,. \tag{4.48}$$

4.9.2 Estimate of the error based on repeated measurements

Combining the quality and reproducibility of the fitted K_0 of the resonance method with the quasi-static measurements, we are relatively certain of the K_0 level of the quasi static measurement. The K_0 and K_∞ are linked, which means that if one of them determined within some error then the other will be determined within the same error.

Based on the discrepancy between repeated measurements, our estimate of the error on the absolute levels is ±5-7% for both DC704 and PPE. Using an average value of the bulk modulus of 4GPa, we thus arrive at

$$0.2\text{GPa} < \Delta K < 0.3\text{GPa}\,, \tag{4.49}$$

which is in agreement with the estimate above.

4.10 Summary and concluding remarks

We have shown how we by modelling and subtraction of features of the bulk transducer can obtain almost seven decades – from a couple of mHz to roughly 10 kHz – of bulk modulus data.

Overall the error estimate is much smaller than what was suggested by Jakobsen & Niss [25], which in part is due to the possibility of comparing two independent methods in the same measurement (the quasi static and the resonance).

To give an idea of the effort of arriving at the datasets presented in Fig. 4.10, we have added up the measuring times of the total number of measurements. The total measuring time for bulk modulus measurements in connection with this work was $\sim$240 days or roughly 5760 hours of effective measuring time. Hopefully, some of work here will make it a little easier to arrive at reproducible and trustworthy results in future measurements.

Having said that, there is definitely still room for improvements and there are problems, that we have not yet understood. For instance, it would improve the quality of the data significantly if we could find and eliminate the source the low frequency noise in $1 - 10$mHz range. Also, the reproducibility is still not fantastic and it would be nice to improve that in the future.

Unfortunately, there is not much hope to expand the lower temperature limit of the method. In this work we have really pushed the limit of the capability of the bulk transducer. When the bulk modulus relaxation time is around 1Hz we start to effects of the liquid not being able flow in through the hole, and from the signature of the "breathing mode" there are some indications that cavities inside the bulk transducer start building up.

5 Shear modulus measurements

The shear modulus measurement is closest to working routinely and several publications have been based on this measurement, e.g. [24, 26–29]. Among the advantages of this measurement (over the bulk modulus measurement) are a much better signal-to-noise ratio, a shorter measurement protocol, and easier handling.

Since this measurement has been used more routinely some standardized software for the data treatment has been developed (by Bo Jakobsen), which has also eased this work considerably. A detailed description of the technique was given by Christensen and Olsen [1] and a thorough analysis of the possible errors of the measurement was given by Jakobsen & Niss [25] and thus only a brief description of the technique will be given here. We discuss the reproducibility of the measurement and give a estimate of error on the absolute levels of the measured shear modulus.

5.1 The shear transducer

The piezo-electric shear modulus gauge (PSG) is constructed of three electrode covered piezo-electric ceramic discs mounted in a layer construction. There is a gap of 0.5mm between the discs, where the liquid is loaded.

When an electric field is applied to the discs they will expand or contract in the radial direction, depending on the polarity of the discs compared to the direction of the electric field.

Electrically the middle disc is connected in parallel with the two outer discs in series as is shown in Fig. 5.1. In the figure small dots indicate the polarity of the piezo-electric discs, and thus when an electric field is applied, the middle disc will move opposite the two outer discs. With this construction the gap between the discs will then be field-free, and the liquid will be subjected to a purely mechanical perturbation.

There will also be a small deformation in the polar direction, but since the plates are in counter phase this will only cause a small translation of the liquid layer. In addition to that the aluminum casing is mechanically soft and will deform easily compared to the liquid.

The partially clamping of the plates due to the liquid is measured as a decrease in the capacitance which can then be related to the shear modulus of the liquid.

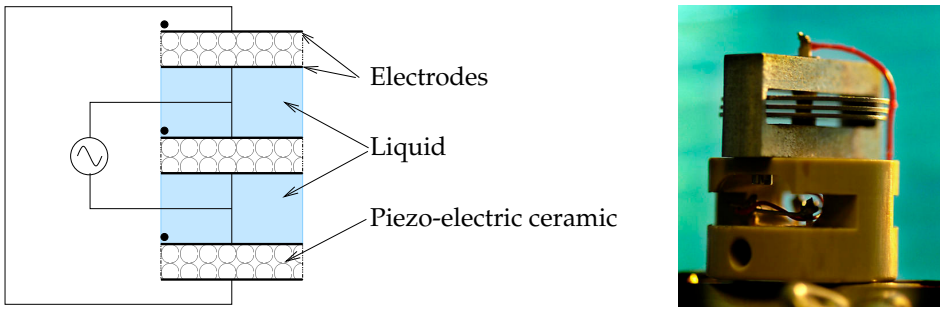

(a) Schematic drawing of the shear transducer. (b) Photo of the shear transducer

Figure 5.1 The shear transducer. (a) The pz discs are electrically connected so the middle disc is in parallel with the two outer discs in series. Physically the three plates are positioned as shown, which has the consequence that the gaps between the discs (where the liquid is loaded) is field-free. The polarity of the disc is marked by a dot on one side of each disc. With this configuration, the middle disc will move opposite to the two outer discs when a field is applied. (b) Photo of the shear transducer. Small holes drilled in the center of the two outer discs allow for the electrical connection to the inner disc. The three discs and hubs are fixed inside a aluminum casing attached to a foot that fits in the cryostat holder.

5.1.1 Raw data

Fig. 5.2 shows the measured capacitance of the liquid filled and the empty cell at room temperature and a temperature in vicinity of the glass transition temperature. At 300K the spectrum of the empty and filled transducer are identical (note that the resonances are actual (radial) resonances of pz discs and not due to the liquid).

As the temperature is lowered the shear modulus of the liquid increase and will cause a partial clamping of the pz discs. This is seen as the drop in capacitance in the low end of the spectrum. The rigidity of the liquid will also change the resonance spectrum, moving the resonances to higher frequencies.

5.1.2 Modelling the PSG

For the PSG the equations of motions for the discs have to solved. We go over the equations and their solutions carefully in appendix C based on the formulation by (but somewhat more detailed than) Christensen & Olsen [1]. Here we give a short summary of the crucial steps and assumptions in the modelling process.

In the three disc construction the middle disc will be subjected to twice the mechanical stress of the outer disc when the cell loaded, due to the presence of the liquid. The middle disc is also subjected twice the electrical field due to the electrical connection of the plates. Together these conditions ensure that the middle disc will always move twice the distance of the outer discs (when the inertia of the liquid can be ignored). Thus there will be a neutral plane in the liquid that remains unaffected by the movement of the discs. This plane could be regarded an infinitely rigid support, and thus the three disc construction can mapped to a one disc construction with infinitely rigid support with 1/3 of the liquid layer thickness and a capacitance corresponding to that of the

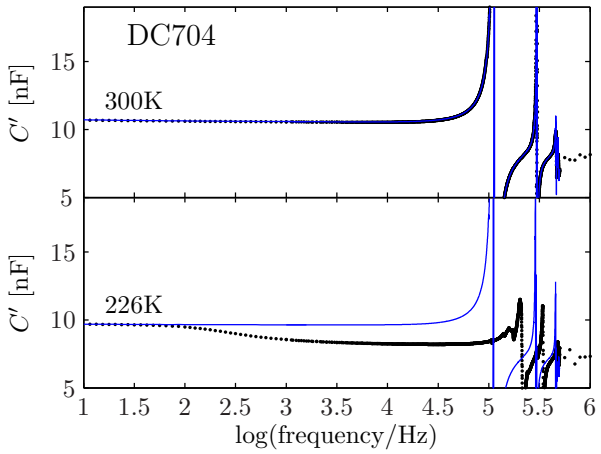

Figure 5.2 Raw data of the empty (full lines) and filled (black dots) PSG at two temperatures. At ambient temperature (300K) the spectrum of the empty and filled transducer are identical. As the temperature is lowered the shear modulus of the liquid increase and will cause a partial clamping of the pz discs. This is seen as the drop in capacitance in the low end of the spectrum. The rigidity of the liquid will also change the resonance spectrum, moving the resonances to higher frequencies.

three disc system, i.e. 3/2 of the capacitance of a single pz disc.

We define F to be the dimensionless measured quantity

$$F = \frac{C_m - C_{cl}}{C_{fr} - C_{cl}} \tag{5.1}$$

where C_m is the measured capacitance and $C_{cl} = C_m(\omega \to \infty)$ is the clamped limit of C_m and $C_{fr} = C_m(\omega \to 0)$ is the free capacitance.

The measured capacitance C_m is the ratio of charge on the electrodes, Q, and the applied voltage, V. The charge is found by integration if the charge density of the electrodes which is given by the elasto-electric compliance matrix (see appendix C or [1] for more details) of the piezo ceramic, and depends on both dielectric end mechanical properties. This results in the dimensionless measured function being determined solely by the radial displacement u_r of the edge of the disc

$$F = a u_r(r_0) \tag{5.2}$$

where a is a constant and r_0 is the radius of the disc.

The displacement, u_r, as a function of the stress that the liquid exerts on the surface of the disc is found by solving the radial equation of motion for a the disc

$$c_{11}\left(r^2\left(u_r''\right) + r u_r' - u_r\right) - \sigma_l \frac{r^2}{\xi} = -\omega^2 r^2 \rho u_r \tag{5.3}$$

where c_{11} is an elastic constant and ρ is the density of the ceramics. In arriving at this equation it is assumed that the tangential stress on the free side is zero and σ_l on side

in contact with the liquid and that the stress gradient across the disc is simply σ_l/ξ, which is reasonable because the disc is thin.

The key assumption now is that the displacement of disc gives a pure shear deformation of the liquid. Then we can write

$$\sigma_l = G(\omega)\frac{u_r(r)}{d} \tag{5.4}$$

where d is thickness of the liquid layer (which in this case 1/3 of the separation between the discs). The volume change of the liquid is on the order of u/r_0, while the shear deformation is u/d, hence the ratio between volume change and shear deformation is on the order of $d/r_0 \ll 1$. We have $r_0 = 1$cm while $d = 0.5/3$mm, and hence the ratio of volume change to shear deformation is less than 2%.

Define the characteristic quantities of the pz discs inertance $M_c = \rho d\xi$, modulus $G_c = c_{11}d\xi/r_0$, and the characteristic frequency $\omega_c = \sqrt{\frac{G_c}{M_c}}$, as well as the following dimensionless quantities

$$V = \frac{G(\omega)}{G_c},\ S = \left(\frac{\omega}{\omega_c}\right)^2 \tag{5.5}$$

where $G(\omega)$ is the shear modulus of the liquid. Then Eq. (5.3) can be reduced to a Bessel differential equation, which is solved with the boundary conditions of zero displacement at the center and zero stress at the edge.

Partial filling of the discs

A complication arises when the liquid does not fill out the entire space between the discs, which is inevitable because the liquid contracts when it is cooled. This can be corrected by solving the above equation with some slightly different boundary conditions (see [1]), which is largely unproblematic. But it does introduce some uncertainty, since the outcome is quite sensitive to the actual radius of the liquid r_l since the largest shear deformation takes place at the edge and the charge collecting area is large at the edge.

We define the filling degree by

$$x_l = \frac{r_l}{r_0} \tag{5.6}$$

then F will be a function of the dimensionless quantities S and V (defined in Eq. (5.5)) as well as the filling degree, $F(S, V, x_l)$.

Dispersion of the ceramics

The weak dispersion of the dielectric constant of the ceramics is accounted for in the same way as in the bulk modulus measurement, namely by assuming that $C_{fr}(\omega)/C_{cl}(\omega)$ is constant and that the dispersion in the liquid measurement is the same as in the reference measurement of the empty transducer. Defining a new function Φ as the ratio of F for the liquid filled measurement and for the reference measurement on the empty transducer we have

$$\Phi = \frac{F(S, V, x_l)}{F(S, 0, 1)} = \frac{C_m^{\text{liq}} - C_{cl}}{C_m^{\text{emp}} - C_{cl}}\,. \tag{5.7}$$

Φ is determined experimentally.

Inversion of the data

Φ can be approximated by an algebraic expression, and in the end the shear modulus is given by the following expression

$$G(\omega) = G_c \frac{a - b\Phi + \sqrt{(a - b\Phi)^2 - 4\Phi c(\Phi - 1)}}{2\Phi c} \tag{5.8}$$

where a, b, and c are constants.

5.2 The shear modulus data

The shear modulus data obtained for DC704 and PPE are shown in Fig. 5.3. The measurements presented here are carried out in the same experimental setup and cryostat (CRYO 5) as the bulk modulus data presented in Fig. 4.10 and the temperatures are selected to overlap with the temperatures in the bulk modulus measurement. The temperature range of the shear measurement is less restricted so the shear modulus data sets go to lower temperature than the bulk modulus data sets do.

The signal-to-noise ratio is evidently much higher in this measurement compared to the bulk modulus measurement.

5.3 Discussion of reproducibility and errors

Compared to the bulk modulus measurement, it was in general easy to get the empty reference measurement to match the liquid measurement.

We do not in the shear modulus measurement have an independent check of the absolute levels, as we did in the bulk modulus measurement where the resonance method provided such a check[1]. However, we do know that the shear modulus should vanish for $\omega \to 0$. This knowledge can be used to fine tune the liquid-reference match by a small scaling of the measured capacitance of the reference by a single factor, usually on the order of 1.005, i.e. a correction in the per mille range.

5.3.1 Filling degree

In the bulk measurement the volume of the sphere does not change with temperature, only density. In the shear measurement, the two liquid layers contract when cooled thus making the effective radius smaller. This has been accounted for in the inversion algorithm by assuming a constant thermal expansion coefficient and an initial filling degree of 100%, i.e. $x_l^{\text{initial}} = 1$.

The filling is done by hand and the filling degree is determined by eye, so there could be variations in the initial filling. In addition to that, the ceramics may absorb some liquid, which means that at the end of the measurement the filling profile can be changed slightly. Jakobsen & Niss [25] carried out a careful analysis of the influence

1 in priciple it should also be possible to obtain a value for the shear modulus by the shift in resonances (in Fig. 5.2) [1], but we have not pursued this possibility here

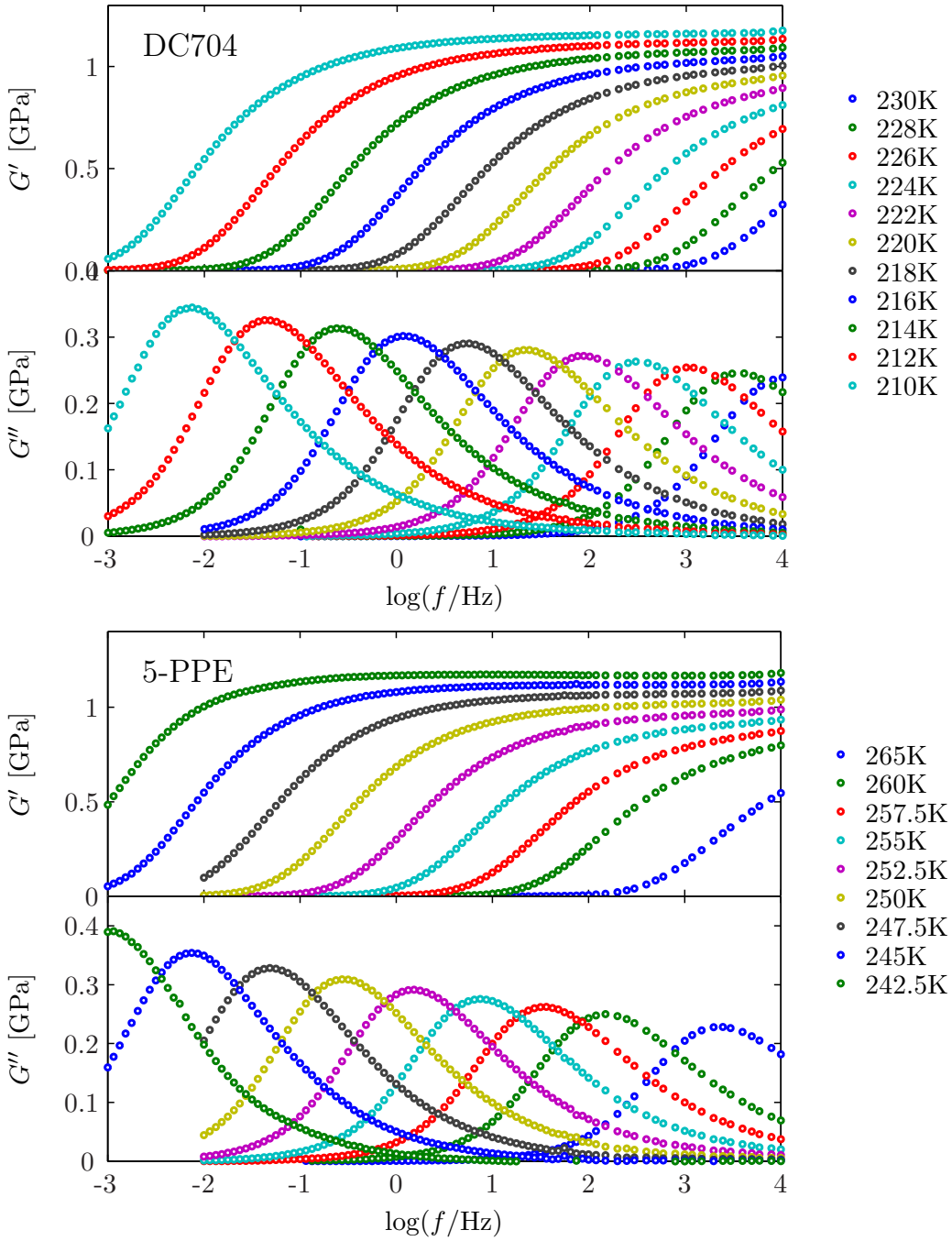

Figure 5.3 Real and imaginary part of the shear modulus of DC704 and 5-PPE for a range of temperatures close to T_g.

an initial filling degree less than 100% ($x_l^{\text{initial}} < 1$) in which they estimated that this could cause a change peak position of up to 0.2 decades and a broadening of the shape.

Christensen [30] has shown that the geometry of the liquid layer (radius $\gg$ thickness) introduces a geometric hindrance of the radial flow when the viscosity of the liquid increases upon cooling. This effectively stops the radial contraction at a fairly high temperature. Thus the assumption of a constant thermal contraction may not hold.

Repeating the data inversion algorithm with different values of fixed radii or small variations in value of the thermal expansion coefficient, did not have a big effect on the absolute levels of the final data, while it may have a some effect on the temperature dependence of the high frequency shear modulus as well the shapes and peak positions.

5.3.2 Repeated measurements

The measurements were repeated several times with different transducers and on different experimental set ups.

In figure 5.4 we show data from numerous measurements on both DC704 and 5PPE (each in different colors). All data sets were produced for this work except for one, which is an old measurement by Niels Boye Olsen (shown in black dashed lines). The temperature steps of his measurement were 2.5K instead of 2K which we used, and consequently the temperatures match only every 10K.

Each dataset is scaled by a single factor to make the absolute levels agree. It is obvious that the shapes of relaxation is almost identical for all measurements. The shape preservation was also noted by Jakobsen & Niss [25], where the difference in absolute levels was ascribed to different degrees of filling.

In table 5.1 we list the measurements shown in Fig. 5.4, relevant information about the measurement, and the factor by which the results of this particular measurements have been scaled to make them agree with the chosen reference. The measurements in CRYO 3 have been shifted according to the procedure described in Appendix B. The measurement by Niels Boye Olsen (black dashed lines) were not shifted on the frequency axis.

For DC704 the scaling factors are within $\pm 6\%$, which we will then take as an estimate of the error on the absolute values of the measurement.

For PPE the measurements seem to separate into two categories: data obtained with the S9 transducer and data obtained with the S7 transducer with almost 10% difference in the absolute levels between the two groups of measurements. This could indicate some systematic error connected with the specific shear transducer used in the measurement (for instance a slightly different disc separation), although the DC704 results do not generally support this picture.

However, a reservation should be made here regarding the reproducibility plot of PPE data. As was the case in the bulk modulus measurement, most of the measurements (those marked with $*$ in table 5.1) are taken with a different bottle of the chemical than the final data presented in Fig. 5.3. The initial measurements all showed problems with something that looked like DC conductivity for temperatures below 0°C. In Fig. 5.4 this shows up as a deviation in the imaginary part at low temperature, where the loss starts to grow.

	Color	Set-up	Transducer	Scaling-factor
DC704	black	CRYO 3	S9	1
	red	CRYO 5	S9	1.06
	cyan	CRYO 3	S4	0.98
	magenta	CRYO 5	S7	0.95
	green	CRYO 5	S7	0.97
	black dashed	x	x	0.97
5PPE	black	CRYO 5	S9	1
	cyan*	CRYO 3	S9	1
	red*	CRYO 3	S7	0.89
	blue*	CRYO 5	S9	1.01
	green*	CRYO 5	S7	0.87

Table 5.1 Table listing all the measurements shown in Fig. 5.4. All measurements were carried out for this work, except for the black dashed of DC704 which is an old measurement by Niels Boye Olsen.

5.4 Final remarks

We have presented numerous data sets for the liquids DC704 and PPE. All of the measurements agree very well regarding the shape and position of loss peaks. The absolute levels agree within $\pm 10\%$. It is very encouraging that the shapes of relaxation and the relative change in absolute levels with temperature is preserved to such a high degree that scaling by one factor makes all data sets collapse. The scaling factors in the case of DC704 were not too dramatic, indicating an error of the measurement of approximately 6%.

The approach to the error estimates has been experimental and "brute force": making a lot of measurements using different measuring cells over a fairly extended period of time to see what variations we get. This has had the advantage of enabling a critical review of the effects of for instance uncertainties of filling degree predicted by Jakobsen & Niss [25], and we show that in general the measurement reproduces better than what their conservative estimates suggests.

A clear improvement of the method would be to include an analysis of the resonances at high frequencies to get an independent measure of the shear modulus. This would provide us with better estimate of the correct absolute levels of the data.

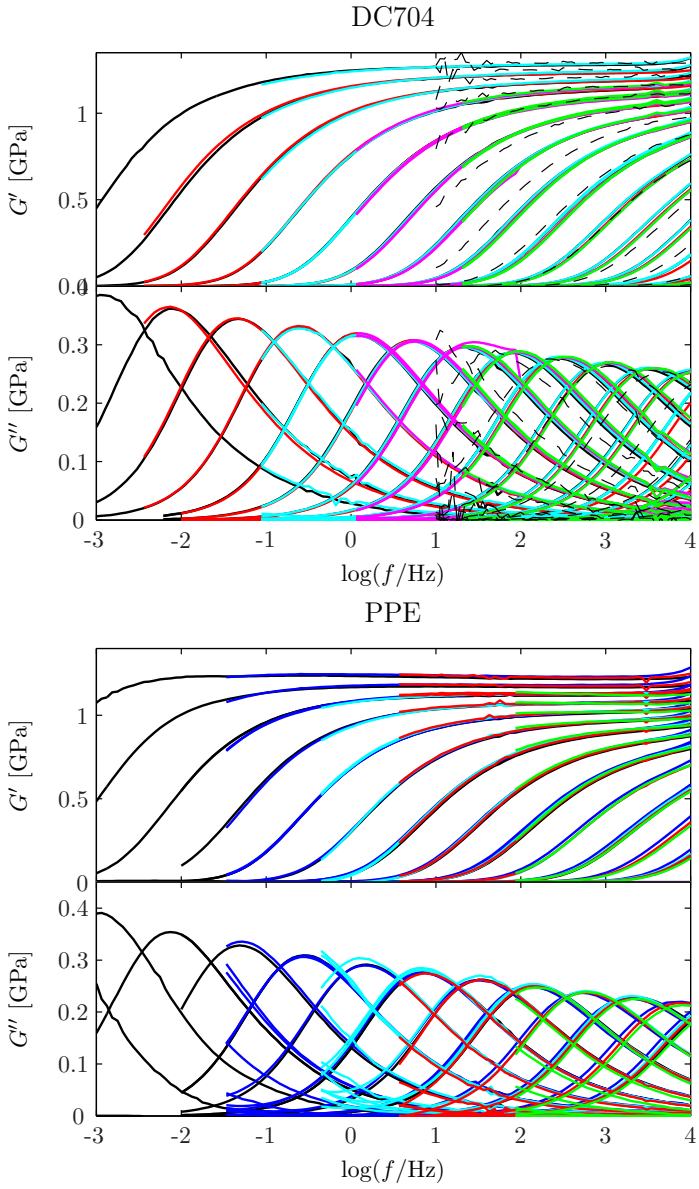

Figure 5.4 Reproducibility of the shear measurement. The measurements (each data set with a different color) are taken with several different transducers and cryostats and each measurement has been scaled by a factor to make the absolute levels agree (details are listed in Table 5.1), and shifted whenever the temperature calibrations were not identical using CRYO 5 as a reference (see Appendix B). The data sets were cut at increasing frequencies to make it visible that these are actually different data sets.

6 Longitudinal modulus measurement: a proof of concept

This final of the three "technical" chapters concerns a new measurement technique that is based on the same principles as the two previous ones. In fact, it requires no new devices just a simple modification of the PSG: flipping the middle disc of the 3 disc construction will cause all three plates to move in the same direction when an electrical field is applied. It will thus not be a pure shear deformation of the liquid between because the liquid will be subjected to a volume change. With this method we will consequently measure some combination of shear and bulk modulus.

Now, the reader may ask: why would we want to do that? We already have methods to measure the bulk and shear moduli, why do we need a third measure of the same two quantities? In fact, there are many good reasons to do that. One good reason is that such a method supplies us with an independent measurement that can be used to check the validity of the first two (especially with respect to absolute levels of the moduli). Another very good reason is that the bulk measurement is a very difficult measurement with a limited temperature range. If we succeed in matching all three measurements, we could in the future skip the tedious and cumbersome bulk modulus measurement and just do the other two and deduce the bulk modulus from that. This would furthermore have the consequence that we would be able to measure the bulk modulus at lower temperatures than now since the new transducer does not suffer from the same limitations as the PBG, plus it is a much faster measurement.

So in principle there are a lot of advantages to this measurement.

The downside is that the modeling and interpretation of data becomes more involved than with the PSG, because some of the simplifying assumptions that were valid for the PSG no longer holds. Unfortunately, this is also the reason why data from this measurement has not been inverted. The process of modelling is simply not quite finalized yet; there are still uncertainties as to what boundary conditions actually hold for this measurement.

In the following we will present raw data from the measurement, confirming that there is a signal, and point out some general observations that might be important for the modelling. The signal strength is compared to that of the two other mechanical measurements, and we conclude by some considerations regarding the modeling.

6.1 The "longitudinal" transducer

Naming this device was not an easy task because it is probably not a "pure" modulus that we measure. For now we will call it the piezo-electric longitudinal modulus gauge (PLG) in analogy with the PSG and PBG, even though the device is probably not measuring a pure longitudinal modulus.

The PLG is almost identical to the shear transducer: we are operating three discs in a layer construction, electrically connected so the voltage over the middle disc is twice the voltage over the two outer discs. The difference between the PSG and the PLG is simply the polarity of the middle disc, which in the PLG has been flipped. This flip will cause the three discs to move in the same direction when an electrical field is applied. Consequently, the volume is now changed under the deformation and it can no longer be assumed a pure shear deformation.

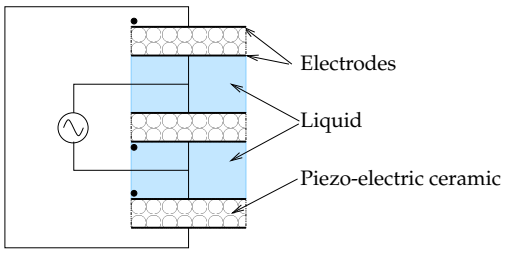

Figure 6.1 Schematic drawing of the piezo electric "longitudinal" gauge.

In Fig. 6.1 we show a schematic drawing of the PLG, where the only difference compared to Fig. 5.1 is the polarity of the middle disc has been flipped. The polarity is marked with a dot at the top or bottom of each disc.

6.2 Raw data

In Fig. 6.2 we show the raw data of six different liquids. All measurements except for PG, is carried out in the same measuring cell and the same cryostat (CRYO 3). The PG measurement was carried out in CRYO 5 using a different shear transducer.

Clearly, there is a signal from the liquid, although it is (expectedly) smaller than that of the shear measurement.

The scales on the axes for all plots are the same, so it is possible to compare the measurements. It can thus be seen that the real part of the capacitance for the liquids with the lowest T_g's is shifted to lower values. This is not surprising since we know that the properties of piezo ceramic are highly temperature dependent. It may however not have been recognized before that this actually influences the signal quality. This is evident when instead we look at the imaginary parts, where the frequency dependence of the ceramic material is quite dramatic at higher temperatures (in our frequency window) while less dramatic at the low temperatures (compare for instance the DEP curves to the PPE data).

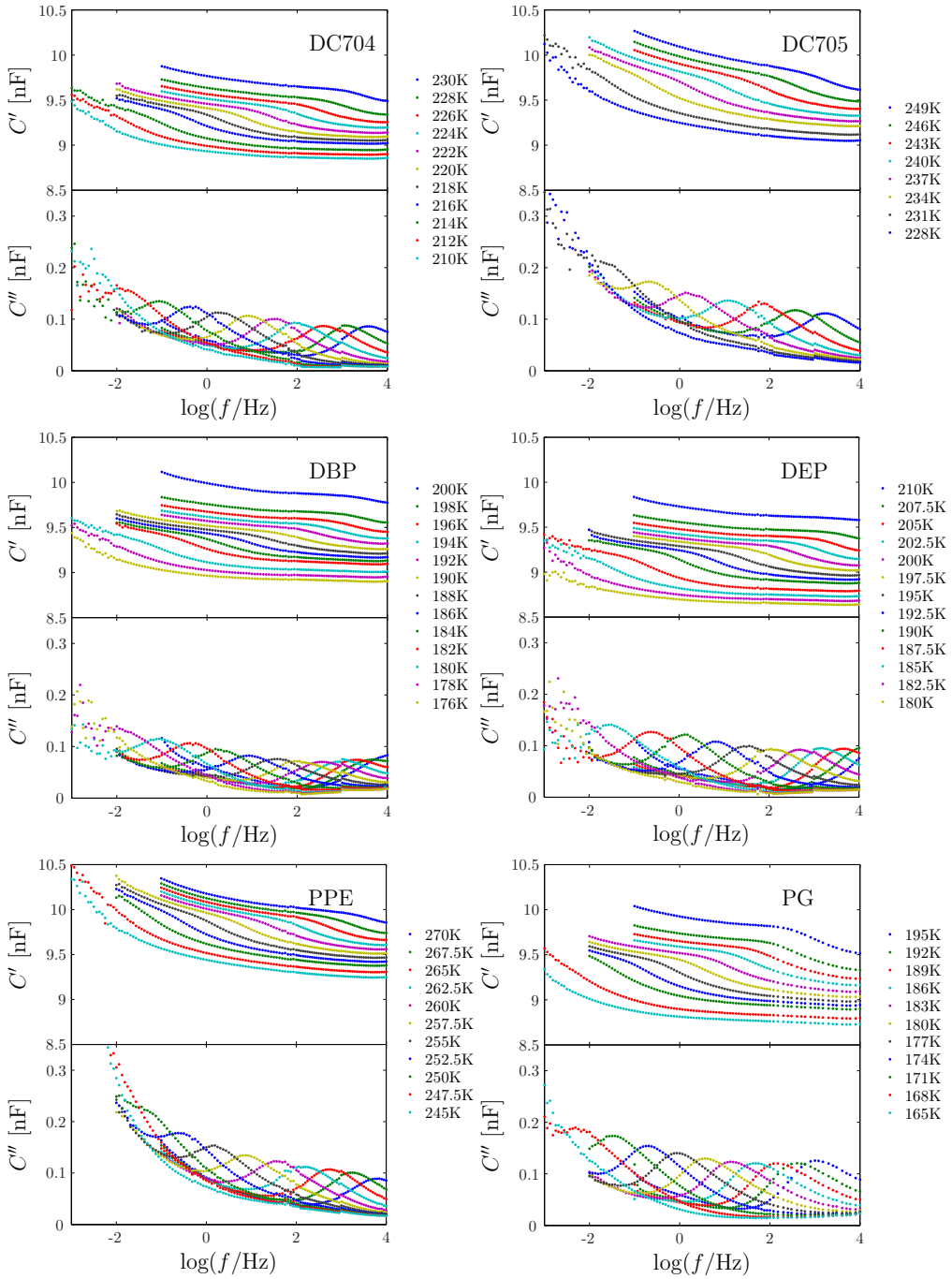

Figure 6.2 Raw data for 6 different molecular glass-formers. We clearly see the partial clamping of the discs due to the liquid, so we conclude that there is signal.

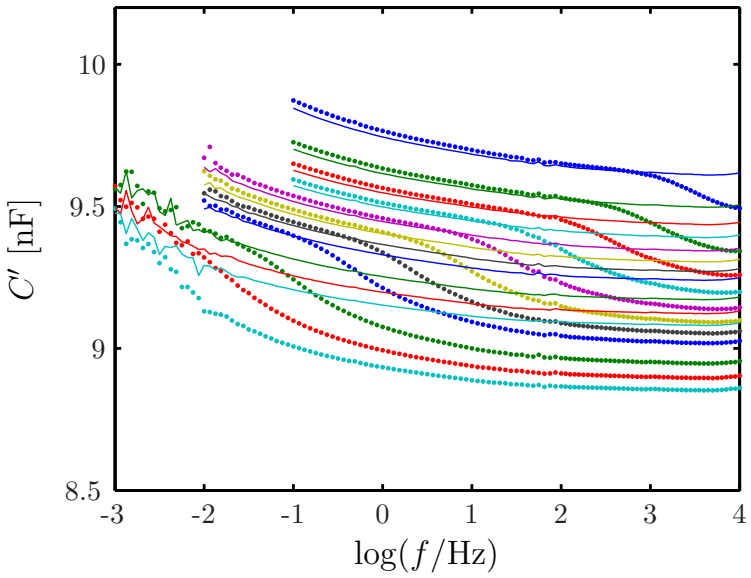

Figure 6.3 Comparing the liquid filled measurement with that of an empty reference. Quite clearly the reference measurement lies below the liquid measurement – a feature that is completely reproducible and general for all the measurements.

There is considerable noise at the lowest frequencies from 1mHz to 10mHz, a quite marked shift from very low noise to very high noise seen very clearly in the imaginary parts of the response, for all measurements in CRYO 3. The single measurement in CRYO 5 (PG) does not suffer quite as bad from this low frequency noise. This is a problem that appears periodically in the bulk modulus measurements as well, but so far has not been encountered in the dielectric or shear modulus measurement.

6.2.1 Liquid-reference match

As was the case with bulk and shear modulus measurements, we need to make a reference measurement with the empty PLG, repeating the same thermal cycle as that of the liquid measurement. Figure 6.3 shows an example of a match between a liquid and a reference measurement.

First of all it should be noticed that the curves of the liquid measurement seem to (almost) line up with the reference at the low frequencies. This tells us that the pz-discs at low frequencies are not clamped, thus there is no signal from the liquid. Since we expect the response of this measurement to be a mixture of bulk and shear modulus, this is perhaps a little bit surprising because the bulk modulus does *not* go to zero at low frequencies. Thus there has to be some kind of flowing mechanism at low frequencies (as is the case with the PBG where the liquid can flow out of the hole at sufficiently low frequencies). We speculate that the liquid at the edge is able to bend inwards and outwards when the discs oscillate at low frequencies; the PLG may have its own “breathing mode”.

Secondly, we notice that the liquid and reference do not match perfectly at low temperatures – in fact the reference curves seem to lie systematically *below* the liquid curves. This is observed in all the measurements and is completely reproducible. With our usual algorithm of eliminating the low frequency dispersion of the piezo ceramics by the reference measurement, this will result in the moduli becoming negative at low frequencies, if used uncorrected.

One possible explanation for this was pointed out already by Christensen and Olsen [1]. The piezo ceramic material is not only sensitive to the temperature and thermal history, but also to the stress history. When we lower the temperature the liquid contracts thereby creating surface tensions on the pz discs, and thus the stress history of the reference and the liquid spectrum can not be the same. Perhaps this effect is more severe in the case of PLG than the PSG.

6.2.2 Reproducibility

For some of the liquids the measurement was repeated (using the same measuring cell). The measurement is very reproducible, as can be seen in Fig. 6.4 where we show two sets of measurements on DC704 (in red and blue) that are nearly identical. In principle we should be able to reduce noise in the measurement by just taking the average of two (or more) sets of measurements. This would be especially valuable to reduce the low frequency noise.

A more thorough evaluation of the reproducibility can not be carried out before we are able to invert the data and can compare the determined moduli.

6.3 Comparing signal strengths of the mechanical measurements

We can define the signal strength as the relaxation strength in the liquid seen in the capacitance compared to the capacitance of the empty cell. The “free” capacitance of the PSG and PLG is $\sim$ 10nF, while it is $\sim$ 25nF in the PBG.

Thus when we look at the imaginary part of the raw “longitudinal” data and compare that to the raw signals of the bulk and shear modulus measurements will give us an idea of the quality of the signal in this new measurement. In Fig. 6.5 this is shown for two temperatures (216K and 224K) for DC704. For the higher temperature we see that the relaxation strength in the shear modulus measurement is approximately six times larger than that of the “longitudinal” measurement. The relaxation strength seen in the bulk measurement appears to be comparable with that of the “longitudinal”, but compared with the free capacitance of the empty cell then the “longitudinal” signal is approximately 2.5 times greater. This is probably also why the noise is visibly larger in the bulk modulus.

When we then turn to the lower temperatures the signal of the “longitudinal” measurement is significantly improved over the bulk measurement, mostly due to complications in the PBG at low temperatures.

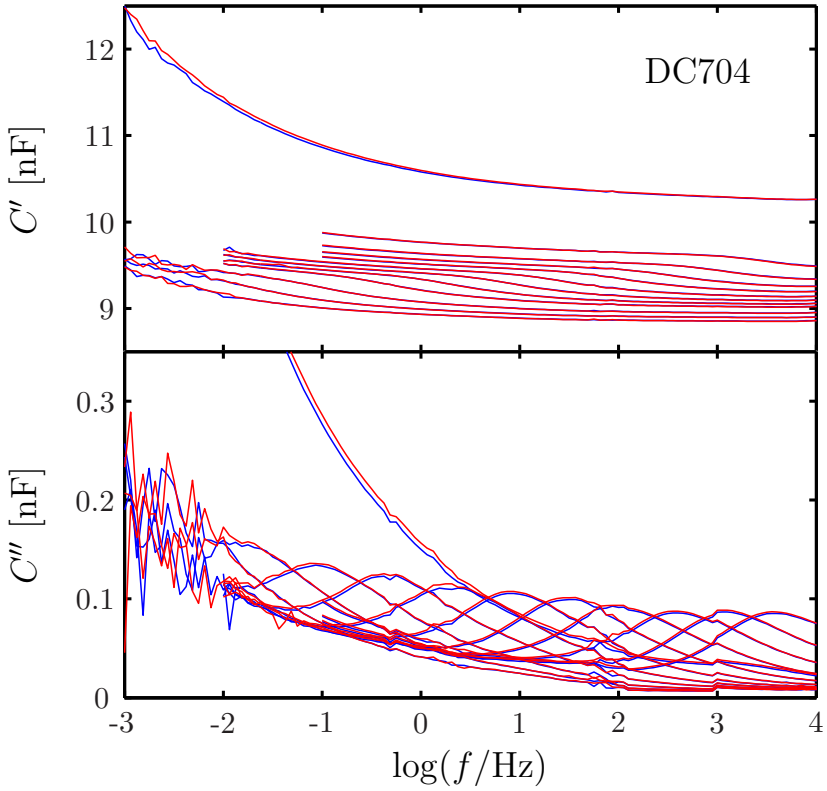

Figure 6.4 The reproducibility of the measurement. Blue and red curves are two different measurement series with identical thermal cycles. The two sets of measurements are close to identical thus establishing that the measurement is reproducible (at least in the same measuring cell).

6.4 Final remarks and outlook

We have shown that there is signal in the PLG. The signal is decent, and thus it makes sense to continue with development and modelling of the technique.

The modeling of the PLG and PSG is parallel for the derivation of the equations of motion of the discs (see appendix C). The measured capacitance of the empty cell should for instance be the same and largely depends on the displacement of the edge of the pz disc. The difference enters when we need to specify the stress on the pz discs due to the presence of the liquid. Here it is less obvious what should be assumed. Perhaps the combination of bulk and shear modulus determined is frequency independent, and most likely it is a function of the radius.

In the modeling of the PLG we can not map the three disc construction to a one disc device in the case of the PLG, which means that we have to solve three equations of motion (one for each disc) instead of just one.

Liquid and reference curves (almost) collapse at low frequencies, which suggest a

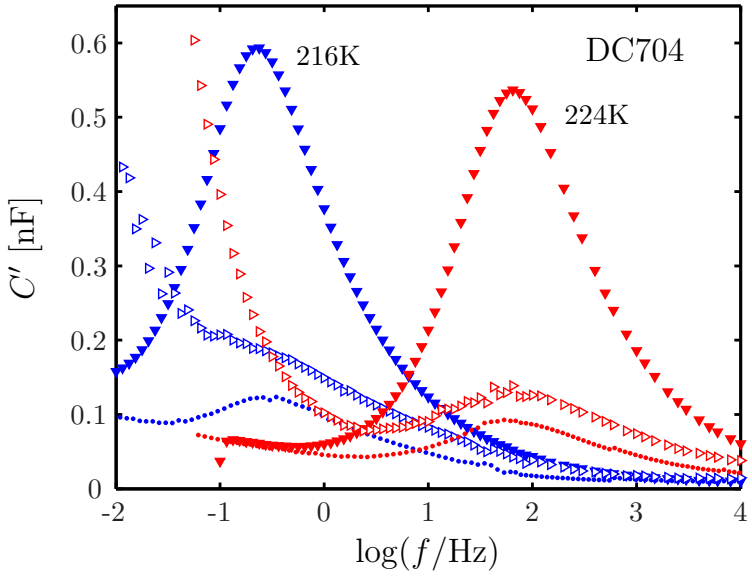

Figure 6.5 Imaginary part of the measured capacitance of the liquid filled PSG (▼), PBG (▷), and PLG (•). The signal in the PLG is roughly 1/6 of that in PSG, but at low temperatures a vast improvement over the signal in the PBG. At higher temperature the signal in the PLG is comparable to that in the PBG, but with less noise.

"breathing mode" that probably needs to be included in the model. Another – less attractive – possible reason for this observation could be the that the signal is largely dominated by the shear modulus.

In the end the modeling of the PLG will be more complicated than the modelling of the PSG, but if successful the PLG could be added as valuable independent check of our existing techniques.

7 Times, shapes, and decoupling in DC704 and PPE

In this chapter we will have a closer look at the data presented in chapter 4 and 5. In section 7.1 we cross-check the measurements with each other, extracting as much information as possible from the measurements. Unfortunately, the "longitudinal modulus" data are not in a finalized form, and thus cannot be used as a check of absolute levels of the shear and bulk modulus measurements.

In sections 7.2 and 7.3 we characterize the present data in terms of time-temperature-superposition, time scales of the alpha relaxation and the spectral shapes, and in section 7.4 we compare the temperature dependence of the time scale of the alpha relaxation found for the bulk and shear modulus relaxation to those of other response functions that can be measured *in the same set-ups* with methods developed in our group as well as the dielectric response.

The possibility of comparing of five different response functions all measured under identical conditions – the same cryostat and the same measuring equipment – is really unique. This kind of comparative analysis is scarce in the literature. Below we will give an overview of related studies.

A large subset of these are aimed at studying the (breakdown of the) Stokes-Einstein (SE) and Debye-Stokes-Einstein (DSE) relations. The SE relation connect the translational diffusion of large (macroscopic) objects in a fluid to the viscosity of the fluid [31]. The SE and DSE relations state that

$$D \propto \frac{T}{\eta} \tag{7.1}$$

where D is the diffusion constant, T is the temperature, and η the viscosity. The constant of proportionality involves Boltzmanns constant and a geometric factor that depends on the shape of the diffusing object and whether the translational or rotational diffusion is studied.

Strictly speaking these relations were derived for a macroscopic sphere suspended in a fluid, but it has been shown to hold even for the self-diffusion of particles in the liquid at high temperatures both in simulations (e.g. by Bordat *et al* [32]) and in experiments, e.g. by Chang & Sillescu [33]. In figure 7.1 we show the results of Chang & Sillescu for six different liquids, where the $D\eta/T$ is shown as a function of temperature scaled with T_g. Clearly, the SE relation is constant at temperatures above $1.2T_g$, but starts to deviate from this below. Similar results have been found by other groups [34–42]. Cicerone & Ediger [36] and later Rajian & Quitevis [42] and Heuberger & Sillescu [43] showed that the SE relation breaks down for small tracer molecules, while it is still valid at low temperatures for large tracer molecules.

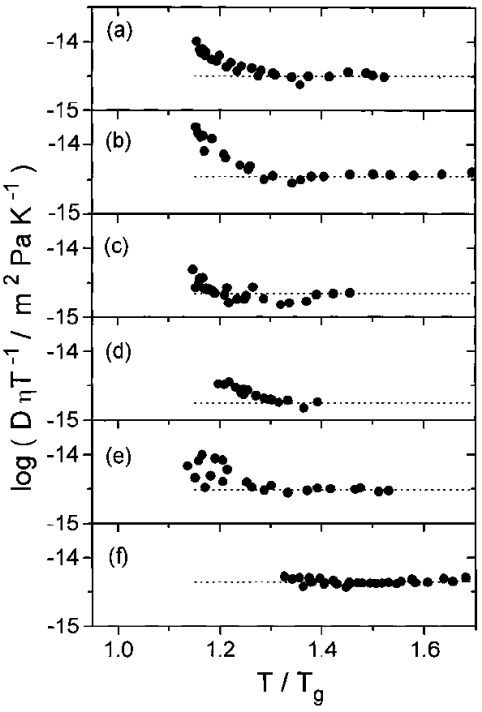

Figure 7.1 Breakdown of the Stokes-Einstein relation. Results of Chang & Sillescu [33] showing $D\eta/T$ as a function of temperature. The SE relation breaks down around $1.2T_g$ in six different liquids: (a) OTP, (b) salol, (c) PDE, (d) CDE, (e) m-TCP, (f) glycerol. From [33]

In other studies time scales of different probes are compared, often through a decoupling index X of relaxation times (τ) or peak (angular) frequencies $f_{\max}$

$$X(\chi_1, \chi_2, T) = \frac{\tau_{\chi_1}(T)}{\tau_{\chi_2}(T)} \quad \text{or} \quad \frac{f^{\chi_1}_{\max}(T)}{f^{\chi_2}_{\max}(T)} \tag{7.2}$$

where χ_1 and χ_2 are two different probes and T is the temperature. If $X \neq 1$ the time scales of the two probes are decoupled. Contrary to investigations of the SE relation, there seems to be no really clear conclusion regarding the temperature dependence of X, which apparently depends on the liquid under investigation and/or the probes used. There are reports of constant decoupling index in measurements, e.g. [7, 44–46], as well as some of a temperature dependent decoupling index, e.g. [47–49].

Sometimes the relaxation time (or peak frequencies) of different probes are simply compared in an Arrhenius plot ($\log \tau$ or $\log \omega_{\max}$ as a function of inverse temperature scaled by T_g) of different probes without explicitly evaluating the decoupling index. We show an example in Fig. 7.2 due to Schröter & Donth [50], who collected data from dielectric, heat capacity, shear retardation and NMR measurements on glycerol.

Fairly often, dielectric measurements and dynamic shear measurements are compared [26, 27, 44, 47, 55–62], which is probably due to two things: (1) this set of probes is

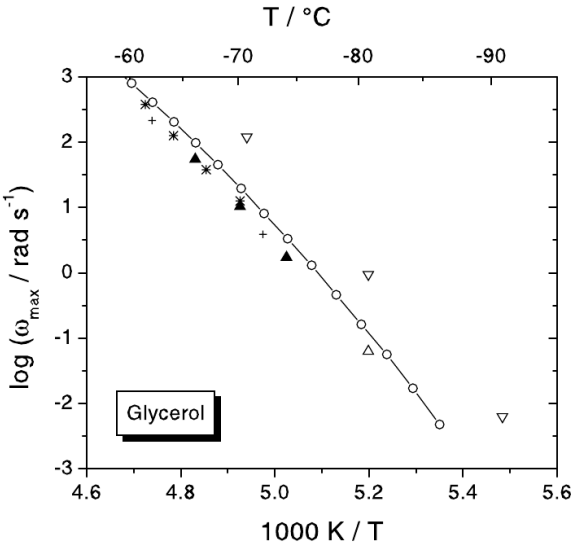

Figure 7.2 Arrhenius plot for glycerol using $\omega_{\max}$ from different probes: dielectric ((○) [51]), heat capacity ((+) [52] and (∗)[53]), maximum in G' ((▽) [50]) , maximum in the retardation contribution to J'' ((△) [50]), and NMR ((▲) [54]). Figure and data sources are from [50].

particularly interesting because they are believed to be closely connected, and (2) these measurements are relatively easy to perform. The Dermant-DiMarzio-Bishop model [63] connects dielectric and shear modulus and was studied, e.g. by Zorn *et al* [44] and Niss *et al* [60].

A smaller subset of comparative studies is involves purely mechanical responses. Christensen & Olsen [24] compared bulk and shear moduli for 1,2,6-hexanetriol with the same methods as in the present thesis, and concluded that bulk modulus relaxation was slower than the shear modulus relaxation, while the spectral shapes were identical within the noise. They also pointed out that different relaxation times of bulk and shear relaxation in consistent with a simple network model where the viscosity in bulk and shear viscosity stem from the same element.

Meng & Simon [20] presented pressure relaxation measurements, and compared the bulk results to shear creep compliance curves (measured by others) in polystyrene. They found that the bulk relaxation occurs in the short time region of the shear response, contrary to the conclusion of Christensen & Olsen.

Bulk and shear modulus relaxation have been compared by several authors using ultrasonic measurements of longitudinal and shear sound waves [14, 64–66]. Based on this procedure Morita *et al* [14] found that the bulk relaxation was roughly 5 times slower than shear relaxation, and Dexter & Matheson [64] reported similar observation. Alig and coworkers [65–67] have derived a theoretical expression for the relation between bulk and shear viscosities of polymers, $\eta^K/\eta^G = 2/3$, but found experimentally that this number was too small.

Yee & Takemori [11] developed a method by which Youngs modulus and Poissons ratio

could be measured on simultaneously on a sample. Combining the measured quantities they could calculate bulk and shear modulus. They did not explicitly state anything about the time scales of shear and bulk relaxation, but their results suggest that they are very similar.

Out of all these studies only a few compared response functions measured in the same experimental setups, and none of those involved more than two different probes.

7.1 Viscosity determined through bulk and shear moduli

We can determine the shear viscosity from the measurement of the shear modulus. Recall that the complex shear modulus may be written as [3]

$$\tilde{G}(i\omega) = G' + iG'' = G' + i\omega\eta^G \tag{7.3}$$

where both the G' and η are frequency-dependent. This means that we can determine the DC shear viscosity as

$$\eta_0^G = \eta(\omega \to 0) = \lim_{\omega\to 0} \frac{G''(\omega)}{\omega}\,. \tag{7.4}$$

The (DC) shear viscosity is proportional to the relaxation time in the temperature dependence according to the Maxwell relation $\tau = \eta/G_\infty$ (see chapter 2, section 2.1.1), since the temperature dependence of G_∞ is small compared to that of the shear viscosity. This procedure was also used in [8].

In Fig. 7.3 we show the $\log(G''(\omega)/\omega)$ as a function of frequency. Approaching the low frequencies (compared to the alpha relaxation time), the curves bend over and eventually settle at a plateau. The limiting value, $\eta(\omega \to 0)$, was taken to be the lowest data point of the curves shown in Fig. 7.3. For the lowest temperature of DC704 and the two lowest temperatures of PPE we do not really see the plateau and this procedure (simply taking the last data point) may thus be underestimating the DC shear viscosity for the lowest temperatures.

We have also a measure of the shear viscosity from the bulk transducer measurements. Recall, that at low frequencies the liquid flows in and out of the hole drilled in the piezo-ceramic shell, and that this Pouseuille flow is governed by the shear viscosity of the liquid (see chapter 4, section 4.4.3). Thus if the dimension of this "tube" (the drilled hole) is known, we should in principle be able to determine a shear viscosity from the "breathing mode" in the bulk modulus measurements.

From Eq. 4.15 we know that the shear viscosity is proportional to the mechanical flow resistance, R_h

$$\eta^G = AR_h \tag{7.5}$$

where $A = \frac{\pi a^4}{8l}$ is purely geometric factor, a and l being the radius and length of the "tube". Specifications from the workshop that produces the measuring cell, the values of these quantities are $a = 0.9$ and $l = 3.75$ (all in mm). This gives $A = 6.9 \times 10^{-11}\mathrm{m}^3$, which is the value we used. But even if we do not know the specifications exactly, the geometric factor is a number that is specific to certain measuring cell (bulk transducer), and thus could be calibrated with one set of measurements and tested with another.

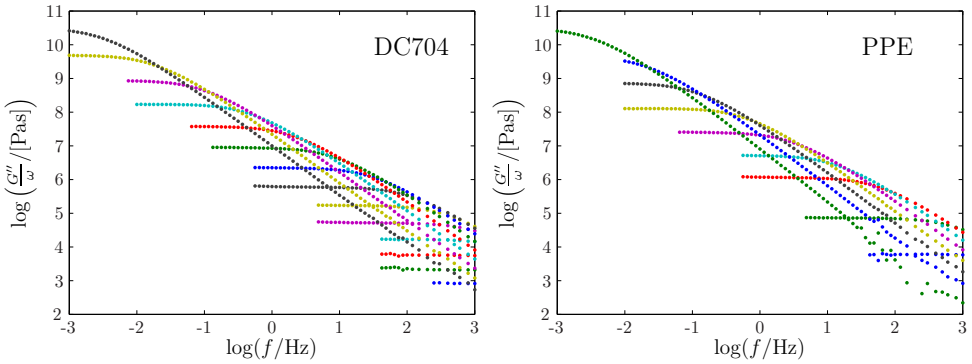

Figure 7.3 Determining the shear viscosity from shear modulus measurements. The figures show G''/ω plotted logarithmically against the frequency. Clearly, this quantity approaches a constant value for $\omega \to 0$. This level is the static shear viscosity.

R_h as a funtion of temperature is determined by the method described in chapter 4, i.e. through the the mechanical impedence, $\tilde{Z} = S/i\omega$, where S is the stiffness found in the bulk transducer measurement (see Eq. (4.31) in chapter 4). R_h can be found as the high frequency foot point of a Nyquist representation (imaginary part versus real part) of the mechanical impedance, or as through the peak position, $Z''_{\max} = 1/2R_h$ (because the "breathing" mode is described by a purely exponential the trace of the impedance in a Nyquist is a semi-circle).

In Fig. 7.4 we show the mechanical impedances in a Nyquist representation with logarithmic axes to fit all data in one window. The peak value is marked with an 'X' for each temperature. Identifying the peak position of course requires the peak to be in the measured frequency window, thus this method is restricted to relatively high temperatures.

Finally, we have a value for the viscosity from the fits of a model to the standing waves (see chapter 4, section 4.5.2, p. 44). These fitted viscosities are somewhat less reliable since they result from a multiparameter fit which was not well reproduced in different measurements; the values for viscosity are for instance not monotonic. In addition, the fitted viscosities are bulk or longitudinal viscosities, must thus be expected to higher than a shear viscosity. We will nevertheless include them for comparison.

All of the shear viscosities determined from the methods mentioned above are plotted together in Fig. 7.5. There is excellent agreement between the values obtained from the shear measurement and those determined from the "breathing" mode of the bulk measurement. The fitted values of the resonance method are – as expected – less than perfect, but also not entirely wrong. In a sense this confirms the validity of the model used for fitting the resonances in the bulk modulus measurement.

It is very encouraging that the methods agree this well with each other. It also means that combining the shear and bulk modulus measurements, we are able to reliably cover the temperature dependence of the shear viscosity over 10 orders of magnitude. Perhaps if we are able to adjust the fitting procedure, we will be able to extend this into the high temperature regions as well, thus making it possible to extract shear

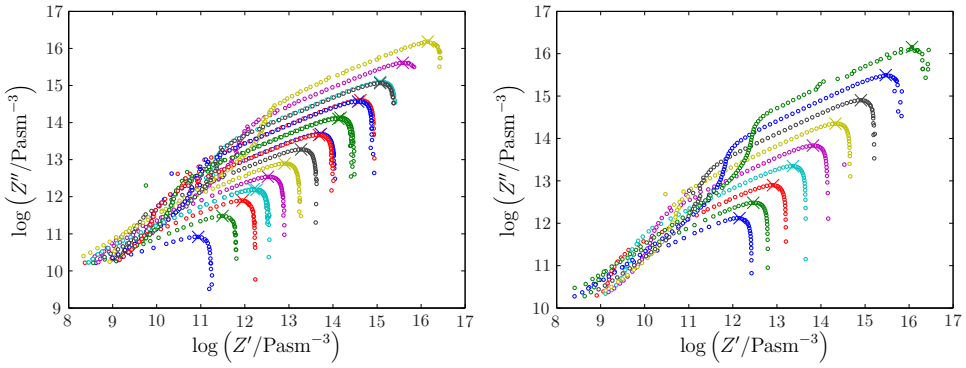

Figure 7.4 Determining the shear viscosity from the "breathing" mode. The flow resistance R can be determined by the high-frequency limit of the mechanical impedence, $\tilde{Z} = V\tilde{S}/i\omega$. But since the "breathing" mode is Debye like, the $\tilde{Z}$ traces out a semi-circle (see Fig. 7.4) and we only need to know the peak position to determine R. Here we used a doublelog plot to fit all data in the same window, which of course will distort the circular shape.

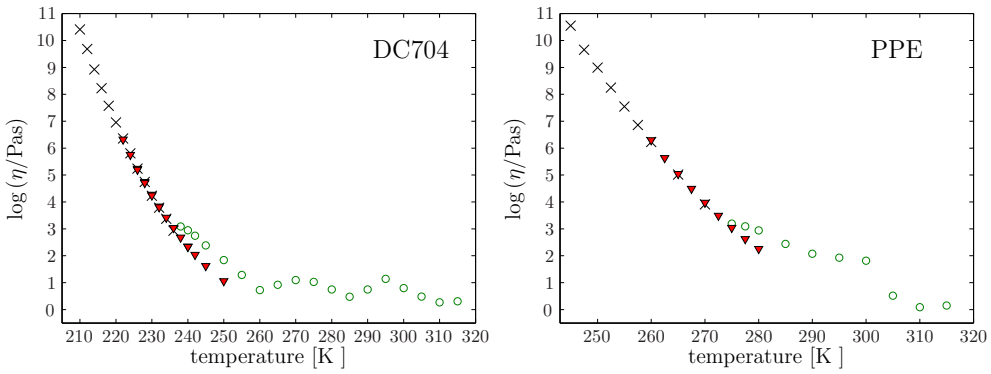

Figure 7.5 Comparing the shear viscosities obtained with different methods. Crosses are determined from the low-frequency limit of the shear modulus Eq. (7.4), full triangles are determined through "breathing" mode of the bulk modulus measurement, and open circles are the fitted values from the resonances of the bulk measurement (see chapter 4, section 4.5.2). These fitted values are obviously less precise than the two other methods. It is on the other hand encouraging to see that the fitted viscosities are not completely wrong either. In general it seems they are a bit too high.

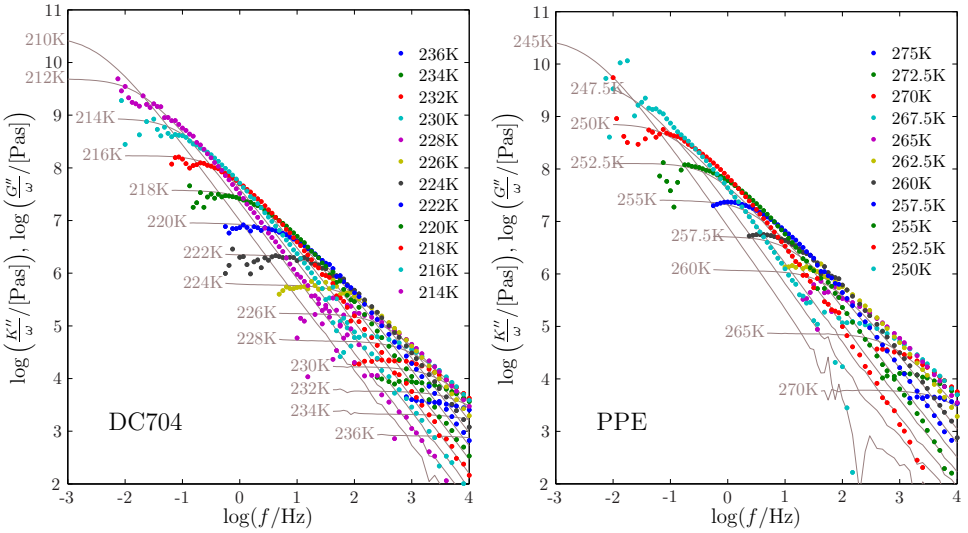

Figure 7.6 Determining the bulk viscosity from bulk modulus measurements. The figures show $\log(K''/\omega)$ plotted logarithmically against the frequency. Clearly, this quantity approaches a constant value for $\omega \to 0$. For comparison we have plotted also the shear viscosity curve (grey lines). In DC704 and we see that the bulk and shear viscosity curves collapse, but for different temperatures. PPE show a similar pattern although the quality of the bulk viscosity curves is less convincing.

viscosities over 12-13 decades, in the same experimental set-up.

The bulk viscosity is defined in the same way as the shear viscosity

$$\tilde{K}(i\omega) = K' + iK'' = K' + i\omega\eta^K \tag{7.6}$$

and in principle, we can determine the DC limit in analogue with Eq. 7.4, $\eta_0^K = \lim_{\omega\to 0} K''/\omega$. In Fig. 7.6 the low frequency limit of the bulk viscosity is shown (colored circles) and the shear viscosity as black lines. The bulk viscosity curves are quite noisy and thus the procedure of taken the last data point for each temperature as the DC limit would result in very noisy curves. To extract a meaningful number from these curves a more advanced approach or some modelling is needed, which we have not done. Interestingly, the bulk and shear viscosity curves apparently collapse *but not for the same temperatures*. For instance the bulk viscosity curve for 220K for DC704 falls on top of the shear viscosity curve for 218K. The quality of the PPE data are not quite as good, but the trend is the same: the bulk and shear viscosity curves are similar but at different temperatures. So bulk and shear viscosities are apparently very similar though not identical. And by coincidence we have chosen the temperature steps in the two experiments with coincide with the difference in viscosity. This observation presents a challenge to theory.

7.2 Time-temperature-superposition

Time-temperature-superposition (TTS) refers to the observation that for many liquids the shape of the relaxation remains unchanged when the temperature is varied, while the position on the time/frequency axis is shifted. It has been suggested that TTS (for the alpha relaxation) applies whenever the alpha relaxation is not influenced by other processes [68].

A standard way of checking for TTS in (frequency domain) data is to make a dimensionless plot of the imaginary part of the response function (the "loss"), i.e. scaling the frequency axis with the relaxation time (or the peak position) and the y-axis by the peak height

$$(\omega/\omega_{\max}, \chi''/\chi''_{\max}) \tag{7.7}$$

where χ here represents a any measured complex response.

If this scaling makes the data collapse then TTS is obeyed. Normally this is a qualitative statement, but a quantitative TTS-measure based on this procedure has been proposed by Nielsen *et al.* [69]. This however required extremely precise (noise-free) data and would not be useful to characterize our mechanical data.

Another less well-known way of checking for TTS is the normalized Cole-Cole plot. A Cole-Cole plot is a parameterized plot $(\chi'(\omega), \chi''(\omega))$ of the complex response. The normalized Cole-Cole plot is then a parameterized plot of relaxation data subtracting the long-time limit and normalized to the relaxation strength. Defining the normalized relaxation function

$$\tilde{F}(\omega) = \frac{\tilde{\chi}(\omega) - \chi_0}{\chi_\infty - \chi_0}\,, \tag{7.8}$$

the normalized Cole-Cole plot is thus $(F'(\omega), F''(\omega))$. The advantage of the normalized Cole-Cole plot is that it includes both the real and imaginary part and thus is a more "complete" representation of the data. Also, in the Cole-Cole plots the entire trace of the data from $\omega \to 0$ to $\omega \to \infty$ is contained in one plot.

In Fig 7.7 we show both of these TTS plots for both shear and bulk modulus relaxation of DC704 and PPE. Left column is bulk modulus data and the right column is the shear modulus data in the different representations. TTS is obeyed in the bulk modulus data for both DC704 and PPE within the noise. In the less noisy shear modulus data it is obvious that while the DC704 data show perfect data collapse the PPE data have small deviations on the high-frequency side of the alpha relaxation peak. There is apparently a wing in the spectrum, which could be due to a small amplitude beta relaxation according to the conjecture of Olsen *et al* [68].

Overall, both bulk and shear relaxation shapes for both DC704 and PPE are very similar. In the shear data we do see a small difference between the two substances: PPE is a bit narrower than the DC704, which in the Cole-Cole representation correspond to a slightly higher peak position. But could the bulk and shear relaxation for each in fact be identical? In Fig. 7.8 we combined the TTS curves of bulk and shear modulus relaxation (bulk data in black symbols and shear data in cyan), and at least for DC704 it looks like the less noisy shear modulus data traces out the curve that the bulk modulus data are scattered around. For the PPE data there are some deviations from this picture around the peak area of the spectrum, but shear and bulk data have the same height in the Cole-Cole representation. The similarity of the bulk and shear

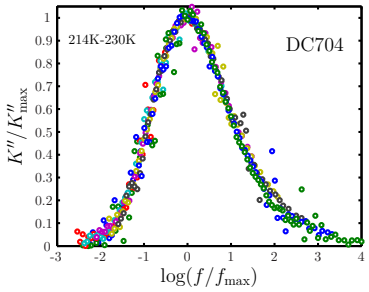

(a) Standard TTS plot for DC704 (bulk).

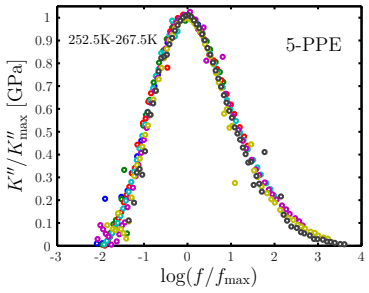

(b) Standard TTS plot for PPE (bulk).

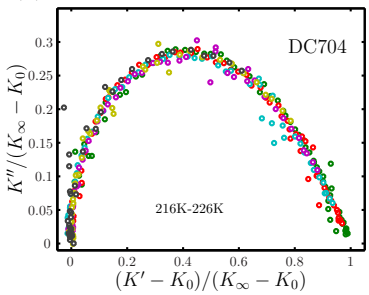

(c) Normalized Cole-Cole plot of DC704 (bulk).

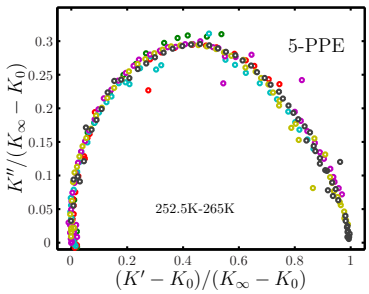

(d) Normalized Cole-Cole plot of PPE (bulk).

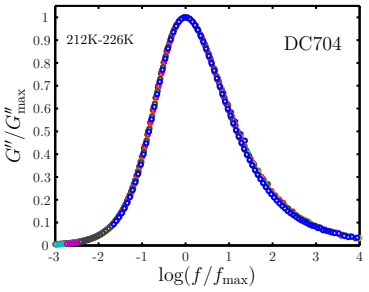

(e) Standard TTS plot for DC704 (shear).

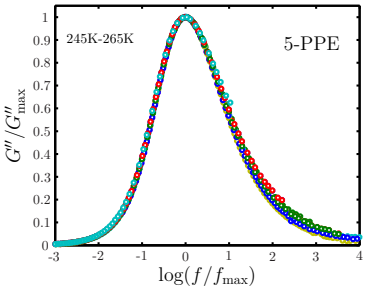

(f) Standard TTS plot for PPE (shear).

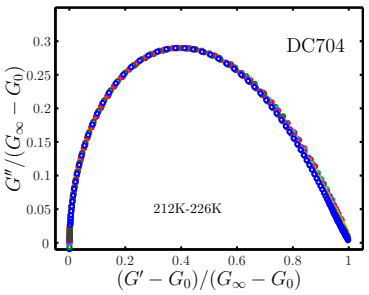

(g) Normalized Cole-Cole plot of DC704 (shear).

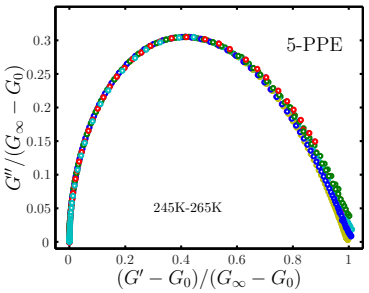

(h) Normalized Cole-Cole plot of PPE (shear).

Figure 7.7 Various TTS plots of the bulk and shear modulus data presented in chapters 4 and 5. Bulk modulus data are quite noisy, but within the noise TTS is obeyed in both DC704 and PPE. With less noise in the shear data, we can see that TTS is perfectly obeyed in DC704, while there is a wing in the PPE (shear) data, but the data seem to converge to a master curve when T is lowered.

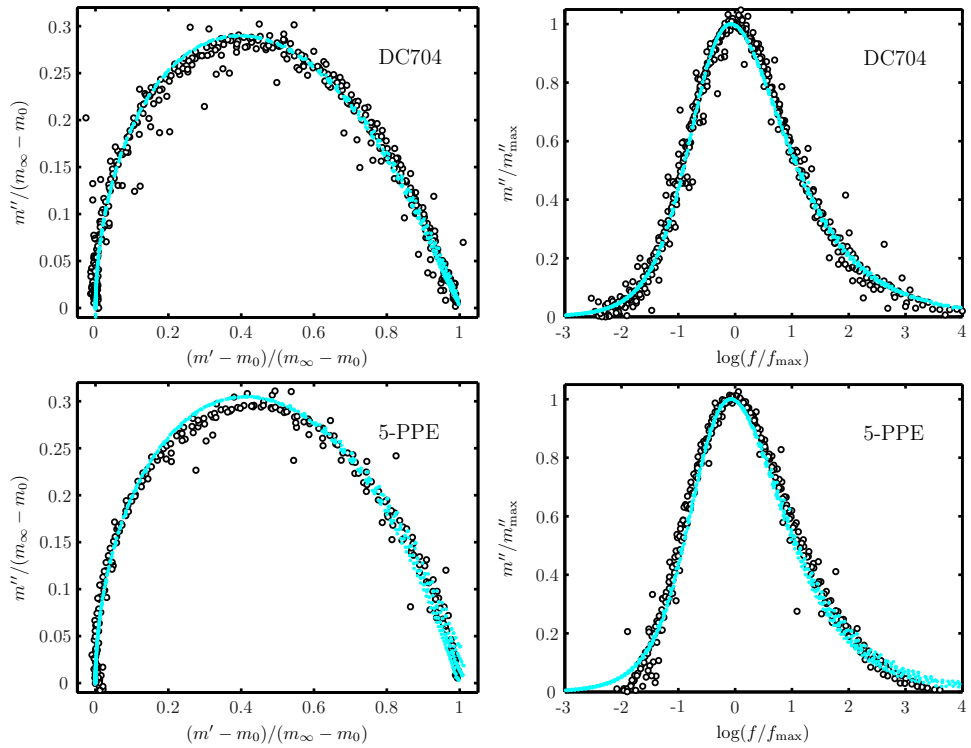

Figure 7.8 Same plots as in Fig. 7.7, but now with bulk and shear data plotted together, bulk data in black symbols and shear data in blue symbols. It seems like the shape of the bulk and shear relaxation is the same, most convincingly in DC704. This could be due to some connection between the shear and bulk moduli, but it could also be because all relaxation are similar for a given substance.

modulus relaxation was already noted by Morita *et al* [14] (in a polymer) and later by Christensen & Olsen [24] (for the alcohol 1,2,6-hexanetriol).

Normally when we present and analyze bulk modulus data we make a low frequency cut off of the data to get rid of the signal due to liquid flowing out of the PZ shell at low frequencies (the "breathing mode", since this feature is unrelated to the bulk modulus relaxation. But as we already explored in the previous section the position of this "breathing" mode is determined by the shear viscosity and a geometric factor. Including this feature in the TTS plot could reveal something about the coupling between shear and bulk viscosities. We scaled the bulk modulus curves to the peak position of the "breathing" mode. In order to do so, the peak must of course be in the frequency window of the measurement. This limits the range of temperatures that can be included in the analysis to the higher temperatures.

In Fig. 7.9 we show the imaginary part of the bulk modulus as a function of frequency, including also the "breathing" mode of the liquid flowing in and out of the hole drilled in the ceramics, as well as all of these curves scaled with the peak position of the "breathing" mode. Being Debye like in nature the "breathing" mode obviously scales,

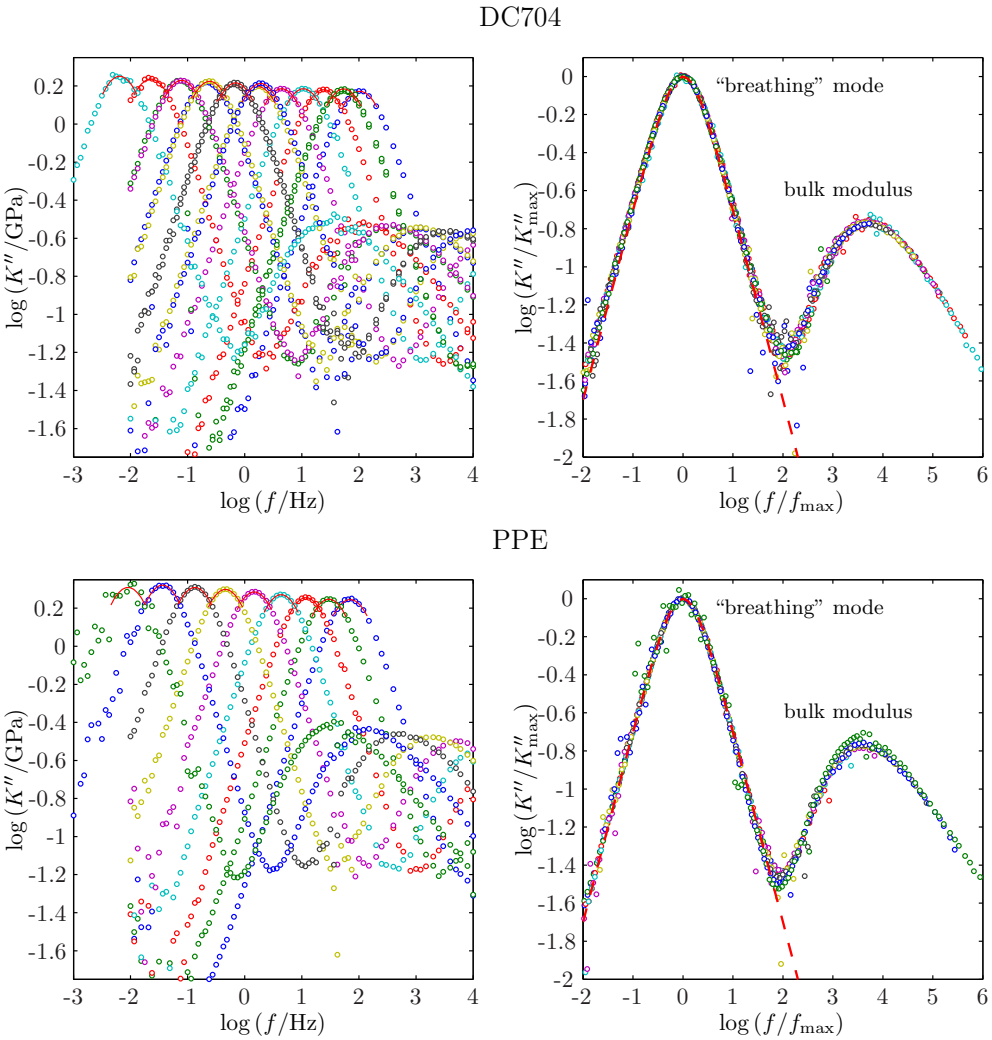

Figure 7.9 Left side shows the imaginary part of the bulk modulus as a function of frequency at different temperatures, including also the "breathing" mode of the liquid flowing in and out of the hole drilled in the ceramics. Right side shows the same spectra scaled to the position of the "breathing" mode. For DC704 there is clearly TTS over the entire region, while PPE shows small deviations from this picture for the lowest temperatures. The red dashed line is a pure Debye curve.

but perhaps more surprising is the fact that this scaling at the same time seem to scale the bulk modulus relaxation. The entire signal collapses to one curve. For DC704 the collapse is close to perfect, both the minimum between the two peaks and the height and position of the bulk modulus relaxation collapse within the noise. For PPE the minimum decreases slightly and the maximum of the bulk modulus relaxation increases with decreasing temperature thus destroying the data collapse. The peak position of the bulk relaxation however seem to be unchanged.

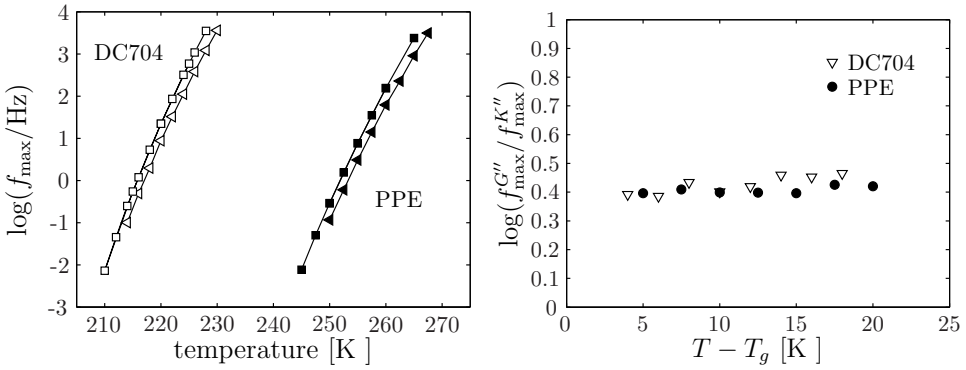

Figure 7.10 Bulk modulus (circles) and shear modulus (squares) loss peak frequencies of DC704 (open symbols) and PPE (full symbols). The shear modulus relaxes 2.5 times (0.4 decades) faster than the bulk modulus.

Time-temperature-superposition for the entire curve suggests that the bulk and shear viscosities follow each other, i.e. their decoupling index in constant over the temperature range included here. Below we will look more into the question of decoupling of time scales.

7.3 Relaxation times and shape parameters

For all measurements it is possible to determine the time scale of the relaxation from the loss peak frequency, $f_{\max}$. If TTS is obeyed this quantity should be proportional to the inverse of the relaxation time. The peak position is determined by fitting a second order polynomial to a some points around maximum data point of the loss. Exactly how many data point are included in the fit depend on the noise. For the shear modulus relaxation a total of five points were sufficient. For the lowest temperature of the bulk modulus data, we included as many as 15. The result is shown in Fig. 7.10, where the full symbols are PPE data and the open symbols are the DC704 data. In both cases the shear modulus relaxes roughly 2.5 times (0.4 decades) faster than the bulk modulus. This agrees well with the conclusion of Christensen & Olsen [24] and Morita *et al.* [14], but not with the relation $\eta^K/\eta^G = 2/3$ derived by Alig and coworkers [65, 67]. Despite the difference in relaxation times, the temperature dependence of bulk and shear relaxation times seems to the same for these two liquids.

In our group it is customary to characterize the shape of the relaxation function in terms of the minimum slope (suggested by Olsen *et al* [68]) and the normalized half width the relaxation (suggested by Dixon *et al* [70]). The minimum slope is defined as the minimum of the logarithmic derivative of the high frequency part of spectrum

$$\alpha_{\min} = \min_{f>f_{\max}} \left(\frac{d \log \chi''}{d \log f} \right) \tag{7.9}$$

which is a negative number giving the high frequency power law behavior of the liquid (see Fig. 13.3 in chapter 13 for an illustration of the procedure). $\alpha_{\min}$ expresses

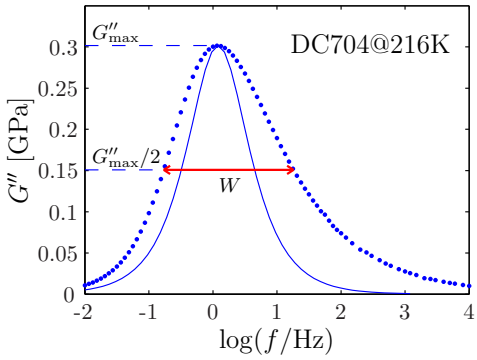

Figure 7.11 Example of the determination of the full width at half maximum. Dots are data points, full curve shows a Debye relaxation (rescaled to make the peak positions collapse), and the red arrow marks the full width at half maximum, W. Usually we normalize this number to the width of a Debye process, w_D.

the "stretching" of the relaxation as does the model parameters β_{SE} and β_{CD} of the stretched exponential function and the Cole-Davidson fitting functions (Eqs. (2.7) and (2.8)), but without assuming any model or functional form of the relaxation.

Determining the minimum slope thus involves taking the numerical derivative of the data, and this only works really well for relatively noise-free measurements. For most dielectric data this is an excellent method to characterize the spectral shapes of relaxation as documented Nielsen *et al* [69]. For shear modulus relaxation data it works relatively well, while the bulk modulus data are simply too noisy for this procedure.

The full width at half maximum W is the width of the relaxation spectrum at half maximum (illustrated in Fig. 7.11). It is more straight forward to determine W and we should be able get obtain value even for the bulk modulus relaxation spectra.

We show the minimum slopes of DC704 and PPE shear relaxation as a function of loss peak frequencies in Fig. 7.12(a) compared to the values obtained in 2005 by Jakobsen *et al* [27] for the same substances (in smaller open symbols). There is excellent agreement between the two sets of data.

In Fig. 7.12(b) we report the widths (normalized to the width of Debye W/W_D), obtained for both bulk and shear modulus measurements. The scatter is quite large for the bulk relaxation values which reflects the relatively large noise in the measurement itself. Within the scatter the bulk and shear measurements agree, which is also what we expect based on the TTS analysis in the previous section. The width of DC704 shear relaxation is more or less constant while the PPE values decrease slightly with decreasing temperature. This again confirms that TTS is well obeyed in DC704 and not in PPE (but the changes are not dramatic).

Both width and minimum slope for DC704 agree very well with previous results, while we observe a discrepancy between widths of the shear relaxation in the present measurements and the values reported in [27] for PPE. The latter are shifted towards lower values (narrower spectral shape), but the temperature dependence (or loss peaks fre-

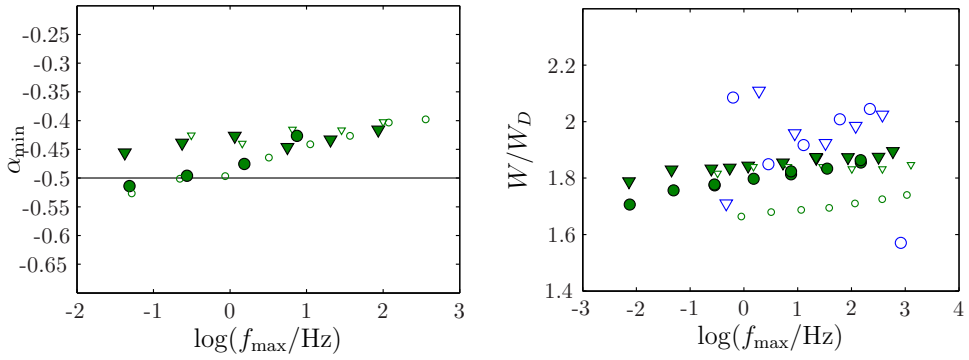

(a) Minimum slopes of the shear modulus relaxation plotted versus the corresponding loss peak frequencies.

(b) Normalized full width at half maximum W/W_D versus the corresponding loss peak frequencies.

Figure 7.12 Spectral shape parameters for DC704 and PPE. Triangles are DC704 data, circles are PPE data, shear modulus data in green and bulk modulus data in blue. Large symbols are from present measurements, small symbols are parameters reported by Jakobsen *et al* [27]. Bulk modulus relaxation data were too noisy to extract any meaningful minimum slope value. There is excellent agreement between present results and previously reported values of the minimum slope and, in the case of DC704, with W. For PPE there is a small discrepancy in the width parameter in absolute numbers, but not in temperature dependence.

quency dependence) is similar. Jakobsen and Niss [25] showed that an imperfect filling of the shear transducer can lead to a spurious broadening of the spectral shape, what could explain this observed discrepancy.

7.4 Time scales of the alpha relaxation in different responses

We have observed that the time scales of the bulk and shear modulus relaxation, although not identical, have a constant decoupling index. Is this surprising? Maybe not, since both responses probe the structural relaxation processes of the liquid.

On the other hand the dynamics of viscous liquids are often stated to be characterized by a break-down of the Stokes-Einstein relation at around $T/T_g \sim 1.2$ [33, 35], and as mentioned in the introduction several experimental studies [33–37, 39–42, 48, 49, 71] find that the decoupling index is temperature dependent.

Others again report no or only weak decoupling of time scales in measurements [7, 44–46]. Jakobsen *et al* [27] report a constant decoupling index of dielectric and shear mechanical relaxation times for some liquids and not for others.

Common for many of these publications is that data from own measurements are compared to literature values. This should always be done with caution. Since the relaxation times and viscosities are extremely temperature dependent even a very small difference in calibration of temperature can lead to a spurious temperature dependence of the decoupling index when T_g is approached.

We illustrate this point in Fig. 7.13 by a simulated relaxation map. The left figure

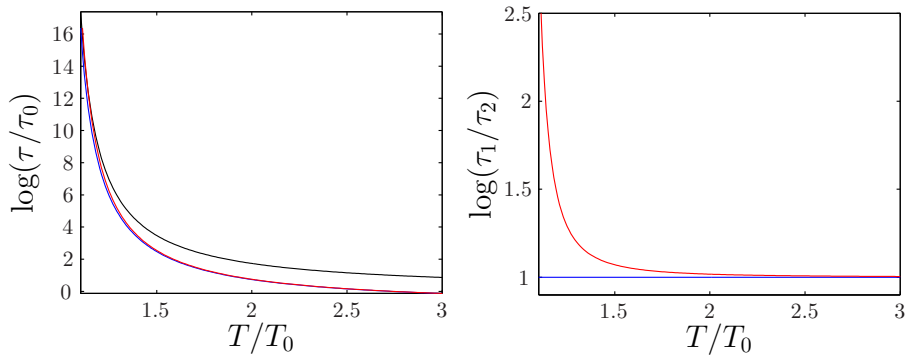

Figure 7.13 Illustration of a spurious temperature dependent decoupling of relaxation times. In the left figure the blue and red curves are both shifted one decade in relaxation time with respect to the black curve. In addition the red curve is shifted 1% on the temperature axes. This shift is barely visible in the ordinary relaxation map. The right figure shows the decoupling index as a function of temperature of the red and blue curves with respect to the black curve. For the blue curve the decoupling index is (of course) constant while the red curve has a dramatic temperature dependence due to the small shift on the temperature axes.

shows a relaxation time curve in black and the identical curve shifted one decade in blue. The red curve is identical to the blue curve except it has been shifted 1% up in temperature. There is hardly any visible difference between the blue and red curve in this plot. But when we look at the decoupling index (defining the black curve as the reference) there is a dramatic difference in the behavior; the decoupling index of the blue curve of course being constant, while red curve increase quite substantially with decreasing temperature.

In our group several different techniques for measuring response functions of viscous liquids have been developed to be measured *in the same set ups*. In addition to the already mentioned methods (mechanical and dielectric spectroscopy techniques) we can measure the longitudinal heat capacity, c_l, and the longitudinal expansion coefficient, α_l. The longitudinal heat capacity, c_l, was measured by Jakobsen *et al* [72] using the 3ω-method. The longitudinal expansion coefficient, α_l, was measured in the time-domain by Kristine Niss [73] using a micro-regulator to make fast ("instantaneous") temperature jumps (the micro regulator is described in [21]). All data were acquired in the same cryostat and experimental set up, except the α_l measurement, which was carried out in a very similar set up. The temperatures of the two cryostats were calibrated by the procedure described in Appendix B and the temperature has been adjusted accordingly.

Thus we are able to compare the time scale of the alpha relaxation for five different responses, all measured under (almost) identical condition. Loss peak frequencies for all the response functions are shown in Fig. 7.14. In the comparison we included also the loss peaks of the compressibility, although the compressibility is simply the inverse of the bulk modulus $\tilde{\kappa}_S = 1/\tilde{K}_S$, and thus not a "new" or independent response function, as well as the (inverse) shear viscosities determined in section 7.1 above. The dashed line is a fit of the dielectric loss peaks to the Avramov equation (chosen due to

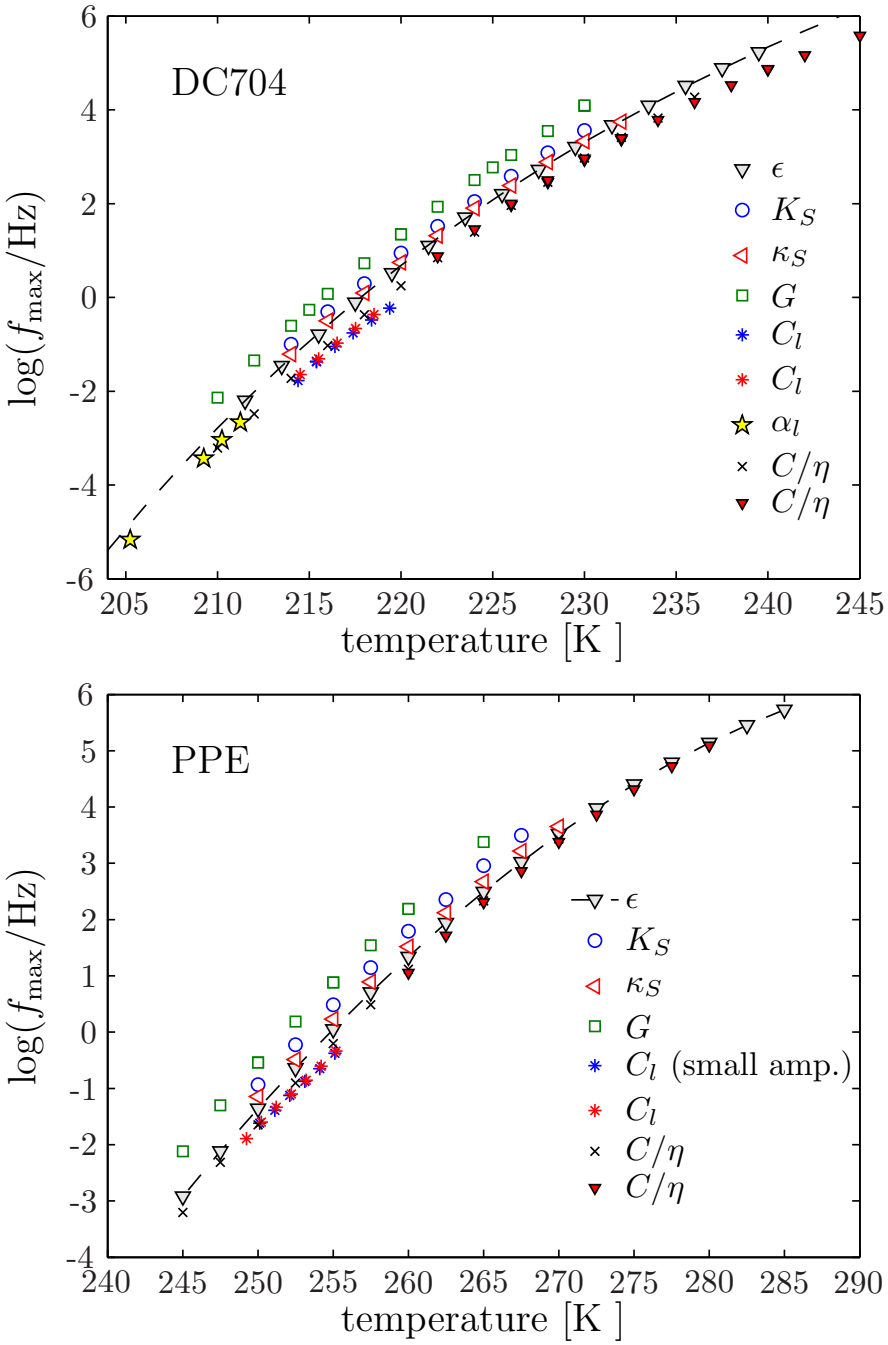

Figure 7.14 Loss peak frequencies for a number of different thermo-visco-elastic response functions all (except for α_l) measured in the same set-up. c_l data is measured using the 3ω-method by Bo Jakobsen [72]. α_l is measured in the time-domain by Kristine Niss [73]. Dashed lines are fits of the dielectric loss peaks to the Avramov equation (see chapter 10).

its superiority over the VFT equation for DC704, see also chapter 10)

$$\tau = \tau_0 \exp\left\{\left(\frac{B}{T}\right)^n\right\} \tag{7.10}$$

with τ_0, B, and n as free fitting parameters.

It is evident that for both DC704 and PPE the different response functions relax on slightly different time scales, though not dramatically different. All relaxation times at a given temperature fall within roughly one decade. It also appears from the figure they have a similar temperature dependence. Because this is difficult to judge from such a relaxation map, we quantify differences in temperature dependence by the decoupling index defined as the logarithm of the ratio of loss peak frequencies, $\log\left(f_{\max}/f^{\epsilon''}_{\max}\right)$, using the dielectric values as a reference because it covers a very wide span of relaxation times.

Unfortunately, not all measurements are taken at the same temperatures, so instead of the actual dielectric loss peaks we used the fit as a reference. A good fit is important in the case of DC704 because we need to extrapolate to be able to estimate the decoupling index of the α_l loss peaks. In the case of PPE all measurements except the heat capacity was measured at the same temperatures. The plotted decoupling indices are thus the ratio of the actual measured peak frequencies. Since the temperature region of the heat capacity measurement was covered by the dielectric measurement, a simple linear interpolation between dielectric loss peaks were used to estimate the decoupling of heat capacity relaxation time.

Fig. 7.15 shows the decoupling indices of all measurements. As already indicated by Fig. 7.14, these are very close to constant. We observe little or no decoupling of time scales in DC704 and PPE for most of the measurements. This is really quite remarkable when the sensitivity of the decoupling index is taken into consideration.

Based Fig. 7.15 we can establish a hierarchy of relaxation times, shear relaxation being the fastest and heat capacity relaxation the slowest

$$\tau_{c_l} > \tau_{\alpha_l} > \tau_\epsilon > \tau_{\kappa_s} > \tau_{K_S} > \tau_G\,. \tag{7.11}$$

This may not necessarily be valid in general. In the literature it seem well established, though, that the dielectric relaxation is slower than the shear modulus relaxation [7, 26, 27, 44, 50, 61] and there also indications of the bulk modulus relaxation in general is slower than the shear relaxation [14, 24, 64].

The inverse viscosities have been scaled by an arbitrary factor C to place the data in the window of the loss peak frequencies and thus the position of these data points is not relevant for this comparison. The viscosities in the decoupling plot seem less constant (especially for PPE) which may be explained by the fact that the proportionality of relaxation time and viscosity is only approximate. The Maxwell model predicts that $\tau = \eta/G_\infty$ and over the temperature interval shown here G_∞ decreases roughly 30% with increasing temperature (see Fig. 9.1). A change of 30% in G_∞ will shift the point of the highest temperature 0.15 decades down with repect to the point at the lowest temperature, which – at least in the case of PPE – is roughly what would bring the viscosities to fall on a horizontal line.

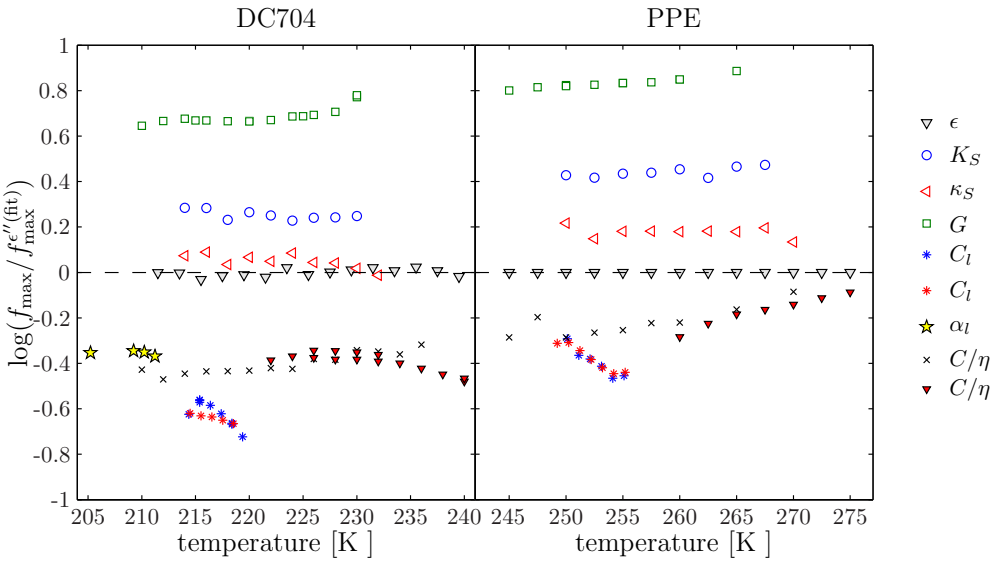

Figure 7.15 Decoupling index for DC704 and PPE of all measured response functions. For DC704 a fit (Eq. (7.10)) of the dielectric relaxation times was used because the dielectric measurement was taken at slightly different temperatures. These plots clearly show that there little or no decoupling of the time scales. The Avramov fit is near perfect for DC704, which is also required if the extrapolation down to the temperatures of the α_l measurement should be trusted.

7.5 Discussion and concluding remarks

Based on the findings in this chapter we can conclude the following:

- The bulk and shear modulus relaxation shapes are almost identical in shape for DC704 and PPE respectively
- TTS is obeyed in DC704 and only small deviations from TTS is seen in PPE
- There is no sign of a β relaxation in either DC704 or PPE (unless the small deviations from TTS is a signature of underlying small amplitude beta process)
- Time scales of of the five different probes presented here decouple, but the decoupling index is constant for time scales at temperatures down to (and actually, in the case of DC704, also somewhat below) the glass transition temperature

DC704 and PPE thus show particularly simple patterns of relaxation. This immediately poses two questions: Why is this? And is it unique?

Probably the coupling of time scales in viscous liquids is not universal. There are strong indications from experiment of a break-down of the Stokes-Einstein relation [33–37, 39–42] and – perhaps more convincing – from simulations [74–82] as T_g is approached. Even though some of reported temperature dependent decoupling index may be explained by experimental uncertainties of the temperature, there are other examples where this is not the case; Jakobsen *et al* [27] for instance report decoupling index for shear and dielectric relaxation in seven different liquids measured in the same

experimental setup, where some liquids display a constant decoupling index and others not. And simulations certainly do not suffer from these problems.

Then we may speculate why it seems to be the case for DC704 and PPE.

A class of viscous liquids with simple dynamics have been identified in computer simulations. They have been termed "strongly correlating liquids" [83] due to their strong correlations between fluctuations of the configurational part of pressure and potential energy at constant volume. The dynamics of these liquids can described in terms of one 'order' parameter. Viscous liquids with one order parameter have been shown to have a "dynamical Prigogine-Defay ratio" equal to unity [84]. The dynamical Prigogine-Defay ratio is defined as a ratio of a combination of (the imaginary part of) three independent thermo-visco-elastic response functions

$$\Lambda \equiv \frac{\kappa_T''(\omega) c_P''(\omega)}{T \left[\alpha_P''(\omega)\right]^2}\,, \tag{7.12}$$

where κ_T'' is the imaginary part of the isothermal compressibility, $c_P''(\omega)$ is the imaginary part of the isobaric specific heat and $\alpha_P''(\omega)$ is the imaginary part of the isobaric expansion coefficient. $\Lambda = 1$ was shown to hold approximately for two computer liquids [85].

If DC704 and PPE belong to this class of liquids, then certain combinations of linear response functions will be proportional and thus have identical relaxation times. Since there are only three independent thermo-visco-elastic response function, the remaining may be calculated from a combination of these three. It seems plausible that the relaxation times from combinations of these three linear response functions may be proportional if they themselves are proportional in frequency. So far, this is just a pure speculation and it remains to be confirmed.

There is however a clear indication that DC704 is a "strongly correlating liquid". In Paper V (p. 289) the density scaling exponent for DC704 is predicted using the same shear modulus, bulk modulus, heat capacity, and expansion coefficient data as in section 7.4 and found to be in agreement with the exponent determined by dielectric measurements under different pressures.

8 Broadband mechanical spectrum of DC704

In this chapter we return to the original idea of measuring the mechanical properties of viscous liquids: combining the low frequency measurements with result from the high frequency techniques developed in the Nelson group at the Department of Chemistry at MIT.

This collaborative work has been underway for several years now and there are still some loose ends, but it is now close to an end.

8.1 Introduction and motivation

The dramatic slowing down with temperature of the structural relaxation in supercooled liquids represents a serious challenge for any theory of supercooling liquids. It is equally challenging experimentally to span that many orders of magnitude in time or frequency. No single technique can cover the entire range of relaxation times and as a result any such attempt must be pieced together by several different techniques.

Dielectric spectroscopy has long been able to cover an impressive 18 orders of magnitude in frequency [86] and routinely cover 9 decades from mHz to MHz. In Fig. 8.1 such a broadband measurement of glycerol by Lunkenheimer and co-workers is shown. Recently, a similarly impressive light scattering study of OTP by Petzold & Rössler [87] follows the alpha relaxation over 16 decades in time over 200K, from just above T_g (245K) to well above the melting temperature (440K), shown in Fig. 8.2.

These extremely broad spectra provide valuable insight into the rich dynamics of viscous liquids: the temperature dependence of the alpha-relaxation time, the evolution of the alpha relaxation shape with temperature, and the emergence of less intense and less temperature dependent relaxation processes once the alpha-relaxation has moved to lower frequencies. A schematic representation of a low-temperature dielectric loss spectrum due to Lunkenheimer *et al* [88] is shown in Fig. 8.3.

Dielectric spectroscopy is a very precise method and results are straight-forward to interpret compared to other types of spectroscopy where the extraction of the desired properties is usually more involved. The abundance of dielectric data in the literature is a proof of the popularity of the technique. But in reality dielectric spectroscopy is a substitute (but a good, reliable, and very precise one) for what we are really interested in, namely the thermodynamic and mechanical response functions, the "true" measures of viscosity.

As a result there has been numerous attempts to connect the dielectric response to the

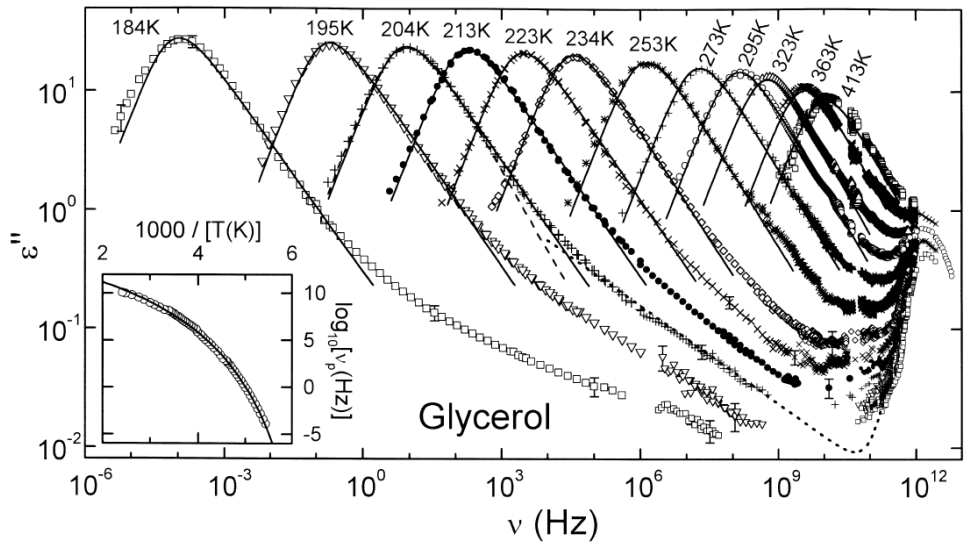

Figure 8.1 Broadband dielectric spectroscopy of glycerol covering 18 decades in frequency. As the temperature is lowered the alpha relaxation process moves down in frequency and broadens. At low temperatures (close to T_g) a wing develops on the high frequency side of the alpha peak. Already at quite high temperatures a fast process (peak around 1THz) separates from the alpha relaxation. This processes is completely temperature independent and get more and more distinct as the temperature is lowered. From [86].

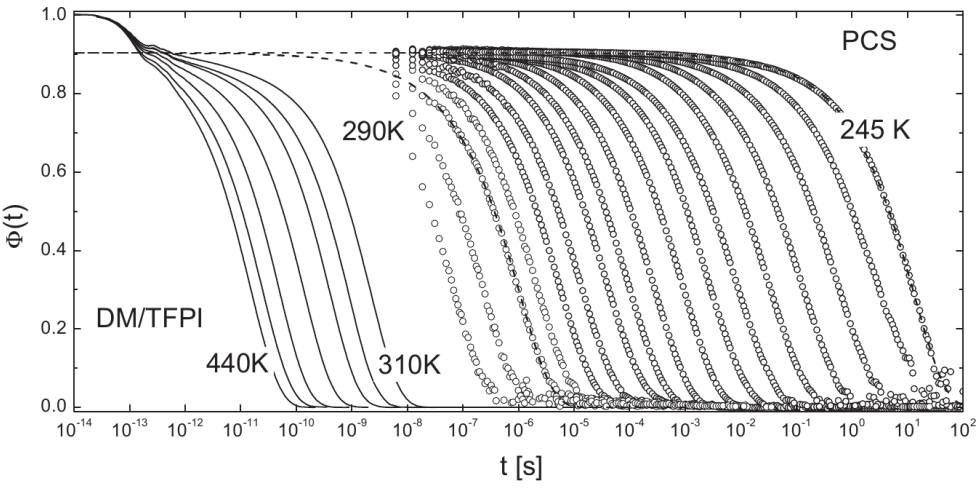

Figure 8.2 Light scattering study of OTP covering 16 decades in time using different light scattering techniques. From [87].

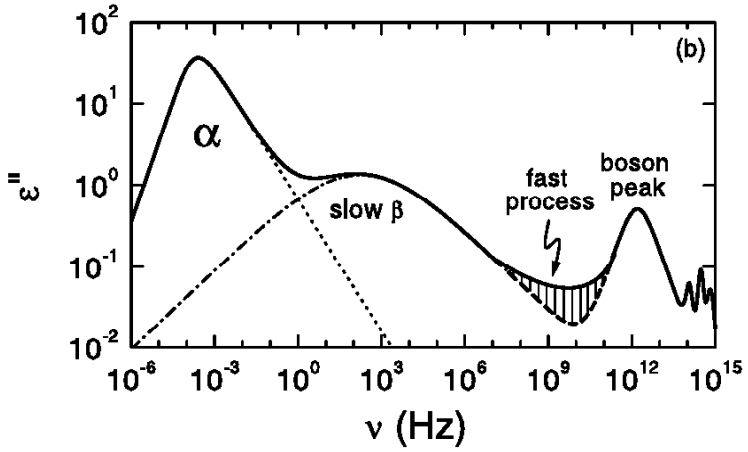

Figure 8.3 A schematic representation of a typical dielectric loss spectrum of a viscous liquid at a temperature just above T_g. At the lowest frequencies we see the alpha relaxation which has a characteristic asymmetric shape with $\omega \propto 1$ on the low frequency side of the peak and $\omega \propto \beta$ where $-1 < \beta < 0$ on the high frequency side of the peak. At slightly higher frequencies a secondary relaxation may appear, which is sometimes called a slow beta or a Johari-Goldstein beta process. This process is less temperature dependent than the alpha relaxation. Around 1 THz a temperature independent peak appears which is referred to as the "microscopic peak" or the Boson peak. In the region just below the Boson peak it is sometimes suggested that additional "fast processes" exist because the loss is higher than what a simple superposition of the present processes would suggest. From [89].

mechanical properties and reveal exactly how they may be related, e.g. [60, 63]. It is demonstrated in chapter 7 that in some liquids the dielectric relaxation time is nearly proportional to the viscosity. For other liquid this may not be the case.

In dielectric measurements spectral shapes can get distorted due to DC conduction thus making it difficult to determine shape parameters and relaxation times. In mono-alcohols the dominant signal is due to an extremely slow Debye process, which is not related to the structural relaxation [28, 90, 91]. In those cases mechanical spectroscopy offers some advantages over dielectric spectroscopy. Mechanical spectroscopy can be applied to any liquid – also the ones with small (or no) dipole moments.

8.1.1 Broadband mechanical spectra in the literature

Mechanical relaxation data spanning many decades have often been constructed by invoking the time-temperature-superposition principle. The frequency (or time) window of a certain technique may be relatively small, but by measuring at different temperatures different parts of the relaxation spectrum is uncovered and then shifting the data to make them collapse onto one master curve, it is possible to "extend" the frequency window (see for instance [92] who claim to cover more than 30 decades). This procedure however only produces one master curve and usually only of the alpha relaxation, and thus does not reveal any information on the temperature evolution of the alpha process or on additional processes. It is questionable if this procedure is valid over

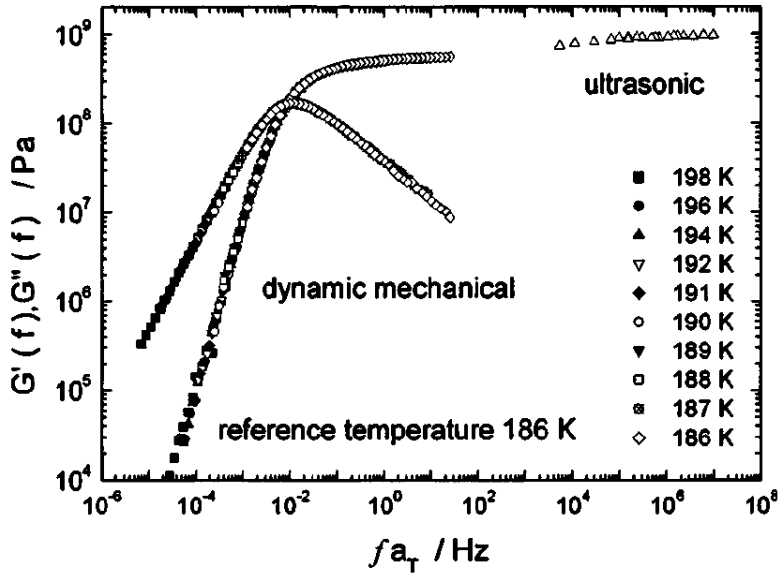

Figure 8.4 A master curve of shear mechanical relaxation in *m*-toluidine using time-temperature superposition of two different measurements, a dynamical shear measurement and an ultrasonic shear measurement giving a total dynamical range of ∼13 decades. From [8].

more than a limited range of temperatures.

Mandanici et al [8] combined two techniques in different dynamical regions with TTS thus avoiding absurd extrapolations. This way almost 13 decades in frequency is reliably covered. But still only as a master curve and not covering a broad range of temperatures.

Read and coworkers have measured tensile creep compliance of aging polymers covering a time span from 10^{-8}s - 10^{5}s corresponding to a frequency window 1.6μHz to 16MHz with a total of four different techniques that together covered most of the region [93, 94]. The polymers were quenched from a temperature above T_g to room temperature ($< T_g$) and the evolution of the beta process some of the alpha process was followed as the sample was aging. The creep compliance of polypropylene measured over 13 decades in time is shown in Fig. 8.5. While the mechanical methods applied in this study were indeed linear response measurements, the sample properties was not studied in equilibrium as a function of temperature, but out of equilibrium as a function of (waiting) time at a fixed temperature.

We thus believe that we are the first to present an attempt at compiling the mechanical counterpart of Fig. 8.1, combining 6 different mechanical spectroscopy techniques spanning 14 decades in frequencies from 1mHz to (almost) 1 THz for an equilibrium liquid. The total temperature range covered is 150-400K.

If matched correctly we will at the same temperatures have access to the short time properties, the high ("infinite") frequency moduli, and the long time properties, i.e.

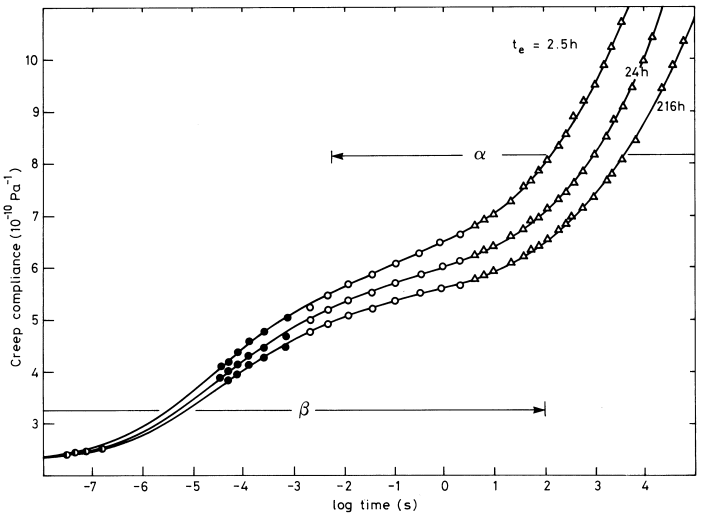

Figure 8.5 Tensile creep compliance measurements on poly(propylene) covering 13 decades in time. The polymer was quenched from 353K to 295K and measured at different aging times. The figure is from [5], the data were also published in [94].

relaxation time and fragility index. This could prove extremely valuable for testing the proposed correlations between high frequency elastic moduli and fragility [95] as well as models suggesting that the alpha relaxation time is controlled by the short time elastic properties, e.g. shoving model [96]. Experimentally one usually only has access to one of the limits and thus a test of such relations rely on assumptions regarding the continuation of the curve (for instance $G''_{max} \propto G_\infty$ in [96]) or on literature values of relaxation times or fragility (e.g. in [97]). Given that these may vary considerably with measured property and preferred definition of T_g, it is advantageous with complete mechanical spectra, where we are sure to link the high frequency moduli to the "correct" values of for instance relaxation times.

8.2 Mechanical spectroscopy techniques used here

In Figure 8.6 we give an overview of various techniques available to us for probing the mechanical properties of a liquid and the frequency range each of them covers.

For some of these methods, certain geometries are natural to work with and certain properties are measured, for other methods other geometries and quantities are convenient. Thus, to match measurements and compile a spectrum, it will be necessary to convertsound velocities into moduli (or vice versa) and measured moduli into other moduli.

In the following subsections we briefly sketch the principles of the techniques used to compile the broadband spectrum of DC704 and specify how to convert between the measured properties.

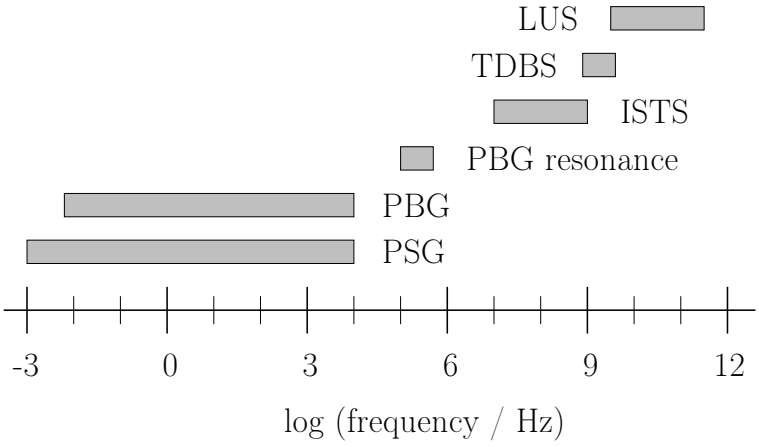

Figure 8.6 Overview a the mechanical spectroscopy techniques used here and their frequency windows. PBG/PSG techniques (presented in chapters 4 and 5) cover roughly seven decades from 1 mHz to 10kHz (the PBG measurements are however quite noisy at the lowest frequencies and the lower limit of this measurements 10mHz rather than 1mHz). Using the resonances in the PBG spectrum we can extend this method into the 100-500kHz region, but only at moderately high temperatures. Impulsive Stimulated Scattering (ISS) techniques can measure both longitudinal and transverse sound velocities and damping in the MHz-GHz region [98, 99]. Laser Ultrasonics (LUS) combined with Time Domain Brillouin Scattering (TDBS) covers from 1Ghz to almost 1THz [100]. This technique measures mainly longitudinal acoustics, but can also measure shear waves [101].

8.2.1 Connection between the complex moduli, sound velocity and sound attenuation

The general equation of motion for an isotropic medium is given by Landau & Lifshitz [6, p. 87]

$$(K + 4/3G)\nabla(\nabla \cdot \mathbf{u}) - G\nabla \times \nabla \times \mathbf{u} = \rho\ddot{\mathbf{u}} \tag{8.1}$$

where $\mathbf{u}$ is the displacement field, ρ is the density, and K and G are the bulk and shear moduli. Assuming a one dimensional geometry we have $\mathbf{u} = (u_x, 0, 0)$, and then Eq. (8.1) reduces to

$$Mu_x'' = \rho\ddot{u}_x \tag{8.2}$$

where the dot means differentiation with respect to time and the apostrophe here means differentiation with respect to x, and $M = K + 4/3G$.

Assuming a harmonic input the displacement field can be written

$$u(x,t) = u_0 e^{i(\omega t + kx)} = u_0 e^{ik((\omega/k)t + x)} \tag{8.3}$$

where the propagation velocity of the wave (the sound velocity) is $c_l = \omega/k$. Inserting this into Eq. (8.2) we obtain

$$Mk^2 = \rho\omega^2 \;\Rightarrow\; c_l = \sqrt{\frac{M}{\rho}}\,. \tag{8.4}$$

But if there is dispersion in the medium M is complex, i.e. the wavevector k (or the frequency) is complex, $k = k' + ik''$

$$e^{i(kx-\omega t)} = e^{i((k'+ik'')x-\omega t)} = e^{-i(\omega t-k'x)}e^{-k''x} \tag{8.5}$$

From this we define the sound velocity velocity as $c_l = \frac{\omega}{k'}$ and the damping coefficient is k''. Using the relation from Eq. (8.4) we get an expression for the sound velocity, c_l, and the acoustic damping α

$$c_l(\omega) = \frac{\omega}{k'(\omega)} = \frac{1}{\mathrm{Re}\left\{\sqrt{\frac{\rho}{M(\omega)}}\right\}}, \quad \alpha(\omega) = k''(\omega) = \omega\,\mathrm{Im}\left\{\sqrt{\frac{\rho}{M(\omega)}}\right\}. \tag{8.6}$$

If we conversely want to calculate the modulus from wave vector k and a measured complex frequency ($\tilde{\omega} = \omega' + i\omega''$), then by Eq. (8.4) we have

$$\tilde{M} = \frac{\rho(\omega'^2 - \omega''^2)}{k^2} + i\frac{2\rho\omega'\omega''}{k^2} \tag{8.7}$$

and conversely if the frequency is fixed and a complex wavevector is measured

$$\tilde{M} = \frac{\rho\omega^2(k' - k'')^2}{|k|^4} + i\frac{2\rho\omega^2 k'k''}{|k|^4}. \tag{8.8}$$

Temperature-dependence of density

Obviously, to calculate back and forth between sound velocities and moduli, we need to know the temperature dependence of the density of the liquid. Since we have not measured this, we will have to use an estimate.

Density is defined as mass divided by volume $\rho = \frac{m}{V}$. If we have a fixed mass and monitor the development with temperature $\rho = \rho(V(T))$. To the first order temperature dependence of the volume can be written

$$\begin{aligned} V(T) &= V_0 + \frac{dV}{dT}(T - T_0) = V_0\left[1 + \frac{1}{V_0}\frac{\partial V}{\partial T}(T - T_0)\right] \\ &= V_0\left[1 + \alpha_p(T - T_0)\right] \end{aligned} \tag{8.9}$$

and we have

$$\rho(T) = \frac{m}{V_0[1 + \alpha_p(T - T_0)]} = \frac{\rho_0}{1 + \alpha_p(T - T_0)}, \tag{8.10}$$

where α_p is the (isobaric) expansion coefficient. The expansion coefficient for liquids is in general somewhere between $5 \cdot 10^{-4}\mathrm{K}^{-1}$ and $10 \cdot 10^{-4}\mathrm{K}^{-1}$. The value for DC704 $\alpha_p = 72 \cdot 10^{-5}\mathrm{K}^{-1}$ is given in [102]. We will assume that the expansion coefficient is temperature independent.

8.2.2 PBG/PSG (mHz-kHz)

These techniques were described in chapters 4 and 5 and they are aimed measuring high moduli (in the MPa-GPa range) and optimized to measure the low frequencies. These

techniques measure the complex bulk and shear modulus, which can be converted into a longitudinal modulus through the relation

$$M = K + 4/3G. \tag{8.11}$$

In these measurements, the frequency is fixed and a complex modulus (complex wavevector) is measured.

8.2.3 Impulsive Stimulated Scattering (MHz-GHz)

In the megahertz frequency range, Impulsive Stimulated Scattering (ISS) techniques can measure both longitudinal and shear sound velocities and damping, depending on the experimental geometry [98]. ISS is a pump-probe experiment where two short laser pulses are overlapped spatially and temporally in the sample to impulsively excite a material response and probe beams then measures the time evolution of the response.

The VVVV geometry refers to the excitation pulses and probe beams all being vertically polarized, VHVH refers to the polarization of the two pump pulses as well as the probe beams being polarized at 90° angles. The technique operated in the VVVV geometry is termed Impulsive Stimulated Thermal Scattering (ISTS). In ISTS, absorption of excitation laser pulses in the liquid results in an impulsive heating and a thermal expansion in the peaks of the generated interference pattern. The expansion launches two counter propagating acoustic waves, whose wavelength matches the excitation interference fringe spacing.

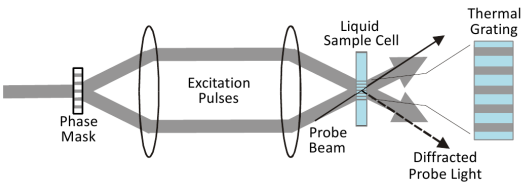

(a) Schematic view of the ISS setup (from [100]). Two light pulses are crossed spatially and temporally in the sample, thus producing an interference pattern. In the VVVV geometry of the experiment (excitation and probe pulses all have the same polarization direction) some heat will be absorbed in the peaks of this interference pattern causing a rapid thermal expansion. This rapid expansion launches two counter propagating acoustic waves which will diffract a probe beam incident on the grating pattern created by the wave.

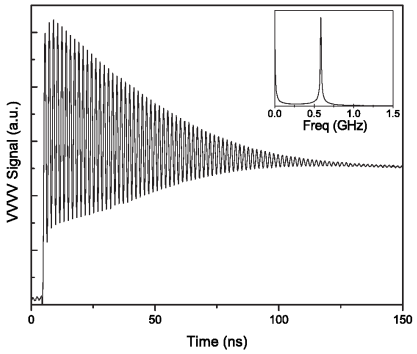

(b) Typical signal of an ISTS measurement. The offset is due to the thermal grating that decays slowly through thermal diffusion, while the oscillations are due to the acoustic waves propagating. The inset shows the Fourier transform of the signal from which the frequency of the oscillations can be determined. From [97].

Figure 8.7 Principle of the Impulsive Stimulated Thermal Scattering (ISTS) technique and an example of the signal output.

Diffraction of a probe laser pulse incident on the grating pattern generated by the acoustic wave arises through the induced changes in the refractive index (which in the

case of ISTS mainly comes from density changes). The signal (an example is shown in Fig. 8.7) shows time-resolved oscillations which eventually decay due to acoustic damping (or if the acoustic wave propagates out of the probing region).

The frequency $\omega(k)$ of the acoustic response at the selected wave-vector k allows for a determination of sound velocity through the dispersion relation $c_l(k) = \omega(k)/k$. The decay of the acoustic oscillation envelope is related to the acoustic attenuation $I(t) \sim \exp(-\gamma t)$. There is also a quasi-steady-state density modulation which decays on a micro second timescale due to diffusion of the heat from the grating peaks to the nulls, which results in an offset of the signal.

In this measurement, the wave vector is fixed and a complex frequency is measured.

8.2.4 Laser Ultrasonics (GHz-THz)

Laser ultrasonics is an analogue to the conventional ultrasonic technique, but it has access to much higher frequencies, typically from a few GHz up to several hundreds of GHz.

In a picosecond laser ultrasonic measurement very short light pulses (typically ∼300fs) irradiates a thin metal film (10-100nm) that acts as a transducer converting the absorbed light to thermal energy. The thermal expansion of the film launches an acoustic wave and the response gets detected through a variably delayed probe pulse. If a material is in contact with the metal film the acoustic pulse will be transmitted into the this material and the mechanical properties of the this material can be studied. Sound velocity of the sample can be determined through a measured round trip time and the damping by comparing the signal intensity of two echoes.

In the set up in the Nelson lab the technique is operated in transmission mode, which means that there is a metal film on both sides of the sample. The pump pulse then generates an acoustic wave on one side of the sample which then propagates through the sample material to the second metal film. The arrival of the strain pulse on the second metal film will cause a small deformation (displacement) of the film which gets detected interferometrically by a variably delayed probe pulse.

When this technique is employed to measure mechanical properties of liquids a multilayer construction is necessary where the liquid is sandwiched between two metal coated substrates. Liquid layer thicknesses varying from a few nanometers to a few microns can be fabricated this way [100].

Narrow band acoustic wave generation

The standard laser ultrasonic technique is a broadband technique, because a short pulse contains many frequencies. In the Nelson group a pulse-shaper was developed to facilitate frequency tuning of the acoustic wave generation. The idea is to split the pulse into a pulse-train of seven pulses with a variable delay between the pulses, where the delay sets the frequency.

The principle of the measurement is sketched in Fig. 8.8, where also a typical signal from such a measurement is shown.

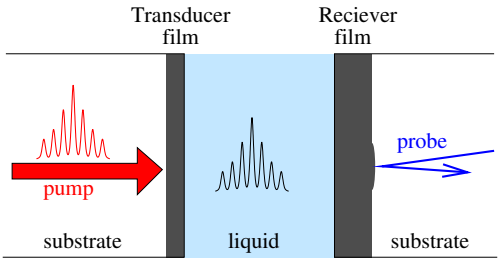

(a) A train of ultra short laser light pulses incident on a thin metal film. The metal film absorbs some of the pump light what causes a sudden heating and thermal expansion of the film. The expansion of the film generates an acoustic wave pattern similar to the shaped light pulse which then propagates across the sample and get detected interferometrically on the receiver film by the probe pulse. The transducer film is usually very thin (10-50nm) to facilitate generation of high frequency acoustic waves, while the receiver film is somewhat thicker ($\sim$ 100nm) to get a high reflection and to hinder probe light penetration into the sample.

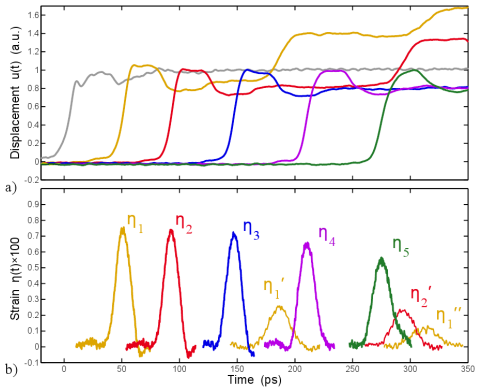

(b) Signal in the LUS measurement. Zero delay time corresponds to the time where the pump pulse hits the transducer film. At a later time the signal arrives at the receiver film which then gets detected interferometrically as a small displacement of the receiver film. Different colors correspond to different liquid layer thicknesses hence the different arrival times. From [100].

Figure 8.8 Principle of the narrow band laser ultrasonic technique and an example of the signal output.

Compared to the broad band approach the narrow band technique enhances the signal at selected frequencies thus improving the signal to noise ratio when a frequency resolved spectrum is sought.

In this measurement the frequency is fixed and a complex wavevector is measured.

Time domain stimulated Brillouin light scattering

It is also possible to monitor the propagation of the strain pulse directly in the liquid, see figure 8.9(a). For this technique the setup is identical to the LUS setup, but the sample sandwich construction is slightly different: in this case there is no receiver metal film and the probe light penetrates into the liquid.

The probe pulse light will be reflected by the transducer film but also by the propagating strain wave. These two parts will interfere constructively or destructively depending on the length of the extra path travelled by light reflected at the film. As the strain pulse propagates through the sample, the two parts of the reflected beam will move in and out of phase, resulting in an oscillatory signal, see figure 8.9(b). As in the ISTS measurement, the frequency of the oscillations ν_B can be related to the sound velocity and the damping of the oscillations to the acoustic damping. The incident angle of the probe beam, θ, the sound velocity of the liquid c_l, and the probe light wave lengths λ, will select out a specific frequency of the oscillations, according to the relation

$$\nu_B = \frac{2nc_l}{\lambda \sin\theta} \tag{8.12}$$

where n is the refractive index of the liquid. Thus there are different possibilities for

tuning the frequency.

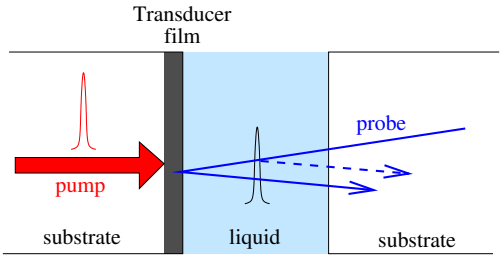

(a) In this configuration the probe light penetrates into the sample and directly probes the acoustic wave as it propagates through the sample. A portion of the light gets reflected by the propagating strain pulse and interferes with the light reflected by the film. As the wavefront propagates, the two reflected beams will alternate between constructive or destructive interference at the detector.

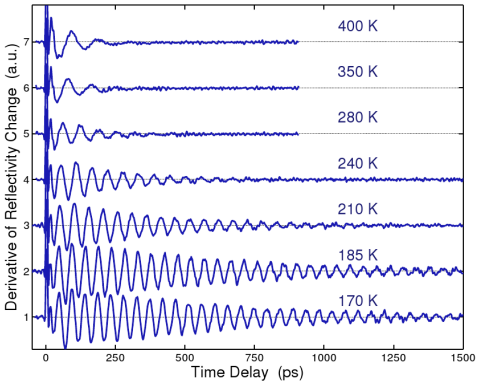

(b) An example of signal from a TDBS measurement. As the temperature decreases the frequency of the oscillations increase and the damping decreases, reflecting an increase in sound velocity and decrease in acoustic damping. From [100]

Figure 8.9 Principle of the Time Domain Brillouin Scattering (TDBS) technique and an example of the signal output. The frequency of the oscillations can be related to the sound velocity of the liquid and the decay to the acoustic damping in the liquid.

This technique is close to standard frequency domain Brillouin scattering; but in the TDBS experiment a stimulated wave is probed instead of thermally induced acoustic waves. And the scattered probe light is not split into frequency components, instead the intensity of the scattered light gets detected, which will average all scattered frequencies.

In this measurement the wave vector is fixed and a complex frequency is measured.

8.3 Matching the measurements

One way to assess how well the data from the different measurements match, is by plotting data as a function of temperature at fixed frequencies or fixed wavelengths. In this representation the measurements are only required to span wide in temperature to get overlap of the different methods, and they do need to overlap in frequency. Plotting the sound velocity or the real part of the modulus as a function of temperature a solid-like level and a liquid-like level should appear and for each selected frequency (or wave vector) there will be a transition from one to the other, happening at a temperature that depends on the frequency: a low frequency/high wave vector the transition happens at low temperatures and vice versa.

In Fig. 8.10 we show the longitudinal sound velocity as measured in the high frequency techniques and calculated using Eq. (8.6) from the measured moduli at low frequencies. The limiting high and low frequency levels of the liquid sound velocity are indicated by dashed lines. Obviously the relaxation strength decreases with increasing temperature

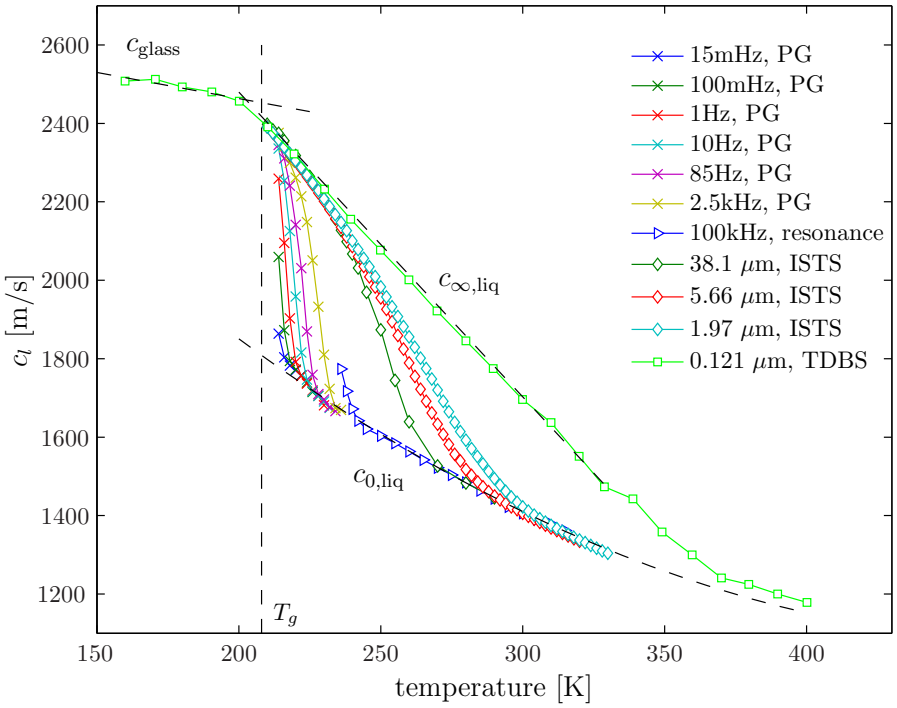

Figure 8.10 The longitudinal sound velocity as a function of temperature at different fixed frequencies or wavelengths. The zero and infinite frequency levels of the liquid sound velocity, $c_{0,\text{liq}}(T)$ and $c_{\infty,\text{liq}}(T)$, are suggested by the dashed lines. The glass transition temperature is marked by a vertical dashed line. In the measurements the glass transition is manifested as a change in slope of the temperature dependence of the "solid-like" sound velocity. The transition from liquid-like to solid-like behavior happens at a lower temperature with lower probe frequency/larger probe wavelength. The agreement between the different methods is excellent.

and the extrapolations of the limiting high and low frequency levels indicate that it vanishes around 400K. We have also indicated a "glass-line" (black dashed line labelled c_{glass} and the glass transition temperature is shown by a vertical dashed line. The glass transition is clearly seen in the measurement as a change in slope from the $c_{\infty,\text{liq}}$-level to the c_{glass} level.

Overall there is good agreement between different methods. The low frequency measurements pointa to a slightly higher and steeper c_∞ level than the high frequency measurements, while the agreement at the c_0 level is remarkable. No corrections of temperature or otherwise were introduced.

We proceed to construct the frequency resolved spectrum, which is shown in Fig. 8.11. Each temperature has been assigned a color ranging from dark blue (lowest temperatures) to dark red (high temperatures). This should make it easier visually to link the high and low frequency regions. In this representation the frequency gap between the high and low frequency methods becomes quite clear. The data points

from the resonance method provide some linking between the two regions, but only in the M_0 level and the beginning of the dispersive region is given by this method. And only the real part as the fitted values of the imaginary parts (the fitted viscosities) are too noisy be meaningful in this context (see section 4.7 (chapter 4) for details on the resonance method).

It is also clear that the different data sets do not fit exactly. As already seen in the (T, c_l)-representation, the low frequency region has a slightly higher K_∞ level than what is measured at the high frequencies, but with the estimated error on the bulk and shear moduli of 4-7% each gives an error of ∼5-10% on the sum, so the deviation is within the error of the of the measurement.

In the MHz region there is a discrepancy between the low temperatures and the higher temperatures, which can probably be explained by the fact that they are from different measurement series. Also the agreement of the ISTS data with the LUS and TDBS data of the GHz region is not perfect; in the real part the ISTS data at intermediate temperatures is lower that what both LUS results and extrapolations from low temperatures suggest. In the imaginary part on the other hand there is apparently no discrepancy between the three high frequency methods.

Also there is some systematic error on the lowest temperatures in the MHz region. These curves should be flat showing the M_∞-level (as the LUS curves at corresponding temperatures do), but instead they bend slightly upwards toward the higher frequencies.

Pink curves are stretched exponential fits that connect the low and high frequency regions for a few selected temperatures. (The curves are fitted "by hand" and are thus not fits in the least squares sense.) The fits give a reasonable interpolation, which shows that there are no additional processes "hiding" in the regions we are currently not covering.

At the lowest temperatures the stretching exponent β was set to 1/2, but with increasing temperature the relaxation narrows. This is really only inferred by the real part of the spectrum where the flatness of the high-frequency end forces the fit to be narrow. In the imaginary part the loss grows with frequency showing the emergence of a spectral feature that is not seen in the real part, and that is independent of temperature. As a consequence the imaginary parts of the stretched exponentials seem quite postulated.

The high frequency spectral feature seen only in the loss is probably the low frequency side of the Boson peak or the "microscopic" peak, which is also found in e.g. dynamic light scattering, dielectric spectroscopy, and neutron scattering around a couple of THz. The amplitude of this peak seems to be higher than the alpha relaxation, which is not the general picture.

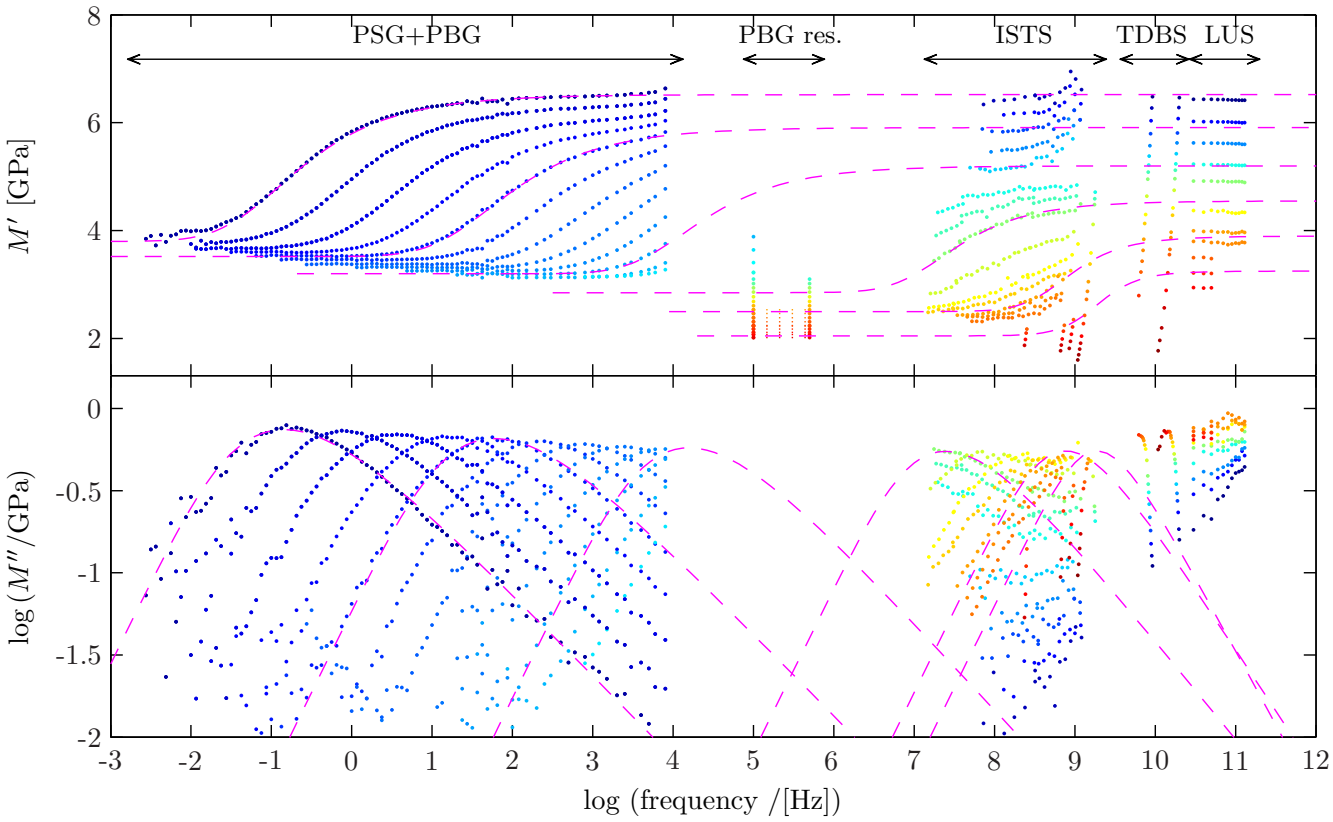

Figure 8.11 Full spectrum showing the frequency dependence of the longitudinal modulus M of DC704 at temperatures from 210K to 400K. Data from 1mHz to 10kHz is found by adding the bulk and shear moduli from the quasi-static method of chapters 4 and 5. Data from 10MHz to 1GHz are taken with Impulsive Stimulated Thermal Scattering (Torchinsky, Johnson), data from 10GHz to 100GHz are time domain Brillouin scattering and laser ultrasonic result, converted to moduli through Eq. (8.7).

8.4 Discussion and outlook

We have presented a broadband mechanical spectrum of DC704 using 6 different experimental techniques covering a total of 14 decades of frequency (although only sparsely from 10kHz to 10MHz) and 200K in temperature. To the best of our knowledge this has never been attempted before using true linear response mechanical measurements on equilibrium liquids. This offers a unique possibility to study that entire relaxational range from the very fluent to the ultra-viscous liquid just above the glass transition.

There are many uncertainties and possible sources of error that could have potentially destroyed a meaningful outcome of the attempt to match that many measurements.

In the low frequency region we need to calculate the longitudinal modulus from the bulk and shear moduli, each of which have uncertainties on the absolute numbers. Tschoegl and Knauss [103] discusses the necessary conditions for determination of any mechanical modulus by calculation from two other. Their strict the experimental protocol demands that the source functions are determined "*simultaneously on the same specimen, under the same conditions of the experimental environment*", furthermore they go on to "add the requirement of *high accuracy and precision.*" We can not claim that we live up to all of these demands, but we are close:

- the low frequency bulk and shear moduli are measured under the same conditions of experimental environment (same lab, same cryostat) though not simultaneously
- the measurements are not carried out on exactly the same specimen, but different specimens from the same bottle. The closest we can come to measuring on the same specimen is filling the two measuring cells at the same time (which was actually sometimes also done)
- we do have a quite high precision in the shear measurement and fairly high in the bulk measurement and the reproducibility of the measurements is fair

We thus argue that in our case such an addition is safe.

When we compile the broadband mechanical spectrum none of these demands are met: the measurement are performed in different labs with different bottles of chemicals, different handling of the liquids, and in different cryostats. In addition to that, the different techniques measure slightly different quantities, thus necessitating a conversion of (some of) the data, and further assumptions in order to make these conversions, e.g. assumptions regarding the temperature dependence of density.

With all of these reservations and uncertainties, it can seem quite miraculous that we can successfully match the measurements. Since we are not in the religious business, we will instead view this as a confirmation of both ends of the spectrum being determined correctly.

To make a convincing statement about the evolution of the dynamical mechanical spectrum of DC704, however, we would like to fill the gap in measurements at frequencies in the kHz to MHz range to connect the high and low frequency measurements.

9 Cauchy (and Cauchy-like) relations

The relation between the stress σ and the strain ϵ tensor for small deformations is linear (Hooke's law)

$$\sigma_{ij} = c_{ijkl}\epsilon_{kl} \tag{9.1}$$

where the indices i, j, k, l runs through the three spatial directions, e.g x, y, z. Thus there are 81 entries in the tensor c and potentially 81 different elastic moduli. However, both stress and strain tensors are symmetric by definition which can be written: $c_{ijkl} = c_{jikl} = c_{ijlk}$. A symmetric second rank tensor has only 6 independent components. Therefore, by collecting the indices i, j and k, l into index pairs (i.e. $xx = 1$, $yy = 2$, $zz = 3$, $yz = 4$, $zx = 5$, $xy = 6$), the elasticity tensor c can be thought of as a 6×6 matrix, thus reducing the number of possible independent elastic moduli to 36. Usually, it is also assumed that the stress tensor can be derived from an elastic potential W [104]

$$\sigma_{ij} = \frac{\partial W}{\partial \epsilon_{ij}} \quad \Rightarrow \quad c_{ijkl} = \frac{\partial^2 W}{\partial \epsilon_{ij} \partial \epsilon_{kl}} \,. \tag{9.2}$$

We thus have the following symmetry: $c_{ijkl} = c_{klij}$, which means that the 6×6 matrix defined above is symmetric. This reduces the number of independent moduli to 21.

For most crystalline structures the symmetry reduces this number further. For instance the hexagonal structure has 5 independent moduli and the cubic only 3 [6]. For an isotropic solid (such as a glass) the number of independent moduli reduces to two, namely $c_{11} = c_{xxxx}$ (the longitudinal modulus) and $c_{44} = c_{yzyz}$ (the shear modulus).

9.1 The Cauchy relations

The Cauchy relations are a set of relations between certain elements of c. The relations are traditionally derived through an assumption of central forces between pairs of molecules (see e.g. [105, p. 245-248]), i.e. that particles/molecules interact through pair-potentials depending only on the distance between them. [1] In compact notation the Cauchy relations can be written [104]

$$c_{ijkl} = c_{ikjl} \tag{9.3}$$

which amounts to 6 relations. In elastic solids these relations are rarely found to hold true except for some noble gas crystals [107], rather the deviations from the Cauchy-relations are studied to obtain information about the nature of the inter-atomic potentials, see e.g. [108, 109].

1 This is not a necessary condition. Weiner *et al* [106] have derived the same relations from an assumption about the deformation of electron density.

In the isotropic case, where the number of independent and nonzero moduli is already reduced to two, the Cauchy relation provides a relation between the two, namely $c_{44} = 3c_{11}$, reducing the number of independent moduli to just one. Expressed in terms of the longitudinal and shear moduli, the Cauchy relation for an isotropic solid states that

$$M = 3G \tag{9.4}$$

or equivalently, since $M = K + 4/3G$, the Cauchy relation is sometimes stated as

$$K = 5/3G\,. \tag{9.5}$$

Intuitively, a relation between the bulk and shear moduli of an isotropic solid is maybe not so surprising. If we imagine a model the material where each molecule is connected to its nearest neighbors by springs (of possibly different spring constants). Then a shearing of the material will involve some of the same springs that are involved in a compression.

9.2 Cauchy relation for liquids

The Cauchy relation is derived for a purely elastic solid and it is unclear how and if it should be applied to liquids. In thin liquids the shear modulus is vanishing (at least not at moderate frequencies, see however [101]), while the bulk modulus still persists. In that case a Cauchy relation would not make sense. For viscous liquids, where the short time / high frequency response to a deformation appears solid-like, a generalization of the Cauchy relation would perhaps be useful.

The most straightforward generalization of the Cauchy relation to the visco-elastic case, where the moduli become frequency-dependent, is perhaps the following

$$K(\omega) = 5/3G(\omega)\,. \tag{9.6}$$

This relation can however not be expected to hold since the two moduli generally relax on different timescales (see chapter 7) and thus can not be proportional for all frequencies. The next obvious attempt would be a translation of the moduli in Eq. (9.4) to the solid-like moduli in the viscoelastic case

$$K_\infty = 5/3G_\infty\,. \tag{9.7}$$

Zwanzig & Mountain [110] derived a relation between the high-frequency elastic moduli of liquids similar to this expression which includes a term that depends on temperature and pressure

$$K_\infty = 5/3G_\infty + 2(P - \rho kT)\,, \tag{9.8}$$

where the added term for the isobaric case in a small temperature interval can be regarded as a constant.

A generalized Cauchy relation between M_∞ and G_∞ was found to describe data well [111]

$$M_\infty = AG_\infty + B \tag{9.9}$$

where A and B are constants. This relation describes data well for many organic glass-formers [112–116], for bulk metallic glasses [117, 118], and even in through irreversible

chemical changes such as sol-gel transition, polymerization, and curing epoxy-systems [119–121], and A is found to be close to 3 (i.e. the proportionality predicted by the Cauchy relation, see Eq. (9.4)).

A "pure" Cauchy relation for viscous liquids was proposed by Fioretto *et al* [116], where the relation is suggested to hold for the relaxations strength rather than the high-frequency moduli

$$\Delta K = 5/3\Delta G \tag{9.10}$$

where $\Delta K = K_\infty - K_0$ and $\Delta G = G_\infty - G_0 = G_\infty$. This has also been observed in several liquids by Tage Christensen and Niels Boye Olsen.

In general, the two expressions in Eq. (9.9) and (9.10) can not both be valid since that would lead to $K_\infty = 5/3G_\infty + K_0$ which again implies K_0 being constant. Clearly, this must be wrong. An exception to this general consideration is stated below. The latter expression Eq. (9.10) is – in spite the lack of theoretical justification – more appealing since it has no adjustable parameters.

Moreover, in the pure Cauchy relation (Eq. (9.10)), unlike the general Cauchy relation, both sides converge to zero for $T \to \infty$, and this relation could thus be valid for any temperature. In contrast the generalized Cauchy relation which must break down once G_∞ vanishes at higher temperatures.

9.3 Experimental data

With our shear and bulk modulus measurements it is possible to test these relations. In Fig. 9.1 shear and bulk modulus data are presented as a function of temperature at a fixed frequencies. All measurements presented in chapter 4 and 5 are included which gives and idea of the error on the limiting values of G_∞, K_∞, and K_0. Inspecting the plots it becomes clear that the temperature interval where we access to all three quantities (G_∞, K_∞, and K_0) is small. To extend the temperature interval some, we approximated the temperature dependence of the three quantities with linear expressions. Thus the straight lines in red and blue with errorbars in Fig. 9.1 represent approximate mean values of the data sets and the errors indicated are between 3% and 7% and chosen to include all measurements. These regression lines can now be used for extrapolation to extend the temperature interval for comparison some.

In Fig. 9.2 these "mean-value" curves are plotted for regions where we trust the fits and their extrapolations. For DC704 this is the temperature interval 210-230K and for PPE the interval shown is 250-270K. The results are consistent with the pure Cauchy relation in Eq. 9.10, though less convincing for DC704. It should be noted that with the assumptions of an affine dependence of G_∞, K_∞, and K_0 on temperature, Eq. 9.9 automatically applies, and thus we have no way of distinguishing between the two relations, although the slope in the two cases obviously can not be the same. In particular, we can conclude that for these two liquids the slope of (G_∞, K_∞) is *not* close to the Cauchy prediction. For DC704 the slope is 2.3 and for PPE it is 3.4 which is far from the $5/3 \approx 1.7$ predicted in the Cauchy relation and reported in the literature.

The assumption that G_∞, K_∞, and K_0 depend linearly on temperature is only valid over a small temperature interval which is most evident for the K_0 level of PPE (see Fig. 9.1), which flattens out at higher temperatures.

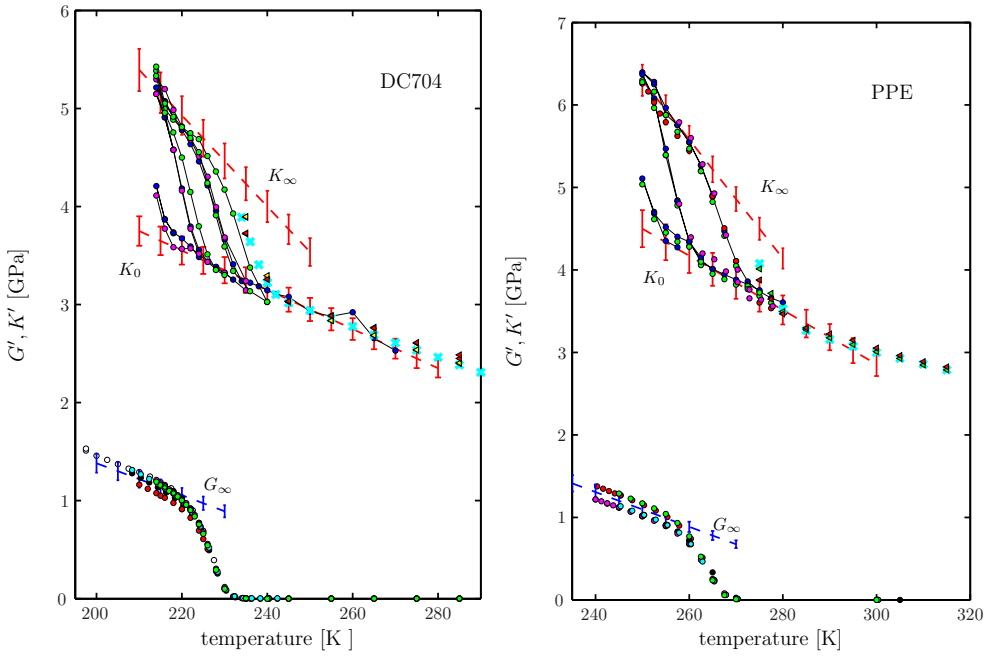

Figure 9.1 The shear and bulk moduli at fixed (high) frequencies as a function of temperature. All measurements of chapters 4 and 5 are included to give an idea of the error. The limiting K_0, K_∞ and G_∞ are approximated by linear fits to a "mean" of all measurements with errorbars (between 3% and 7 %) to include all measurements.

9.4 Discussion and concluding remarks

We have shown that the "pure" Cauhcy relation and the generalized Cauchy relation can not both in general be valid, except in the case where K_0, K_∞ and G_∞ all depend linearly on temperature. For small temperature intervals (like in our case) the generalized Cauchy relation almost trivially holds.

The data for PPE and DC704 are thus not in conflict with the generalized Cauchy relation, but this is not too surprising, given that we used linear approximations and extrapolations of the limiting high and low frequency moduli. The slopes of the (G_∞, K_∞)-curves are however not close to the Cauchy prediction.

Our data however clearly shows that $K_0(T) \propto T$ (Fig. 9.1) is not valid over the entire measured temperature interval, and probably the same is true for the instantaneous values of bulk and shear moduli. We thus find it unlikely that the generalized Cauchy relation should hold over broader temperature intervals.

Perhaps more surprisingly, the data provides support for the "pure" Cauhcy relation (Eq. (9.10)). For PPE the agreement of the data with this prediction of is very convincing.

Clearly, the relation $K(\omega, T) = 5/3G(\omega, T)$ proposed in Eq. 9.7 does not hold. It does however seem like the shape of the $(K(\omega, T), G(\omega, T))$ curves (at least for DC704)

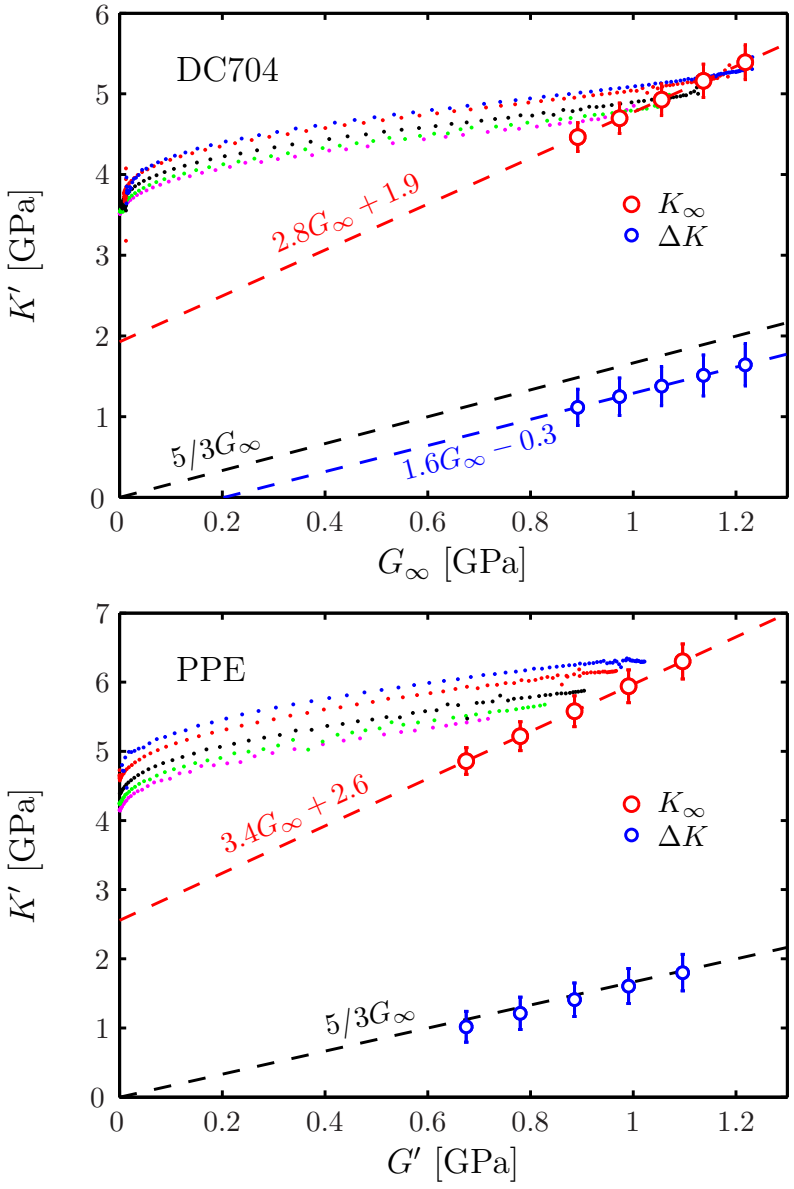

Figure 9.2 Various Cauchy-relations plotted for DC704 and PPE. In both, the dots are $(G(\omega), K(\omega))$ for different temperatures, red circles are the generalized Cauchy relation (G_∞, K_∞), and blue circles are the "pure" Cauchy relation $(\Delta G, \Delta K)$. The fits to the general Cauchy relation is shown as a full line and the "pure" Cauchy relation prediction as a dashed line. Clearly, Eq. (9.7) does not give unified description of the data, although the shape of the $(G(\omega), K(\omega))$ curves seems to be preserved

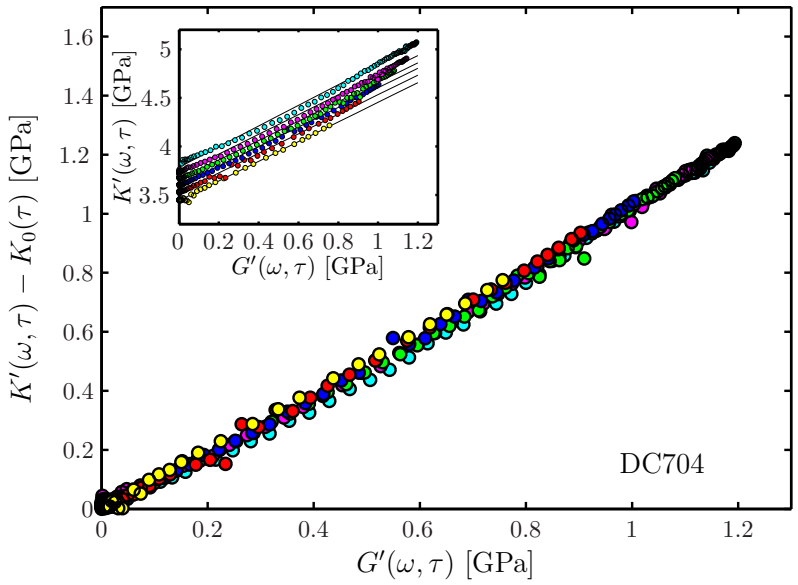

Figure 9.3 A Cauchy-like relation appears to be valid for DC704. The inset shows the real part of the frequency-dependent bulk modulus for a given relaxation time plotted against frequency dependent the shear modulus at the same relaxation time. Each color is a different fixed relaxation time. Each curve was fitted by a straight line (in black). The main figure shows that the same curves all collapse when the intercept subtracted, i.e. plotting $(G'(\omega,\tau), K'(\omega,\tau) - K_0(\tau))$. For high values of τ (corresponding to low temperatures) there is a slight curvature in the data, but this can be ascribed to the match of relaxation times being imperfect.

is preserved for different values of T. Already in chapter 7, we have a hint that the shape of bulk and the shear moduli are (close to) identical, while the relaxation time at a given temperature is different (the shear modulus is "faster"). This explains the shape preservation of $(K(\omega,T), G(\omega,T))$. It also means that if we compare bulk and shear modulus relaxation spectra for temperatures *with the same relaxation time* the two should be proportional. Plotting $(G(\omega,\tau), K(\omega,\tau))$ should thus give straight lines. The intercept would then correspond to the K_0 level for the given relaxation time. Of course the lines would then not collapse for different pairs of G and K curves since K_0 depends on temperature.

We tested this for DC704 where by pure luck the relaxation times of the bulk and shear moduli were separated approximately by the temperature steps ΔT used in the measurement, i.e. $\tau_{\text{bulk}}(T) = \tau_{\text{shear}}(T + \Delta T)$. The inset of Fig. 9.3 shows $(K'(\omega,\tau), G'(\omega,\tau))$ for different values of τ (symbols) as well as their fits (black lines). All fits have slopes close 1 (between 0.99 and 1.01). For some of the higher values of τ (corresponding to low temperatures) there is a slight curvature in the data, but this can be ascribed to the match of relaxation times being imperfect.

Subtracting the intercept (the $K_0(\tau)$) all the data point collapse onto one line with slope ~ 1, which is shown in the main figure. Although the factor of proportionality is

strikingly close to one, this is probably not significant and will depend on the particular set of measurements plotted together – recall that the spread in absolute values (unlike the shape) is substantial for these data.

So it seems that at least for some simple liquids the following relation between bulk and shear moduli

$$K'(\omega,\tau) - K_0(\tau) \propto G'(\omega,\tau) \tag{9.11}$$

may be valid. We can call this a "dynamical" or an "isochronal" Cauchy relation. Note that this relation also implies proportionality between the relaxation strengths (for a fixed relaxation time) which is simply the limit for $\omega \to \infty$. Measurements on other liquids as well as a more careful matching of relaxation times would however be required to further investigate/establish this relation.

Bibliography

[1] T. Christensen and N. B. Olsen. A rheometer for the measurement of high shear modulus covering more than seven decades of frequency below 50 khz. *Review of Scientific Instruments*, 66(10):5019–5031, 1995.

[2] T. Christensen and N. B. Olsen. Determination of the frequency-dependent bulk modulus of glycerol using a piezoelectric spherical shell. *Physical Review B*, 49(21):15396–15399, 1994.

[3] G. Harrison. *The Dynamic Properties of Supercooled Liquids*. Academic Press, 1976.

[4] J. D. Ferry. *Viscoelastic properties of polymers*. John Wiley & Sons, Inc, 1980.

[5] B. W. Rossiter and R. C. Baetzold, editors. *Determination of elastic and mechanical properties*. John Wiley & Sons, Inc, 1991.

[6] L. D. Landau and E. M. Lifshitz. *Theory of Elasticity*. Elsevier, 1986.

[7] R. D. Deegan, R. L. Leheny, N. Menon, S. R. Nagel, and D. C. Venerus. Dynamic shear modulus of tricresyl phosphate and squalane. *Journal of Physical Chemistry B*, 103:4066–4070, 1999.

[8] A. Mandanici, X. Shi, G. B. McKenna, and M. Cutroni. Slow dynamics of supercooled *m*-toluidine investigated by mechanical spectroscopy. *Journal of Chemical Physics*, 122:114501, 2005.

[9] K. Schröter, S. A. Hutcheson, X. Shi, A. Mandanici, and G. B. McKenna. Dynamic shear modulus of glycerol: corrections due to intrument compliance. *Journal of Chemical Physics*, 125:214507, 2006.

[10] S. A. Hutcheson and G. B. McKenna. The measurement of mechanical properties of glycerol, *m*-toluidine, and sucrose benzoate under consideration of corrected theometer compliance: An in-depth study and review. *Journal of Chemical Physics*, 129:074502, 2008.

[11] A. F. Yee and M. T. Takemori. Dynamic bulk and shear relaxation in glassy polymers. I. Experimental techniques and results. *Journal of Polymer Science: Polymer Physics Edition*, 20:205–224, 1982.

[12] D. G. Ivey, B. A. Mrowca, and W. Guth. Propagation of ultrasonic bulk waves in high polymers. *Journal of Applied Physics*, 20:486–492, 1949.

[13] R. S. Marvin, R. Aldrich, and H. S. Sack. The dynamics bulk viscosity of polyisobutylene. *Journal of Applied Physics*, 25:1213–1218, 1954.

[14] E. Morita, R. Kono, and H. Yoshizak. Bulk and shear relaxation processes in poly-i-butyl methacrylate. *Japanese Journal of Applied Physics*, 7:451, 1968.

[15] G. Goldbach and G. Rehage. Die Volumenretardation des Polystyrols nach Drück- und Temperatursprüngen. *Rheologica Acta*, 6:30–53, 1967.

[16] Y. Meng, P. Bernazzani, P. A. O'Connell, G. B. McKenna, and S. L. Simon. A new pressurizable dilatometer for measuring the time-dependent bulk modulus

and pressure-volume-temperature properties of polymeric materials. *Review of Scientific Instruments*, 80:053903, 2009.

[17] J. E. McKinney, S. Edelman, and R. S. Marvin. Apparatus for the direct determination of the dynamic bulk modulus. *Journal of Applied Physics*, 27:425–430, 1956.

[18] T. H. Deng and W. G. Knauss. The temperature and frequency dependence of the bulk compliance of poly(vinyl acetate). A re-examination. *Mechanics of Time-Dependent Materials*, 1:33–49, 1997.

[19] S. B. Sane and W. G. Knauss. The time-dependent bulk response of poly (methyl methacrylate). *Mechanics of Time-Dependent Materials*, 5:293–324, 2001.

[20] Y. Meng and S. L. Simon. Pressure relaxation of polystyrene and its comparison to the shear response. *Journal of Polymer Science: Part B: Polymer Physics*, 45:3375–3385, 2007.

[21] B. Igarashi, T. Christensen, E. H. Larsen, N. B. Olsen, I. H. Pedersen, T. Rasmussen, and J. Dyre. A cryostat and temperature control system optimized for measuring relaxations of glass-forming liquids. *Review of Scientific Instruments*, 79:045105, 2008.

[22] B. Igarashi, T. Christensen, E. H. Larsen, N. B. Olsen, I. H. Pedersen, T. Rasmussen, and J. Dyre. An impedence-measurement setup optimized for measuring relaxations of glass-forming liquids. *Review of Scientific Instruments*, 79:045106, 2008.

[23] A. L. Fetter and J. D. Walecka. *Theoretical Mechanics of Particles and Continua*. Dover Publications, 2003.

[24] T. Christensen and N. B. Olsen. Quasistatic measurements of the frequency-dependent bulk and shear modulus of supercooled liquids. *Journal of Non-Crystalline Solids*, 172-174:362–364, 1994.

[25] B. Jakobsen and K. Niss. Dielectric and shear mechanical relaxation in glass forming liquids. Master's thesis, Roskilde University, 2003.

[26] T. Christensen and N. B. Olsen. Comparativemeasurements of the electrical and shear mechanical response in some supercooled liquids. *Journal of Non-Crystalline Solids*, 172-174:357–361, 1994.

[27] B. Jakobsen, K. Niss, and N. B. Olsen. Dielectric and shear mechanical alpha and beta relaxations in seven glass-forming liquids. *Journal of Chemical Physics*, 123(23):234511, 2005.

[28] B. Jakobsen, C. Maggi, T. Christensen, and J. C. Dyre. Investigation of the shear-mechanical and dielectric relaxation processes in two monoalcohols close to the glass transition. *Journal of Chemical Physics*, 129:184502, 2008.

[29] C. Maggi, B. Jakobsen, T. Christensen, N. B. Olsen, and J. C. Dyre. Supercooled liquid dynamics studied via shear-mechanical spectroscopy. *Journal of Physical Chemistry B*, 112:16320–16325, 2008.

[30] T. Christensen. personal communication.

[31] A. Einstein. *Investigations on the Theory of Brownian motion*. Dover, 1956.

[32] P. Bordat, F. Affouard, M. Descamps, and F. Müller-Plathe. The brakdown of the Stokes-Einstein relation in supercooled binary liquids. *Journal of Physics: Condensed Matter*, 15:5397–5407, 2003.

[33] I. Chang and H. Sillescu. Heterogeneity at the glass transition: Translational and rotational self diffusion. *Journal Physical Chemistry B*, 101:8794–8801, 1997.

[34] E. Rössler. Indications for a change of diffusion mechanism in supercooled liquids. *Physcial Review Letters*, 65:1595–1598, 1990.

[35] F. Fujara, B. Geil, H. Sillescu, and G. Fleischer. Translational and rotational diffusion in supercooled orthoterphenyl close to the glass transition. *Zeitschrift für Physik B: Condensed Matter*, 88:195–204, 1992.

[36] M. T. Cicerone and M. D. Ediger. Enhanced translation of probe molecules in supercooled o-terphenyl: Signature of spatially heterogenous dynamics? *Journal of Chemical Physics*, 104:7210–7218, 1996.

[37] D. B. Hall, A. Dhinojwala, and J. M. Torkelson. Translation-rotation paradox for diffusion in glass-forming polymers: The role of the temperature dependence of the relaxation time distribution. *Physical Review Letters*, 79:103–106, 1997.

[38] L. Andreozzi, A. Di Schino, M. Giordano, and D. Leporini. Evidence of a fractional Debye-Stokes-Einstein law in supercooled o-terphenyl. *Europhysics Letters*, 38:669–674, 1997.

[39] A. Voronel, E. Veliyulin, V. Sh. Machavariani, A. Kisliuk, and D. Quitmann. Fractional Stokes-Einstein law for ionic transport in liquids. *Physical Review Letters*, 80:2630–2633, 1998.

[40] S. Corezzi, E. Campani, P. A. Rolla, S. Capaccioli, and D. Fioretto. Changes in the dynamics of supercooled systems revealed by dielectric spectroscopy. *Journal of Chemical Physics*, 111:9343–9351, 1999.

[41] C. H. Wang and S. S. Gong. Tracer diffusion in salol in the supercooled state. *Journal of Chemical Physics*, 117:4896–4900, 2002.

[42] J. R. Rajian and E. L. Quitevis. Translational diffusion in sucrose benzoate near the glass transition: Probe size dependence in the breakdown of the Stokes-einsten equation. *Journal of Chemical Physics*, 126:224506, 2007.

[43] G. Heuberger and H. Sillescu. Size depedence of tracer diffusion in supercooled liquids. *Journal Physical Chemistry*, 100:15255–15260, 1996.

[44] R. Zorn, F. I. Mopsik, G. B. McKenna, L. Willner, and D. Richter. Dynamics of polybutadienes with different microstructures. 2. Dielectric response and comparisons with rheological behavior. *Journal of Chemical Physics*, 107:3645–3655, 1997.

[45] W. Suchanski, S. Jurga, T. Pakula, M. Paluch, and J. Ziolo. Molecular dynamics in supercooled di-isobutyl phthalate close to the glass transition. *Journal of Physics: Condensed Matter*, 12:9551–9562, 2000.

[46] C. Dreyfus, S. Murugavel, R. Gupta, M. Massot, R. M. Pick, and H. Z. Cummins. Brillouin scattering study of inorganic glass-forming liquids. *Philosophical Magazine B*, 82:263–271, 2002.

[47] R. Kono, T. A. Litovitz, and G. E. McDuffe. Comparison of dielectric and mechanical relaxation processes in glycerol -*n*-propanol mixtures. *Journal of Chemical Physics*, 45:1790–1796, 1966.

[48] E. Rössler and P. Eiermann. Reorientational dynamics in supercooled *m*-tricresyl phosphate: Its relation to main and secondary relaxation – ^{31}p magnetic resonance study of relaxation, line shape, and stimulated echo. *Journal of Chemical Physics*, 100:5237–5248, 1993.

[49] J. C. Hooker and J. M. Torkelson. Coupling of probe reorientation dynamics and rotor motions to polymer relaxation as sensed by second harmonic generation and fluorescence. *Macromolecules*, 28:7683–7692, 1995.

[50] K. Schröter and E. Donth. Comparison of shear response with other properties at the dynamic glass transition of different glassformers. *Journal of Non-Crystalline Solids*, 307-310:270–280, 2002.

[51] F. Stickel. PhD thesis, Johannes Gutenburg University, Mainz, 1995.

[52] N. O. Birge and S. R: Nagel. Specific-heat spectroscopy of the glass transition. *Physical Review Letters*, 54:2674–2677, 1985.

[53] J. Korus. PhD thesis, University of Halle, 1997.

[54] S. A. Reinsberg, X. H. Qui, M. Wilhelm, H. W. Spiess, and M. D: Ediger. Length scale of dynamic heterogeneity in supercooled glycerol near T_g. *Journal of Chemical Physics*, 114:7299–7302, 2001.

[55] C. T. Moynihan, N. Balitactac, L. Boone, and T. A. Litovitz. Comparison of shear and conductivity relaxation times for concentrated lithium chloride solutions. *Journal of Chemical Physics*, 55:3013–3019, 1971.

[56] J. Colmenero, A. Alegria, P. G. Santangelo, K. L. Ngai, and C. M. Roland. Detailed correspondences between dielectric and mechanical relaxations in poly(vinylethylene). *Macromolecules*, 27:407–210, 1994.

[57] M. Cutroni and A. Mandanici. Mechanical and dielectric behavior of some ionic glasses. *Solid State Ionics*, 105:149–157, 1998.

[58] M. Cutroni and A. Mandanici. The α-relaxation process in simple glass forming liquid m-toluidine. II. The temperature dependence of the mechanical response. *Journal of Chemical Physics*, 114:7124–7129, 2001.

[59] P. Pötschke, M. Abdel-Goad, I. Alig, S. Dudkin, and D. Lellinger. Rheological and dielectric characterization of melt mixed polycarbonate-multiwalled carbon nanotube composites. *Polymer*, 45:8863–8870, 2004.

[60] K. Niss, B. Jakobsen, and N. B. Olsen. Dielectric and shear mechanical relaxations in glass-forming liquids: A test of the Gemant-DiMarzio-Bishop model. *Journal of Chemical Physics*, 123:234510, 2005.

[61] A. Mandanici, R. Richert, M. Cutroni, X. Shi, S. A. Hutcheson, and G. B. McKenna. Relaxational features of supercooled and glassy m-toluidine. *Journal of Non-Crystalline Solids*, 352:4729–4734, 2006.

[62] S. Pawlus, M. Mierzwa, M. Paluch S. J. Rzoska, and C. M. Roland. Dielectric and mechanical relaxation in isooctylcyanobiphenyl (8*ocb). *Journal of Physics: Condensed Matter*, 22:235101, 2010.

[63] E. A. DiMarzio and M. Bishop. Connection between the macroscopic electric and mechanical susceptibilities. *Journal of Chemical Physics*, 60:3802–3811, 1974.

[64] A. R. Dexter and A. J. Matheson. Viscoelastic relaxation of the bulk modulus in two supercooled benzene derivatives. *Journal of Chemical Physics*, 54:3463–3471, 1971.

[65] V. A. Solovyev, Y. S. Manucharov, and I. Alig. On the origin of the volume viscosity liquid polymeric systems. *Acta Polymerica*, 8:513–516, 1989.

[66] I. Alig, F. Stieber, A. D. Bakhramov, Y. S. Manucharov, S. A. Manucharova, and V. A. Solovyev. Entanglement behavior in dynamic bulk and shear properties as studied by acoustic methods. *Polymer*, 31:877–881, 1990.

[67] M. Schulz and I. Alig. Influence of stochastic environments of Gaussian chains on dynamic shear and bulk properties. *Journal of Chemical Physics*, 97:2772–2776, 1992.

[68] N. B. Olsen, T. Christensen, and J. C. Dyre. Time-temperature superposition in viscous liquids. *Physical Review Letters*, 86(7):1271–1274, 2001.

[69] A. I. Nielsen, T. Christensen, B. Jakobsen, K. Niss, N. B. Olsen, R. Richert, and J. C. Dyre. Prevalence of approximate $\sqrt{t}$ relaxation for the dielectric alpha process in viscous organic liquids. *Journal of Chemical Physics*, 130:154508, 2009.

[70] P. K. Dixon, L. Wu, S. R. Nagel, B. D. Williams, and J. P. Carini. Scaling in the relaxation of supercooled liquids. *Physcial Review Letters*, 65:1108–1111, 1990.

[71] E. L. Gjersing, S. Sen, P. Yu, and B. G. Aitken. Anomalously large decoupling of rotational and shear relaxation in a molecular glass. *Physcial Review E*, 76:214202, 2007.

[72] Bo Jakobsen, N. B. Olsen, and T. Christensen. Frequency-dependent specific heat from thermal effusion in sphercial geometry. *Physical Review E*, 81:061505, 2010.

[73] K. Niss. in preparation.

[74] D. Thirumalai and R. D. Mountain. Activated dynamics, loss of ergodicity, and transport in supercooled liquids. *Physcial Review E*, 47:479–489, 1993.

[75] L. Angelani, G. Parisi, G. Ruocco, and G. Viliani. Connected network of minima as a model glass: Long time dynamics. *Physcial Review Letters*, 81:4648–4651, 1998.

[76] M. Nicodemi and A. Coniglio. Macroscopic glassy relaxations and microscopic motions in a frustrated lattice gas. *Physical Review E*, 57:R39–R42, 1998.

[77] R. Yamamoto and A. Onuki. Dynamics of highly supercooled liquids: Heterogeneity, rheology, and diffusion. *Physical Revew E*, 58:3515–3529, 1998.

[78] P. Allegrini, J. F. Douglas, , and S. C. Glotzer. Dynamic entropy as a measure of caging and persistent particle motion in supercooled liquids. *Physical Revew E*, 60:5714–5724, 1999.

[79] S. C. Glotzer, V. N. Novikov, and T. S. Schrøder. Time-dependent, four-point density correlation function description of dynamical heterogeneity and decoupling in supercooled liquids. *Journal of Chemical Physics*, 112:509–512, 2000.

[80] C. D. Michele and D. Leporini. Viscous flow and jump dynamics in molecular supercooled liquids. i. translations. *Physical Revew E*, 63:036701, 2001.

[81] T. Ködderman, R. Ludwig, and D. Paschek. On the validity of Stokes-Einstein and Stokes-Einstein-Debye relations in ionic liquids and ionic-liquid mixtures. *European Journal of Chemical Physics and Physical Chemistry*, 9:1851–1858, 2008.

[82] D. Jeong, M. Y. Choi, H. J. Kim, and Y. Jung. Fragility, Stokes-Einstein violation, and correlated local excitations in a coarse-grained model of an ionic liquid. *Physical Chemistry Chemical Physics: Physical Chemistry of Ionic Liquids*, 12:2001–2010, 2010.

[83] N. P. Bailey, T. Christensen, B. Jakobsen, K. Niss, N. B. Olsen, U. R. Pedersen, T. B. Scrøder, and J. C. Dyre. Glass-forming liquids: one or more 'order' parameters? *Journal of Physics: Condensed Matter*, 20:244113, 2008.

[84] N. L. Ellegaard, T. Christensen, P. V. Christiansen, N. B. Olsen, U. R. Pedersen, T. B. Schröder, and J. C. Dyre. Single-order-parameter description of glass-forming liquids: A one-frequency test. *Journal of Chemical Physics*, 126:074502, 2007.

[85] U. R. Pedersen, T. Christensen, T. B. Schøder, and J. C. Dyre. Feasibility of a single-parameter description of equilibrium viscous liquid dynamics. *Physcial Review E*, 77:011201, 2008.

[86] U. Schneider, P. Lunkenheimer, R. Brand, and A. Loidl. Dielectric and far-infrared spectroscopy of glycerol. *Journal of Non-Crystalline Solids*, 235-237:173–179, 1998.

[87] N. Petzold and E. A. Rössler. Light scattering study on the glass former o-terphenyl. *Journal of Chemical Physics*, 133:124512, 2010.

[88] P. Lunkenheimer, U. Schneider, R. Brand, and A. Loidl. Glassy dynamics. *Contemporary Physics*, 41:15–36, 2000.

[89] P. Lunkenheimer and A. Loidl. Dielectric spectroscopy of glass-foming materials: α-relaxation and excess wing. *Chemical Physics*, 284:205–219, 2002.

[90] S. S. N. Murthy and M. Tyagi. Experimental study of the high frequency relaxation process in monohydroxy alcohols. *Journal of Chemical Physics*, 117:3837–3847, 2002.

[91] L. M. Wang and R. Richert. Dynamics of glass-forming liquids. IX. Structural versus dielectric relaxation in monohydroxy alcohols. *Journal of Chemical Physics*, 121:22, 2004.

[92] G. A. Arzoumanidis and K. M. Liechti. Linear viscoelastic property measurement and its significance for some nonlinear viscoelastic models. *Mechanics of Time-Dependent Materials*, 7:209–250, 2003.

[93] B. E. Read, G. D. Dean, and P. E. Tomlins. Effects of physical ageing on creep in polypropylene. *Polymer*, 29:2159–2169, 1988.

[94] B. E. Read. Analysis of creep and physical aging in glassy polymers. *Journal of Non-Crystalline Solids*, 131-133:408–419, 1991.

[95] V. N. Novikov and A. P. Sokolov. Poisson's ratio and the fragility of glass-forming liquids. *Nature*, 431:961–963, 2004.

[96] J. C. Dyre, N. B. Olsen, and T. Christensen. Local elastic expansion model for viscous-flow activation energies of glass-forming molecular liquids. *Physical Review B*, 53:2171–2174, 1996.

[97] D. H. Torchinsky, J. A. Johnson, and K. A. Nelson. A direct test of the correlation between elastic parameters and fragility of ten glass formers and their relationship to elastic models of the glass transition. *Journal of Chemical Physics*, 130:064502, 2009.

[98] Y-X. Yan and K. A. Nelson. Impulsive stimulated light scattering. II. Comparison to frequency-domain light-scattering spectroscopy. *Journal of Chemical Physics*, 87:6257–6266, 1987.

[99] Y. Yang and K. A. Nelson. Impulsive stimulated light scattering from glass-forming liquids. I. Generalized hydrodynamics approach. *Journal of Chemical Physics*, 103:7722–7731, 1995.

[100] C. Klieber. *Ultrafast photo-acoustic spectroscopy of supercooled liquids*. PhD thesis, Massachusetts Institute of Technology, 2010.

[101] T. Pezeril, C. Klieber, S. Andrieu, and K. A. Nelson. Optical generation of gigahertz-frequency shear acoustic waves in liquid glycerol. *Physical Review Letters*, 102:107402, 2009.

[102] R. H. Orcutt. Interlot density variation of a siloxane manometer fluid. *Journal of Vacuum Science Technology*, 10:506–506, 1973.

[103] N. W. Tschoegl and W. G. Knauss. Poisson's ratio in linear viscoelasticity – a critical review. *Mechanics of Time-Dependent Materials*, 6:3–51, 2002.

[104] F. W. Hehl and Y. Itin. The Cauchy relations in linear elasticity theory. *Journal of Elasticity*, 66:185–192, 2002.

[105] M. Born and K. Huang. *Dynamical theory of crystal lattices*. Oxford University Press, 1954.

[106] J. H. Weiner. Hellmann-Feynman theorem, elastic moduli, and Cauchy relations. *Physical Review B*, 24:845–848, 1981.

[107] E. V. Zarochentsev, E. P Troitskaya, and Val. V. Chabanenko. Elastic constant of noble-gas crystals under pressure and the Cauchy relations. *Physics of the Solid State*, 46:249–253, 2004.

[108] S. V. Sinogeikin and J. B. Bass. Single-crystal elasticity of MgO at high pressure. *Physical Review B*, 59:R14141–R14144, 1999.

[109] K. J. McClellan, F. Chu, J. M. Roper, and I. Shindo. Room temperature single crystal elastic constant of boron carbide. *Journal of Materials Science*, 36:3403–3407, 2001.

[110] R. Zwanzig and R. D. Mountain. High-frequency elastic moduli of simple fluids. *Journal of Chemical Physics*, 43:4464–4471, 1965.

[111] J. K. Krüger, J. Balle, T. Britz, A. le Coutre, R. Peter, R. Bactavatchalou, and J. Schreiber. Cauchy-like relation between elastic constants in amorphous materials. *Physical Review B*, 66:012206, 2002.

[112] J. K. Krüger, T. Britz, A. le Coutre, J. Baller, W. Possart, P. Alnot, and R. Sanctuary. Different glassy states, as indicated by a violation of the generalized Cauchy relation. *New Journal of Physics*, 5:80.1–80.11, 2003.

[113] F. Scarponi, L. Comez, D. Fioretto, and L. Palmieri. Brillouin light scattering from transverse and longitudinal acoustic waves in glycerol. *Physical Review B*, 70:054203, 2004.

[114] J. K. Krüger, U. Müller, R. Bactavatchalou, J. Mainka, C. Gilow, W. Possart, A. Tschöpe, P. Alnot, D. Rouxel, R. Sanctuary, and B. Wetzel. The generalized Cauchy relation as an universal property of the amorphous state. *Journal de Physique IV*, 129:45–49, 2005.

[115] R. Bactavatchalou, P. Alnot, J. Baller, M. Kolle, U. Müller, M. Philipp, W. Possart, D. Rouxel, R. Sanctuary, A. Tschöpe, Ch. Vergnat, B. Wetzel, and J. K. Krüger. The generalized Cauchy relation: a probe for local structure in materials with isotropic symmetry. *Journal of Physics: Conference Series*, 40:111–117, 2006.

[116] D. Fioretto, S. Corezzi, S. Caponi, F. Scarponi, G. Monaco, A. Fontana, and L. Palmieri. Cauchy relation in relaxing liquids. *Journal of Chemical Physics*, 128:214502, 2008.

[117] P. Wen, J. P. Johari, R. J. Wang, and W. H. Wang. Change in vibrational properties of bulk metallic glass with time. *Physcial Review B*, 73:224203, 2006.

[118] E. Pineda and D. Crespo. Elastic properties behaviour of metallic glasses. *Reviews on Advanced Materials Science*, 18:173–176, 2008.

[119] H. Yamura, M. Matsukawa, T. Otani, and N. Ohtori. Brillouin scattering study on the elastic properties of epoxy adhesive layer. *Japanese Journal of Applied Physics*, 38:3175–3178, 1999.

[120] M. Philipp, U. Müller, R. J. Jiménez Riobóo, J. Baller, R. Sanctuary, W. Possart, and J. K. Krüger. Interphases, gelation, vitrification, porous glasses and the generalized Cauchy relation: epoxy/silica nanocomposites. *New Journal of Physics*, 11:023015, 2009.

[121] M. Philipp, C. Vergnat, U. Müller, R. Sanctuary, J. Baller, W. Possart, P. Alnot, and J. K. Krüger. Second order elasticity at hypersonic frequencies of reactive polyurethanes as seen by generalized Cauchy relations. *Journal of Physics: Condensed Matter*, 21:031506, 2009.

Part II

Temperature dependence of dielectric relaxation time

10 Dynamic divergence? – an analysis of a large set of dielectric data

This chapter presents an analysis of a large set of relaxation time data obtained through dielectric spectroscopy. Most of the results were published in [1], but more details will be provided here as well as some new findings. The paper is enclosed as Paper II, p. 265.

Compared to Paper II [1] there are a few minor changes. Symbols and colors for each dataset has been redefined, thus figures and tables will not be identical to the ones presented in [1]. The dataset for 5PPE has been replaced by a dataset with a much broader temperature range (was taken subsequently in connection with the mechanical measurements) and the dataset for PHIQ has been removed (as we later discovered that *per*-hydro-isoquinoline is in fact the same as *deca*-hydro-isoquinoline).

10.1 Non-Arrhenius behavior of the relaxation time

The focus of this chapter is on the non-Arrhenius temperature dependence of the relaxation time τ. τ generally increases more rapidly upon cooling than predicted by the well-known Arrhenius equation that characterizes, e.g., the reaction time of a chemical reaction as a function of temperature. Thus if the activation energy ΔE is defined by

$$\tau(T) = \tau_0 \exp\left(\frac{\Delta E(T)}{k_B T}\right) , \tag{10.1}$$

(where k_B is Boltzmann's constant, T is temperature, and τ_0 is the pre-exponential factor) one usually observes that $\Delta E(T)$ increases upon cooling. To the best of our knowledge there are no liquids where ΔE decreases upon cooling.

The most widely used fit to data is the Vogel-Fulcher-Tammann (VFT) equation dating back to the 1920's [2–4]:

$$\tau(T) = \tau_0 \exp\left(\frac{A}{T - T_0}\right) , \tag{10.2}$$

where A and T_0 (and sometimes τ_0) are fitting parameters. This equation predicts a divergence of the liquid relaxation time at $T = T_0$. By its very nature this prediction cannot be conclusively verified because, if true, close to T_0 the liquid would require much longer time to equilibrate than a human life time. Experimentalists often do not focus very much on the interpretation of T_0, but pragmatically regard the VFT equation as just a convenient fit to data. Many theorists, on the other hand, were inspired by the VFT equation to develop theories predicting a phase transition at T_0 to some sort of ideal glassy state with infinite relaxation time [5].

10.1.1 The entropy model

Probably, the most famous of models predicting a phase transition to a state of infinite relaxation time is the Adam-Gibbs entropy model[6]. This model predicts that the temperature dependence of the apparent activation energy is inversely proportional to the configurational entropy

$$\Delta E \propto \frac{1}{S_c} \tag{10.3}$$

where the configurational entropy is defined as the entropy minus the vibrational part, $S_c = S - S_{\text{vib}} \approx S_{\text{liquid}} - S_{\text{glass}}$.

This is justified as follows [7]: Any molecular rearrangement is a thermally activated transition that involves all molecules of a "cooperatively rearranging region." Such a region is defined as a "subsystem of the sample which, upon a sufficient fluctuation in energy (or, more correctly, enthalpy), can rearrange into another configuration independently of its environment." Three crucial assumptions go into the model: (1) The activation energy is proportional to region volume. This is justified by writing the change in Gibbs free energy upon activation as a chemical potential change $\Delta\mu$ times volume and assuming that "in a good approximation the dependence of $\Delta\mu$ on temperature and region volume can be neglected." (2) There is a lower limit to the size of a cooperatively rearranging region since it must have at least two configurations "available to it, one in which the region resides before the transition and another one to which it may move." (3) The cooperatively rearranging regions are "independent and equivalent subsystems", i.e., there are only insignificant interactions of any given region with its surroundings. Then the configurational entropy of the entire sample is simply a sum of the regional entropies, which are proportional to region size.

At some finite temperature the critical size is thus expected to become macroscopic, because the entropy of the liquid decreases faster than the entropy of the glass. At zero configurational entropy only one (or very few) configurations are available to the whole system.

The entropy can be found by integrating the heat-capacity and thus the configurational entropy can be found by integrating the configurational part of the heat-capacity. The configurational heat capacity may be defined as the difference between the heat-capacity of liquid and that of the glass, $\Delta C_p = C_p^{\text{liq}} - C_p^{\text{glass}}$. Assuming that this quantity does not change much in the vicinity of T_g we may write

$$S_c(T) \approx \Delta C_p \int_{T_0}^{T} \frac{1}{T'}\, dT' = \Delta C_p \ln(T/T_0) \tag{10.4}$$

assuming $S_c(T_0) = 0$. Close to T_0 (where $\delta T =: T - T_0 \to 0$) we may expand this expression to the first order to obtain

$$\ln\left(\frac{1}{1-\delta T/T}\right) \approx \ln\left(1 + \delta T/T\right) \approx \delta T/T \tag{10.5}$$

and we arrive at

$$\Delta E \propto \frac{1}{S_c} \propto \frac{T}{T - T_0} \tag{10.6}$$

when approaching T_0. This expression is exactly the functional form for the temperature-dependence of the relaxation time suggested by the VFT equation.

There are both theoretical and experimental objections to this model, some of which we have summarized in [7] (enclosed Paper II p. 265).

10.1.2 Other models

The Adam-Gibbs entropy model is not the only phenomenological macroscopic model for the viscous slowing down of super-cooled liquids. Some of them are compatible with a relaxation time diverging at a finite temperature, others not.

The free volume model by Cohen, Turnbull, and Grest[8, 9] predicts that the free energy of activation is inversely proportional to the free volume, v_f, defined as the volume within its cage less the volume of the molecule

$$\Delta E \propto \frac{1}{v_f(T)}. \tag{10.7}$$

This expression obviously diverges if the free volume v_f goes to zero, for instance if the volume of the molecule is assumed to be independent of the temperature while the total volume decreases due to thermal contraction.

The volume of a molecule is however not very well-defined (except in the case of hard spheres). In the denominator of Eq. (10.7) two large numbers, namely the volume of the sample and the total volume occupied by the molecules, are subtracted from each other to give a small number. The inverse of their difference is consequently extremely sensitive to the exact definition of molecular volume.

There are also various elastic models (summarized in a review by Dyre [10]), the shoving model by Dyre, Olsen & Christensen [11] being the most recent. The central assumption of this model is that the energy necessary to make a flow event in supercooled liquids is due to a deformation of the surroundings of the rearranging molecules, making room for the molecules to rearrange. Assuming a purely radial local volume increase gives a pure shear deformation of the surroundings. The free energy of activation in this framework is thus proportional to the instantaneous shear modulus, G_∞

$$\Delta E \propto G_\infty(T). \tag{10.8}$$

According to this model the increase in $G_\infty(T)$ with decreasing temperature (as the liquid "stiffens") is sufficient to explain the temperature dependence of the relaxation time. Elastic models are difficult to unite with the idea of a diverging relaxation time, since this would imply that the liquid at some finite temperature should become infinitely rigid.

10.2 Status of the VFT divergence

The Adam-Gibbs entropy theory from 1965 predicts a second order phase transition at $T = T_0$ to a state of zero configurational entropy – a unique glassy state – and infinite relaxation time [6]. Later, leading theorists like Edwards [12, 13], Anderson [14] and, more recently, Bouchaud in 2004 [15] and Wolynes in 2007 [16], have all investigated and developed this intriguing scenario much further. The list of theoretical

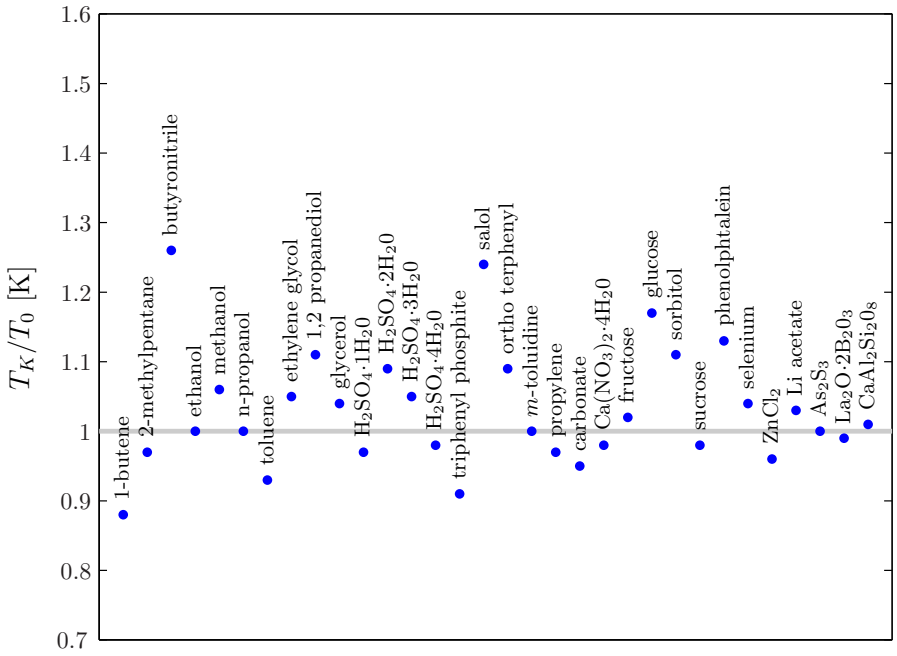

Figure 10.1 The ratio of the Kauzmann temperature, T_K, and the VFT divergence temperature, T_0, for a number of glass-forming liquids. There is an almost perfect correlation between T_K and T_0. Data reported in [32].

publications stating more or less explicitly that the goal of the work is to *produce a VFT law* continues (e.g. [17–25]).

Although there are diverging opinions from other well-known theorists [26–29], it remains an attractive idea that the dramatic slowing down of relaxations is caused by an underlying phase transition to a state with infinite relaxation time; the fact that data are usually well fitted by the VFT equation has reinforced this idea over many years now.

Support for the idea of a "dynamic divergence" at $T = T_0$ traditionally came from the reported equality of T_0 and the Kauzmann temperature T_K, the temperature where the liquid phase entropy by extrapolation is identical to the crystal phase entropy [30–32]. Fig. 10.1 shows a seemingly perfect correlation between T_0 of the VFT equation and the Kauzmann temperature T_K for a collection of liquids (data reported in [32]).

In 2003 Tanaka presented a compilation of data showing, however, that $T_0 = T_K$ is not confirmed by experiment [33] and the deviation seems to increase the "stronger" the liquid. These data are shown in Fig. 10.2 where T_K/T_0 is plotted as a function of the parameter D (sometimes referred to as the "fragility parameter". The connection to Angell's fragility index (see chapter 2, Eq. (2.6) for a definition) comes from writing the VFT equation in the following way

$$\tau = \tau_0 \exp\left(\frac{DT_0}{T - T_0}\right). \tag{10.9}$$

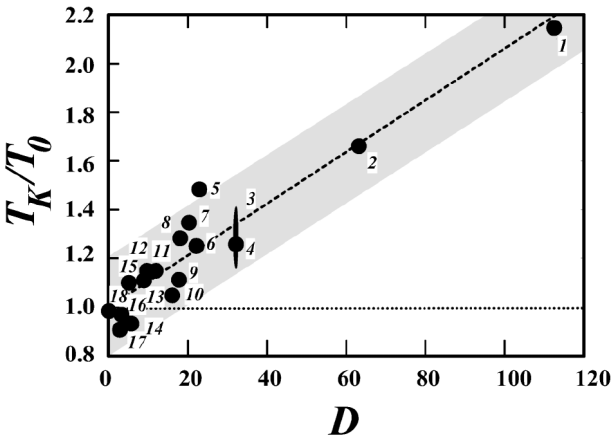

1. GeO_2
2. SiO_2
3. $ZnCl_2$
4. butyronitrile
5. $Zr_{46.75}Ti_{8.25}Cu_{7.5}Ni_{10}Be_{27.5}$
6. $Mg_{65}Cu_{25}Y_{10}$
7. $Zr_{41.2}Ti_{13.8}Cu_{12.5}Ni_{10}Be_{22.5}$
8. $Pd_{40}Ni_{40}P_{20}$
9. 1,2-propane diol
10. ethylene glycol
11. $Cu_{47}Ti_{34}Zr_{11}Ni_8$
12. glycerol
13. sorbitol
14. toluene
15. *o*-terphenyl
16. propylene carbonate
17. triphenyl phosphite
18. sucrose

Figure 10.2 The ratio T_K/T_0 as a function of the parameter D (which can be seen as a measure of fragility) for 18 different liquids (see Ref. [33] for details and references on the liquids). Evidently, T_0 is not equal to T_K and the deviation from equality is increasing with increasing D, corresponding to decreasing fragility index. Figure from [33].

Calculating Angell's fragility index of this expression gives $D = \left(\frac{T_g}{T_0} + \frac{T_0}{T_g} - 2\right) m_A$. This means that we have the following

$$\begin{aligned} &D \text{ large} \quad \text{for } \frac{T_g}{T_0} \text{ large ('strong' liquids)} \\ &D \text{ small} \quad \text{for } \frac{T_g}{T_0} \to 1 \text{ ('fragile' liquids).} \end{aligned} \tag{10.10}$$

The trend with larger deviations for strong liquid may not be so surprising, since strong liquids are characterized by obeying a near Arrhenius temperature dependence of the relaxation time. Thus fitting these data with the VFT equation would reveal a T_0 close to 0K. At the same time strong liquids often have high glass transition temperatures $\sim 500 - 1000K$ and correspondingly high T_K.

Regardless of the conclusion of such studies, it is an indisputable fact that they are comparing two temperatures, *none of which are directly measured.* The determination of T_K involves extrapolations of data and T_0 is a parameter from a nonlinear fit. This again underlines how difficult it is to conclusively test the existence of a phase transition below T_g to a totally arrested phase. Below, we rely on experimental facts for the temperature dependence of the dynamics and ask: How convincing is the evidence for the dynamical divergence predicted by the VFT equation?

10.3 Method

It is not possible to directly test the existence of a T_0, since the rapid increase in relaxation time with decreasing temperature makes the equilibration of the liquid much below T_g exceed normal laboratory time scales. So instead of any direct evidence we have to look to circumstantial evidence. We thus return to the fact that the VFT

equation originally introduced as a convenient fitting function for the non-Arrhenius temperature dependence of relaxation times or viscosities.

We believe that if a T_0 indeed exists – and thus theories predicting a VFT like expression for the temperature dependence of the relaxation time are correct – it is reasonable to expect that the VFT equation should fit relaxation time data better than any other simple equations with the same number of fitting parameters.

In order to quantify how well the VFT equation fits data we compare the VFT equation to another popular fitting function [34–36] that is now known as the Avramov equation:

$$\tau(T) = \tau_0 \exp\left\{\left(\frac{B}{T}\right)^n\right\} . \tag{10.11}$$

Versions of the Avramov equation has in the past been used with fixed values of n [37–39]. Letting n be a fitting parameter, however, the Avramov equation has three fitting parameters (two with dimension, and one dimensionless) just as the VFT equation, but no dynamic divergence.

Although the prefactor τ_0 is often regarded as a fitting parameter, we chose to fix it to a physically reasonable value, which leaves only two free fitting parameters in the two equations (see in section 10.5 below for an elaboration on this constraint).

The pre-exponential factor in the Arrhenius equation is interpreted as a microscopic entity related to the *attempt* frequency of crossing some barrier opposing the rearrangement of particles, while the exponential (Boltzmann) factor is the probability of success. τ_0 is thus expected to have phonon like timescales, $10^{-15}\text{s} - 10^{-12}\text{s}$, so we chose to fix $\tau_0 = 10^{-14}\text{s}$.

10.3.1 Selection of relaxation time data

For this method to work accurate data are needed. Dielectric relaxation measurements give the some of the most precise relaxation time data, much more accurate than data from other relaxation processes or from viscosity measurements. For practical reasons the best dielectric data for ultra-viscous liquids come from experiments on molecular organic liquids; these liquids are often easily super-cooled and they are usually convenient to work with.

The analysis is based on an impressive database of dielectric measurements compiled by Albena Nielsen. Some datasets were measured by Albena herself, some by Niels Boye Olsen, and the rest were collected from leading experimental groups: the groups of Peter Lunkenheimer, Ernst Rössler, Ranko Richert, Marian Paluch, and Ricardo Diaz-Calleja.

From the dielectric loss data we identified the relaxation time τ as the inverse loss peak frequency, $\tau \equiv 1/f_{\max}$. The loss peak frequencies were determined by fitting a parabola to the top five data points of the dielectric loss at each temperature. The frequency at which this parabola take its maximum value was defined to be the loss peak frequency (see Fig. 10.3). This method has the advantage of being independent of models, robust, and easy to implement, i.e. identification of this peak frequency can be completely automated. So although the inverse loss peak frequency is not identical to an average relaxation time or even proportional to it (if TTS is not obeyed), it

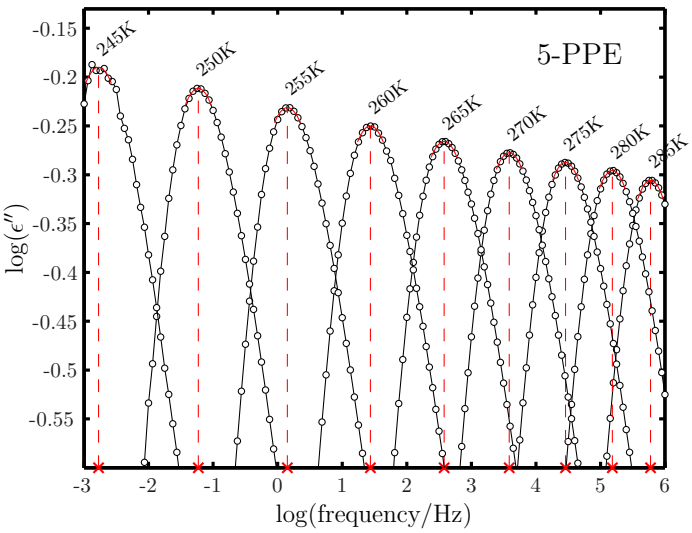

Figure 10.3 Example of the determination of loss peak frequencies (here 5-PPE). For each temperature the data point of maximum value of the dielectric loss is identified. Then a parabola is fitted to this point and two points on either side. The loss peak is now defined as the maximum of this parabola. The plot shows the data (black circles), the fitted parabolas (red solid line), and the maximum of parabolas (red crosses).

nevertheless represents a characteristic time for the liquid and it can be identified in an unbiased way.

The fitting region was limited to relaxation times between 1 μs and 1000 s. This was done for two reasons. First, we compare different fits to different data sets, and restricting the fitting region ensures that all data sets lie in more or less the same dynamical region. Secondly, the restriction was introduced in order to ensure that we do not compare different types of dynamic behavior; otherwise there is the risk that one ultimately tests the two equations ability to interpolate between two different types of dynamic behavior. Thus the lower limit (1 μs) was chosen to ensure that the dynamics are well within the "landscape" dominated domain [40, 41], i.e. well below the crossover temperature (the T_c of mode-coupling theory [26, 42, 43]). The upper limit (1000 s) was chosen to ensure that all data are true equilibrium data. A further requirement was that only data sets covering at least four decades with a minimum of 5 different temperatures were included in the analysis.

In addition, some materials were discarded from the analysis prior to this selection process:

- The analysis was limited to non-polymeric systems because the polymer glass transition may be fundamentally different from the liquid-glass transition [44].
- It is well-established [45–47] that the dominating dielectric process (an intense Debye like process sometimes referred to as the α'-process) in mono-alcohols is not related to the structural glass transition thus making it difficult to accurately determine the peak-position of the true α-process

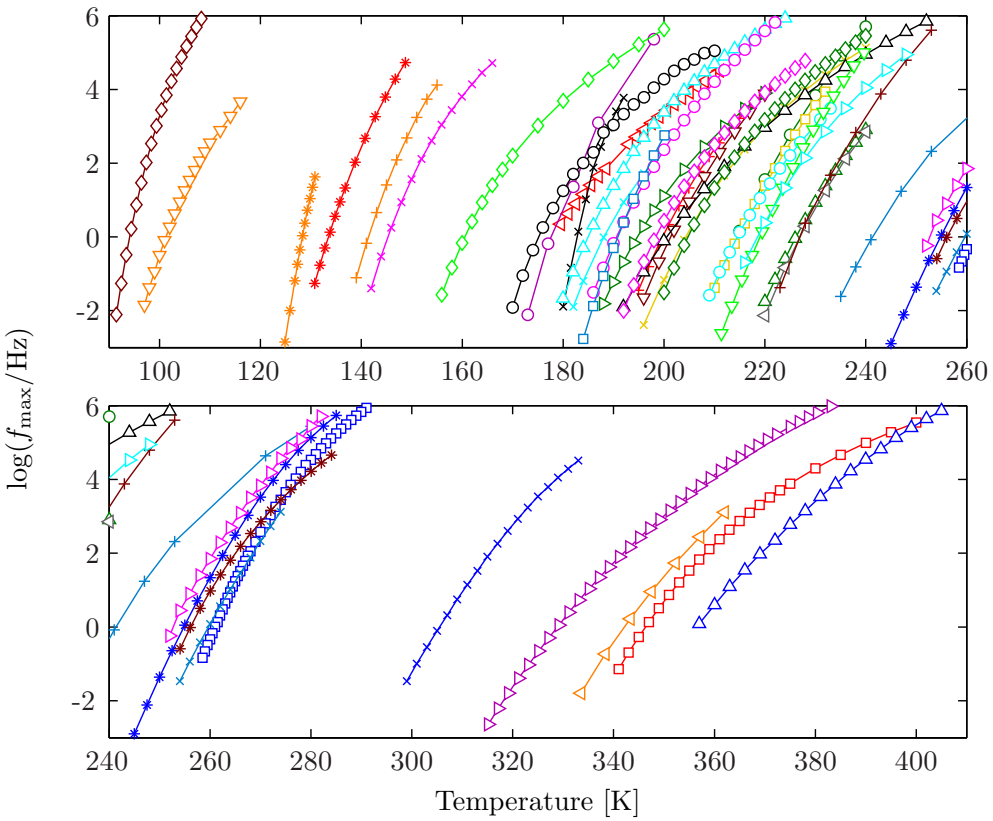

Figure 10.4 The figure shows the data sets used in the analysis (for table of liquids and corresponding symbols, see table 10.1). All liquids clearly exhibit the non-Arrhenius temperature dependence of the relaxation time that generally characterizes ultraviscous liquids.

- Although the dielectric (and other) properties of plastic crystals are similar to those of super-cooled liquids they are not liquids, these systems are *crystalline*, and the origin of the complex dielectric relaxation spectrum is not structural disorder but orientational disorder of an otherwise ordered crystal

Out of an initial selection of datasets for more than 60 different liquids, only 41 met these demands.

Fig. 10.4 shows the analyzed data. Although the analysis was limited to organic liquids, the datasets span quite large region of T_g's (from roughly 90K to about 340K). All liquids exhibit the characteristic non-Arrhenius behavior with a relaxation time that upon cooling increases stronger than predicted by the Arrhenius equation (fragility index of the liquids lie in the region $40 - 160$). All liquids, symbols, and references to where the data were first published are listed in Table 10.1.

10.3.2 Sensitivity of parameters in the models

One initial check to make before we start the fitting routines is the sensitivity of the model output to the fitting parameters. Normally, this is done if one wants an idea of how much fitted values of the parameters can be trusted – especially if the physical interpretation of a fitted value is meaningful. Obviously, if the model is insensitive to some parameter, the fitted value has little meaning.

This is of course not particularly interesting if the equations were merely regarded as fitting functions, but since we are looking for evidence for the existence of a T_0 this is relevant.

The sensitivity matrix (see appendix D) is a matrix with columns corresponding to the number of fitting parameters and rows corresponding to the number of data points, and each entry is the derivative of the model with respect to one of the parameters evaluated in a specific point.

The logarithmic derivatives of the VFT equation is given by

$$\frac{\partial \ln \tau_{\mathrm{VFT}}}{\partial \ln A} = \frac{A}{T - T_0}, \qquad \frac{\partial \ln \tau_{\mathrm{VFT}}}{\partial \ln T_0} = \frac{AT_0}{(T - T_0)^2}. \tag{10.12}$$

And in the case of the Avramov equation we get

$$\frac{\partial \ln \tau_{\mathrm{Avramov}}}{\partial \ln n} = n \left(\frac{B}{T}\right)^n \ln\left(\frac{B}{T}\right), \qquad \frac{\partial \ln \tau_{\mathrm{Avramov}}}{\partial \ln B} = \left(\frac{B}{T}\right)^n \left(\frac{1}{n}\right). \tag{10.13}$$

In the case of the VFT equation, the sensitivity matrix (for a liquid with N data points) will look like this

$$S_{\mathrm{VFT}} = \begin{pmatrix} \frac{A}{T_1 - T_0} & \frac{AT_0}{(T_1 - T_0)^2} \\ \frac{A}{T_2 - T_0} & \frac{AT_0}{(T_2 - T_0)^2} \\ \vdots & \vdots \\ \frac{A}{T_N - T_0} & \frac{AT_0}{(T_N - T_0)^2} \end{pmatrix} \tag{10.14}$$

Evaluation the sensitivity matrices for several liquids with some initial guesses for the parameters reveals that both the VFT and Avramov equations are sensitive to both their parameters.

10.3.3 Correlations between parameters

The next step is a check for correlations between parameters. Again, if two parameters are close to 100% correlated it is not possible to determine each of them uniquely – only a combination.

A standard way to check for correlations between parameters is the normalized covariance matrix (see appendix D). This is a symmetric matrix with ones in the diagonal and the ij^{th} entry shows the correlation between parameter i and j. Since we are only dealing with two parameters this is a 2×2-matrix with only one interesting entry (the off-diagonal element).

For the VFT equation this gives the following correlation factor between A and T_0

$$c = \frac{\sum_{l=1}^{N} \left(\frac{1}{T_l - T_0}\right)^3}{\sqrt{\sum_{l=1}^{N} \left(\frac{1}{T_l - T_0}\right)^4 \sum_{l=1}^{N} \left(\frac{1}{T_l - T_0}\right)^2}} \tag{10.15}$$

where the subscript l denotes the points where the model was calculated. It is obvious that $|c| \leq 1$. We can also see that if we have only one point, the two parameters then $|c| = 1$. Of course increasing the number of (data) points will decrease the correlation, but the sums in Eq. (10.15) will always be dominated by the data point(s) closest to T_0, and one would consequently expect the correlation factor to be close to one.

Indeed, evaluating c for a number of datasets with some initial guesses for parameters, reveals that the two parameters for both VFT and Avramov equations are highly correlated ($c > 0.95$). From this analysis it seem that there is little hope to determine T_0 (or any of the other parameters) uniquely, but in the stability test of the section below the picture is a little less pessimistic.

10.3.4 Details of the fitting routines

The VFT and Avramov equations were fitted to data using the least-squares method. The procedure for selecting data sets for the analysis, as well as the subsequent fitting procedures, were fully automated via MatLab routines.

Initial guesses to feed the fitting routines were established via a linearization of both equations

$$\text{VFT-equation:} \qquad \frac{1}{\ln \frac{\tau}{\tau_0}} = \frac{1}{A} T - \frac{T_0}{A} \tag{10.16}$$

$$\text{Avramov equation:} \qquad \ln \ln \frac{\tau}{\tau_0} = \ln B - n \ln T \tag{10.17}$$

The linear regression ($y = ax + b$) to this representation provides us with initial guesses for the fitting parameters since calculation shows

$$n = -a, \;\; B = \exp(b) \tag{10.18}$$

for the Avramov equation, and in the case of the VFT equation we obtain

$$A = \frac{1}{a}, \;\; T_0 = -\frac{b}{a}. \tag{10.19}$$

We checked the robustness of the fits by varying the parameters 70% to either side from these initial guesses. In Fig. 10.5 we show a representative example of the outcome.

Fits to the Avramov equation are very stable. Varying the initial guess 70% to either side of the guess presented above in Eq. (10.18), yields the same average error with very little variation in the fitted values for the fitting parameters (see figure 10.5, right column). To illustrate how small the deviations are for the Avramov equation we plotted the fitted values for B and n minus the average value. The deviation (in absolute numbers) for n is thus $\sim 10^{-8}$ and $\sim 10^{-6}$K for B (for *all* liquids), i.e. for

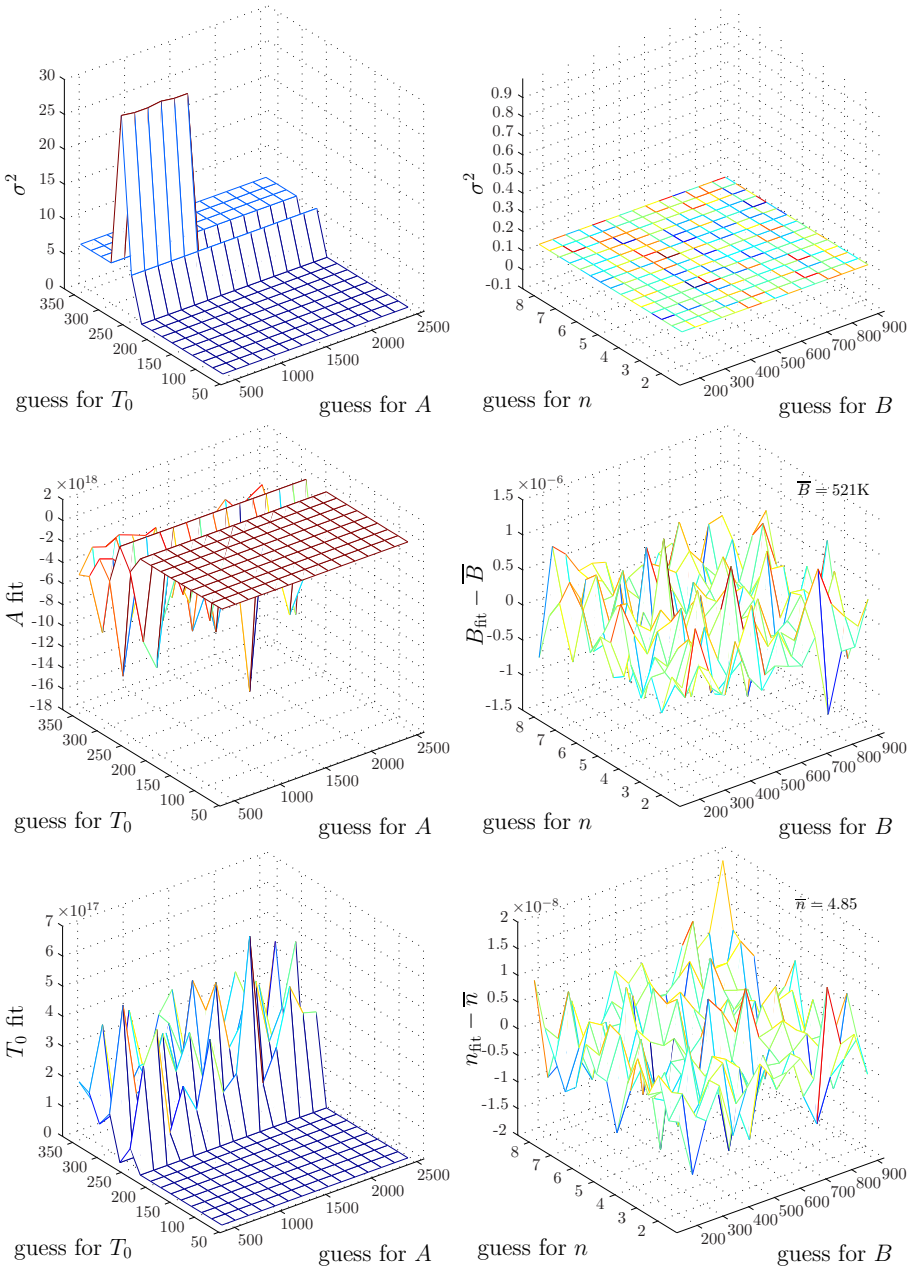

Figure 10.5 Example (5-PPE) of the robustness of the fits (left column: VFT equation, right column: Avramov equation). Top row shows the squared standard deviation (defined in Eq. (10.20)) plotted against the initial guesses of the parameters, second and third rows show the fitted values of the parameters as a function of the initial guesses.

all practical matters the fits give identical parameters. The VFT equation shows a similar stability as long as the guess for T_0 is not too close the lowest temperature of the dataset. If this condition is not met, the fits go crazy, giving rise to high standard deviations and nonsense values for the fitted parameters.

The correlations between parameters is also evident doing this analysis – the stability plots for the fitted values of the parameters are practically mirror images of each other (although it can be difficult to see in the 3D plots). Having said that though it is also quite clear that the variations in the parameters are very small, so as stated above, it is safe say that the parameters are uniquely determined (for reasonable initial guesses).

These conclusions are of course completely dependent on the fitting algorithm. We used a predefined function in MatLab, `fminsearch`, which (as we have shown) is sufficiently robust.

10.4 Analysis and results

Examples of fits are shown in Fig. 10.6 with VFT fits in solid lines and Avramov fits in dashed lines. Overall, both equations fit well. For a detailed comparison of the two fitting functions we use the standard deviation formula

$$\sigma = \sqrt{\frac{1}{N-p}\sum_{i=1}^{N}\left(\log(\tau_{\mathrm{fit},i}) - \log(\tau_{\mathrm{data},i})\right)^2} \tag{10.20}$$

where N is the number of data points and $p = 2$ is the number of degrees of freedom. Fig. 10.7 shows σ_{VFT} and $\sigma_{\mathrm{Avramov}}$ for all liquids. For clarity the numbers are sorted in descending order from "worst fit" to "best fit", a clever suggestion of Ulf R. Pedersen. Arranging the numbers in this manner makes any differences in the fitting ability between the two equations visually clearer. However, this also means that two points on a vertical line are not necessarily from the same liquid and should not be compared. In this representation it is clear the VFT equation generally fits data better than the Avramov equation.

Inspecting the fits (in Fig. 10.6 as well as those not shown) shows that deviations are rather systematic. Thus highly non-Arrhenius liquids, i.e. data sets with large curvature, are generally poorly fitted by the Avramov equation. Apparently, the Avramov equation is not able to "bend" enough to capture the curvature of these data sets. Is this a signal of the dynamic divergence predicted by the VFT equation? In order to look into this question we investigate how the activation energy changes with temperature by use of the temperature index defined [48] by

$$I \;=\; -\frac{d\ln\Delta E}{d\ln T}\,. \tag{10.21}$$

The temperature index quantifies the activation-energy temperature dependence in a way that is independent of the unit system, much like the Grüneisen parameter of the solid state physics. If for instance the temperature index is five, lowering the temperature by 1% leads to a 5% increase of activation energy. The temperature index is related to Angell's fragility index by

$$m_A = c(1 + I(T_g)) \tag{10.22}$$

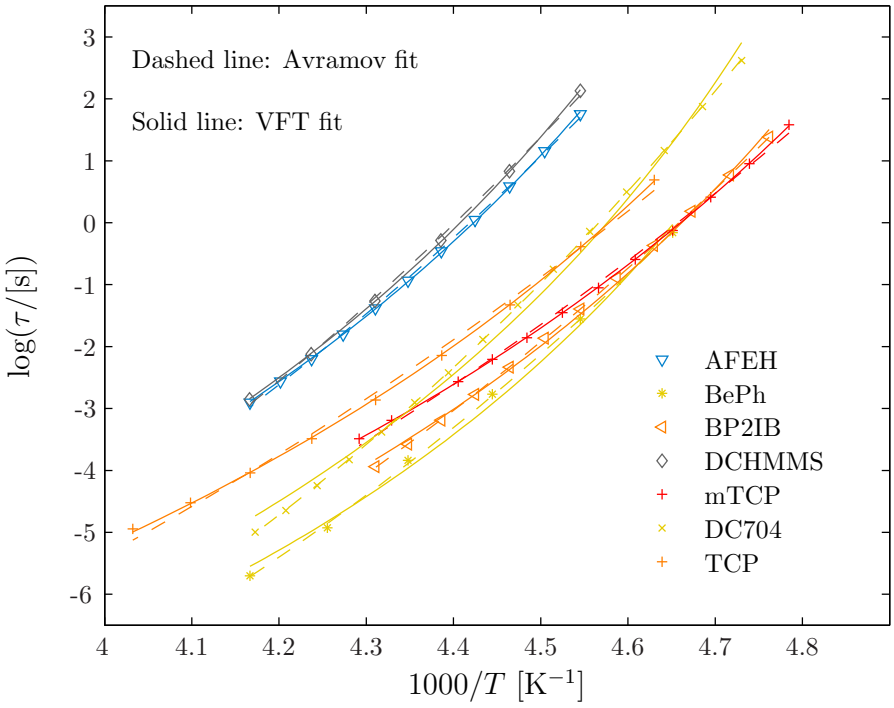

Figure 10.6 Examples of fits with the VFT equation (solid lines) and the Avramov equation (dashed lines). In some cases it is hard to distinguish between the two fits, but there are examples where VFT equation is superior to the Avramov equation and vice versa. In all cases both equations fit rather nicely.

where $c = \log_{10}(\tau(T_g)/\tau_0) = 16$ if $\tau_0 = 10^{-14}$ and the glass transition temperature is defined by $\tau(T_g) = 100$ s.

For the Avramov equation the temperature index is constant, $I^{\text{Avramov}} = n - 1$. For the VFT equation one finds

$$I^{\text{VFT}} = \frac{T_0}{T - T_0}\,. \tag{10.23}$$

Thus the VFT temperature index increases upon cooling and it diverges at $T = T_0$. Fig. 10.8 shows the numerically calculated temperature indices. For nine out of ten liquids the temperature index increases with decreasing temperature. This explains why the VFT equation fits data better than the Avramov equation.

The temperature index is also useful for throwing light on how strong the evidence for the existence of a dynamic divergence is. First, we chose the eight liquids that are best fitted by the Avramov equation. Fig. 10.9 (left) shows the actual and the VFT-predicted temperature indices for these liquids. There is very little agreement between the fits and the actual values; in some cases (i.e. DC704 and TPE) it seems almost ridiculous to impose a VFT functional form. If we instead look at some of the liquids that are best fitted by the VFT equation (Fig. 10.9 right) we can on one hand

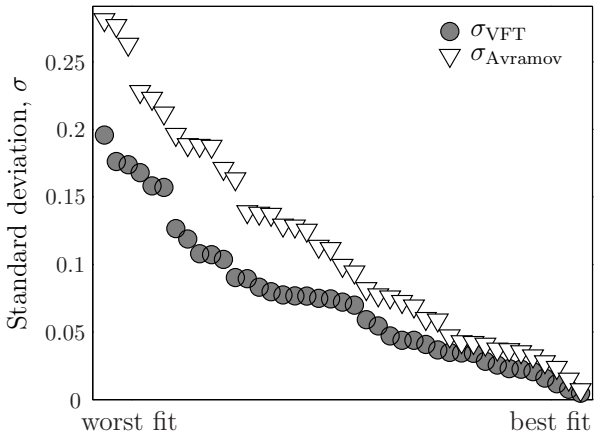

Figure 10.7 Standard deviation from fits to data of the VFT equation and the Avramov equation. For clarity the numbers have been arranged in descending order for each of the two fits. As a consequence two points on a vertical axes do not in general belong to the same liquid. Plotted this way it is evident that the VFT-equation on average fits data better than the Avramov equation.

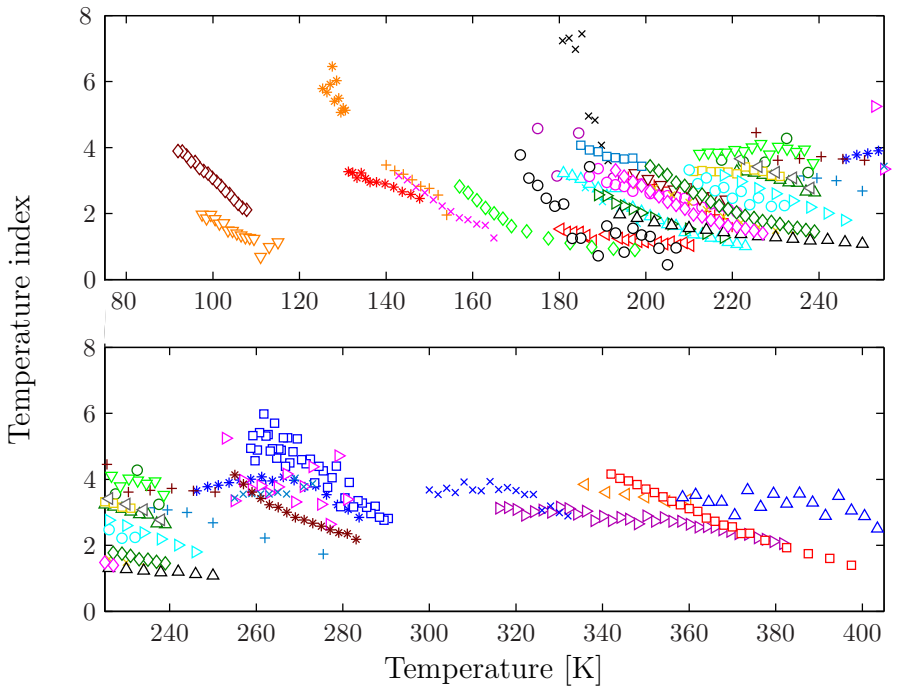

Figure 10.8 The graph shows the temperature index (eq. 10.21) as a function of temperature for all liquids. With a few exceptions, the temperature index increases with decreasing temperature. This feature is captured by the VFT equation while the Avramov equation predicts a temperature independent index.

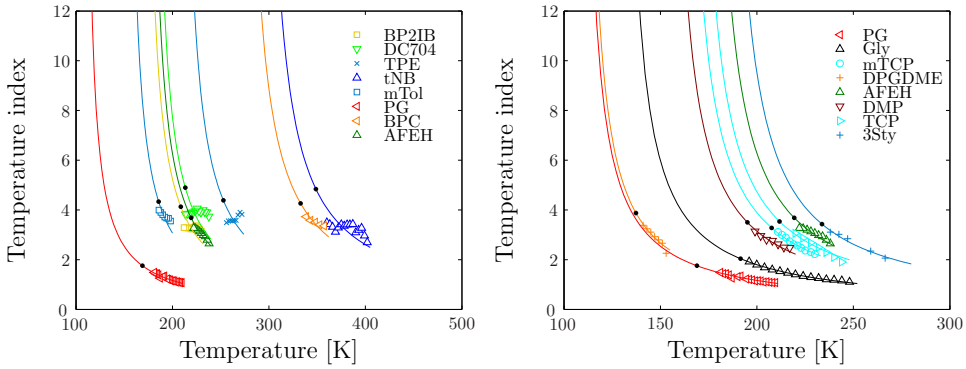

Figure 10.9 The temperature index for the liquids where VFT equation (right), respectively the Avramov equation (left), fits best. The full lines show the VFT predicted temperature indices that diverge at a finite temperature. There is little compelling evidence for such a divergence in the data. In both subfigures the black dot marks the glass transition temperature determined by an extrapolation of the VFT equation to $\tau = 100$s.

say, the data are not inconsistent with a dynamic divergence. On the other hand, one cannot reasonably say that there is compelling evidence for the VFT extrapolation.

10.4.1 Fitting of different dynamic regions

Now we have more or less established that the evidence for a dynamic divergence is inconclusive. Another question that could be relevant for clarifying the issue is: how much do the fitting parameters change with the fitting region? If we have a correct model we would expect that the fitting parameters do not depend too much on the fitted region.

For this analysis we selected datasets that span a wide dynamical window. Instead of the selection criteria used above we selected the liquids spanning at least 5.5 decades in the region where $10^{-3} < \tau < 10^{6}$ and measured at least 9 different temperatures. 21 datasets met these requirements.

Fig. 10.10 shows the fitting parameters of the VFT and Avramov equations fitted to different dynamical regions ($[10^{-6}-10^{0}]$s, $[10^{-5}-10^{1}]$s, $[10^{-4}-10^{2}]$s, and $[10^{-3}-10^{3}]$s), normalized to the fitted value at the highest temperatures (shortest times) of the given parameter. From these plots we can see that for the Avramov equation the changes in fitting parameters with changing dynamical region is systematic as well as monotonic: lowering the temperature region that is fitted, leads to an increase in n while B decreases (with a few exceptions showing no change). This is also what we would expect because the temperature index is increasing with decreasing temperature and $I^{\text{Avramov}} = n - 1$.

For the VFT equation there seems to be no clear trend in the changes in fitted values, although the changes are monotonic. It is however clear that there is a correlation between A and T_0 (as we already predicted earlier); when one increases, the other one will decrease and vice versa. A maximum of 10% change in T_0, however, may not

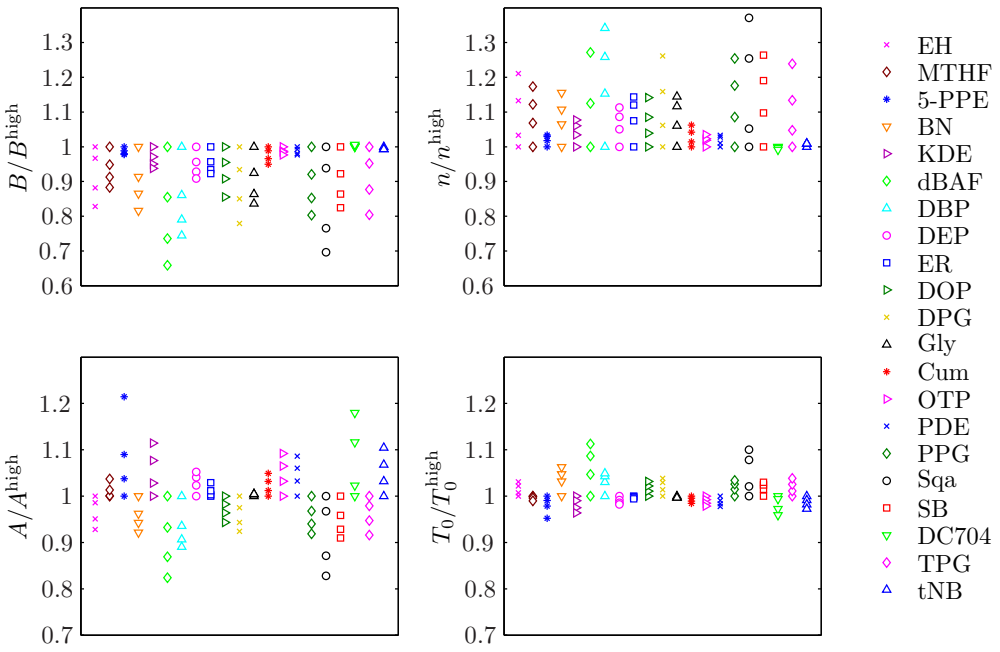

Figure 10.10 The fitting parameters of the VFT and Avramov equations fitted to different dynamical regions ($[10^{-6} - 10^{0}]$s, $[10^{-5} - 10^{1}$s], $[10^{-4} - 10^{2}]$s, and $[10^{-3} - 10^{3}]$s), normalized to the fitted value at the highest temperatures (shortest times) of the given parameter.

be significant enough to draw any conclusions regarding the evidence for a dynamic divergence.

10.5 Influence of the choice of pre-factor

So far we have not treated the pre-factor, τ_0, as a fitting parameter. The choice of τ_0 does however influence the fitting results. There are several ways of examining this. One is to vary the fixed value and monitor the changes in fitting ability of the VFT and the Avramov equations. Another is to let the pre-factor be a free fitting parameter. Below we will explore both options.

Starting with the former, Fig. 10.11 shows the sum of deviations for all 41 liquids when varying the τ_0 from 10^{-6}s to 10^{-20}s for both the VFT and the Avramov equation. The fits are clearly quite sensitive to this parameter, both curves have an asymmetric shape rising sharply when τ_0 increases and also somewhat less dramatically when τ_0 is lowered. In between the two extremes there is a minimum for both equations, occurring in the case of the Avramov equation around $10^{-10} - 10^{-9}$s, and in the case of the VFT equation around $10^{-15} - 10^{-14}$s. One could say that the physically meaningful pre-factor are friendlier to the VFT equation than the Avramov equation. However, the two curves cross at $\tau_0 = 10^{-12}$s, which means that for this choice of pre-factor Avramov equation fits the data just as well the VFT equation.

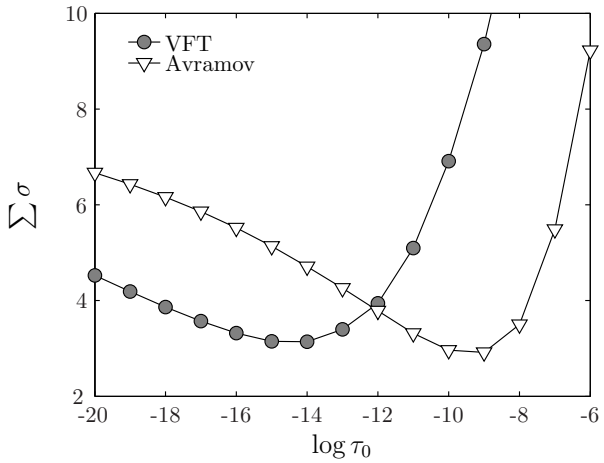

Figure 10.11 The sum of deviations for all liquids in the study for different choices of the pre-factor τ_0. The fits are clearly quite sensitive to this parameter.

The choice of pre-factor also influences the temperature index. This is illustrated in Fig. 10.12 where the temperature index for cumene is plotted for τ_0 varying as above. Not only does the absolute values change quite a bit; also the temperature dependence of the index does in some cases change from increasing with decreasing temperature to the opposite. Interestingly, there exists a value of τ_0 for which the temperature index is constant (marked with a dashed line). This observation also holds true for almost all other liquids studied here (see Fig. 10.16 for further support of this postulate). This is by no means trivial. But it also shows that the temperature index is quite sensitive to the choice of pre-factor. On the one hand this represents the most serious objection to using the temperature index method of quantifying the temperature changes of activation energy. On the other hand for physically reasonable values of τ_0 the overall picture is pretty clear.

Now we will turn to the other option for examining the influence of the choice of pre-factor: letting τ_0 be a free fitting parameter. In Fig. 10.13 the results of this is shown and it is evident that with three free fitting parameters, there is absolutely no reason to prefer the VFT equation over the Avramov equation. The inset shows a histogram over the fitted pre-factors and as one would expect from figure 10.11 the "distribution" peaks around 10^{-9}s for the Avramov equation while the VFT "distribution" peaks around 10^{-12}s, but has a somewhat higher mean value.

10.5.1 What can and cannot be learned from different data representations?

In the following we will present two temperature derivative analysis methods and apply them to our sets of data. In contrast to the temperature index analysis, there are no assumptions regarding the pre-factor and thus it is merely a way presenting data – in fact they correspond to (as we will show) a linearisation of the VFT equation and the Avramov equation, respectively, with three fitting parameters (two for the linear regression and one for the constant of integration).

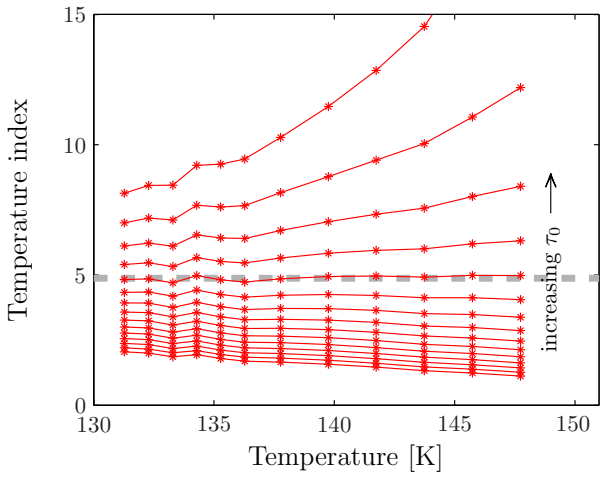

Figure 10.12 An example (here cumene) of the influence the choice of τ_0 has for the temperature index. It is evident that a low pre-factor ($\tau_0 < 10^{-11}$) results in an index that increases with decreasing temperature where as the exact opposite behavior can be obtained with a high pre-factor ($\tau_0 > 10^{-9}$); in between there is a choice of pre-factor that gives a constant index (in this case $\tau_0 \approx 10^{-10}$). This behavior is general.

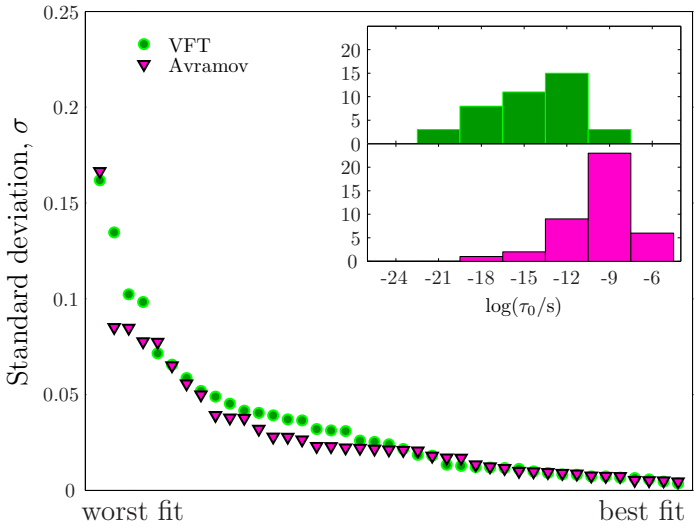

Figure 10.13 Error of the fits varying all three parameters (including the pre-factor, τ_0) of the VFT and Avramov equations. The inset shows a histogram over the fitted values of the pre-factor; as one would expect from figure 10.11 the "distribution" peaks around 10^{-9} for the Avramov equation while the VFT "distribution" peaks around 10^{-12}, but has a somewhat lower mean value.

The first is a commonly used way plotting relaxation time data, sometimes called Stickel-analysis after the author of [49]. The analysis is based on the VFT equation: we observe that if the temperature dependence of the relaxation time can be described by the VFT equation, then we can write

$$\frac{d}{dT}\ln\tau^{\mathrm{VFT}} = \frac{d}{dT}\left\{\frac{A}{T-T_0}\right\} = -\frac{A}{(T-T_0)^2} \tag{10.24}$$

and thus we have

$$s := \left(-\frac{d\ln\tau}{dT}\right)^{-1/2} = \frac{1}{\sqrt{A}}(T-T_0) \tag{10.25}$$

i.e. plotting (T, s) we should get a straight line, if the VFT equation is a correct description of data. This rarely gives a straight line if a large dynamical window is considered. The main point made by Stickel *et al* [49] was in fact that the VFT equation alone could not describe the entire data set.

In our case we have restricted ourselves to the viscous region just above T_g, so let us nevertheless proceed to carry out this analysis on the data we have used here. The results can be inspected in Fig. 10.14. The x-axis has been shifted by T_g to squeeze the data sets a little closer together. Most data sets seem to follow a relatively straight line, although there are also examples of clear deviations from that, e.g. PDE, KDE, 5-PPE, and MTHF are all distinctly convex.

The Stickel plot offers an easy way of determining T_0: this is simply the intersection of the extrapolation of a straight line through the data points with the x-axis. If T_0 has a physical meaning it should not depend (too much) on which points are included in the fit. We do an analysis similar to that of section 10.4.1 and determine T_0 for the different dynamical regions.

In Fig. 10.15(a) a Stickel plot of the same subset of data used in section 10.4.1 is shown. From Fig. 10.15(b) it is obvious that for most liquids T_0 changes quite significantly depending on the fitting region. For most liquids, T_0 decreases, the fitting region moves to lower temperatures. For a few it decreases or remains more or less constant. It also seems to be a gradual change rather than a kink between two different "VFT regions". In Fig. 10.15(c) we show two extreme examples of changes in T_0; for dBAF T_0 increases when the temperature region fitted is lowered, while 5-PPE shows the opposite behavior. The dotted line is a linear regression line to the entire region (gives the "average" T_0).

The general problem with this analysis is that the Stickel plot visually understates how dramatic a divergence is. At the same time it emphasizes the high temperatures, which is unfortunate since the relaxation time dramatically changes when T_g is approached while not much is happening at higher temperatures. So plotting a quantity like s linearly in temperature may lead to some unjustified extrapolations: It is easy to ascribe a "wiggle" at the end of this curve to noise, while in fact this is where the interesting physics is going on (and also where the VFT equation is expected to work).

A clever way of focussing on the timescales rather than the temperatures, is to put $\log f_{\max}$ (or $\log\tau$) on the x-axis. Defining a temperature dependent fragility (much like the temperature index) one gets a quantity that does not depend on the choice of pre-factor:

$$m(T) := \frac{d\log f_p}{d\ln T} \tag{10.26}$$

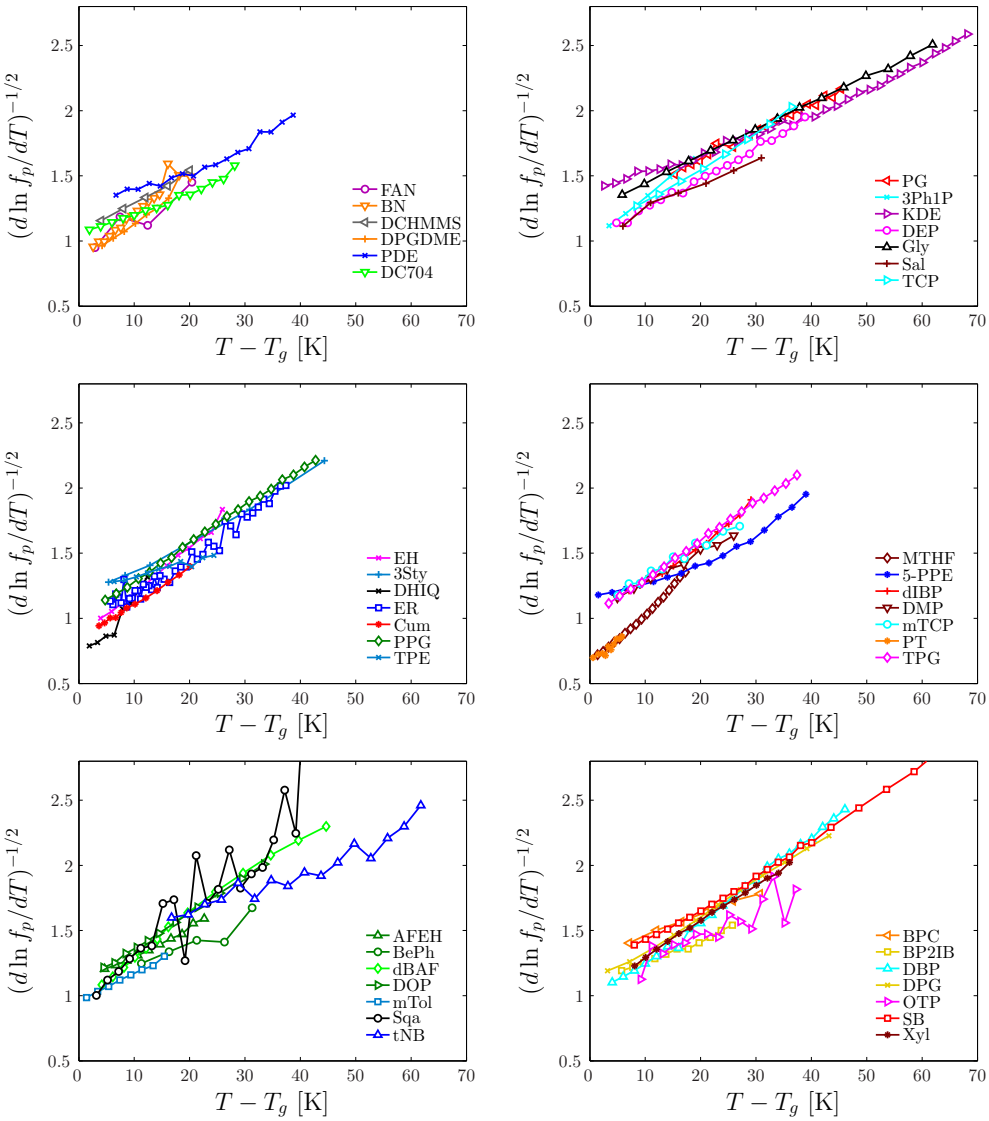

Figure 10.14 Here the Stickel-plots for all of the data sets used in the analysis. The x-axes is shifted by T_g to squeeze the datasets closer together. The data were split in six windows to avoid too busy plots.

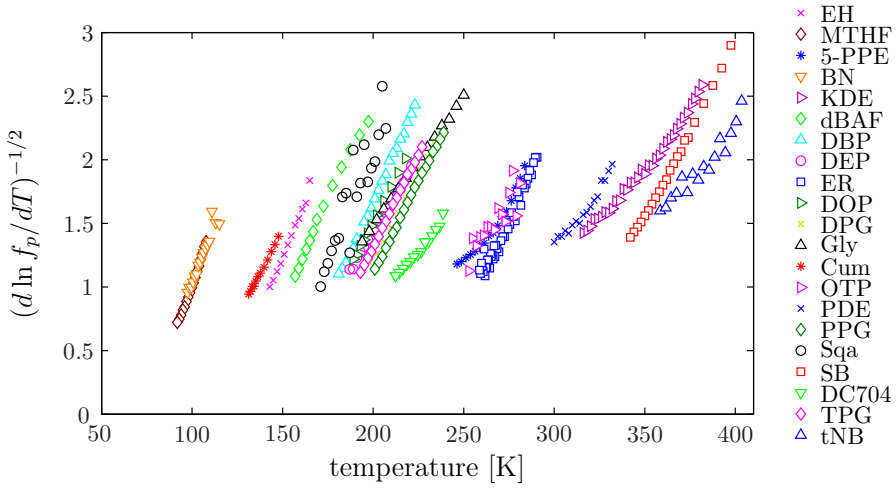

(a) Regular Stickel-plot for the 21 liquids covering the largest dynamical range.

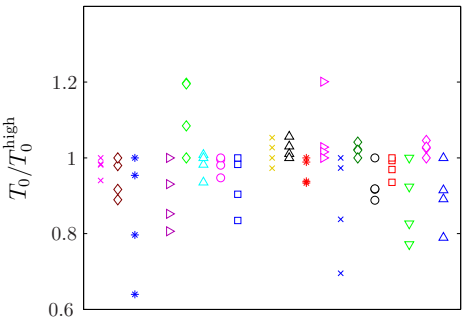

(b) T_0 for different fitting regions

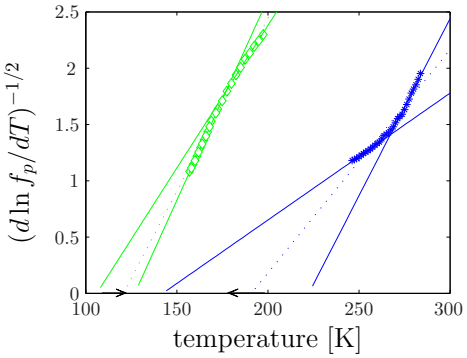

(c) Two examples of how T_0 changes

Figure 10.15 T_0's dependence on the fitting region in the Stickel plot. Left figure shows the fitted T_0 for different fitting regions (normalized to the high temperature value) for 21 liquids. Right figure shows two extreme examples of changing T_0: PPE where T_0 decreases dramatically, and dBAF with the opposite behavior. Dashed lines is a linear regression line to the entire region and thus gives the "average" T_0-value.

where f_p is the loss peak frequency. Taking the value of this function at T_g will give us the Angell fragility index

$$m(T_g) = \left.\frac{d\log f_p}{d\ln T}\right|_{T_g} = \left.\frac{d\log(1/f_p)}{Td(1/T)}\right|_{T_g} = \left.\frac{d\log(1/f_p)}{d(T_g/T)}\right|_{T_g} = m_A \tag{10.27}$$

with our definition of relaxation time, $\tau = \frac{1}{f_{\max}}$.

It was discovered by Niels Boye Olsen that data seem to follow a straight line if this quantity was plotted as a function of the logarithmic loss peak frequency. This is shown in Fig. 10.16.

It seems we have the following

$$\frac{d\log f_p}{d\ln T} = a\log f_p + b\,, \tag{10.28}$$

and if we integrate this we get

$$f_{\max}(T) = 10^{-b/a}\exp\left\{\frac{\ln 10\exp(aC)}{a}T^a\right\} \tag{10.29}$$

where C is a constant of integration. With the following definitions: $n = -a$, $B = -\ln 10^{-1/a}\exp(-C)$ and $f_0 = 10^{-b/a}$, this is exactly the Avramov equation.

So although the connection is more subtle than in the Stickel analysis, the "fragility" analysis is a way of linearizing the Avramov equation.

Two things are worth noting in this context. 1) It is obvious that the Angell's fragility index is *not* a material constant (such as a melting temperature), but highly dependent on the definition of T_g. If the definition of T_g instead of $\tau(T_g) = 100s$ were $\tau(T_g) = 1s$ then m would be lower. 2) It is also obvious that the curves in the "fragility" plot do not have the same temperature dependence. Most seem to follow straight lines in this plot, only with different slopes. This means that some of these lines will cross each other and thus changing the definition of T_g should in principle affect (and possibly spoil) many correlations found between fragility and other quantities.

However, for all liquids m is a decreasing function of $\log f_{\max}$. This means that to some extent some correlation with fragility index will not be entirely lost if the definition of T_g changes. In Fig. 10.17 we have illustrated this by correlating m at the usual definition of T_g with m at a definition of $\tau(T_g) = 1$s. The dashed line represents perfect correlation, and each data point is a liquid. Clearly, the correlation is not completely lost, although the data points now are a somewhat scattered.

10.6 Fitting functions without divergence

The previous section showed that there is no reason to prefer the VFT equation over the Avramov equation when all three parameters are allowed to vary, and hence no sign of a dynamic divergence (according to the ansatz we have made).

But one might ask: is this a fair argument? We fixed the pre-factor precisely to ensure a possible physical interpretation of the parameter T_0, and should we now be willing to accept unphysical values of the pre-factor?

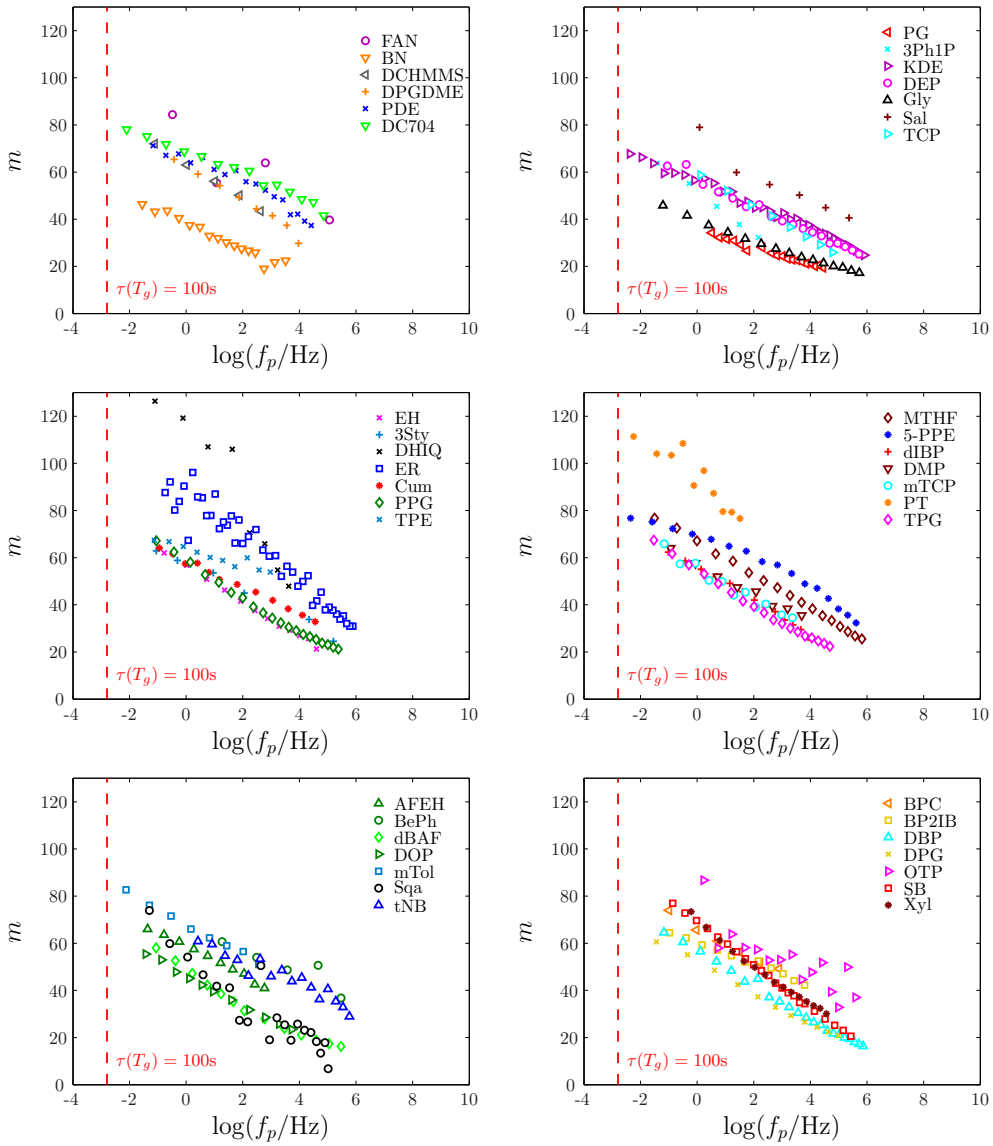

Figure 10.16 Fragility-index (defined as $m_T \equiv \frac{d \log f_{\max}}{d \ln T}$) a function of temperature. At T_g this corresponds to fragility index defined by Angell. The vertical lines mark the glass transition defined via the equation $\tau(T_g) = 100$s.

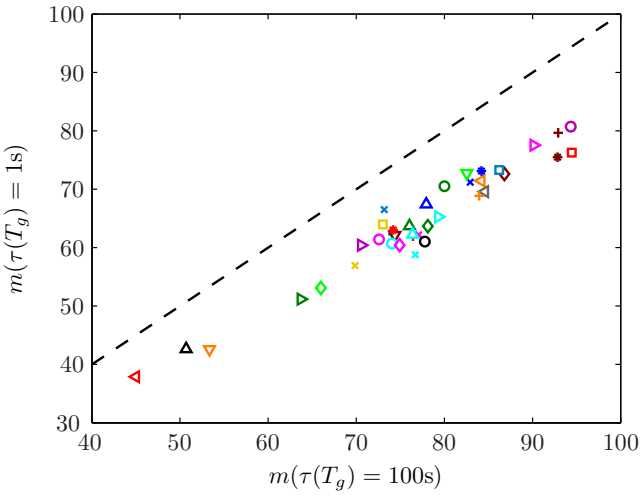

Figure 10.17 The correlation of m with the usual definition of T_g with m with a different definition of T_g. The dashed line represents a perfect correlation. Clearly, the correlation is not entirely lost when the definition of T_g is changed, but significant scatter is introduced.

Maybe not, and thus we proceed to construct a fitting function that has an increasing temperature index upon cooling, but no dynamic divergence (recall that our analysis in section 10.4 showed that the superiority of the VFT fits were due to it's prediction of an increasing $I(T)$ with decreasing temperature). If we, however, want to compare any such function to the VFT equation, the number of free fitting parameters should be the same. Since one free parameter is reserved to the constant of integration, we are left with one, and thus it is a game of finding monotonically decreasing functions of only one parameter (which for instance rules out a linear expression). We consider to such functions, $I = \frac{T_1 - T}{T}$ (FF1) and $I = \left(\frac{T_2}{T}\right)^2$ (FF2). By integration one finds

$$\Delta E \propto T \exp\left(\frac{T_1}{T}\right) \quad \text{(FF1)} \tag{10.30}$$

$$\Delta E \propto \exp\left(\frac{T_2^2}{2T^2}\right) \quad \text{(FF2)} \tag{10.31}$$

In Fig. 10.18 the standard deviations from fit to data of the VFT equation and the two fitting functions, FF1 and FF2, are shown, and it is clear that FF1 and FF2 fits data at least as well as the VFT-equation. In Fig. 10.19 we show the same liquids as in Fig. 10.9 (i.e. the eight liquids best fitted by the Avramov (upper panel) and VFT (lower panel) equations) and we see that the FF1 and FF2 predictions are in good agreement with the data and makes what seems reasonable extrapolations to lower temperatures compared to the VFT equation.

We can also subject these new functions to the same analysis as in section 10.5, and we find that FF1 and FF2 in all areas perform at least as well as the VFT equation. In Fig. 10.20 we show the dependence of the choice of pre-factor (compare Fig. 10.11). We clearly see that FF1 and FF2 fits as well as the VFT equation for low values of the

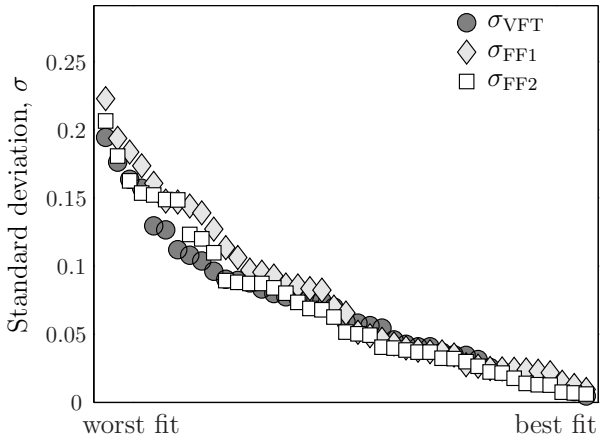

Figure 10.18 The figures shows the mean squared distance from data point to the fit for the VFT equation compared to the new fitting functions, FF1 (Eq. (10.30)) and FF2 (Eq. (10.31)). There is no significant difference in the ability to fit data between the three functions.

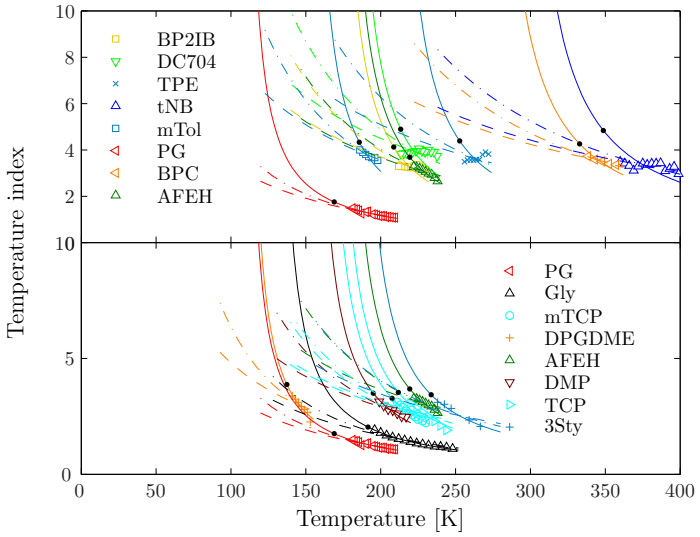

Figure 10.19 The temperature index for the liquids where Avramov equation (upper panel), respectively the VFT equation (lower panel), fits best. Dashed lines are the predicted temperature index for FF1, and dash-dotted lines are the FF2 prediction.

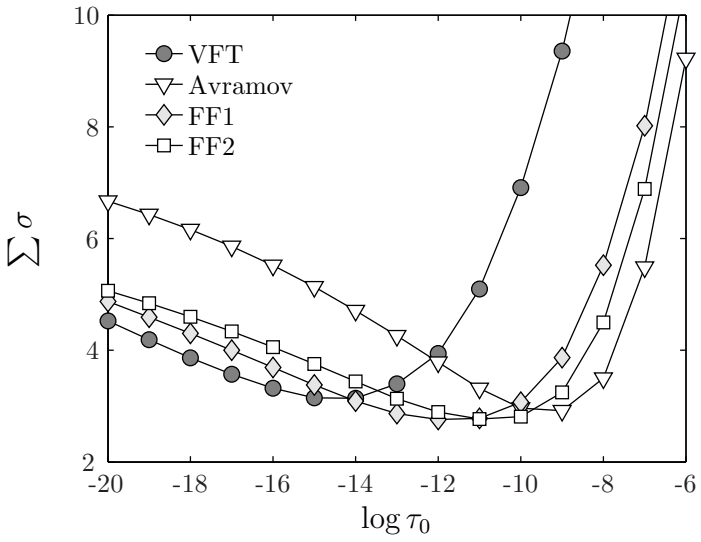

Figure 10.20 The sum of deviations for all liquids in the study for different choices of the pre-factor τ_0. The fits are clearly quite sensitive to this parameter, but for the physically meaningful values of τ_0 the conclusion is that the VFT equation fits better than the Avramov equation.

pre-factor, better for intermediate, and as well as the Avramov equation for the really high values of the pre-factor.

These two fitting functions, FF1 and FF2, were chosen rather arbitrarily and too much emphasis should not be put on the functional form of these. Interestingly, however, a recent publication from Mauro *et al.* [50] arrive at an expression for the temperature dependence of the activation energy quite similar to FF1

$$\Delta E(T)/k_B = K \exp\left(\frac{C}{T}\right). \tag{10.32}$$

10.7 Discussion and conclusions

We have shown that for a large body of dielectric data, the VFT-equation and the Avramov-equation both generally fit very well, but the VFT-equation on average fits slightly better *when the pre-factor τ_0 is fixed at a physcially reasonable value.* If this restriction is relaxed the two functions fit data equally well.

It was also shown that (for physically meaningful values of τ_0) the temperature index with few exceptions increases upon cooling, an interesting fact by itself. This means that not only is the activation energy increasing with decreasing temperature, it is increasing with increasing rate. This feature is captured by the VFT equation, while the Avramov equation predicts a constant temperature index. Other fitting functions with an increasing temperature index and no dynamic divergence are shown to fit data at least as well as the VFT equation.

This fact indicates that there is no convincing evidence for a dynamic divergence at a finite temperature. As pointed out already by Harrison, both the Avramov and the VFT equations are convenient for interpolation of experimental data, but extrapolation outside the experimental range should not be carried out with any degree of confidence, nor should any physical meaning necessarily be assigned to these equations [34].

We limited the analysis to a dynamical region where we believe the dynamics are dominated by the energy-landscape. It can of course be discussed where exactly is the cross-over in dynamics is taking place, but the conclusions drawn here are still valid if one restricts the fitting region to the ultra-viscous region ($10^{-3} < \tau < 10^{3}$), as we show in Fig. 10.21.

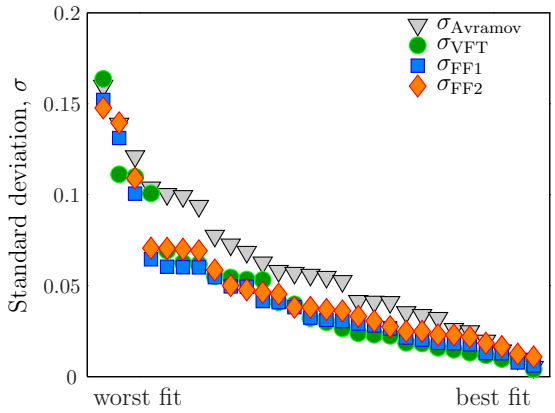

Figure 10.21 The mean squared error of VFT and Avramov equations as well as FF1 and FF2 when restricting the fitting region to the ultra-viscous region just above T_g (10^{-3}s $< \tau < 10^{3}$). This decreased the number of liquids to 28, but the result are very similar. If anything, restricting the fitting region closed the gap between the VFT equation and the Avramov equation.

A clever way to extend the range of relaxation times beyond those obtainable by linear relaxation experiments is to consider results from ageing experiments. Studies by McKenna, Simon, Plazek and co-workers – mainly on polymeric systems – show that the VFT prediction is not followed when systems are aged into equilibrium by annealing for sufficiently long time slightly below the glass-transition temperature [51–53]. In Fig. 10.22 we show their results on the molecular glass-former *m*-toluidine and a polymer, polystyrene.

Although the accuracy of these experiments is not comparable to that of dielectric relaxation experiments on the metastable equilibrium phase, it was nevertheless possible to conclude that the relaxation times deviate from the VFT equation by always increasing less markedly when lowering temperature than predicted by the VFT equation. These results are fully consistent with the above conclusion and including polymeric systems in the analysis would not have changed the outcome [54, 55].

In this study only organic glass-formers were studied. However, a related study by Mauro *et al* [50] on a range of oxide glasses show similar results. These authors find that in general the VFT and Avramov equations fit equally well (varying all three

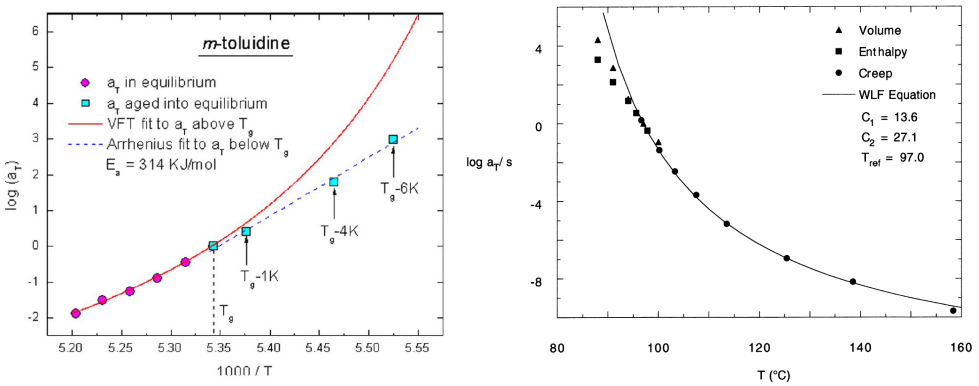

(a) From [51]. (b) From [52].

Figure 10.22 Data for m-toluidine (a) and polystyrene (b) showing that when then the sample is aged into equilibrium below T_g the relaxation time increases less than predicted by VFT equation fitted to relaxation time data below T_g.

parameters), but extrapolations to low temperatures of fits to viscosity data at high temperatures predict too high, respectively too low, T_g's. They suggest a new equation for describing viscosity data (mentioned previously, see Eq. (10.32)) and show that this equation give more reasonable prediction of T_g as well as of the pre-factor. So it seems that conclusions drawn here based on organic liquid data are also valid for oxide glasses.

We conclude that the data analyzed – the most accurate presently available for any class of glass-forming liquids – do not give convincing indications of any dynamic divergences. Consequently, the temperature T_0 of the VFT equation cannot be assigned any fundamental significance. In our opinion, theories predicting a dynamic divergence of the VFT form should be reconsidered.

Liquid	Abr.	Symb.	Temp. int.(K)	f_{max} int. (Hz)	I int.	Ref.
1,2-propandiol (propylene-glycol)	PG	◁	180 ; 211	0.34 ; 4.51	1.03 ; 1.53	[56]
2-ethyl-hexylamine	EH	×	142 ; 166	−1.4 ; 4.72	1.26 ; 3.15	[57]
2-methyl-tetrahydrofurane	MTHF	◇	91 ; 108	−2.1 ; 5.92	2.11 ; 3.89	[56]
2-phenyl-5-acetomethyl-5-ethyl-1,3-dioxocyclohexane	AFEH	△	220 ; 240	−1.75 ; 2.91	2.64 ; 3.28	[56]
3,3,4,4-benzophenonetetracarboxylic dianhydride	BPC	◁	334 ; 362	−1.79 ; 3.11	3.33 ; 3.85	[58]
3-fluoro-aniline	FAN	○	173 ; 198	−2.11 ; 5.36	3.08 ; 4.58	[59]
3-phenyl-1-propanol	3Ph1P	×	182 ; 200	−1.89 ; 2.38	1.7 ; 3.1	[1]
3-styrene	3Sty	+	235 ; 280	−1.61 ; 5.44	1.73 ; 3.14	[60]
5-polyphenyl-ether	5-PPE	*	245 ; 285	−2.9 ; 5.73	2.84 ; 4.08	this work
benzophenone	BePh	○	215 ; 240	0.16 ; 5.7	3.24 ; 4.27	[61]
biphenyl-2yl-isobutylate	BP2IB	□	210 ; 232	−1.38 ; 3.94	3.13 ; 3.41	[56]
butyronitrile	BN	▽	97 ; 116	−1.85 ; 3.66	0.68 ; 1.97	[62]
cresolphthalein-dimethylether	KDE	▷	315 ; 383	−2.64 ; 5.98	2.05 ; 3.16	[63]
decahydroisoquinoline	DHIQ	×	180 ; 192	−1.89 ; 3.78	3.6 ; 7.45	[64]
di-iso-butyl-phtalate	dIBP	+	195 ; 221	−1.44 ; 4.02	1.59 ; 3.12	[56]
dibutyl-ammonium-formide	dBAF	◇	156 ; 200	−1.57 ; 5.63	0.89 ; 2.82	[65]
dibutyl-phtalate	DBP	△	180 ; 224	−1.67 ; 5.93	1.01 ; 3.22	[66]
dicyclohexyl-methyl-2-methylsuccinate	DCHMMS	◁	220 ; 240	−2.13 ; 2.85	2.77 ; 3.66	[67]
diethyl-phtalate	DEP	○	186 ; 222	−1.51 ; 5.81	2.04 ; 3.36	[1]
diglycidyl-ether-of-bisphenol A (epoxy-resin)	ER	□	259 ; 291	−0.83 ; 5.94	2.76 ; 5.98	[68]
dimethyl-phtalate	DMP	▽	196 ; 220	−1.65 ; 3.87	2.42 ; 3.23	[1]
dioctyl-phtalate	DOP	▷	188 ; 220	−1.81 ; 3.9	1.27 ; 2.57	[56]
dipropylene-glycol	DPG	×	196 ; 240	−2.39 ; 5.13	1.3 ; 2.84	[1]
dipropylene-glycol-dimethyl-ether	DPGDME	+	139 ; 155	−1.11 ; 4.12	1.96 ; 3.47	[56]

glycerol	Gly	△	192 ; 252	−1.89 ; 5.85	1.08 ; 1.97	[66]
isopropyl-benzene	Cum	∗	131 ; 149	−1.26 ; 4.73	2.46 ; 3.27	[56]
m-tricresyl-phosphate	mTCP	○	209 ; 233	−1.58 ; 3.49	2.22 ; 3.32	[69]
m-toluidine	mTol	□	184 ; 200	−2.77 ; 2.76	3.43 ; 4.07	[1]
o-terphenyl	OTP	▷	252 ; 282	−0.24 ; 5.71	2.64 ; 5.25	[70]
phenolphthalein-dimethylether	PDE	×	299 ; 333	−1.47 ; 4.51	2.89 ; 3.93	[71]
phenyl-salicylate (salol)	Sal	+	223 ; 253	−1.38 ; 5.6	3.62 ; 4.45	[72]
polypropylene-glycol	PPG	◇	200 ; 240	−1.51 ; 5.46	1.45 ; 3.43	[66]
pyridine-toluene	PT	∗	125 ; 131	−2.85 ; 1.63	5.07 ; 6.46	[66]
squalane	Sqa	○	170 ; 210	−1.92 ; 5.05	−0.25 ; 3.77	[64]
sucrose-benzonate	SB	□	341 ; 400	−1.14 ; 5.54	1.39 ; 4.16	[73]
tetraphenyl-tetramethyl-trisiloxane	DC704	▽	211 ; 240	−2.62 ; 5	3.53 ; 4.11	[64]
tricresyl-phosphate	TCP	▷	216 ; 248	−0.69 ; 4.95	1.8 ; 3.16	[1]
triphenyl-ethylene	TPE	×	254 ; 274	−1.47 ; 3.13	3.43 ; 4.04	[64]
tripropylene-glycol	TPG	◇	192 ; 228	−2.01 ; 4.78	1.4 ; 3.31	[66]
trisnaphthylbenzene	tNB	△	357 ; 405	0.09 ; 5.86	2.51 ; 3.67	[74]
xylitol	Xyl	∗	254 ; 284	−0.59 ; 4.66	2.18 ; 4.13	[56]

Table 10.1: Trivial name, abbreviation, and symbols used in the figures. The table also includes information such as the dynamical interval available, the temperature interval, temperature index interval, and references to where the data were first published.

Bibliography

[1] T. Hecksher, A. I. Nielsen, N. B. Olsen, and J. C. Dyre. Little evidence for dynamic divergences in ultraviscous molecular liquids. *Nature Physics*, 4(9):737–741, 2008.

[2] H. Vogel. Das temperaturabhängigkeitsgesetz der viskosität von flüssigkeiten. *Physikalische Zeitschrift*, 22:645–646, 1921.

[3] G. S. Fulcher. Analysis of recent measurements of the viscosity of glasses. *Journal of American Ceramic Society*, 8:339–355, 1925.

[4] G. Tammann. Glasses as supercooled liquids. *Journal of the Society of Glass Technology*, 9:166–185, 1925.

[5] C. A. Angell. Oxide glasses in light of ideal glass concept .I. Ideal and nonideal transitions and departures from ideality. *Journal of the American Ceramic Society*, 51(3):117, 1968.

[6] G. Adams and J. H. Gibbs. On the temperature dependence of cooperative relaxation properties in glass-forming liquids. *Journal of Chemical Physics*, 43(1):139–146, 1965.

[7] J. C. Dyre, T. Hecksher, and K. Niss. A brief critique of the Adam-Gibbs entropy model. *Journal of Non-Crystalline Solids*, 355:624–627, 2009.

[8] M. H. Cohen and D. Turnbull. Molecular transport in liquids and glasses. *Journal of Chemical Physics*, 31:1164–1169, 1959.

[9] M. H. Cohen and G. S. Grest. Liquid-glass transition, a free volume approach. *Physical Review B*, 20:1077–1098, 1979.

[10] J. C. Dyre. The glass transition and elastic models of glass-forming liquids. *Reviews of Modern Physics*, 78(3):953–972, 2006.

[11] J. C. Dyre, N. B. Olsen, and T. Christensen. Local elastic expansion model for viscous-flow activation energies of glass-forming molecular liquids. *Physical Review B*, 53:2171–2174, 1996.

[12] S. F. Edwards. Theory of glasses. *Polymer*, 17:933–937, 1976.

[13] S. F. Edwards. The glass transition. *International Journal of Modern Physics B*, 6(10):1587–1594, 1992.

[14] P. W. Anderson. *Ill-Condensed Matter*, chapter Lectures on Amorphous Systems, pages 159–261. North-Holland, 1979.

[15] J. Bouchaud and G. Biroli. On the Adam-Gibbs-Kirkpatrick-Thirumalai-Wolynes scenario for the viscosity increase in glasses. *Journal of Chemical Physics*, 121(15):7347–7354, 2004.

[16] V. Lubchenko and P. G. Wolynes. Theory of structural glasses and supercooled liquids. *Annual Review of Physical Chemistry*, 58:235–266, 2007.

[17] J. S. Langer. Dynamics and thermodynamics of the glass transition. *Physical Review E*, 73:041504, 2006.

[18] R. R. Nigmatullin. Theory of dielectric relaxation in non-crystalline solids: from a set of micromotion to the averaged collective motion in the mesoscale region. *Physica B: Condensed Matter*, 358(1-4):201–215, 2005.

[19] J. S. Langer and A. Lemaitre. Dynamic model of super-Arrhenius relaxation rates in glassy materials. *Physical Review Letters*, 94:175701, 2005.

[20] L. Dagdug. A theoretical framework for the Vogel-Fulscher-Tammann equation for covalent network glasses derived by the stichastic matrix method. *Journal of Physics: Condensed Matter*, 12:9573–9589, 2000.

[21] J. Rault. Origin of the Vogel-Fulcher-Tammann law in glass-forming materials: the α-β bifurcation. *Journal of Non-Crystalline Solids*, 271:177–217, 2000.

[22] T. Kitamura. The origin of the Vogel-Fulcher law near the liquid-glass transition. *Physica A*, 262:16–34, 1999.

[23] H. Tanaka. A simple physical picture of the liquid-glass transition. *Journal of Chemical Physics*, 105(20):9375–9378, 1996.

[24] H. Carmesin. Slow dynamics at the liquid-glass transition. *Physica A*, 201:25–29, 1993.

[25] U. Mohanty. On the nature of supercooled and glassy states of matter. *Physica A*, 177:345–355, 1991.

[26] W. Götze and L. Sjögren. Relaxation processes in supercooled liquids. *Reports on Progess in Physics*, 55(3):241–376, 1992.

[27] F. H. Stillinger. Supercooled liquids, glass transition and the Kauzmann paradox. *Journal of Chemical Physics*, 88(12):7818–7825, 1988.

[28] D. Kivelson, G. Tarjus, X. Zhao, and S. A. Kivelson. Fitting of viscosity: Distinguishing the temperature dependences predicted by various models of supercooled liquids. *Physical Review E*, 53(1):751–758, 1996.

[29] J. P. Gallahan and D. Chandler. Coarse-grained microscopic model of glass-formers. *Proceedings of the National Academy of Sciences of the United Stated of America*, 100(17):9710–9714, 2003.

[30] C. A. Angell and D. L. Smith. Test of the entropy basis of the Vogel-Tamman-Fulcher equation – dielectric relaxation of polyalcohols near T_g. *Journal of Physical Chemistry*, 86(19):3845–3852, 1982.

[31] R. Richert and C. A. Angell. Dynamics of glass-forming liquids. V. On the link between molecular dynamics and configurational entropy. *Journal of Chemical Physics*, 108(21):9016–9026, 1998.

[32] C. A. Angell. Entropy and fragility in supercooling liquids. *Journal of Research of the National Institute of Standards and Technology*, 102(2):171–185, 1997.

[33] H. Tanaka. Relation between thermodynamics and kinetics of glass-formin liquids. *Physical Review Letters*, 90(5):055701, 2003.

[34] G. Harrison. *The Dynamic Properties of Supercooled Liquids*. Academic Press, 1976.

[35] I. Avramov and A. Milchev. Effect of disorder on diffusion and viscosity in condensed systems. *Journal of Non-Crystalline Solids*, 104:253–260, 1988.

[36] I. Avramov. Viscosity in disordered media. *Journal of Non-Crystalline Solids*, 351:3163–3173, 2005.

[37] H. Bässler. Viscous flow in supercooled liquids analyzed in terms of transport theory for random media with energetic disorder. *Physical Review Letters*, 58(8):767–770, 1987.

[38] T. A. Litovitz. Temperature dependence of the viscosity of associated liquids. *Journal of Chemical Physics*, 30(7):1088–1089, 1952.

[39] A.J. Barlow and J. Lamb. The visco-elastic behaviour of lubricating oils under cyclic shearing stress. *Proceeding of the Royal Society of London. Series A, Mathematical and Physical Sciences*, 253(1272):52–69, 1959.

[40] F. H. Stillinger. A topographic view of supercooled liquid and glass formation. *Science*, 267:1935–1939, 1995.

[41] T. B. Schrøder, S. Sastry, J.C. Dyre, and S. C. Glotzer. Crossover to potential energy landscape dominated dynamics in a model glass-forming liquid. *Journal of Chemical Physics*, 112(22):9834–9840, 2000.

[42] C. A. Angell. Perspective on the glass transition. *Journal of Physics and Chemistry of Solids*, 49(8):863–871, 1988.

[43] S. P. Singh and S. P. Das. Characteristic temperatures of glassy behavior in a simple liquid. *Journal of Physics: Condensed Matter*, 19:246107, 2007.

[44] J. Dyre. Ten themes of viscous liquid dynamics. *Journal of Physics: Condensed Matter*, 19:205105, 2007.

[45] S. S. N. Murthy and M. Tyagi. Experimental study of the high frequency relaxation process in monohydroxy alcohols. *Journal of Chemical Physics*, 117:3837–3847, 2002.

[46] L. M. Wang and R. Richert. Dynamics of glass-forming liquids. IX. Structural versus dielectric relaxation in monohydroxy alcohols. *Journal of Chemical Physics*, 121:22, 2004.

[47] B. Jakobsen, C. Maggi, T. Christensen, and J. C. Dyre. Investigation of the shear-mechanical and dielectric relaxation processes in two monoalcohols close to the glass transition. *Journal of Chemical Physics*, 129:184502, 2008.

[48] J. C. Dyre and N. B. Olsen. Landscape equivalent of the shoving model. *Physical Review B*, 69:042501, 2004.

[49] F. Stickel, E. W. Fischer, and R. Richert. Dynamics of glass-forming liquids. I. Temperature-derivative analysis of dielectric data. *Journal of Chemical Physics*, 102(15):6251–6257, 1995.

[50] J. C. Mauro, Y. Yue, A. J. Ellison, P. K. Gupta, and D. G. Allan. Viscosity of glass-forming liquids. *Proceeding of the National Academy of Sciences of the United States of America*, 106:19780–19784, 2009.

[51] P. A. O'Connell and G. B. McKenna. Arrhenius-type temperature dependence of the segmental relaxation below t_g. *Journal of Chemical Physics*, 110:11054, 1999.

[52] S. L. Simon, J. W. Sobieski, and D. J. Plazek. Volume and enthalpy recovery of polystyrene. *Polymer*, 42:2555–2567, 2001.

[53] X. F. Shi, A. Mandanici, and G. B. McKenna. Shear stress relaxation and physical aging study of simple glass-forming materials. *Journal of Chemical Physics*, 125:174507, 2005.

[54] G. B. McKenna. Diverging views on the glass transition. *Nature Physics*, 4:673–674, 2008.

[55] S. L. Simon and G. B. McKenna. Experimental evidence against the existence of an ideal glass transition. *Journal of Non-Crystalline Solids*, 355:672–675, 2009.

[56] A. I. Nielsen, T. Christensen, B. Jakobsen, K. Niss, N. B. Olsen, R. Richert, and J. C. Dyre. Prevalence of approximate $\sqrt{t}$ relaxation for the dielectric alpha process in viscous organic liquids. *Journal of Chemical Physics*, 130:154508, 2009.

[57] L.-M. Wang and R. Richert. Debye type relaxation and the glass transition of alcohols. *Journal of Physical Chemistry B*, 109(22):11091–11094, 2005.

[58] K. L. Ngai and M. Paluch. Classification of secondary relaxation in glass-formers based on dynamical properties. *Journal of Chemical Physics*, 120(2):857–873, 2004.

[59] J. Wiedersich, T. Blochowicz, S. Benkhof, A. Kudlik, N. V. Surovtsev, C. Tschirwitz, V. N. Novikov, and E. A. Rössler. Fast and slow relaxation processes in glasses. *Journal of Physics: Condensed Matter*, 11:A147–A156, 1999.

[60] T. Blochowicz. *Broadband Dielectric Spectroscopy in Neat and Binary Molecular Glass Formers Frequency and Time Domain Spectroscopy, Non-Resonant Spectral Hole Burning*. PhD thesis, Universitat Bayreuth, 2003.

[61] P. Lunkenheimer, R. Wehn, and A. Loidl. Dielectric spectroscopy on aging glasses. *Journal of Non-Crystalline Solids*, 352:4941–4945, 2006.

[62] N. Ito, K. Duvvuri, D. V. Matyushov, and R. Richert. Solvent response and dielectric relaxation in supercooled butyronitrile. *Journal of Chemical Physics*, 125(2):024504, 2006.

[63] M. Paluch, K. L. Ngai, and S. Hensel-Bielowka. Pressure and temperature dependences of the relaxation dynamics of cresolphthalein-dimethylether: Evidence of contributions from thermodynamics and molecular interactions. *Journal of Chemical Physics*, 114(24):10872–10883, 2001.

[64] B. Jakobsen, K. Niss, and N. B. Olsen. Dielectric and shear mechanical alpha and beta relaxations in seven glass-forming liquids. *Journal of Chemical Physics*, 123(23):234511, 2005.

[65] N. Ito, W. Huang, and R. Richert. Dynamics of a supercooled ionic liquid studied by optical and dielectric spectroscopy. *Journal of Physical Chemistry B*, 110(9):4371–4377, 2006.

[66] N. B. Olsen, T. Christensen, and J. C. Dyre. Time-temperature superposition in viscous liquids. *Physical Review Letters*, 86(7):1271–1274, 2001.

[67] R. Diaz-Calleja, A. Garcia-Bernabe, M. J. Sanchis, and L. F. del Castillo. Interconversion of mechanical and dielectrical relaxation measurements for dicyclohexylmethyl-2-methyl succinate. *Physcial Review E*, 72(5):051505, 2005.

[68] M. Mierzwa, S. Pawlus ANS M. Paluch, E. Kaminska, and K. L. Ngai. Correlation between primary and secondary johari-goldstein relaxations in supercooled liquids: Invariance to changes in thermodynamic conditions. *Journal of Chemical Physics*, 128:044512, 2008.

[69] T. Blochowicz, C. Gainaru, P. Medick, C. Tschirwitz, and E. A. Rossler. The dynamic susceptibility in glass forming molecular liquids: The search for universal relaxation patterns ii. *Journal of Chemical Physics*, 124(13):134503, 2006.

[70] R. Richert. On the dielectric susceptibility spectra of supercooled o-terphenyl. *Journal of Chemical Physics*, 123:154502, 2005.

[71] S. Hensel-Bielowka and M. Paluch. Origin of the high-frequency contributions to the dielectric loss in supercooled liquids. *Physical Review Letters*, 89(2):025704, 2002.

[72] C. Gainaru, A. Rivera, S. Putselyk, G. Eska, and E. A. Rössler. Low-temperature dielectric relaxation of molecular glasses: Crossover from the nearly constant loss to the tunneling regime. *Physical Review B*, 72(17):174203, 2005.

[73] J. R. Rajian, W. Huang, R. Richert, and E. L. Quitevis. Enhanced translational diffusion of rubrene in sucrose benzoate. *Journal of Chemical Physics*, 124(1):014510, 2006.

[74] R. Richert, K. Duvvuri, and L.-T. Duong. Dynamics of glass-forming liquids. VII. Dielectric relaxation of supercooled tris-naphthylbenzene, squalane and decahydroisoquinoline. *Journal of Chemical Physics*, 118(4):1828–1836, 2003.

Part III

Linear and nonlinear relaxation

11 The out-of-equilibrium dynamics

In the previous parts of the thesis we have been addressing the properties of the (metastable) equilibrium liquid. For many purposes – both in application and from a more fundamental point of view – it is also extremely interesting what happens when the liquid is taken out of equilibrium, i.e. when it forms a glass.

The glass transition is a kinetic event; by definition a glass is simply a highly viscous liquid that has not yet had time to equilibrate [1–6]. Any glass thus relaxes towards the equilibrium liquid state. Equilibrium can only be reached on laboratory time scales, however, if the glass is kept at a temperature not too far below the glass transition region.

The change of materials properties over time is referred to as aging. Aging of purely physical properties is termed "physical aging" to distinguish it from other time-dependent processes such as chemical degradation [7].

Aging of glasses is a nonlinear phenomenon, because the aging rate is structure dependent and itself evolves with time when the structure changes as equilibrium is gradually approached [7–16]. Thus aging studies provide information beyond that obtained by linear-response experiments like, e.g., dielectric relaxation measurements.

In the following sections we give an overview of phenomenology that characterizes relaxation of viscous liquids close to and below the glass transition temperature.

11.1 Aging effects

Figure 11.1 illustrates the change of some measured property p (typically volume or enthalpy) of a liquid cooled through the glass transition. The liquid coefficient is defined by the slope of the cooling curve in the liquid state

$$\alpha_p^{\mathrm{liq}} = \left(\frac{\partial p}{\partial T}\right)_{eq} \tag{11.1}$$

and a corresponding coefficient can phenomenologically be defined for the glass, $\alpha_p^{\mathrm{gl}} = \left(\frac{\partial p}{\partial T}\right)_{\mathrm{gl}}$. Since the glass is not in equilibrium this is however not a thermo-dynamically well-defined quantity. If p is volume then α_p is the thermal expansion, and if p is enthalpy then α_p is the heat capacity. Usually, the liquid coefficient is larger than the glassy coefficient, $\alpha_p^{\mathrm{liq}} > \alpha_p^{\mathrm{gl}}$.

In the liquid and glassy regions (far above and far below T_g, respectively) thermal cycling is reversible, i.e. the same path is followed during cooling and reheating. In the glass transition region this is not the case; when a liquid is cooled and re-heated across

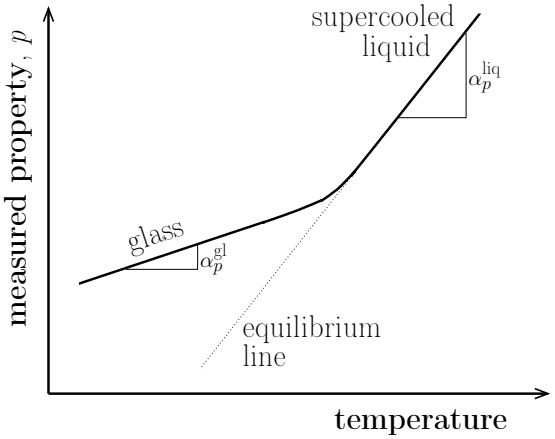

Figure 11.1 Cooling curve following the property p for a continuously cooled liquid. When the structural relaxation time becomes comparable with the inverse cooling rate the liquid will not have time to fully relax to equilibrium and the measured property will start to deviate from the equilibrium line.

the glass transition region a hysteresis is observed, as shown in Fig. 11.2. When the liquid is cooled through the glass transition region, the measured property p gradually changes slope from the liquid value α_p^{liq} to the glassy value α_p^{gl}. During re-heating a different path is followed: when the glass transition region is approached p stays below the cooling curve, then at a higher temperature it approaches the liquid line with a much steeper slope, see Fig. 11.2(a). In the derivative (Fig. 11.2(b)) the cooling curve is a gradual change from the (high) liquid value to the (low) glassy value. The hysteresis shows up in the re-heating as an undershoot approaching the glass transition region and an overshoot towards the liquid level. How large the under- and overshoots are depends on the cooling and heating rates: a slow cooling rate and fast re-heating rate gives a small undershoot and a large overshoot, while a fast cooling and subsequent slow heating gives a large undershoot and a small overshoot. The hysteresis effect is a consequence of the glass aging (or relaxing) irreversibly towards the (meta-stable) equilibrium state during the thermal cycle.

This relaxation can be studied in a more controlled way by temperature step experiments. In Fig. 11.3(a) a schematic representation of a temperature step experiment is shown. At $t = 0$ a temperature step from T_1 to T_2 is imposed on the liquid. The liquid responds instantaneously to the temperature step following the glass line – it is quenched out of equilibrium. Then an isothermal relaxation towards equilibrium follows. The overall change in p is given by $\Delta p = \alpha_p^{\mathrm{liq}}(T_2 - T_1)$ and the instantaneous (glassy) change is given by $\Delta p_g = \alpha_p^{\mathrm{gl}}(T_2 - T_1)$. The purely structural part of the response is thus given by $\Delta p_s = \Delta\alpha_p(T_2 - T_1)$ where $\Delta\alpha_p$ is defined as the difference between the liquid and glassy coefficient. In Fig. 11.3(b) the temperature step and the measured property p is shown as a function of temperature.

Of course a temperature step in a real experiment cannot be instantaneous because heat diffusion takes time. A temperature step can however be regarded “instantaneous” if the temperature is established homogeneously through the liquid, before any structural

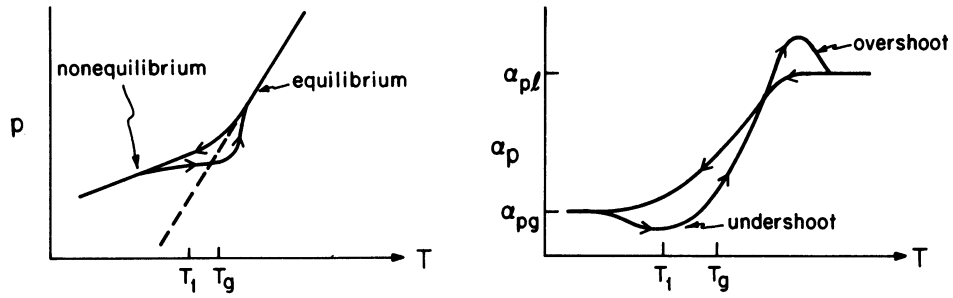

(a) Cooling and reheating (b) Derivative of p

Figure 11.2 The hysteresis observed when a glass is thermally cycled across the glass transition region. In the glass transition region the heating curve lies below the cooling curve. If the heating rate is slow it will start to relax toward the equilibrium line (giving rise to a large undershoot in the derivative) and then follow the equilibrium line. If the heating rate is fast no structural changes takes place in the beginning and the heating curve continues the glassy line and only later catches up with the liquid line. This gives a large overshoot in the derivative. From [13]

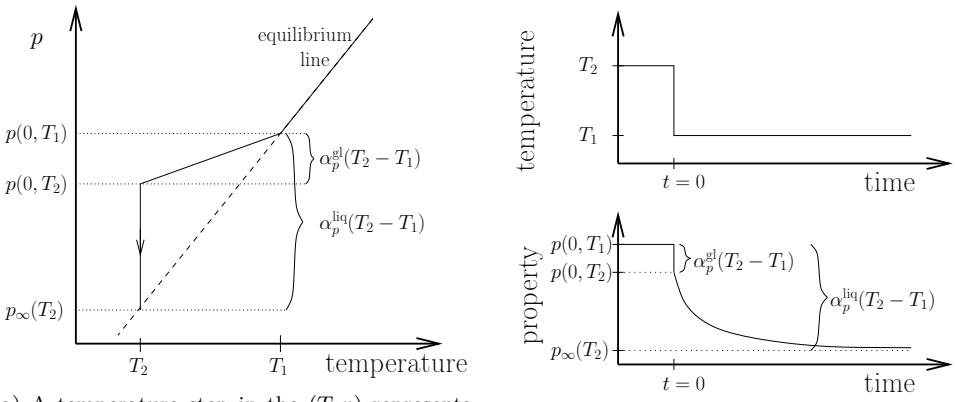

(a) A temperature step in the (T,p) representation.

(b) A temperature step as a function of time.

Figure 11.3 A schematic representation a temperature step experiment. The material is initially in equilibrium. At time $t = 0$ the temperature is changed from T_1 to T_2. The measured property p responds by an instantaneous jump from $p(0,T_1)$ to $p(0,T_2)$ followed by a slow structural relaxation towards equilibrium at the new temperature, $p_\infty(T_2)$. The overall change in p is given by the liquids coefficient times the change in temperature.

relaxation takes place. This will allow for an "ideal aging experiment" [17, 18], which is defined as an aging experiment where the full relaxation curve is monitored. Doing an ideal aging experiment is thus a matter of generating large separation between the heat diffusion time and the structural relaxation time, e.g. by a small sample and/or low temperatures.

11.1.1 Non-linearity

We stated that aging is a non-linear phenomenon. What does that mean? Let us start by summarizing what a linear response means. Define the input (how we perturb the system) as θ and the output as p (the property we measure). In the simplest case the output is proportional to the input

$$p(t) = r\theta(t) \tag{11.2}$$

and the proportionality factor r is called the response.

If the system has a time-dependent response (i.e. relaxing systems) then the simple relation in Eq. 11.2 will be replaced by a convolution of the response function with the input history

$$p(t) = \int_{-\infty}^{t} r(t-t')\dot{\theta}(t')\,dt' \,. \tag{11.3}$$

This is the definition of a linear response. Eq. 11.2 is thus the special case of Eq. 11.3 where $r(t)$ is constant. This could be the response of a purely elastic solid to a deformation.

A particularly simple instance of the above occurs when the input is a Heaviside step function, $\theta(t) = \theta_0\varphi(t)$, where $\varphi(t) = \begin{cases} 0 & t < 0 \\ 1 & t > 0 \end{cases}$. Then input-output relation becomes

$$\begin{aligned} p(t) &= \int_{-\infty}^{t} r(t-t')\theta_0\dot{\varphi}(t')\,dt' \\ &= \theta_0 \int_{-\infty}^{t} r(t-t')\delta(t')\,dt' = \theta_0 r(t) \end{aligned} \tag{11.4}$$

i.e. the shape of the response function is measured directly. In particular, Eq. (11.4) means that for different magnitudes (and sign) of θ_0 we measure the same output.

If the input is the temperature, this relation rarely holds for viscous liquids. Even for small temperature steps, the response depends both on the sign and magnitude of the temperature step. In Fig. 11.4 this shown by a temperature up and a temperature down jump to the same temperature (figure from [9]). The two responses are clearly not mirror symmetric, the down jump appearing quite flat and reaching equilibrium much faster than the up-jump. The up-jump – while slower in the beginning – has a much steeper approach to equilibrium.

This is the so-called fictive-temperature effect described already by Tool in the 1940's [19], an effect which comes from the fact that the relaxation rate is structure dependent and itself evolves with time: A temperature down jump is "auto-retarded" [9] because as the structure ages, the aging rate decreases. In contrast, a temperature up jump is "auto-accelerated" because as the structure ages, the aging rate increases [9].

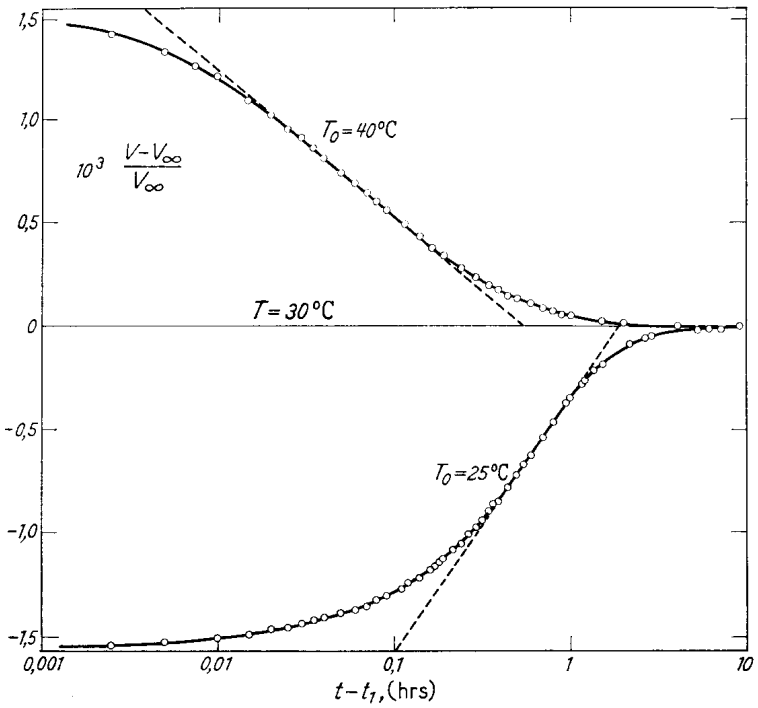

Figure 11.4 The asymmetry of approach following a temperature up-jump and down-jump to the same temperature. This asymmetry shows that the response to even small temperature steps is nonlinear. The asymmetry arises because a down-jump is "auto-retarded": for every time-step the intrinsic relaxation time becomes slower and slower, approaching the equilibrium value of the set temperature, giving rise to a stretching of the curve. The up-jump on the other hand is "auto-accelerated": the intrinsic relaxation time is increasing as the equilibrium value is approached, thus revealing a sharper (or more compressed) curve shape. From [9].

The retardation or acceleration of the structural relaxation is thus a consequence of a large difference in the relaxation time at initial temperature T_1 and the final temperature T_2. How large or small does a temperature step need to be before the measured response becomes nonlinear? Obviously, small enough that the relaxation time does not change too much, $\tau(T_2)/\tau(T_1) \approx 1$.

Assuming an Arrhenius expression for the equilibrium relaxation time $\tau(T) = \tau_0 \exp\left(\frac{T_A}{T}\right)$, where T_A is the activation temperature simply defined by activation energy divided by Boltzmann's constant, the change of the temperature by some percentage r will result in the following change of relaxation time

$$\tau(T(1+r)) = \tau_0 \exp\left(\frac{T_A}{T(1+r)}\right) = \tau_0 \left\{\exp\left(\frac{T_A}{T}\right)\right\}^{\frac{1}{1+r}} \tag{11.5}$$

and we can express $\tau(T(1+r))$ in terms of $\tau(T)$

$$\tau(T(1+r)) = \tau(T)\left\{\exp\left(\frac{T_A}{T}\right)\right\}^{\frac{r}{1+r}} \tag{11.6}$$

T_A is on the order of 10^4 and T of 10^2 and thus by insertion we see that a 10% change of temperature will result in an increase in relaxation time by a factor of almost 10^4. A change of 1% gives an increase by a factor 3, and only with a change in temperature less than one permille, can we expect a roughly linear response in a temperature step experiment.

11.1.2 Relaxation function and relaxation rate

From the measured property p in a temperature step experiment we can define a relaxation function subtracting the value approached at long times and normalizing by the overall change [13, 17]

$$R(t) = \frac{p(t,T_2) - p_\infty(T_2)}{p(0,T_1) - p_\infty(T_2)}, \tag{11.7}$$

where p_∞ refers to the value approached for $t \to \infty$, i.e. the equilibrium value at the T_2.

For any relaxation function $R(t)$ the Kovacs-McKenna (KM) relaxation rate $\Gamma(t)$ is defined [9, 14] by

$$\Gamma(t) \equiv -\frac{d\ln R}{dt} = -\frac{1}{R}\frac{dR}{dt}, \tag{11.8}$$

which is sometimes referred to as the inverse effective relaxation time, $\Gamma = 1/\tau_{\text{eff}}$. The KM relaxation rate gives the relative change of the relaxation function with time and is independent of normalization. For a simple exponential relaxation function, $R(t) = \exp(-t/\tau)$, the KM relaxation rate is constant: $\Gamma(t) = 1/\tau$. For the stretched-exponential, $R(t) = \exp[-(t/\tau)^\beta]$ $(0 < \beta < 1)$ the KM relaxation rate is $\Gamma(t) = (\beta/\tau)(t/\tau)^{\beta-1}$ that decreases monotonically to zero as $t \to \infty$.

A convenient representation of aging data is a parameterized plot of the logarithm of the KM relaxation rate versus the relaxation function, a so-called Kovacs-McKenna plot. We show the original plot presented by Kovacs [9] in Fig. 11.5.

Kovacs [9] measured volume changes and did not use a normalized relaxation function, but the relative volume change $\delta = (V - V_\infty)/V_\infty$ as the x-axis. Thus for all the up jumps we have $\delta < 0$ because volume is increasing, while $(\delta > 0)$ for down jumps. In the Kovacs plot the difference between up jumps and down jumps then becomes very obvious: for down jumps the KM relaxation rate is monotonically decreasing, while the KM relaxation rate for up jumps approach equilibrium in a much flatter manner – for large up jumps the relaxation rate may even become non-monotonic: first decreasing and then increasing.

In this figure it appears that temperature up and down jumps to the same temperature do not always approach the same KM relaxation rate at long times. This gap between terminal relaxation rates is sometimes referred to as the "expansion gap" or the "τ-effective paradox". The existence of an expansion gap has been a matter of debate

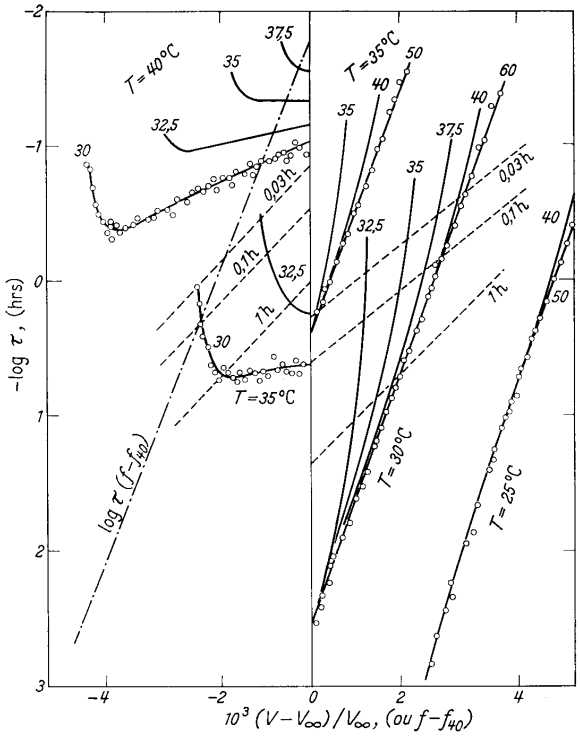

Figure 11.5 The Kovacs-McKenna plot. This is parameterized plot of the KM relaxation rate (defined in Eq. (11.8)) as a function of the relaxation function. The figure also illustrates the so-called τ-effective paradox (sometimes also called the expansion gap), which is the observation that apparently KM relaxation rate is not approaching the same value following temperature jumps to the same temperature from above and below. From [9].

[20–23]. Kolla & Simon [18] recently concluded, however, that there is no expansion gap for $t \to \infty$; they attributed the reported expansion gap to the fact that Kovacs' was unable to examine departures from equilibrium that were small enough to show the convergence of time scales.

11.1.3 Memory effect

In a cross-over experiment the input to the system gets a little more complicated. In Fig. 11.6 we give a schematic representation of a cross-over experiment. The input now consists of two consecutive temperature steps of opposite sign. The initial measured response is identical to that of Fig. 11.3. At a later time t_1 the temperature is changed to a temperature T_3 characterized by the equilibrium value of $p_\infty(T_3)$ being identical to the measured $p(t_1, T_2)$. If the system has no "memory" of the past input, it should immediately be in equilibrium and thus the p should not change. What is observed is instead a hump: p changes in the opposite direction followed by a decay back the equilibrium value at T_3. This is sometimes called the memory effect.

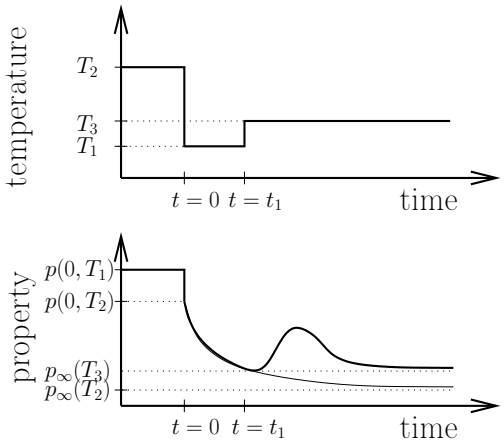

Figure 11.6 Schematic representation of the memory effect in a cross-over experiment. At $t = 0$ the temperature is changed from T_1 to T_2 and the measured property starts adjusting to the new temperature. At time $t = t_1$ (before equilibrium is reached) the temperature is changed to T_3, the temperature where the equilibrium value of the property is equal to value at that instant, $p_\infty(T_3) = p(t_1, T_2)$. If the system has no "memory" of the past the material should instantly be in equilibrium. Instead what is observed is a "hump": the value changes after the temperature is adjusted, then decays back to the same value.

The memory effect in a cross-over experiment has been convincingly demonstrated, e.g. by Kovacs [9] for poly-vinyl-acetate, and by Macedo & Napolitano [24] and Spinner and Napolitano [25] for borosilicate glass. The data of Kovacs *et al* [26] for several cross-over experiments, where initial and final temperatures, T_1 and T_3, are fixed, while the intermediate temperature T_2 is varied. The memory effect grow with the amplitude of the consecutive up- and down-jumps and apparently all the curves from different temperature inputs merge at sufficiently long time with the curve of a simple quench from T_1 to T_3.

11.2 The Tool-Narayanaswamy formalism

Already in 1931 Tool introduced the idea of a "fictive" temperature (actually he called it "equilibrium" temperature at that time and only later was the term "fictive" temperature adopted) as a measure of the structural state of a glass [27]. Later, in the 1940's this idea developed into the model described below [19]. The definition of the fictive temperature is depicted in Fig. 11.8, where we show a cooling curve of $p(T)$ (but temperature history is not important for the definition).

The fictive temperature is the temperature of the intersection of the projection of the point $(T_1, p(T_1))$ in the (T, p)-plot onto the extrapolated equilibrium line using the slope of the glass line. T_f is thus the equilibrium temperature from which the system must be quenched to obtain the property $p(T_1)$. Thus the limiting value of T_f is T_g for a continuously cooled system.

By this definition the fictive temperature changes continuously from initial temperature

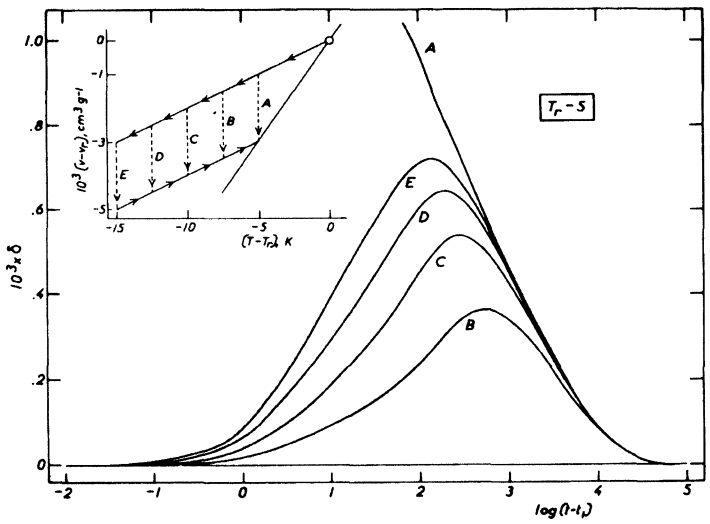

Figure 11.7 Data from cross-over experiments. The inset shows the input sequence: (A) is a simple 5K temperature down jump, (B)-(E) are cross-over experiments with increasing amplitude on the temperature steps both down- and subsequent up-jumps, such that the final temperature in all cases is the same. Large figure shows the corresponding volume response to the temperature inputs. The larger the amplitude of the jump cycle is, the larger is the memory effect. From [26].

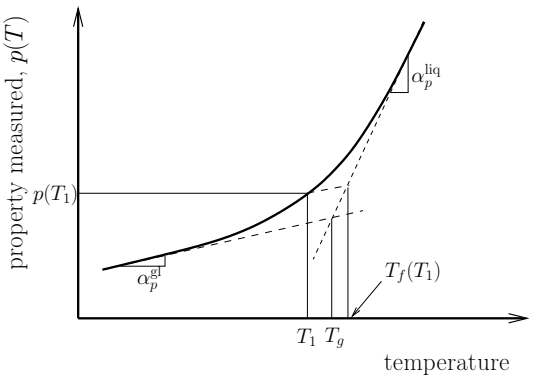

Figure 11.8 Definition of the fictive temperature, T_f. The slope of the measured property in the liquid state $\partial p/\partial T = \alpha_p^{\mathrm{liq}}$ is higher than that of the glassy state, α_p^{gl}. The fictive temperature is found by extrapolating a line with the slope α_p^{gl} to intersect with the equilibrium line (the line with slope α_p^{liq} extrapolated to lower temperatures). For very low temperatures T_f reaches it limiting value T_g. Adapted from [13].

T_1 to the final temperature T_2 after a temperature step (see Fig. 11.9) following the

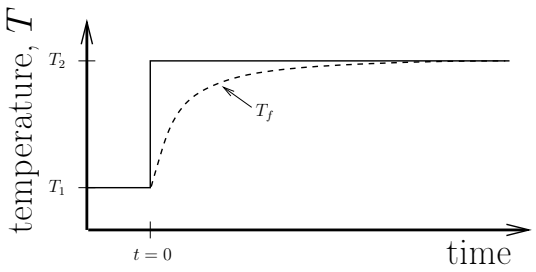

Figure 11.9 Evolution of the fictive temperature following a temperature step. With the definition of the fictive temperature provided in Fig. 11.8, this quantity will decay monotonically from T_1 to T_2 following the relaxational part of the response function of the measured property p. Adapted from [28]

structural part of the measured property p. We have that [17]

$$R_p(t) = \frac{p(t, T_2) - p_\infty(T_2)}{p(0, T_2) - p_\infty(T_2)} = \frac{T_f - T_2}{T_1 - T_2}\,. \tag{11.9}$$

The difference between this definition of a relaxation function and Eq. (11.7) is just the normalization: Eq. (11.7) was normalized to the overall change in Δp, and the above relaxation function is normalized to the structural part, Δp_s.

Tool proposed the following equation to describe the time-dependence of the fictive temperature (and thereby the relaxation function) [19]

$$\frac{dT_f}{dt} = \frac{T - T_f}{\tau} \tag{11.10}$$

where $\tau = \tau(T, T_f)$ is a function of both temperature and fictive temperature and suggested the following expression for τ [19]

$$\tau = k \exp\left(-A_1 T - A_2 T_f\right) \tag{11.11}$$

where k, A_1, and A_2 are constants. With some minor modifications Eqs. (11.10) and (11.11) can also describe situation where a liquid is cooled or heated at constant rates. Tool demonstrated that his equation gave a reasonable description of heating rate data [19].

The model can however not explain the cross-over experiment. It was then concluded that the model was too simple, having only one "order-parameter" (namely T_f) and that more advanced approaches were needed to describe the aging phenomenology [13].

Narayanaswamy's idea [17, 29] was that since the nonlinearity of structural relaxation was due to a change in relaxation rate, then linearity could be restored by using the reduced time. If the structural clock rate is denoted by $\gamma(t) = 1/\tau(t)$, the reduced time $\tilde{t}$ is defined [13, 17–23, 30] by

$$\tilde{t}(t) \;=\; \int_{-\infty}^{t} \gamma(T(t'), T_f(t'))dt'\,, \tag{11.12}$$

where the lower bound is arbitrary. $\tilde{t}$ is sometimes called the "material time" or the time measured on "the internal clock".

Assuming now that the response of a material is linear except from the time dependence of the relaxation rate γ and that time-aging-time superposition (TAS) holds (so that R is retains its form when temperature is changed — even out of equilibrium), we can describe the aging of the property as a linear convolution integral in the reduced time $\tilde{t}$

$$p\left(T,\tilde{t}\right) = p_\infty(T) - \Delta\alpha_p \int_{-\infty}^{\tilde{t}} R\left(\tilde{t}-\tilde{t}'\right) \frac{dT}{d\tilde{t}}\, d\tilde{t}\,, \tag{11.13}$$

where $\Delta\alpha_p = \alpha_p^{\mathrm{liq}} - \alpha_p^{\mathrm{gl}}$. Consequently, fictive temperature is given by a similar expression

$$T_f = T - \int_{-\infty}^{\tilde{t}} R\left(\tilde{t}-\tilde{t}'\right) \frac{dT}{d\tilde{t}}\, d\tilde{t}\,. \tag{11.14}$$

If R is assumed to be a pure exponential $R(\tilde{t}) = \exp(-\tilde{t})$ then Eq. (11.14) reduces to Tool's equation (Eq. (11.10)).

In principle, $R(\tilde{t})$ could be measured by making linear temperature steps, but in practice this requires extremely good temperature control and high measurement precision and is not very feasible. Instead, the stretched exponential (SE) function has proven to be a quite successful expression for the linear relaxation function

$$R(\tilde{t}) = \exp\left(-\tilde{t}^{\beta}\right)\,. \tag{11.15}$$

Narayanaswamy [17] also suggested an expression the dependence of relaxation rate on temperature and fictive temperature based on the Arrhenius equation

$$\gamma(T,T_f) = \gamma_0 \exp\left(-x\frac{\Delta E}{k_B T} - (1-x)\frac{\Delta E}{k_B T_f}\right)\,, \tag{11.16}$$

where x is a number between 0 and 1 and ΔE is the activation energy.[1] Equation (11.16) reduces to the Arrhenius equation when $T = T_f$. There is no theoretical justification for this form, but it has been shown to describe data well by numerous authors [17, 29, 31]. The Arrhenius equation in general is inadequate to express the temperature dependence of the equilibrium relaxation time, but for a small temperature interval, such as a temperature step in an aging experiment, it is a good approximation.

Later other functional forms of $\gamma_s(T,T_f)$ have been suggested based on extensions of different models of the temperature dependence of the equilibrium relaxation time (Mauro *et al* [32] compares 5 different). None of these are theoretically justified either. Below we list two examples that are based the Adam-Gibbs model and the Avramov model that we encountered in part II

$$\begin{aligned}
&\text{Avramov equation: } \gamma(T,T_f) = \gamma_0 \exp\left\{-\left(\frac{T_*}{T_f}\right)^g \left(\frac{T_f}{T}\right)^h\right\} \\
&\text{Adam-Gibbs equation: } \gamma(T,T_f) = \gamma_0 \exp\left\{\left(\frac{T_*}{T\left(1-\frac{T_0}{T_f}\right)}\right)\right\}
\end{aligned} \tag{11.17}$$

1 This notation is actually not due to Narayanaswamy, but his expression is equivalent to this.

It should be noted that the Avramov expression has four fitting parameters (γ_0, T_*, g, and h) compared to the Arrhenius expression and the Adam-Gibbs expression that have only three fitting parameters, $\gamma_0, \Delta E, x$ and γ_0, T_A, T_0 respectively.

Scherer [33] showed for aging data on a range of oxide glasses that the Arrhenius expression introduced by Narayanaswamy and the Adam-Gibbs expression fit data equally well.

11.2.1 Fitting heating rate curves

In the following we implement the TN model presented above on to fit a set of heating rate data from the literature. Partly to demonstrate what we can get out of such analysis and how well it works, and partly to test a new relaxation function (emerging from the analysis of aging experiment in the next chapter) that we call the exponential $\sqrt{t}$ relaxation function

$$R(t) = \exp\left[-c\sqrt{\tilde{t}} - \tilde{t}\right]. \tag{11.18}$$

This function has a long time exponential decay and seems to give a better description of the relaxation function than the SE function in a temperature step experiment [34] (see Paper III, p. 269). Thus it would be interesting to see if this function also gives a better fit to other types of aging experiments, like the cross-over experiment and DSC heating curves. A similar function was suggested by Hornbøll *et al* [35], introducing an exponential cut off to the SE function but without fixing the stretching exponent, β. Hornbøll *et al* showed that the TN model using their function gave a superior fit to hyper quenched glasses. However, their fit involves one extra parameter, the β of the SE function, which is normally fixed.

As an example of heating rate data we will use the B_2O_3 data of DeBolt *et al* [31] (presented in Fig. 4 of [31]). They consist of three heating rate curves of a sample; All were heated at a constant heating rate of $q_h = 10$K/min, subsequent to a cooling by different cooling rates ($q_c = 40, 10, 2$K/min). The data clearly show the hysteresis described earlier in the form of a undershoot and overshoot in the derivative of the fictive temperature.

For the relaxation rate's dependence of temperature and fictive temperature, we will use the expression suggested by Narayanaswamy (Eq. (11.16)), which is also what was done in the paper, and as the relaxation function we will use both the SE function and the exponential $\sqrt{t}$ function. We then have a total of four fitting parameters: $\gamma_0, \Delta E, x$ of Eq. (11.16) and one shape parameter for each of the relaxation functions, β and c respectively. In principle, ΔE and γ_0 can be determined by equilibrium relaxation data in the relevant temperature interval to reduce the number of fitting parameters and ensure a physical interpretation of the model, but since we do not have the equilibrium data they were treated as fitting parameters.

All three data sets were fitted simultaneously and the result are shown in Fig. 11.10. Figure 11.10(a) shows the data as they were presented in [31] as well as the fits to the TN-model. The curves in color represent fits to the exponential $\sqrt{t}$ function and the fits using the SE function are shown as a black full line. Obviously, the TN-model captures all the features of the glass transition hysteresis and apparently, the choice of relaxation function makes little difference. The fitted parameters are listed in table 11.1 as well as the χ^2 value. The fitted parameters for the Arrhenius expression are

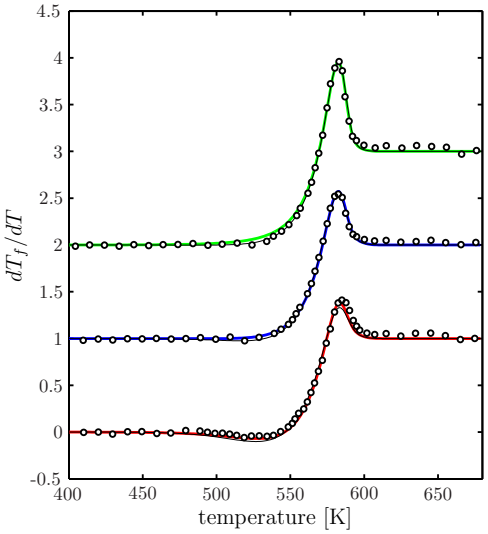

(a) Data and fits (have been shifted vertically for clarity).

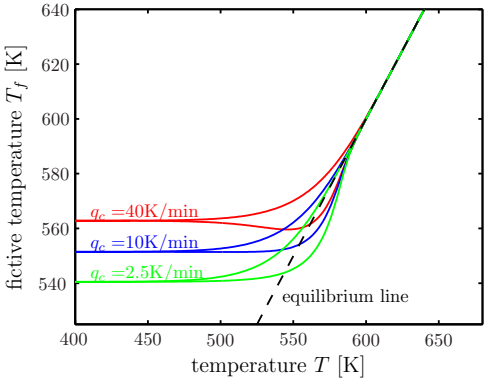

(b) Simulated fictive temperature.

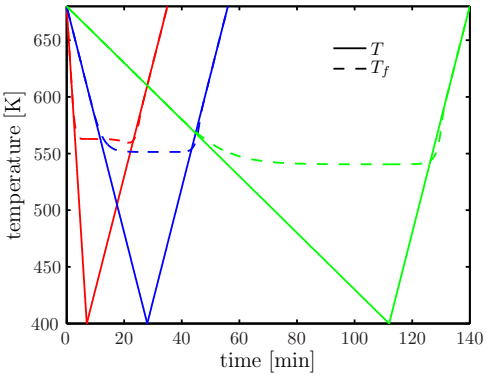

(c) Actual and fictive temperature through cooling and re-heating of the sample.

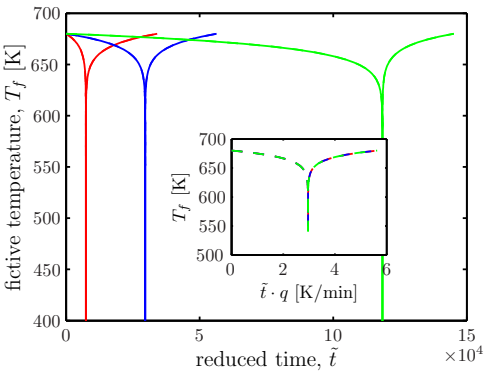

(d) Actual and fictive temperature as a function of reduced time (the curves are identical except the fictive temperature in the dip stops at a higher temperature). The inset shows how the same curves collapse when the reduced time is scaled by the cooling/heating rate.

Figure 11.10 Fitting the B_2O_3 by DeBolt *et al* reported in [31] data using the TN model. The samples have been cooled at different rates ($q_c = 40, 10, 2.5$K/min) and subsequently reheated at the same rate ($q_h = 10$ K/min). Data points (circles) are shown in (a) as well as the TN fits using the $\exp\sqrt{t}$ relaxation function (in color) and the stretched exponential (black lines). Fitting parameters are given in table 11.1. Both functions fit the data excellently, but the standard deviation shows that the $\exp\sqrt{t}$ relaxation function fits slightly better. (b-d) shows the fitted T_f curves (both cooling and re-heating) as a function of time, temperature, and reduced time. In the beginning T and T_f are identical, but around T_g the fictive temperature "freezes" in and does not change before the temperature again is increased.

not very different in the two cases, and the shape parameters both predict a relatively narrow relaxation functions, so the fits are consistent with each other. The pre-factors γ_0 are extremely high, which can probably be explained by the fact that it is a relatively small temperature interval around T_g where the Arrhenius expression is important, and a non-Arrhenius relaxation times are fitted to an Arrhenius expression in the vicinity of T_g, the result would be a very steep curve with a high γ_0.

	$\gamma_0 \left[\frac{1}{\mathrm{s}}\right]$	$\Delta E/k_B$ [K]	x	β	c	χ^2
SE	$2.2 \cdot 10^{29}$	$4.0 \cdot 10^4$	0.52	0.71		0.18
SE [31]	$1.5 \cdot 10^{33}$	$4.5 \cdot 10^4$	0.40	0.65		
$\exp\sqrt{t}$	$7.7 \cdot 10^{27}$	$3.7 \cdot 10^4$	0.56		0.79	0.15

Table 11.1 Fitting parameters from fitting TN model to B_2O_3 data from DeBolt *et al* [31] including the parameters obtained by DeBolt *et al*. Our fitted values of the parameters deviate from those of DeBolt *et al*, but they did not use a least-square method for fitting.

The heating rate experiment is not as well-defined and controlled experiment as the temperature step experiment. Thermal gradients will inevitably arise when a sample is continuously cooled. This problem gets bigger for a faster cooling rate, and this may explain the relatively poor fit to the sample with the highest cooling rate (data in bottom of Fig. 11.10(a)), compared to the fits to the slower cooling rates. How severe this problem is, of course also depends on sample size compared to heat diffusion length.

11.2.2 Shift factors and TAS

The TN-model can of course also be applied to temperature step experiments, where normally the reduced time is calculated by numerical integration of Eq. 11.12 using one of the proposed expressions for the clock rate's dependence of fictive and real temperatures (e.g. Eq. (11.16) or (11.17)). The measured curve directly gives the relaxation of the fictive temperature (Eq. (11.9)).

There is however a clever way of determining an out-of-equilibrium relaxation rate directly from experimental data instead of via modelling. This approach is mathematically equivalent to the TAS concept [36–40] and is sometimes referred to as the method of reduced variables.

The procedure was traditionally implemented by first using the short-time response of for instance a mechanical perturbation to take a "snap-shot" of the structure during a temperature step experiment [22, 41–43]. These curves are then shifted horizontally on the time axes in order to determine the aging-time shift factors, a_{T_f}. Assuming time-aging time superposition, the shift factors are proportional to the structural relaxation time. Thus, the reduced time is found via an equation equivalent to Eq. (11.12), $\tilde{t} = \int_0^t (a_{T_f}(t'))^{-1}\, dt$ [26].

Struik defined the proper protocols for doing this [12], which is illustrated in Fig. 11.11(a). He suggested that a series of square perturbations be applied to the aging sample at different aging times. The duration of the perturbation t_i should be substantially lower than current aging time T_{a_i}, more specifically $t_i/t_{a_i} < 0.1$. In Fig. 11.11(b) we show an example where the shift factors have been determined in an aging experiment by O'Connell *et al* [38]. The figure shows that the TAS assumption hold since all the measured short time responses can be collapsed to one master curve.

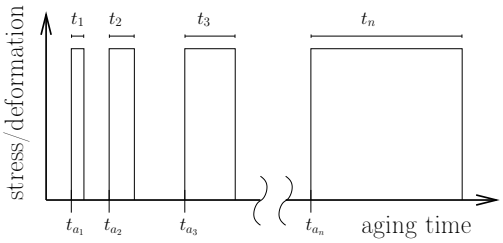

(a) Struik's protocol [12] for determining shift factors. Adapted from [44]

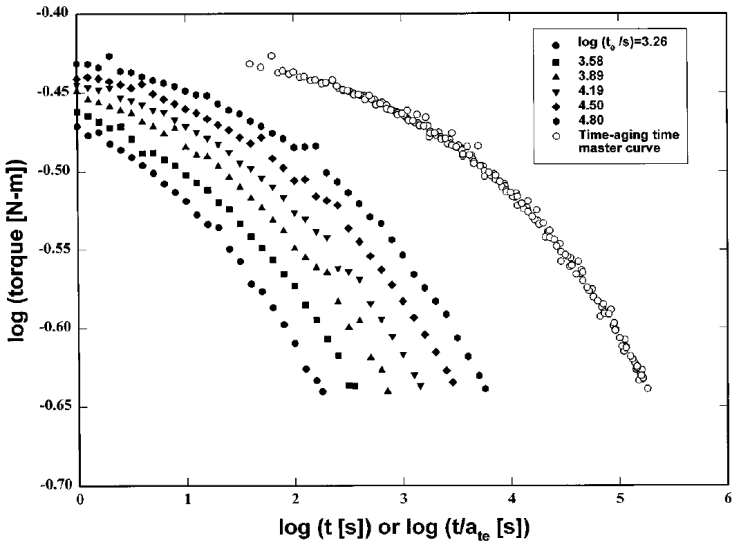

(b) Determining the out-of-equilibrium relaxation rates via shift factors. From [38]

Figure 11.11 Time-aging-time superposition (TAS) to determine shift factors. (a) Struik's protocol for determining the short time response of an aging sample, according to which the duration of the perturbation should be roughly 1/10th of the current aging time. (b) An example from O'Connell *et al* that implements this procedure determine the shift factors. Clearly, TAS principle is obeyed in this case since the curves collapse to master curve when shifted appropriately along the time axis.

11.3 Concluding remarks

The existence of a material time is an old idea that predates Narayanaswamy; thus the well-known time-temperature superposition concept may be regarded as a "linear" internal clock hypothesis. Narayanaswamy's insight was to generalize this to describe aging, which is a highly non-linear phenomenon.

The TN formalism is standard for interpreting aging experiments and used routinely used in industry for predicting aging effects [35, 45, 46]. Nevertheless, it is not known whether – and in which sense – the internal clock exists, or if it should merely be regarded as a convenient mathematical construction. The TN formalism is for instance difficult to unite with the idea that the dynamics of a viscous liquid is heterogeneous.

Usually, it is assumed that different probes can have different internal clocks. Roe & Millman showed a difference in enthalpy and volume relaxation [47] and similar results have been found by others [22, 43, 48].

In the following chapter we propose a test to resolve some of these questions.

12 Testing the internal clock hypothesis

This chapter presents aging experiments on five organic liquids for temperature up and down jumps (section 12.2), which were published in [34]. Several paragraphs of this chapter are identical and almost all of the figures to those of the paper, but there are some changes: most of the background material has been omitted since it was covered in the previous chapter, and a section on the approach Lunkenheimer *et al* has been added. The measurement presented here were carried out by Niels Boye Olsen.

In section 12.4 a new test of the existence of an internal clock is proposed. In contrast to most earlier works this test makes no assumptions regarding which quantity controls the internal clock's rate or the mathematical form of the relaxation function. This section demonstrates that all five liquids have internal clocks. Section 12.6 extends the data analysis in order to study whether the long-time relaxation is stretched or simple exponential. Section 12.7 shows that within the experimental uncertainties the long-time simple exponential structural relaxation has the same rate as the long-time exponential decay of the dipole autocorrelation function. A discussion of noise and systematic errors in the data analysis is given in section 12.8. Finally, section 12.9 gives a summary and some concluding remarks.

12.1 Introduction and motivation

A typical aging experiment consists of a temperature step, i.e., a rapid decrease or increase of temperature to a new, constant value. Ideally, such a temperature step should be instantaneous. In practical terms this means that the new temperature should be established as constant in time and homogeneous throughout the sample before any structural relaxation has taken place. If this is achieved and if sufficient time is available, it is possible to monitor the complete relaxation to equilibrium of the physical property being probed. An experimental protocol that measures the complete relaxation curve will be referred to as an "ideal aging experiment" [18].

What are the requirements for an ideal aging experiment? First, there should be good temperature control and the setup should allow for rapid thermal equilibration following a temperature jump. Secondly, a physical observable is needed that may be monitored quickly and accurately and which, preferably, changes significantly even for rather small temperature changes. The latter property allows for studying aging following temperature jumps that are of order just one percent in absolute units, which is enough for most ultra-viscous liquids to become highly nonlinear. The organic liquids studied in here have glass transition temperatures in the region 170K-200K and most temperature jumps presented are just one or two Kelvin jumps.

In order to make faster temperature-jump experiments possible, we designed a dielec-

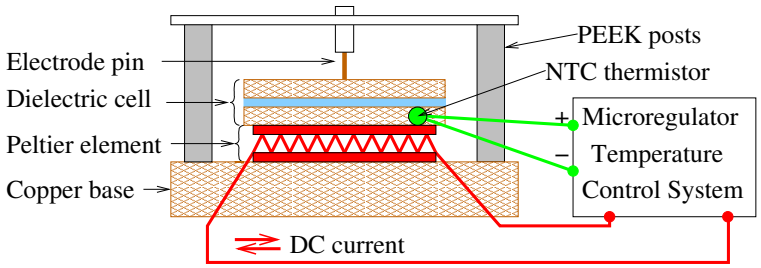

Figure 12.1 Schematic drawing of the dielectric measuring cell with the microregulator. The liquid is deposited in the (50 μm) gap between the disks of the dielectric cell. The Peltier element heats or cools the dielectric cell, depending on the direction of the electrical current powering the element. The current is controlled by an analog temperature-control system that receives temperature feedback information from an NTC thermistor embedded in one disc of the dielectric cell. A stainless steel electrode pin keeps the cell pressed against the Peltier element and provides electrical connection to one of the disks. The dielectric measuring cell is placed in the main cryostat.

tric cell based on a Peltier thermoelectric element by means of which the heat flow is controlled via electrical currents (Fig. 12.1) [49]. The characteristic thermal equilibration time of this "microregulator" is two seconds. This is almost a factor of hundred times faster than that of conventional equipment, which usually involves much larger heat diffusion lengths; our liquid layer is just 50 μm thick and the use of a Peltier element minimizes heat diffusion lengths outside of the liquid layer. In the microregulator temperature may be kept constant over weeks, keeping fluctuations below 100 μK [49, 50]. The experimental setup is detailed in Refs. [49] and [50], which describe the microregulator, the surrounding cryostat, and the electronics used for measuring the frequency-dependent dielectric response.

For monitoring aging we chose to measure the dielectric loss (the imaginary part of the dielectric constant) at a fixed frequency. With modern equipment this quantity may be measured quickly and accurately. For a viscous liquid of molecules with a permanent dipole moment, a large frequency range exists in which the dielectric loss changes considerably for small temperature variations. The dielectric loss was used previously for monitoring aging by several groups, e.g., by Johari [51], Schlosser and Schönhals [52], Alegria *et* al. [53–55], Leheny *et* al. [36, 56], Cangialosi *et* al. [57], Lunkenheimer *et* al. [58–60], D'Angelo *et* al. [61], and Serghei and Kremer [62].

12.2 Experimental results and initial data analysis

We studied aging of the following five organic liquids: Dibutyl phthalate (DBP), diethyl phthalate (DEP), 2,3-epoxy propyl-phenyl-ether (2,3-epoxy), 5-phenyl-4-ether (5-PPE), and triphenyl phosphite (TPP). These liquids are excellent glass formers. In order to ensure complete equilibrium before each measurement, the sample was kept at the temperature in question until there were no detectable changes of the dielectric properties.

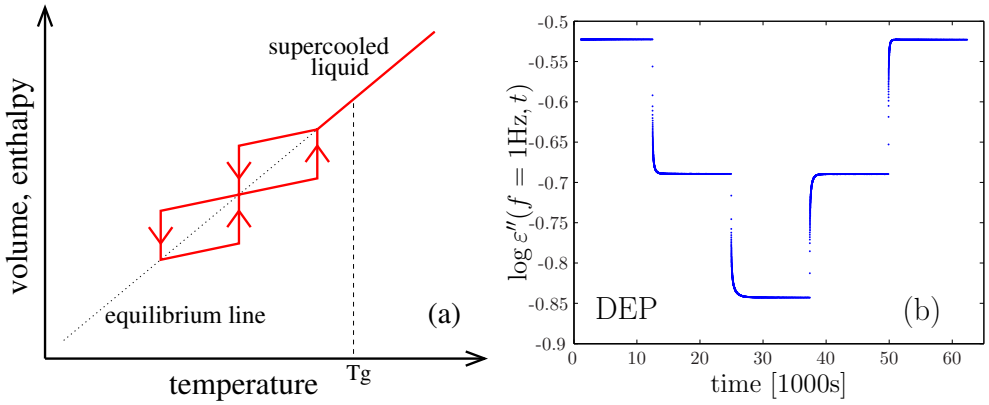

Figure 12.2 A typical measurement. (a) Schematic representation of the protocol in which the sample is first aged to complete equilibrium to a temperature slightly below the calorimetric glass transition temperature T_g, a process that typically takes weeks, followed by two down temperature jumps and two up temperature jumps. (b) Data from measurements on DEP following this protocol, jumping from 184K to 183K, further to 182K, and back to 183K and finally to 184K. The dielectric loss ε'' was measured as a function of time at the frequency $f = 1\text{H}z$. The duration of the measurement depends on the temperature range, i.e., how long it takes to equilibrate the sample fully after a temperature jump. Following this procedure we know the relaxation functions as well as the equilibrium values of the dielectric losses at the temperatures in question.

Aging was studied by monitoring how the dielectric loss at a fixed frequency, $\varepsilon''(f)$, develops as a function of time following a temperature jump. In order to avoid the liquid aging significantly during the measurement of a single frequency response data point, the monitoring frequency f must be considerably higher than the inverse structural relaxation time that is of order the inverse alpha loss-peak frequency; thus the monitoring frequency must be much larger than the loss-peak frequency. For the data analysis of sections 12.3 and 12.4 to apply, however, f must also be sufficiently below any contribution(s) from potential beta processes. These constraints vary with the liquid and the selected temperature range, and the choice of f was optimized for each liquid. For all five liquids the optimal f is in the Hertz range.

Measurements consist of consecutive temperature jumps of (usually) one or two Kelvin, in most cases with two down/up jumps followed by two up/down jumps. This is illustrated in Fig. 12.2, which in (b) shows the raw data obtained for DEP. Here $f = 1\text{Hz}$ and the temperature jumps are one Kelvin. The temperature protocol ensures that data are obtained for one up and one down jump to the same temperature. The duration of each measurement varies with the relaxation time of the liquid in question at the measured temperatures. A time-consuming part of the experiment is the initial aging to complete equilibrium at some target temperature just below the calorimetric glass transition temperature, which in most cases required weeks of annealing. In all cases care was taken to ensure that the loss at one temperature was monitored until the sample had reached complete equilibrium; only thereafter was temperature changed to a new value. In section 12.8 possible sources of errors in the experiments.

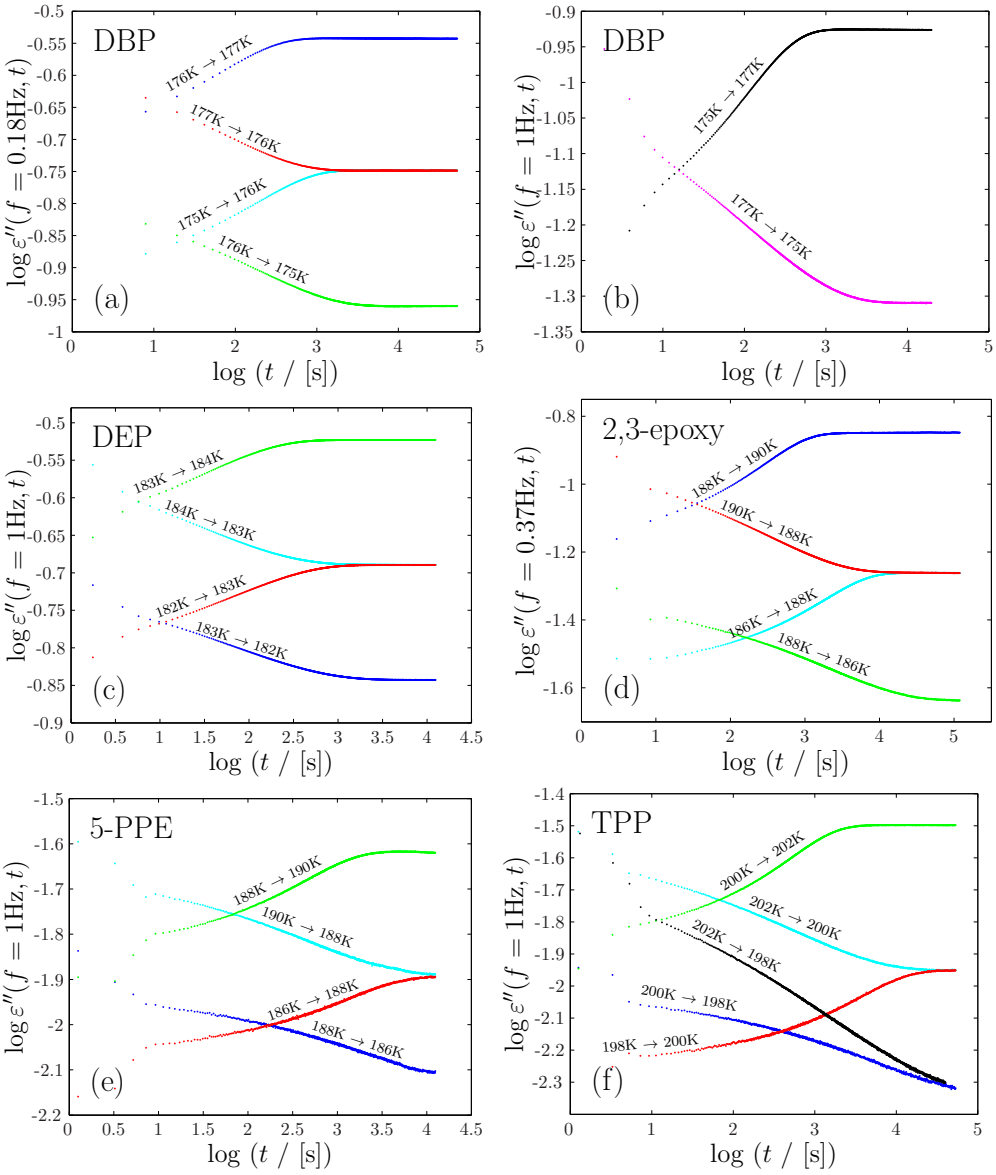

Figure 12.3 Monitoring aging by measuring the dielectric loss at a fixed frequency. This figure presents the full set of data upon which the paper's analysis is based. The data are given in log-log (base 10) plots showing the dielectric loss as a function of time. In all cases the starting situation ("$t = 0$") is that of thermal equilibrium, a condition that is ensured by annealing for such long time that no observable change is seen in the dielectric loss. (a) Dibutyl phthalate (DBP). A series of measurements at $f = 0.18$Hz stepping 1K from 177K and 175K to 176K, as well as the reverse. (b) DBP stepping from 175K to 177K and back, this time monitored at $f = 1$Hz. (c) Diethyl phtalate (DEP) ($f = 1$Hz). (d) 2,3-epoxy propyl-phenylether (2,3-epoxy) ($f = 1$Hz). (e) 5-polyphenyl-ether (PPE) ($f = 1$Hz). (f) Triphenyl phosphite (TPP) ($f = 1$Hz).

Figures 12.3(a)-(f) show the data. Two data sets were included for DBP, with aging monitored at different frequencies. Note that aging for down jumps to a given temperature is faster than for an up jump ending at the same temperature (compare, e.g., the two jumps to 200 K in Fig. 12.3(f)), which is due to the fictive temperature effects described in the previous chapter. The fact that the fictive-temperature effect is clearly visible in Fig. 12.3 shows that even relatively small temperature jumps of 1K or 2K are highly nonlinear.

For any experiment monitoring the relaxation of some quantity towards its equilibrium value, the normalized relaxation function $R(t)$ is defined by subtracting the long-time (equilibrium) limit of the quantity in question and subsequently normalizing by the overall relaxation strength [13, 17]. For a temperature jump from T_1 to T_2 starting from equilibrium the normalized relaxation function is given by

$$R(t) \;=\; \frac{\log \varepsilon''_{f_m}(T_2,t) - \log \varepsilon''_{f_m}(T_2,t\to\infty)}{\log \varepsilon''_{f_m}(T_1,t=0) - \log \varepsilon''_{f_m}(T_2,t\to\infty)}\,, \tag{12.1}$$

where f_m denotes the fixed frequency at which the dielectric loss is measured.

Taking now DBP as an example, Fig. 12.4(a) shows as functions of time the normalized relaxation functions for all six temperature jumps of Fig. 12.3(a) and (b). Figure 12.4(b) shows the corresponding KM relaxation rates (see Eq. (11.8)). At long times there is considerable noise in the KM rates because the relaxation rate is difficult to determine by numerical differentiation when the noise becomes comparable to $R(t)$ [21]. In order to eliminate unreliable long-time $\Gamma(t)$ data points we introduced a cut-off at 0.5% from equilibrium for all data sets. Despite the long-time noise it is clear that for up and down jumps ending at the same temperature (175, 176, or 177 K) the KM relaxation rates eventually approach the same number. This shows that there is no expansion gap as Kovacs proposed in 1963 based on experiments monitoring relaxation by measuring volume changes [9]. Figure 12.4(c) is a parameterized plot of $(R(t), \log(\Gamma(t)))$ which – except for the normalization of R introduced here – was the data representation originally used by Kovacs [9] (see Fig. 11.5 in the previous chapter). Again, it is clear that up and down jumps to the same temperature approach the same KM relaxation rate at long times ($R \to 0$). This observation is in agreement with the conclusion of Kolla & Simon [18], that the expansion gap vanishes for $t \to \infty$.

12.3 The internal clock hypothesis

According to the TN formalism, for all temperature jumps applied to a given system – small or large, up or down – the normalized relaxation function is a unique function of the material time that has passed since the jump was initiated at $\tilde{t} = 0$: $R = R(\tilde{t})$. In applications of the TN formalism one often allows for different material times to control the aging of different quantities (with the function $R(\tilde{t})$ varying with the quantity that is being monitored). But if an internal clock *really* exists, a common material time must control all relaxations. In particular, the relaxation of the clock-rate activation energy itself during aging must be controlled by the same material time that controls the dielectric aging process. A major point of paper III is to check against experiments the consequences of assuming that an internal clock exists. The next subsections develop a theory for testing this.

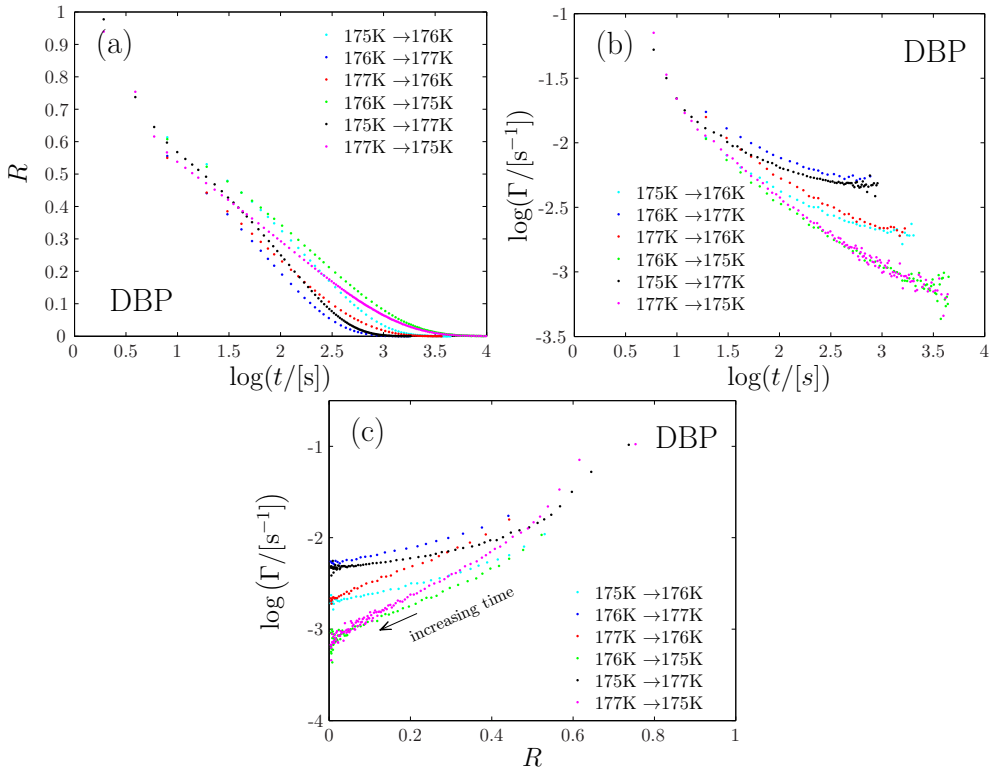

Figure 12.4 (a) Normalized relaxation functions for DBP as functions of log(time). (b) The Kovacs-McKenna (KM) relaxation rates Γ defined in Eq. (11.8) for these data, as functions of log(time). Up and down jumps ending at 176 K give the same relaxation rate at long times, showing that there is no so-called expansion gap as proposed by Kovacs in 1963 [9]. (c) Parameterized plot of $(R(t), \Gamma(t))$. Again, it is seen that different temperature jumps to the same temperature approach the same relaxation rate at long times (small R).

Determining the structural clock rate $\gamma_s(t)$ in the TN formalims usually involves some mathematical modelling, fitting of data, or assumption regarding what controls the relaxation [10, 13, 17, 63]. In Sec. 12.4 we develop a test of the internal clock hypothesis which does not require such procedures, but proceeds directly from data without explicitly determining the material time, $\tilde{t}(t)$. First, however, it is necessary to define precisely both the dielectric relaxation rate, γ_d, in an out-of-equilibrium situation and the structural clock rate, γ_s.

12.3.1 Defining the dielectric relaxation rate for out-of-equilibrium situations

The five liquids studied are all good glass formers that obey time-temperature superposition (TTS) for their main (alpha) process to a good approximation. Moreover, they all have a high-frequency decay of the loss that to a good approximation may be described by a power-law, $\varepsilon''(f) \propto f^{-n}$, where n is close to 1/2. In Fig. 12.5(a-b)

we show equilibrium dielectric loss curves at different temperatures for DBP and how they collapse when scaled with the loss peak position. It was conjectured some time ago that a high-frequency exponent of $-1/2$ reflects the generic properties of the pure alpha process obeying TTS (i.e., whenever the influence of additional relaxation processes is negligible) [64], a conjecture that was strengthened by a recent study involving more than 300 dielectric spectra [65]. For the below data analysis the exponent n was identified as the minimum slope [65] of the log-log plotted dielectric loss curve above the loss peak, evaluated at the temperature where the loss peak is 0.1 Hz (shown for DBP in Fig. 12.6(a)). The values for n thus obtained are listed in Table 12.1.

	DBP	DEP	2,3-epoxy	5-PPE	TPP
β	0.506	0.483	0.550	0.507	0.495

Table 12.1 The high-frequency slopes n used in the data analysis.

The inverse power-law high-frequency dielectric loss is used to monitor the dielectric relaxation rate $\gamma_d(t)$ as the structure ages following a temperature jump. This is done by proceeding as follows. First, we define the dielectric relaxation rate for the equilibrium liquid, γ_d, as the angular dielectric loss-peak frequency:

$$\gamma_d \equiv 2\pi f_{\max}\,, \tag{12.2}$$

where $f_{\max}$ is the loss-peak frequency. If temperature is lowered in a step experiment, the dielectric loss curve gradually moves to lower frequencies as the system ages and relaxes to equilibrium. How to define a dielectric relaxation rate γ_d for this out-of-equilibrium situation? It is not possible to continuously monitor the entire loss curve, because the aging takes place on the same time scale as that of the dielectric loss, implying that linear-response measurements around the loss peak frequency are not well defined (i.e., a harmonic input does not result in a harmonic output). To circumvent this problem, the intuitive idea is that how much the dielectric relaxation rate has changed may be determined from how much the loss has changed at some fixed frequency in the high-frequency power-law region, which is illustrated in Fig. 12.6(a). Mathematically, this corresponds to defining $\gamma_d(t)$ from the high-frequency equilibrium expression as follows

$$\varepsilon''(f,t) \;\propto\; (f/\gamma_d(t))^{-n}\,. \tag{12.3}$$

Thus by probing the dielectric loss at the fixed frequency f, the dielectric relaxation rate may be determined during aging from

$$\log\gamma_d(t) \;=\; \frac{1}{n}\log\varepsilon''(f,t) + A\,. \tag{12.4}$$

The calibration constant A is found by using equilibrium data from higher temperatures where the loss peak is within the observable frequency range. Figure 12.6(b) shows that the procedure of predicting the peak position by the measuring the dielectric loss at a fixed frequency indeed is valid; the loss peak positions for the spectra where the peak position is in the frequency window is shown in green triangles, while the predicted peak positions using the dielectric loss at different fixed frequencies are shown in black symbols. All curves line up at low temperatures (i.e. when the alpha peak has moved past the "probing" frequency) thus confirming the procedure.

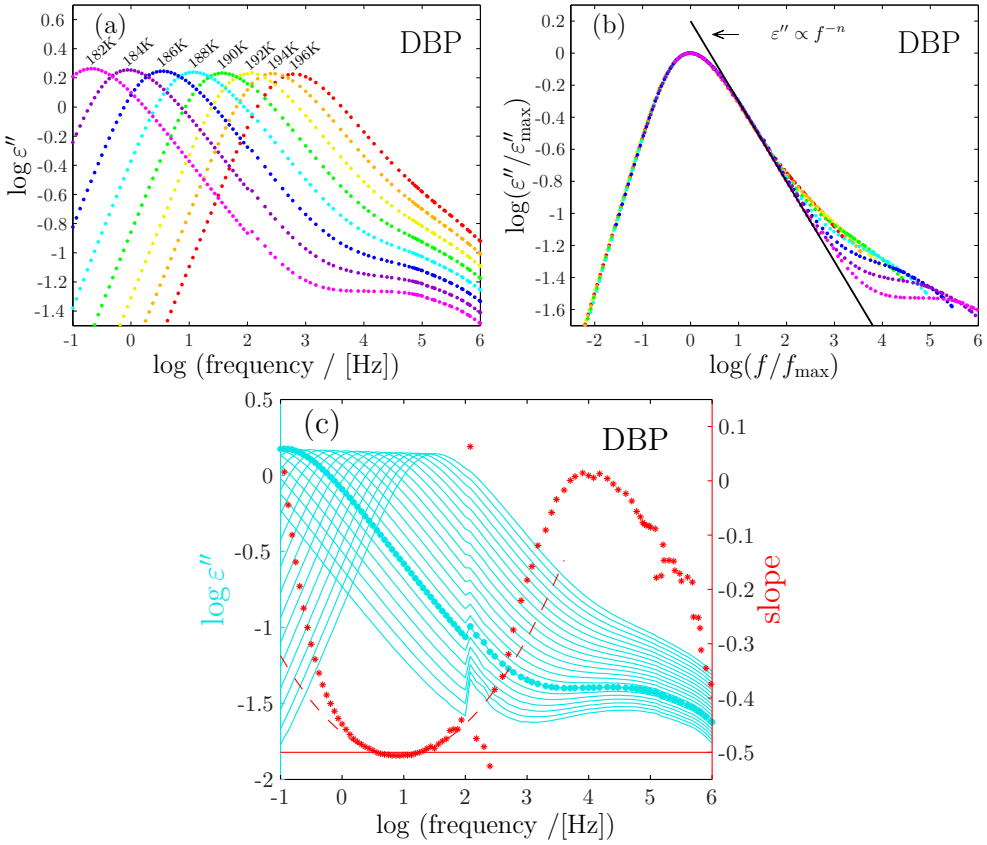

Figure 12.5 (a) Dielectric loss spectra for DBP above T_g (i.e., equilibrium data). (b) TTS plot of the same spectra illustrating that the high-frequency wing of the alpha (main) process approaches a slope of roughly $-1/2$ as temperature is lowered [64, 65]. All five liquids have high-frequency slopes close to $-1/2$, but this fact is not important for the analysis. (c) Illustration of the procedure used to determine the inverse power-law exponent n, which is identified as the minimum slope of the dielectric loss curve in a log-log plot at the temperature where the loss-peak frequency is 0.1 Hz (blue dotted curve). The red data points give the numerical slopes of this curve, and the red dashed curve is a parabola fitted to the bottom points of the slope; the analytic minimum of the parabola determines the minimum slope [65].

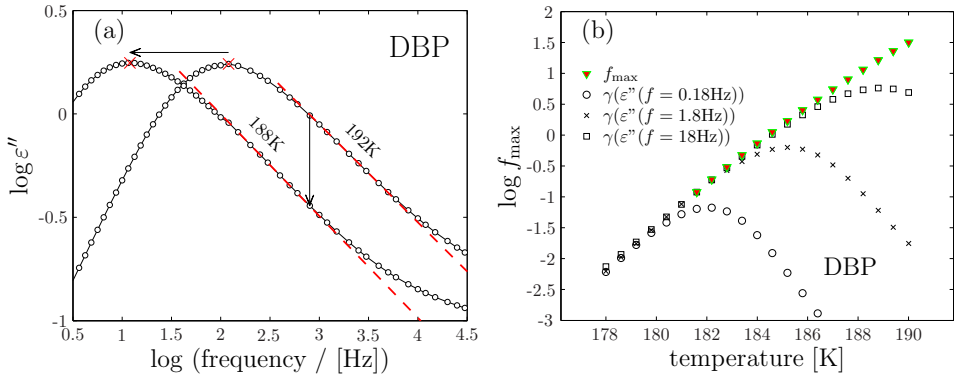

Figure 12.6 (a) Illustration of how one utilizes the fact that the loss varies as f^{-n} at high frequencies to measure the dielectric loss-peak frequency that by definition gives the dielectric clock rate, also during aging (Eq. (12.4)).(b) The loss-peak frequencies determined from the equilibrium spectra (green) and the predicted peak-positions using Eq. (12.4) below (corresponding to γ_d) at different measuring frequency. The curves line up at low temperatures, showing that this procedure determines the correct loss-peak frequency.

Although the above ideas seem straightforward, from a conceptual point of view one may question the validity of the concept of a dielectric relaxation rate in a situation where the structure ages on the same time scale as the dipoles relax. In order to specify the precise assumptions needed to justify defining $\gamma_d(t)$ via Eq. (12.4), we reason as follows. According to linear-response theory, for a system in thermal equilibrium the measured output is calculated from a convolution integral involving the input before the measuring time. A convenient way to summarize time-temperature superposition (TTS) for the equilibrium liquid is to formulate the convolution integral in terms of a dielectric "material" time $\tilde{t}$: If γ_d is the equilibrium liquid's dielectric relaxation rate (Eq. (12.2)), the dielectric material time is defined from the actual time t by

$$\tilde{t} = \gamma_d t\,. \tag{12.5}$$

In terms of $\tilde{t}$, since in a standard dielectric experiment the input variable is the electric field $\mathbf{E}$ and the output is the displacement vector $\mathbf{D}$, the convolution integral is of the form

$$\mathbf{D}(\tilde{t}) = \int_0^\infty \mathbf{E}(\tilde{t}-\tilde{t}')\psi(\tilde{t}')d\tilde{t}'\,. \tag{12.6}$$

Equation (12.6) describes TTS because it implies that, except for an overall time/frequency scaling, the same frequency-dependent dielectric constant is observed at different temperatures (we ignore the temperature dependence of the overall loss, an approximation which introduces a relative error into the data treatment well below 1% over the range of temperatures studied).

In Eq. (12.6), which applies at equilibrium whenever TTS applies, the dielectric material time is defined from the actual time by scaling with γ_d (Eq. (12.5)). In the out-of-equilibrium situation following a temperature jump, the simplest assumption

is that Eq. (12.6) also applies, however with a generalized dielectric material time involving a time-dependent dielectric relaxation rate $\gamma_d(t)$, i.e.,

$$d\tilde{t} \,=\, \gamma_d(t)dt\,. \tag{12.7}$$

As the system gradually equilibrates at the new temperature, the dielectric relaxation rate $\gamma_d(t)$ approaches the equilibrium liquid's loss-peak angular frequency at the new temperature. The equilibrium liquid's power-law dielectric loss $\varepsilon'' \propto f^{-n}$ applies in a range of frequencies obeying $f \gg f_{\max}$. Since by Eq. (12.6) $\varepsilon(\tilde{\omega}) = \int_0^\infty \psi(\tilde{t}')\exp(-i\tilde{\omega}\tilde{t}')d\tilde{t}'$ where $\tilde{\omega} = \omega/\gamma_d$, the equilibrium liquid's loss obeys $\varepsilon'' \propto \tilde{\omega}^{-n}$ for $\tilde{\omega} \gg 1$. By the mathematical Tauberian theorem this implies that $\psi(\tilde{t}') \propto (\tilde{t}')^{n-1}$ whenever $\tilde{t}' \ll 1$. The proposed generalization of Eq. (12.6) to out-of-equilibrium situations now mathematically implies that the dielectric relaxation rate $\gamma_d(t)$ is given by Eq. (12.3) (or Eq. (12.4)). Assuming the simplest generalization of TTS to out-of-equilibrium situations, we have thus defined a generalized dielectric relaxation rate; moreover we have shown how to measure it by monitoring the high-frequency dielectric loss at a fixed frequency using the inverse power-law approximation.

The procedure described above for determining the dielectric clock rate is equivalent to the time-aging time superposition [36–40] (described in chapter 11), where the short-time response of a perturbation of the liquid during an aging experiment is used to determine the shift factors [22, 41–43].

In the following we relate $\gamma_d(t)$ to the TN structural relaxation clock rate $\gamma_s(t)$, but first the latter quantity needs to be precisely defined.

12.3.2 Defining the structural relaxation clock rate

The structural relaxation clock rate $\gamma_s(t)$ determines the structural relaxation's material time in the TN formalism. Just as was the case for the generalized dielectric relaxation rate, it is not *a priori* obvious that any $\gamma_s(t)$ may be defined; the eventual test of the existence of $\gamma_s(t)$ is whether a consistent description is arrived at by assuming its existence. Assuming for the moment that this is the case, we define the structural relaxation clock rate's time-dependent activation (free) energy $E(t)$ by writing

$$\gamma_s(t) \,=\, \gamma_0 e^{-E(t)/k_B T} \;(\gamma_0 = 10^{14}\mathrm{s}^{-1})\,. \tag{12.8}$$

The activation energy $E(t)$ depends on the structure and evolves during the structural relaxation. Consider the case of structural relaxation induced by a general temperature variation. According to the TN formalism the aging of the activation energy is described by a linear convolution integral over the temperature history involving a material time $\tilde{t}_s$ defined by the analogue of Eq. (12.7),

$$d\tilde{t}_s \,=\, \gamma_s(t)dt\,. \tag{12.9}$$

Including for convenience the inverse temperature in the below equation, the linear convolution integral for the activation energy's evolution induced by a temperature variation, $T(t) = T_0 + \Delta T(t)$, is given by an expression of the form

$$\Delta(E/k_BT)(\tilde{t}_s) \;=\; \int_0^\infty \Delta T(\tilde{t}_s - \tilde{t}'_s)\phi(\tilde{t}'_s)d\tilde{t}'_s\,. \tag{12.10}$$

12.3.3 Assuming the existence of an internal clock

A main purpose of this work was to investigate the consequences of assuming that an internal clock exists. This assumption implies that the same material time controls dielectric aging via Eq. (12.6) and aging of the structural relaxation clock rate via Eq. (12.10), i.e., that for any aging experiment one has

$$\gamma_s(t) \;\propto\; \gamma_d(t)\,. \tag{12.11}$$

A clock works by counting repeated physical processes, and two clocks measure the same physical time if the number of ticks counted by the clocks are proportional for all time intervals. Thus both above-defined clock rates γ_d and γ_s are defined only up to a proportionality: The physical content of Eqs. (12.6) and (12.10) is invariant if the reduced times are redefined by multiplying by some number. Nevertheless, Eq. (12.11) is not trivial; thus Eqs. (12.6) and (12.10) may both apply with different definitions of the reduced time. As mentioned, the TN formalism is often used assuming that different physical quantities (e.g., volume and enthalpy) relax with rates that are not proportional [13, 22, 43, 48].

If Eq. (12.11) applies, we find via Eqs. (12.3) and (12.8) that after a temperature jump to temperature T the logarithm of the measured loss is given by

$$\ln\varepsilon''(f_{\max}, t) \;=\; -n\,\frac{E(t)}{k_BT} + C\,, \tag{12.12}$$

and that this quantity relaxes following a material time whose rate may be determined from Eq. (12.4). We proceed to derive a test of this prediction. If this is fulfilled, the internal clock hypothesis will be regarded as confirmed.

12.4 A test for the existence of an internal clock

In this section we show that the existence of an internal clock, i.e., the assumption that the dielectric clock rate is proportional to the structural relaxation clock rate (Eq. (12.11)), can be tested without evaluating $\tilde{t}$ explicitly and without fitting data to analytical functions.

First, we define a dimensionless KM relaxation rate by replacing time in Eq. (11.8) by the reduced structural relaxation time,

$$\tilde{\Gamma} \equiv -\frac{d\ln R}{d\tilde{t}_s}\,. \tag{12.13}$$

According to the TN formalism, for all temperature jumps $R(\tilde{t}_s)$ is the same function of $\tilde{t}_s$. This implies that $\tilde{\Gamma}(\tilde{t}_s)$ is the same for all jumps. By eliminating $\tilde{t}_s$, $\tilde{\Gamma}$ is a unique function of R:

$$\tilde{\Gamma} \;=\; \Phi(R)\,. \tag{12.14}$$

Thus one way of testing whether the TN formalism applies is to check whether $\tilde{\Gamma}$ is a unique function of the normalized relaxation function for different temperature jumps. To do this we express the dimensionless KM relaxation rate in terms of the real unit KM relaxation rate,

$$\tilde{\Gamma}(\tilde{t}) = -\frac{d\ln R}{dt}\frac{dt}{d\tilde{t}_s} = \frac{\Gamma(t)}{\gamma_s(t)}\,. \tag{12.15}$$

If an internal clock exists, $\gamma_s(t)$ may be evaluated from its proportionality to the dielectric relaxation rate Eq. (12.11), which is accessible via Eq. (12.4). Note that the unknown proportionality constant in Eq. (12.11) is irrelevant because, as mentioned, clock rates are only defined up to a proportionality constant (in Sec. 12.7 we discuss the possibility of absolute calibration of the structural and dielectric clock rates). Thus, if $\gamma_s(t) \propto \gamma_d(t)$, then $\tilde{\Gamma}$ may be calculated directly from a temperature jump experiment's data via Eq. (12.15), since $\Gamma(t)$ and $\gamma_d(t)$ are determined both from $\ln\varepsilon''(f_m,t)$ via Eqs. (11.8) and (12.4), respectively.

Defining the proportionality constant between the two rates to be unity, $\gamma_s(t) = \gamma_d(t)$, the results for the KM relaxation rates $\Gamma(R)$ and the dimensionless KM relaxation rates $\tilde{\Gamma}(R)$ are plotted in Fig. 12.7. For all five liquids the results are consistent with the internal clock hypothesis. Even the 4K down jump for TPP – corresponding to a clock-rate variation of almost two orders of magnitude – falls nicely onto the master curve. The spread in KM relaxation rates as $R \cong 0$ is approached at long times reflects the already mentioned fact that relaxation rates cannot be determined reliably by numerical differentiation when the noise becomes comparable to the distance to equilibrium.

Once the existence of an internal clock has been demonstrated, it is natural to evaluate the reduced time $\tilde{t}$ explicitly by integration in order to determine $R(\tilde{t})$. As shown in Fig. 12.8 this gives the data collapse predicted by the TN formalism. For the numerical integration one must either include short-time transient points, where the sample still undergoes temperature equilibration, or omit the initial measurements. The error introduced from this uncertainty influences all values of $\tilde{t}$. This is one reason to prefer the "direct" test of the internal clock hypothesis of Fig. 12.7; another reason is that the direct test is simpler because it avoids evaluating the material time $\tilde{t}$.

12.5 The approach of Lunkenheimer *et al*

Lunkenheimer and coworkers recently studied aging by monitoring the dielectric loss [58–60]. They found that the relaxation curves $R(t)$ to a good approximation may be described by a stretched-exponential relaxation function which, as a new feature, introduces a time-dependent characteristic time $\tau(t)$: $R(t) = \exp\left[-(t/\tau(t))^{\beta}\right]$. The nonlinear stretching exponent β was found to be identical to that derived from the linear dielectric relaxation function. This is a novel approach to aging studies. However, it does not lend any obvious physical interpretation to $\tau(t)$, which has the appearance of a "global" averaged relaxation time representing the entire aging process until time t. It is mathematically incompatible with the TN-formalism. In terms of a "reduced

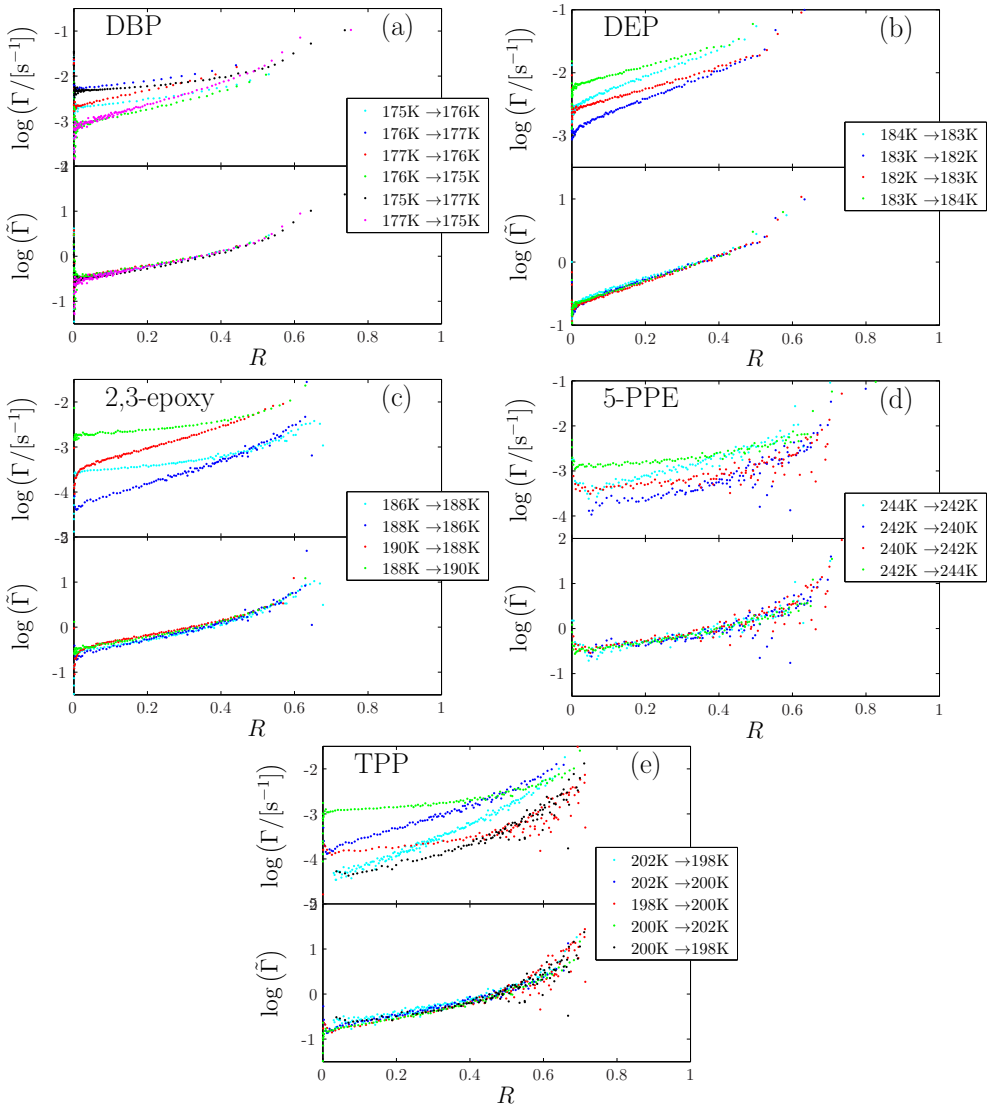

Figure 12.7 Kovacs-McKenna (KM) relaxation rates Γ and its dimensionless version $\tilde{\Gamma}(\tilde{t}) = \Gamma(t)/\gamma_d(t)$ (defined in Eq. (12.13) and calculated from data via the internal-clock hypothesis, $\gamma_s(t) = \gamma_d(t)$) as functions of the normalized relaxation functions R for the five liquids. For each liquid the upper subfigure shows $\Gamma(R)$, the lower subfigure shows $\tilde{\Gamma}(R)$. In all cases there is data collapse of $\tilde{\Gamma}(R)$ within experimental errors. This confirms the existence of an internal clock for these liquids.

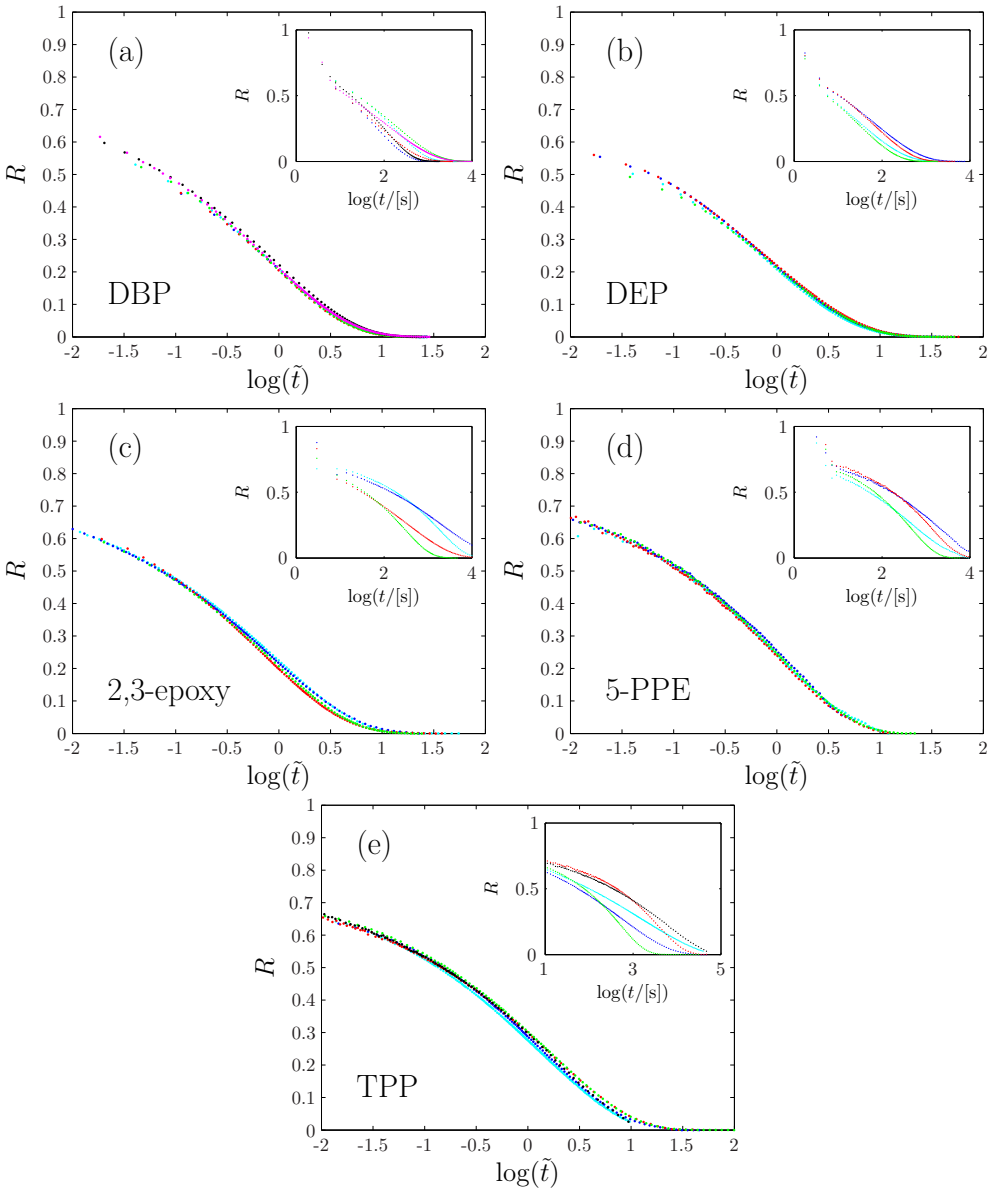

Figure 12.8 The traditional way of demonstrating TN data collapse by plotting the normalized relaxation functions as function of the reduced time, $R(\tilde{t})$. The insets show the normalized relaxation functions plotted against real time, $R(t)$.

time" the definition with this approach would read

$$\tilde{t} = t/\tau(t) = \gamma(t)t \tag{12.16}$$

which can not be valid at same time as the TN formulation of a reduced time in Eq. (11.12).

Since with our data we have direct access to the relaxation rate γ we can of course also test this approach. Figure 12.9 shows that this approach does not work nearly as well as TN-formalism for PPE. Further inspection reveals that Eq. (12.16) gives fairly good data collapse for temperature down-jump, and for temperature up-jumps respectively (compare with Fig. 12.8), but not an overall collapse.

Lunkenheimer and co-workers a recursive definition of the clock rate was used, which in our notation reads

$$\gamma(t) = [\gamma(t=0) - \gamma(t\to\infty)] \exp\left\{-(t/\tau(t))^{\beta_{age}}\right\} + \gamma(t\to\infty)\,, \tag{12.17}$$

where $\gamma(t=0)$, $\gamma(t\to\infty)$ and β_{age} were treated as fitting parameters. We have not tested this method of determining the clock rate which strictly speaking could give a different result than what we show in Fig. 12.9.

The approach of Lunkenheimer and co-workers [58–60] clearly does not work as well as the TN formalism when using the clock rate measured directly. From a pragmatic point of view this concept is also less useful than the TN formalism, since it is unclear how it should be applied to more complicated thermal histories.

12.6 Long-time asymptotic behavior of the structural relaxation

Inspecting the shape of the dimensionless KM relaxation rate as a function of the normalized relaxation function in Fig. 12.7 shows that the aging is not exponential, because that would imply a constant KM relaxation rate. The stretched-exponential function, $\exp[-\tilde{t}^{\beta}]$, is commonly used for fitting relaxation functions. It is difficult to get reliable data on the long-time behavior of structural relaxations, but our data allow one to get such data with fair accuracy. Figure 12.7 shows that $\tilde{\Gamma}(R) \to$ const. at long times ($R \to 0$) for all five liquids. This is also evident from the DBP data for which Fig. 12.10(a) shows the dimensionless Kovacs plots, a stretched exponential (red line), and Eq. (12.19) (blue line) with the values of the fit parameters listed in Table 12.2. The KM relaxation rate for the same data is in Fig. 12.10(b), where again is included a test of the fit by the stretched-exponential relaxation function (red straight line). Although the data become noisy at long times, they do show a bend over at long times that is inconsistent with the stretched exponential relaxation function – the KM relaxation rates approach a finite value at long times. The blue curve in Fig. 12.10 (b) is the "exponential $\sqrt{t}$" relaxation function detailed below.

The fact that the KM relaxation rates converge to finite values means that the relaxation function at long times follows a simple exponential decay. To model this mathematically with as few parameters as possible, we fitted the data to the following "exponential $\sqrt{t}$" relaxation function that retains features of a stretched exponential with exponent 1/2, but has a long-time simple exponential decay [35, 66]:

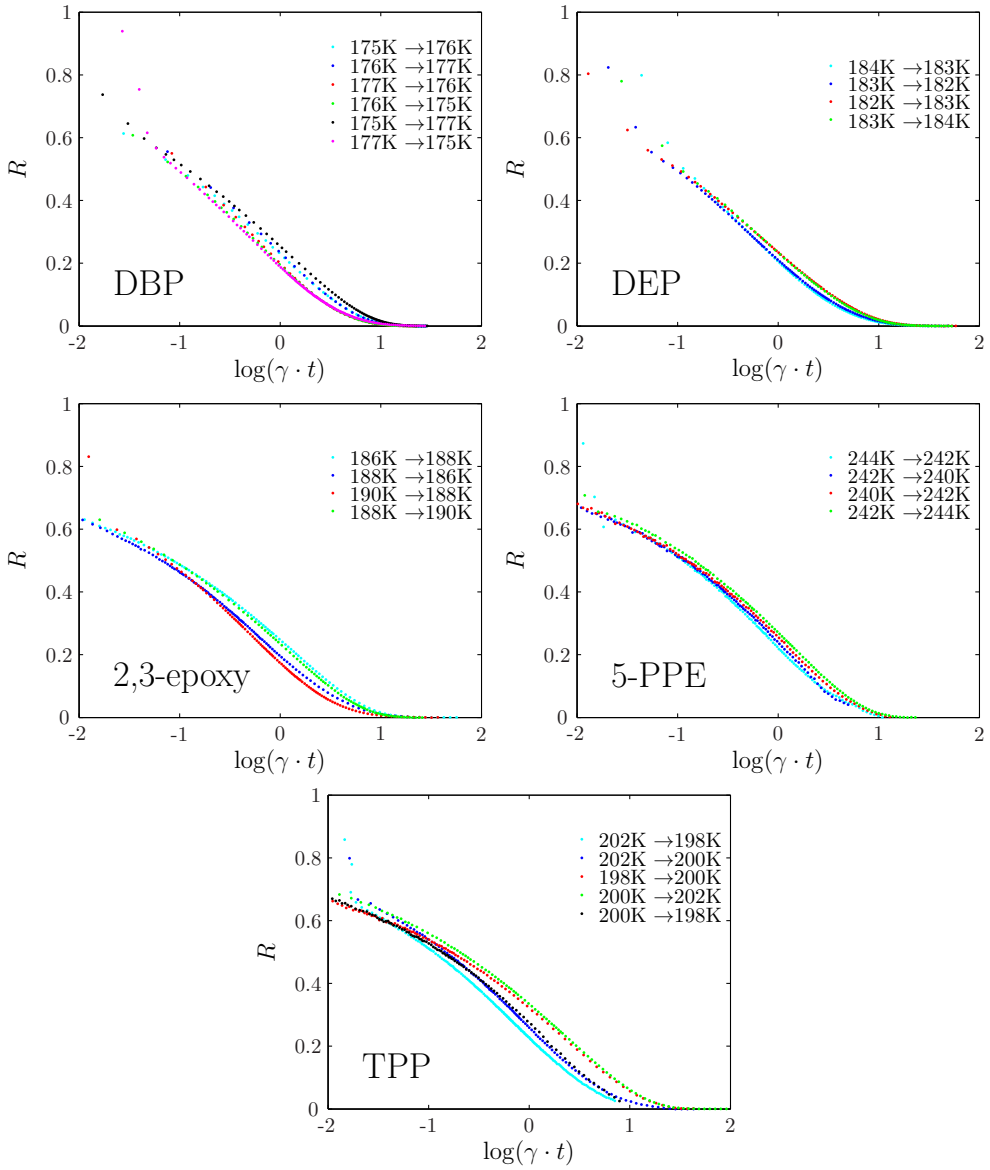

Figure 12.9 The result of using the definition of a reduced time of Eq. (12.16). Although it does gather the curves the data collapse is not as convincing as in Fig. 12.8.

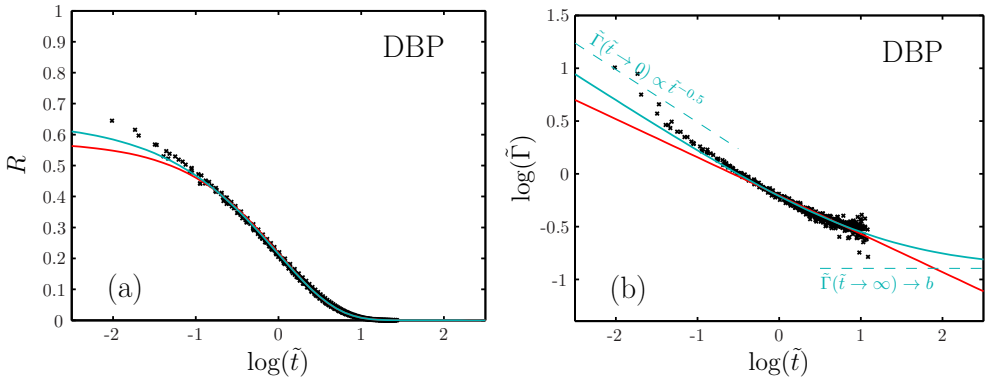

Figure 12.10 Fits of the "exponential $\sqrt{t}$ relaxation" function (Eq. (12.19)) (blue) and the stretched exponential ($R(\tilde{t}) = \exp\left(-a_{\rm se} - (b_{\rm se}\tilde{t})^{c_{\rm se}}\right)$) (red) to DBP data. (a) In the standard representation showing R as a function of $\log(\tilde{t})$ it is hard to distinguish the two fitting functions. (b) Relaxation rates as functions of the (reduced) times in a log-log plot. In this representation the stretched exponential function is a straight line, while the exponential $\sqrt{t}$ relaxation function of Eq. (12.19) has a "banana" shape: at short times it gives a straight line with slope $-1/2$, at long times it bends over and eventually levels off to a constant value. The two asymptotes are marked with dashed lines. Although the measurements are noisy at long times, we conclude that the data do not follow a straight line, but have a curved shape similar to the one suggested by the exponential $\sqrt{t}$ relaxation function.

$$R(\tilde{t}) = \exp\left(-A - B\tilde{t} - C\tilde{t}^{1/2}\right) . \tag{12.18}$$

Here A, B, and C are fitting parameters. The number A reflects the fact that, due to fast relaxations, the normalized relaxation function R does not start at unity at the shortest experimentally accessible times. The case $B = 0$ gives a stretched exponential with exponent $1/2$, the $C = 0$ case gives an ordinary exponential decay. At short times one has $R(\tilde{t}) \cong 1 - A - C\tilde{t}^{1/2}$, which justifies the name "exponential $\sqrt{t}$ relaxation function" (see Ref. [65] and its references to $\sqrt{t}$ relaxation in other contexts). Equation (12.18) may be rewritten in the more convenient form

$$R(\tilde{t}) = \exp\left(-a - b\tilde{t} - c(b\tilde{t})^{1/2}\right) \tag{12.19}$$

where $a = A$, $b = B$, and $c = C/\sqrt{B}$. Recast in this form, it is clear that b merely adjusts the time scale and that c is the only genuine shape parameter.

12.7 Calibrating the dielectric clock rate

The results obtained so far may be summarized as follows. The TN formalism predicts that the dimensionless KM relaxation rate (Eq. (12.13)) is a unique function of R for the relaxation towards equilibrium following any temperature jump. This can be tested only, however, if one is able to determine the structural relaxation clock rate $\gamma_s(t)$. This can be done either by some assumption about the clock rate's structure dependence – a common procedure – or, as above, by the internal clock hypothesis,

	DBP	DEP	2,3-epoxy	5-PPE	TPP
a	0.44	0.48	0.37	0.38	0.34
b	0.13	0.05	0.06	0.15	0.03
c	2.7	4.4	4.6	2.2	5.2
a_{kww}	0.55	0.55	0.42	0.45	0.38
b_{kww}	0.96	0.95	1.27	0.90	0.76
c_{kww}	0.64	0.57	0.56	0.64	0.54

Table 12.2 Values of fitted parameters of Eq. (12.19)

	DBP	DEP	2,3-epoxy	5-PPE	TPP
$\sigma^{\exp\sqrt{t}}_{\log(R)}$	0.041	0.029	0.042	0.023	0.026
$\sigma^{\exp\sqrt{t}}_{\log(\tilde{\Gamma})}$	0.052	0.028	0.081	0.172	0.111
$\sigma^{\mathrm{kww}}_{\log(R)}$	0.043	0.030	0.042	0.026	0.026
$\sigma^{\mathrm{kww}}_{\log(\tilde{\Gamma})}$	0.074	0.037	0.092	0.186	0.116

Table 12.3 Test of how well the two functions fit data, where superscript "exp $\sqrt{t}$" is the exponential $\sqrt{t}$ relaxation function of Eq. (12.19) and superscript "str exp" is the stretched exponential relaxation function. The quality of the fits is measured via the standard mean-square deviation σ for fitting, respectively, $\log(R)$ as a function of time and $\log(\Gamma)$ as a function of time. The exponential $\sqrt{t}$ relaxation function provides a somewhat better fit than the stretched exponential.

$\gamma_s(t) \propto \gamma_d(t)$, where the dielectric relaxation rate is determined from data via Eq. (12.4). The data do collapse as predicted by the internal clock hypothesis, confirming the existence of such a clock for all five liquids.

As emphasized, a clock rate is determined only up to a proportionality constant, i.e., two clocks measure the same physical time if their numbers of "ticks" are proportional for all time intervals. Still, one may ask whether some sort of absolute calibration of the dielectric and structural relaxation clock rates is possible. We defined the dielectric relaxation rate in equilibrium, γ_d, as the dielectric angular loss-peak frequency (Eq. (12.2)). This is convenient because the loss-peak frequency can easily be determined accurately. A characteristic feature of the dielectric losses of supercooled organic liquids is their pronounced asymmetry: Whereas the loss decays as a non-trivial power-law above the loss-peak frequency, at low frequencies the loss almost follows the Debye function ($\varepsilon''(\omega) \propto \omega$). Via the fluctuation-dissipation theorem the low-frequency behavior corresponds to a simple exponential long-time decay of the equilibrium dipole autocorrelation function. Inspired by the recent work of Gainaru *et* al. [67] it is obvious to ask whether redefining γ_d to be the rate of this long-time decay would imply that $\tilde{\Gamma} \to 1$ asymptotically at long times. In other words: Is the long-time exponential structural-relaxation clock rate equal to the exponential long-time decay of the equilibrium dipole autocorrelation function? Because the liquids studied here all obey TTS, such a recalibration of γ_d corresponds to multiplying each liquid's equilibrium γ_d (defined by Eq. (12.2)) by a fixed constant. This is illustrated in Fig. 12.11.

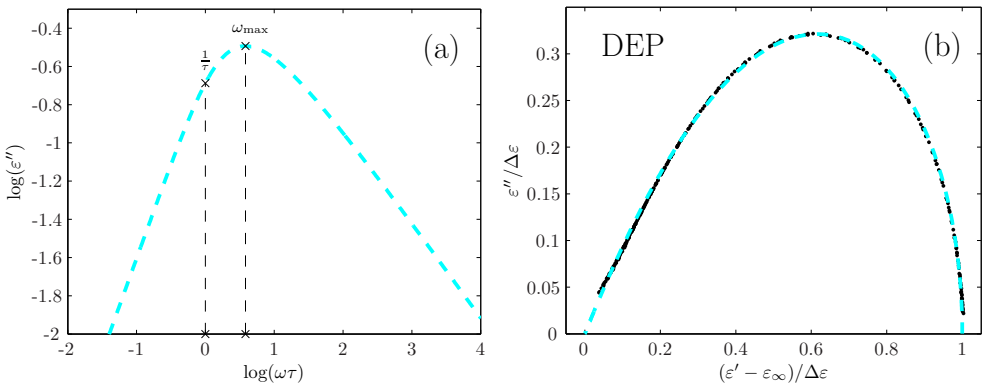

Figure 12.11 (a) Illustration of the difference between the two calibrations of the dielectric relaxation rate γ_d, using either the loss-peak angular frequency or the rate of the long-time exponential decay of the dipole autocorrelation function giving the low-frequency Debye behavior. (b) Normalized Cole-Cole plot of the dielectric loss of DEP (black dots) versus that of the "exponential $\sqrt{t}$ relaxation" model (Eq. (12.19)) used to fit the dielectric data at the following temperatures: 206 K, 207 K, 208 K, 209 K, 210 K, 211 K (blue dashed line).

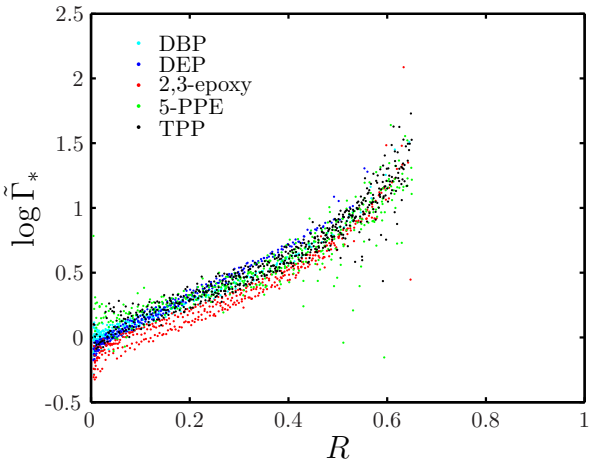

Figure 12.12 Dimensionless Kovacs plots including data for all temperature jumps of the five liquids, using the alternative calibration of the dielectric relaxation rate corresponding to scaling data with the long-time dielectric relaxation rate. This procedure "lifts" the curves of Fig. 12.7 such that the dimensionless KM relaxation rates all terminate at approximately one at long times ($R \to 0$).

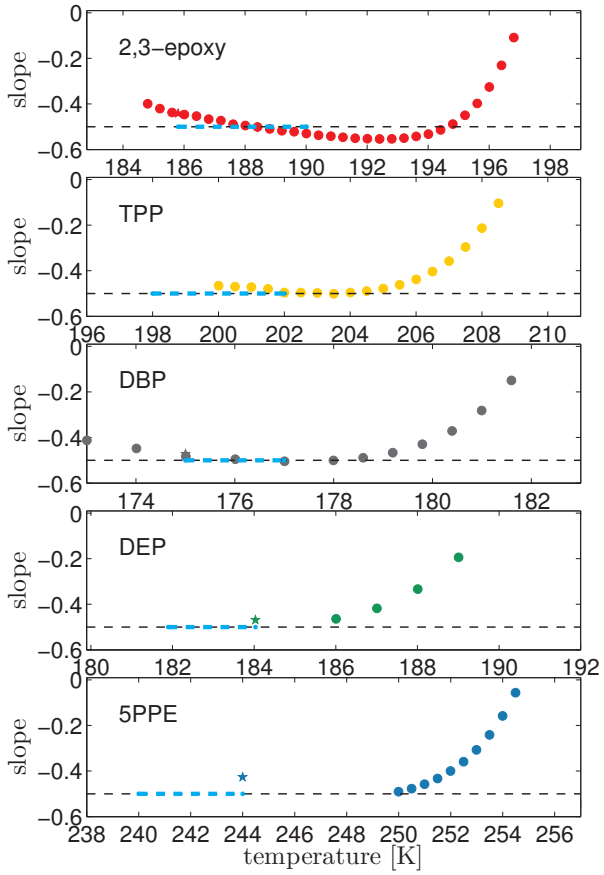

Figure 12.13 The slopes of the equilibrium log-log plotted dielectric losses at the measuring frequencies as functions of temperature. The aging interval is marked with a blue dashed line. For each frequency there is a temperature window where the slope is constant. In this way the measuring frequency and temperature jumps can be fine tuned such that the proposed method for finding the clock rate applies.

For each liquid the recalibration constant is obtained as follows. Assuming Eq. (12.19) for the equilibrium dipole autocorrelation function, the liquid's dielectric loss was fitted by the Laplace transform of the negative time-derivative of this function, which interestingly provides an excellent fit to the dielectric data of all five liquids (compare Fig. 12.11(b)). In Fig. 12.12 we show the result of applying this re-calibration of the dielectric relaxation rate in the analysis of Sec. 12.4. Within experimental uncertainties all recalibrated KM relaxation rates converge to one at long times ($R \to 0$). This suggests an underlying unity in the description of aging for the liquids examined in this paper.

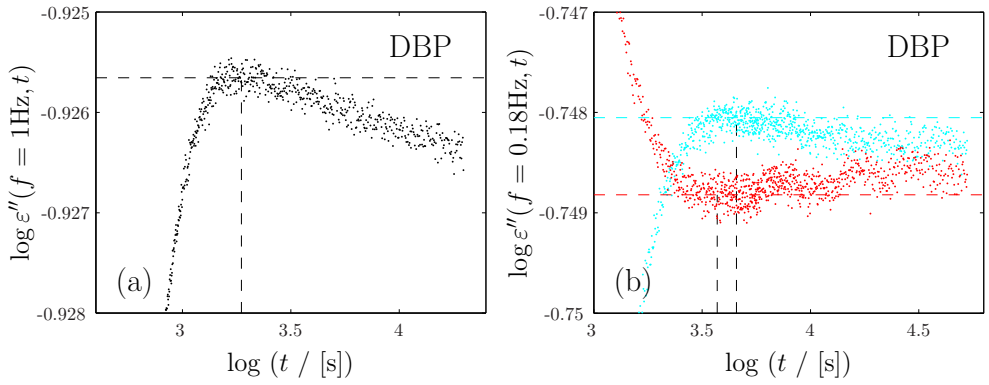

Figure 12.14 Examples of the issues with determining the long $\varepsilon''(f_m, t \to \infty)$ limit of the data. (a) Zoom of the tail of the 2K up jump to 175K for DBP (data of Fig. 12.3(b)). There is a small drift at long times, which is due to the slow (compared to the alpha relaxation time) radial flow of the liquid in the measuring cell. The dashed vertical line marks where the data were cutoff and the dashed horizontal line marks the $\epsilon''(f_m, t \to \infty)$ level used in the analysis. (b) Zoom of the approach to equilibrium for the 1K up and down jump to 176K. There is a small overshoot in the up-jump and a small undershoot in the down-jump before the two curves eventually approach the same value (as they should). The vertical lines show where the data were cut off at the bottom of the over- or undershoot.

12.8 Systematic errors and noise

We discuss here the some sources of errors of the data and the analysis presented in this study. For a general and systematic analysis of errors and noise of the measurement we refer to Igarashi *et al* [49, 50].

The geometry of the measuring cell (disc radius much larger than disc separation) introduces an extremely slow radial contraction which in equilibrium dielectric measurements can be neglected. For aging experiments it poses a problem because it introduces a small drift at long times, which distorts the curve shape of the aging relaxation function and complicates the determination of the value approached at long times. In Fig. 12.14 a zoom of the tail of the DBP data from Fig. 12.3(b) is shown. The drift is small, but clearly visible. After a temperature step the curve should level off to a constant (equilibrium) value, instead the curve appears slightly slanted. The drift coming from the initial quench may be reduced by annealing for long time before starting a measurement (typically over several weeks), which we did.

A further source of error is that in some cases we also observe a small overshoot when approaching equilibrium. We do not currently have an explanation for this, but it may be due to something other than the drift. Whenever a small drift or an overshoot was present, we chose to cut the data shortly after reaching its maximum/minimum and $\varepsilon''(t \to \infty)$ was adjusted accordingly. This is illustrated in Fig. 12.14 where the $\varepsilon''(t \to \infty)$ is marked by a horizontal dashed line and the cut-offs by a vertical dashed line. Ideally, of course, the level approached from above and below should be identical, but the deviation is in the permille range.

The signal-to-noise ratio depends on the (dielectric) relaxation strength (correspond-

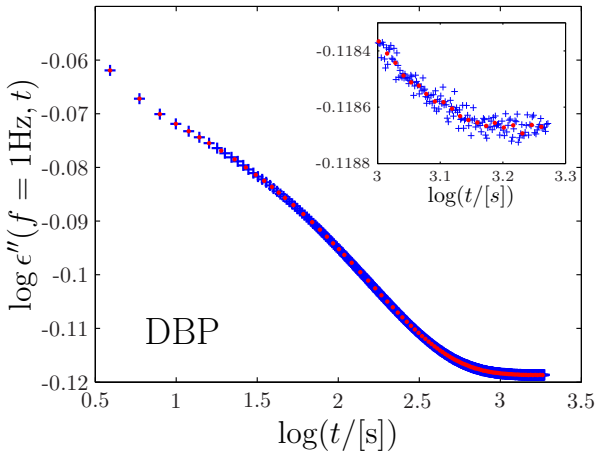

Figure 12.15 Illustration of the smoothing procedure described in the text. Blue +'s are the measured data points, red ·'s are the averaged data points used in the analysis. The algorithm minimizes the distortion of the curve shape by averaging over few (or no) data points in the beginning and more data points towards the end of the relaxation. Inset shows a zoom on the tail of the relaxation curve.

ing to the absolute level of the dielectric loss) of the liquids studied. Thus, there is more noise in the data for TPP and 5-PPE, which have relatively small dielectric relaxation strengths, compared to DBP, DEP, and 2,3-epoxy, which have larger relaxation strengths.

Although the precision of a dielectric measurement is high with barely any visible noise in the relaxation curve, we still encounter noise problems when taking the numerical derivatives of these curves. Averaging over even few data points distorts the curve shapes at short times, but it is necessary (and also less problematic) to average over more data points in the long time tails of these curves. To deal with this problem we designed an algorithm to average over a number of data points that increases with aging time, i.e., no averaging of the first data points and ending up averaging over 8 (in the case of DBP and 2,3-epoxy) or 16 (in the case of DEP, 5-PPE, and TPP) data points in the tail. This procedure is illustrated in Figure 12.15.

In Fig. 12.13 we show the slope of the equilibrium dielectric loss at the measuring frequencies of the aging experiment as a function of temperature. The temperature intervals used in the aging experiments are marked with a blue line. For each frequency there is a temperature window where the slope is constant (close to $-1/2$). In this way the measuring frequency and temperature jumps can be fine-tuned such that the proposed method for finding the clock rate is valid. The graphs show that not all measurements are carried out in the optimal regions. The slopes vary a little in the aging temperature interval studied for some of the liquids, and they are not entirely identical to the value above T_g. Thus the conditions for the proposed method for determining the clock rate are not fulfilled in all cases. However, one can still obtain data collapse using a slightly incorrect inverse power-law exponent since the error made is the same for all data points. The error simply results in a vertical shift of the curves

in Fig. 12.7 and a horizontal shift in Fig. 12.8. A slight variation of the power-law exponent in the measured temperature interval will influence the shape of the master curve and may explain why the data collapse is not perfect.

12.9 Concluding remarks

We have shown how the internal clock hypothesis can be checked in a test that neither involves free parameters nor the fitting of data to some mathematical expression. The test is based on assuming the standard Tool-Narayanaswamy formalism for structural relaxation studied by monitoring the liquids' dielectric loss at a fixed frequency in the Hertz range, following temperature up and down jumps. Based on data for five organic liquids we conclude that: 1) All liquids age consistent with the TN formalism; 2) All liquids have an internal clock; 3) No liquid exhibits an expansion gap; 4) All liquids have exponential long-time relaxation; 5) The long-time structural-relaxation clock rate equals that of the long-time simple exponential decay of the dipole autocorrelation function.

Our finding that the liquids have exponential long-time relaxation is consistent with several classical viscoelastic and aging models; for instance is the KAHR model [26] based on a box distribution of relaxation times, which implies the existence of a longest relaxation time and thus an exponential long-time relaxation. It is also worth emphasizing that, in contrast to reports for other materials (e.g., oxide glasses) where there is evidence that the material clock does not tick the same way for all processes, the data presented here are consistent with the existence of a unique material time. We have shown that the structural relaxation rate is proportional to the dielectric relaxation rate for five organic supercooled liquids, and the fact that the structural relaxation was monitored by measuring the dielectric loss is, in our opinion, probably not important. Nevertheless, it would be interesting to study for instance volume relaxation for the same liquids to investigate whether there really is a common material clock for these liquids. We finally note that, in contrast to the well-known TNM formalism of Moynihan *et al.* [10], the analysis applied here does not require one or more fictive temperatures.

The emphasis of the data analysis was on using data directly without having to fit to analytical functions. This is why we determined the dielectric clock rate from the loss-peak angular frequency (Eq. (12.2)) and the exponent β as the minimum slope of the dielectric loss at the temperature where the loss peak frequency is 0.1 Hz (Table 12.1). If this purist approach is relaxed a bit, however, further interesting features appear. Thus if the dielectric clock rate is instead determined from the dielectric loss' low-frequency Debye-like behavior, all KM relaxation rates converge to unity at long times (Fig. 12.12). Moreover, since the minimum slopes are not completely temperature independent, but converge to the in Ref. [65] conjectured generic value of $-1/2$ at the lowest temperatures (Fig. 12.13), one may ask what happens if the exponent β of Eq. (12.4) is replaced by $-1/2$. The result of repeating the entire analysis with this high-frequency exponent is shown in Fig. 12.16. The main effect is to lift the 2,3-epoxy data, the liquid whose exponent β was furthest from $-1/2$. Since the long-time structural relaxation clock rate, if identical to the redefined dielectric relaxation rate, should approach the latter from above, this figure is consistent with the conclusion that the two rates are identical.

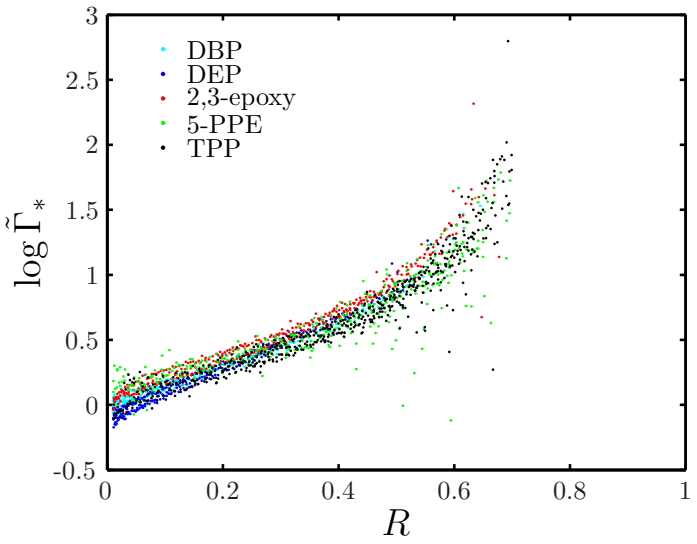

Figure 12.16 Dimensionless Kovacs plots including data for all temperature jumps of the five liquids, using the alternative calibration of the dielectric relaxation rate corresponding to scaling data with the long-time dielectric relaxation rate and assuming for all liquids the high-frequency exponent of the dielectric loss $-1/2$ [65].

In current state-of-the-art aging experiments the characteristic thermal equilibration time τ is at least 100 s, if τ is defined from the long-time thermal-diffusion-limited approach to equilibrium $\sim \exp(-t/\tau)$. This reflects the fact that heat conduction is a notoriously slow process. Experience shows that in order to monitor an almost complete aging curve at least four decades of time must be covered; for instance the typical aging function $\exp(-K\sqrt{t})$ decays from 97% to 3% over four decades of time. Thus with present methods, one needs at least of order $100\,\mathrm{s} \times 10^4 = 10^6\,\mathrm{s}$ to have an almost ideal temperature down-jump experiment. This is more than a week. Clearly much is to be gained if it were possible to equilibrate sample temperatures faster.

13 Single parameter relaxation functions

In the last roughly twenty years the stretched-exponential function has become an icon of relaxation phenomena. If the normalized relaxation function is denoted by $R(t)$, the stretched exponential (SE) relaxation function is defined by

$$R(t) = \exp\left[-(t/\tau)^{\beta}\right] \tag{13.1}$$

where $0 < \beta < 1$ is the so-called stretching exponent and τ a characteristic time.

The use of this function goes back to Kohlrausch more than 150 years ago [68], and the stretched exponential function is sometimes referred to as the Kohlrausch or the Kohlrausch-Williams-Watts (KWW) relaxation function [69]. The stretched exponential function has been rediscovered several times in quite different contexts. In 2009 alone more than 100 papers appeared that fitted experimental data or computer simulations to a stretched exponential in physics, chemistry, materials science, engineering sciences, etc. The interesting history of the stretched exponential function was recently reviewed by Cardona et al. [70].

The popularity of the SE function comes from the fact that it provides a good single-parameter fit to many relaxation data. Mathematically, if the stretched exponential function is written as a weighted sum over exponentials with different relaxation times, the relaxation-time distribution is asymmetric and dominated by the shorter relaxation times when plotted on a logarithmic scale. This characteristic asymmetry is found in numerous experiments. We believe that this fact, in conjunction with the SE functions purely mathematical beauty, accounts for the popularity of the stretched exponential for fitting data whenever a single- parameter representation is sought. Once relaxation data have been fitted by a stretched exponential, it is common procedure to correlate the stretching exponent β to various other characteristics of the system in question (see, e.g., [71, 72]). The fact that Eq. 13.1 fits many data quite well has catalyzed theorists to contemplate why this is, and there are now many derivations of this function. An overview of some of these may be found in Phillip's review from 1996 [73].

While it is well known that the stretched exponential rarely fits data perfectly, its common use is explicitly or implicitly justified from a belief that may be summarized as follows:

> The stretched-exponential function provides the best overall single-parameter fit to relaxation data.

It is this statement that we wish to test.

13.1 Alternatives to the stretched exponential

In the previous chapter another function emerged, that seem to capture the asymptotic high and low frequency behavior of the studied liquids better than the stretched exponential. We call it the "exponential $\sqrt{t}$" relaxation function. The exponential $\sqrt{t}$ relaxation function is constructed by multiplying a stretched exponential function with $\beta = 1/2$ by a simple exponential.

The stretching exponent is fixed to $1/2$ because there are indications that dielectric relaxation is characterized by an inherent more or less universal high-frequency slope of $-1/2$ [64, 65, 74]. At the same time data are generally closer to Debye behavior at low frequencies than predicted by the stretched exponential function, indicating the existence of an effective long-time cutoff in the relaxation time distribution; thus the introduction of an additional simple exponential function in Eq. 13.2.

The mathematical expression for the exponential $\sqrt{t}$ relaxation function is

$$R(t) = \exp\left[-C\sqrt{t/\tau} - t/\tau\right]. \tag{13.2}$$

The dimensionless parameter C governs when one function "takes over" from the other. For small C's we get a narrow distribution of relaxation times and a narrow dielectric loss peak, for large C's the loss peak broadens to eventually become as broad as that of the $\beta = 1/2$ SE function. This function has the same number of parameters as the SE functions, namely one dimensionless parameter relating to the shape of the dielectric loss peak in a log-log plot, one τ that gives the characteristic relaxation time.

The "exponential $\sqrt{t}$ relaxation" function is similar to the "modified stretched exponential" introduced by Saglanmak *et al* [66] and the "composite relaxation function" introduced by Hornbøll *et al* [35] which both are functions that combine the stretched exponential with a long-time exponential cut-off.

Cole-Davidson (CD) relaxation function [75] is another popular fitting function, and judging from Fig. 13.1, it could well represent a challenge the SE function. The figure is taken from Nielsen *et al* [65] and shows the minimum slope (see below for a definition) plotted against the width of the dielectric loss peak as well as the predictions of the CD and SE functions. The data in the analysis lies between the two lines predicted by CD and SE, but significantly closer to the CD prediction. The CD relaxation is purely empirical and invented to fit non-Debye dielectric relaxation data. It is given in the frequency domain as follows

$$\varepsilon(\omega) = \varepsilon_\infty + \frac{\Delta\varepsilon}{(1 + i\omega\tau)^{\beta_{\mathrm{CD}}}}. \tag{13.3}$$

Again τ is a characteristic time, β_{CD} is a dimensionless shape parameter, $\Delta\epsilon$ is the relaxation strength, and ε_∞ is the high frequency limiting value of the dielectric constant. The CD relaxation function also has a rather sharp cut off in relaxation times, but the shape parameter allows for different limiting high-frequency power-laws.

The last of the one-parameter functions we will study is the model for generic dielectric alpha relaxation proposed by Dyre [76]. In the frequency domain the generic alpha (GA) relaxation function is given by a sum of Debye term and a term involving the

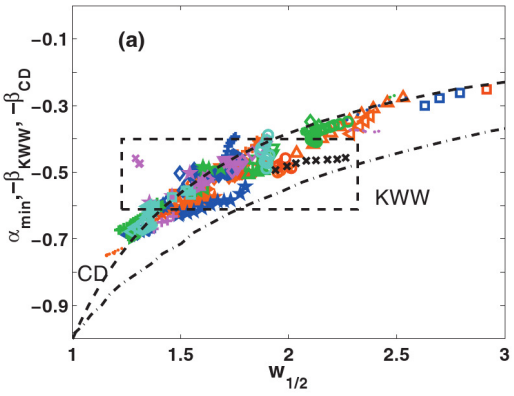

Figure 13.1 Figure from Nielsen *et al* [65] showing the minimum slope (Eq. (13.5)) plotted against the half-width of the data as well as the predictions of the CD and SE functions. Based on this figure one would guess that the CD function was probably a better choice than the SE function for fitting these data.

square root of a Debye

$$\varepsilon(\omega) = \varepsilon_\infty + \Delta\varepsilon \left[C \left(\frac{1}{\sqrt{1+i\omega\tau}} + \frac{1}{\sqrt{2+\sqrt{1+i\omega\tau}}} \right) + \frac{1}{1+i\omega\tau} \right] \tag{13.4}$$

As with the CD function, we have three parameters fixing position and magnitude of the spectrum (τ,$\Delta\epsilon$, and ϵ_∞) and a single shape parameter, C. The GA function also predicts a high frequency loss with a square root dependence of the frequency, $\epsilon'' \propto \omega^{-1/2}$, as does the exponential $\sqrt{t}$ relaxation function. And the C parameter plays much the same role as the C parameter from the exponential $\sqrt{t}$ relaxation function: it determines when the Debye behavior dominates.

As the only function mentioned here this function is theoretically derived. However, it has hardly received any attention in the community and thus it is not known if it gives a good fit to data.

13.2 Data selection procedure

By far the most accurate relaxation data are those of dielectric relaxation measurements, a technique that today routinely covers frequencies from mHz to MHz (and beyond, if required). For super-cooled, glass-forming organic liquids, in particular, abundant amounts of dielectric relaxation data are available today. For the below analysis we included data for 53 organic glass-forming liquids, altogether 429 different spectra (each liquid has several spectra referring to different temperatures). The data sets were collected from leading groups and supplemented by own data. The liquids in study are listed in Table 13.1.

The analysis is based on data for the dielectric loss as a function of frequency at different temperatures. The analysis focuses on the main (alpha) dielectric loss peak, because

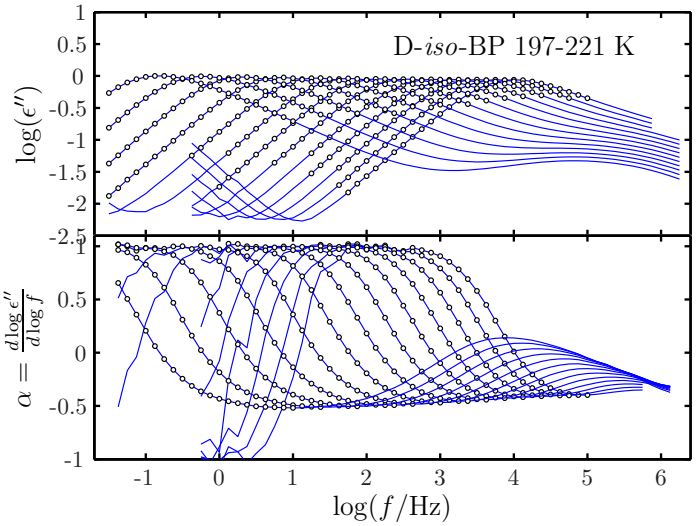

Figure 13.2 An example of how we selected the subset of data points to be included in the analysis. The data points used for the fits go from the inflection point on the low-frequency side of the alpha peak to the inflection point on the high-frequency side.

the one-parameter relaxation functions can only fit a single loss peak. Moreover, since the SE function predicts a loss that in a log-log plot has no inflection points, we fitted the data's low-frequency inflection point below the loss-peak frequency to the high-frequency-inflection point. As an example, Fig. 13.2 shows dielectric relaxation data for di-iso-butyl phthalate at different temperatures in a log-log plot (blue curves, upper panel). At high temperatures (the spectra to the right) one observes an increase of the loss at low frequencies; this is due to the commonly observed DC conduction. At low temperatures the beta process is visible. The data range for fitting must be limited to exclude both phenomena, which is obtained by fitting from low-frequency to high-frequency inflection point. The lower panel of Fig. 13.2 shows the numerical point-by-point slope of the data, i.e.

$$\alpha = \frac{d\log\epsilon''}{d\log\omega}. \tag{13.5}$$

From this we determined the relevant frequency range at each temperature, marked by the black symbols in both panels.

The logarithmic derivative is also the key the to determining the minimum slope [64, 65, 74], defined as the minimum of the α in Eq. (13.5) on the high frequency side of the loss peak. For most liquids there is so little noise in the spectrum that even the numerical derivative is smooth. But for a some liquids (typically those with a relatively weak dielectric relaxation strength) the derivative is so noisy that just picking the minimum of the numerical derivative would not give a reasonable value. We show an example, cumene (IsoPB) at 130K, in Fig. 13.3. To avoid these erroneous $\alpha_{\min}$ values we introduced a smoothing of the curve by a moving point average, averaging over 3 point of either side of the current point. This is shown as the pink full line in the figure. We

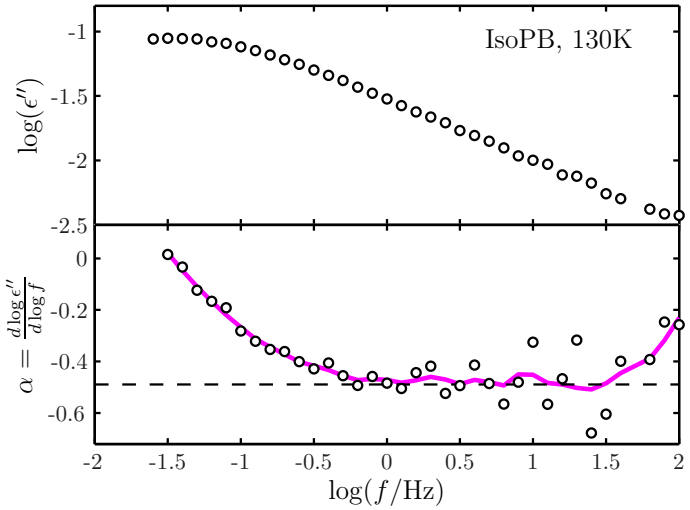

Figure 13.3 Procedure to find the minimum slope of the dielectric loss. Top panel show the data in a log-log plots. Bottom panel shows the numerical derivative. Just taking the minimum of the derivative would obviously give a wrong minimum slope due to noise scatter. The full line is a moving average of the derivative and the minimum of this will yield a "correct" minimum slope. We have marked this value by the dashed line.

now set $\alpha_{\min}$ equal to the minimum of the smoothed derivative (on the high frequency side of the dielectric loss), but only if the neighboring values are close. Otherwise, this point is discarded and the new minimum value is chosen and so on until all demands are met.

The minimum slope, $\alpha_{\min}$, is a measure of the true high frequency power law behavior of the spectrum.

13.3 Details of the fitting routines

When fitting an equation to data, one often has different choices to make, that may influence the results. First choice we have already made, namely what data-points to include in the analysis. The next important choice to make is what function we want to minimize. In our case there are two rather different options: we can either minimize the mean squared distance from fit to data logarithmically or linearly. The first option will focus on the asymptotic low- and high-frequency behavior and the second will focus mainly on the peak area. To minimize the influence of additional (beta) processes our initial incentive was to do the linear fit, but in the end we did both.

All fitting routines were performed with the 'fminsearch' function in MatLab which uses a simplex search method. We found this algorithm to give the most stable results.

In the case of dielectric relaxation, the normalized relaxation function R(t) gives the relaxation to equilibrium as function of time after application of a constant electric field. In general, from R(t) the complex frequency-dependent dielectric constant $\epsilon(\omega)$

is given by

$$\epsilon(\omega) = \epsilon_\infty + \Delta\epsilon \left[\mathcal{L}\left\{-\frac{dR(t)}{dt}\right\}\right](\omega) \tag{13.6}$$

$$= \epsilon_\infty + \Delta\epsilon \left(1 - i\omega \int_0^\infty R(t)\exp(-i\omega t)\,dt\right) \tag{13.7}$$

where ω is the angular frequency, $[\mathcal{L}f]$ the Laplace transform operator, ϵ_∞ is the high-frequency loss, and $\Delta\epsilon$ the dielectric loss strength.

For calculating the Laplace transform accurately when $R(t)$ is the stretched exponential relaxation function, which may be numerically tricky, we used Wuttke's numerical C-routine *libkww* [77].

For calculating the Laplace transform when $R(t)$ is the exponential $\sqrt{t}$ function, we used a combination of the semi-analytical Laplace transform and a numerical integration method (details can be found in Appendix E). The semi-analytical expression is given by a rather complicated expression involving the complex errorfunction:

$$\begin{aligned}\epsilon(\omega) =& \epsilon_\infty + \Delta\epsilon \left[\frac{1}{C^2}\frac{1}{1+i\omega\tau}\right. \\ &- \frac{1}{2C^2}\frac{\sqrt{\pi}}{\sqrt{1+i\omega\tau}^3}\exp\left(\frac{1}{4(1+i\omega\tau)}\right)\operatorname{erfc}\left(\frac{1}{2\sqrt{1+i\omega\tau}}\right) \\ &\left.+\frac{1}{2}\frac{\sqrt{\pi}}{\sqrt{1+i\omega\tau}}\exp\left(\frac{1}{4(1+i\omega\tau)}\right)\operatorname{erfc}\left(\frac{1}{2\sqrt{1+i\omega\tau}}\right)\right].\end{aligned} \tag{13.8}$$

With a rational approximation for the complex errorfunction this gives the correct Laplace transform for values of $C < 5$.

13.4 Comparing fits to data

Before presenting the overall picture that compares the SE relaxation function to the exponential $\sqrt{t}$, the CD, and the GA functions, Fig. 13.4 gives examples of fits of these functions to dielectric loss data. To demonstrate the wide range of behaviors that a successful fitting function must capture, the figure shows the spectrum with the highest $\alpha_{\min}$ (top), the lowest $\alpha_{\min}$ (bottom), and the spectrum with $\alpha_{\min}$ closest to 1/2.

In general all 4 four functions show impressive fits for most liquids. For the few cases where dc-conductivity severely interferes with the low frequency power-law ($\epsilon'' \propto \omega$), e.g. for DCHMS, isoeugenol, and 246MTH or if the beta-relaxation mixes with the alpha, e.g. in TolPyr at high temperatures (shown in the top of Fig. 13.4), the fits are relatively poor. This is of course to be expected since all four function predicts an asymmetric shape of the imaginary part of the dielectric constant with a limiting high-frequency power-law exponent equal to 1 and a flatter high-frequency side.

In these cases the SE function usually outperforms the other fitting functions. But this does not necessarily mean that the SE function is a better function; since all four functions aim at fitting the "true" alpha process, the fact that SE is able to capture both beta relaxation and DC-conduction interfering with the alpha process just means that it is flexible.

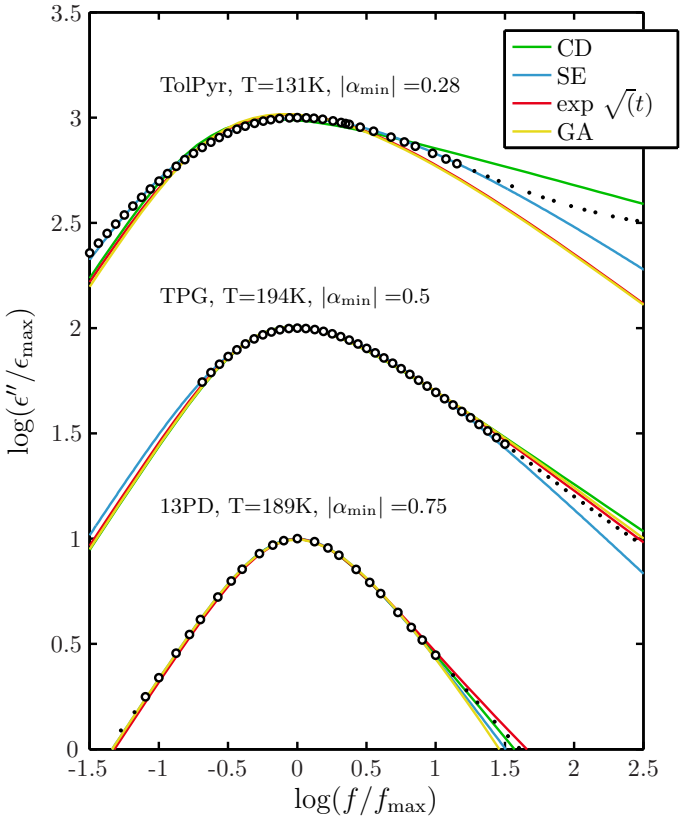

Figure 13.4 Examples of fits. We have plotted the spectrum with the highest $|\alpha_{\min}|$ (top), the lowest $|\alpha_{\min}|$ (bottom), and the spectrum with $|\alpha_{\min}|$ closest to 1/2.

To quantify the quality of the fits we used the standard deviation formula

$$\sigma^2 = \frac{1}{N-n}\sum_{i=1}^{N}\left(\frac{\epsilon''_{\text{fit},i} - \epsilon''_{\text{data},i}}{\epsilon''_{\text{data,max}}}\right)^2 \tag{13.9}$$

(13.10)

where N is the number data points and $n = 1(3?)$ is the number of degrees of freedom (i.e. number of free fitting parameters).

Figure 13.5 compares the fits of the four fitting functions for all 429 spectra as well as average for the 53 liquids. We show both the results from linear fitting (top) and results from the fitting logarithmically (bottom). In all plots the we have sorted spectra/liquids according to quality of the fits.

The conclusions that can be drawn from this analysis are

- the results are surprisingly similar for the logarithmic and the linear fit
- the CD and the GA functions show roughly the same overall fitting ability

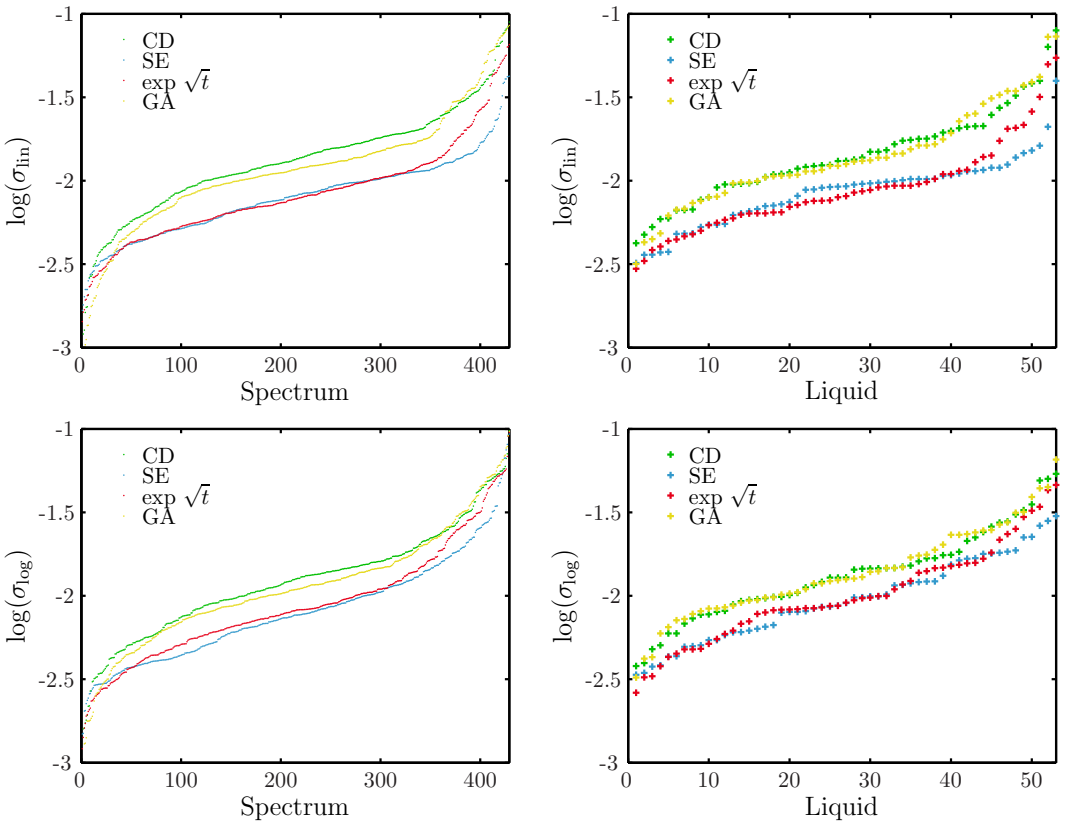

Figure 13.5 Quality of the fits of four different one-parameter relaxation function (Eq. (13.1 - 13.4)) to dielectric relaxation spectra arranged in increasing order. Top and bottom, left: results for each spectrum fitted linearly and logarithmically, respectively. Top and bottom, right: linear and logarithmic fitting results averaged for each liquid. Label on the y-axes σ_{lin} / σ_{log} refer to the fitting method (linear or logarithmic).

- the performance of the exponential $\sqrt{t}$ and the SE functions is significantly better and *roughly the same* for the two

But clearly, there are also a number of spectra/liquids for which the SE function fits significantly better. They all lie in the end of the relatively poor fits and they are primarily the very broad spectra. An example of such a spectrum is TolPyr at 131K shown in the top of Fig. 13.4. In this case, however, the broad spectral shape is not intrinsic to the alpha relaxation, but due to an intense beta process. At lower temperatures where the alpha and beta processes are well separated, this liquid approaches $\epsilon'' \propto \omega^{-1/2}$ for $f > f_{\max}$.

From the analysis of quality of the fits it should be noted that the exponential $\sqrt{t}$ function gives good fits even to data that are relatively broad (with minimum slope $\alpha_{\min} < 0.4$). In fact, Fig. 13.6 shows that there is very little correlation at all between the quality of the fits (both linear and logarithmic) of any of the fitting functions and $\alpha_{\min}$, i.e. the asymptotic high frequency power law. One would not a priori expect

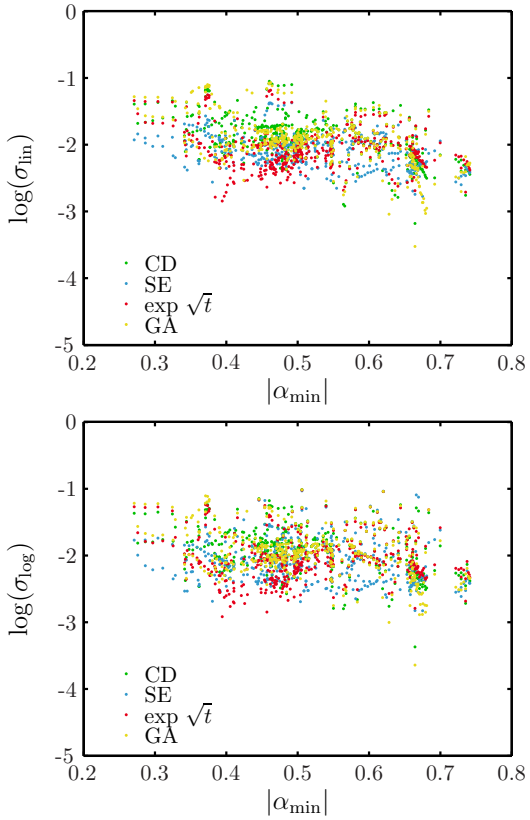

Figure 13.6 Correlations – or the lack of – between the α_{min} and quality of the fits. Contrary to intuition there seems to be almost no correlation between quality of the fits and the limiting high frequency power law; all functions fit more or less equally well in the whole α_{min}-range – both in the linear and logarithmic fitting procedure.

this because the exponential $\sqrt{t}$ function (and the GA function for that matter) by construction has an asymptotic high-frequency slope of $-1/2$. But over the fitting range chosen (from inflection point to inflection point in the log-log plot of the dielectric loss) the exponential $\sqrt{t}$ function is able to fit even relatively broad loss peaks. It would make little sense to expand the fitting range, because it is likely that beyond the high-frequency inflection point the main relaxation process is influenced by one or more additional high-frequency relaxation processes.

13.5 Final remarks and conclusions

We have presented fitting results for two relaxation functions with simple expressions in the time domain and two functions with simple expressions in the frequency domain. It seems that the functions that are given in the time domain fit the data better than the ones given in the frequency domain. If this is just a curious coincidence or if there is some meaning to that is unclear.

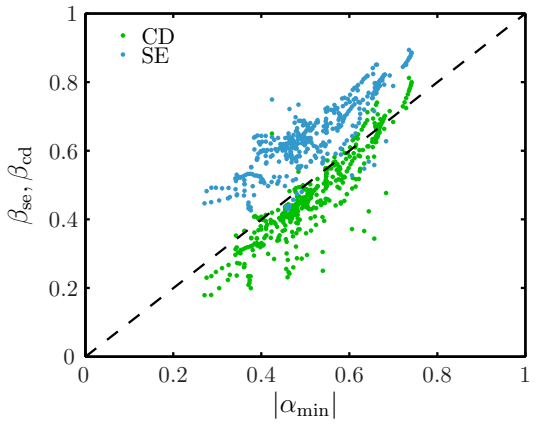

Figure 13.7 The correlation between the fitted β-parameters of the CD and SE functions and $\alpha_{\min}$. Both CD and SE functions seem to compensate for being too narrow and too broad, respectively, by adjusting the β-parameter.

As shown in Fig. 13.6 there is very little correlation between the asymptotic high frequency behavior of the liquid and the fitting ability of *any of the functions*. The standard deviations are spread from $10^{-3} - 10^{-1}$ in the whole range of $\alpha_{\min}$s. This is even the case for the logarithmic fits, which emphasizes the high- and low frequency asymptotic behavior of the liquids, where one would naively expect that the CD and SE functions would have a clear advantage over the GA and exponential $\sqrt{t}$ function.

This may partly be explained by the fact that the functions are fitted to relatively few data points around the peak. Thus the shape-parameter of the SE function β_{SE} (and the CD function for that matter) is really just adjusting the width of the peak and not fitting the asymptotic behavior or the tail. Support for this interpretation is found in Fig. 13.7, where the fitted values of β_{SE} and β_{CD} is plotted versus the minimum slope for each fitted spectrum. The figure shows that while there is some correlation between the asymptotic high-frequency powerlaw behavior of the spectrum and the fits, β_{SE} is always higher than the minimum slope and β_{CD} is systematically lower.

In conclusion, the stretched exponential function in this analysis did not stand out as an exceptionally good fitting function. The SE function does not fit data much better than other single-parameter fitting functions. In fact, the exponential $\sqrt{t}$ function – maybe a little surprising – performed as well as the SE function. This questions whether there is any fundamental significance of β parameter in the stretched exponential – the most important role of the β is merely, it seems, to adjust the width of the relaxation spectrum.

Liquid	Abbreviation	Reference
1,2-propanediol (propylene-glycol)	PG	[65]
1,3-propane-diol	13PD	[65]
2-methyl-tetrahydrofuran	MTHF	[65]
2,3-dimethyl-pentane	23DMP	[78]
2,3-epoxy-propyl-phenylether	23EPPE	[65]
2,4,6-trimethyl-heptane	246TMH	[78]
2-methyl-pentane-2,4-diol	2MP24D	[65]
2-phenyl-5-acetomethyl-5-ethyl-1,3-dioxocyclohexane	APAED	[65]
3-flouroaniline	3FAN	[79]
3-methyl-heptane	3MH	[78]
3-methyl-pentane	3MP	[78]
3-methyl-phosphate	3MPh	[80]
4-methyl-heptane	4MH	[78]
4,7,10-trioxatridecane-1,13-diamine	TODDA	[65]
4-tertbutyl-pyridine	4TBP	[80]
5-phenyl-4-ether	5PPE	this work
α-phenyl-o-cresol	PoC	[65]
benzophenone	BP	[81]
biphenyl-2yl-isobutylate	IB2BF	[65]
butyronitrile	Butyronitrile	[82]
cyclo-octanol	CO	[83]
dicyclohexyl-2-methyl succinate	DCMMS	[84]
dicyclohexyl-methyl-2-methyl succinate	DCHMS	[65]
dibutyl-ammonium-fomide	DBAF	[85]
dibutyl phtalate	DBP	[65]
diethyl phtalate	DEP	[65]
diglycidyl-ether of bisphenol	DGEBA	[86]
di-*iso*-butyl phtalate	DisoBP	[65]
dioctyl phtalate	DOP	[65]
dimethyl phtalate	DMP	this work
dioctyl phtalate	DOP	[65]
dipropylene-dimethyl-glycol-dimethyl-ether	DPGDME	[65]
ethylene-glycol	EG	[87]
glycerol	glycerol	[64]
isoeugenol	Isoeugenol	[65]
isopropyl-bezene (cumene)	IsoPB	[65]
m-tricresyl-phosphate	mTCP	[88]
methyl-m-toluate	MMT	[65]
n-ϵ-methyl-caprolactam	nMC	[65]
n-propyl-benzene	nPB	[65]
orto-carborane	ortoCarborane	[89]
pentachloronitrobenzene	PCB	[90]
polypropylene-glycol	PPG	[64]
propylene-carbonate	PC	[91]
sucrose-benzoate	SB	[92]
tetramethyl-tetraphenyl-trisiloxane (dc704)	DC704	[74]
toluene-pyridine mixture	TolPyr	[64]
tricresyl-phosphate	TCP	[65]
triphenyl-ethylene	TPE	[74]
triphenyl phosphite	TPP	[64]
tripropylene glycol	TPG	this work
tris-naphtyl-benzene	TNB	[93]
xylitol	Xylitol	[65]

Table 13.1 List of all liquids studied providing the relevant references.

Bibliography

[1] Walter Kauzmann. The nature of the glassy state and the behavior of liquids at low temperatures. *Chemical Review*, 43:219–256, 1948.

[2] P. G. Debenedetti. *Metastable liquids : concepts and principles*. Princeton, N.J. : Princeton University Press, 1996.

[3] C. A. Angell, K. L. Ngai, G. B. McKenna, P. F. McMillan, and S. W. Martin. Relaxation in glassforming liquids and amorphous solids. *Journal of Applied Physics*, 88:3113–3157, 2000.

[4] C. Alba-Simionesco. Salient properties of glassforming liquids close to the glass transition. *Comptes Rendus de l'Academie des Sciences (Serie IV)*, 2:203–216, 2001.

[5] W. Kob. *Proceedings of Les Houches Summer School of Theoretical Physics, Session LXXVII, 1-26 July, 2002*, chapter Slow relaxations and non-equilibrium dynamics in condensed matter. Springer, Berlin, 2004.

[6] J. C. Dyre. The glass transition and elastic models of glass-forming liquids. *Reviews of Modern Physics*, 78(3):953–972, 2006.

[7] I. A. Hodge. Physical aging in polymer glasses. *Science*, 267:1945–1947, 1995.

[8] A. J. Kovacs. La contraction isotherme du volume des polymères amorphes. *Journal of Polymer Science*, 30:131–147, 1958.

[9] A. J. Kovacs. Transition vitreuse dans les polymeres amorphes. Etude phenomenologique. *Fortschritte der Hochpolymeren-Forschung*, 3(3):394–507, 1963.

[10] C. T. Moynihan, A. J. Easteal, M.a. DeBolt, and J. Tucker. Dependence of the fictive temperature of glass on cooling rate. *American Ceramic Society*, 59:12–16, 1976.

[11] O. V. Mazurin. Relaxation phenomena in glass. *Journal of Non-Crystalline Solids*, 25:129–169, 1977.

[12] L. C. E. Struik. *Physical Aging in Amorphous Polymers and Other Materials*. Elsevier, Amsterdam, 1978.

[13] G. W. Scherer. *Relaxation in Glass and Composites*. Wiley, New York, 1986.

[14] G. B. McKenna. On the physics required for prediction of the long-term performance of polymers and their composites. *Journal of Research of the National Institute of Standards and Technology*, 99:169–189, 1994.

[15] I. M. Hodge. Enthalpy relaxation and recovery in amorphous materials. *Journal of Non-Crystalline Solids*, 169(3):211 – 266, 1994.

[16] I. Avramov. Kinetics of structural relaxation of glass-forming melts. *Thermochimica Acta*, 280:363–382, 1996.

[17] O. S. Narayanaswamy. A model of structural relaxation in glass. *Journal of the American Ceramic Society*, 54(10):491–498, 1971.

[18] S. Kolla and S. L. Simon. The τ-effective paradox: new measurements towards a resolution. *Polymer*, 46:733–739, 2005.

[19] A. Q. Tool. Relation between inelastic deformability and thermal expansion of glass in its annealing range. *Journal of American Ceramic Society*, 29:240–253, 1946.

[20] R. W. Rendell, K. L. Ngai, G. R. Fong, and J. J. Aklonis. Volume recovery near the glass transition temperature in polyvinyl acetate – predictions of a coupling model. *Macromolecules*, 20:1070–1083, 1987.

[21] L. C. E. Struik. Volume-recovery theory: 1. Kovacs' τ-effective paradox. *Polymer*, 38(18):4677 – 4685, 1997.

[22] G. B. McKenna, Y. Leterrier, and C. R. Schultheisz. The evolution of material properties during physical aging. *Polymer Engineering and Science*, 35:403–410, 1995.

[23] G. B. McKenna, M. G. Vangel, A. L. Rukhin, S. D. Leigh, B. Lotz, and C. Straupe. The tau-effective paradox revisited: an extended analysis of kovacs' volume recovery data on poly(vinyl acetate). *Polymer*, 40:5183–5205, 1999.

[24] P. B. Macedo and A. Napolitano. Effects of a distribution of volume relaxation times in annealing of bsc glass. *Journal of Research of the National Bureau of Standards Section A-Physics*, 71A:231–238, 1967.

[25] S. Spinner and A. Napolitano. Further studies in the annealing of a borosilicate glass. *Journal of Research of the National Bureau of Standards Section A-Physics and Chemistry*, 70A:147–152, 1966.

[26] A. J. Kovacs, J. J. Aklonis, J. M. Hutchinson, and A. R. Ramos. Isobaric volume and enthalpy recovery of glasses. ii. a transparent multiparameter theory. *Journal of Polymer Science: Polymer Physics Edition*, 17:1097–1162, 1979.

[27] A. Q. Tool and C. G. Eichlin. Variations caused in the heating curves of glass by heat treatment. *Journal of the American Veramic Society*, 14(4):276–308, 1931.

[28] C. T. Moynihan, S. N. Crichton, and S. M. Opalka. Linear and non-linear structural relaxation. *Journal of Non-Crystalline Solids*, 131-133:420–434, 1991.

[29] O. S. Narayanaswamy and R. Gardon. Calculation of rediduall stresses in glass. *Journal of American Ceramic Society*, pages 554–558, 1969.

[30] I. L. Hopkins. Stress relaxation or creep of linear viscoelastic substances under varying temperature. *Journal of Polymer Science*, 28:631–633, 1958.

[31] M. A. DeBolt, A. J. Easteal, P. B. Macedo, and C. T. Moynihan. Analysis of structural relaxation in glass using rate heating data. *Journal of the American Ceramic Society*, 59:16–21, 1976.

[32] J. C. Mauro, D. C. Allan, and M. Potuzak. Non-equilibrium viscosity of glass. *Physical Revew B*, 80:094204, 2009.

[33] G. W. Scherer. Volume relaxation far from equilibrium. *Journal of American Ceramic Society*, 69:374–381, 1986.

[34] T. Hecksher, N. B. Olsen, K. Niss, and J. C. Dyre. Physical aging studied by a device allowing for rapid thermal equilibration. *Journal of Chemical Physics*, in press, 2010.

[35] L. Hornbøll, T. Knudsen, Y. Yue, and X. Guo. Heterogenous enthalpy relaxation in glasses far from equilibrium. *Chemical Physics Letters*, 494:37–40, 2010.

[36] R. L. Leheny and S. R. Nagel. Frequency-domain study of physicak aging in a simple liquid. *Physcial Review B*, 57:5154–5162, 1998.

[37] R. D. Bradshaw and L. C. Brinson. Physical aging in polymers and polymer composites: An analysis and method for time-aging time superposition. *Polymer Engineering and Science*, 37:31–44, 1997.

[38] P. A. O'Connell and G. B. McKenna. Large deformation response of polycarbonate: Time-temperature time-aging time and time-strain superposition. *Polymer Engineering and Science*, 37(9):1485–1495, 1997.

[39] A. Lee and J. D. Lichtenhan. Viscoelastic responses of polyhedral oligosilsesquioxane reinforced epoxy systems. *Macromolecules*, 31:4970–4974, 1998.

[40] P. A. O'Connell and G. B. McKenna. Arrhenius-type temperature dependence of the segmental relaxation below t_g. *Journal of Chemical Physics*, 110:11054, 1999.

[41] A. J. Kovacs, R. A. Stratton, and J. D. Ferry. Dynamic mechanical properties of polyvinyl acetate in shear in the glass transition temperature range. *Journal of Physical Chemistry*, 67(1):152–161, 1963.

[42] J. Beckmann and G. B. McKenna. Physical aging kinestics of syndiotactic polystyrene as determined from creep behavior. *Polymer Engineering and Science*, 37(9):1459–1468, 1997.

[43] I. Echeverria, P. L. Kolek, D. J. Plazek, and S. L. Simon. Enthalpy recovery, creep and creep-recovery measurements during physical aging of amorphous selenium. *Journal of Non-Crystalline Solids*, 324:242–255, 2003.

[44] M. L. Cerrada and G. B. McKenna. Physical aging of amorphous PEN: Isothermal, isochronal and isostructural results. *Macromolecules*, 38(8):3065–3076, 2000.

[45] J. J. Tribone, J. M. O'Reilly, and J. Greener. Analysis of enthalpy relaxation in poly(methyl methacrylate): effects of tacticity, deuteration, and thermal history. *Macromolecules*, 19:1732–1739, 1986.

[46] I. M. Hogde. Adam-gibbs formulation of enthalpy relaxation near the glass transition. *Journal of Research of the National Institute of Standards and Technology*, 102:195–205, 1997.

[47] R. Roe and G. M. Millman. Physical aging in polystyrene: Comparison of the changes in creep behavior with the enthalpy relaxation. *Polymer Engineering and Science*, 23:318–322, 1983.

[48] S. L. Simon, D. J. Plazek, J. W. Sobieski, and E. T. McGregor. Physical aging of a polyetherimide: Volume recovery and its comparison to creep and enthalpy measurements. *Journal of Polymer Science Part B-Polymer Physics*, 35:929–936, 1997.

[49] B. Igarashi, T. Christensen, E. H. Larsen, N. B. Olsen, I. H. Pedersen, T. Rasmussen, and J. Dyre. A cryostat and temperature control system optimized for measuring relaxations of glass-forming liquids. *Review of Scientific Instruments*, 79:045105, 2008.

[50] B. Igarashi, T. Christensen, E. H. Larsen, N. B. Olsen, I. H. Pedersen, T. Rasmussen, and J. Dyre. An impedence-measurement setup optimized for measuring relaxations of glass-forming liquids. *Review of Scientific Instruments*, 79:045106, 2008.

[51] G. P. Johari. Effect of annealing on the secondary relaxations in glasses. *Journal of Chemical Physics*, 77:4619–4626, 1982.

[52] E. Schlosser and A. Schönhals. Dielectric relaxation during physical aging. *Polymer*, 32:2135–2140, 1991.

[53] A. Alegria, E. Guerrica-Echevarria, L. Goitiandia, I. Telleria, and J. Colmenero. α-relaxation in the glass-transition range of amorphous polymers. 1. temperature behavior across the glass transition. *Macromolecules*, 28:1516–1527, 1995.

[54] A. Alegria, L. Goitiandia, I. Telleria, and J. Colmenero. α-relaxation in the glass-transition range of amorphous polymers. 2. influence of physical aging on the dielectric relaxation. *Macromolecules*, 30:3881–3887, 1997.

[55] L. Goitiandia and A. Alegria. The adam-gibbs equation and the our-of-equilibrium α-relaxation of glass forming systems. *Journal of Chemical Physics*, 121:1636–1643, 2004.

[56] H. Yardimci and R. L. Leheny. Memory in an aging molecular glass. *Europhysics Letters*, 62:203–209, 2003.

[57] D. Cangialosi, W. Wübbenhorst, J. Groenewold, E. Mendes, and S. J. Picken. Diffusion mechanism for physical aging of polycarbonate far below the glass transition temperature studied by means of dielectric spectroscopy. *Journal of Non-Crystalline Solids*, 351:2605, 2005.

[58] P. Lunkenheimer, R. Wehn, and A. Loidl. Glassy aging dynamics. *Physical Review Letters*, 95:055702, 2005.

[59] P. Lunkenheimer, R. Wehn, and A. Loidl. Dielectric spectroscopy on aging glasses. *Journal of Non-Crystalline Solids*, 352:4941–4945, 2006.

[60] R. Wehn, P. Lunkenheimer, and A. Loidl. Broadband dielectric spectroscopy and aging of glass formers. *Journal of Non-Crystalline Solids*, 353:3862–3870, 2007.

[61] P. D'Angelo, M. Barra, M. Nicodemi, and A. Cassinese. Phase transitions and aging phenomena in dielectriclike polymeric materials investigated by ac measurements. *Journal of Applied Physics*, 101:044910, 2007.

[62] A. Serghei and F. Kremer. Metastable states of glassy dynamics, possibly mimicking confinement-effects in thin polymer films. *Macromolecular Chemistry and Physics*, 209:810–817, 2008.

[63] N. B. Olsen, J. C. Dyre, and T. E. Christensen. Structural relaxation monitored by instantaneous shear modulus. *Physical Review Letters*, 81:1031–1033, 1998.

[64] N. B. Olsen, T. Christensen, and J. C. Dyre. Time-temperature superposition in viscous liquids. *Physical Review Letters*, 86(7):1271–1274, 2001.

[65] A. I. Nielsen, T. Christensen, B. Jakobsen, K. Niss, N. B. Olsen, R. Richert, and J. C. Dyre. Prevalence of approximate $\sqrt{t}$ relaxation for the dielectric alpha process in viscous organic liquids. *Journal of Chemical Physics*, 130:154508, 2009.

[66] N. Saglanmak, A. I. Nielsen, N. B. Olsen, J. C. Dyre, and K. Niss. An electrical circuit model of the alpha-beta merging seen in dielectric relaxation of ultraviscous liquid. *Journal of Chemical Physics*, 132:024503, 2010.

[67] Catalin Gainaru, Robret Kahlau, Ernst A. Rössler, and Roland Böhmer. Evolution of excess wing and β-processes in simple glass-fomers. *Journal of Chemical Physics*, 131:184510, 2009.

[68] R. Kohlrausch. Theorie des elektrischen Rückstandes in der Leidner Flasche. *Annalen der Physik und Chemie (Poggendorff)*, 91:179–213, 1854.

[69] G. Williams and D. C. Watts. Non-symmetrical dielectric relaxation behavior arising from a simple empirical decay function. *Transaction of the Faraday Society*, 66:80, 1970.

[70] M. Cardona, R. V. Chamberlin, and W. Marx. The history of the stretched exponential function. *Annalen der Physik*, 16:842–845, 2007.

[71] K. L. Ngai. Universality of low-frequency fluctuation, dissipation and relaxation properties of condensed matter. i. *Comments on Solid State Physics*, 9:127, 1979.

[72] R. Böhmer, K. L. Ngai, C. A. Angell, and D. J. Plazek. Nonexponential relaxation in strong and fragile glass-formers. *Journal of Chemical Physics*, 99:4201, 1993.

[73] J. C. Phillips. Stretched exponential relaxation in molecular and electronic glasses. *Reports on Progess in Physics*, 59:1133, 1996.

[74] B. Jakobsen, K. Niss, and N. B. Olsen. Dielectric and shear mechanical alpha and beta relaxations in seven glass-forming liquids. *Journal of Chemical Physics*, 123(23):234511, 2005.

[75] D. W. Davidson and R. H. Cole. Dielectric relaxation in glycerine. *Journal of Chemical Physics*, 18:1417–1417, 1950.

[76] J. C. Dyre. A model for the generic alpha relaxation of viscous liquids. *Europhysics Letters*, 71:646–650, 2005.

[77] J. Wuttke. Fourier transform of the stretched exponential function: Analytic error estimates, double exponential transform, and open-source implementation libkww. http://arXiv.org/abs/0911.4796, November 2009.

[78] S. Shahriari, A. Mandanici, L.-M. Wang, and R. Richert. Dynamics of glass-forming liquids. viii. dielectric signature of probe rotation and bulk dynamics in branched alkanes. *Journal of Chemical Physics*, 121:8960–8967, 2004.

[79] J. Wiedersich, T. Blochowicz, S. Benkhof, A. Kudlik, N. V. Surovtsev, C. Tschirwitz, V. N. Novikov, and E. A. Rössler. Fast and slow relaxation processes in glasses. *Journal of Physics: Condensed Matter*, 11:A147–A156, 1999.

[80] T. Blochowicz, C. Gainaru, P. Medick, C. Tschirwitz, and E. A. Rossler. The dynamic susceptibility in glass forming molecular liquids: The search for universal relaxation patterns ii. *Journal of Chemical Physics*, 124(13):134503, 2006.

[81] P. Lunkenheimer, L. C. Cardo, M. Köhler, and A. Loidl. Broadband dielectric spectroscopy on benzophenone: α relaxation, β relaxation, and mode coupling theory. *Physical Review E*, 77:031506, 2008.

[82] N. Ito, K. Duvvuri, D. V. Matyushov, and R. Richert. Solvent response and dielectric relaxation in supercooled butyronitrile. *Journal of Chemical Physics*, 125(2):024504, 2006.

[83] R. Brand, P. Lunkenheimer, and A. Loidl. Relaxations and fast dynamics of the plastic crystal cyclo-octanol investigated by broadband dielectric spectroscopy. *Physical Review B*, 56:5713?5716, 1997.

[84] R. Diaz-Calleja, A. Garcia-Bernabe, M. J. Sanchis, and L. F. del Castillo. Interconversion of mechanical and dielectrical relaxation measurements for dicyclohexylmethyl-2-methyl succinate. *Physcial Review E*, 72(5):051505, 2005.

[85] N. Ito, W. Huang, and R. Richert. Dynamics of a supercooled ionic liquid studied by optical and dielectric spectroscopy. *Journal of Physical Chemistry B*, 110(9):4371–4377, 2006.

[86] M. Mierzwa, S. Pawlus ANS M. Paluch, E. Kaminska, and K. L. Ngai. Correlation between primary and secondary johari-goldstein relaxations in supercooled liquids: Invariance to changes in thermodynamic conditions. *Journal of Chemical Physics*, 128:044512, 2008.

[87] T. Blochowicz, C. Tschirwitz, S. Benkhof, and E. A. Rössler. Susceptibility functions for slow relaxation processes in supercooled liquids and the search for universal relaxation patterns. *Journal of Chemical Physics*, 118:7544, 2003.

[88] T. Hecksher, A. I. Nielsen, N. B. Olsen, and J. C. Dyre. Little evidence for dynamic divergences in ultraviscous molecular liquids. *Nature Physics*, 4(9):737–741, 2008.

[89] R. Brand, P. Lunkenheimer, U. Schneider, and A. Loidl. Is there an excess wing in the dielectric loss of plastic crystals? *Physical. Review Letters*, 82:1951?1954, 1999.

[90] R. Brand, P. Lunkenheimer, and A. Loidl. Relaxation dynamics in plastic crystals. *Journal of Chemical Physics*, 116:10386–10401, 2002.

[91] L.-M. Wang, V. Velikov, and C. A. Angell. Direct determination of kinetic fragility indices of glassforming liquids by differential scanning calorimetry: Kinetic versus thermodynamic fragilities. *Journal of Chemical Physics*, 117:10184–10192, 2002.

[92] J. R. Rajian, W. Huang, R. Richert, and E. L. Quitevis. Enhanced translational diffusion of rubrene in sucrose benzoate. *Journal of Chemical Physics*, 124(1):014510, 2006.

[93] R. Richert, K. Duvvuri, and L.-T. Duong. Dynamics of glass-forming liquids. VII. Dielectric relaxation of supercooled tris-naphthylbenzene, squalane and decahydroisoquinoline. *Journal of Chemical Physics*, 118(4):1828–1836, 2003.

14 Summary and outlook

In the introduction the "big questions" of the field was stated in the form of the three non's: non-Arrhenius temperature dependence of the relaxation time, non-exponential relaxation, and the non-linearity of the relaxation upon even small temperature steps. This thesis has touched upon all of these topics, so it would be appropriate to sum up how (in my view) this work has contributed to a resolution of these questions.

Non-Arrhenius temperature dependence of the relaxation time: The standard fitting function for fitting the non-Arrhenius data is the VFT equation. Originally this equation was introduced as a convenient fit to data, but since then several theories and models have produced similar formulas, indicating a fundamental significance of the divergence temperature T_0. The analysis in Part II of this thesis of a large set of relaxation time data does however not favor the VFT equation over other fitting functions without dynamic divergences at a finite temperature. This strongly suggest that theorists should look in other directions.

Non-exponential relaxation: It was conjectured by Olsen *et al* [1] that an asymptotic high frequency powerlaw with exponent $-1/2$ may be generic to the alpha relaxation once it is well separated from other processes. This conjecture was further strengthened by the work of Nielsen *et al* [2], who for a large body of dielectric data showed the prevalence of the square root.

Here a new fitting function (the exponential $\sqrt{t}$ relaxation function) was suggested that combines the short time $\sqrt{t}$ relaxation with a long time exponential tail. This function has a generic high frequency loss and an adjustable width. The long time exponential decay may be intuitively rationalized in the following way: at long times (beyond the alpha relaxation time) the molecular structure is continuously changing and it is difficult to imagine that there would be any "memory" left. With no memory, the relaxation must terminate exponentially.

Fitting the exponential $\sqrt{t}$ relaxation function to a large set of equilibrium dielectric data, as well as other single parameter fitting functions, showed that this overall gave a good description of data, even spectra with asymptotic high frequency power law with exponents well below or above 1/2. This study also questions the fundamental significance of the stretched exponential function (and the associated β shape parameter), since the SE did not stand out as an exceptionally good fitting function.

---

[1] N. B. Olsen, T. Christensen, and J. C. Dyre. Time-temperature superposition in viscous liquids. *Physical Review Letters*, 86(7):1271-1274, 2001

[2] A. I. Nielsen, T. Christensen, B. Jakobsen, K. Niss, N. B. Olsen, R. Richert, and J. C. Dyre. Prevalence of the approximate $\sqrt{t}$ relaxation for the dielectric alpha process in viscous organic liquids. *Journal of Chemical Physics*, 130:154508, 2009

Non-linearity: In chapter 12 a series of "ideal aging experiments" was analyzed in term of the Tool-Narayanaswamy formalism. The result confirms – as numerous other experiments on glasses – that the structural non-linear relaxation can be linearized in terms of the reduced time, the internal clock. We believe however that it is the first time that this has been shown directly without any assumptions of fictive temperatures or explicit evaluation of the reduced time.
It was further shown that – at least for the studied liquids – the internal clock apparently has a real physical meaning. This was inferred by the fact that assuming proportionality of the generalized dielectric relaxation rate and the structural relaxation rate lead to linearization of the structural relaxation. This implies that the TN formalism may have a deeper theoretical foundation.

In addition to these "traditional" questions, the careful mechanical measurements (as described in Part I) have contributed to the first experimental test of a prediction of the theory of strongly correlating liquids.

14.1 Outlook

The following is a list of open questions and obvious continuation of the present work:

A: The observed similarities of the bulk and shear modulus relaxation is quite intriguing and similar measurements should be carried out on more substances. Obviously, we would like to know how general this is. Is it linked to TTS? Or to a single-order-parameter-ness? What about the β-process? The β-process has so far not been observed in a bulk modulus measurement, and documenting it is interesting in itself.

B: The isochronal or dynamic Cauchy relation found for DC704 should be checked in other liquids. Temperatures must of course be carefully matched such that bulk and shear moduli are measured at the same relaxation times. We suggest the following procedure: bulk and shear measurements are carried out at convenient temperatures. The relaxation times/loss peak freuqencies for the two quantities are plotted and via this plot the loss peaks of the bulk modulus is projected horizontally onto the shear curve, and the corresponding temperatures for a shear measurement with the same peak position can be found.

C: The aging experiments presented in chapter 12 indicate that the (structural) relaxation in liquids terminates exponentially. This is very interesting and should be examined closer. Measurements with even higher resolution than those presented in chapter 12 should be able to resolve whether the structural relaxation at long times is in fact exponential.
Another – more empirical – way of testing the exponential cut off is to use the new empirical function (the exponential $\sqrt{t}$) in the TN model to fit data from cross-over experiments. This experiment i particularly sensitive to functional form of the relaxation.

D: Pursuing the modelling of the "longitudinal" transducer is probably worth the effort. It would be extremely valuable to have a third independent measurement of

the mechanical properties. In [A] and [B] we would depend on accurate measurements not only with respect to noise, but also absolute values measured.

E: We showed that for five different response functions the decoupling of relaxation times was temperature independent down to T_g in two liquids and we conjectured that this may be due to the fact that the studied liquids belongs to the class of strongly correlating liquids. The connection between the proportionality between certain combinations of thermo-mechanical response functions and proportionality of the relaxation time of all other responses should to be justified theoretically.

Part IV

Appendices

A Energy bonds and linear response

In the following we give a very brief introduction to linear response theory and the use of electrical networks as a modelling tool for both mechanical, electrical and thermal.

A.1 Linear response

When we perturb a system usually the system reacts in some way, that can be measured. We define the input and the output by φ and γ. A linear response is defined by

$$\gamma(t) = \int_{-\infty}^{t} R(t-t')d\varphi(t') = \int_{-\infty}^{t} R(t-t')\dot{\varphi}(t')\,dt' \tag{A.1}$$

where $R(t)$ is the systems response or relaxation function. This function can be measured directly if the input is a Heaviside step input.

By a change of variables ($\tau = t - t'$) this is equivalent to

$$\gamma(t) = \int_{0}^{\infty} R(\tau)\dot{\varphi}(t-\tau)\,d\tau\,. \tag{A.2}$$

The FD theorem ensures (if we choose the input and measured output as a conjugate pair of variables) that whenever a perturbation is linear then the measured response is directly proportional to the mean squared fluctuations in equilibrium of the measured quantity.

If the input is harmonic $\varphi(t) = \mathrm{Re}\left\{\varphi_0 e^{i\omega t}\right\}$ then the output will also be harmonic, $\gamma(t) = \mathrm{Re}\left\{\gamma_0 e^{i\omega t}\right\}$. Then by insertion we get

$$\gamma_0 e^{i\omega t} = \int_{0}^{\infty} R(\tau)\frac{d}{dt}\left(\varphi_0 e^{i\omega(t-\tau)}\right)\,d\tau = i\omega\varphi_0 e^{i\omega t}\int_{0}^{\infty} R(\tau)e^{i\omega\tau}\,d\tau \tag{A.3}$$

and we see that $\gamma_0/\varphi_0 = i\omega\int_0^\infty R(\tau)e^{i\omega\tau}\,d\tau$. The response function in the frequency domain is thus the Laplace transform of the derivative of the time domain response function.

A.2 Energy bond graphs

Energy bond graphs is a powerful modelling tool (for a thorough introduction see Christiansen [1, 2]). It is a generalization of the analogues there are between mechanical and electrical networks to embrace all kinds of linear response (and even – with some

modification – non-linear) situations. Throughout this thesis the electrical elements will be used to depict the models (also mechanical models) used although a more general set of elements and flow-charts has been developed [1, 2].

An energy bond is a set of conjugate variable, i.e. two quantities whose product has dimension of energy pr time. Examples of energy bond pairs include the thermodynamic pairs temperature & entropy (T, S) and volume & pressure (V, p), but it could also be electrical voltage & current (U, I).

For this ultrashort tutorial we will adopt the notation of Christiansen [1] and define all properties in terms of a generalized voltage denoted by e and a generalized current denoted by f, which could be any of the above pairs. The e variable is characterized by being invariant under time-reversal, while f variable changes sign. From the e and f variables we may integrate to find the generalized momentum $p = \int e\,dt$ and generalized charge $q = \int f\,dt$.

The possible response function using one of these variables as input and measuring the other is listed in the table below.

	e	p	q	f
e	x	x	compliance, $\tilde{J}$	admittance, $\tilde{Y}$
p	x	x	admittance, $\tilde{Y}$	lightness, $\tilde{F}$
q	stiffness, $\tilde{S}$	impedance, $\tilde{Z}$	x	x
f	impedance, $\tilde{Z}$	inertance, $\tilde{M}$	x	x

All these response functions are mathematically equivalent. For the complex response functions (i.e. in the frequency domain) it is easy to go from one response function to another

$$\tilde{Z} = \frac{e}{f} = \frac{1}{f/e} = \frac{1}{\tilde{Y}} \tag{A.4}$$

since integration and differentiation in the frequency-domain reduces to multiplying or dividing by the Laplace-frequency, $s = i\omega$

$$\tilde{Z} = s\tilde{M} = \frac{1}{s}\tilde{S}, \quad \tilde{Y} = s\tilde{J} = \frac{1}{s}\tilde{F} \tag{A.5}$$

A.2.1 The electrical analogue

The most common building blocks of an electrical networks are the resistor R giving the proportionality between voltage (e) and current (f), the capacitor C giving the proportionality between voltage (e) and charge (q), and the inductor L giving the proportionality between voltage (e) and charge acceleration (df/dt).

With these rules we can easily work out what the impedance, admittance, etc. are of the building blocks of these networks

	$\tilde{Y}$	$\tilde{J}$	$\tilde{Z}$	$\tilde{S}$
inductor, L	$\frac{1}{sL}$	$\frac{1}{s^2L}$	sL	s^2L
resistor, R	$\frac{1}{R}$	$\frac{1}{sR}$	R	sR
capacitor C	sC	C	$\frac{1}{sC}$	$\frac{1}{C}$

In an electrical network the impedance is added of elements in series and admittance is added for elements in parallel.

B Temperature calibration and stability

The temperature stability in the cryostats are of course very important since the properties of super-cooled liquids are extremely temperature dependent.

We have been working on two different set ups, that we internally have labelled CRYO 3 and CRYO 5. CRYO 3 is a nitrogen cooled cryostat that has to be refilled manually every day, where as CRYO 5 has a cooling pump system that works continuously (a "refrigerator cryostat").

Here we will show some measurements documenting the temperature stability of the two cryostats, and we will show how the absolute temperature of the two cryostats compare, i.e. if the calibration of them is identical or if there are differences.

B.1 Temperature stability of CRYO 3

Beside the overall temperature stability of the cryostat, it is for the nitrogen cryostat interesting to know how much refilling of nitrogen influences the temperature.

Using a NTC resistor as a thermometer (REF) we tested the temperature stability of nitrogen cryostat that was used for many of the measurements presented in this thesis.

Initially we filled up the nitrogen chamber at room temperature to see how this affects the temperature inside the cryostat. In Fig. B.1 the result is shown. Initially, a few large oscillations with an amplitude of almost 0.3K is seen, then the amplitude of the oscillations decrease and after 30 minutes the temperature inside the cryostat is stable within 10mK.

Fig. B.2 shows a quench from 295K to 275K. The resulting cooling rate is close to constant. As the final temperature is approached there are a few oscillations and after 20 minutes the temperature is stable in the cryostat chamber.

Together Fig. B.1 and B.2 show that the initial filling of nitrogen is quite dramatic and takes longer time to adjust than a quench large quench in temperature once the whole set-up has adjusted to the nitrogen fill.

So what happens when we refill the nitrogen chamber during a measurement? Fig. B.3 shows an example of that, and evidently a refill during a measurement can be felt inside the cryostat chamber, but it is a modest effect that last only a couple of minutes and has a maximum amplitude of $\sim$ 50mK.

The last measurement was a long time stability check of the temperature. The result is shown in Fig. B.4. Over a period of 50 hours the temperature is stable within $\sim$ 30mK with oscillations on many timescales, but most evidently is a very slow oscillation with

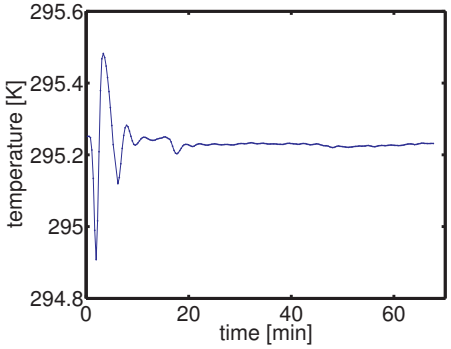

Figure B.1 Temperature as a function of time after the initial nitrogen filling of the cryostats nitrogen chamber.

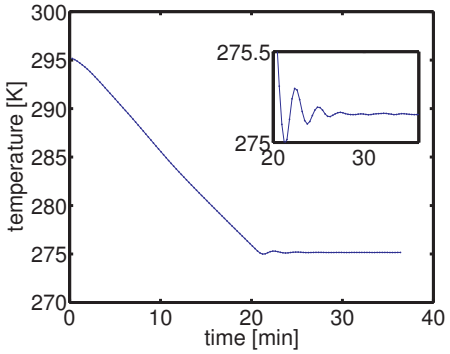

Figure B.2 Ramping from ambient temperature to 275K. The set temperature is reached within 20 minutes and completely stable within 30 minutes. The inset show a zoom at the final approach.

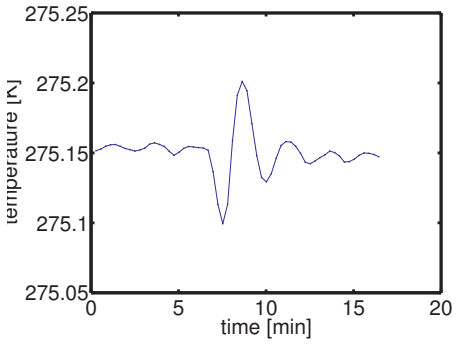

Figure B.3 The temperature was stabilized at 275K, and at $t \approx 6$min the nitrogen chamber is refilled. The refill has a small and short-lived influence on the temperature.

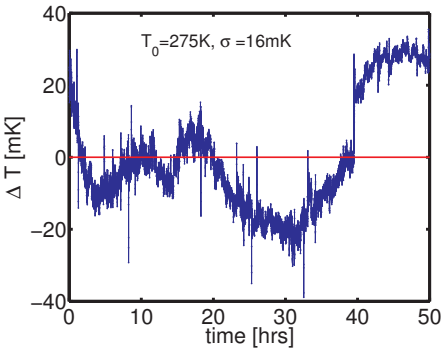

Figure B.4 Long time measurement of the temperature stability of CRYO 3 (nitrogen cryostat).

a period of almost 40 hours. Apparently, the tank did not run out of nitrogen in the 50 hours this measurement lasted. It is however likely that the tank would not last this long at a lower set temperature.

B.2 Temperature stability of CRYO 5

Fig. B.5 show the temperature variation in CRYO 5 over a period of 24 hours measured using the same method as above. The temperature of this cryostat is extremely stable: except for a few spikes in ΔT of less than 10mK, the temperature is stable within a few mK for the entire period with no slow oscillations. The standard deviation for this measurement i 1mK(!), more than 10 times better than the nitrogen cryostat. This is quite impressive even though it is easier to keep the temperature stable at room temperature than below.

The measurement was carried out by Bo jakobsen.

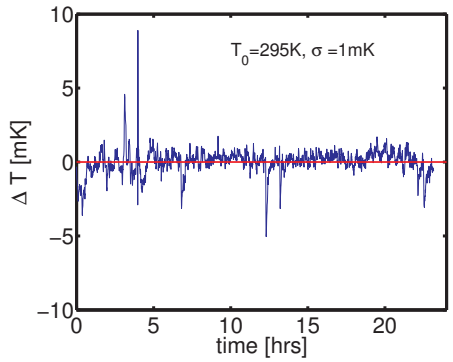

Figure B.5 Long time temperature stability of CRYO 5. The temperature in this cryostat is extremely stable. Except for a few spikes in ΔT of less than 10mK, the temperature is stable within a few mK. The measurement was carried out by Bo jakobsen.

B.3 Temperature calibration between CRYO 3 and CRYO 5

A clever way of comparing the absolute temperature calibration of the two cryostats is to use a dielectric measurement of some liquid. Since the dielectric relaxation is extremely temperature dependent, such a measurement will give a very precise measure of the temperature.

I used 5-PPE (a very convenient choice) as a probe, and measured a full temperature cycle in CRYO 5. Then I moved the holder with the filled dielectric cell attached to CRYO 3 and repeated the measurement. The result is a collection of curves that should be identical if the absolute temperature calibration for the two cryostats is the same. If this is not the case, the two measurements will be shifted.

Figure B.6 show the dielectric loss spectrum for 5-PPE measured in CRYO 3 (red) and CRYO 5 (blue). The exact same thermal cycle was measured in both cryostats and the plots show that the absolute temperature calibration for the two cryostats is not identical. To the left the dielectric loss spectra are shown as measured. The blue curves are shifted slightly to the left of the red curve. To the left we show the same curves but now the red curves have been shifted 0.13 decades to the right to make them overlap with the blue curves. This works to some degree but the overlap is not perfect at high temperatures. This could either be due the non-Arrheniusness of the liquid, but it could also be because the difference in calibrated absolute temperature is not the same.

To make a qualitative statement of the differences in temperature calibration we plot the loss peaks against the temperature to see how much we need to shift the temperature axis to make this overlap. Top panel of Fig. B.7 show the loss peak frequencies as a function of temperature for both measurements without shift. In the bottom panel the measurement in CRYO 3 (red) is shifted 0.35K up, which makes the two curve overlap completely. We thus conclude that the temperature calibration shift between CRYO 3 and CRYO 5 is constant (at least down to 245K).

The conclusion is that for a quite large range of temperatures it is safe to just make a

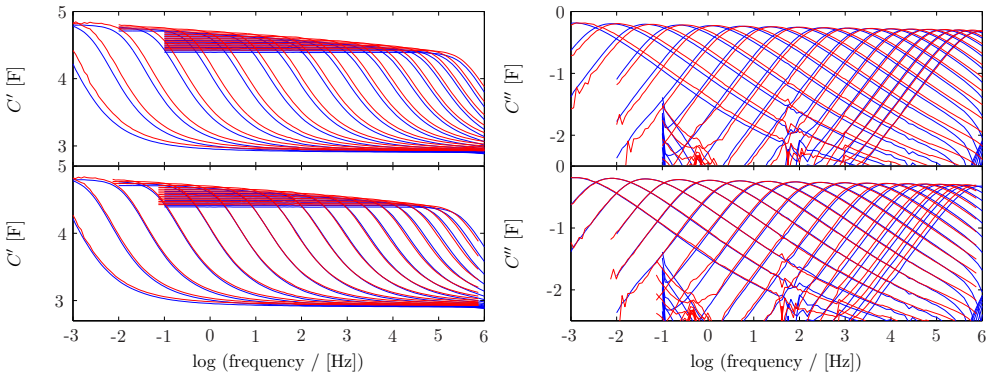

Figure B.6 Dielectric spectrum of 5-PPE from 245K-287.5K in steps of 2.5K. Measurement in CRYO 3 is shown in red and measurement in CRYO 5 is shown blue. In the bottom panels the CRYO 3 measurement has been shifted a little 0.13 decade to the left.

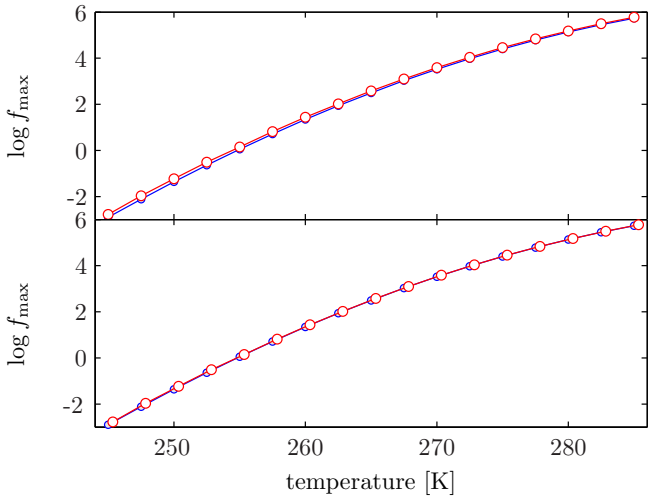

Figure B.7 Top panel: loss peak frequencies as a function of temperature. Bottom panel: same as top only with the red curve shifted +0.35K to make the two curves collapse.

shift along the frequency axis, but the shift is truly in the temperature.

C Theory of the piezo-electric transducer discs

C.1 Derivation of the equations

The equation are set up in cylindrical coordinates (r, ϕ, z). These refer – in the neighborhood of $r = (r\cos\phi)e_x + (r\sin\phi)e_y + ze_z$ – to the radial e_r, the azimuthal e_ϕ and the axial e_z unit vectors. A point in the material lies at r before the displacement and at r' after. The displacement field is $u(r) = r' - r = u_r e_r + u_\phi e_\phi + u_z e_z$. The strain tensor then becomes

$$\begin{aligned}
&\epsilon_{rr} = \frac{\partial u_r}{\partial r},\ \epsilon_{\phi\phi} = \frac{1}{r}\frac{\partial u_\phi}{\partial \phi} + \frac{u_r}{r},\ e_{zz} = \frac{\partial u_z}{\partial z},\\
&\epsilon_{\phi z} = \frac{1}{2}\left(\frac{1}{r}\frac{\partial u_z}{\partial \phi} + \frac{\partial u_\phi}{\partial z}\right),\ \epsilon_{rz} = \frac{1}{2}\left(\frac{\partial u_r}{\partial z} + \frac{\partial u_z}{\partial r}\right),\\
&\epsilon_{r\phi} = \frac{1}{2}\left(\frac{\partial u_\phi}{\partial r} - \frac{u_\phi}{r} + \frac{1}{r}\frac{\partial u_r}{\partial \phi}\right)
\end{aligned} \tag{C.1}$$

The cylindical geometry gives $u_\phi = 0$ and independence of u_r and u_z on ϕ, and thus we have

$$\begin{aligned}
&\epsilon_{rr} = \frac{\partial u_r}{\partial r},\ \epsilon_{\phi\phi} = \frac{u_r}{r},\ e_{zz} = \frac{\partial u_z}{\partial z},\\
&\epsilon_{\phi z} = \epsilon_{r\phi} = 0,\ \epsilon_{rz} = \frac{1}{2}\left(\frac{\partial u_r}{\partial z} + \frac{\partial u_z}{\partial r}\right)
\end{aligned} \tag{C.2}$$

The components e_{zz} and e_{rz} are not vanishing but they do not enter the problem.

The elastoelectric compliance matrix of a piezoceramic with axial symmetry along the pole axis has the same form as that of a crystal class $6mm$. This has the favorable

property of a decoupling into four parts, namely

$$\begin{pmatrix}\epsilon_{\phi z}\\ D_\phi\end{pmatrix} = \begin{pmatrix}s_{44} & d_{15}\\ d_{15} & \epsilon_{11}^T\end{pmatrix}\begin{pmatrix}\sigma_{\phi z}\\ E_\phi\end{pmatrix} \tag{C.3}$$

$$\begin{pmatrix}\epsilon_{rz}\\ D_r\end{pmatrix} = \begin{pmatrix}s_{44} & d_{15}\\ d_{15} & \epsilon_{11}^T\end{pmatrix}\begin{pmatrix}\sigma_{rz}\\ E_r\end{pmatrix} \tag{C.4}$$

$$\epsilon_{r\phi} = 2(s_{11} - s_{12})\sigma_{r\phi} \tag{C.5}$$

$$\begin{pmatrix}\epsilon_{rr}\\ \epsilon_{\phi\phi}\\ \epsilon_{zz}\\ D_z\end{pmatrix} = \begin{pmatrix}s_{11} & s_{12} & s_{13} & d_{13}\\ s_{12} & s_{11} & s_{13} & d_{13}\\ s_{13} & s_{13} & s_{33} & d_{33}\\ d_{13} & d_{13} & d_{33} & \epsilon_{33}^T\end{pmatrix}\begin{pmatrix}\sigma_{rr}\\ \sigma_{\phi\phi}\\ \sigma_{zz}\\ E_z\end{pmatrix} \tag{C.6}$$

where the superscript T on the dielectric constant indicates constant tension. A change among the variables in eq. (C.6) can thus be made without involving the coefficients of eqs. (C.3-C.5)

A further simplification can be made as the piezoceramic disc is free to move in the z direction, i.e. $\sigma_{zz} = 0$ on the surface. Also the gradient $\partial/\partial z u_{zz}$ will be zero at frequencies well below the first thickness resonance, and we have $u_{zz} = 0$ throughout the pz-disc. The ratio between the first thickness resonance and the first radial resonance is approximately $R/\xi = 20$ which means that this condition holds even at the lowest radial resonances. Thus we will only consider the following relations

$$\begin{pmatrix}\epsilon_{rr}\\ \epsilon_{\phi\phi}\\ D_z\end{pmatrix} = \begin{pmatrix}s_{11} & s_{12} & d_{13}\\ s_{12} & s_{11} & d_{13}\\ d_{13} & d_{13} & \epsilon_{33}^T\end{pmatrix}\begin{pmatrix}\sigma_{rr}\\ \sigma_{\phi\phi}\\ E_z\end{pmatrix} \tag{C.7}$$

If we instead choose the input variables to be ϵ_{rr}, $\epsilon_{\phi\phi}$ and E_z, then

$$\begin{pmatrix}\sigma_{rr}\\ \sigma_{\phi\phi}\\ D_z\end{pmatrix} = \begin{pmatrix}c_{11} & c_{12} & -e_{13}\\ c_{12} & c_{11} & -e_{13}\\ e_{13} & e_{13} & \epsilon_{33}^S\end{pmatrix}\begin{pmatrix}\epsilon_{rr}\\ \epsilon_{\phi\phi}\\ E_z\end{pmatrix} \tag{C.8}$$

where the superscript S indicates constant strain in the r and ϕ directions and constant tension in the z direction. Denoting Poissons' ratio by $p = s_{12}/s_{11}$ and the planar coupling factor by [3, p. 291]

$$k_p = \left(\frac{2d_{33}^2}{\epsilon_{33}^T(s_{11} + s_{12})}\right)^{1/2} \tag{C.9}$$

we can express the new matrix entries in terms of the old in the following way

$$\begin{aligned} c_{11} &= \frac{1}{s_{11} + ps_{12}},\ c_{11} = \frac{p}{s_{11} + ps_{12}},\\ e_{13} &= \frac{d_{13}}{s_{11} + s_{12}},\ \epsilon_{33}^s = \epsilon_{33}^T(1 - k_p^2) \end{aligned} \tag{C.10}$$

The coupling factor k_p is a dimensionless measure of the strength of the piezo-electric effect. A value close to one means strong coupling between the electrical and the mechanical properties.

The measured quantity is the capacitance of the pz disc, $C_m = Q/U$, where $U = E_z\xi$ and Q is given by integrating

$$Q = \int_0^{R_0} 2\pi r D_z(r)\, d. \tag{C.11}$$

One limit is the special case where the ceramic is free to move, i.e. there are no internal stresses in the disc. We call this the free capacitance, C_f, and it is defined by $\sigma_{rr} = \sigma_{\phi\phi} = \sigma_{zz} = 0$ and thus becomes

$$\begin{aligned} C_f = \frac{Q}{U} &= \frac{\int_0^{R_0} 2\pi r D_z(r)\, dr}{E_z\xi} = \frac{\int_0^{R_0} 2\pi r \epsilon_{33}^T E_z\, dr}{E_z\xi} \\ &= \frac{\pi\epsilon_{33}^T}{\xi}\int_0^{R_0} 2r\, dr = \pi\epsilon_{33}^T\frac{R_0^2}{\xi}. \end{aligned} \tag{C.12}$$

Likewise we can define the clamped capacitance, i.e. where the disc is not able to move radially or transversely, while the stress in the z-direction remains zero. The clamped capacitance is defined by $\epsilon_{rr} = \epsilon_{\phi\phi} = 0$ and $\sigma_{zz} = 0$ and becomes

$$C_{cl} = \pi\epsilon_{33}^S\frac{R_0^2}{\xi}. \tag{C.13}$$

Combining the expressions for C_f and C_{cl} with Eq. (C.10) we have

$$\frac{C_{cl}}{C_f} = \frac{\epsilon_{33}^S}{\epsilon_{33}^T} = 1 - k_p^2 \tag{C.14}$$

In between those limiting scenarios we must integrate the full expression for D_z

$$Q = \int_0^{R_0} 2\pi r D_z(r)\, dr = \int_0^{R_0} 2\pi r \left(e_{13}\epsilon_{rr} + e_{13}\epsilon_{\phi\phi} + \epsilon_{33}^S E_z\right) dr \tag{C.15}$$

Substituting the strains with the displacement field expressions in Eq. (C.2) we obtain

$$\begin{aligned} Q &= \int_0^{R_0} 2\pi r \left(e_{13}\frac{\partial u_r}{\partial r} + e_{13}\frac{u_r}{r} + \epsilon_{33}^S E_z\right) dr \\ &= 2\pi e_{13}\left(\int_0^{R_0} r\frac{\partial u_r}{\partial r}\, dr + \int_0^{R_0} r\frac{u_r}{r}\, dr\right) + \epsilon_{33}^S E_z \pi R_0^2 \end{aligned} \tag{C.16}$$

Partial integration of the first integral finally brings us to

$$\begin{aligned} Q &= 2\pi e_{13}\left(R_0 u_r(R_0) - \int_0^{R_0} u_r\, dr + \int_0^{R_0} r\frac{u_r}{r}\, dr\right) + \epsilon_{33}^S E_z \pi R_0^2 \\ &= 2\pi e_{13} R_0 u_r(R_0) + \epsilon_{33}^S E_z \pi R_0^2 \end{aligned} \tag{C.17}$$

The measured capacitance of the pz disc may then be written as

$$\begin{aligned} C_m = \frac{Q}{U} = \frac{Q}{E_z\xi} &= \frac{2\pi e_{13} R_0 u_r(R_0) + \epsilon_{33}^S E_z \pi R_0^2}{E_z\xi} \\ &= \frac{2\pi e_{13} R_0}{E_z\xi} u_r(R_0) + \epsilon_{33}^S \pi\frac{R_0^2}{\xi} = \frac{2\pi e_{13} R_0}{E_z\xi} u_r(R_0) + C_{cl} \end{aligned} \tag{C.18}$$

We introduce the dimensionless quantity $F \equiv \frac{C_m - C_{cl}}{C_f - C_{cl}}$, and rewrite it with the expression of Eq. (C.14)

$$\begin{aligned} F &= \frac{C_m/C_{cl} - 1}{C_f/C_{cl} - 1} = \frac{C_m/C_{cl} - 1}{1/(1-k_p^2) - 1} \\ &= \frac{C_m/C_{cl} - 1}{1/(1-k_p^2) - 1} = \frac{C_m/C_{cl} - 1}{k_p^2/(1-k_p^2)} = \left(\frac{C_m}{C_{cl}} - 1\right) \frac{1-k_p^2}{k_p^2} \end{aligned} \tag{C.19}$$

Using the expression for C_m (Eq. (C.18)) and C_{cl} (Eq. (C.13)), we now arrive at the following expression for F

$$F = \frac{\frac{2\pi e_{13} R_0}{E_z \xi} u_r(R_0)}{\pi \epsilon_{33}^S \frac{R_0^2}{\xi}} \frac{1-k_p^2}{k_p^2} = \frac{2e_{13}}{\epsilon_{33}^S E_z R_0} u_r(R_0) \frac{1-k_p^2}{k_p^2} \tag{C.20}$$

Substituting Eq. (C.10) for ϵ_{33}^S and e_{13} and Eq. (C.9) for k_p we end up with

$$\begin{aligned} F &= \frac{2e_{13}}{\epsilon_{33}^T (1-k_p^2) E_z R_0} u_r(R_0) \frac{1-k_p^2}{k_p^2} = \frac{2e_{13}}{\epsilon_{33}^T E_z R_0} u_r(R_0) \frac{1}{k_p^2} \\ &= \frac{2\frac{d_{13}}{s_{11}+s_{12}}}{\epsilon_{33}^T E_z R_0} u_r(R_0) \frac{\epsilon_{33}^T (s_{11}+s_{12})}{2d_{13}^2} = \frac{1}{E_z R_0 d_{13}} u_r(R_0) \end{aligned} \tag{C.21}$$

By Eq. C.20 F is given by the measured capacitance and it now remains to find the displacement at the edge as a function of the rigidity of the liquid.

We will now consider a differential element of the pz disc (see Fig. C.1). The resulting force pr. volume transmitted through the surfaces is the divergence of the stress-tensor. The expression for this divergence in cylindrical coordiantes is

$$\nabla \cdot \underline{\underline{\sigma}} = \frac{1}{r} \frac{\partial}{\partial r} (r\sigma_{rr}) - \frac{1}{r} \sigma_{\phi\phi} + \frac{1}{r} \frac{\partial}{\partial \phi} \sigma_{r\phi} + \frac{\partial}{\partial z} \sigma_{rz} \tag{C.22}$$

where the third term in our case is zero since by Eq. (C.5) $\sigma_{r\phi} \propto \epsilon_{r\phi} = 0$. Setting this equal to the density times the (radial) acceleration we arrive at the radial equation of motion for the disc

$$\frac{1}{r} \frac{\partial}{\partial r} (r\sigma_{rr}) - \frac{1}{r} \sigma_{\phi\phi} + \frac{\partial}{\partial z} \sigma_{rz} = \rho \frac{\partial^2}{\partial t^2} u_r \tag{C.23}$$

The tangential stress σ_{rz} on the free side(s) is zero and $-\sigma_l$ on the sides that are in contact with the liquid. Because the disc is thin $\xi \ll R_0$ the gradient $\frac{\partial}{\partial z}\sigma_{rz}$ is approximated by $-\sigma_l/\xi$.

In the following a harmonic time-variation in $\tilde{E}_z = E_z e^{i\omega t}$ and $\tilde{u}_r = u_r e^{i\omega t}$ and u_r and E_z will from now on refer to the amplitude of these fields.

$$\frac{1}{r} \frac{\partial}{\partial r} (r\sigma_{rr}) - \frac{1}{r} \sigma_{\phi\phi} - \frac{1}{\xi} \sigma_l = -\omega^2 \rho u_r \tag{C.24}$$

Using Eq. (C.8), i.e.

$$\begin{aligned} \sigma_{rr} &= c_{11}\epsilon_{rr} + c_{12}\epsilon_{\phi\phi} - e_{13}E_z \\ \sigma_{\phi\phi} &= c_{12}\epsilon_{rr} + c_{11}\epsilon_{\phi\phi} - e_{13}E_z \end{aligned} \tag{C.25}$$

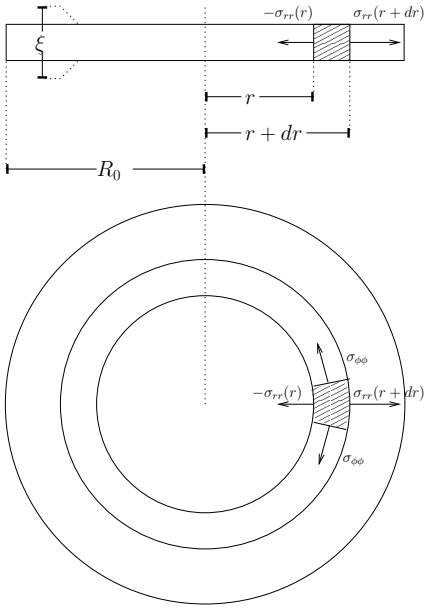

Figure C.1 A sketch of the pz disc seen from the side and from the top. The shades areas represent a differential element of the disc and the arrows shows the stresses that are acting on the surfaces of this element. The thickness of the disc is ξ and the radius R_0.

combined with Eq. (C.2), i.e.

$$\epsilon_{rr} = \frac{\partial u_r}{\partial r}, \qquad \epsilon_{\phi\phi} = \frac{u_r}{r} \tag{C.26}$$

we can rewrite Eq. (C.24) purely in terms of the displacement

$$\begin{aligned} -\rho\omega^2 u_r &= \frac{1}{r}\frac{\partial}{\partial r}\left(r\left(c_{11}\frac{\partial u_r}{\partial r} + c_{12}\frac{u_r}{r} - e_{13}E_z\right)\right) - \frac{1}{r}\left(c_{12}\frac{\partial u_r}{\partial r} + c_{11}\frac{u_r}{r} - e_{13}E_z\right) - \frac{1}{\xi}\sigma_l \\ &= c_{11}\frac{\partial^2 u_r}{\partial r^2} + c_{12}\frac{1}{r^2}\left(r\frac{\partial u_r}{\partial r} - u_r\right) - 0 + \frac{1}{r}\left(c_{11}\frac{\partial u_r}{\partial r} + c_{12}\frac{u_r}{r} - e_{13}E_z\right) \\ &\quad - \frac{1}{r}\left(c_{12}\frac{\partial u_r}{\partial r} + c_{11}\frac{u_r}{r} - e_{13}E_z\right) - \frac{1}{\xi}\sigma_l \end{aligned} \tag{C.27}$$

where most of the terms cancel out and we end up with

$$c_{11}\left(\frac{\partial^2 u_r}{\partial r^2} + \frac{1}{r}\frac{\partial u_r}{\partial r} - \frac{u_r}{r^2}\right) - \frac{1}{\xi}\sigma_l = -\rho\omega^2 u_r \tag{C.28}$$

To make the equations a little more compact we define the differential operator $\mathcal{P}$

$$\mathcal{P} = r^2\left(\frac{\partial}{\partial r}\right)^2 + r\frac{\partial}{\partial r} - 1 \tag{C.29}$$

The equations of motion for differential element of the discs between r and $r+dr$ (see Fig. C.2)

$$\begin{aligned} c_{11}\mathcal{P}\left[u_1\right] - \sigma_1\frac{r^2}{\xi_1} &= -\omega^2 r^2\rho_1 u_1 \\ c_{11}\mathcal{P}\left[u_2\right] - (\sigma_2^+ + \sigma_2^-)\frac{r^2}{\xi_2} &= -\omega^2 r^2\rho_2 u_2 \\ c_{11}\mathcal{P}\left[u_3\right] - \sigma_3\frac{r^2}{\xi_3} &= -\omega^2 r^2\rho_3 u_3 \end{aligned} \tag{C.30}$$

where in principle the thickness of the pz-discs ξ and the distance between discs d could differ, but in practice we will assume these quantities to be the same for all discs and gaps.

Now we need to express the stress from the liquid σ_l (which of course will be different for the shear transducer compared to the longitudinal transducer), apply the appropriate boundary conditions and finally solve the equations.

C.2 Solving the equations for the shear transducer

In Fig. C.2 we show a cross-section of a differential element between r and $r+dr$ of the three disc construction for the PSG. In this geometry, there will be a plane in the liquid that remains unperturbed by the deformation imposed by the pz-discs (illustrated with red dash-dotted lines in Fig. C.2) at 1/3 of the layer thickness, d/3. This plane can be regarded as an infinitely rigid support, and the problem of finding the dependence of the measured electrical capacitance on the liquid properties can be mapped onto a one-disc device (with 3/2 of the capacitance of a single disc) and infinitely rigid support.

In this case we only have to solve one equation

$$\mathcal{P}\left[u_r\right] + \left(\frac{\rho r^2\omega^2}{c_{11}}\right)u_r - \frac{r^2}{c_{11}\xi}\sigma_l = 0 \tag{C.31}$$

Now we assume that the deformation of the liquid is pure shear and only the component $\epsilon_{rz}^{\mathrm{liq}}$ is nonzero, i.e. that the volume change in the deformation is negligible

We then have

$$\sigma_l = 2G(\omega)\epsilon_{rz}^{\mathrm{liq}} = G(\omega)\frac{u_r}{d} \tag{C.32}$$

where G is the shear modulus of the liquid. Inserting this into Eq. (C.31)

$$\mathcal{P}\left[u_r\right] + r^2\left(\frac{\rho\omega^2}{c_{11}} - \frac{G(\omega)}{c_{11}d\xi}\right)u_r = 0. \tag{C.33}$$

The boundary conditions of this differential equation are zero displacement at the center $u_r(0) = 0$ and zero stress at the edge $\sigma_{rr}(R_0) = 0$. Using Eqs. C.2 and C.8 this

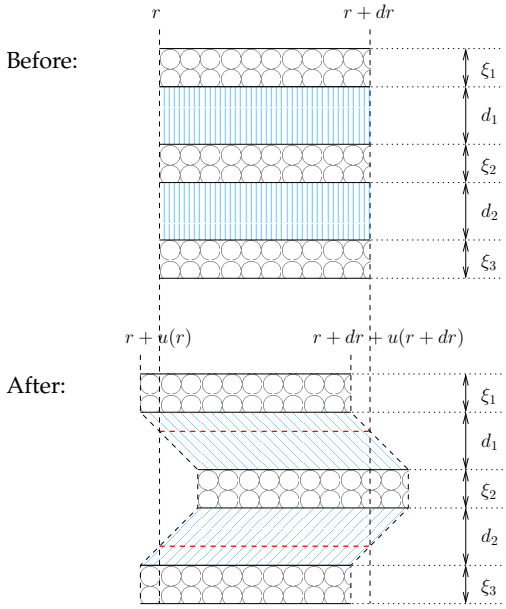

Figure C.2 A cross-section of a differential element between r and $r + dr$ of the three disc construction for the PSG, shown before and after a field is applied to the discs.

can be written in terms of displacement

$$\begin{aligned}\sigma_{rr} &= c_{11}\epsilon_{rr} + c_{12}\epsilon_{\phi\phi} - e_{13}E_z \\ &= \frac{1}{s_{11}+ps_{12}}\epsilon_{rr} + \frac{p}{s_{11}+ps_{12}}\epsilon_{\phi\phi} - \frac{d_{13}}{s_{11}+s_{12}}E_z \\ &= \frac{1}{s_{11}+ps_{12}}\frac{\partial u_r}{\partial r} + \frac{p}{s_{11}+ps_{12}}\frac{u_r}{r} - \frac{d_{13}}{s_{11}+s_{12}}E_z\end{aligned} \tag{C.34}$$

which then gives

$$\frac{\partial u_r}{\partial r}(R_0) + \frac{p}{R_0}u_r = \frac{d_{13}(s_{11}+ps_{12})}{s_{11}+s_{12}}E_z = d_{13}(1+p)E_z. \tag{C.35}$$

The problem becomes dimensionless with the following two definitions

$$x = r/R_0, \;\; e(x) = \frac{1}{(1+p)d_{13}E_zR_0}u(R_0x) \tag{C.36}$$

which gives

$$\begin{aligned}e'(x) &= \tfrac{d}{dx}\left(\frac{1}{(1+p)d_{13}E_zR_0}u(R_0x)\right) \\ &= \frac{1}{(1+p)d_{13}E_zR_0}u'(R_0x)R_0 = \frac{1}{(1+p)d_{13}E_z}u'(R_0x) \\ e''(x) &= \frac{R_0}{(1+p)d_{13}E_z}u''(R_0x)\end{aligned} \tag{C.37}$$

The characteristic quantities is defined as follows

$$\text{modulus:} \quad G_c = \frac{c_{11} d\xi}{R_0^2} \tag{C.38}$$

$$\text{inertance:} \quad M_c = \rho d\xi \tag{C.39}$$

$$\text{frequency:} \quad \omega_c = \sqrt{\frac{G_c}{M_c}} = \sqrt{\frac{c_{11}}{\rho R_0^2}} \tag{C.40}$$

together with

$$V = \frac{G(\omega)}{G_c}, \;\; S = \left(\frac{\omega}{\omega_c}\right)^2, \;\; k^2 = S - V \tag{C.41}$$

and Eq. C.33 becomes a first order Bessel differential equation

$$\begin{aligned}
0 &= \mathcal{P}\left[u_r\right] + r^2 \left(\frac{\rho\omega^2}{c_{11}} - \frac{G(\omega)}{c_{11} d\xi}\right) u_r = \mathcal{P}\left[u_r\right] + \frac{r^2}{R_0^2}\left(\frac{R_0^2 \rho\omega^2}{c_{11}} - \frac{R_0^2 G(\omega)}{c_{11} d\xi}\right) u_r \\
&= \frac{1}{(1+p) d_{13} E_z R_0} \mathcal{P}\left[u_r\right] + x^2 \frac{1}{(1+p) d_{13} E_z R_0} \left(\frac{\omega^2}{\omega_c^2} - \frac{G(\omega)}{G_c}\right) u_r \\
&= \frac{1}{(1+p) d_{13} E_z R_0} \left(r^2 \frac{\partial^2}{\partial r^2} u_r + r \frac{\partial}{\partial r} u_r - u_r\right) + k^2 x^2 e(x) \\
&= \frac{1}{(1+p) d_{13} E_z R_0} \left(r^2 \frac{\partial^2}{\partial x^2} u_r \left(\frac{dx}{dr}\right)^2 + r \frac{\partial}{\partial x} u_r \frac{dx}{dr} - u_r\right) + k^2 x^2 e(x) \\
&= x^2 e''(x) + x e'(x) - e(x) + k^2 x^2 e(x) = x^2 e''(x) + e'(x) + (k^2 x^2 - 1) e(x)
\end{aligned} \tag{C.42}$$

with the boundary conditions

$$e(0) = 0, \quad e'(1) + p e(1) = 1 \tag{C.43}$$

In this formulation the dimensionless measured capacitance in Eq. (C.20) becomes

$$F(\omega) = (1+p) e(1) \tag{C.44}$$

The general solution to this differential equation

$$e(x) = A J_1(kx) + B Y_1(kx) \tag{C.45}$$

where J_n and Y_n are a Bessel functions of the first order (first and second kind respectively). Applying the first boundary condition reveals $B = 0$, while the second boundary condition gives

$$A = \left[k J_1'(k) + p J_1(k)\right]^{-1} \tag{C.46}$$

Through recurrence formulas for Bessel functions the following general expression for the derivative is found

$$J_n'(x) = J_{n-1}(x) - \frac{n}{x} J_n(x) \tag{C.47}$$

and a can thus be expressed

$$A = \left[k\left(J_0(k) - \frac{1}{k} J_1(k)\right) + p J_1(k)\right]^{-1} = \left[k J_0(k) + (p-1) J_1(k)\right]^{-1} \tag{C.48}$$

Thus the measured capacitance can be written

$$C_m = C_{cl}\left[(1+p)\frac{J_1(k)}{kJ_0(k)+(p-1)J_1(k)}\frac{k_p^2}{1-k_p^2}+1\right] \tag{C.49}$$

where k is given from Eq. (C.38)-(C.41).

D Nonlinear optimization

This is a note based on [4, 5] on some technical and mathematical issues of doing fits of models to data.

Quite generally a model y is some function of the input x and the parameters θ

$$y = f(x;\theta)\,. \tag{D.1}$$

Often such a mathematical model is used to predict something, i.e. when we know the parameters, we can predict the outcome of a certain input. But often we are interested in solving the *inverse* problem: given the input and the output, what were the parameters? This kind of problem is often *ill-posed*, i.e. there may be many equally good solutions and they may not be stable.

If we write the data Y and the associated model output y can be written as column vectors

$$\begin{aligned} Y &= (Y(x_1), Y(x_2), \ldots, Y(x_N))^T \\ y &= (y(x_1), y(x_2), \ldots, y(x_N))^T \end{aligned} \tag{D.2}$$

we can estimate the parameters by minimizing the least squares cost between the computed and measured values of the model output. The least squares cost (which also approximate the model variance) is given by

$$\sigma^2 = \frac{1}{N-n}\sum_{l=1}^{N} |y(x_l) - Y(x_l)|^2 \tag{D.3}$$

where N is the number of observations and n is the number of parameters.

To ensure that this procedure is meaningful we can check two things: is the model sensitive to the parameters? And are the parameters correlated?

D.1 Parameter sensitivity

The sensitivity of the model output y to the model parameters θ can be predicted from the matrix

$$S = \frac{\partial y}{\partial \theta} = \left(\frac{\partial y}{\partial \theta_1} \;\; \frac{\partial y}{\partial \theta_2} \;\; \cdots \;\; \frac{\partial y}{\partial \theta_n} \right) . \tag{D.4}$$

If the absolute values of the parameters are very different (i.e. differs by orders of magnitude) the columns of this matrix becomes comparable if one instead uses the

logarithmic derivatives

$$S = \frac{\partial \ln y}{\partial \ln \theta} = \left(\frac{\partial \ln y}{\partial \ln \theta_1} \quad \frac{\partial \ln y}{\partial \ln \theta_2} \quad \cdots \quad \frac{\partial \ln y}{\partial \ln \theta_n} \right) . \tag{D.5}$$

If the elements in one column is close to zero the model is insensitive to that parameter.

D.2 Correlations between parameters

If 2 parameters in a model are correlated (in a sense that will be defined below) then it is not possible to determine a unique value of these parameters. A very simple example of such a correlation would be a linear model in this form

$$y = (\theta_1 + \theta_2)x. \tag{D.6}$$

In this case it is obvious that only the sum of the parameters can be determined – not the actual values of θ_1 and θ_2. In other cases it might be more difficult to asses whether to parameters are correlated or not.

A standard tool for quantifying the "correlatedness" of parameters is using the covariance matrix

$$C = \left(S^T S \right)^{-1}. \tag{D.7}$$

The correlation matrix c is then obtained as follows

$$c_{i,j} = \frac{C_{i,j}}{\sqrt{C_{i,i} C_{j,j}}} \tag{D.8}$$

where $-1 \leq c_{i,j} \leq 1$. c is a symmetric matrix with ones in the diagonal. Two parameters are correlated if $|c_{i,j}| \sim 1$.

E Analytical and numerical Laplace transforms

Definition of the Laplace transform:

$$[\mathcal{L}f](s) = \int_0^\infty e^{-st} f(t)\, dt =: F(s). \tag{E.1}$$

When we use the Laplace transforms presented here, we will with no further hesitation use $s = i\omega$

General rules for the Laplace transform

$$\text{linearity: } [\mathcal{L}(af + bg)](s) = a[\mathcal{L}f](s) + b[\mathcal{L}g](s) \tag{E.2}$$

$$\text{differentiation: } \left[\mathcal{L}\frac{d}{dt}f\right](s) = sF(s) - f(0) \tag{E.3}$$

$$\text{convolution: } [\mathcal{L}(f \circ g)](s) = F(s)G(s) \tag{E.4}$$

Laplace transforms of some special functions

$$\left[\mathcal{L}e^{-t/\tau}\right](s) = \frac{1}{1 + s\tau} \tag{E.5}$$

E.1 Analytic transforms

E.1.1 The stretched exponential

The response function in the frequency domain corresponding to a relaxation function in the time domain is given by the Laplace transform of the derivative of the relaxation function.

In general there is no analytical solution for the stretched exponential, $R(t) = \exp\left\{-\left(\frac{t}{\tau}\right)^\beta\right\}$. However, for $\beta = 0.5$ it is possible to arrive at a semi-analytical expression

$$[\mathcal{L}R](s) = \int_0^\infty e^{-st} e^{-\sqrt{t/\tau}}\, dt \tag{E.6}$$

Change of variables, $\xi = \sqrt{t/\tau} \Rightarrow d\xi = -\frac{1}{2\sqrt{t/\tau}}\, dt$

$$[\mathcal{L}R](s) = -2\int_0^\infty \xi e^{-s\tau\xi^2} e^{-\xi}\, d\xi \tag{E.7}$$

Now we re-write this

$$[\mathcal{L}R](s) = -2\int_0^\infty \xi e^{-s\tau\xi^2-\xi}\,d\xi \tag{E.8}$$

$$= -2\left[\int_0^\infty \xi e^{-s\tau\xi^2-\xi}\,d\xi + \frac{1}{2s\tau}\int_0^\infty e^{-s\tau\xi^2-\xi}\,d\xi - \frac{1}{2s\tau}\int_0^\infty e^{-s\tau\xi^2-\xi}\,d\xi\right] \tag{E.9}$$

$$= -2\left[\int_0^\infty \left(\xi + \frac{1}{2s\tau}\right) e^{-s\tau\xi^2-\xi}\,d\xi - \frac{1}{2s\tau}\int_0^\infty e^{-s\tau\xi^2-\xi}\,d\xi\right] \tag{E.10}$$

$$= -2\left[\frac{1}{2s\tau}\int_0^\infty (2s\tau\xi+1)\, e^{-s\tau\xi^2-\xi}\,d\xi - \frac{1}{2s\tau}\int_0^\infty e^{-s\tau\xi^2-\xi}\,d\xi\right] \tag{E.11}$$

$$= -\frac{1}{s\tau}\int_0^\infty (2s\tau\xi+1)\, e^{-s\tau\xi^2-\xi}\,d\xi + \frac{1}{s\tau}\int_0^\infty e^{-s\tau\xi^2-\xi}\,d\xi \tag{E.12}$$

The second part of this integral is a standard definite integral and can be looked up in tables. The first part of this sum can be solved with a change of variables, $y = s\tau\xi^2 + \xi \Rightarrow dy = (2s\tau\xi+1)d\xi$, to give

$$-\frac{1}{s\tau}\int_0^\infty (2s\tau\xi+1)\, e^{-s\tau\xi^2}e^{-\xi}\,d\xi = -\frac{1}{s\tau}\int_0^\infty e^{-y}\,dy = \frac{1}{s\tau} \tag{E.13}$$

In total we obtain

$$[\mathcal{L}R](s) = \frac{1}{s\tau}\left[1 + \frac{1}{2}\sqrt{\frac{\pi}{s\tau}}e^{1/4s\tau}\mathrm{erfc}\left(\frac{1}{\sqrt{4s\tau}}\right)\right] \tag{E.14}$$

E.1.2 The derivative of the stretched exponential

Normally we are not interested in the Laplace transform of the relaxation function, $R(t)$, but rather the negative derivative of this

$$\left[\mathcal{L}\left(-\tfrac{d}{dt}R\right)\right](s) = \int_0^\infty e^{-st}\frac{e^{-\sqrt{t/\tau}}}{2\sqrt{t/\tau}}\,dt \tag{E.15}$$

Change of variables, $\xi = \sqrt{t/\tau} \Rightarrow d\xi = -\frac{1}{2\sqrt{t/\tau}}\,dt$

$$\left[\mathcal{L}\left(-\tfrac{d}{dt}R\right)\right](s) = -\int_0^\infty e^{-s\tau\xi^2}e^{-\xi}\,d\xi \tag{E.16}$$

This integral is a standard definite integral (same as above)

$$\left[\mathcal{L}\left(-\tfrac{d}{dt}R\right)\right](s) = -\frac{1}{2}\sqrt{\frac{\pi}{s\tau}}e^{1/4s\tau}\mathrm{erfc}\left(\frac{1}{\sqrt{4s\tau}}\right). \tag{E.17}$$

As a check, we can try solving this with the rule of differentiation

$$\left[\mathcal{L}\left(-\tfrac{d}{dt}R\right)\right](s) = 1 - s\tau\,[\mathcal{L}R] \tag{E.18}$$

$$= 1 - s\tau\left\{\frac{1}{s\tau}\left[1 + \frac{1}{2}\sqrt{\frac{\pi}{s\tau}}e^{1/4s\tau}\mathrm{erfc}\left(\frac{1}{\sqrt{4s\tau}}\right)\right]\right\} \tag{E.19}$$

$$= -\frac{1}{2}\sqrt{\frac{\pi}{s\tau}}e^{1/4s\tau}\mathrm{erfc}\left(\frac{1}{\sqrt{4s\tau}}\right). \tag{E.20}$$

and have established that the two methods arrive at the same expression.

E.1.3 The exponential $\sqrt{t}$ relaxation function

The exponential $\sqrt{t}$ relaxation function

$$R(t) = e^{-C\sqrt{t/\tau}-t/\tau} \Rightarrow \tfrac{d}{dt}R = -e^{-C\sqrt{t/\tau}-t/\tau}\left(\tfrac{C}{2\sqrt{t/\tau}}+1\right) \tag{E.21}$$

This is the stretched exponential multiplied by a simple exponential. This function too has a semi-analytical expression that can be derived on the basis of the above.

$$\left[\mathcal{L}\tfrac{d}{dt}r\right](s) = -\int_0^\infty e^{-st}e^{-C\sqrt{t/\tau}-t/\tau}\left(\frac{C}{2\sqrt{t/\tau}}+1\right)dt \tag{E.22}$$

$$= -C\int_0^\infty e^{-st}\frac{e^{-C\sqrt{t/\tau}-t/\tau}}{2\sqrt{t/\tau}}\,dt - \int_0^\infty e^{-st}e^{-C\sqrt{t/\tau}-t/\tau}\,dt \tag{E.23}$$

Change of variable, $\xi = \sqrt{t/\tau}$ gives

$$\left[\mathcal{L}\tfrac{d}{dt}r\right](s) = -C\int_0^\infty e^{-s\tau\xi^2}e^{-C\xi-\xi^2}\,d\xi - \int_0^\infty e^{-s\tau\xi^2}e^{-C\xi-\xi^2}2\xi\,d\xi \tag{E.24}$$

Denoting $\tilde{s} = s\tau + 1$ we simplify this to obtain

$$\left[\mathcal{L}\tfrac{d}{dt}r\right](s) = -C\int_0^\infty e^{-\tilde{s}\xi^2-C\xi}\,d\xi - 2\int_0^\infty \xi e^{-\tilde{s}\xi^2-C\xi}\,d\xi \tag{E.25}$$

First part of this integral we already know and the second part may also be looked up in standard tables. So at last we arrive at

$$\left[\mathcal{L}\tfrac{d}{dt}r\right](s) = \frac{C}{2}\sqrt{\frac{\pi}{\tilde{s}}}e^{1/4\tilde{s}}\mathrm{erfc}\left(\frac{C^2}{\sqrt{4\tilde{s}}}\right) - 2\int_0^\infty \xi e^{-\tilde{s}\xi^2-C\xi}\,d\xi \tag{E.26}$$

E.2 Numerical transforms

A straight-forward way to obtain a Laplace transform is using the FFT (Fast Fourier Transform) defined in MatLab. This gives reasonable curves, but has severe problems in the high- and low-frequency limits. The disadvantage of such an approach is that the whole curve is given at once; it is not possible to calculate the transform at a given frequency – which is what we want for fitting purposes.

E.2.1 'Sum-of-exponentials' method

A mathematical theorem ("Bernsteins Theorem") states that function that are completely monotone may be written as a (possibly infinite) sum of exponentials

$$f(t) = \int_0^\infty G(\ln\tau)e^{-t/\tau}\,d\ln\tau \tag{E.27}$$

The advantage of that with respect to the Laplace transform is obvious: the Laplace transform is a linear operation and thus the transform of a sum of exponentials, will be a sum of the transform of the exponential function (Eq. E.5). This gives a simple expression

$$F(s) = [\mathcal{L}f](s) = \left[\mathcal{L}\left(\int_0^\infty G(\ln\tau)e^{-t/\tau}\,d\ln\tau\right)\right] \tag{E.28}$$

$$= \int_0^\infty G(\ln\tau)\left[\mathcal{L}e^{-t/\tau}\right](s)\,d\ln\tau \tag{E.29}$$

$$= \int_0^\infty G(\ln\tau)\frac{1}{1+s\tau}\,d\ln\tau \tag{E.30}$$

Bello *et al* [6] have compiled a list of this distribution of relaxation times for some of the popular fitting functions. In the case of the stretched exponential in general, $R(t) = \exp\left[-(t/\tau_0)^\beta\right]$ the expression is somewhat complicated

$$G(\ln\tau) = \frac{1}{\pi}\int_0^\infty e^{-x}e^{-u\cos(\pi\beta)}\sin(u\sin(\pi\beta))\,dx \tag{E.31}$$

where $u = \left(\frac{x\tau}{\tau_0}\right)^\beta$. For $\beta = 1/2$ the expression is very simple

$$G(\ln\tau) = \left(\frac{\tau}{4\pi\tau_0}\right)^{1/2}. \tag{E.32}$$

This expression can now be used as a basis to calculate the Laplace transform of the exponential $\sqrt{t}$ relaxation function. Maggi [7] has done this, and the result is

$$G(\ln\tau) = \Theta(\tau_0-\tau)\frac{1}{\mathcal{N}}\frac{\tau_0}{4\pi\tau(\tau_0-\tau)}\sqrt{\frac{C^2\tau}{\pi(\tau_0-\tau)}}\exp\left\{-\frac{C^2\tau}{4(\tau_0-\tau)}\right\} \tag{E.33}$$

where $\Theta(x)$ is the Heaviside step-function and $\mathcal{N}$ is normalization factor

$$\mathcal{N} = \int_0^{\tau_0}\frac{\tau_0}{4\pi\tau(\tau_0-\tau)}\sqrt{\frac{C^2\tau}{\pi(\tau_0-\tau)}}\exp\left\{-\frac{C^2\tau}{4(\tau_0-\tau)}\right\}d\tau. \tag{E.34}$$

Bibliography

[1] P. V. Christiansen. *Dynamik og diagrammer –introduktion til energy-bond-graph formalismen.* IMFUFA, Roskilde University, 1978.

[2] P. V. Christiansen. *Energy Bond Graphs. The glass bead game of physics. A comprehensive thesis in three parts.* IMFUFA, Roskilde University, 2005.

[3] B. Jaffe, W. R. Cook, and H. Jaffe. *Piezoelectric Ceramics.* Academic Press London, 1971.

[4] C. T. Kelley. *Iterative methods for optimization.* SIAM - Frontiers in Applied Mathematics, 1999.

[5] M. S. Olufsen and Johnny Ottesen. Patient specific patameter estimation and heart rate regulation. *Annals of Biomedical Engineering*, 2010.

[6] A. Bello, E.. Laredo, and M. Grimau. Distribution of relaxation times from dielectric spectroscopy using monte carlo simulated annealing: Application to α-pvdf. *Physical Review B*, 60:12764–12774, 1999.

[7] C. Maggi. *Experimental Studies of Supercooled Liquids, Gels and Glasses.* PhD thesis, Roskilde University, 2010.

F Reprint of publications

ARTICLES

Little evidence for dynamic divergences in ultraviscous molecular liquids

TINA HECKSHER, ALBENA I. NIELSEN, NIELS BOYE OLSEN AND JEPPE C. DYRE*
DNRF Centre 'Glass and Time', IMFUFA, Department of Sciences, Roskilde University, Postbox 260, DK-4000 Roskilde, Denmark
*e-mail: dyre@ruc.dk

Published online: 27 July 2008; doi:10.1038/nphys1033

The physics of the ultraviscous liquid phase preceding glass formation continues to pose major problems that remain unsolved. It is actively debated, for instance, whether the marked increase of the relaxation time reflects an underlying phase transition to a state of infinite relaxation time. To elucidate the empirical evidence for this intriguing scenario, some of the most accurate relaxation-time data available for any class of ultraviscous liquids—those obtained by dielectric relaxation experiments on organic liquids just above the glass transition—were compiled. Analysis of data for 42 liquids shows that there is no compelling evidence for the Vogel–Fulcher–Tammann (VFT) prediction that the relaxation time diverges at a finite temperature. We conclude that theories with a dynamic divergence of the VFT form lack a direct experimental basis.

All liquids may be supercooled. In some cases, the liquid crystallizes spontaneously. In other cases, a marked increase in viscosity and relaxation time is observed on continued cooling, and the liquid eventually solidifies into a glass—a frozen liquid. Which of the two scenarios that prevails depends on the cooling rate. The ultraviscous liquid phase preceding glass formation has universal physical properties, independent of the nature of the chemical bonds involved: metal bonds, ionic bonds, covalent bonds, van der Waals bonds or hydrogen bonds. The universalities and the lack of understanding of the basic phenomenology continue to make this research field attractive to physicists, chemists and materials scientists alike.

The universal features[1–7] that characterize ultraviscous supercooled liquids relate, in particular, to the time dependence of relaxation functions and to the temperature dependence of the relaxation time. The former is not our focus here; it is reflected in the fact that relaxation functions are generally well fitted by the so-called stretched exponential function. The focus below is on the relaxation time, which increases markedly on cooling into the ultraviscous phase, sometimes by more than a factor of ten when temperature is lowered by just 1%. Figure 1 shows the relaxation time as a function of temperature for some typical molecular liquids. This figure raises the question: Does the relaxation time diverge at finite temperatures or only as $T \to 0$?

The average relaxation time τ is generally non-Arrhenius. That is, on cooling, τ almost always increases faster than predicted by the well-known Arrhenius equation. This is the mathematical expression that characterizes, for example, the temperature dependence of a chemical reaction time in terms of an activation energy. For ultraviscous liquids, if the temperature-dependent activation energy $\Delta E(T)$ is defined by the Arrhenius expression

$$\tau(T) = \tau_0 \exp\left(\frac{\Delta E(T)}{k_B T}\right), \qquad (1)$$

it is generally found that $\Delta E(T)$ increases significantly on cooling. To the best of our knowledge, there are no liquids where ΔE decreases, which is in itself a striking fact.

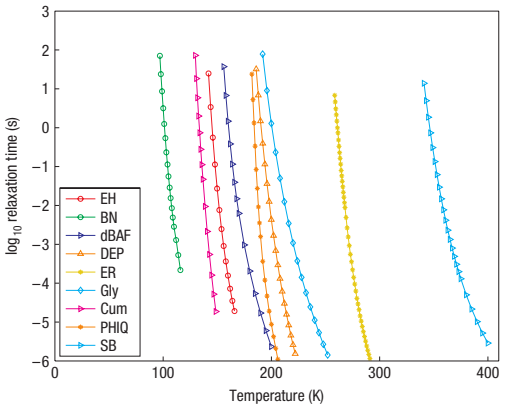

Figure 1 Relaxation time as a function of temperature for typical organic liquids supercooled into the ultraviscous phase. The relaxation time was determined as the inverse dielectric loss-peak frequency, identified by fitting data in a log–log plot around the maximum with a parabola. If a linear scale were used, the relaxation time would increase almost vertically on cooling; even on a log scale, the increase is marked. The question investigated in this article is whether or not there is reason to believe that the relaxation time diverges at some finite temperature. The full lines are drawn as guides to the eye. Table 1 explains the liquid abbreviations.

THE VFT EQUATION

The function most widely used to fit relaxation-time data is the Vogel–Fulcher–Tammann (VFT) equation dating back to the 1920s (refs 8–10):

$$\tau = \tau_0 \exp\left(\frac{A}{T - T_0}\right) \qquad (T_0 < T). \qquad (2)$$

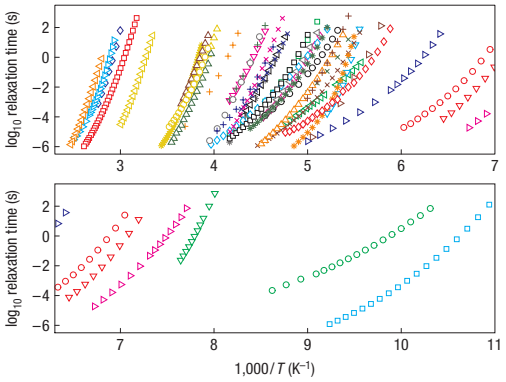

Figure 2 Relaxation time data identified from dielectric loss peaks for all of the 42 organic ultraviscous liquids used in the analysis. Both panels show the logarithm of the dielectric relaxation time as a function of inverse temperature. A straight line in this plot signals an Arrhenius temperature dependence. The liquids all exhibit the non-Arrhenius temperature dependence of the relaxation time that characterizes ultraviscous liquids. The symbols are explained in Table 1.

Table 1 Liquids included in the analysis. The name of each liquid, its abbreviation and the symbol used in the figures are listed. More details (including references, temperature, frequency intervals and some further information) are provided in the Supplementary Information.

Liquid	Abbreviation	Symbol
1,2-propandiol (propylene-glycol)	PG	◁
2-ethyl-hexylamine	EH	○
2-methyl-tetrahydrofurane	MTHF	□
2-phenyl-5-acetomethyl-5-ethyl-1,3-dioxocyclohexane	AFEH	▽
3,3,4,4-benzophenonetetracarboxylic dianhydride	BPC	◇
3-fluoro-aniline	FAN	▷
3-phenyl-1-propanol	3Ph1P	×
3-styrene	3Sty	+
5-polyphenyl-ether	5-PPE	△
benzophenone	BePh	*
biphenyl-2yl-isobutylate	BP2IB	◁
butyronitrile	BN	○
cresolphthalein-dimethylether	KDE	□
decahydroisoquinoline	DHIQ	▽
di-iso-butyl-phtalate	dIBP	◇
dibutyl-ammonium-formide	dBAF	▷
dibutyl-phtalate	DBP	×
dicyclohexyl-methyl-2-methylsuccinate	DCHMMS	+
diethyl-phtalate	DEP	△
diglycidyl-ether-of-bisphenol A (epoxy-resin)	ER	*
dimethyl-phtalate	DMP	◁
dioctyl-phtalate	DOP	○
dipropylene-glycol	DPG	□
dipropylene-glycol-dimethyl-ether	DPGDME	▽
glycerol	Gly	◇
isopropyl-benzene	Cum	▷
m-tricresyl-phosphate	mTCP	×
m-toluene	mTol	+
o-terphenyl	OTP	△
perhydroisoquinoline	PHIQ	*
phenolphthalein-dimethylether	PDE	◁
phenyl-salicylate (salol)	Sal	○
polypropylene-glycol	PPG	□
pyridine–toluene mixture	PT	▽
squalane	Sqa	◇
sucrose-benzonate	SB	▷
tetraphenyl-tetramethyl-trisiloxane	DC704	×
tricresyl-phosphate	TCP	+
triphenyl-ethylene	TPE	△
tripropylene-glycol	TPG	*
trisnaphthylbenzene	tNB	◁
xylitol	Xyl	○

This corresponds to an activation energy that increases on cooling as $\Delta E \propto T/(T - T_0)$. Although the VFT equation has few adjustable parameters, it generally gives quite good fits to data. The coefficients of the VFT equation were considered in the landmark paper published in 1955 by Williams, Landel and Ferry[11] that discussed the non-Arrhenius problem in terms of the free-volume model. In the 1970s, there were reports that the VFT equation breaks down at temperatures with long relaxation times (large viscosities)[12,13]. These 'early warnings' were to some extent forgotten or repressed, perhaps because probing the relaxation time accurately through viscosity measurements is difficult at high viscosities.

Experimentalists often regard the VFT equation as just a convenient fit to data[12]. Many theorists, on the other hand, were inspired by the VFT equation to develop theories predicting a phase transition at T_0 to a state with infinite relaxation time[14]. The first such approach was the famous Adam–Gibbs entropy model from 1965 predicting a second-order phase transition at $T = T_0$ to a state of zero configurational entropy and infinite relaxation time[15,16], a unique 'ideal glass'. A number of simplifying assumptions go into the Adam–Gibbs formalism, and in 1997 it was argued by DiMarzio and Yang[17] that even if the Adam–Gibbs idea of an underlying phase transition is accepted, the relaxation time remains finite at the transition temperature. Very recently, mathematically rigorous theorems derived by Eckmann and Procaccia[18] show that for two-dimensional soft-sphere mixtures, at least, the configurational entropy stays positive for $T > 0$.

Leading theorists such as Edwards[19,20], Anderson[21] and, more recently, Bouchaud and Biroli in 2004 (ref. 22) and Lubchenko and Wolynes in 2007 (ref. 23) have developed dynamic divergence scenarios far beyond Adam and Gibbs'. Although there are differing opinions from other famous theorists[24–27], it remains a popular idea that the marked slowing down on cooling reflects an underlying phase transition to a state of infinite relaxation time. The fact that data are usually well fitted by the VFT equation has reinforced this idea over many years[28]. Our aim is to provide an in-depth investigation of the evidence for dynamic divergences of the VFT form. Before detailing the data analysis, it should be noted that support for the idea of a dynamic divergence traditionally came from several papers reporting near equality of the VFT fitting parameter T_0 and the Kauzmann temperature T_K, the temperature where the liquid phase entropy by extrapolation below the glass transition becomes identical to the crystal phase entropy[29–31]. In 2003, however, Tanaka presented a compilation of data showing that $T_0 = T_K$ is not confirmed by experiment[32].

As is evident from the above, an important question of contemporary glass science is the following: Is there experimental evidence for the dynamic divergence predicted by the VFT equation? Answering this is important, because if there is an underlying dynamic divergence, this obviously explains the marked relaxation-time increase on cooling. By its very nature the question is subtle, however, because if the equilibrium liquid relaxation time diverges at some finite temperature, it is impossible to equilibrate the liquid at or close to that temperature. This means that no experiment can conclusively prove the existence of a dynamic divergence. To cut this science–philosophical Gordian knot, we take the following pragmatic viewpoint: the conjecture of a diverging

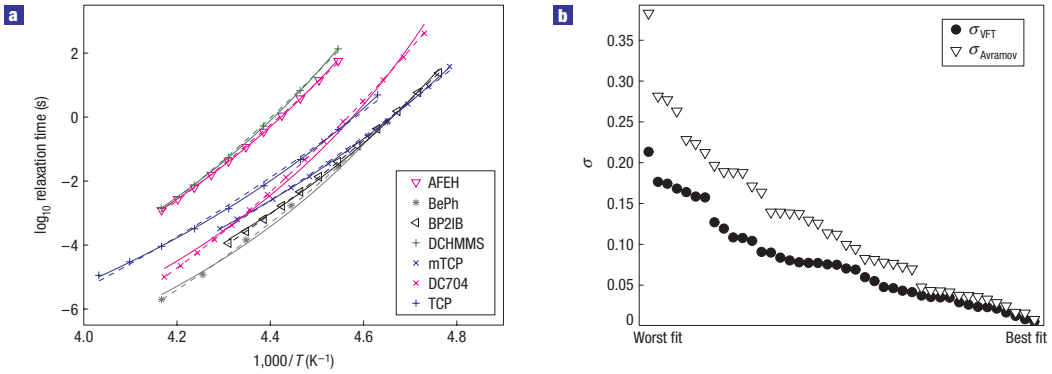

Figure 3 The VFT and Avramov equations compared with data. a, Examples of fits with the VFT equation (solid lines) and the Avramov equation (dashed lines). **b**, Standard deviation from fits to data of the two equations. The *x* axis represents the 42 liquids sorted in descending order of standard deviation for each of the two fitting functions; thus, a given position on the *x* axis generally corresponds to two different liquids. On average, the VFT equation fits data better than does the Avramov equation.

relaxation time of VFT form will be regarded as probably correct if—and only if—the VFT equation fits data considerably better than do other mathematically simple functions with the same number of fitting parameters and no dynamic divergence. To investigate this, data for a large number of liquids are needed.

DATA ANALYSIS

Accurate data are required to assess whether or not the VFT prediction of a diverging relaxation time is confirmed by experiment. Dielectric relaxation measurements give the most precise relaxation-time data, far more accurate than data from other relaxation processes or from viscosity measurements. For practical reasons, the best dielectric data for ultraviscous liquids are for organic liquids; such liquids are often easily supercooled and quite convenient to work with. Monoalcohols were omitted from the analysis because their dominant dielectric relaxation process does not relate to the calorimetric glass transition[33].

To quantify how well the VFT equation fits data, we compared the VFT equation with another popular fitting function[34–39] that is now known as the Avramov equation:

$$\tau(T) = \tau_0 \exp\left(\frac{B}{T^n}\right). \qquad (3)$$

Like the VFT equation, the Avramov equation has two parameters in addition to the prefactor τ_0, but it has no dynamic divergence. The prefactor is usually regarded as a free parameter, but we chose to fix it to $\tau_0 = 10^{-14}$ s (ref. 40). The below conclusions are not sensitive to the exact value of τ_0 if it is insisted that it should have a physically reasonable value, that is, be in (or just slightly outside) the range 10^{-14}–10^{-13} s.

At any given temperature, from the dielectric loss as a function of frequency, we define the liquid relaxation time τ as the inverse loss-peak frequency. The last of these is identified by fitting loss data as a function of log frequency close to the maximum loss with a parabola. Figure 2 shows all data analysed. All liquids exhibit the characteristic non-Arrhenius behaviour with a relaxation time that increases stronger on cooling than predicted by the Arrhenius equation (that is, equation (1) with temperature-independent activation energy). A list of all liquids included in the analysis and their corresponding symbols is given in Table 1; more details are provided in the Supplementary Information.

The fitting region was restricted to relaxation times between 1 μs and 1,000 s. This was done to avoid comparing different types of dynamic behaviour—otherwise there is the risk that we ultimately test the two equations' ability to interpolate between two different dynamics. The lower limit (1 μs) was chosen to ensure that the dynamics are well within the 'landscape dominated' domain[41,42]. The upper limit (1,000 s) was chosen to ensure that all data are true equilibrium data. A further requirement was that only data sets covering at least four decades in time measured at five or more temperatures were included in the analysis. Out of an initial collection of data for 62 liquids, 42 met these demands. The liquids represent some of the most commonly studied organic glass formers; their dielectric properties were measured by leading groups in the field. These data were supplemented by some new measurements of ours.

Equations (2) and (3) were fitted to data using the least-squares method. The procedures for selecting data and the subsequent fitting procedures were automated through MatLab routines. Examples of fits are shown in Fig. 3a with VFT fits as solid lines and Avramov fits as dashed lines. Both equations fit well with little visible difference. For a quantitative comparison of the two fitting functions, we used the standard deviation formula, $\sigma^2 = 1/(N-n)\sum_i(\log_{10}(\tau_{\mathrm{fit},i}) - \log_{10}(\tau_{\mathrm{data},i}))^2$, where N is the number of data points and $n = 2$ is the number of degrees of freedom. Figure 3b shows σ_{VFT} and $\sigma_{\mathrm{Avramov}}$ for all liquids, where the σ values for clarity are sorted in descending order for both fits. The VFT equation generally fits data better than does the Avramov equation.

Inspecting the fits closely—in Fig. 3a as well as those not shown—reveals that deviations are systematic. Thus, highly non-Arrhenius liquids, that is, data sets with large curvature, are generally poorly fitted by the Avramov equation. Apparently, the Avramov equation is not able to 'bend' enough to capture the curvature of these data sets. Is that a signal of the dynamic divergence predicted by the VFT equation? To investigate this possibility, we calculated how the activation energy changes with temperature using the temperature index defined[43] by

$$I = -\frac{\mathrm{d}\ln\Delta E}{\mathrm{d}\ln T}. \qquad (4)$$

The temperature index quantifies the activation-energy temperature dependence in a way that is independent of the

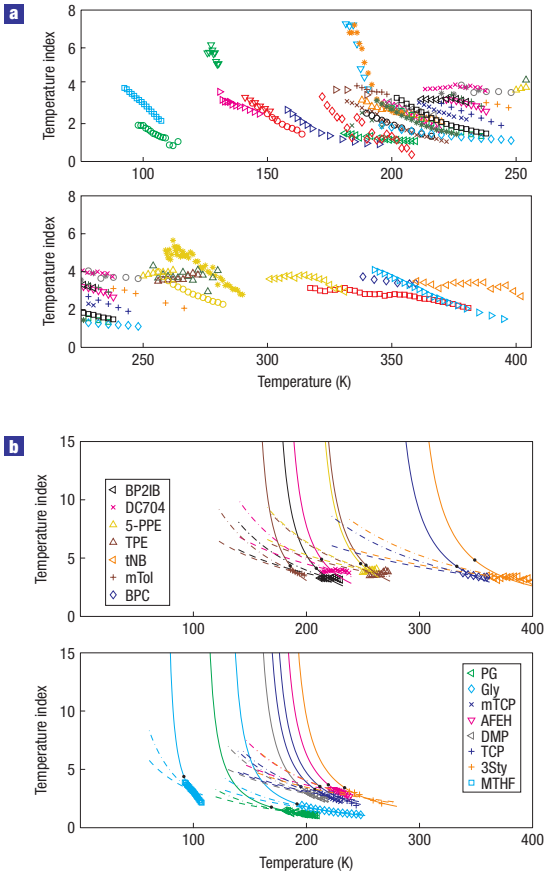

Figure 4 Temperature indices. This quantity (equation (4)) measures how fast the activation energy increases on cooling; it is plotted as a function of temperature. **a**, Temperature indices for all liquids. With few exceptions, the temperature index increases with decreasing temperature. This explains why the VFT equation fits data better than does the Avramov equation, which predicts a temperature-independent index. **b**, Temperature indices for the eight liquids where the Avramov equation (upper panel), respectively the VFT equation (lower panel), fits best. The full lines give the VFT-predicted temperature indices (equation (5)), the dashed–dotted and dashed lines, respectively, give the predictions of the two fitting functions FF1 and FF2 that do not have dynamic divergences (equations (6) and (7)). In both subfigures, the black circles mark the glass-transition temperature for each liquid.

unit system, like the Grüneisen parameter of solid-state physics quantifies the effects of thermal expansion. If for instance the temperature index is four, lowering the temperature by 1% leads to a 4% increase of the activation energy. If the glass transition temperature is defined by $\tau(T_g) = 100\,\mathrm{s}$, the temperature index is related to Angell's fragility $m \equiv \mathrm{d}\log_{10}(\tau)/\mathrm{d}(T_g/T)|_{T_g}$ by $m = c(1+I(T_g))$, where $c = \log_{10}(\tau(T_g)/\tau_0) = 16$ (ref. 43).

For the Avramov equation, the temperature index is constant, $I_{\mathrm{Avramov}} = n-1$. For the VFT equation, we find

$$I_{\mathrm{VFT}} = \frac{T_0}{T-T_0}. \qquad (5)$$

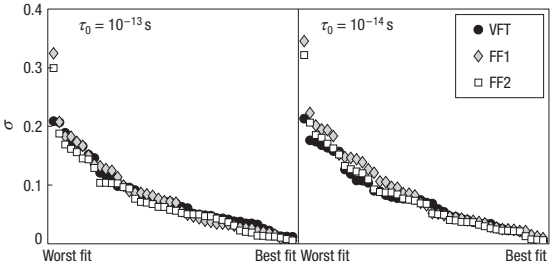

Figure 5 Standard deviation from fits to data of the VFT equation and two alternative fitting functions with the same number of parameters but no dynamic divergence, FF1 and FF2 of equations (6) and (7). The *x* axis represents the liquids sorted in descending order of standard deviation for each fitting function. For both choices of physically reasonable prefactors, the three functions fit equally well. The worst-fit outlier is perhydroisoquinoline, one of the most fragile (non-Arrhenius) liquids in the collection (compare Fig. 1).

Thus, the VFT temperature index increases on cooling and diverges at $T = T_0$. Figure 4a shows temperature indices for all 42 liquids as functions of temperature. For the vast majority of liquids, the temperature index increases with decreasing temperature. This explains why the VFT equation fits data better than the Avramov equation.

The temperature index is also useful for shedding light on how strong the evidence for a dynamic divergence is. Figure 4b (upper panel) shows the actual and the VFT-predicted temperature indices for the eight liquids that are best fitted by the Avramov equation; the lower panel shows those liquids that are best fitted by the VFT equation. The data are not inconsistent with the dynamic divergence predicted by the VFT equation, but we cannot reasonably say that there is compelling evidence for a divergent temperature index as predicted by the VFT equation. The dashed–dotted and dashed lines are the temperature indices of the two below fitting functions.

We proceed to compare the VFT function to two alternative fitting functions with temperature indices that increase on cooling, but without divergence at a non-zero temperature. Fitting functions one and two (FF1 and FF2) reflect the following temperature indices: $I = (T_1/T)^2$ and $I = (T_2 - T)/T$ $(T < T_2)$, respectively. Integrating these expressions via equation (4) leads to

$$\Delta E(T) \propto \exp\left[\frac{T_1^2}{2T^2}\right] \qquad (\mathrm{FF1}), \qquad (6)$$

$$\Delta E(T) \propto T\exp\left[\frac{T_2}{T}\right] \qquad (\mathrm{FF2}). \qquad (7)$$

Figure 5 shows the standard deviations from fitting these two functions to data compared with the VFT equation. The panels show results from two different prefactors, $\tau_0 = 10^{-13}$ s and $\tau_0 = 10^{-14}$ s. In both cases the three functions fit equally well.

OUTLOOK

The analysis was limited to non-polymeric systems because the polymer glass transition may be fundamentally different from the liquid–glass transition. The VFT equation was often used also for the polymer glass transition, however, where it is generally

known as the Williams–Landel–Ferry equation[11]. A clever way to extend the range of relaxation times beyond those obtainable by linear relaxation experiments is to consider results from ageing experiments. Studies by McKenna, Simon, Plazek and co-workers mainly on polymeric systems show that the VFT prediction is not followed when systems are aged into equilibrium by annealing for sufficiently long time slightly below the glass-transition temperature[44–47]. Although the accuracy of these experiments is not comparable to that of dielectric relaxation experiments on the metastable equilibrium phase, it was nevertheless possible to conclude that the relaxation times deviate from the VFT equation by always increasing less markedly when lowering temperature than predicted by the VFT equation. These results are fully consistent with the above conclusion.

It is not possible to rule out that there is a dynamic divergence of the VFT form, but our findings give no indications of such a divergence. It is instructive to compare the situation to that of a second-order phase transition. This is associated with a dynamic divergence where the (maximum) relaxation time diverges as an inverse power law of the temperature distance to the transition temperature (critical slowing down). Thus, right at the phase transition, the relaxation time is infinite. Although it is not possible to experimentally definitively prove this dynamic divergence, nobody doubts it. This is because (1) the predicted mathematical form is supported by experiment, (2) the dynamic critical exponents fit theoretical predictions and (3) there is a fundamental understanding of what is going on and why relaxations slow down when the transition is approached. For ultraviscous liquids, there is no such generally agreed simple and universal model. Here, the logic was traditionally reversed. The observation that data are well fitted by the VFT equation was used to justify a search for models with a dynamic divergence. Our findings indicate that this is probably not a fruitful route. Thus, with Occam's razor in mind—'it is vain to do with more what can be done with fewer'—we suggest that in the search for the correct theory for ultraviscous liquid dynamics, theories not predicting a dynamic divergence of the VFT form should be focused on.

Received 22 February 2008; accepted 24 June 2008; published 27 July 2008.

References

1. Brawer, S. *Relaxation in Viscous Liquids and Glasses* (American Ceramic Society, Columbus, 1985).
2. Debenedetti, P. G. *Metastable Liquids: Concepts and Principles* (Princeton Univ. Press, Princeton, 1996).
3. Ediger, M. D., Angell, C. A. & Nagel, S. R. Supercooled liquids and glasses. *J. Phys. Chem.* **100**, 13200–13212 (1996).
4. Angell, C. A., Ngai, K. L., McKenna, G. B., McMillan, P. F. & Martin, S. W. Relaxation in glassforming liquids and amorphous solids. *J. Appl. Phys.* **88**, 3113–3157 (2000).
5. Debenedetti, P. G. & Stillinger, F. H. Supercooled liquids and the glass transition. *Nature* **410**, 259–267 (2001).
6. Binder, K. & Kob, W. *Glassy Materials and Disordered Solids: An Introduction to their Statistical Mechanics* (World Scientific, Singapore, 2005).
7. Dyre, J. C. The glass transition and elastic models of glass-forming liquids. *Rev. Mod. Phys.* **78**, 953–972 (2006).
8. Vogel, H. Das Temperaturabhängigkeitsgesetz der Viskosität von Flüssigkeiten. *Phys. Zeit.* **22**, 645–646 (1921).
9. Fulcher, G. S. Analysis of recent measurements of the viscosity of glasses. *J. Am. Ceram. Soc.* **8**, 339–355 (1925).
10. Tammann, G. Glasses as supercooled liquids. *J. Soc. Glass Technol.* **9**, 166–185 (1925).
11. Williams, M. L., Landel, R. F. & Ferry, J. D. The temperature dependence of relaxation mechanisms in amorphous polymers and other glass-forming liquids. *J. Am. Chem. Soc.* **77**, 3701–3707 (1955).
12. Laughlin, W. T. & Uhlman, D. R. Viscous flow in simple organic liquids. *J. Phys. Chem.* **76**, 2317–2325 (1972).
13. Breitling, S. M. & Magill, J. H. A model for the Magill-Li viscosity-temperature relation. *J. Appl. Phys.* **45**, 4167–4171 (1974).
14. Angell, C. A. Oxide glasses in light of the ideal glass concept. I. Ideal and nonideal transitions and departures from ideality. *J. Am. Ceram. Soc.* **51**, 117–125 (1968).
15. Gibbs, J. H. & DiMarzio, E. A. Nature of the glass transition and the glassy state. *J. Chem. Phys.* **28**, 373–383 (1958).
16. Adams, G. & Gibbs, J. H. On the temperature dependence of cooperative relaxation properties in glass-forming liquids. *J. Chem. Phys.* **43**, 139–146 (1965).
17. DiMarzio, E. A. & Yang, A. J. M. Configurational entropy approach to the kinetics of glasses. *J. Res. Natl Inst. Stand. Technol.* **102**, 135–157 (1997).
18. Eckmann, J.-P. & Procaccia, I. Ergodicity and slowing down in glass-forming systems with soft potentials: No finite-temperature singularities. Preprint at <http://arxiv.org/abs/0802.4346> (2008).
19. Edwards, S. F. Theory of glasses. *Polymer* **17**, 933–937 (1976).
20. Edwards, S. F. The glass transition. *Int. J. Mod. Phys. B* **6**, 1587–1594 (1992).
21. Anderson, P. W. in *Ill-Condensed Matter* (eds Balian, R., Maynard, R. & Toulouse, G.) 159–261 (North-Holland, Amsterdam, 1979).
22. Bouchaud, J. P. & Biroli, G. On the Adam–Gibbs–Kirkpatrick–Thirumalai–Wolynes scenario for the viscosity increase in glasses. *J. Chem. Phys.* **121**, 7347–7354 (2004).
23. Lubchenko, V. & Wolynes, P. G. Theory of structural glasses and supercooled liquids. *Ann. Rev. Phys. Chem.* **58**, 235–266 (2007).
24. Götze, W. & Sjögren, L. Relaxation processes in supercooled liquids. *Rep. Prog. Phys.* **55**, 241–376 (1992).
25. Stillinger, F. H. Supercooled liquids, glass transition and the Kauzmann paradox. *J. Chem. Phys.* **88**, 7818–7825 (1988).
26. Kivelson, D., Tarjus, G., Zhao, X. & Kivelson, S. A. Fitting of viscosity: Distinguishing the temperature dependences predicted by various models of supercooled liquids. *Phys. Rev. E* **53**, 751–758 (1996).
27. Garrahan, J. P. & Chandler, D. Coarse-grained microscopic model of glass-formers. *Proc. Natl Acad. Sci.* **100**, 9710–9714 (2003).
28. Langer, J. S. The mysterious glass transition. *Phys. Today* 8–9 (February 2007).
29. Angell, C. A. & Smith, D. L. Test of the entropy basis of the Vogel–Tammann–Fulcher equation—dielectric relaxation of polyalcohols near T_G. *J. Phys. Chem.* **86**, 3845–3852 (1982).
30. Richert, R. & Angell, C. A. Dynamics of glass-forming liquids. V. On the link between molecular dynamics and configurational entropy. *J. Chem. Phys.* **108**, 9016–9026 (1998).
31. Angell, C. A. Entropy and fragility in supercooling liquids. *J. Res. Natl Inst. Stand. Technol.* **102**, 171–185 (1997).
32. Tanaka, H. Relation between thermodynamics and kinetics of glass-forming liquids. *Phys. Rev. Lett.* **90**, 055701 (2003).
33. Huth, H., Wang, L.-M., Schick, C. & Richert, R. Comparing calorimetric and dielectric polarization modes in viscous 2-ethyl-1-hexanol. *J. Chem. Phys.* **126**, 104503 (2007).
34. Harrison, G. *The Dynamic Properties of Supercooled Liquids* (Academic, New York, 1976).
35. Avramov, I. Viscosity in disordered media. *J. Non-Cryst. Solids* **351**, 3163–3173 (2005).
36. Bässler, H. Viscous flow in supercooled liquids analyzed in terms of transport theory for random media with energetic disorder. *Phys. Rev. Lett.* **58**, 767–770 (1987).
37. Litovitz, T. A. Temperature dependence of the viscosity of associated liquids. *J. Chem. Phys.* **7**, 1088–1089 (1952).
38. Barlow, A. J. & Lamb, J. The visco-elastic behaviour of lubricating oils under cyclic shearing stress. *Proc. R. Soc. A* **253**, 52–69 (1959).
39. Barlow, A. J., Lamb, J. & Matheson, A. J. Viscous behaviour of supercooled liquids. *Proc. R. Soc. A* **292**, 322–342 (1966).
40. Stickel, F., Fischer, E. W. & Richert, R. Dynamics of glass-forming liquids. I . Temperature-derivative analysis of dielectric data. *J. Chem. Phys.* **102**, 6251–6257 (1995).
41. Stillinger, F. H. A topographic view of supercooled liquid and glass formation. *Science* **267**, 1935–1939 (1995).
42. Schrøder, T. B., Sastry, S., Dyre, J. C. & Glotzer, S. C. Crossover to potential energy landscape dominated dynamics in a model glass-forming liquid. *J. Chem. Phys.* **22**, 9834–9840 (2000).
43. Dyre, J. C. & Olsen, N. B. Landscape equivalent of the shoving model. *Phys. Rev. B* **69**, 042501 (2004).
44. O'Connell, P. A. & McKenna, G. B. Arrhenius-like temperature dependence of the segmental relaxation below T_g. *J. Chem. Phys.* **110**, 11054–11060 (1999).
45. Shi, X. F., Mandanici, A. & McKenna, G. B. Shear stress relaxation and physical aging study on simple glass-forming materials. *J. Chem. Phys.* **125**, 174507 (2005).
46. Simon, S. L., Sobieski, J. W. & Plazek, D. J. Volume and enthalpy recovery of polystyrene. *Polymer* **42**, 2555–2567 (2001).
47. Echeverria, I., Kolek, P. L., Plazek, D. J. & Simon, S. L. Enthalpy recovery, creep and creep-recovery measurements during physical aging of amorphous selenium. *J. Non-Cryst. Solids* **324**, 242–255 (2003).

Supplementary Information accompanies this paper on www.nature.com/naturephysics.

Acknowledgements

For kindly providing data to this study, we are indebted to S. Benkhof, T. Blochowicz, T. Christensen, L. F. del Castillo, R. Diaz-Calleja, L.-T. Duong, K. Duvvuri, G. Eska, C. Gainaru, A. Garcia-Bernabe, S. Hensel-Bielowka, W. Huang, N. Ito, B. Jakobsen, E. Kaminska, M. Koehler, A. Kudlik, A. Loidl, P. Lunkenheimer, D. V. Matyushov, M. Mierzwa, P. Medick, K. L. Ngai, K. Niss, V. N. Novikov, M. Paluch, S. Pawlus, L. C. Pardo, S. Putselyk, E. L. Quitevis, J. R. Rajian, R. Richert, A. Rivera, E. A. Rössler, M. J. Sanchis, N.V. Surovtsev, C. Tschirwitz, L.-M. Wang and J. Wiedersich. The centre for viscous liquid dynamics 'Glass and Time' is sponsored by the Danish National Research Foundation (DNRF).

Author contributions

Project planning and data analysis were carried out by T.H. and J.C.D., experimental work by A.I.N. and N.B.O.

Author information

Reprints and permission information is available online at http://npg.nature.com/reprintsandpermissions. Correspondence and requests for materials should be addressed to J.C.D.

Journal of Non-Crystalline Solids 355 (2009) 624–627

Contents lists available at ScienceDirect

Journal of Non-Crystalline Solids

journal homepage: www.elsevier.com/locate/jnoncrysol

A brief critique of the Adam–Gibbs entropy model

Jeppe C. Dyre *, Tina Hechsher, Kristine Niss

DNRF Centre 'Glass and Time,' IMFUFA (Building 27), Department of Sciences, Roskilde University, Postbox 260, DK-4000 Roskilde, Denmark

ARTICLE INFO

Article history:
Available online 10 April 2009

PACS:
64.70.Pf

Keywords:
Glass formation
Glass transition

ABSTRACT

This paper critically discusses the entropy model proposed by Adam and Gibbs in 1965 for the dramatic temperature dependence of glass-forming liquids' average relaxation time, which is one of the most influential models during the last four decades. We discuss the Adam–Gibbs model's theoretical bases as well as its reported experimental model confirmations; in the process of doing this a number of problems with the model are identified.

1. Introduction

Any liquid forms a glass when supercooled rapidly enough to avoid crystallization [1–15]. Glass formation is an example of the 'falling-out-of-equilibrium' that takes place for any system the relaxation time of which exceeds laboratory time scales [16]. This phenomenon does not in itself present subtle scientific questions, in our opinion, although there may well be interesting relaxations taking place at T_g affecting details of the glass structure [17]. The ultraviscous liquid in metastable equilibrium above T_g, on the other hand, does present fundamental scientific challenges. The two most important questions relating to the ultraviscous liquid phase preceding glass formation are: (1) What causes the non-exponential relaxations usually observed? (2) What causes the non-Arrhenius temperature dependence of the average (alpha) relaxation time τ? This paper addresses one of the classical answers to the latter question.

Most viscous liquids require temperature dependence of the activation energy $\Delta E = \Delta E(T)$ if the Arrhenius expression is accepted,

$$\tau(T) = \tau_0 \exp\left(\frac{\Delta E(T)}{k_B T}\right). \quad (1)$$

Molten pure silica and a few other liquids have almost temperature-independent activation energy, but for all other liquids the activation energy increases upon cooling. An unbiased measure of how fast the activation energy increases is the 'temperature index' defined [18] by $I = -d\ln\Delta E/d\ln T \geqslant 0$. The standard measure of the degree of non-Arrhenius behavior is Angell's fragility m defined by $m = d\log\tau/d(T_g/T)|_{T=T_g}$ [19–21], a quantity that however only refers to liquid properties right at T_g. If the glass transition temperature (by definition) is taken as the temperature where $\tau = 100$ s and $\tau_0 = 10^{-14}$ s, Arrhenius behavior corresponds to $m = 16$. In the index terminology Arrhenius behavior corresponds to $I = 0$. Generally, the following relation allows one to calculate the fragility from the index at T_g: $m = 16[1 + I(T_g)]$ [18].

In the broad research field 'viscous liquids and the glass transition' there is no general agreement about the origin of the non-Arrhenius behavior of viscous liquids. It may well be that no simple, universally valid model or theory exists, but many workers in the field including ourselves prefer to think that such a model exists. This is a reasonable assumption, because ultraviscous liquids approaching the glass transition have physical properties that do not depend on whether the liquid is bonded by covalent bonds, ionic bonds, van der Waals bonds, hydrogen bonds, or metallic bonds [1–15] (we prefer to exclude the often studied polymer glass transition because it is not a liquid–glass transition, but it is noteworthy that this transition has several properties in common with the liquid–glass transition).

Whenever an important scientific problem is unsolved, there is usually not one, but many models allegedly solving the problem. The non-Arrhenius behavior of glass-forming liquids is no exception. Classical phenomenological models relate the relaxation time to other macroscopic liquid properties, like the configurational entropy [22,23], the free volume [24–27], the energy [6,17,28–32], or the high-frequency elastic constants [33–37]. More recently, these were supplemented by models that have more fundamental basis like, e.g., the mode-coupling theory [13,38], the random-first-order-transition theory (RFOT) [39,40], energy-landscape based models [41–45], frustration-based approaches [46], the entropic barrier hopping theory [47], kinetically constrained models [48,49], etc.

* Corresponding author.
E-mail address: dyre@ruc.dk (J.C. Dyre).

0022-3093/$ - see front matter © 2009 Elsevier B.V. All rights reserved.
doi:10.1016/j.jnoncrysol.2009.01.039

This paper deals with one of the most popular classical models, the Adam–Gibbs entropy model [23]. We first briefly review the model and how it was traditionally supported by experiment (Section 2). In Section 3 critiques of the model are presented, relating to both the model's theoretical basis and its experimental validation. Many of these arguments have been made before, but we felt it would be useful to collect them into one paper. Section 4 concludes.

2. The Adam–Gibbs entropy model

2.1. Assumptions and model prediction

According to the Adam–Gibbs model the liquid's relaxation time is controlled by the configurational entropy $S_c(T)$. This quantity is defined by subtracting the vibrational entropy, $S_{vib}(T)$, from the entropy S: $S_c(T) = S(T) - S_{vib}(T)$. This separation of entropy into two contributions is much in the spirit of the energy landscape paradigm that was subsequently formulated by Goldstein [41] and Stillinger [50], where vibrations around a potential energy minimum (an inherent state) are occasionally interrupted by thermally activated transitions to another minimum.

The Adam–Gibbs model's activation energy obeys

$$\Delta E(T) \propto \frac{1}{S_c(T)}. \tag{2}$$

This is justified as follows. Any molecular rearrangement is a thermally activated transition that involves all molecules of a 'cooperatively rearranging region.' Such a region is defined as a 'subsystem of the sample which, upon a sufficient fluctuation in energy (or, more correctly, enthalpy), can rearrange into another configuration independently of its environment.' Three crucial ideas/assumptions go into the model: (1) The activation energy is proportional to region volume. This is justified by writing the change in Gibbs free energy upon activation as a chemical potential change $\Delta\mu$ times volume and assuming that 'in a good approximation the dependence of $\Delta\mu$ on temperature and region volume can be neglected.' (2) There is a lower limit to the size of a cooperatively rearranging region since it must have at least two configurations 'available to it, one in which the region resides before the transition and another one to which it may move.' (3) The cooperatively rearranging regions are 'independent and equivalent subsystems,' i.e., there are only insignificant interactions of any given region with its surroundings.

2.2. The model's attractive scenario

The Adam–Gibbs model connects two of the most fundamental concepts of physics: *Entropy* and *Time*. The model is aesthetically attractive by having this property – the only other *quantitative* connection of entropy and time that we can think of is that of black hole thermodynamics as theorized by Hawking and others (the fact that entropy cannot decrease for an isolated system is a *qualitative* entropy-time connection). The entropy model has the further beauty of connecting the observed dramatic slowing down to the Kauzmann paradox and the theory of phase transitions. Recall that the Kauzmann paradox is the observation that the supercooled liquid's excess entropy S_{exc} (the liquid entropy minus the crystal entropy at the same temperature) extrapolates to zero at a temperature T_K not far below T_g [3]. Unless something rather dramatic happens invalidating this extrapolation, the liquid's entropy would fall below the crystal's if the liquid could be equilibrated close to and below T_K. But if – as usually done – the excess entropy is identified with the configurational entropy (a point returned to below),

$$S_{exc}(T) \cong S_c(T), \tag{3}$$

the Adam–Gibbs (AG) model solves the Kauzmann paradox: By Eq. (2) the relaxation time diverges to infinity as the liquid is cooled towards T_K. This means that the liquid cannot equilibrate close to T_K, implying that the glass transition must take place above T_K, no matter how slowly the liquid is cooled.

Based on Eq. (3) the AG model presents a scenario that predicts an underlying phase transition to a state of zero configurational entropy and infinite relaxation time. Thus the model explains the dramatic relaxation-time increase as a consequence of the approach to a phase transition. The predicted slowing down extends over a broader temperature range and is much more dramatic than the usual critical slowing down for second order phase transitions where $\tau \propto |T - T_c|^{-x}$ [51], but the idea is the same. In this way, the paradigm of second order phase transitions comes into play for the glass transition problem.

The above explains the AG model's attraction in general, theoretical terms. Its main attraction, however, is probably the fact that it appears to explain experiments. We shall not detail the evidence for this here, but refer the reader to the several excellent reviews [8,10,11,52]. In many cases the experimental evidence for the AG model relates it to the Vogel–Fulcher–Tammann (VFT) empirical equation for the relaxation time:

$$\tau(T) = \tau_0 \exp\left(\frac{A}{T - T_0}\right). \tag{4}$$

Close to T_K the configurational entropy $S_c(T)$ may be expanded to first order: $S_c(T) \propto T - T_K$, implying that to lowest order the AG model predicts

$$T_K = T_0. \tag{5}$$

This prediction has been compared to experiment on many liquids. The general picture reported in numerous papers is that the AG model is obeyed for most, if not all systems studied [52,53]. These include chemically quite different systems with widely differing glass transition temperatures.

3. Critiques of the AG entropy model

3.1. Model assumptions

As mentioned, the three basic assumptions of the AG model are: (1) The activation energy is proportional to the region volume, $\Delta E(T) \propto V_{reg}(T)$. (2) A region must have at least two configurations, i.e., its configurational entropy is larger than $k_B \ln 2$; (3) The 'region assumption' that regions are *independent* and *equivalent* subsystems of the liquid. None of points (1)–(3) are compelling: Molecular rearrangements take place in almost perfect crystals via diffusing vacancies or interstitials, and in a plastic crystal, for instance, one might well have molecular reorientations happening without either Assumption (1) or (2) being obeyed. This is also an example where Assumption (3) breaks down. Even if Assumption (3) holds, however, it is not necessary that a region must have a minimum configurational entropy in order to allow for transitions; also for a low configurational entropy a region would have many states 'available to it' if differing energies are allowed for.

Assumption (1), which is responsible for the non-Arrhenius behavior and the relaxation time divergence as $T \to T_K$, was justified by the suggestion that the chemical potential difference between initial and transition state (barrier) is region-size independent. The question is how well defined a chemical potential difference is for this situation particularly in view of the small region sizes inferred from experiment that makes it difficult to justify ignoring the interactions with the surroundings, see below.

Finally, returning to the region Assumption (3) we note that it can only be justified if regions are very large. As an analogue, note that even for rather large 'regions,' nucleation theory must take into account interactions with the surrounding liquid in order to arrive at realistic predictions. It is not clear why the same should not be done in the Adam–Gibbs theory; indeed, this is done in the more sophisticated RFOT entropy model of Wolynes and coworkers [39,40].

Suppose that we nevertheless accept Assumptions (1)–(3) and go ahead by comparing to experiment. When this is done one typically arrives at regions containing 4–8 molecules [11,54] close to the glass transition. At higher temperatures regions must be even smaller, because it is the increasing regions size upon cooling that is responsible for the non-Arrhenius behavior. The small region sizes of experiment presents a serious challenge to the AG entropy model, because such small regions cannot reasonably be regarded as independent with region-region interactions that may be ignored; every molecule must interact with molecules of other regions as much as with the molecules within its region.

Suppose that one nevertheless accepts the AG idea that the configurational entropy controls the relaxation time's temperature dependence and also accepts Eq. (3) that allows for the entropy model to be tested in experiment. Then, as mentioned, the relaxation time becomes infinite at T_K where the equilibrium state of the liquid has zero configurational entropy – the 'ideal glass' state [55,56]. This state cannot be reached experimentally, of course, but one may still ask what is its nature. A state of zero entropy is unique like a perfect crystal, so one would expect that some simple description of it can be given. Except for the random close packing of hard spheres (the uniqueness of which is questioned), we are not aware of attempts to describe the ideal glassy state in structural terms. This does not rule out that such a description exists, but one would imagine it to be fairly simple (like a quasi-crystal) and thus to have been identified long ago.

3.2. The AG entropy model's experimental validation

Despite the above arguments, suppose that we accept the AG entropy model's prediction Eq. (2). Unfortunately, configurational entropy cannot be measured. For many years this problem was solved by arguing as follows: "The vibrational properties of glass and crystal are very similar, and very similar to the liquid's high-frequency vibrational properties (i.e., on time scales much shorter than those of the alpha (main) relaxation time). Since the crystalline state has practically zero configurational entropy, the crystal entropy provides a good estimate of the liquid's vibrational entropy. Thus by subtracting crystal entropy from liquid entropy one finds the liquid's configurational entropy (Eq. (3))".

There is now a growing recognition that the above reasoning is problematic [15,57–59]. Dating back to the 1950s, in fact, it was known from sound velocity measurements that the liquid's high-frequency sound velocity is generally much more temperature dependent than that of the crystal or glass phases [5,60,61]. It is easy to understand why this is so if one adopts the simple-minded assumption that the high-frequency sound velocity is a function of density: The thermal expansion coefficient is generally considerably larger in the liquid than in the solid phases (crystal or glass). In this simple approach, the vibrational entropy is a (logarithmic) function of the vibrational force constants that determine the high-frequency sound velocity, so the vibrational entropy is considerably more temperature dependent in the liquid than in the crystal. This severely weakens Eq. (3). An illustration of the problem with Eq. (3) is the fact that it is not generally true that a liquid must have larger entropy than the same temperature crystal: Both in the cases involving so-called inverse melting [62,63] and for the classical hard sphere system, the crystalline phase has larger entropy than the liquid.

Suppose that we nevertheless accept Eq. (3). Then at the Kauzmann temperature T_K there is a second order phase transition to the ideal glassy state – if the liquid has the infinite time needed to equilibrate. But T_K is identified by extrapolation, and one may well question how reliable the extrapolation is. This question arises, in particular, if one accepts that T_g is close to a genuine phase transition as predicted by the AG model. It seems quite possible that the liquid entropy may 'bend over' and stay above the crystalline entropy right down to zero temperature [64–66]. This would imply $T_K = 0$.

Suppose that we nevertheless accept that data conform to Eq. (5) – the intriguing connection of a purely dynamic temperature (T_0) with a purely thermodynamic one (T_K). Very recently the VFT equation's predicted divergence was questioned in a paper that compiled accurate data for the dielectric relaxation time's temperature dependence for 42 organic liquids [67]. The conclusion was that, while the VFT equation does work well as a mathematically simple representation of data, there is no evidence for any dynamic divergence; in other words, there is no evidence that T_0 exists [68].

Suppose that we nevertheless accept both the extrapolation usually carried out in order to identify T_K and the existence of the VFT T_0. Then a simple experimental test of the entropy model is the prediction Eq. (5). Numerous papers published the last 30 years have reported confirmation of Eq. (5); indeed this appears to be one of the strongest experimental arguments for the AG entropy model. In 2003, however, Tanaka compiled a large amount of data and concluded that Eq. (5) is disobeyed [69].

4. Concluding remarks

The classical Adam–Gibbs scenario presents several challenges. Thus if entropy is the variable controlling the relaxation time, it seems that more advanced approaches are needed. There are, however, alternatives like the elastic models that date back to the 1940s [15]. According to the shoving model [15,33], one of the elastic models, the activation energy is proportional to the instantaneous shear modulus G_∞. This quantity is quite temperature dependent in viscous liquids, in fact precisely enough to explain the non-Arrhenius behavior [70]. Since G_∞ cannot diverge, there is no underlying phase transition, so the elastic model scenario differs qualitatively from that of the AG entropy model.

References

[1] G. Tammann, J. Soc. Glass Technol. 9 (1925) 166.
[2] F. Simon, Z. Anorg. Allg. Chem. 203 (1931) 219.
[3] W. Kauzmann, Chem. Rev. 43 (1948) 219.
[4] G.P. Johari, J. Chem. Educ. 51 (1974) 23.
[5] G. Harrison, The Dynamic Properties of Supercooled Liquids, Academic, New York, 1976.
[6] S. Brawer, Relaxation in Viscous Liquids and Glasses, American Ceramic Society, Columbus, Ohio, 1985.
[7] G.W. Scherer, Relaxation in Glass and Composites, Wiley, New York, 1986.
[8] C.A. Angell, J. Non-Cryst. Solids 131 (1991) 13.
[9] P.G. Debenedetti, Metastable Liquids: Concepts and Principles, Princeton University Press, Princeton, 1996.
[10] C.A. Angell, K.L. Ngai, G.B. McKenna, P.F. McMillan, S.W. Martin, J. Appl. Phys. 88 (2000) 3113.
[11] C. Alba-Simionesco, C. R. Acad. Sci. Paris (Ser. IV) 2 (2001) 203.
[12] E. Donth, The Glass Transition, Springer, Berlin, 2001.
[13] S.P. Das, Rev. Mod. Phys. 76 (2004) 785.
[14] K. Binder, W. Kob, Glassy Materials and Disordered Solids: An Introduction to their Statistical Mechanics, World Scientific, Singapore, 2005.
[15] J.C. Dyre, Rev. Mod. Phys. 78 (2006) 953.
[16] J.C. Dyre, Phys. Today (January) (2008) 15.
[17] J.C. Dyre, Phys. Rev. Lett. 58 (1987) 792.
[18] J.C. Dyre, N.B. Olsen, Phys. Rev. E 69 (2004) 042501.
[19] D.J. Plazek, K.L. Ngai, Macromolecules 24 (1991) 1222.

[20] R. Böhmer, K.L. Ngai, C.A. Angell, D.J. Plazek, J. Chem. Phys. 99 (1993) 4201.
[21] G. Ruocco, F. Sciortino, F. Zamponi, C. De Michele, T. Scopigno, J. Chem. Phys. 120 (2004) 10666.
[22] J.H. Gibbs, E.A. DiMarzio, J. Chem. Phys. 28 (1958) 373.
[23] G. Adam, J.H. Gibbs, J. Chem. Phys. 43 (1965) 139.
[24] A.K. Doolittle, J. Appl. Phys. 22 (1951) 1471.
[25] M.H. Cohen, D. Turnbull, J. Chem. Phys. 31 (1959) 1164.
[26] A.J. Kovacs, Fortsch. Hochpolym.-Forsch. 3 (1963) 394.
[27] G.S. Grest, M.H. Cohen, in: I. Prigogine, S.A. Rice (Eds.), Advances in Chemical Physics, vol. 48, Wiley, New York, 1981, p. 455.
[28] M. Goldstein, Faraday Symp. Chem. Soc. 6 (1972) 7.
[29] S.V. Nemilov, Sov. J. Glass Phys. Chem. 4 (1978) 113.
[30] J.P. Bouchaud, J. Phys. I 2 (1992) 1705.
[31] J.C. Dyre, Phys. Rev. B 51 (1995) 12276.
[32] G. Diezemann, J. Chem. Phys. 107 (1997) 10112.
[33] J.C. Dyre, N.B. Olsen, T. Christensen, Phys. Rev. B 53 (1996) 2171.
[34] A. Tobolsky, R.E. Powell, H. Eyring, in: R.E. Burk, O. Grummit (Eds.), Frontiers in Chemistry, vol. 1, Interscience, New York, 1943, p. 125.
[35] M. Mooney, Trans. Soc. Rheol. 1 (1957) 63.
[36] F. Bueche, J. Chem. Phys. 30 (1959) 748.
[37] S.V. Nemilov, Russ. J. Phys. Chem. 42 (1968) 726.
[38] W. Götze, L. Sjögren, Rep. Prog. Phys. 55 (1992) 241.
[39] J.P. Bouchaud, G. Biroli, J. Chem. Phys. 121 (2004) 7347.
[40] V. Lubchenko, P.G. Wolynes, Ann. Rev. Phys. Chem. 58 (2007) 235.
[41] M. Goldstein, J. Chem. Phys. 51 (1969) 3728.
[42] F.H. Stillinger, Science 267 (1995) 1935.
[43] P.G. Debenedetti, F.H. Stillinger, Nature 410 (2001) 259.
[44] D.J. Wales, Energy Landscapes, Cambridge University Press, Cambridge, 2003.
[45] F. Sciortino, J. Stat. Mech., Art. No. P05015 (2005).
[46] G. Tarjus, S.A. Kivelson, Z. Nussinov, P. Viot, J. Phys.: Condens. Matter 17 (2005) R1143.
[47] K.S. Schweizer, E.J. Saltzman, J. Phys. Chem. B 108 (2004) 19729.
[48] G.H. Fredrickson, Ann. Rev. Phys. Chem. 39 (1988) 149.
[49] J.P. Garrahan, D. Chandler, Proc. Natl. Acad. Sci. 100 (2003) 9710.
[50] F.H. Stillinger, T.A. Weber, Phys. Rev. A 28 (1983) 2408.
[51] N. Goldenfeld, Lectures on Phase Transitions and the Renormalization Group, Addison-Wesley, Reading, MA, 1992.
[52] G.B. McKenna, S.C. Glotzer (Eds.), Proceedings of the Conference 40 Years of Entropy and the Glass Transition on J. Res. Natl. Inst. Stand. Technol., 102 (2), (March–April, 1997) (Several excellent papers on the entropy model are found in the proceedings).
[53] P. Richet, Geochim. Cosmochim. Acta 48 (1984) 471.
[54] O. Yamamuro, I. Tsukushi, A. Lindqvist, S. Takahara, M. Ishikawa, T. Matsuo, J. Phys. Chem. B 102 (1998) 1605.
[55] C.A. Angell, J. Am. Ceram. Soc. 51 (1968) 117.
[56] G.N. Greaves, S. Sen, Adv. Phys. 56 (2007) 1.
[57] M. Goldstein, J. Chem. Phys. 64 (1976) 4767.
[58] L.-M. Martinez, C.A. Angell, Nature 410 (2001) 663.
[59] G.P. Johari, J. Chem. Phys. 116 (2002) 2043.
[60] T.A. Litovitz, J. Acoust. Soc. Am. 31 (1959) 681.
[61] A.F.M. Barton, Adv. Mol. Relax. Process. 4 (1972) 87.
[62] K. Mortensen, W. Brown, B. Nordén, Phys. Rev. Lett. 68 (1992) 2340.
[63] F.H. Stillinger, P.G. Debenedetti, Biophys. Chem. 105 (2003) 211.
[64] P.D. Gujrati, M. Goldstein, J. Chem. Phys. 74 (1981) 2596.
[65] F.H. Stillinger, P.G. Debenedetti, T.M. Truskett, J. Phys. Chem. B 105 (2001) 11809.
[66] J.P. Eckmann, I. Procaccia, Phys. Rev. E 78 (2008) 011503.
[67] T. Hecksher, A.I. Nielsen, N.B. Olsen, J.C. Dyre, Nat. Phys. 4 (2008) 737.
[68] S.L. Simon, J.W. Sobieski, D.J. Plazek, Polymer 42 (2001) 2555.
[69] H. Tanaka, Phys. Rev. Lett. 90 (2003) 055701 .
[70] D.H. Torchinsky, J.A. Johnson, K.A. Nelson, J. Chem. Phys. 130 (2009) 064502.

THE JOURNAL OF CHEMICAL PHYSICS **133**, 174514 (2010)

Physical aging of molecular glasses studied by a device allowing for rapid thermal equilibration

Tina Hecksher,[a] Niels Boye Olsen,[b] Kristine Niss,[c] and Jeppe C. Dyre[d]
Department of Sciences, DNRF Centre "Glass and Time," IMFUFA, Roskilde University, P.O. Box 260, DK-4000 Roskilde, Denmark

(Received 9 June 2010; accepted 14 August 2010; published online 5 November 2010)

Aging to the equilibrium liquid state of organic glasses is studied. The glasses were prepared by cooling the liquid to temperatures just below the glass transition. Aging following a temperature jump was studied by measuring the dielectric loss at a fixed frequency using a microregulator in which temperature is controlled by means of a Peltier element. Compared to conventional equipment, the new device adds almost two orders of magnitude to the span of observable aging times. Data for the following five glass-forming liquids are presented: dibutyl phthalate, diethyl phthalate, 2,3-epoxy propyl-phenyl-ether, 5-polyphenyl-ether, and triphenyl phosphite. The aging data were analyzed using the Tool–Narayanaswamy formalism. The following features are found for all five liquids: (1) The liquid has an "internal clock," a fact that is established by showing that aging is controlled by the same material time that controls the dielectric properties. (2) There are no so-called expansion gaps between the long-time limits of the relaxation rates following up and down jumps to the same temperature. (3) At long times, the structural relaxation appears to follow a simple exponential decay. (4) For small temperature steps, the rate of the long-time exponential structural relaxation is identical to that of the long-time decay of the dipole autocorrelation function. © *2010 American Institute of Physics*. [doi:10.1063/1.3487646]

I. INTRODUCTION

The change of materials properties over time is referred to as aging. Aging phenomena often involve chemical degradation, but there are also several instances of purely physical property changes. Understanding physical aging is important for many materials applications. Moreover, physical aging presents fundamental scientific challenges and provides valuable insight into materials properties. This paper shows that by utilizing the Peltier thermoelectric effect, physical aging may be studied at considerably shorter times than has so far been possible. The new setup adds almost two decades to the span of aging times compared to what may be obtained by conventional equipment in the same observation time.

A prime example of aging is that of a viscous liquid's physical properties relaxing slowly towards equilibrium when a perturbation is applied to the equilibrated liquid close to its glass transition. In equilibrium, a liquid's properties do not change with time, of course (the fact that the liquids studied below are supercooled and thus technically only in quasiequilibrium is not important because no crystallization was observed). If the temperature is changed, properties gradually adjust themselves to new equilibrium values. If the temperature is lowered, a glass is produced; recall that by definition, a glass is nothing but a highly viscous liquid that has not yet had time to equilibrate.[1–6] Any glass ages toward the equilibrium liquid state. This state can only be reached on laboratory time scales, however, if the glass is kept just below the glass transition temperature; contrary to popular myth, windows do not flow observably.

Aging is a nonlinear phenomenon. This is because the aging rate is structure dependent and itself evolves with time when the structure changes as equilibrium is gradually approached.[7–16] Thus, aging studies provide information beyond that obtained by linear-response experiments such as, e.g., dielectric relaxation measurements. There are good reasons to believe that on the microscopic level, aging is heterogeneous;[17–19] the below analysis is, however, entirely macroscopic and does not discuss possible microscopic interpretations of the observed aging phenomena (see, e.g., Refs. 20 and 21).

A typical aging experiment consists of a temperature step, i.e., a rapid decrease or increase of temperature to a new, constant value. Ideally, such a temperature step should be instantaneous; more precisely, the new temperature should be established as constant in time and homogeneous throughout the sample before any structural relaxation has taken place. If this is achieved and if sufficient time is available, it is possible to monitor the complete relaxation to equilibrium of the physical property being probed. An experimental protocol that measures the complete relaxation curve will be referred to as an "ideal aging experiment."[22]

What are the requirements for an ideal aging experiment? First, there should be good temperature control and the setup should allow for rapid thermal equilibration following a temperature jump. Second, a physical observable is needed that may be monitored quickly and accurately and

[a]Electronic mail: tihe@ruc.dk.
[b]Electronic mail: nbo@ruc.dk.
[c]Electronic mail: kniss@ruc.dk.
[d]Electronic mail: dyre@ruc.dk.

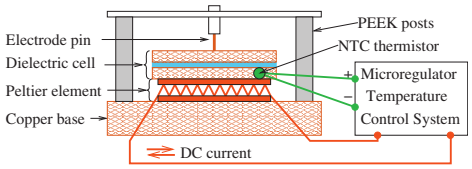

FIG. 1. Schematic drawing of the dielectric measuring cell with the microregulator. The liquid is deposited in the (50 μm) gap between the disks of the dielectric cell. The Peltier element heats or cools the dielectric cell, depending on the direction of the electrical current powering the element. The current is controlled by an analog temperature-control system that receives temperature feedback information from an NTC thermistor embedded in one disk of the dielectric cell. A stainless steel electrode pin keeps the cell pressed against the Peltier element and provides electrical connection to one of the disks. The dielectric measuring cell is placed in the main cryostat. Details of the setup are described in Refs. 23 and 24.

which, preferably, changes significantly even for small temperature changes. The latter property allows for studying aging following temperature jumps that are of order just 1% in absolute units, which is enough for most ultraviscous liquids to become highly nonlinear. The organic liquids studied in this paper have glass transition temperatures in the region 170–200 K and most temperature jumps are 1 or 2 K jumps.

In current state-of-the-art aging experiments, the characteristic thermal equilibration time τ is at least 100 s if τ is defined from the long-time thermal-diffusion-limited approach to equilibrium $\sim\exp(-t/\tau)$. This reflects the fact that heat conduction is a notoriously slow process. Experience shows that in order to monitor an almost complete aging curve, at least four decades of time must be covered; for instance, the typical aging function $\exp(-K\sqrt{t})$ decays from 97% to 3% over four decades of time. Thus with present methods, one needs at least of order 100 s $\times 10^4 = 10^6$ s for an almost ideal temperature down-jump experiment. This is more than a week. Clearly, much is to be gained if it were possible to equilibrate sample temperatures faster.

In order to make possible faster temperature-jump experiments, we designed a dielectric cell based on a Peltier thermoelectric element by means of which the heat flow is controlled via electrical currents (Fig. 1).[23] The characteristic thermal equilibration time of the microregulator is 2 s. This is almost a factor of a hundred times faster than that of conventional equipment, which usually involves much larger heat diffusion lengths; our liquid layer is 50 μm thick and the use of a Peltier element minimizes heat diffusion lengths outside of the liquid layer. In the microregulator, the temperature may be kept constant over weeks, keeping fluctuations below 100 μK.[23,24]

For monitoring aging we chose to measure the dielectric loss (the negative imaginary part of the dielectric constant) at a fixed frequency. With modern equipment, this quantity may be measured quickly and accurately; our electronics setup is detailed in Ref. 24. Moreover, for a viscous liquid of molecules with a permanent dipole moment, a frequency range exists in which the dielectric loss changes considerably for small temperature variations. The dielectric loss was used previously for monitoring aging by several groups, e.g., by Johari,[25] Schlosser and Schönhals,[26] Alegria *et al.*,[27–29] Leheny *et al.*,[30,31] Cangialosi *et al.*,[32] Lunkenheimer *et al.*,[33–35] D'Angelo *et al.*,[36] and Serghei and Kremer.[37]

This paper presents ideal aging experiments on five organic liquids with both temperature up and down jumps (Sec. II). As mentioned, the temperature jumps are of order 1% and, aging is monitored by measuring the dielectric loss at a fixed frequency in the hertz range. In Sec. III we give a mathematical formulation of the reduced time concept. This is sometimes referred to as the material time or, perhaps more intuitively appealing, the time measured on an "internal" clock, i.e., a clock with clock rate varying with temperature and with the annealing state of the sample. We here follow Narayanaswamy's[38] seminal paper from 1971 and go into some detail in order to make the text easier to read for nonexperts in aging. In Sec. IV a new test of the existence of an internal clock is proposed. In contrast to most earlier works, this test makes no assumptions regarding which quantity controls the internal clock's rate or the mathematical form of the relaxation function. This section demonstrates that all five liquids have internal clocks. Section V extends the data analysis in order to study whether the long-time relaxation is stretched or simple exponential. Section VI shows that within the experimental uncertainties, the long-time simple exponential structural relaxation has the same rate as the long-time exponential decay of the dipole autocorrelation function. Finally, Sec. VII gives a summary and a few concluding remarks. A discussion of noise and systematic errors in the data analysis is given in the Appendix.

II. EXPERIMENTAL RESULTS AND INITIAL DATA ANALYSIS

The experimental setup is detailed in Refs. 23 and 24, which describe the microregulator, the surrounding cryostat, and the electronics used for measuring the frequency-dependent dielectric response. We studied aging of the following five organic liquids: dibutyl phthalate ("DBP"), diethyl phthalate ("DEP"), 2,3-epoxy propyl-phenyl-ether ("2,3-epoxy"), 5-polyphenyl-ether ("5-PPE"), and triphenyl phosphite ("TPP"). These liquids are all excellent glass formers. In order to ensure complete equilibrium before each measurement, the sample was kept at the temperature in question until there were no detectable changes of the dielectric properties.

Aging was studied by monitoring how the dielectric loss at a fixed frequency $\varepsilon''(f)$ develops as a function of time following a temperature jump. In order to avoid the liquid aging significantly during the measurement of a single frequency response data point, the monitoring frequency f must be considerably higher than the inverse structural relaxation time, which is of order of the inverse main (alpha) loss-peak frequency; thus the monitoring frequency must be much larger than the loss-peak frequency. For the data analysis of Secs. III and IV to apply, however, f must also be sufficiently below any contribution(s) from potential beta processes. These constraints vary with the liquid and the selected temperature range, and the choice of f was optimized for each liquid. For all five liquids the optimal f is in the Hertz range.

Measurements consist of consecutive temperature jumps

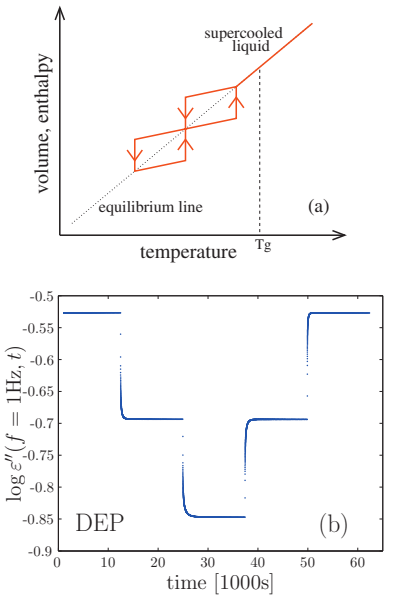

FIG. 2. A typical measurement. (a) Schematic representation of the protocol in which the sample is first aged to complete equilibrium at a temperature slightly below the calorimetric glass transition temperature T_g, a process that typically takes weeks, followed by two down temperature jumps and two up temperature jumps. (b) Data from measurements for DEP following this protocol, jumping from 184 to 183 K, further to 182 K, back to 183 K, and finally to 184 K. The dielectric loss ε'' was measured as a function of time at the frequency $f=1$ Hz. The duration of the measurement depends on the temperature range, i.e., how long it takes to equilibrate the sample fully after a temperature jump. Following this procedure, we know the relaxation functions as well as the equilibrium values of the dielectric losses at the temperatures in question. Throughout this paper log refers to the logarithm with base 10.

of (usually) 1 or 2 K, in most cases with two down/up jumps followed by two up/down jumps. This is illustrated in Fig. 2, which in Fig. 2(b) shows the raw data obtained for DEP. Here $f=1$ Hz and the temperature jumps are 1 K. The temperature protocol ensures that data are obtained for one up and one down jump to the same temperature. The duration of each measurement varies with the relaxation time of the liquid in question at the measured temperatures. A time-consuming part of the experiment is the initial aging to complete equilibrium at the target temperature just below the calorimetric glass transition temperature, which in most cases required weeks of annealing. In all cases, care was taken to ensure that the loss at one temperature was monitored until the sample had reached equilibrium; only thereafter was temperature changed to a new value. The Appendix discusses possible sources of errors in the experiments.

Figures 3(a)–3(f) show the data on which the paper is based. Two data sets were included for DBP, with aging monitored at different frequencies. Note that aging for down jumps to a given temperature is faster than for an up jump to the same temperature [compare, e.g., the two jumps to 200 K in Fig. 3(f)]. This is the so-called fictive-temperature effect described already by Tool[39] in the 1940s, an effect which comes from the fact that the relaxation rate is structure dependent and itself evolves with time: A down jump is "autoretarded"[8] because as the structure ages, the aging rate decreases. In contrast, an up jump is "autoaccelerated" because as the structure ages, the aging rate increases.[8] These are nonlinear effects that are characteristic for structural relaxation of single-component systems (but not, e.g., for aging involving composition fluctuations in binary systems). The fictive-temperature effect is clearly visible in Fig. 3, which shows that even relatively small temperature jumps are highly nonlinear, reflecting the fact that the equilibrium relaxation time is strongly temperature dependent for glass-forming liquids.

For any experiment monitoring the relaxation of some quantity toward its equilibrium value, the normalized relaxation function $R(t)$ is defined by subtracting the long-time (equilibrium) limit of the quantity in question and subsequently normalizing by the overall relaxation strength.[12,38] In the DEP case, for instance, for which the quantity monitored is $\log \varepsilon''(f=1\ \text{Hz})$, for a temperature jump from T_1 to T_2 starting from equilibrium the normalized relaxation function is given by

$$R(t) = \frac{\log \varepsilon''(1\ \text{Hz}, T_2, t) - \log \varepsilon''(1\ \text{Hz}, T_2, t \to \infty)}{\log \varepsilon''(1\ \text{Hz}, T_1, t=0) - \log \varepsilon''(1\ \text{Hz}, T_2, t \to \infty)}. \quad (1)$$

The Kovacs–McKenna (KM) relaxation rate $\Gamma(t)$ is defined[8,13] by

$$\Gamma(t) \equiv -\frac{d \ln R}{dt} = -\frac{1}{R}\frac{dR}{dt}. \quad (2)$$

The KM relaxation rate gives the relative change of the relaxation function with time and has the convenient property of being independent of the normalization. For a simple exponential relaxation function $R(t)=\exp(-t/\tau)$, the KM relaxation rate is constant: $\Gamma(t)=1/\tau$. In general, the KM relaxation rate changes with time. For both for temperature up and down jumps, we found that $\Gamma(t)$ decreases with time (for large up jumps this does not have to be the case). A popular analytical fitting function is the stretched exponential $R(t)=\exp[-(t/\tau)^{\beta}]$ $(0<\beta<1)$; this function has $\Gamma(t)=(\beta/\tau)\times(t/\tau)^{\beta-1}$ that decreases monotonically to zero as $t\to\infty$.

Taking DBP as an example, Fig. 4(a) shows as functions of time the normalized relaxation functions for all six temperature jumps of Figs. 3(a) and 3(b). Figure 4(b) shows the corresponding KM relaxation rates. At long times there is considerable noise in the KM rate because this quantity is difficult to determine by numerical differentiation when the noise becomes comparable to $R(t)$.[41] In order to eliminate unreliable long-time $\Gamma(t)$ data points, we introduced a cutoff at 0.5% from equilibrium for all data sets. Despite the long-time noise, it is clear that for up and down jumps ending at the same temperature (175, 176, or 177 K), the KM relaxation rates eventually approach the same number. This shows that there is no so-called expansion gap as Kovacs[8] proposed in 1963 based on experiments monitoring relaxation by measuring volume changes. Figure 4(c) gives a parametrized plot of $(R(t), \log(\Gamma(t)))$ which, except for the normalization of R introduced here, was the data representation originally used by Kovacs.[8] Again, it is clear that up and down jumps to the same temperature approach the same KM relaxation rate at

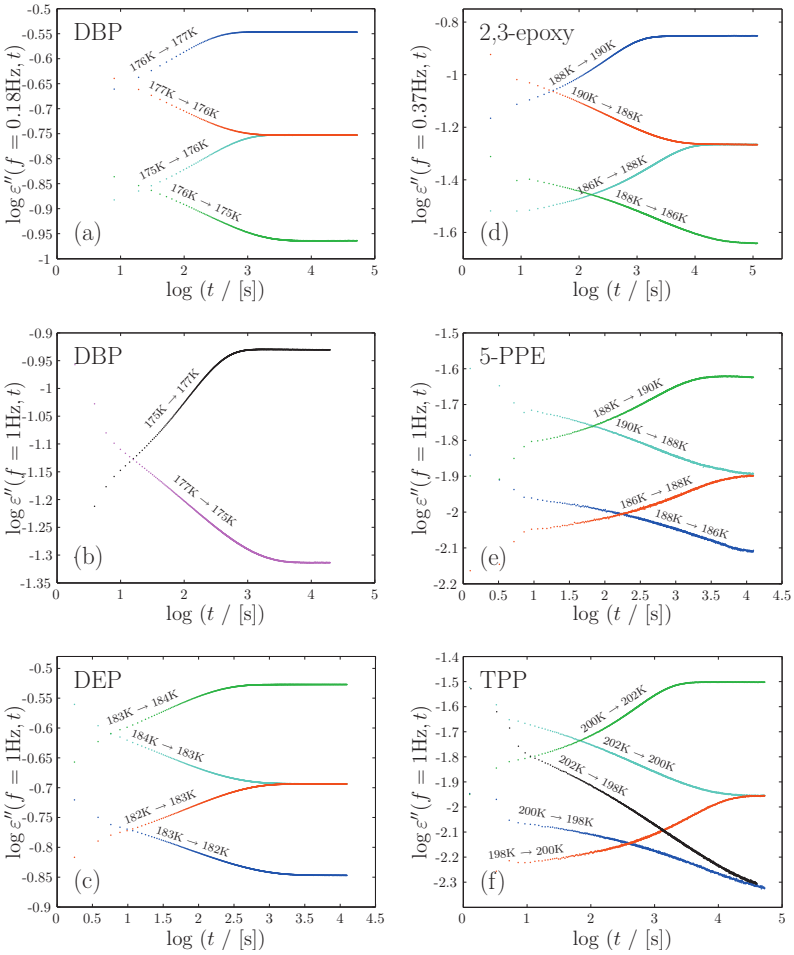

FIG. 3. Monitoring aging by measuring the dielectric loss at a fixed frequency. This figure presents the full set of data on which the paper's analysis is based (Ref. 40). The data are given in log-log (base 10) plots showing the dielectric loss as a function of time. In all cases, the starting situation ("$t=0$") is that of thermal equilibrium, a condition that is ensured by annealing for such a long time that no observable change is seen in the dielectric loss. (a) DBP. A series of measurements at $f=0.18$ Hz, stepping 1 K from 177 K and 175 K to 176 K, as well as the reverse. (b) DBP stepping from 175 to 177 K and back, this time monitored at $f=1$ Hz. (c) DEP ($f=1$ Hz). (d) 2,3-epoxy ($f=1$ Hz). (e) 5-PPE ($f=1$ Hz). (f) TPP ($f=1$ Hz).

long times ($R\rightarrow 0$). The existence of an expansion gap has been a matter of debate.[41–44] Kolla and Simon[22] recently concluded, however, that there is no expansion gap for $t\rightarrow\infty$; they attributed the reported expansion gap to the fact that Kovacs was unable to examine departures from equilibrium that were small enough to show the convergence of time scales. Our findings confirm this.

III. THE INTERNAL CLOCK HYPOTHESIS

For interpreting the data we use the Tool–Narayanaswamy (TN) formalism, which dates back to Tool's works in the 1940s and matured with Narayanaswamy's seminal paper from 1971.[12,38,39,45] The TN formalism interprets aging in terms of a so-called material time. The main feature of the TN formalism is that it describes aging in terms of a linear convolution integral, even when the aging is highly nonlinear. The formalism generally works well, although from a fundamental point of view it is still somewhat of a mystery why this is.

Lunkenheimer and co-workers[33–35] recently studied aging also by monitoring the dielectric loss. They found that the relaxation curves $R(t)$ to a good approximation may be described by a stretched-exponential relaxation function which, as a new feature, introduces a time-dependent characteristic time $\tau(t)$: $R(t)=\exp[-(t/\tau(t))^{\beta}]$. Interestingly, the nonlinear stretching exponent β was found to be identical to that derived from the linear dielectric relaxation function. This is a novel approach to aging studies. However, it does not lend any obvious physical interpretation to $\tau(t)$, which has the appearance of an averaged relaxation time representing the entire aging process until time t.

The TN approach's material time may be thought of as time measured on a clock with rate changing as sample properties evolve with time. The material time is analogous to the proper time concept of relativity theory, the reading on a clock following a (possibly accelerated) observer's world line; from an inertial system one would say that the clock rate varies with the observer's velocity, but the moving observer would dispute this. The existence of a material time is an old idea that predates Narayanaswamy; thus the well-known time-temperature superposition concept may be regarded as a "linear" internal clock hypothesis. Narayanaswamy's brilliant insight was to generalize this to describe aging, which is a highly nonlinear phenomenon.

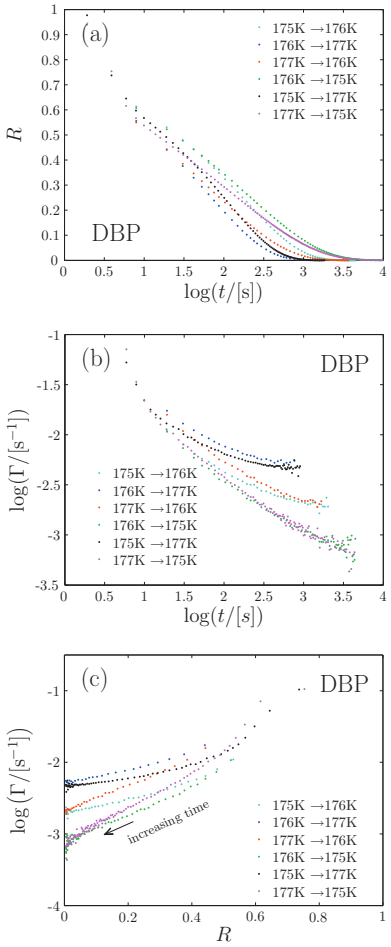

FIG. 4. (a) Normalized relaxation functions for DBP as functions of log (time). (b) The KM relaxation rates Γ defined in Eq. (2) for these data, as functions of log(time). Up and down jumps ending at 176 K give the same relaxation rate at long times, showing that there is no so-called expansion gap as proposed by Kovacs in 1963 (Ref. 8). (c) Parametrized plot of $(R(t),\Gamma(t))$. Again, it is seen that different temperature jumps to the same temperature approach the same relaxation rate at long times (small R).

The material time, which will be denoted by $\tilde{t}$, is time measured using a unit that itself evolves with time. If the structural clock rate is denoted by $\gamma_s(t)$, the material time $\tilde{t}$ is defined[12,22,38,39,41–45] by

$$d\tilde{t} = \gamma_s(t)dt. \tag{3}$$

This means that

$$\tilde{t}(t) = \int_{-\infty}^{t} \gamma_s(t)dt, \tag{4}$$

where the lower bound is, of course, arbitrary. The TN formalism is standard for interpreting aging experiments and used routinely in industry for predicting aging effects.[46–48] Nevertheless, it is not known whether—and in which sense—the internal clock exists, or if it should merely be regarded as a convenient mathematical construction.

According to the TN formalism, for all temperature jumps applied to a given system in equilibrium—small or large, up or down—the normalized relaxation function is a unique function of the material time that has passed since the jump was initiated at $\tilde{t}=0$: $R=R(\tilde{t})$. In applications of the TN formalism, one often allows for different material times to control the aging of different quantities (with also the function $R(\tilde{t})$ varying with which quantity that is being monitored). But if an internal clock *really* exists, a common material time must control all relaxations. In particular, the relaxation of the clock-rate activation energy itself during aging must be controlled by the same material time that controls the dielectric aging process (details are given below). A major point of this paper is to check against experiments the consequences of assuming that an internal clock exists. The next subsections develop a theory for testing this.

Determining the structural clock rate $\gamma_s(t)$ in the TN formalisms usually involves some mathematical modeling, fitting of data, or assumption regarding what controls the relaxation.[9,12,38,49] In Sec. IV we develop a test of the internal clock hypothesis which does not require such procedures, but proceeds directly from data without explicitly determining $\tilde{t}(t)$. First, however, it is necessary to define precisely both the dielectric relaxation rate in an out-of-equilibrium situation and the structural relaxation clock rate.

A. Defining the dielectric relaxation rate for out-of-equilibrium situations

The five liquids studied all obey time-temperature superposition (TTS) for their main (alpha) process to a good approximation. Moreover, they all have a high-frequency decay of the loss that to a good approximation may be described by a power-law $\varepsilon''(f) \propto f^{-\beta}$, where β is close to 1/2. It was conjectured some time ago that a high-frequency exponent of $-1/2$ reflects the generic properties of the pure alpha process obeying TTS (i.e., whenever the influence of additional relaxation processes is negligible),[50] a conjecture that was strengthened by a recent study involving more than 300 dielectric spectra.[51] For the data analysis below, the exponent β was identified as the minimum slope[51] of the log-log plotted dielectric loss curve above the loss peak, evaluated at the temperature where the loss peak is 0.1 Hz (Fig. 5). The β values thus obtained are listed in Table I.

The inverse power-law high-frequency dielectric loss, compare Fig. 6(a), is used to monitor the dielectric relaxation rate $\gamma_d(t)$ as the structure ages following a temperature jumps. This is done by proceeding as follows. First, we define the dielectric relaxation rate for the equilibrium liquid γ_d as the dielectric loss-peak angular frequency

$$\gamma_d \equiv 2\pi f_m, \tag{5}$$

where f_m is the loss-peak frequency. If the temperature is lowered in a step experiment, the dielectric loss curve gradually moves to lower frequencies as the system ages and relaxes to equilibrium. How to define a dielectric relaxation rate γ_d for this out-of-equilibrium situation? It is not possible to continuously monitor the entire loss curve. This is because the aging takes place on the same time scale as that of the

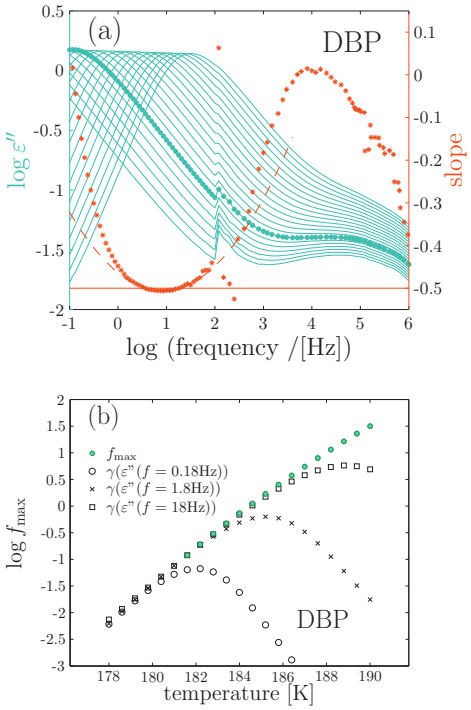

FIG. 5. (a) Illustration of the procedure used to determine the inverse power-law exponent β, which is identified as the minimum slope of the dielectric loss curve in a log-log plot at the temperature where the loss-peak frequency is 0.1 Hz (blue dotted curve). The red data points give the numerical slopes of this curve and the red dashed curve is a parabola fitted to the bottom points of the slope; the analytic minimum of the parabola determines the minimum slope (Ref. 51). (b) The loss-peak frequencies determined from the equilibrium spectra (green) and the predicted peak positions using Eq. (7) (corresponding to γ_d) at different measuring frequencies. The curves line up at low temperatures, showing that this procedure determines the correct loss-peak frequency.

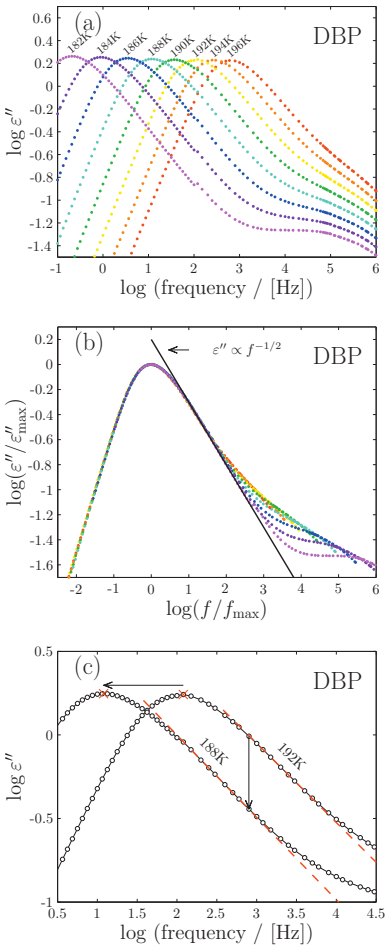

FIG. 6. (a) Dielectric loss spectra for DBP above T_g (i.e., equilibrium data). (b) TTS plot of the same spectra illustrating that the high-frequency wing of the alpha (main) process approaches a slope of $-1/2$ as the temperature is lowered (Refs. 50 and 51). All five liquids have high-frequency slopes close to $-1/2$, but this fact is not important for the analysis. (c) Illustration of how one utilizes the fact that the loss varies as $f^{-\beta}$ at high frequencies to measure the dielectric loss-peak frequency that by definition gives the dielectric clock rate during aging [Eq. (7)].

dielectric loss, implying that linear-response measurements around the loss-peak frequency are not well defined (i.e., a harmonic input does not result in a harmonic output). To circumvent this problem, the intuitive idea is that how much the dielectric relaxation rate has changed may be determined from how much the loss has changed at some fixed frequency in the high-frequency power-law region [Fig. 6(c)]. Mathematically, this corresponds to defining $\gamma_d(t)$ from the high-frequency equilibrium expression as follows:

$$\varepsilon''(f,t) \propto (f/\gamma_d(t))^{-\beta}. \tag{6}$$

Thus by probing the dielectric loss at the fixed frequency f, the dielectric relaxation rate may be determined during aging from

$$\log \gamma_d(t) = \frac{1}{\beta}\log \varepsilon''(f,t) + A. \tag{7}$$

The calibration constant A is found by using equilibrium data from higher temperatures where the loss peak is within the observable frequency range.

It should be emphasized that it is not a new idea to monitor aging by measurements at a frequency much larger than the reciprocal structural relaxation time; for instance, Struik[11] long ago discussed the proper protocols for doing this.

Although the above ideas seem straightforward, from a fundamental point of view one may question the validity of the concept of a dielectric relaxation rate in a situation where the structure ages on the same time scale as the dipoles relax. In order to specify the precise assumptions needed to justify

TABLE I. The high-frequency slopes β used in the data analysis.

	DBP	DEP	2,3-epoxy	5-PPE	TPP
β	0.506	0.483	0.550	0.507	0.495

defining $\gamma_d(t)$ via Eq. (7), we reason as follows. According to linear-response theory, for a system in thermal equilibrium the measured output is calculated from a convolution integral involving the input before the measuring time. A convenient way to summarize TTS for the equilibrium liquid is to formulate the convolution integral in terms of a dielectric "material" time $\tilde{t}$: If γ_d is the equilibrium liquid's dielectric relaxation rate [Eq. (5)], the dielectric material time is defined from the actual time t by

$$\tilde{t} = \gamma_d t. \tag{8}$$

In terms of $\tilde{t}$, since in a standard dielectric experiment the input variable is the electric field **E** and the output is the displacement vector **D**, the convolution integral is of the form

$$\mathbf{D}(\tilde{t}) = \int_0^\infty \mathbf{E}(\tilde{t}-\tilde{t}')\psi(\tilde{t}')d\tilde{t}'. \tag{9}$$

Equation (9) describes TTS because it implies that except for an overall time/frequency scaling, the same frequency-dependent dielectric constant is observed at different temperatures (we ignore the temperature dependence of the overall loss, an approximation which introduces a relative error into the data treatment well below 1% over the range of temperatures studied).

In Eq. (9), which applies at equilibrium whenever TTS is obeyed, the dielectric material time is defined from the actual time by scaling with γ_d [Eq. (8)]. In the out-of-equilibrium situation following a temperature jump, the simplest assumption is that Eq. (9) also applies, but with a generalized dielectric material time involving a time-dependent dielectric relaxation rate $\gamma_d(t)$, i.e.,

$$d\tilde{t} = \gamma_d(t)dt. \tag{10}$$

As the system gradually equilibrates at the new temperature, the dielectric relaxation rate $\gamma_d(t)$ approaches the equilibrium liquid's loss-peak angular frequency at the new temperature. The equilibrium liquid's power-law dielectric loss $\varepsilon'' \propto f^{-\beta}$ applies in a range of frequencies obeying $f \gg f_m$. Since by Eq. (9) $\varepsilon(\tilde{\omega}) = \int_0^\infty \psi(\tilde{t}')\exp(-i\tilde{\omega}\tilde{t}')d\tilde{t}'$, where $\tilde{\omega} = \omega/\gamma_d$, the equilibrium liquid's loss obeys $\varepsilon'' \propto \tilde{\omega}^{-\beta}$ for $\tilde{\omega} \gg 1$. By the mathematical Tauberian theorem, this implies that $\psi(\tilde{t}') \propto (\tilde{t}')^{\beta-1}$ whenever $\tilde{t}' \ll 1$. The proposed generalization of Eq. (9) to out-of-equilibrium situations now mathematically implies that the dielectric relaxation rate $\gamma_d(t)$ is given by Eq. (6). In summary, assuming the simplest generalization of TTS to out-of-equilibrium situations, a generalized dielectric relaxation rate has been defined; moreover, we have shown how to measure it by monitoring the high-frequency dielectric loss at a fixed frequency using the inverse power-law approximation.

The idea of determining an out-of-equilibrium relaxation rate directly from experimental data instead of via modeling is mathematically equivalent to the so-called time-aging time superposition.[29,52–55] This is traditionally[43,56–58] implemented by first using the short-time response of, for instance, a mechanical perturbation to take a "snap-shot" of the structure during a volume-recovery experiment. These curves are then shifted horizontally on the time axes in order to determine the aging-time shift factors, α_{T_f}. Assuming time-aging time superposition, the shift factors are proportional to the structural relaxation time. Thus, the reduced time is found via an equation equivalent to Eq. (10), $\tilde{t} = \int_0^t (a_{T_f}(t'))^{-1}dt$.[59]

In Sec. III B, we relate $\gamma_d(t)$ to the TN structural relaxation clock rate $\gamma_s(t)$, but first the latter quantity needs to be defined precisely.

B. Defining the structural relaxation clock rate

The structural relaxation clock rate $\gamma_s(t)$ determines the structural relaxation's material time in the TN formalism. Just as was the case for the generalized dielectric relaxation rate, it is not *a priori* obvious that any $\gamma_s(t)$ may be defined; the test of the existence of $\gamma_s(t)$ is whether a consistent description is arrived at by assuming its existence. Assuming for the moment that this is the case, we define the structural relaxation clock rate's time-dependent activation (free) energy $E(t)$ by writing

$$\gamma_s(t) = \gamma_0 e^{-E(t)/k_B T} (\gamma_0 = 10^{14}\ \mathrm{s}^{-1}). \tag{11}$$

The activation energy $E(t)$ depends on the structure and evolves during the structural relaxation. Consider the case of structural relaxation induced by a general temperature variation. According to the TN formalism, the aging of the activation energy is described by a linear convolution integral over the temperature history involving a material time $\tilde{t}_s$ defined by the analog of Eq. (10),

$$d\tilde{t}_s = \gamma_s(t)dt. \tag{12}$$

Including for convenience the inverse temperature in the below equation, the linear convolution integral for the activation energy's evolution induced by a temperature variation $T(t) = T_0 + \Delta T(t)$ is given by an expression of the form

$$\Delta(E/k_B T)(\tilde{t}_s) = \int_0^\infty \Delta T(\tilde{t}_s - \tilde{t}_s')\phi(\tilde{t}_s')d\tilde{t}_s'. \tag{13}$$

C. Assuming the existence of an internal clock

A main purpose of this paper is to investigate the consequences of assuming that an internal clock exists. This assumption implies that the same material time controls dielectric aging via Eq. (9) and aging of the structural relaxation clock rate via Eqs. (11) and (13), i.e., that for any aging experiment one has

$$\gamma_s(t) \propto \gamma_d(t). \tag{14}$$

A clock works by counting repeated physical processes, and two clocks measure the same physical time if the number of ticks counted by the clocks are proportional for all time intervals. Thus both the above-defined clock rates γ_d and γ_s are defined only up to a proportionality: The physical content of Eqs. (9) and (13) is invariant if the reduced times are redefined by multiplying by some number. Nevertheless, Eq. (14) is not trivial; thus Eqs. (9) and (13) may both apply with different definitions of the reduced time. As mentioned, the TN formalism is often used assuming that different physical

quantities (e.g., volume and enthalpy) relax with rates that are not proportional.[12]

If Eq. (14) applies, we find via Eqs. (6) and (11) that after a temperature jump to temperature T the logarithm of the measured loss is given by

$$\ln \varepsilon''(f,t) = -\beta \frac{E(t)}{k_B T} + C \tag{15}$$

and that this quantity relaxes controlled by a material time whose rate may be determined from Eq. (7). We proceed to derive a test of this prediction.

IV. A TEST FOR THE EXISTENCE OF AN INTERNAL CLOCK

In this section we show that the existence of an internal clock, i.e., the assumption that the dielectric clock rate is proportional to the structural relaxation clock rate [Eq. (14)] can be tested without evaluating $\tilde{t}$ explicitly and without fitting data to analytical functions.

First, we define a dimensionless KM relaxation rate by replacing time in Eq. (2) by the reduced structural relaxation time

$$\tilde{\Gamma} \equiv -\frac{d \ln R}{d\tilde{t}_s}. \tag{16}$$

According to the TN formalism, for all temperature jumps $R(\tilde{t}_s)$ is the same function of $\tilde{t}_s$. This implies that $\tilde{\Gamma}(\tilde{t}_s)$ is the same for all jumps. By eliminating $\tilde{t}_s$, $\tilde{\Gamma}$ is a unique function of R

$$\tilde{\Gamma} = \Phi(R). \tag{17}$$

Thus, one way of testing whether the TN formalism applies is to check whether $\tilde{\Gamma}$ is indeed a unique function of the normalized relaxation function for different temperature jumps. To do this we express the dimensionless KM relaxation rate in terms of the real-unit KM relaxation rate

$$\tilde{\Gamma}(\tilde{t}) = -\frac{d \ln R}{dt}\frac{dt}{d\tilde{t}_s} = \frac{\Gamma(t)}{\gamma_s(t)}. \tag{18}$$

If an internal clock exists, $\gamma_s(t)$ may be evaluated from its proportionality to the dielectric relaxation rate Eq. (14), which is accessible via Eq. (7). Note that the unknown proportionality constant in Eq. (14) is irrelevant because, as mentioned, clock rates are only defined up to a proportionality constant (in Sec. VI we discuss the possibility of absolute calibration of the structural and dielectric clock rates). In summary, if $\gamma_s(t) \propto \gamma_d(t)$, via Eq. (18) $\tilde{\Gamma}$ may be calculated directly from a temperature-jump experiment's data, since $\Gamma(t)$ and $\gamma_d(t)$ are both determined from $\ln \varepsilon''(f,t)$ via Eqs. (2) and (7), respectively.

Defining the proportionality constant between the two rates to be unity, $\gamma_s(t) = \gamma_d(t)$, the results for the KM relaxation rates $\Gamma(R)$ and the dimensionless KM relaxation rates $\tilde{\Gamma}(R)$ are plotted in Fig. 7. For all five liquids the results are consistent with the internal clock hypothesis. Even the 4 K down jump for TPP—corresponding to a clock-rate change of almost two orders of magnitude—falls nicely onto the master curve. The spread in KM relaxation rates as $R \cong 0$ is approached at long times reflects the already mentioned fact that relaxation rates cannot be determined reliably by numerical differentiation when the noise becomes comparable to the distance to equilibrium.

Once the existence of an internal clock has been demonstrated, it is natural to evaluate the reduced time $\tilde{t}$ explicitly by integration in order to determine $R(\tilde{t})$. As shown in Fig. 8, this gives the data collapse predicted by the TN formalism. For the numerical integration, one must either include short-time transient points, where the sample still undergoes temperature equilibration, or omit the initial measurements. The error introduced from this uncertainty influences all values of $\tilde{t}$. This is one reason to prefer the "direct" test of the internal clock hypothesis of Fig. 7; another reason is that the direct test is simpler by not evaluating the material time $\tilde{t}$.

V. LONG-TIME ASYMPTOTIC BEHAVIOR OF THE STRUCTURAL RELAXATION

Inspecting the shape of the dimensionless KM relaxation rate as a function of the normalized relaxation function in Fig. 7 shows that the aging is not exponential because that would imply a constant KM relaxation rate. The stretched-exponential function $\exp[-\tilde{t}^{\beta}]$ is commonly used for fitting relaxation functions. It is difficult to get reliable data on the long-time behavior of structural relaxations, but our data allow one to get such data with fair accuracy. Figure 7 shows that $\tilde{\Gamma}(R) \to$ Const. at long times ($R \to 0$) for all five liquids. This is also evident from the DBP data for which Fig. 9(a) shows the dimensionless Kovacs plots, a stretched exponential (red line), and Eq. (20) (blue line) with the values of the fit parameters listed in Table II. The KM relaxation rate for the same data is shown in Fig. 9(b), where a test of the fit by the stretched-exponential relaxation function (red straight line) is again included. Although the data become noisy at long times, they indicate a bend over at long times that is not consistent with the stretched-exponential relaxation function; the KM relaxation rates appear to approach a finite value at long times. The blue curve in Fig. 9(b) is the "exponential $\sqrt{t}$" relaxation function detailed below [Eq. (20)].

The fact that the KM relaxation rates appear to converge to finite values means that the relaxation function at long times follows a simple exponential decay. To model this mathematically with as few parameters as possible, we fitted the data to the following "exponential $\sqrt{t}$" relaxation function, which retains features of a stretched exponential with exponent 1/2 but has a long-time simple exponential decay:[48,60]

$$R(\tilde{t}) = \exp(-A - B\tilde{t} - C\tilde{t}^{1/2}). \tag{19}$$

Here A, B, and C are fitting parameters. The number A reflects the fact that due to fast relaxations, the normalized relaxation function R does not start at unity at the shortest experimentally accessible times. The case $B=0$ gives a stretched exponential with exponent 1/2 and the $C=0$ case gives an ordinary exponential decay. At short times one has $R(\tilde{t}) \cong 1 - A - C\tilde{t}^{1/2}$, which justifies the name "exponential $\sqrt{t}$

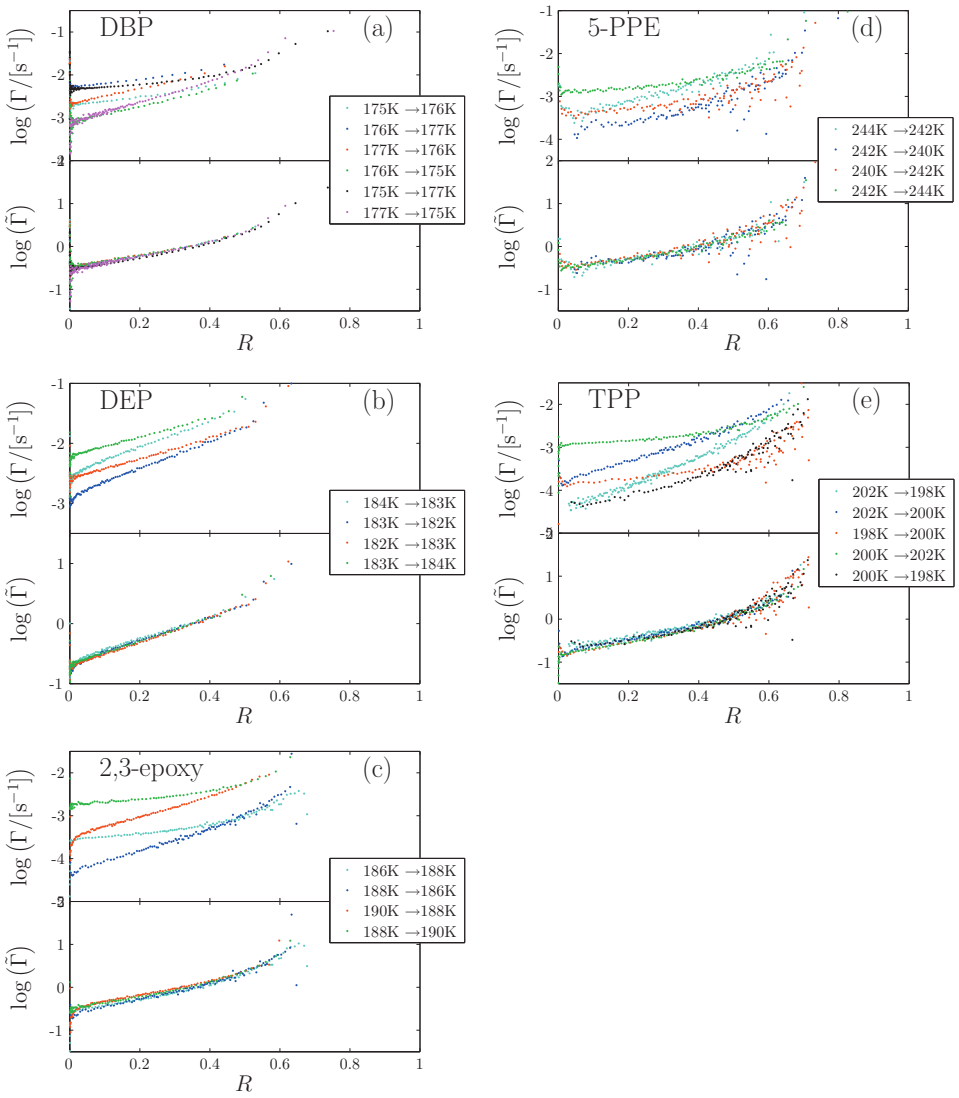

FIG. 7. Kovacs-McKenna (KM) relaxation rates Γ and its dimensionless version $\tilde{\Gamma}(\tilde{t})=\Gamma(t)/\gamma_d(t)$ [defined in Eq. (16) and calculated from data via the internal clock hypothesis $\gamma_s(t)=\gamma_d(t)$] as functions of the normalized relaxation functions R for the five liquids. For each liquid, the upper subfigure shows $\Gamma(R)$ and the lower subfigure shows $\tilde{\Gamma}(R)$. In all cases there is data collapse of $\tilde{\Gamma}(R)$ within experimental errors. This confirms the existence of an internal clock for these liquids.

relaxation function" (see Ref. 51 and references therein to $\sqrt{t}$ relaxation in other contexts). Equation (19) may be rewritten as

$$R(\tilde{t}) = \exp(-a - b\tilde{t} - c(b\tilde{t})^{1/2}), \tag{20}$$

where $a=A$, $b=B$, and $c=C/\sqrt{B}$. Recast in this form, it is clear that b merely adjusts the time scale and that c is the only genuine shape parameter. Table III quantifies how well analytical relaxation functions fit data, concluding that Eq. (20) fits data somewhat better than the standard stretched exponential relaxation function.

VI. CALIBRATING THE DIELECTRIC CLOCK RATE

The results obtained so far may be summarized as follows. The TN formalism predicts that the dimensionless KM relaxation rate [Eq. (16)] is a unique function of R for the relaxation toward equilibrium following any temperature jump. This can be tested only, however, if one is able to determine the structural relaxation clock rate $\gamma_s(t)$. This can be done either by some assumption about the clock rate's structure dependence, a commonly used procedure, or, as above, by the internal clock hypothesis $\gamma_s(t) \propto \gamma_d(t)$, where the dielectric relaxation rate is determined from data via Eq.

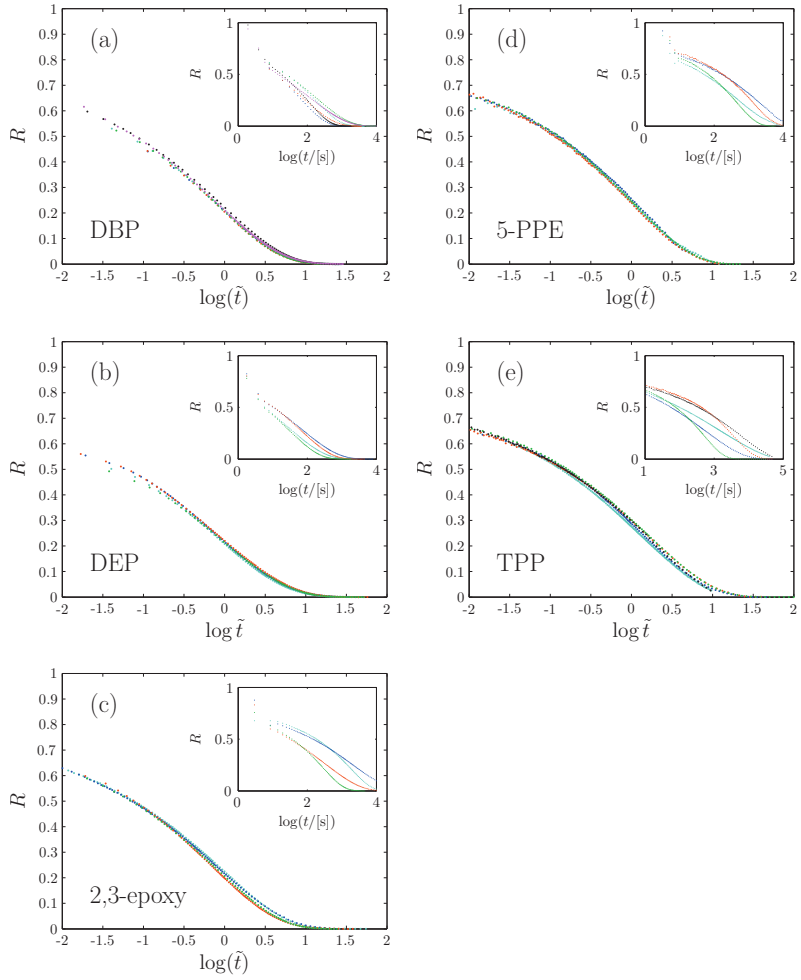

FIG. 8. The traditional way of demonstrating TN data collapse by plotting the normalized relaxation functions as function of the reduced time $R(\tilde{t})$. The insets show the normalized relaxation functions plotted against real time $R(t)$.

(7). The data do collapse as predicted by the internal clock hypothesis, confirming the existence of such a clock for all five liquids.

As emphasized, a clock rate is determined only up to a proportionality constant, i.e., two clocks measure the same physical time if their numbers of "ticks" are proportional for all time intervals. Still, one may ask whether some sort of absolute calibration of the dielectric and structural relaxation clock rates is possible. We defined the dielectric relaxation rate in equilibrium γ_d as the dielectric angular loss-peak frequency [Eq. (5)]. This is convenient because the loss-peak frequency can easily be determined accurately. A characteristic feature of the dielectric losses of supercooled organic liquids is their pronounced asymmetry. Whereas the loss decays as a nontrivial power-law above the loss-peak frequency, at low frequencies the loss almost follows the Debye function ($\varepsilon''(\omega) \propto \omega$). Via the fluctuation-dissipation theorem, the low-frequency behavior corresponds to a simple exponential long-time decay of the equilibrium dipole autocorrelation function. Inspired by the recent work of Gainaru *et al.*,[61] it is obvious to ask whether redefining γ_d to be the rate of this long-time decay and assuming equality in Eq. (14) would imply that $\tilde{\Gamma} \to 1$ asymptotically at long times. In other words: Is the long-time exponential structural relaxation clock rate equal to the exponential long-time decay of the equilibrium dipole autocorrelation function? Because the liquids studied here all obey TTS, such a recalibration of γ_d corresponds to multiplying each liquid's equilibrium γ_d [Eq. (5)] by a fixed constant. This is illustrated in Fig. 10.

For each liquid, the recalibration constant is obtained as follows. Assuming Eq. (20) for the equilibrium dipole autocorrelation function, the liquid's dielectric loss was fitted by the Laplace transform of the negative time-derivative of this function (which interestingly provides an excellent fit to the dielectric data of all five liquids [compare Fig. 10(b)], a fit that is better than that of standard single-parameter fitting functions). In Fig. 11 we show the result of applying this recalibration of the dielectric relaxation rate in the analysis of Sec. IV. Within experimental uncertainties, all recalibrated KM relaxation rates converge to one at long times ($R \to 0$). This suggests an underlying unity in the description of aging for the liquids examined in this paper.

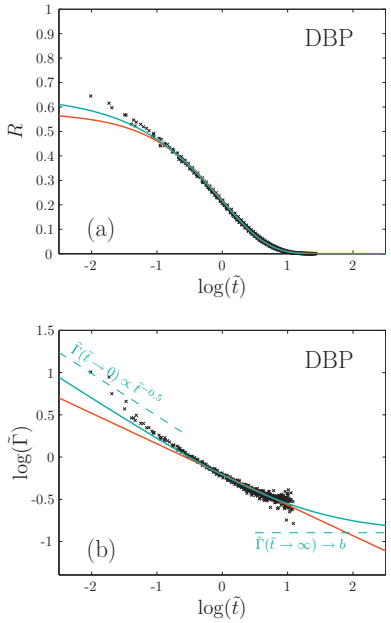

FIG. 9. Fits of the exponential $\sqrt{t}$ relaxation function [Eq. (20)] (blue) and the stretched exponential (red) to DBP data. (a) In the standard representation showing R as a function of $\log(\tilde{t})$ it is hard to distinguish the two fitting functions. (b) Relaxation rates as functions of the (reduced) times in a log-log plot. In this representation, the stretched-exponential function is a straight line, while the exponential $\sqrt{t}$ relaxation function of Eq. (20) has a "banana" shape: at short times it gives a straight line with slope $-1/2$ and at long times it bends over and eventually levels off to a constant value. The two asymptotes are marked with dashed lines. Although the measurements are noisy at long times, the data do not appear to follow a straight line, but have a curved shape similar to the one of the exponential $\sqrt{t}$ relaxation function.

VII. CONCLUDING REMARKS

We have shown how the internal clock hypothesis can be checked in a test that neither involves free parameters nor the fitting of data to some mathematical expression. The test is based on assuming the standard Tool–Narayanaswamy formalism for structural relaxation studied by monitoring the liquids' dielectric loss at a fixed frequency in the Hertz range, following temperature up and down jumps. Based on data for five organic liquids we conclude that within the experimental uncertainties (1) all liquids age consistent with the TN formalism; (2) all liquids have an internal clock; (3) no liquid exhibits an expansion gap; (4) all liquids appear to have exponential long-time relaxation; and (5) the long-time structural relaxation clock rate equals that of the long-time simple exponential decay of the dipole autocorrelation function.

TABLE II. Values of fitted parameters of Eq. (20).

	DBP	DEP	2,3-epoxy	5-PPE	TPP
a	0.42	0.46	0.37	0.35	0.33
b	0.11	0.04	0.06	0.13	0.02
c	3.1	5.1	4.7	2.6	6.2

TABLE III. Test of how well the two functions fit data, where superscript "exp$\sqrt{t}$" is the exponential $\sqrt{t}$ relaxation function of Eq. (20) and superscript "str exp" is the stretched-exponential relaxation function. The quality of the fits is measured via the standard mean-square deviation σ for fitting, respectively, $\log(R)$ as a function of time and $\log(\Gamma)$ as a function of time. The exponential $\sqrt{t}$ relaxation function provides a somewhat better fit than does the stretched exponential.

	DBP	DEP	2,3-epoxy	5-PPE	TPP
$\sigma^{\exp\sqrt{t}}_{\log(R)}$	0.041	0.029	0.042	0.023	0.026
$\sigma^{\text{str exp}}_{\log(R)}$	0.043	0.030	0.042	0.026	0.026
$\sigma^{\exp\sqrt{t}}_{\log(\tilde{\Gamma})}$	0.052	0.028	0.081	0.172	0.111
$\sigma^{\text{str exp}}_{\log(\tilde{\Gamma})}$	0.074	0.037	0.092	0.186	0.116

Our finding that the liquids appears to have exponential long-time relaxation is consistent with several classical viscoelastic and aging models, for instance, the famous Kovacs-Aklonis-Hutchinson-Ramos (KAHR) model[59] based on a box distribution of relaxation times, which implies the existence of a longest relaxation time and thus an exponential long-time relaxation. It is also worth emphasizing that, in contrast to reports for other materials (e.g., oxide glasses) for which there is evidence that the material clock does not tick the same way for all processes, the data presented here are consistent with the existence of a unique material time. We have shown that the structural relaxation rate is proportional to the dielectric relaxation rate for five organic supercooled

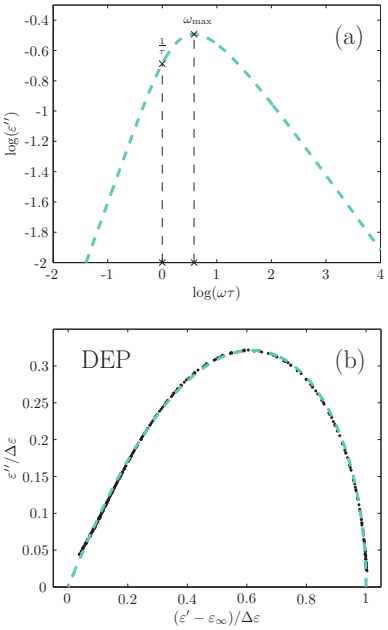

FIG. 10. (a) Illustration of the difference between the two calibrations of the dielectric relaxation rate γ_d, using either the loss-peak angular frequency or the rate of the long-time exponential decay of the dipole autocorrelation function giving the low-frequency Debye behavior. (b) Normalized Cole–Cole plot of the dielectric loss of DEP (black dots) vs that of the exponential $\sqrt{t}$ relaxation function [Eq. (20)] used to fit the dielectric data at the following temperatures: 206, 207, 208, 209, 210, and 211 K (blue dashed line).

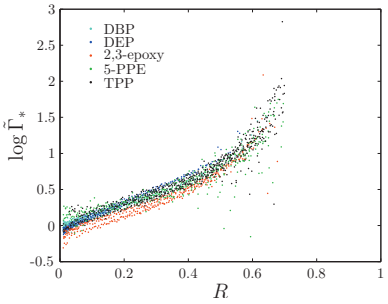

FIG. 11. Dimensionless Kovacs plots including data for all temperature jumps of the five liquids, using the alternative calibration of the dielectric relaxation rate corresponding to scaling data with the long-time dielectric relaxation rate. This procedure "lifts" the curves of Fig. 7 such that the dimensionless KM relaxation rates all terminate at approximately one at long times ($R \rightarrow 0$).

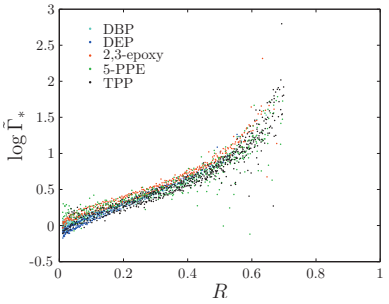

FIG. 13. Dimensionless Kovacs plots including data for all temperature jumps of the five liquids, using the alternative calibration of the dielectric relaxation rate corresponding to scaling data with the long-time dielectric relaxation rate and assuming for all liquids the high-frequency exponent of the dielectric loss $-1/2$ (Ref. 51).

liquids. The fact that the structural relaxation was monitored by measuring the dielectric loss is, in our opinion, not important. Nevertheless, it would be interesting to study, for instance, volume relaxation for the same liquids to investigate whether there is really a common material clock for these liquids. We finally note that in contrast to the well-known Tool-Narayanaswamy-Moynihan (TNM) formalism of Moynihan *et al.*,[9] the analysis applied here does not require one or more fictive temperatures. In this sense our approach is closer in spirit to the KAHR approach (which is known, however, to be mathematically equivalent to the TNM formalism).

The emphasis of the data analysis was on using data directly without having to fit to analytical functions. This is

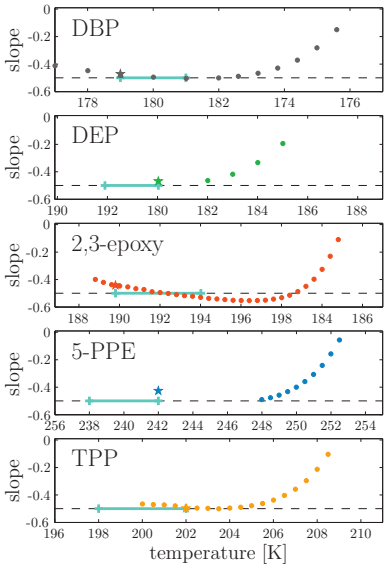

FIG. 12. The slopes of the equilibrium log-log plotted dielectric losses at the measuring frequencies as functions of temperature. The aging interval is marked with a blue dashed line. There is a temperature window where the slope is almost constant. In this way, the measuring frequency and temperature jumps can be fine-tuned such that the proposed method for determining the clock rate applies.

why we determine the dielectric clock rate from the loss-peak angular frequency [Eq. (5)] and the exponent β as the minimum slope of the dielectric loss at the temperature where the loss-peak frequency is 0.1 Hz (Table I). If this purist approach is relaxed a bit, however, further interesting features appear. Thus if the dielectric clock rate is instead determined from the dielectric loss' low-frequency Debye-like behavior, all KM relaxation rates converge to unity at long times (Fig. 11). Moreover, since the minimum slopes are not completely temperature independent, but converge to the (in Ref. 51) conjectured generic value of $-1/2$ at the lowest temperatures (Fig. 12), one may ask what happens if the exponent β of Eq. (7) is replaced by $-1/2$. The result of repeating the entire analysis with this high-frequency exponent is shown in Fig. 13. The main effect is to lift the 2,3-epoxy data, the liquid whose exponent β was furthest from $-1/2$. Since the long-time structural relaxation clock rate, if identical to the redefined dielectric relaxation rate, should approach the latter from above, this figure is consistent with the conclusion that the two rates are identical.

By modern microengineering it should be possible to extend aging experiments to even shorter times, thus making it realistic to perform a series of ideal temperature-jump experiments over just hours. When this is eventually realized, it is not unlikely that aging studies could become routine on par with, e.g., present-day dielectric measurements.

ACKNOWLEDGMENTS

The center for viscous liquid dynamics "Glass and Time" is sponsored by the Danish National Research Foundation (DNRF).

APPENDIX: SYSTEMATIC ERRORS AND NOISE

We discuss here the some sources of errors of the data and the analysis. For a general and systematic analysis of errors and noise of the measurement, we refer to Refs. 23 and 24.

The geometry of the measuring cell (disk radius much larger than disk separation) introduces an extremely slow radial contraction which in equilibrium dielectric measurements can be neglected. For aging experiments it poses a

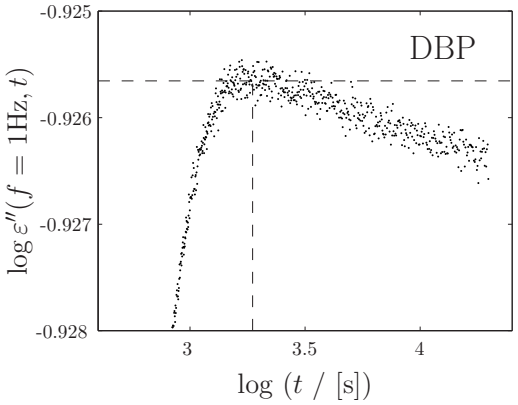

FIG. 14. Zoom of the tail of the 2 K up jump to 175 K for DBP [data of Fig. 3(b)]. There is a small drift at long times, which is due to the slow (compared to the alpha relaxation time) radial flow of the liquid in the measuring cell. The dashed vertical line marks where the data were cut off and the dashed horizontal line marks the $\epsilon''(t\to\infty)$ level used in the analysis.

problem because it introduces a small drift at long times, which distorts the curve shape of the aging relaxation function and complicates the determination of the value approached at long times. In Fig. 14 a zoom of the tail of the (upper) DBP data from Fig. 3(b) is shown. The drift is small but clearly visible. After a temperature step, the curve should level off to a constant (equilibrium) value; instead the curve appears slightly slanted. The drift coming from the initial quench may be reduced by annealing for a long time before starting a measurement, which we did (typically over several weeks). A further source of error is that in some cases a small overshoot is observed when approaching equilibrium. We do not currently have an explanation for this, but it may be due to something other than the drift. Whenever a small drift or an overshoot was present, we chose to cut the data shortly after reaching the maximum/minimum and $\varepsilon''(t\to\infty)$ was adjusted accordingly. This is illustrated in Fig. 14 where the $\varepsilon''(t\to\infty)$ is marked by a horizontal dashed line and the cutoffs by a vertical dashed line.

The signal-to-noise ratio depends on the (dielectric) relaxation strength (corresponding to the absolute level of the dielectric loss) of the liquids studied. Thus, there is more noise in the data for TPP and 5-PPE, which have relatively small dielectric relaxation strengths, than for DBP, DEP, and 2,3-epoxy, which have larger relaxation strengths.

Although the precision of a dielectric measurement is high with barely any visible noise in the relaxation curve, we still encountered noise problems when taking the numerical derivatives of these curves. Averaging over even few data points distorts the curve shapes at short times, but it is necessary (and also less problematic) to average over more data points in the long-time tails of these curves. To deal with this problem, we designed an algorithm to average over a number of data points that increases with aging time, i.e., no averaging of the first data points and averaging over 8 (in the case of DBP and 2,3-epoxy) or 16 (in the case of DEP, 5-PPE, and TPP) data points in the tail. This procedure is illustrated in Fig. 15.

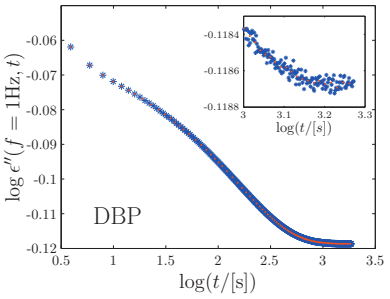

FIG. 15. Illustration of the smoothing procedure described in the text. The algorithm minimizes the distortion of the curve shape by averaging over few (or no) data points in the beginning and over more data points toward the end of the relaxation.

In Fig. 12 we show the slope of the equilibrium dielectric loss at the measuring frequencies of the aging experiment as a function of temperature. The temperature intervals used in the aging experiments are marked with a light blue line. For each frequency there is a temperature window where the slope is constant (close to $-1/2$). In this way the measuring frequency and temperature jumps can be fine-tuned such that the proposed method for finding the clock rate is valid. The graphs show that not all measurements were carried out in the optimal regions. The slopes vary in the aging temperature interval studied for some of the liquids and they are not entirely identical to the value above T_g. Thus the conditions for the proposed method for determining the clock rate are not rigorously fulfilled in all cases. However, one will still obtain data collapse using a slightly incorrect inverse power-law exponent since the error made is the same for all data points. The error simply results in a vertical shift of the curves in Fig. 7 and a horizontal shift in Fig. 8. Note finally that a slight variation of the power-law exponent in the measured temperature interval will influence the shape of the master curve and may explain why the data collapse is not perfect.

[1] W. Kauzmann, Chem. Rev. (Washington, D.C.) **43**, 219 (1948).
[2] P. G. Debenedetti, *Metastable Liquids: Concepts and Principles* (Princeton University Press, Princeton, 1996).
[3] C. A. Angell, K. L. Ngai, G. B. McKenna, P. F. McMillan, and S. W. Martin, J. Appl. Phys. **88**, 3113 (2000).
[4] C. Alba-Simionesco, C. R. Acad. Sci. Paris, Ser. IV **2**, 203 (2001).
[5] W. Kob, "Slow relaxations and nonequilibrium dynamics in condensed matter," in *Proceedings of the Les Houches Summer School of Theoretical Physics, Session LXXVII*, 1–26 July 2002, edited by J.-L. Barrat, M. Feigelman, J. Kurchan, and J. Dalibard (Springer, Berlin, 2004), p. 199.
[6] J. C. Dyre, Rev. Mod. Phys. **78**, 953 (2006).
[7] A. J. Kovacs, J. Polym. Sci., Polym. Phys. Ed. **30**, 131 (1958).
[8] A. J. Kovacs, Fortschr. Hochpolym.-Forsch. **3**, 394 (1963).
[9] C. T. Moynihan, P. B. Macedo, C. J. Montrose, P. K. Gupta, M. A. DeBolt, J. F. Dill, B. E. Dom, P. W. Drake, A. J. Easteal, P. B. Elterman, R. P. Moeller, H. Sasabe, and J. A. Wilder, Ann. N.Y. Acad. Sci. **279**, 15 (1976).
[10] O. V. Mazurin, J. Non-Cryst. Solids **25**, 129 (1977).
[11] L. C. E. Struik, *Physical Aging in Amorphous Polymers and Other Materials* (Elsevier, Amsterdam, 1978).
[12] G. W. Scherer, *Relaxation in Glass and Composites* (Wiley, New York, 1986).
[13] G. B. McKenna, J. Res. Natl. Inst. Stand. Technol. **99**, 169 (1994).
[14] I. M. Hodge, J. Non-Cryst. Solids **169**, 211 (1994).
[15] I. M. Hodge, Science **267**, 1945 (1995).

[16] I. Avramov, Thermochim. Acta **280–281**, 363 (1996).
[17] M. D. Ediger, Annu. Rev. Phys. Chem. **51**, 99 (2000).
[18] R. Richert, J. Phys.: Condens. Matter **14**, R703 (2002).
[19] W. Huang and R. Richert, J. Chem. Phys. **130**, 194509 (2009).
[20] G. Diezemann, J. Chem. Phys. **123**, 204510 (2005).
[21] R. Richert, Phys. Rev. Lett. **104**, 085702 (2010).
[22] S. Kolla and S. L. Simon, Polymer **46**, 733 (2005).
[23] B. Igarashi, T. Christensen, E. H. Larsen, N. B. Olsen, I. H. Pedersen, T. Rasmussen, and J. C. Dyre, Rev. Sci. Instrum. **79**, 045105 (2008).
[24] B. Igarashi, T. Christensen, E. H. Larsen, N. B. Olsen, I. H. Pedersen, T. Rasmussen, and J. C. Dyre, Rev. Sci. Instrum. **79**, 045106 (2008).
[25] G. P. Johari, J. Chem. Phys. **77**, 4619 (1982).
[26] E. Schlosser and A. Schönhals, Polymer **32**, 2135 (1991).
[27] A. Alegria, E. Guerrica-Echevarria, L. Goitiandia, I. Telleria, and J. Colmenero, Macromolecules **28**, 1516 (1995).
[28] A. Alegría, L. Goitiandia, I. Telleria, and J. Colmenero, Macromolecules **30**, 3881 (1997).
[29] L. Goitiandia and A. Alegria, J. Chem. Phys. **121**, 1636 (2004).
[30] R. L. Leheny and S. R. Nagel, Phys. Rev. B **57**, 5154 (1998).
[31] H. Yardimci and R. L. Leheny, Europhys. Lett. **62**, 203 (2003).
[32] D. Cangialosi, M. Wübbenhorst, J. Groenewold, E. Mendes, and S. J. Picken, J. Non-Cryst. Solids **351**, 2605 (2005).
[33] P. Lunkenheimer, R. Wehn, U. Schneider, and A. Loidl, Phys. Rev. Lett. **95**, 055702 (2005).
[34] P. Lunkenheimer, R. Wehn, and A. Loidl, J. Non-Cryst. Solids **352**, 4941 (2006).
[35] R. Wehn, P. Lunkenheimer, and A. Loidl, J. Non-Cryst. Solids **353**, 3862 (2007).
[36] P. D'Angelo, M. Barra, M. Nicodemi, and A. Cassinese, J. Appl. Phys. **101**, 044910 (2007).
[37] A. Serghei and F. Kremer, Macromol. Chem. Phys. **209**, 810 (2008).
[38] O. S. Narayanaswamy, J. Am. Ceram. Soc. **54**, 491 (1971).
[39] A. Q. Tool, J. Am. Ceram. Soc. **29**, 240 (1946).
[40] See http://glass.ruc.dk/data for the raw data.
[41] L. C. E. Struik, Polymer **38**, 4677 (1997).
[42] R. W. Rendell, K. L. Ngai, G. R. Fong, and J. J. Aklonis, Macromolecules **20**, 1070 (1987).
[43] G. B. McKenna, Y. Leterrier, and C. R. Schultheisz, Polym. Eng. Sci. **35**, 403 (1995).
[44] G. B. McKenna, M. G. Vangel, A. L. Rukhin, S. D. Leigh, B. Lotz, and C. Straupe, Polymer **40**, 5183 (1999).
[45] I. L. Hopkins, J. Polym. Sci., Polym. Phys. Ed. **28**, 631 (1958).
[46] J. J. Tribone, J. M. O'Reilly, and J. Greener, Macromolecules **19**, 1732 (1986).
[47] I. M. Hodge, J. Res. Natl. Inst. Stand. Technol. **102**, 195 (1997).
[48] L. Hornbøll, T. Knusen, Y. Yue, and X. Guo, Chem. Phys. Lett. **494**, 37 (2010).
[49] N. B. Olsen, J. C. Dyre, and T. Christensen, Phys. Rev. Lett. **81**, 1031 (1998).
[50] N. B. Olsen, T. Christensen, and J. C. Dyre, Phys. Rev. Lett. **86**, 1271 (2001).
[51] A. I. Nielsen, T. Christensen, B. Jakobsen, K. Niss, N. B. Olsen, R. Richert, and J. C. Dyre, J. Chem. Phys. **130**, 154508 (2009).
[52] R. D. Bradshaw and L. C. Brinson, Polym. Eng. Sci. **37**, 31 (1997).
[53] P. A. O'Connell and G. B. McKenna, Polym. Eng. Sci. **37**, 1485 (1997).
[54] A. Lee and J. D. Lichtenhan, Macromolecules **31**, 4970 (1998).
[55] P. A. O'Connell and G. B. McKenna, J. Chem. Phys. **110**, 11054 (1999).
[56] A. J. Kovacs, R. A. Stratton, and J. D. Ferry, J. Phys. Chem. **67**, 152 (1963).
[57] J. Beckmann, G. B. McKenna, B. G. Landes, D. H. Bank, and R. A. Bubeck, Polym. Eng. Sci. **37**, 1459 (1997).
[58] I. Echeverría, P. L. Kolek, D. J. Plazek, and S. L. Simon, J. Non-Cryst. Solids **324**, 242 (2003).
[59] A. J. Kovacs, J. J. Aklonis, J. M. Hutchinson, and A. R. Ramos, J. Polym. Sci., Part B: Polym. Phys **17**, 1097 (1979).
[60] N. Sağlanmak, A. I. Nielsen, N. B. Olsen, J. C. Dyre, and K. Niss, J. Chem. Phys. **132**, 024503 (2010).
[61] C. Gainaru, R. Kahlau, E. A. Rössler, and R. Böhmer, J. Chem. Phys. **131**, 184510 (2009).

ARTICLE IN PRESS
NOC-14892; No of Pages 5

Journal of Non-Crystalline Solids xxx (2010) xxx–xxx

Contents lists available at ScienceDirect

Journal of Non-Crystalline Solids

journal homepage: www.elsevier.com/ locate/ jnoncrysol

A combined measurement of thermal and mechanical relaxation

Tage Christensen *, Bo Jakobsen, Jon Papini, Tina Hecksher, Jeppe C. Dyre, Niels Boye Olsen

DNRF Centre "Glass and Time", IMFUFA, Department of Sciences, Roskilde University, Postbox 260, DK-4000 Roskilde, Denmark

ARTICLE INFO

Article history:
Received 18 April 2010
Received in revised form 29 June 2010
Available online xxxx

Keywords:
Glass transition;
Thermoviscoelasticity;
Prigogine–Defay ratio

ABSTRACT

In order to describe relaxation the thermodynamic coefficient $\frac{1}{\beta_S} = \left(\frac{\partial V}{\partial S}\right)_p$ can be generalized into a complex frequency-dependent cross response function. We explore theoretically the possibility of measuring $\frac{1}{\beta_S}(\omega)$ for a supercooled liquid near the glass transition. This is done by placing a thermistor in the middle of the liquid which itself is contained in a spherical piezoelectric shell. The piezoelectric voltage response to a thermal power generated in the thermistor is found to be proportional to $\frac{1}{\beta_S}(\omega)$ but factors pertaining to heat diffusion and adiabatic compressibility $\kappa_S(\omega)$ do also intervene. We estimate a measurable piezoelectric voltage of 1 mV to be generated at 1 Hz for a heating power of 0.3 mW. Together with $\kappa_S(\omega)$ and the longitudinal specific heat $c_l(\omega)$ which may also be found in the same setup a complete triple of thermoviscoelastic response functions may be determined when supplemented with shear modulus data.

1. Introduction

The recent finding [1] that a class of liquids — the strongly correlating liquids — may be described by a single "order" parameter makes it urgent to devise methods that measure thermal and mechanical relaxation and their interconnection. It would be an advantage if they can be measured in the same setup on the same sample. The classical Prigogine–Defay test of a one "order" parameter description has recently been rigorously reformulated for the equilibrium liquid in terms of (four) Dynamic Prigogine–Defay ratios [2]. One of these, $\Lambda_{sp} = -(T_0/c_p)''(\kappa_S)''/((1/\beta_S)'')^2$ is from an experimental viewpoint the easiest to access. It contains the complex frequency-dependent specific heat $c_p(\omega)$, adiabatic compressibility $\kappa_S(\omega)$ and adiabatic pressure coefficient $\beta_S(\omega) \equiv (\delta p(\omega)/\delta T(\omega))_S$. We can measure $\kappa_S(\omega)$ by the so-called piezoelectric bulk modulus gauge (PBG) [3]. The PBG is a hollow sphere with a thin wall of a piezoelectric ceramic material. Pressure/volume changes of a contained liquid are detectable due to the piezoelectric effect. In the middle of the PBG we have now added a thermistor by which we can measure the longitudinal heat capacity $c_l(\omega)$ via the effusivity [4,5]. In this paper we study theoretically what can be deduced by combining the two sensors, i.e. how does the expansion of the liquid upon heating in the centre affect the piezoelectric shell.

2. Thermomechanical response of a differential volume element

The thermal interaction with matter is described in terms of the conjugated variables temperature, T and entropy, S. We name the interaction as an energy bond. It is a scalar bond since the variables are scalars. The mechanical interaction is described in terms of the strain and stress tensors but this interaction can be separated in a pure scalar part by the trace of these tensors and the deviatoric traceless part of these tensors. The conjugated variables of the scalar mechanical energy bond may then be taken as volume, V and minus pressure, $-p$. The deviatoric parts of the strain and stress tensors describe shear deformations and are not coupled to the scalar parts for symmetry reasons (The Curie–Prigogine principle [6–8]) but the scalar bonds however are coupled. The response δS and δV to perturbations δT and $-\delta p$ defines the constitutive properties of matter:

$$dV/V_0 = -\kappa_T dp + \alpha_p dT \tag{1}$$

$$dS/V_0 = -\alpha_p dp + \frac{1}{T_0} c_p dT \tag{2}$$

Since the perturbations excite thermal and acoustical waves the constitutive equations are defined for a differential volume element, V_0 of a linear dimension, R much smaller than the characteristic thermal diffusion length and acoustical wave length associated with the time scale of the perturbations (Figs. 1 and 2).

Eqs. (1) and (2) are valid in equilibrium thermodynamics. When it comes to describing the relaxation of supercooled liquids they are replaced with corresponding equations of linear irreversible thermodynamics

$$dV(t)/V_0 = -\int_{-\infty}^{t} \kappa_T(t-t')dp(t') + \int_{-\infty}^{t} \alpha_p(t-t')dT(t') \tag{3}$$

* Corresponding author.
E-mail address: tec@ruc.dk (T. Christensen).

0022-3093/$ – see front matter © 2010 Elsevier B.V. All rights reserved.
doi:10.1016/j.jnoncrysol.2010.07.051

Please cite this article as: T. Christensen, et al., A combined measurement of thermal and mechanical relaxation, J. Non-Cryst. Solids (2010), doi:10.1016/j.jnoncrysol.2010.07.051

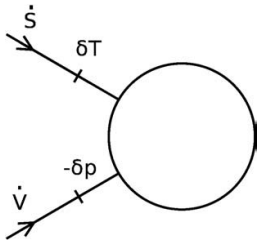

Fig. 1. The two scalar energetic interactions with a differential volume element. Differential means that the wavelengths of the thermal and mechanical perturbations are much longer than the dimensions of the volume element.

$$dS(t)/V_0 = -\int_{-\infty}^{t}\alpha_p(t-t')dp(t') + \int_{-\infty}^{t}\frac{1}{T_0}c_p(t-t')dT(t') \tag{4}$$

The thermodynamic coefficients are now replaced by response functions. These relaxing response functions may be consider in the frequency domain instead by defining e.g. the complex frequency-dependent compressibility as:

$$\kappa_T(\omega) = i\omega\int_0^\infty \kappa_T(t)e^{-i\omega t}dt. \tag{5}$$

Now dV, dS, dp and dT should be interpreted as the complex amplitudes of harmonically varying perturbations and the constitutive equations of linear irreversible thermodynamics (3) and (4) becomes

$$dV/V_0 = -\kappa_T(\omega)dp + \alpha_p(\omega)dT \tag{6}$$

$$dS/V_0 = -\alpha_p(\omega)dp + \frac{1}{T_0}c_p(\omega)dT \tag{7}$$

They can now be treated exactly like the equilibrium Eqs. (1) and (2). The response functions like $\kappa_T(\omega)$ and $c_p(\omega)/T_0$ pertaining to the conjugated variables of a single energy bond are auto response functions. $\alpha_p(\omega)$ on the other hand is a cross response function connecting a variable from the thermal bond to a variable from the mechanical bond. The three functions give a complete description of the thermomechanical response. For relaxing system they are not completely independent since the knowledge of the cross response function and one of the auto response functions for all frequencies makes it possible to calculate the other auto response function [9,10]. Moreover if the liquid relaxation is described by a single order parameter the relaxational part of the triple of relaxation functions are proportional and the dynamic Prigogine–Defay ratio [2]

$$\Lambda_{Tp} = \frac{c_p''\kappa_T''}{T_0\left(\alpha_p''\right)^2} \tag{8}$$

is equal to 1.

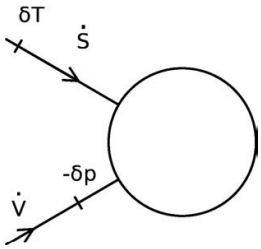

Fig. 2. Another response situation. Here entropy and pressure are the input variables and marked on the energy bond nearest to the system. In Fig. (1) temperature and pressure were the input variables.

There are three other different possibilities of pairs of independent controlling variables than $(dT,-dp)$, namely (dS,dV), $(dS,-dp)$, (dT,dV) leading to other triples of response functions and other variants of the dynamic Prigogine–Defay ratio. It is thus convenient to introduce the four auto response functions (connecting conjugated variables of the same bond),

$$c_V = \frac{T}{V}\left(\frac{\partial S}{\partial T}\right)_V \quad , \quad c_p = \frac{T}{V}\left(\frac{\partial S}{\partial T}\right)_p$$

$$\kappa_T = -\frac{1}{V}\left(\frac{\partial V}{\partial p}\right)_T \quad , \quad \kappa_S = -\frac{1}{V}\left(\frac{\partial V}{\partial p}\right)_S$$

and the four cross response functions (connecting variables of different bonds),

$$\alpha_p = \frac{1}{V}\left(\frac{\partial V}{\partial T}\right)_p = -\frac{1}{V}\left(\frac{\partial S}{\partial p}\right)_T,$$

$$\frac{1}{\alpha_S} = -V\left(\frac{\partial T}{\partial V}\right)_S = V\left(\frac{\partial p}{\partial S}\right)_V,$$

$$\beta_V = \left(\frac{\partial p}{\partial T}\right)_V = \left(\frac{\partial S}{\partial V}\right)_T,$$

$$\frac{1}{\beta_S} = \left(\frac{\partial T}{\partial p}\right)_S = \left(\frac{\partial V}{\partial S}\right)_p$$

Strictly speaking – defining these 8 functions as partial derivatives – they are at first just constant real thermodynamic coefficients but they may be generalized into complex functions just like $\kappa_T(\omega)$, $\alpha_p(\omega)$ and $c_p(\omega)$ and they are thought of in this sense in the following. An extensive table of relations between these functions is given in the appendix of reference [4]. Here we just notice that β_S is related to α_p and c_p by

$$\frac{1}{T_0\beta_S} = \frac{\alpha_p}{c_p}. \tag{9}$$

All of the response functions can be related to fluctuations of the thermodynamic variables [11]. For example $1/\beta_S$ is proportional to correlations between temperature and volume fluctuations. It was recently found [1] that a class of liquids — the strongly correlating liquids — may be described by a single "order" parameter and it was explicitly shown [12] by computer NVT simulations of the Kob–Andersen binary Lennard–Jones system that

$$\Lambda_{TV}(\omega) = -\frac{c_V''\left(\frac{1}{\kappa_T}\right)''}{T_0(\beta_V'')^2} \tag{10}$$

was 1 within 20%.

As we shall see it will probably be the triple $T_0/c_p(\omega), \kappa_S(\omega), 1/\beta_S$ that is experimentally easiest accessible and it will be the *Sp*-variant of the Prigogine–Defay ratio

$$\Lambda_{Sp} = -\frac{\left(\frac{T_0}{c_p}\right)''\kappa_S''}{\left(\left(\frac{1}{\beta_S}\right)''\right)^2} \tag{11}$$

that shall test the one-parameter'ness of real liquids.

3. Thermomechanical response of a finite spherical volume element

When considering a real experiment with perturbations varying at a frequency $f=\omega/(2\pi)$ it is not always possible to be in a situation of homogeneous fields. The wavelength of sound λ_{sound} and the heat diffusion length, $|l_D|$ may be comparable to or smaller than the sample size R. If we consider frequencies below 1 kHz then roughly $\lambda_{sound}>1$m

Please cite this article as: T. Christensen, et al., A combined measurement of thermal and mechanical relaxation, J. Non-Cryst. Solids (2010), doi:10.1016/j.jnoncrysol.2010.07.051

and for $R<1$cm we can neglect mechanical waves i.e. neglect inertia in the continuum description [4]. However the heat diffusion length, $|l_D| = |\sqrt{D/(i\omega)}|$ of a supercooled liquid with a typical heat diffusion constant of $D=0.1\text{mm}^2/\text{s}$ varies from $4\mu m$ to 4mm when frequency varies from 1 kHz to 1 mHz and thus heat diffusion cannot be neglected for a sample size of 1 cm. By the coupling between the temperature field and the strain field that α_p induces, the strain and stress fields also become inhomogeneous. This implies that even in spherical geometry the two pressures, the radial $\delta p_r = -\sigma_{rr}$ and the mean (hydrostatic) $\delta p = -1/3(\sigma_{rr}+\sigma_{\theta\theta}+\sigma_{\varphi\varphi})$ are not equal if shear modulus is comparable to bulk modulus. When interacting mechanically with a sphere through its surface we don't have access to δp but only to δp_r. For this reason shear modulus enters – via the boundary conditions – the description of the thermomechanical response of a finite sphere although it wasn't present in the thermomechanical response of a differential volume element, Eqs. (6) and (7). Consider generally a finite amount of liquid lying in between radii r_1 and r_2 depicted in Fig. 3. In the inertia-free limit the general problem of the relation between the variables, radial pressure, δp_r, temperature change, δT, volume displacement, δV and entropy displacement, δS at the two radii has been solved [4] in the frequency domain in terms of a transfer matrix:

$$\begin{pmatrix} \delta p_r \\ \delta T \\ \delta V \\ \delta S \end{pmatrix}_{r_2} = \mathbf{T}(r_2, r_1) \begin{pmatrix} \delta p_r \\ \delta T \\ \delta V \\ \delta S \end{pmatrix}_{r_1} \tag{12}$$

In general $\mathbf{T}$ is a complicated object. An interesting result was found when two conditions hold: 1) frequencies are high enough to be in the "thermally thick limit" with respect to r_2, i.e. $|l_D| \ll r_2$ and 2) $r_1 \ll r_2$: When studying in this case the combined response to thermal stimuli at radius r_1 and mechanical stimuli at radius r_2 one can neglect the mechanical boundary condition at r_1 and the thermal boundary condition at radius r_2 ending up with a reduced transfer matrix given as

$$\begin{pmatrix} \delta T \\ \delta S \end{pmatrix}_{r_1} = \begin{pmatrix} i\omega Z_{th} T_0 V_2 \kappa_S \beta_S & i\omega Z_{th} T_0 \beta_S \\ V_2 \kappa_S \beta_S & \beta_S \end{pmatrix} \begin{pmatrix} \delta p_r \\ \delta V \end{pmatrix}_{r_2}, \tag{13}$$

where $V_2 = \frac{4\pi}{3} r_2^3$ and Z_{th} is the thermal impedance,

$$Z_{\text{th}}(\omega) = \frac{1}{4\pi\lambda r_1 \left(1 + \sqrt{i\omega r_1^2 c_l(\omega)/\lambda}\right)}, \tag{14}$$

λ is the heat conductivity. The specific heat, c_l entering the thermal impedance is the so-called longitudinal specific heat. c_l is the amount of heat absorbed per Kelvin upon a temperature increment if the associated expansion is forced to be longitudinal. This is in contrast to the isobaric specific heat for which the expansion is isotropic. The longitudinal specific heat can be related to the isochoric specific heat, c_V by [4]

$$c_l = \frac{\frac{1}{\kappa_S} + \frac{4}{3}G}{\frac{1}{\kappa_T} + \frac{4}{3}G} c_V, \tag{15}$$

where G is shear modulus. Using the identities [4]

$$\frac{c_p}{c_V} = \frac{\kappa_T}{\kappa_S} \quad \text{and} \quad \kappa_T - \kappa_S = \frac{c_p}{T_0 \beta_S^2} \tag{16}$$

together with (15) the deviation between the longitudinal specific heat and isobaric specific heat may be expressed by

$$\frac{1}{c_p} = \frac{1}{c_l} - \frac{1}{T_0 \beta_S^2} \frac{\frac{4}{3}G}{1 + \frac{4}{3}G\kappa_S}. \tag{17}$$

This expression has the advantage of giving $c_p(\omega)$ in terms of the quantities $c_l(\omega), \kappa_S(\omega), \beta_S(\omega)$ and $G(\omega)$ that are possible to access experimentally by our new device supplemented with the Piezoelectric Shear modulus Gauge [13].

Eq. (13) is equivalent to equation (138) of reference [4]. The determinant of (13) is zero although a transfer matrix relating proper conjugated variables should have determinant 1. The reason is that we are studying a limiting case where $|i\omega Z_{\text{th}} T_0 V_2 \kappa_S \beta_S^2| \gg 1$. Thus the inverse relation is

$$\begin{pmatrix} \delta p_r \\ \delta V \end{pmatrix}_{r_2} = \begin{pmatrix} \beta_S & -i\omega Z_{th} T_0 \beta_S \\ -V_2 \kappa_S \beta_S & i\omega Z_{th} T_0 V_2 \kappa_S \beta_S \end{pmatrix} \begin{pmatrix} \delta T \\ \delta S \end{pmatrix}_{r_1}, \tag{18}$$

This is equivalent to equation (139) of reference [4], but there was a typo: the common T_0 factor in the matrix of that formula should be deleted. The simplified transfer matrix can be represented by the equivalent diagram of Fig. 4. The equivalent diagram is in a sense a more correct description since it leads to a transfer matrix deviating from Eq. (13) by a negligible term that however endows it with a determinant of 1.

4. The combined experiment

The adiabatic compressibility $\kappa_S(\omega)$ can be measured using the piezoelectric bulk modulus gauge (PBG) [3]. The PBG is a hollow sphere of radius 1 cm with a thin wall of a piezoelectric ceramic material. The thickness t is 0.5 mm. The sphere may be filled by a liquid at elevated temperature, where it is fluent. The PBG transforms the mechanical compliance of the liquid into an electric compliance (the capacitance), that can be simply measured by an LCR-meter or by other means. In order to make combined thermomechanical experiments we have placed a thermistor in the middle of the PBG (see Fig. 5). By the thermistor itself we can measure the longitudinal heat capacity $c_l(\omega)$ via the effusivity [5]. Combining the two devices makes it, in principle, possible to get the cross response function $1/\beta_S$. That is, nearly all ingredients of Λ_{Sp} can be found for the same sample in the same device. However if $c_l(\omega)$ differs significantly from $c_p(\omega)$ [4] as

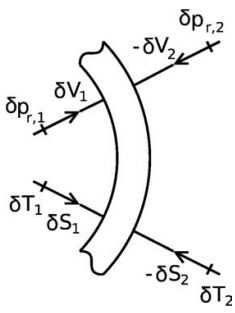

Fig. 3. Depiction of the four thermal and mechanical interactions at the boundaries at r_1 and r_2 in spherical geometry.

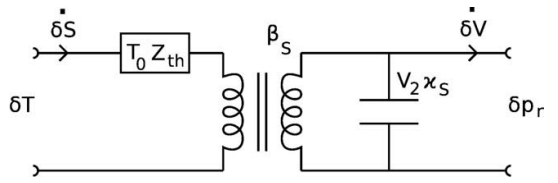

Fig. 4. Equivalent diagram of the liquid.

Please cite this article as: T. Christensen, et al., A combined measurement of thermal and mechanical relaxation, J. Non-Cryst. Solids (2010), doi:10.1016/j.jnoncrysol.2010.07.051

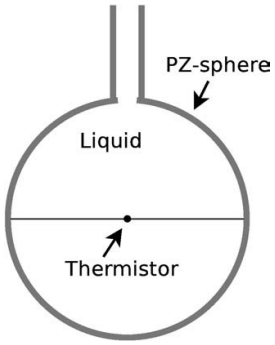

Fig. 5. The combined measurement of c_l, κ_S, β_S.

may be judged by Eq. (17) a supplementary measurement of the shear modulus is needed. We may produce an oscillating heat current with amplitude P_{th} by Joule heating in the thermistor and measure the piezoelectric voltage U_{pz} generated in the PBG as the liquid attempts to expand. This voltage contain information on $1/\beta_S = \left(\frac{\partial V}{\partial S}\right)_p$ but it is also dependent of the thermal interaction of the thermistor with the liquid and the mechanical interaction of the liquid with the PBG. In order to filter these factors out we may look at the equivalent diagram, Fig. 6 of the whole system. For simplicity we model the thermistor as an ideal heat generator in parallel with its heat capacitance C_0 of approximately 5.5×10^{-5} J/K. (For a more detailed model of the thermal structure of the thermistor, see reference [5]). In the equivalence diagram in Fig. 6 the PBG consist of a mechanical compliance, C_m, a transducer ratio, T_{pz} and an electric (clamped) capacitance C_e. They can be expressed [3] in terms of the dielectric constant, ϵ_{33}, the elastic compliance, $(s_{11}+s_{12})/2$ and the piezoelectric constant, d_{13} of the piezoelectric material pz29 together with the radius, r_2 and shell thickness, t (see Table 1).

By the equivalence diagram one finds that the generated piezoelectric voltage amplitude U_{pz} measured by a voltmeter of high impedance ($I_{pz}=0$) in response to a heat current amplitude P_{th} generated in the thermistor becomes

$$\left(\frac{U_{pz}}{P_{th}}\right)_{I_{pz}=0} = \frac{T_{pz}}{C_e i\omega}\frac{1}{(1+C_0 i\omega Z_{th}(\omega))\left(1+\left(1+T_{pz}^2\frac{C_m}{C_e}\right)\frac{V_2\kappa_S(\omega)}{C_m}\right)} \qquad (19)$$

$$\frac{1}{T_0\beta_S(\omega)}$$

We see that in principle β_S may be found by this third cross experiment with a thermistor in the PBG. However the signal is also influenced in its frequency dependence by the thermal impedance of the liquid and the adiabatic compressibility but both of these can be found by the experiments of the thermistor alone respectively the PBG alone. The frequency dependence in the thermal impedance has a characteristic diffusion time constant that is almost independent of the change of c_l at the glass transition whereas the factor containing the compressibility of course will change the position of its characteristic time scale as temperature is changed. It is interesting to estimate this signal. At 1 Hz $C_0 Z_{th}$ is of the order of 1 and so is the factor containing the compressibility. From the values in the Table 1 we find $\frac{T_{pz}}{C_e} = 10^{11}\mathrm{Vm}^{-3}$. Typical values of the expansion coefficient and the specific heat of a liquid are $\alpha_p = 5\times10^{-4}\mathrm{K}^{-1}$ and $c_p = 2\times10^6\mathrm{JK}^{-1}\mathrm{m}^{-3}$ and thus $\frac{1}{T_0\beta_S} = \frac{\alpha_p}{c_p} = 2.5\times10^{-10}\mathrm{m}^3\mathrm{J}^{-1}$. From this we find $\frac{T_{pz}}{C_e}\frac{1}{T_0\beta_S} = 25\,\mathrm{V/J}$. Using a power amplitude P_{th} of 0.3 mW in order to keep temperature change in the centre below 1 K we thus expect a signal of the order of 1 mV at 1 Hz which is readily detectable.

Table 1
Properties and lumped parameters of the piezoelectric bulk modulus gauge modeled in Fig. 6.

r_2		9.5×10^{-3} m
t		0.5×10^{-3} m
ϵ_{33}		26×10^{-9} F/m
$\frac{s_{11}+s_{12}}{2}$		6×10^{-12} m^2/N
d_{13}		26×10^{-9} C/N
k_p	$\frac{d_{13}}{\sqrt{\epsilon_{33}(s_{11}+s_{12})/2}}$	0.64
C_m	$\frac{s_{11}+s_{12}}{2}\frac{4\pi r_2^4}{t}$	1.5×10^{-15} m^3/Pa
T_{pz}	$\frac{2d_{13}}{(s_{11}+s_{12})}\frac{1}{r_2}$	4×10^3 C/m^3
C_e	$\epsilon_{33}\left(1-k_p^2\right)\frac{4\pi r_2^3}{t}$	40×10^{-9} F

5. Conclusion

Of the four dynamic Prigogine–Defay ratios one special namely, $\Lambda_{sp} = -(T_0/c_p)''(\kappa_S)''/((1/\beta_S)'')^2$ seems from an experimental viewpoint to be the most directly accessible. By combining the devices of the two techniques 1) measurement of the adiabatic compressibility $\kappa_S(\omega)$ with the Piezoelectric Bulk modulus Gauge and 2) measurement of the longitudinal specific heat $c_l(\omega)$ by thermal effusion in spherical geometry a third cross response function, $1/\beta_S(\omega)$ may be measured. That is, nearly all ingredients of Λ_{sp} could be found for the same sample in the same device. However $c_l(\omega)$ may differ from $c_p(\omega)$ [4], in which case a supplementary measurement of the shear modulus is needed.

References

[1] U.R. Pedersen, T. Christensen, T. Schrøder, J.C. Dyre, Feasibility of a single-parameter description of equilibrium viscous liquid dynamics, Phys. Rev. E 77 (2008) 011201.
[2] N.L. Ellegaard, T. Christensen, P.V. Christiansen, N.B. Olsen, U.R. Pedersen, T.B. Schrøder, J.C. Dyre, Single-order-parameter description of glass-forming liquids: a one-frequency test, J. Chem. Phys. 126 (2007) 074502.

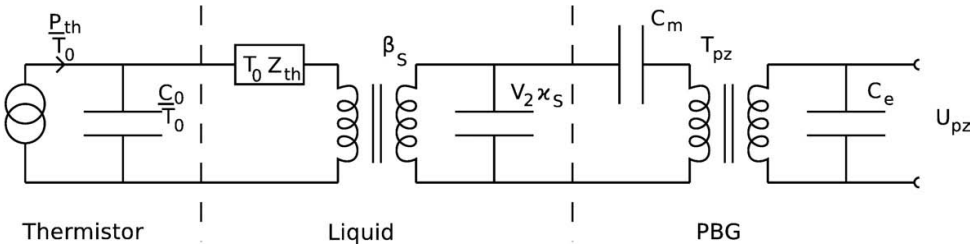

Fig. 6. Equivalent diagram of the liquid in contact with the thermistor and the piezoelectric shell (PBG).

Please cite this article as: T. Christensen, et al., A combined measurement of thermal and mechanical relaxation, J. Non-Cryst. Solids (2010), doi:10.1016/j.jnoncrysol.2010.07.051

[3] T. Christensen, N.B. Olsen, Determination of the frequency-dependent bulk modulus of glycerol using a piezoelectric spherical-shell, Phys. Rev. B 49 (1994) 15396.
[4] T. Christensen, J.C. Dyre, Solution of the spherically symmetric linear thermo-viscoelatic problem in the inertia-free limit, Phys. Rev. E 78 (2008) 021501.
[5] B. Jakobsen, N.B. Olsen, T. Christensen, Frequency dependent specific heat from thermal effusion in spherical geometry, Phys. Rev. E 81 (2010) 061505.
[6] P. Curie, Oeuvres, Societe Francaise de Physique, Paris, 1908.
[7] I. Prigogine, Etude Thermodynamique des Phenomenes Irreversibles, Desoer, Liege, 1947.
[8] S.R.D. Groot, P. Mazur, Non-equilibrium Thermodynamics, North-Holland Publishing Co., Amsterdam, 1962.
[9] N.P. Bailey, T. Christensen, B. Jakobsen, K. Niss, N.B. Olsen, U.R. Pedersen, T.B. Schrøder, J.C. Dyre, Glass-forming liquids: one or more "order" parameters? J. Phys. Condens. Matter 20 (2008) 244113.
[10] J. Meixner, H.G. Reik, in: S. Flügge (Ed.), Principen der Thermodynamik und Statistik, Handbuch der Physik, vol. 3, Springer, Berlin, 1959.
[11] T.B. Schrøder, N.P. Bailey, U.R. Pedersen, N. Gnan, J.C. Dyre, Pressure–energy correlations in liquids. III. Statistical mechanics and thermodynamics of liquids with hidden scale invariance. J. Chem. Phys. 131 (2009) 234503.
[12] N.P. Bailey, U.R. Pedersen, N. Gnan, T.B. Schrøder, J.C. Dyre, Pressure–energy correlations in liquids. II. Analysis and consequences. J. Chem. Phys. 129 (2008) 184508.
[13] T. Christensen, N.B. Olsen, A rheometer for the measurement of a high-shear modulus covering more than 7 decades of frequency below 50 kHz, Rev. Sci. Instrum. 66 (1995) 5019–5031.

Please cite this article as: T. Christensen, et al., A combined measurement of thermal and mechanical relaxation, J. Non-Cryst. Solids (2010), doi:10.1016/j.jnoncrysol.2010.07.051

Predicting the density-scaling exponent of a glass-forming liquid from Prigogine-Defay ratio measurements

Ditte Gundermann[1], Ulf R. Pedersen[1,2], Tina Hecksher[1], Nicholas Bailey[1], Bo Jakobsen[1], Tage Christensen[1], Niels B. Olsen[1], Thomas B. Schrøder[1], Daniel Fragiadakis[3], Riccardo Casalini[3], C. Michael Roland[3], Jeppe C. Dyre[1], and Kristine Niss[1]

[1]*DNRF Centre Glass and Time, IMFUFA, Department of Sciences, Roskilde University, Postbox 260, DK-4000 Roskilde, Denmark*

[2]*Department of Chemistry, University of California, Berkeley, California 94720-1460, USA*

[3]*Chemistry Division, Naval Research Laboratory, Washington, DC 20375-5342, USA*

(Dated: November 22, 2010)

The fundamental question in glass-science is to understand the dramatic temperature and density dependence of the relaxation time of glass-forming liquids. The recently established "density scaling" provides an expression for the relative importance of temperature and density in controlling the relaxation time. We demonstrate experimentally and theoretically that the density scaling exponent can be found from thermoviscoelastic linear-response data at a single state point for approximately single-parameter liquids. Consistent with this a compilation of all available literature data for the Prigogine-Defay ratio shows that van der Waals bonded liquids and polymers are approximately single-parameter liquids, whereas associative and network-forming liquids are not.

Many liquids are known to exhibit peculiar, sometimes even spectacular behavior. Water is a notorious example with its many intriguing anomalies [1, 2]. This raises the question: Do liquids exist with "simple" behavior and what characterizes such behavior? A recent series of papers [3–7] proposed such a class of liquids, "strongly correlating liquids", which are effectively single parameter liquids [8]. The possible existence of single parameter liquids [9] has important implications, particularly for solving long-standing fundamental questions related to the glass-transition [10].

In this paper we present an experimental test of a striking prediction for strongly correlating liquids, namely that the density scaling exponent – characterizing how to scale density and temperature between different state points to have the relaxation time fall on a master curve [11–15] – may be calculated from equilibrium fluctuations at a single state point [7]. The equilibrium fluctuations are probed via the fluctuation-dissipation theorem, which relates linear-response functions to fluctuations. The experiments were performed on a van der Waals bonded and stable glass-forming liquid, Tetramethyltetraphenyltrisiloxane (DC704), which is a commercial silicon oil. The paper goes on to present a reinterpretation of the classic Prigogine-Defay ratio, showing that many other systems are strongly correlating, *i.e.* approximately single parameter liquids. All together, this paper suggests that van der Waals liquids are strongly correlating, confirming the long-held general view that these liquids are simpler than associated liquids. In contrast, network-forming liquids like water, glycerol, or silica are much more complex.

Temperature and volume both play important roles for the viscous slowing down as the glass transition is approached [16–18]. The first measurements of viscosity under pressure date back to Bridgman [19], but only during the last decade has a substantial amount of data become available on viscous liquid dynamics at different pressures (see, e.g., 11–15, and [20]). The most important experimental finding is probably *density scaling*, i.e., that the temperature (T) and density (ρ) dependence of the relaxation time for many liquids may be described in terms of the single scaling variable $\rho^{\gamma_{\text{scale}}}/T$ [11–15]. This scaling is valid, e.g., for van der Waals liquids, but not for hydrogen-bonded liquids [21]. A simple explanation can be given for strongly correlating liquids. Such liquids are characterized by an almost proportionality between the isochoric fluctuations of the virial W and the potential energy U [3–5]. Moreover strongly correlating liquids have "isomorphs", which are curves in the phase diagram along which a number of properties – including the dynamics – are almost invariant [7]. The isomorph concept directly leads to density scaling: A strongly correlating liquid's isomorphs obey the equation $\rho^{\gamma_{\text{isom}}}/T = \text{Const.}$, for which γ_{isom} is determined from the isochoric equilibrium fluctuations' almost proportionality between virial W and potential energy U, $\Delta W(t) \cong \gamma_{\text{isom}} \Delta U(t)$. In particularly the relaxation time is a function of $\rho^{\gamma_{\text{isom}}}/T$. The predicted agreement between the exponent found from the fluctuations, γ_{isom}, and the density scaling exponent, γ_{scale}, was verified for some computer-simulated liquids [22, 23], but never tested experimentally. Such a test is demanding, however, because it involves new and unique measurements of frequency-dependent viscoelastic response functions.

Figure 1 (a) shows the dielectric relaxation time for DC704 as a function of density for different isotherms and data taken at the atmospheric pressure isobar. pVT-data were used to calculate the density at the different pressure-temperature points. Density scaling is demonstrated in Fig 1 (b), showing that all data collapse onto a master curve when plotted as a function of the scaling variable $\Gamma = T/\rho^{\gamma_{\text{scale}}}$ ($\gamma_{\text{scale}} = 6.1 \pm 0.2$).

Turning now to the isomorph prediction, the almost

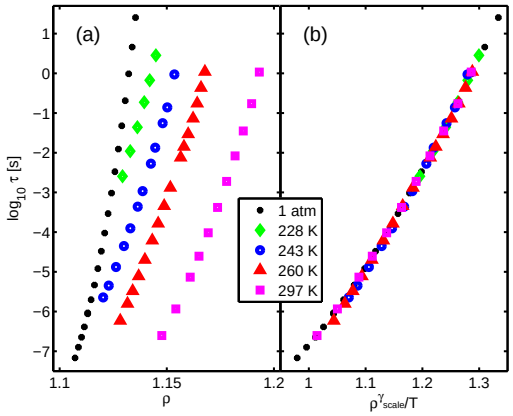

FIG. 1. (a) The dielectric relaxation time ($\tau = 1/\omega_{max}$) as a function of density along different isotherms and along the atmospheric pressure isobar for DC704. (b) Relaxation time as a function of $\rho^{\gamma_{\rm scale}}/T$ for DC704 where $\gamma_{\rm scale} = 6.1$ gives the best collapse of the relaxation times.

proportionality of the equilibrium fluctuations $\Delta W(t) \cong \gamma_{\rm isom}\Delta U(t)$ suggests the following expression for $\gamma_{\rm isom}$ [7] (where sharp brackets indicate NVT ensemble averages)

$$\gamma_{\rm isom} \equiv \frac{\langle \Delta W \Delta U\rangle}{\langle (\Delta U)^2\rangle}. \qquad (1)$$

In order to find this quantity from linear thermoviscoelastic measurements we reason as follows: The virial and the potential energy give the configurational parts of the pressure and energy, respectively. A characteristic of viscous liquids is time-scale separation. Fluctuations of the kinetic terms, which are related to vibrations, decorrelate on a much faster time scale than the fluctuations of configurational terms. Consequently, if one averages the fluctuations in pressure and energy over a time scale much longer than that of the vibrations – but much shorter than the alpha relaxation time – one gets the fluctuations of the configurational terms. For such averages it follows that $\langle \Delta W \Delta U\rangle / \left\langle (\Delta U)^2\right\rangle \simeq V\langle \Delta p \Delta E\rangle / \left\langle (\Delta E)^2\right\rangle$. This brings us closer to something that can be accessed experimentally, because fluctuations in pressure and energy determine the thermoviscoelastic linear-response functions via the fluctuation-dissipation theorem: $V\langle \Delta p \Delta E\rangle / \left\langle (\Delta E)^2\right\rangle = (\beta_V^{liquid} - \beta_V^{solid})/(c_V^{liquid} - c_V^{solid})$, where $\beta_V = (\partial P/\partial T)_V$ is the pressure coefficient. The "solid" response is understood here as the high-frequency (short-time) limit of the relevant frequency-dependent linear-response of the equilibrium liquid (still probing the system at times much longer than phonon times). Thus

$$\gamma_{\rm isom} = \frac{\beta_V(\omega\to 0) - \beta_V(\omega\to\infty)}{c_V(\omega\to 0) - c_V(\omega\to\infty)}. \qquad (2)$$

The two linear thermoviscoelastic response functions $\beta_V(\omega)$ and $c_V(\omega)$ refer to constant-volume measurements. Experiments, however, are usually performed under constant pressure. This problem can be overcome by measuring three independent thermoviscoelastic dynamic response functions, subsequently calculating $\beta_V(\omega)$ and $c_V(\omega)$ using standard thermodynamic relations (where the frequency-dependent versions of the Maxwell relations are the corresponding Onsager relations). A further complication is that even constant-pressure conditions are difficult to obtain for ultraviscous liquids, because the sample thermal expansion is often limited in some spatial directions [24]. This implies that even $c_p(\omega)$ is not measured directly; rather it is the so-called longitudinal heat capacity $c_l(\omega)$ that is measured in most setups [24], and we also measure $\alpha_l(\omega)$ instead of $\alpha_p(\omega)$. Fortunately knowledge of the frequency-dependent shear modulus $G(\omega)$ allows one to calculate $c_p(\omega)$ from data. In summary, to arrive at $\gamma_{\rm isom}$ we measured the following four frequency-dependent linear thermoviscoelastic response functions: The adiabatic bulk modulus $K_s(\omega)$, the longitudinal heat capacity $c_l(\omega)$, the longitudinal expansion coefficient $\alpha_l(\omega)$, and the shear modulus $G(\omega)$.

The (frequency-dependent) shear modulus was measured using a piezoelectric transducer [25], the adiabatic bulk modulus with a similar technique [26], and the longitudinal heat capacity was measured using the 3ω-method in a spherical geometry [27]. The expansion coefficient was measured in the time domain using capacitative dilatometry [28, 29].

Examples of measured frequency-dependent linear responses are shown in Fig. 2. In principle we need only data at one state point to determine $\gamma_{\rm isom}$ from Eq. 2. In practice, we used several temperatures to estimate reliably the temperature dependence of the solid and liquid levels. This was done to be able to extrapolate the DC704 expansion coefficient, which was obtained at lower temperatures than the other response functions. The reference temperature used is $T = 214$ K. This temperature is close to the calorimetric glass transition temperature of DC704, but it should be emphasized that we measure the linear response of the equilibrium liquid. The solid and liquid limits of $\beta_V(\omega)$ and $c_V(\omega)$ were calculated from the high- and low-frequency limits of the four measured thermoviscoelastic response functions, respectively, by solving the following four equations with four unknowns (where all below quantities are frequency-dependent and use is made of the relation $\beta_V = \alpha_p K_T$):

$$c_l = \frac{1+\frac{4G}{3K_S}}{1+\frac{4G}{3K_T}}c_p \quad \alpha_l = \frac{\alpha_p}{1+\frac{4G}{3K_T}}$$
$$c_V = c_p - T\alpha_p^2 K_T \quad K_S = K_T\frac{c_p}{c_V}. \qquad (3)$$

The values of the measured solid and liquid levels at the reference temperature are reported in Tab. I. When sub-

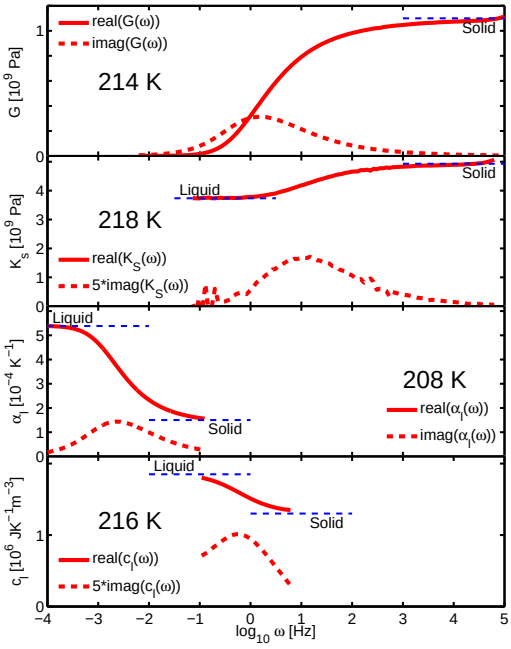

FIG. 2. Examples of frequency-dependent real and imaginary parts of thermoviscoelastic response functions of DC704, illustrating the experimental challenge associated with checking the isomorph prediction. (a) The shear modulus, $G(\omega)$. (b) The adiabatic bulk modulus, $K_S(\omega)$. (c) The longitudinal heat capacity, $c_l(\omega)$. (d) The longitudinal expansion coefficient $\alpha_l(\omega)$, for which data were Laplace transformed in order to give all data in the frequency representation although measurements are in the time domain [29]. In order to place the relaxation region in the observed frequency window, we show data at a temperature that varies with response function.

stituted into Eq. (2) we find that the isomorph prediction for the density scaling exponent of DC704 is $\gamma_{\rm isom} = 6.2 \pm 2$, in good agreement with the density-scaling exponent $\gamma_{\rm scale}6.1 \pm 0.2$ (Fig. 1(b)). The uncertainty on $\gamma_{\rm isom}$ is large because measuring the absolute values of the frequency-dependent thermo-viscoelastic response functions is still very challenging. However, even considering the large uncertainty on the predicted exponent $\gamma_{\rm isom}$, it is quite striking that it agrees with the exponent found from density scaling. The agreement implies that thermoviscoelastic linear-response measurements at one single ambient-pressure state point can be used to predict the density-scaling exponent which descres the density and temperature dependence of relaxation times varying from the micro- to kilo-seconds, measured at pressures up to 400 MPa over a 30 K temperature range. This is a main conclusion of the present paper.

The WU correlation coefficient of the NVT ensemble, $R = \langle \Delta W \Delta U \rangle / \sqrt{\langle (\Delta U)^2 \rangle \langle (\Delta W)^2 \rangle}$, measures how

	DC704 (214 K)
$c_l^{\rm liq}\,[10^6 J/(Km^3)]$	1.65±0.15
$c_l^{\rm sol}\,[10^6 J/(Km^3)]$	1.35±0.05
$K_S^{\rm liq}\,[10^9 Pa]$	4.0±0.05
$K_S^{\rm sol}\,[10^9 Pa]$	5.2±0.05
$\alpha_l^{\rm liq}\,[10^-3K^{-1}]$	0.45±0.04
$\alpha_l^{\rm sol}\,[10^-3K^{-1}]$	0.1±0.01
$G^{\rm liq}\,[10^9 Pa]$	0
$G^{\rm sol}\,[10^9 Pa]$	1.1±0.05
$\Pi_{pT}^{\rm lin}$	1.1±0.3
$\Pi_{VT}^{\rm lin}$	1.2±0.6
R	0.92
$\gamma_{\rm isom}$	6.2 ± 2
$\gamma_{\rm scale}$	6.1 ± 0.2

TABLE I. The values of measured solid and liquid levels of the thermo-mechanical response functions of DC704 at (214 K). These data are used to calculate the predicted exponent $\gamma_{\rm isom}$, which is compared to the exponent found from density scaling $\gamma_{\rm scale}$.

strong the WU correlations are in a liquid and therefore gives a measure of how well we can expect it to follow the isomorph theory. Expressing the R in terms of linear-response functions one realizes that R is directly given by the linear NVT Prigogine-Defay (PD) ratio [30], $\Pi_{VT}^{\rm lin}$:

$$R = \frac{\beta_V^{\rm liq} - \beta_V^{\rm sol}}{\sqrt{-(K_T^{\rm liq} - K_T^{\rm sol})(c_V^{\rm liq} - c_V^{\rm sol})/T}} = \frac{1}{\sqrt{\Pi_{VT}^{\rm lin}}}. \quad (4)$$

The PD-ratio equals unity if the liquid is a single-parameter liquid [9]. Thus a perfectly correlating liquid is what was traditionally referred to as a single- parameter liquid [8]. Earlier studies of the PD-ratio gave no physical interpretation of values different from unity, even if these were close to one. The above interpretation of the linear NVT-PD-ratio as given by the correlation coefficient now shows that the PD-ratio provides a measure of how strongly correlating a given liquid is.

When the linear NVT PD-ratio is exactly unity, other linear PD-ratios, e.g., the experimentally relevant linear NpT PD-ratio, are also one [30]. When $\Pi_{VT}^{\rm lin}$ is not strictly one, there is no such result, but by continuity we surmise that $\Pi_{pT}^{\rm lin}$ is close to unity if and only if $\Pi_{VT}^{\rm lin}$ is. For DC704 we find $\Pi_{pT}^{\rm lin} = 1.1 \pm 0.3$ and $\Pi_{VT}^{\rm lin} = 1.2 \pm 0.6$, consistent with this conjecture.

Neither the linear NVT-PD nor the linear NpT-PD ratios have been reported prior to this study, but there are numerous reports in the literature on the classic (NpT) PD-ratio. This quantity is calculated using temperature-extrapolated liquid and glassy static responses, where the glassy response is defined from the low-temperature ($T < T_g$) solid response rather than the high frequency

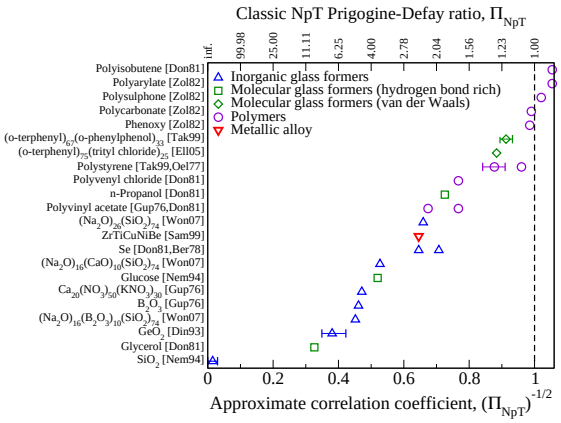

FIG. 3. Literature values of the classical (NpT) Prigogine-Defay ratios $\Pi_{pT}^{\text{classic}}$ of 22 glass formers. Liquids are sorted (along y-axis) with respect to (highest reported) value of the ratio and includes inorganic glass formers (triangles pointing up), hydrogen bond rich molecular liquids (squares), van der Waals bonded molecular liquids (diamonds), polymers (circles), and a metallic alloy (triangle pointing down). The inverse square root of the classic NpT Prigogine-Defay ratio gives an estimate for the correlation coefficient (lower x-axis). Strong correlations are found in van der Waals bonded molecular liquids and polymers. See the supplementary material for references.

level of the equilibrium liquid:

$$\Pi_{pT}^{\text{classic}} \equiv \frac{(\kappa_T^{liq}(T_g) - \kappa_T^{glass}(T_g))(c_p^{liq}(T_g) - c_p^{glass}(T_g))}{T_g(\alpha_p^{liq}(T_g) - \alpha_p^{glass}(T_g))^2}. \quad (5)$$

Here $\kappa_T = 1/K_T$ is the isothermal compressibility and "(T_g)" indicates an extrapolation to the glass transition temperature. Although the classical PD-ratio is not really well-defined from a theoretical point of view [30], it does provide an experimentally much easier route for investigating strong correlations than measuring the proper frequency-dependent linear thermoviscoelastic response functions at one temperature. Thus in the lack of linear PD-ratio data we compiled all available literature data on the classical PD-ratio.

Figure 3 shows the literature values for 22 glass formers, including polymers, a metallic alloy, inorganic and molecular liquids (both hydrogen-bond rich and van der Waals bonded). The systems are sorted after their PD-ratio. In analogy with the NVT case, we define an approximate correlation coefficient of the NpT ensemble as the inverse square-root of the NpT PD-ratio. Network-bonded inorganic glass formers such as silica glasses and hydrogen-bond rich molecular liquids (e.g., glycerol and glucose) have large PD-ratios, whereas van der Waals bonded liquids, exemplified by the two mixtures with o-terphenyl as the major constituent and polymers, have PD-ratios close to one. This confirms the conjecture that van der Waals bonded liquids are strongly correlating, while associative and network-forming liquids are not [5, 6]. It is interesting also to compare propanol and glycerol, which have the same backbone of three carbon atoms, but one and three hydroxyl-groups respectively. Propanol with only one hydroxyl group and therefore fewer hydrogen bonds has a much smaller PD-ratio than glycerol. This pattern is consistent with computer simulation results, where strongly correlating liquids are found to be liquids without directional bonding or competing interactions [4].

The glassy and liquid extrapolated response values used to calculate the classic Prigogine-Defay ratio provides an alternative less well defined way of calculating γ_{isom} [31]. Data of this type is scarce in literature and we need samples where the density-scaling exponent is also available. We did the analysis on a the data of a mixture 67% o-terphenyl and 33% o-phenylphenol from a nice paper by Takahara *et al.*[32]. This mixture is a strongly correlating liquid with $\Pi_{pT}^{\text{classic}} = 1.20$ [32]. We find $\gamma_{\text{isom}} = 5.4 \pm 1$ compared to $\gamma_{\text{scale}} = 6.2 \pm 0.2$ [13], see supplementary material for details.

In summary, we presented the first experimental evidence that a strongly correlating liquid exists and that it obeys the isomorph predictions. Specifically, the scaling exponent found from linear-response data agrees with the exponent found from density scaling for a van der Waals bonded silicone liquid. We moreover connected the classical PD-ratio with the correlation coefficient and found that literature data support the general conjecture that van der Waals bonded liquids are strongly correlating, whereas liquids with significant directional bonding are not. These findings suggest that the liquids with "simple" behavior are the strongly correlating liquids.

[1] P. G. Debenedetti, J. Phys.: Condens. Matter **15**, R1669 (2003).
[2] C. A. Angell, Science **319**, 582 (2008).
[3] U. R. Pedersen and N. B. andT. B. Schrøder andJ. C. Dyre, Phys. Rev. Lett. **100**, 015701 (2008).
[4] N. P. Bailey, U. R. Pedersen, T. B. S. N. Gnan, and J. C. Dyre, J. Chem. Phys. **129**, 184507 (2008).
[5] N. P. Bailey, U. R. Pedersen, T. B. S. N. Gnan, and J. C. Dyre, J. Chem. Phys. **129**, 184508 (2008).
[6] T. B. Schrøder, N. P. Bailey, U. R. Pedersen, N. Gnan, and J. C. Dyre, J. Chem. Phys. **131**, 234503 (2009).
[7] N. Gnan, T. B. Schrøder, U. R. Pedersen, N. P. Bailey, and J. C. Dyre, J. Chem. Phys. **131**, 234504 (2009).
[8] N. P. Bailey, T. Christensen, B. Jakobsen, K. Niss, N. B. Olsen, U. R. Pedersen, T. B. Schrøder, and J. C. Dyre, J. Phys.: Condens. Matter **20**, 244113 (2008).

[9] R. O. Davies and G. O. Jones, Adv. Phys. **2**, 370 (1953).
I. Prigogine and R. Defay, Chemical Thermodynamics (Longman, London) (1954).
M. Goldstein, J. Chem. Phys. **39**, 3369 (1963).
E. Donth, The Glass Transition Springer (2001).
I. M. Hodge, J. Non-Cryst. Solids **169**, 211 (1994).
C. T. Moynihan and P. K. Gupta, J. Non-Cryst. Solids **29**, 143 (1978).
T. M. Nieuwenhuizen, Phys. Rev. Lett. **79**, 1317 (1997).
J. I. Berg and A. R. Cooper, J. Chem. Phys. **68**, 4481 (1978).
A. Lion and J. Peters, Thermochim. Acta **500**, 76 (2010).
L. Wondraczek, S. Krolikowski, and H. Behrens, J. Chem. Phys. **130**, 204506 (2009).

[10] H. N. Lee, K. Paeng, , S. F. Swallen, and M. D. Ediger, Science **323**, 231 (2003).
T. Scopigno, G. Ruocco, F. Sette, and G. Monaco, Science **302**, 849 (2003).
L. Berthier, G. Biroli, J. P. Bouchaud, L. Cipelletti, D. E. Masri, D. L'hote, F. Ladieu, and M. Perino, Science **310**, 1797 (2005).
J. C. Dyre, Rev. Mod. Phys. **78**, 953 (2006).
L. Berthier, G. Biroli, J.-P. Bouchaud, L. Cipelletti, and W. van Saarloos, eds., *Dynamical heterogeneities in glasses, colloids, and granular media* (Oxford University Press, to appear).
K. L. Ngai, *Relaxation and Diffusion in Complex Systems (Partially Ordered Systems)* (Springer, 2010).
G. Floudas, M. Paluch, A. Grzybowski, and K. Ngai, *Molecular Dynamics of Glass-Forming Systems: Effects of Pressure (Advances in Dielectrics)* (Springer, 2010).

[11] C. Alba-Simionesco, A. Cailliaux, A. Alegria, and G. Tarjus, Europhys. Lett. **68**, 58 (2004).

[12] C. Dreyfus, A. L. grand, J. Gapinski, W. Steffen, and A. Patkowski, Eur. Phys. J. B **42**, 309 (2004).

[13] C. M. Roland, S. Hensel-Bielowka, M. Paluch, and R. Casalini, Rep. Prog. Phys. **68**, 1405 (2005).

[14] A. Reiser, G. Kasper, and S. Hunklinger, Phys. Rev. B **72**, 094204 (2005).

[15] R. Casalini and C. M. Roland, Phys. Rev. E **69**, 062501 (2004).

[16] M. L. Ferrer, C. Lawrence, B. G. Demirjian, D. Kivelson, C. Alba-Simionesco, and G. Tarjus, J. Chem. Phys. **109**, 8010 (1998).

[17] C. Alba-Simionesco, D. Kivelson, and G. Tarjus, J. Chem. Phys. **116**, 5033 (2002).

[18] C. M. Roland, Macromol **43**, 7875 (2010).

[19] P. W. Bridgman, Proc. of the Am. Chem. Soc. **77**, 129 (1949).

[20] G. Floudas, K. Mpoukouvalas, and P. Papadopoulos, J. Chem. Phys. **124**, 074905 (2006).

[21] C. M. Roland, R. Casalini, R. Bergman, and J. Mattsson, Phys. Rev. B **77**, 012201 (2008).

[22] D. Coslovich and C. M. Roland, J. Chem. Phys **131**, 151103 (2009).

[23] T. B. Schrøder, U. R. Pedersen, N. P. Bailey, S. Toxvaerd, and J. C. Dyre, Phys. Rev. E **80**, 04150 (2009).

[24] T. Christensen, N. B. Olsen, and J. C. Dyre, Phys. Rev. E **75**, 041502 (2007).

[25] T. Christensen and N. B. Olsen, Rev. Sci. Instr. **66**, 5019 (1995).

[26] T. Christensen and N. B. Olsen, Phys. Rev. B **49**, 15396 (1994).

[27] B. Jakobsen, N. B. Olsen, and T. Christensen, Phys. Rev. E **81**, 061505 (2010).

[28] C. Bauer, R. Bohmer, Moreno-Flores, R. Richert, H. Sillescu, and D. Neher, Phys. Rev. E **61**, 1755 (2000).

[29] K. Niss, N. B. Olsen, and J. C. Dyre, in preperation (2010).

[30] N. L. Ellegaard, T. Christensen, P. V. Christiansen, N. B. Olsen, U. R. Pedersen, T. B. Schrøder, and J. C. Dyre, J. Chem. Phys. **126**, 074502 (2007).

[31] This type of expression for γ_{scale} was also found in Ref. [33] by assuming an entropy basis for the dynamics.

[32] S. Takahara, M. Ishikawa, O. Yamamuro, and T. Matsuo, J. Phys. Chem. B **103**, 792 (1999).

[33] R. Casalini, U. Mohanty, and C. M. Roland, J. Chem. Phys. **125**, 14505 (2006).